Thèse présentée en vue d'obtenir le titre de

DOCTEUR DE L'ECOLE NATIONALE SUPERIEURE DES MINES DE PARIS

par

Samuel FOREST

Spécialité: Sciences et Génie des Matériaux

Modèles Mécaniques de la Déformation Hétérogène des Monocristaux

Mémoire Provisoire

Jury composé de:

Albrecht BERTRAM
René de BORST
Georges CAILLETAUD
Philippe PILVIN
Paul ROUGEE
François SIDOROFF
Erwin STEIN
Cristian TEODOSIU
André ZAOUI

A qui de droit
Acknowledgements
Danksagung

Le présent travail a été effectué au Centre des Matériaux de l'Ecole des Mines de Paris et au Bundesanstalt für Materialforschung und -prüfung (BAM-Berlin).

Je remercie Georges Cailletaud de m'avoir guidé, dès la fin de mes études d'ingénieur, dans l'étude du Monocristal, sujet fascinant s'il en est, et de m'avoir laissé une grande liberté pour explorer les plus beaux domaines de la Mécanique. Je remercie Philippe Pilvin pour l'aide qu'il m'a apporté tout au long du parcours. Il m'a fait bénéficier de sa grande culture mécanicienne. J'ai pu profiter de la riche expérience du groupe SiN en lois de comportement et des outils numériques exceptionnels que sont les logiciels SiDoLo et ZéBuLoN. Merci à Jacques Besson de m'avoir converti à TEX. Je remercie Michel Gaudet pour son soutien informatique dans des conditions souvent difficiles.

Je remercie mon Professeur André Pineau des conseils qu'il m'a prodigué sur les questions les plus fondamentales, de la Recherche à la Philosophie...

J'ai eu la chance de rencontrer à plusieurs reprises Paul Rougée pour de passionnantes discussions. Je le remercie de prendre part à ce jury.

Je remercie F. Sidoroff d'avoir accepté de se pencher sur mon travail.

Je remercie Cristian Teodosiu d'avoir accepté de rapporter sur ce travail.

M. André Zaoui m'a enseigné, depuis mon DEA, combien il faut de rigueur pour aborder les problèmes de micro-mécanique. Je le remercie d'avoir accepté de participer au jury.

I thank Prof. René de Borst for accepting to serve as a referee for my doctoral thesis. This work is part of Brite-Euram project BRE2-CT92-0176, entitled "Development of microstructure based viscoplastic models for an advanced design of single crystal hot section components". This was the occasion for very stimulating exchanges between France, Germany and Greece.

Ich danke Herrn Prof. Albrecht Bertram für die vielen interessanten Diskussionen seit meinem ersten Praktikum bei der BAM und für die Mitwirkung bei diesem Verfahren.

Ich danke Herrn Prof. Stein dafür, daß er sich bereit erklärt hat, diese Arbeit zu begutachten.

Jürgen Olschewski und der ganzen Abteilung V.31 danke ich für das wunderschöne Jahr in Berlin, einer faszinierenden und zugleich wundersamen Hauptstadt der Mechanik und Physik.

Dank Rainer Sievert habe ich gelernt, daß es höhere Kontinua gibt... Er hat mir seine ganze Literatur zur Verfügung gestellt und wir haben uns stundenlang unterhalten.

Aber der Schlüssel zu unserer Forschung liegt wahrscheinlich auch in den Tiefen der theoretischen Physik. Die möchte ich bei Wolfgang Dreyer lernen!

Ich danke Herrn Dr. Ziebs und der ganzen Abteilung V.21 dafür, daß ich an dem spannenden experimentellen Programm über Einkristalle bei der BAM teilnehmen konnte.

Ich danke Bettina, Florent, et mes parents, für ihre ständige Unterstützung. Florent fängt erst an, mit dem Mottschen Teppich zu spielen...

"Nous verrons que l'intelligence humaine se sent chez elle
tant qu'on la laisse parmi les objets inertes,
plus spécialement parmi les solides,
où notre action trouve son point d'appui
et notre industrie ses instruments de travail,
que nos concepts ont été formés à l'image des solides,
que notre logique est surtout la logique des solides,
que, par là-même, notre intelligence triomphe dans la géométrie,
où se révèle la parenté de la pensée logique avec la matière inerte,
et où l'intelligence n'a qu'à suivre son mouvement naturel,
pour aller de découverte en découverte
avec la certitude que l'expérience marche derrière elle
et lui donnera invariablement raison."

H. Bergson, L'Evolution Créatrice.

"Der Romantiker studiert das Leben,
wie der Mahler, Musiker und Mechaniker Farbe, Töne und Kraft.
Sorgfältiges Studium des Lebens macht den Romantiker,
wie sorgfältiges Studium von Farbe, Gestaltung, Ton und Kraft
den Mahler, Musiker und Mechaniker."

Novalis, Das Allgemeine Brouillon, *No. 1073.*

MODELES MECANIQUES DE LA DEFORMATION HETEROGENE DES MONOCRISTAUX

Table of contents

Part B

A COSSERAT THEORY FOR SINGLE CRYSTALS

Part C

NON-HOMOGENEOUS DEFORMATION OF TWO-PHASE SINGLE CRYSTALS

Introduction

The validity of a constitutive model in materials mechanics is often assessed in regard of its ability to satisfactorily describe the homogeneous deformation of the material under various loading conditions. In crystal plasticity much attention has been focused on the anisotropic tensile, compressive and shear behaviour of single crystals. The associated crystal lattice rotation can be measured and compared to model prediction. In each case maintaining a zone of homogeneous deformation in a specimen during testing turns out to be a difficult experimental task. The main objective of the present work is to show that the question of the pertinence of such mechanical modelling can only be settled if the model response is considered under conditions for which deformation becomes non-homogeneous. For that purpose, structural calculations are needed in order to work out the associated stress and strain fields. The confrontation with experiment is then all the more difficult that local strain measurements are necessary. Non-homogeneous deformation may arise as a result of particular loading conditions (the case of torsion of single crystals will be extensively investigated in this work) or of a bifurcation from an initially homogeneous strain state. A bifurcation analysis of the retained constitutive equations provides valuable information for the critical assessment of the model. Do the bifurcation modes have a physical meaning? Are they observed experimentally? When can bifurcation occur?

The ability of classical crystal plasticity models to describe some aspects of the non-homogeneous deformation of single crystal is examined closely in this work and further developments are proposed to come up to any detected deficiency.

The phenomenological approach to constitutive modelling in continuum mechanics can be regarded as a subject of geometry. It consists in recognizing geometrical forms which may result from many complex physical mechanisms. The yield surface in plasticity is such a geometrical object. It has no literal physical reality but comes out in a process akin to Thom's morphogenesis [Thom 1970]. The description of the evolution of these sophisticated forms requires the same virtuosity as geometry in mathematics.

However, the actual physical mechanisms that are responsible for the deformation of solids cannot be left aside if any improvement of the predictive character of constitutive models is to be gained. The elementary physical processes at the various involved length scales ranging from dislocation cores to the specimen size must be identified. The "curse of dimensionality" prevents us from taking all these various length scales into account. A mixed approach is usually retained: some relevant physical features are introduced into the modelling and the remaining constitutive equations have a phenomenological character. Such a compromise must be reached for a large range of model validity in terms of loading conditions and for the predictive capability of the model out of its identification domain. Regarding single crystals, the slip processes due to collective dislocation motion according to a discrete number of slip systems has been acknowledged in this work, but internal variables are used to account for the hardening behaviour, that could not be directly derived from microscopic dislocation mechanisms. Their evolution rules are of phenomenological type and enable us to simultaneously describe the tensile, cyclic and

even creep behaviour of single crystals. Nevertheless the retained evolution equations for internal variables are very similar to that obtained by some phenomenological reasoning on dislocation populations (see section A.3.2.1. for instance). The description of the anisotropic response of single crystals is entirely based on the role of cristallography in the kinematics. We have indeed given up introducing a detailed description of the microstructure of the material, but special attention has been paid on the presence of a coherent second phase in a single crystal material (part C).

The geometric objects classified by Thom describe how forms can evolve and bifurcate one into another. The same applies to the objects of continuum mechanics and the analysis of the structural stability of the constitutive models has become a major field of research. Potier-Ferry [1985] for instance has proposed a tentative catastrophe theory of plasticity and fracture. Structural stability means robustness of the phase portrait by perturbating not only initial conditions but also the set of equations itself or constants that intervene in them. At some singular point the uniqueness or stability of the solution of the boundary value problem may be lost and a bifurcation analysis can help interpreting unstable physical phenomena such as ratchetting (instability due to the loading conditions) or buckling (instability triggered by some geometrical imperfection). The mathematical tools are that of non linear dynamics [Thompson, Stewart 1986]. The linear or non-linear stability analysis has become a standard procedure in engineering sciences. It can be performed at the macroscopic level, like in [Hill, Hutchinson 1975], where the bifurcation analysis deals with both constitutive equations and equilibrium conditions, or at the microscopic level [Balke, Estrin 1994]. The strongly non-linear balance equations studied in the latter are recalled in section A.1 and the associated bifurcation modes are usually interpreted in terms of dislocation structures. In practice, bifurcation is triggered by any imperfection, geometrical or material heterogeneity, and the simulations presented in this work follow some particular bifurcation branches as indicated on the following drawing, after Demazure [1989]:

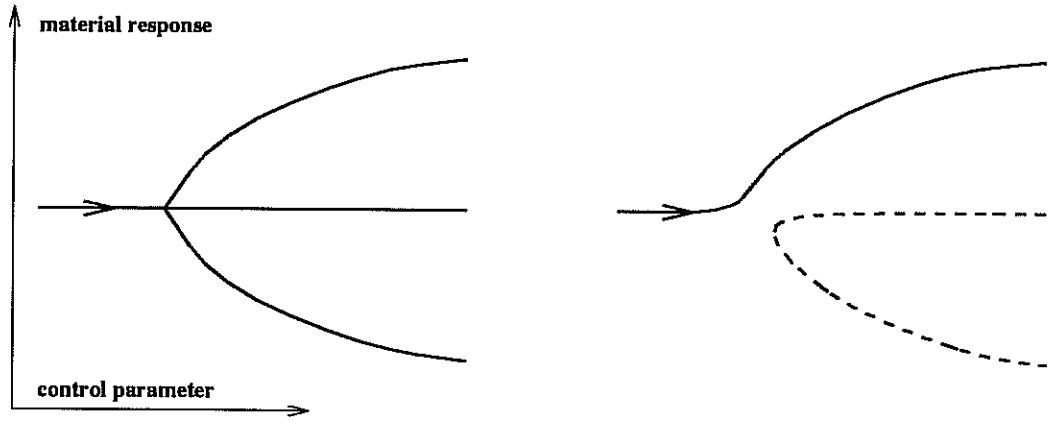

In our work, the control parameter will be the hardening modulus of the material.

An accurate modelling of non-homogeneous deformation of materials constitutes the missing link between the description of material behaviour and damage or fracture

mechanics. The localization of deformation in narrow shear bands or necking zones is often a direct precursor to ductile fracture through profuse void formation and growth within the bands. According to Chang, Asaro [1981], the formation of shear bands is an entirely natural and perhaps inevitable occurence in ductile single crystals. Although the details of these localization processes are certainly affected by microstructure, the generality of the phenomenon suggests that the underlying causes for it may well result from more general mechanical characteristics. It explains why the point of view adopted by the main stream of research during twenty years is the hypothesis that localization of deformation can be regarded as a result of a bifurcation in the constitutive description from an initially homogeneous state. Deformation can also localize in single crystals at the very beginning of plastic flow. Intense slip bands may form that play a significant role in fatigue. The stress is laid in this work on the prediction of these particular bifurcation modes and their simulation using the Finite Element method.

In part A, we mention first some results from literature regarding the stability analysis at the microscale and at the macroscale. The questions of uniqueness and stability are tackled within the framework of isothermal non-associated elastoplasticity at small strains. Under this assumption, it appears in particular that material softening is necessary for general bifurcation modes to occur in the case of associated plasticity. Preliminary calculations are presented to simulate some bifurcation modes predicted in literature. The two-dimensional and three-dimensional cases are distinguished. Bifurcation modes in single crystals have been extensively studied in the last twenty years in the case of single and double slip at large strain. Asaro and Rice [1977] have proved that bifurcation can occur while the material is still hardening. This is due to local geometric softening associated whith lattice rotation. However, coarse slip bands can be observed much earlier than predicted, and they can even appear with the first burst of plastic flow. To model these phenomena, we have introduced local material softening to trigger localization, and we remain within the framework of small strains. A bifurcation analysis in the case of multislip configurations is presented for f.c.c. single crystals. And the predicted bifurcation modes are simulated using the FE method for several three-dimensional slip configurations corresponding to the actual geometry of f.c.c. crystals. Particular attention is devoted to the influence of boundaries, interfaces and latent hardening on slip band formation. Although bifurcation is assumed to occur after very small amounts of deformation, we extend the model to the large strain framework to investigate the effect of local lattice rotation. This is the occasion for a review and comparison of various crystal plasticity models at large strain. A pragmatic formulation of the model using rotating frames is proposed, and the role of the corotational frame in crystal plasticity is pointed out.

In part B, it is shown that a precise description of strong lattice rotation gradients at the continuum level requires an extension of classical crystal plasticity. For that purpose we resort to the mechanics of generalized continua and we propose a Cosserat framework for the description of plastic lattice curvature and torsion at finite deformation. In addition to the usual internal variables that are more or less similar to scalar dislocation densities, internal variables accounting for lattice curvature and torsion are introduced that can be directly related to the dislocation density tensor coming from the continuum theory of

dislocations [Nye 1953]. The link between the additional internal variables and Ashby's geometrically necessary dislocations is enlightened. A bifurcation analysis is then carried out for explicit constitutive equations within the Cosserat framework, and the results are compared to the classical case.

Single crystals hardened by a second coherent phase can deform macroscopically in a rather homogeneous way, while strong deformation gradients develop at the microscopic scale. This happens for instance in single crystal nickel-base superalloys at high temperatures. Such materials are extensively used for hot section components in jet engines or stationary turbines. It is then of the utmost importance to have a precise idea of stress and strain in each phase with a view to damage modelling and fatigue life prediction. However, the modelling must remain simple enough to permit an implementation in a FE code for structural calculations (turbine blades ...). That is why we resort to homogenization techniques and consider only mean values of stress and strain over each phase within the representative volume element (part C). Some results on the effective elastic behaviour of non-homogeneous materials and their tentative extensions to the non-linear case are recalled at the beginning of part C. To compute the stress in each phase, we concentrate on the self-consistent scheme which presents us with a difficult problem in the special case of elastoviscoplasticity. The proposed method, that we have called "quasi-self-consistent" modelling, assumes explicit constitutive equations for the homogeneous equivalent medium. An optimization process ensures that a so-called "self-consistency" condition is fulfilled up to a certain tolerance for a given loading path. The resulting model is then validated for other complex loading conditions. Attention is first paid to the cyclic, proportional and non-proportional, uniaxial and multiaxial behaviour of two-phase isotropic materials. The approach is very general and can be applied to other multiphase materials. The main difficulty in the case of two-phase single crystals lies in the validation of the extension of the model to the anisotropic case. The method requires FE calculations over a representative cell embedded in the homogeneous equivalent medium, so that the morphology of individual phases can be taken into account to some extent. Nevertheless, in the case of single crystal nickel-base superalloy, the shape of the precipitates evolves in a way that depends on loading conditions, misfit and elastic properties of each phase (see [Pineau 1976] and [Dreyer, Olschewski 1994]). These aspects could not be incorporated in the modelling.

The various aspects of non-homogeneous deformation of single crystals tackled in this work are illustrated in the case of single crystal nickel-base superalloy SC16 (part D). The mechanical tests have been performed at BAM - Berlin in the group V.12, within the framework of a Brite-Euram project.

At room temperature, SC16 single crystals under tension deform strongly non-homogeneously at the macroscopic scale: experimental evidence of slip band propagation along the specimen gauge is provided. The results obtained in part A are applied to this particular situation. The importance of local strain measurements is exemplified by the interpretation of tension-torsion tests on SC16 single crystals. In that case a quantitative comparison between FE calculations and local strain measurements is possible. In contrast, deformation under tension at high temperature (950°C) remains

homogeneous and the parameters of the two-phase model developed in part C are identified to describe the behaviour of SC16 under tensile, cyclic (and creep) loading conditions.

The general final discussion provides also the conclusions and prospects. The notations used throughout this work are explained in Appendix 1.

Part A

LOCALIZATION PHENOMENA IN SINGLE CRYSTALS AT INCIPIENT PLASTICITY

1 Non-homogeneous deformation of single crystals : a review of dislocation patterns and physical mechanisms

1.1 Stability analysis at the microscale

1.1.1 Formation of dislocation structures

The evidence of instabilities and pattern formation is overwhelming in the field of plastic deformation of metals. Applied stresses may induce a self-organization of dislocation populations that leads to localization of deformation. An understanding of the collective behaviour of dislocations can be reached through a stability analysis of various physical mechanisms involved at the microscale.

For that purpose, Walgraef and Aifantis [1988] studied the evolution of local variables such as the density of mobile dislocations ρ_m and the density of trapped dislocations ρ_i. Their analysis is restricted to the case of single slip with a view to predicting the formation of *persistent slip bands* (PSB) in grains or single crystals under cyclic loading. Several physical mechanisms are taken into account, namely the pinning of mobile dislocations at obstacles, the freeing of trapped dislocations and the production of dislocations by sources. This analysis leads to a system of coupled non-linear differential equations :

$$\frac{\partial \rho_i}{\partial t} = g(\rho_i) - b\rho_i + \gamma \rho_m {\rho_i}^2 + D_i \Delta \rho_i \tag{1}$$

$$\frac{\partial \rho_m}{\partial t} = b\rho_i - \gamma \rho_m {\rho_i}^2 + D_m \Delta \rho_m \tag{2}$$

where b, γ, and g are material parameters or functions, the Laplacians account for dislocation diffusion processes.

The steady state corresponds to homogeneous densities of dislocations ρ_{0i} and ρ_{0m}. Its stability is studied through the behaviour of its perturbations. Only one spatial dimension, the direction of primary slip, is considered since PSBs are essentially one-dimensional structures. It can be shown that two types of dislocation patterns become possible as soon as critical values of the freeing rate b, used there as bifurcation control parameter, are reached. The first one called "Turning instability" leads to spatial patterning with the wave length :

$$\lambda_c = 2\pi (D_m D_i / a\gamma \rho_{0i})^{1/4} \tag{3}$$

where $a = -g'(\rho_{0i})$.

This mode may account for dislocation ladder structures inside PSBs. The second one, associated with a Hopf bifurcation, corresponds to homogeneous temporal oscillations that have been observed experimentally in the form of *strain bursts*, causing serrations on the load-displacement curve, for slow increases of stress intensity or low creation rates of dislocations.

Experimental observations show that a PSB consists of a large number of slip planes forming a flat lamella which may eventually extend across the whole specimen section. Only dislocations with Burgers vectors of the primary slip system are required for the formation of a PSB. A periodic arrangement of dislocation walls consists of edge dislocation dipoles and multipoles. The PSB is embedded with a less regular vein and matrix structure (figure 1). Other "labyrinth" structures may also be observed. In copper crystals fatigued at room temperature, the dislocation density in the walls is of the order of $10^{15}\,\mathrm{m}^{-2}$, against $10^{13}\,\mathrm{m}^{-2}$ in the channels. The mutual distance between the walls and the wall thickness are about 1.3 and $0.15\,\mu\mathrm{m}$ respectively. The width of both veins and channels in the matrix is of the order of $1.2\,\mu\mathrm{m}$. The width of the PSBs is about $1.2\,\mu\mathrm{m}$ whereas the whole succession of PSBs with veins and matrix, walls and channels can extend to 0.1 mm wide regions. Hu and Teodosiu [1993] perform a similar stability analysis for single and double slip. They start from a balance equation of dipole density, relating the density of dislocations of a given system α, the resolved shear stress and the shearing rate:

$$\frac{\partial \rho_\alpha}{\partial t} + D_\alpha \frac{\partial^2 \tau_\alpha}{\partial x_\alpha^2} = h_\alpha(\rho_\alpha)\dot{\gamma}_\alpha \tag{4}$$

They introduce a non-local work-hardening rule that requires a cut-off distance for elastic interaction between dislocations. Once again, the initial homogeneous solution gives way to pattern formation. In the case of single slip a bundle-like or wall-like structure perpendicular to the slip direction is obtained. When double slip occurs, taking into account of dislocation junction density leads to the formation of a *cell structure* at the beginning of deformation. The cell structure pertains after unloading thanks to the presence of sessile junctions. Another striking example of dynamic non-homogeneous pattern formation is the propagation of *Portevin-Le Chatelier* bands in some substitutional and interstitial solid solution alloys during straining with constant strain rate or stress rate. Macroscopically PLCs manifest themselves in serrated deformation curves. Stress drops or strain bursts are connected with deformation bands initiated usually at one specimen end and propagating through the gauge length with a constant velocity (figure 2). This usually occurs when the strain rate sensitivity is negative. The microscopic mechanism leading to a negative strain rate sensitivity is the so-called dynamic strain-aging: solute atoms segregate to mobile dislocations during the waiting time for localized obstacles to be overcome by thermal activation. Estrin and Kubin [1988] and Aifantis [1987] give a macroscopic interpretation of the phenomenon but Aifantis adds to the uniaxial phenomenological constitutive equation a spatial term accounting for the non-homogeneous deformation pattern throughout the specimen at instant t:

$$\sigma = h\varepsilon + f(\dot{\varepsilon}) + C\Delta\varepsilon \tag{5}$$

A loop-type function f depicts the rate sensitivity due to the interaction between mobile dislocations, solute atoms and obstacles. Then the search for travelling wave solutions leads to an estimation of the PLC band propagation speed ([Zbib, Aifantis 1988]).

1.1.2 Local strain hardening

Estrin and Kubin [1986] have investigated averaged properties of dislocations over a local volume in order to calculate a local strain hardening. They found that these local

mechanical properties differ from the bulk properties obtained by measuring the overall strain hardening in a macroscopic specimen. This difference is especially pronounced at small strains and can be attributed to the inherently non-uniform character of plastic deformation by slip. The local volume can be regarded as the elementary volume of continuum mechanics. To be specific, we take a volume of about $(10\,\mu\mathrm{m})^3$ for Al, Cu single crystals. The state parameters are the mobile dislocation density ρ_m and the relatively immobile forest dislocation density ρ_f. The equation that relates mechanical variables and dislocation densities is the Orowan equation:

$$\dot{\varepsilon} = \rho_m b v \tag{6}$$

with its Arrhenius kinetic form :

$$\dot{\varepsilon} = A\rho_m \exp \frac{(\sigma - \sigma_f)V}{kT} \tag{7}$$

where

$$\sigma_f = \alpha\mu b\sqrt{\rho_f} \tag{8}$$

and V is the activation volume. Derivation of equation 7 yields

$$\dot{\sigma} = \frac{kT}{V}\frac{\ddot{\varepsilon}}{\dot{\varepsilon}} + h\dot{\varepsilon} \tag{9}$$

where

$$h = h^+ + h^- = \alpha\mu b\Big(\frac{\partial\sqrt{\rho_f}}{\partial\varepsilon}\Big)_{|\,\dot{\varepsilon}} - \frac{kT}{V}\Big(\frac{\partial \ln \rho_m}{\partial\varepsilon}\Big)_{|\,\dot{\varepsilon}} \tag{10}$$

The first term h^+ results from a continuous increase of immobile dislocation density whereas h^- is associated with generation or release of mobile dislocations and represents a softening component. The local volume is chosen so that slip can be assumed to be uniformly distributed, which requires deformation greater than 10^{-3}. The retained balance equations for dislocation densities are the following:

$$\frac{d\rho_m}{d\varepsilon} = \frac{C_1}{b^2}\frac{\rho_f}{\rho_m} - C_2\rho_m - \frac{C_3}{b}\sqrt{\rho_f} \tag{11}$$

$$\frac{d\rho_f}{d\varepsilon} = C_2\rho_m + \frac{C_3}{b}\sqrt{\rho_f} - C_4\rho_f \tag{12}$$

C_1 represents a production term with forest obstacles acting as pinning points for fixed dislocation sources. C_2 accounts for interaction between mobile dislocations, such as trapping of edge dipoles or mutual annihilation of two screws by cross-slip. C_3 corresponds to the immobilization of mobile dislocations with a mean free path proportional to $1/\sqrt{\rho_f}$ on a spatially organized forest structure (Frank net, cell walls or subboundaries...). Lastly C_4 describes the arrangement and annihilation of forest dislocations (by climb, cross-slip...). C_1 and C_3 are constant whereas C_2 and C_4 are strain rate and temperature dependent. Starting from initial values $\rho_m^i = 10^7\,\mathrm{m}^{-2}$, $\rho_f^i = 10^{10}\,\mathrm{m}^{-2}$, the forest density reaches with this model a saturation value $\rho_f^s = 10^{14}\,\mathrm{m}^{-2}$. Solving this differential system yields the evolution of local strain hardening $h(\varepsilon)$. The competition of hardening and softening terms gives rise to three distinct domains (figure 3):

(i) for $\varepsilon < \varepsilon_0$, h^- is predominant, due to the initial multiplication of dislocations; for the hardening rate to be positive at the beginning of deformation, the strain rate sensitivity $\frac{kT}{V}$ must be vanishingly small.

(*ii*) for $\varepsilon_0 < \varepsilon < \varepsilon_M$, the strain rate is positive and increases due to ρ_f being far from saturation while ρ_m approaches saturation.

(*iii*) for $\varepsilon > \varepsilon_M$, the strain hardening decreases under the influence of dynamic recovery.

Then a bifurcation analysis based on the study of possible growth of local fluctuations, shows that the stability domain of uniform deformation is contained in (though smaller than) the region of positive hardening rate. In the first domain, uniform slip is unstable. It is suggested that this behaviour is typical of the occurence of individual slip lines or slip bands. In contrast the instability reached at the end of the third domain for large deformations (Considère instability) will lead to non-uniform deformation like necking or shear banding. Thus plastic deformation will necessarily start in a non-uniform fashion. However the total strain accumulated locally during this non-uniform stage is limited, being of the order of ε_0. The specimen will only retain a memory of such a localization in the form of a scar on the surface. This will play an essential role in fatigue damage.

1.2 Softening mechanisms

The previous analysis in terms of local averaged dislocation densities shows that plastic deformation in a local volume will always start with a yield drop. This initial localization is the cause of slip patterning consisting in non-correlated individual slip lines and slip bands formation. Several physical mechanisms favour an initial local softening. Once a dislocation has been moving, it leaves behind a more penetrable stucture in which subsequent deformation will localize. This is especially true in the case of the shearing of precipitates: the passage of a dislocation reduces the cross-sectional area to be sheared in subsequent events, which may eventually lead to precipitate instability and dissolution in the matrix. The initial burst of moving dislocations also causes a breakdown of the forest dislocation structure.

Metals with a high stacking-fault energy like aluminium ($200\,\mathrm{m}J\,\mathrm{m}^{-2}$) deform with homogeneous glide. In contrast a low stacking-fault energy ($20\,\mathrm{m}J\,\mathrm{m}^{-2}$ in steel) favours dislocation dissociation, making cross-slip more difficult and thus slip more planar. In Nickel base superalloys the very high antiphase boundary energy in γ' phase ($300\,\mathrm{m}J\,\mathrm{m}^{-2}$, see [Pope, Ezz 1984]) allows the cutting of precipitates only by superdislocations that can not cross-slip. If we suppose that the critical resolved shear stress on a slip system s is of the form:

$$\tau_c^s = \mu b \sqrt{\sum_r a^{sr} \rho^r} \tag{13}$$

then planar slip or low stacking fault energy implies an anisotropic matrix a^{ij} [Franciosi, Zaoui 1982]. This will result in an anisotropic hardening matrix h^{ij} in the model for single crystals used in this work.

According to [Szczerba, Korbel 1987] also, softening has a local character and leads to slip localization along a softened path for dislocations. Furthermore they propose a softening mechanism at the end of stage II (double slip): the unlocking of Lomer-Cottrell barriers. Canova, Kubin and Brechet [1993] have simulated the mechanisms by which precipitate shearing or the destruction of short range order lead to glide softening and strain localization. Glide softening occurs through a feed-back process. The shearing of a slip plane by gliding dislocations reduces the local glide resistance by decreasing either the average precipitate radius or the degree of short range order in the solid solution.

This induces slip localization and these spatial instabilities may lead to a reduction of strain hardening, sometimes to plastic instabilities on the deformation curves. The stress required for overcoming spherical coherent precipitates is

$$\tau_c = \tau_0 R_0^{3/2} / \lambda^{1/2} \tag{14}$$

where R_0 is the initial radius of precipitates and λ the spacing between precipitates. The shearing of precipitates leads to a reduced radius:

$$R = R_0(1 - \frac{\gamma}{\gamma_0}) \tag{15}$$

In their numerical simulations, Canova, Kubin and Brechet do not explicitely introduce individual events like the shearing of a precipitate by a dislocation, because the required computing efficiency is still beyond reach (the curse of dimensionality...), but instead they use a softening evolution of the local friction stress:

$$\delta\tau_{fi} = -(\tau_{fi} - \tau_p)\frac{\delta\gamma_i}{\gamma_0} \tag{16}$$

for the increment i (τ_p is the intrinsic Peierls friction stress, about 2 MPa for copper). Segments of edge and screw dislocations are placed on a three-dimensional f.c.c. lattice. The elementary length scale is taken as the critical annihilation distance for edge dislocations $y_e = 1.5\,\text{nm}$. The 3D space is tiled with such elementary cells building up a crystal of size $(10\,\mu\text{m})^3$, containing 5800 slip planes. The simulations show the formation of slip bands (width about $2.6\,\mu\text{m}$) subdivided into clusters of slip lines. The width of the bands increases linearly with strain. Deformation further proceeds until the local glide resistance becomes equal to that of the virgin parts of the crystal. New slip zones are initiated by two mechanisms: the nucleation of fresh slip zones in other parts of the crystal or the expansion of the initial band in a Lüders-like manner.

1.3 Characteristic lengths for slip bands

1.3.1 The heterogeneous nature of slip

To make possible the connection between microscopic mechanisms and the macroscopic mechanical behaviour, one of the main difficulties to be overcome arises directly from the intrinsically heterogeneous nature of slip: deformation of crystalline solids occurs by the development of discrete shear slip steps visible sometimes by the nacked eye. Neuhäuser [1983] gives a very precise typology of these discrete phenomena, that take place at various length scales. A *glide band* is a cluster of surface steps resulting from single or few dislocations on closely spaced neighbouring planes. This gives rise to a rather homogeneous deformation of the specimen. In contrast a *slip band* is a cluster of some sharp offsets corresponding to the emergence of many dislocations on a few close crystallographic planes (figures 4a and b). Each slip step in the slip band is called *slip line* produced by the movement of closely correlated dislocation groups. Often the slip bands are again clustered in units called *slip band bundles* which will be of particular interest in the present work since slip band bundles may have a macroscopic size (about 0.1 mm, see D.1.1.). The size of these plastic discrete patterns ranges from tens of Å for slip lines to about 1 mm for slip band bundles and Piobert-Lüders bands (figures 4c and d).

The dynamics of slip band formation in single crystals has been studied by Neuhäuser [1988] using slip line cinematography to observe the growth of steps on the crystal surface. A fractal dimension can be given to specify the irregular profile of the surface, using for instance the following definition:

$$N = FB^D \tag{17}$$

where B is the number of equal sized boxes filling the whole crystal length and N the number of boxes containing at least one event, here a slip line (for this box method, see [Gouyet 1992]). A fractal dimension $D = 0.7$ has been found for neutron irradiated Copper single crystals. In neutron irradiated materials, non-homogeneous slip is intensified by the fact that dislocations cutting through obstacles partially destroy them so that further dislocations find an easier path on the same plane than on other slip planes. But we have seen that this analysis applies also for precipitate shearing or destruction of short range order.

The deformation dynamics of macroscopic specimens cannot be understood simply by application of the dynamics of single dislocations. The interaction between dislocations due to the long range elastic stress and the collective motion of dislocations must be taken into account. This may explain the stepwise growth of slip lines and slip bands. Slip bands develop in distances of a few μm space free from slip and this channel regions become active only after the stress has increased efficiently, and thus after saturation of step heights to final value in slip lines. The essential process in slip band broadening is cross-slip. In the case of single slip, dislocations may cross the whole section but in multiple slip oriented crystals, a spherical or polygonal cell structure develops that delimits slip zones on the slip planes.

The activation of new slip bands at a long distance from preexisting ones and the growth of slip band bundles up to a certain slip band density often result in the propagation of a so-called *Piobert-Lüders band* along the length of the specimen in tension, for both single crystals and polycrystals. The propagation of Piobert-Lüders bands is governed by the gradient of stress at the front where the cross-section is significantly reduced (figure 4d), the induced slip plane rotation and the bending moment. Two types of Piobert-Lüders bands are observed: the front of the G-bands (for Glide) is parallel to the primary slip plane, whereas the K-bands (for Kink) are perpendicular to it. K-bands involve cross-slip mechanisms and show much stronger instability, giving load drops on the load-displacement curve.

Ashby [1971] derives characteristic lengths for slip lines in plastically non-homogeneous crystals, that are two-phase alloys in which one phase deforms less than the other. He considers two populations of dislocations: geometrically necessary dislocations with density ρ^G and statistically stored dislocations with density ρ^S (see also [François, Pineau, Zaoui 1991]). The presence of non-deforming particles induces the formation of a geometrically necessary dislocation array required for compatible deformation of particles and matrix. Density ρ^G can be estimated for some simple situations, such as the shearing of a matrix with equiaxed particles:

$$\rho^G = \frac{f}{r}\frac{4\gamma}{b} \tag{18}$$

r being the radius of the particle and f the volume fraction of particles. More generally,

a geometric slip distance can be introduced such that:

$$\rho^G = \frac{1}{\lambda^G}\frac{4\gamma}{b} \tag{19}$$

where λ^G is characteristic of the microstructure and strain independent. ρ^G is expected to dominate over ρ^S at small strains. On figure 5, λ^G ranges from 0.4μm to 0.1mm according to the volume fraction and accounts for the non-homogeneous plastic deformation at the beginning of deformation. For polycrystals, λ^G can be considered equal to the grain size.

1.3.2 Slip bands and kink bands in f.c.c. single crystals

The deformation modes of f.c.c. single crystals have been extensively studied in the fifties and sixties because of the success of electron microscopy. The most detailed analyses of the behaviour of single crystal go back to this period if one excepts earlier pionneering works of Elam, Taylor, Schmid... The authors distinguish three stages in the tensile deformation of single crystals oriented for single slip. Mader [1957] reports a homogeneous distribution of slip bands in aluminium single crystals during stage I. During stage II slip lines bundles form and the deformation becomes heterogeneous. Slip lines of the secondary systems are observed. As early as 1954, Liebfried and Haasen have seen the necessity to take the non-homogeneous deformation into account for the modelling of the mechanical behaviour of single crystals. Intense shear bands and some kink bands appear at stage III while traces of cross-slip are observed. Kink bands are also reported in [Mader, Seeger 1960]: they are perpendicular to the glide direction (figure 6). Similar deformation modes are observed in copper for different temperatures. Kink bands are also mentionned by Jaoul [1965] and Friedel [1964], who called them *"bandes en genou"*. Mader and Seeger consider that kink bands are not spurious effects but the natural result of some dislocation motion. Within kink bands slip occurs on the primary system but the secondary system can also be activated. Secondary slip in kink bands has also been noted by Garstone, Honeycombe and Greetham [1955] after 4% of deformation in aluminium crystals. They remark that no kink bands are observed in crystals oriented for polyslip. The presence of kink bands induce an asterism in X-ray Laue photographs.

1.3.3 The concept of active slip volume

We have emphasized the discrete and non-homogeneous character of plastic deformation. Korbel [1985] has even coined the word *"plaston"* and for him the overall deformation results from the contributions of distributed localized zones or "plastons"! A far more relevant notion is that of *active slip volume* introduced by Schwink [1966]. It is the volume V_a of the crystal specimen where slip is actually taking place at a given moment and enables us to define the true shear strain rate for single slip:

$$\dot{\gamma}_{true} = \frac{\dot{\varepsilon}\, l_0}{\cos\chi \cos\lambda\, l_a} \tag{20}$$

where the active slip length is $l_a = V_a/Q$ (cross section of the specimen) and l_0 is the length of the specimen.

V_a depends on strain rate and temperature. V_a increases with strain rate with an upper and lower limit. The dislocation density used in the Orowan equation:

$$\dot{\gamma}_{true} = \overline{\rho}_m b \overline{v} \tag{21}$$

must then be the local density:

$$\overline{\rho}_m = L_a / V_a \tag{22}$$

V_a can be measured by light microscopy or slip line cinematography [Neuhäuser 1983].

Estrin and Kubin [1986] relate the notion of active slip volume and that of local strain hardening rate, using the following homogenization procedure:

$$< \varepsilon >= \frac{1}{l_a} \int_0^{l_a} \varepsilon(x,t)\, dx \tag{23}$$

The strain hardening rate $H = \left(\frac{\partial \sigma}{\partial < \varepsilon >}\right)_{|< \dot{\varepsilon} >}$ is then

$$\frac{H}{l} = \left[\int_0^l \frac{dx}{h(x,t)}\right]^{-1} \tag{24}$$

where h is the local strain hardening rate. h, of the order of $10^{-4}\mu$ according to Estrin and Kubin's calculations (see 1.1.2.), is much smaller than the macroscopically observed hardening rate far from saturation. This readily becomes clear if one makes use of the notion of active slip volume or length l_a. Typically,

$$\frac{H}{l} \sim \frac{h}{l_a} \tag{25}$$

$$\frac{h}{H} \sim \beta = \frac{l_a}{l} \tag{26}$$

Estrin and Kubin conclude that typical values for β are 1/25 to 1/15 and other values can be found from experimental measurements of active slip volumes in [Neuhäuser 1983].

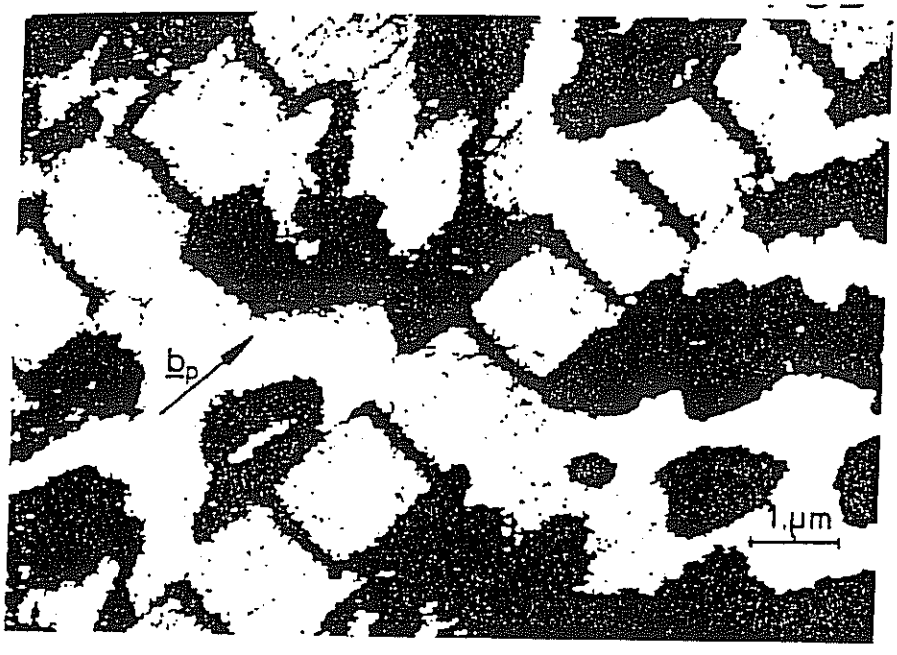

Figure A.1: Microstructure of persistent slip bands in coppper single crystals (after [Mughrabi 1981]).

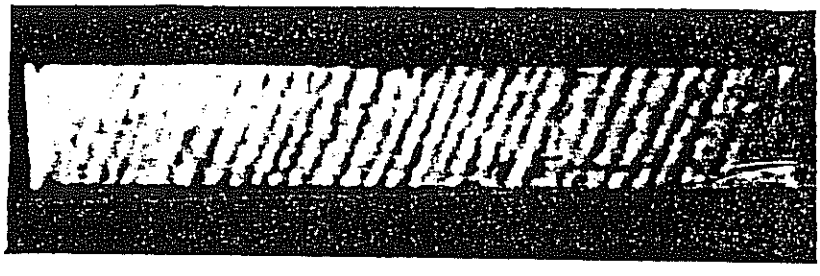

Figure A.2: Video record of Portevin-Le Chatelier bands in polycrystalline Al-Mg at room temperature (after [Estrin, Kubin 1988]).

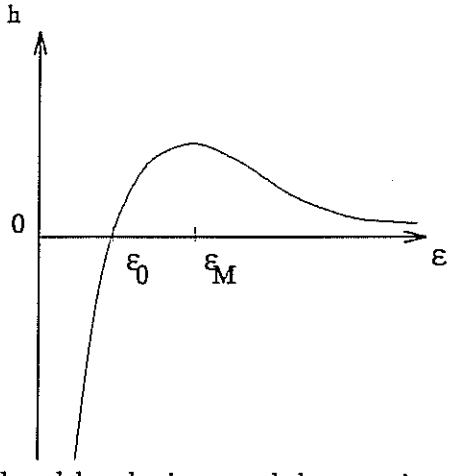

Figure A.3: Variation of the local hardening modulus as given by a non linear analysis of dislocation density evolution (after [Estrin, Kubin 1986]).

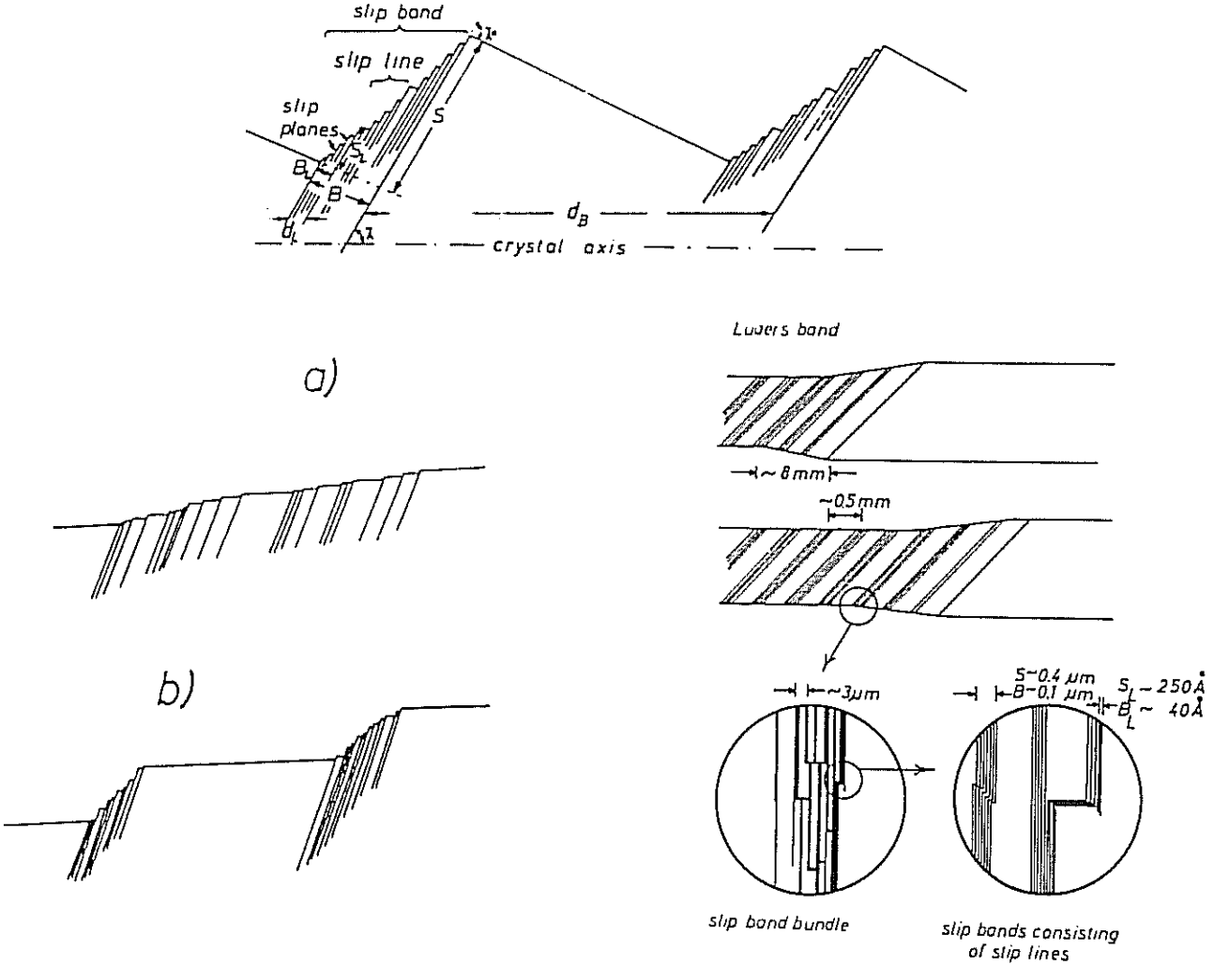

Figure A.4a,b,c and d: Hierarchy from individual to clustered slip bands in single crystals (after Neuhauser [1983] and [1988]).

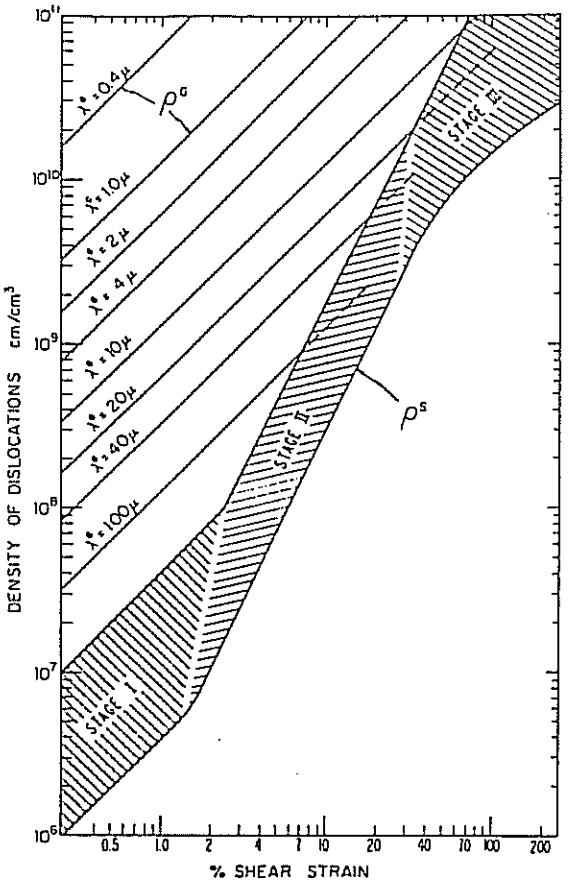

Figure A.5: Evolution of the statistically stored and geometrically necessary dislocation densities with strain (after [Ashby 1971]).

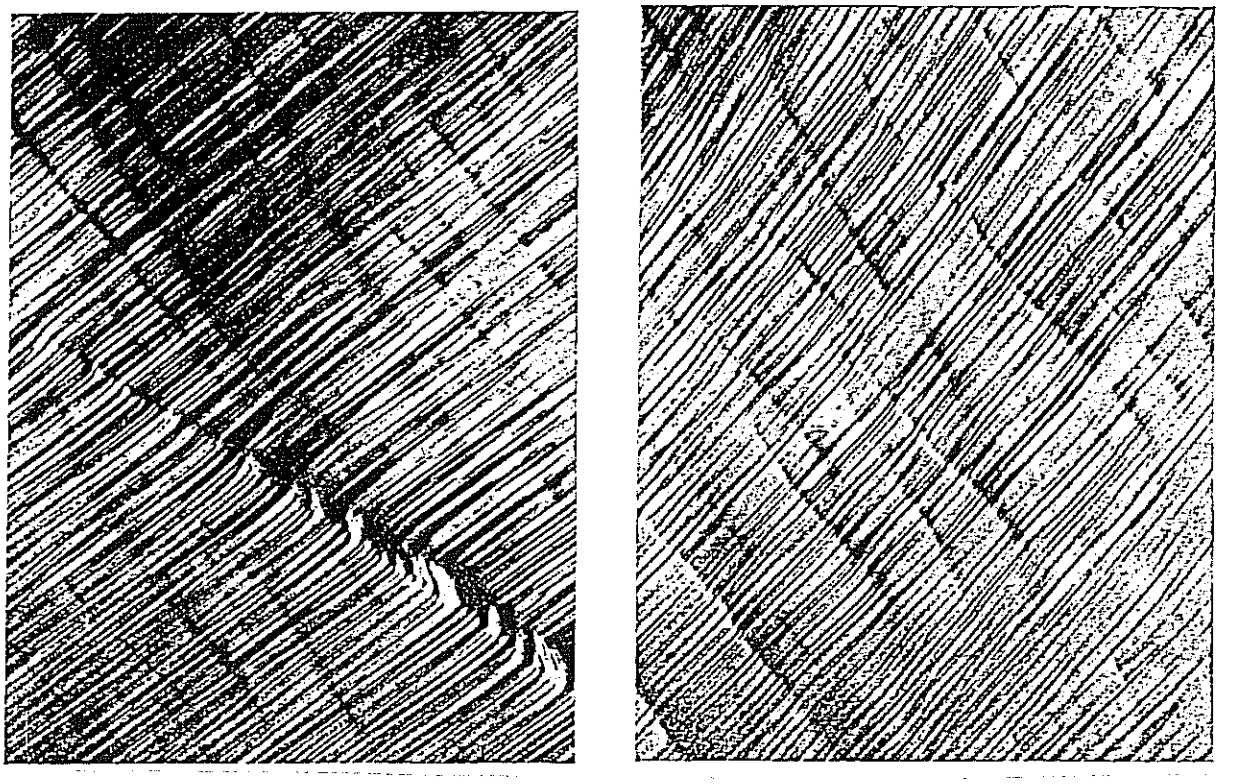

Figure A.6: Slip bands and kink bands at stage III of tension in a single crystal (1 cm = 30 μm, after [Mader, Seeger 1960]).

2 Bifurcation modes in elastoplasticity at small strains

2.1 Formulation of the boundary value problem

2.1.1 Linear incremental formulation

Under small strain conditions, the total strain rate can be decomposed into an elastic and a plastic part

$$\dot{\underset{\sim}{\varepsilon}} = \dot{\underset{\sim}{\varepsilon}}^e + \dot{\underset{\sim}{\varepsilon}}^p \tag{27}$$

The constitutive behaviour of an elastoplastic solid is then described by

- the elastic law

$$\dot{\underset{\sim}{\sigma}} = \underset{\sim\sim}{\mathbf{E}} \, \dot{\underset{\sim}{\varepsilon}}^e \tag{28}$$

  where $\underset{\sim\sim}{\mathbf{E}}$ is the four-rank elasticity tensor
- the yield function $f(\underset{\sim}{\sigma}, \underset{\sim}{\alpha})$, where $\underset{\sim}{\alpha}$ represents the set of hardening variables
- the plastic flow rule

$$\dot{\underset{\sim}{\varepsilon}}^p = \dot{\lambda} \, \underset{\sim}{\mathbf{P}} \tag{29}$$

- the evolution equations of the hardening variables that are assumed to have the form

$$\dot{\underset{\sim}{\alpha}} = \dot{\lambda} \, \underset{\sim}{\mathbf{h}} \tag{30}$$

The plastic loading condition reads

$$\dot{\lambda} > 0 \tag{31}$$

The consistency conditions are

$$f = 0 \quad \text{and} \quad \dot{f} = 0 \tag{32}$$

It follows

$$\dot{f} = \underset{\sim}{\mathbf{N}} : \dot{\underset{\sim}{\sigma}} - \dot{\lambda} \, H \tag{33}$$

where

$$\underset{\sim}{\mathbf{N}} = \frac{\partial f}{\partial \underset{\sim}{\sigma}} \tag{34}$$

$$H = -\frac{\partial f}{\partial \underset{\sim}{\alpha}} : \underset{\sim}{\mathbf{h}} \tag{35}$$

H is the hardening modulus. Non-associated plasticity means that $\underset{\sim}{\mathbf{P}} \neq \underset{\sim}{\mathbf{N}}$. As a result

$$\dot{\lambda} = \frac{\underset{\sim}{\mathbf{N}} : \dot{\underset{\sim}{\sigma}}}{H} \tag{36}$$

If the material has a hardening behaviour ($H > 0$), the plastic loading condition can be written

$$\underset{\sim}{\mathbf{N}} : \dot{\underset{\sim}{\sigma}} > 0 \tag{37}$$

This does not hold for strain-softening materials for which we derive from 27, 28 and 33

$$\dot{\lambda} = \frac{\underset{\sim}{\mathbf{N}} : \underset{\sim\sim}{\mathbf{E}} : \dot{\underset{\sim}{\varepsilon}}}{H + \underset{\sim}{\mathbf{N}} : \underset{\sim\sim}{\mathbf{E}} : \underset{\sim}{\mathbf{P}}} \tag{38}$$

Provided that

$$H + \underset{\sim}{\mathbf{N}} : \underset{\approx}{\mathbf{E}} : \underset{\sim}{\mathbf{P}} > 0 \tag{39}$$

(no "snap-back" behaviour), the plastic loading condition 31 becomes

$$\underset{\sim}{\mathbf{N}} : \underset{\approx}{\mathbf{E}} : \dot{\underset{\sim}{\varepsilon}} \; > \; 0 \tag{40}$$

The constitutive equations take then the incremental form:

$$\dot{\underset{\sim}{\sigma}} = \underset{\approx}{\mathbf{L}} : \dot{\underset{\sim}{\varepsilon}} \tag{41}$$

where

$$\underset{\approx}{\mathbf{L}} = \underset{\approx}{\mathbf{E}} \quad \text{if} \quad f < 0 \quad \text{or} \quad (f = 0 \quad \text{and} \quad \underset{\sim}{\mathbf{N}} : \underset{\approx}{\mathbf{E}} : \dot{\underset{\sim}{\varepsilon}} \leq 0) \tag{42}$$

$$\underset{\approx}{\mathbf{L}} = \underset{\approx}{\mathbf{D}} \quad \text{if} \quad f = 0 \quad \text{and} \quad \underset{\sim}{\mathbf{N}} : \underset{\approx}{\mathbf{E}} : \dot{\underset{\sim}{\varepsilon}} > 0 \tag{43}$$

with

$$\underset{\approx}{\mathbf{D}} = \underset{\approx}{\mathbf{E}} - \frac{(\underset{\approx}{\mathbf{E}} : \underset{\sim}{\mathbf{P}}) \otimes (\underset{\sim}{\mathbf{N}} : \underset{\approx}{\mathbf{E}})}{H + \underset{\sim}{\mathbf{N}} : \underset{\approx}{\mathbf{E}} : \underset{\sim}{\mathbf{P}}} \tag{44}$$

2.1.2 Formulation of the rate problem

For given fields of the rates of body forces $\dot{f}$, surfaces forces $\dot{\underline{F}}$ on the part $\partial_1\mathcal{B}$ of the boundary of the domain $\mathcal{B}$, and displacements $\underline{V}$ on $\partial_2\mathcal{B}$, the rate problem consists in finding the displacement rates $\underline{v}$ in $\mathcal{B}$ satisfying:

$$\begin{cases} \dot{\underset{\sim}{\varepsilon}} = \frac{1}{2}(\underset{\sim}{\nabla}\underline{v} + \underset{\sim}{\nabla}^t\underline{v}) \\ \underline{\text{div}}\ \dot{\underset{\sim}{\sigma}} + \dot{\underline{f}} = 0 \\ \dot{\underset{\sim}{\sigma}} = \underset{\approx}{\mathbf{L}} : \dot{\underset{\sim}{\varepsilon}} \\ \dot{\underset{\sim}{\sigma}}\ \underline{n} = \dot{\underline{F}} \quad \text{on} \quad \partial\mathcal{B}_1 \\ \underline{v} = \underline{V} \quad \text{on} \quad \partial\mathcal{B}_2 \end{cases} \tag{$\mathcal{P}$}$$

The problem $(\mathcal{P})$ is non-linear because of relations 42 and 43.

2.2 Loss of uniqueness; general bifurcation modes

2.2.1 Hill's condition

Let $(\underset{\sim}{\sigma}_A, \underset{\sim}{\varepsilon}_A)$ and $(\underset{\sim}{\sigma}_B, \underset{\sim}{\varepsilon}_B)$ be two distinct solutions of the boundary value problem and let us consider the differences $\Delta\underset{\sim}{\sigma} = \underset{\sim}{\sigma}_A - \underset{\sim}{\sigma}_B$ and $\Delta\underset{\sim}{\varepsilon} = \underset{\sim}{\varepsilon}_A - \underset{\sim}{\varepsilon}_B$. The associated velocity field $\Delta\underline{\mathbf{v}}$ vanishes on the part of the boundary of the solid $\mathcal{B}$ where the velocity is prescribed and is therefore a kinematically admissible velocity field in the expression of the principle of virtual power. Applying the principle of virtual power successively to solutions A and B on body $\mathcal{B}$, Hill [1958] gets a necessary condition for loss of uniqueness:

$$\int_{\mathcal{B}} \Delta\dot{\underset{\sim}{\sigma}} : \Delta\dot{\underset{\sim}{\varepsilon}}\, dV = 0 \tag{45}$$

A local sufficient condition for uniqueness is then

$$\dot{\underset{\sim}{\sigma}} : \dot{\underset{\sim}{\varepsilon}} > 0 \tag{46}$$

for all kinematically admissible velocity fields. This condition is called positiveness of the local second-order work and a review of the uniqueness problem is given in [Vardoulakis 1994]. When a linear incremental formulation of the constitutive equations like 41 exists, the positiveness of the local second-order work is equivalent to the definite positiveness of the four-rank tensor $\underset{\approx}{\mathbf{D}}^s$, where s denotes symmetrisation. A necessary condition for the local loss of uniqueness is then

$$\text{Det } \underset{\approx}{\mathbf{D}}^s = 0 \tag{47}$$

When uniqueness is lost, general bifurcation modes (like necking, plastic buckling...) become possible. These modes can be diffuse or localized deformation modes. However bifurcation modes associated with strain rate jumps at the boundary of the bifurcated zone may occur only later. The corresponding bifurcation criteria will be derived in section 2.4.

2.2.2 General bifurcation modes in non-associated elastoplasticity

Neilsen and Schreyer [1993] have performed a spectral analysis of the elastoplastic tangent tensors $\underset{\approx}{\mathbf{D}}$ and $\underset{\approx}{\mathbf{D}}^s$ in order to obtain explicit criteria for the possible loss of uniqueness and the associated bifurcation modes. $\underset{\approx}{\mathbf{D}}$ has six symmetric eigentensors and three skew-symmetric ones. Let $\underset{\sim}{\mathbf{x}}_i$ be the six orthogonal symmetric eigentensors and ω_i the respective eigenvalues ranged in the increasing order. Every bifurcation mode can be written $\dot{\underset{\sim}{\varepsilon}} = \alpha_i \underset{\sim}{\mathbf{x}}_i$. Uniqueness may be lost as soon as

$$\dot{\underset{\sim}{\varepsilon}} : \underset{\approx}{\mathbf{D}} : \dot{\underset{\sim}{\varepsilon}} = \alpha_i^2 \omega_i = 0 \tag{48}$$

This occurs for the first time when $\omega_1 = 0$. The associated bifurcation mode is proportional to $\underset{\sim}{\mathbf{x}}_1$ and is called fundamental mode. When $\omega_1 < 0$, other bifurcation modes become possible. As a basis of the second-rank symmetric tensors, we can take the eigentensors of the elasticity tensor $\underset{\approx}{\mathbf{E}}$ for instance. In the isotropic case, $3k$ (bulk modulus) is an eigenvalue of first order, $\underset{\sim}{\mathbf{1}}$ being the associated eigentensor and 2μ (shear modulus) is an eigenvalue of order 5. One can choose five basis tensors of the deviatoric space

$$[\underset{\sim}{\mathbf{e}}_1] = \frac{1}{\sqrt{6}}\begin{bmatrix} -1 & 0 & 0 \\ 0 & 2 & 0 \\ 0 & 0 & -1 \end{bmatrix} \quad [\underset{\sim}{\mathbf{e}}_2] = \frac{1}{\sqrt{2}}\begin{bmatrix} -1 & 0 & 0 \\ 0 & 0 & 0 \\ 0 & 0 & 1 \end{bmatrix} \quad [\underset{\sim}{\mathbf{e}}_3] = \frac{1}{\sqrt{2}}\begin{bmatrix} 0 & 1 & 0 \\ 1 & 0 & 0 \\ 0 & 0 & 0 \end{bmatrix}$$

$$[\underset{\sim}{\mathbf{e}}_4] = \frac{1}{\sqrt{2}}\begin{bmatrix} 0 & 0 & 1 \\ 0 & 0 & 0 \\ 1 & 0 & 0 \end{bmatrix} \quad [\underset{\sim}{\mathbf{e}}_5] = \frac{1}{\sqrt{2}}\begin{bmatrix} 0 & 0 & 0 \\ 0 & 0 & 1 \\ 0 & 1 & 0 \end{bmatrix} \tag{49}$$

In a special case we try now to find the critical hardening modulus H^u for which uniqueness may be lost. Let us assume for simplicity that $\underset{\sim}{\mathbf{P}}$ and $\underset{\sim}{\mathbf{N}}$ are in the space generated by the tensors $\underset{\sim}{\mathbf{e}}_1$ and $\underset{\sim}{\mathbf{e}}_2$

$$\underset{\sim}{\mathbf{P}} = p_1 \underset{\sim}{\mathbf{e}}_1 + p_2 \underset{\sim}{\mathbf{e}}_2 \tag{50}$$

$(\lambda_i, \underset{\sim}{\mathbf{e}}_i)$ and $(\omega_i, \underset{\sim}{\mathbf{x}}_i)$ still being the eigenvalues and eigentensors of $\underset{\approx}{\mathbf{E}}$ and $\underset{\sim}{\mathbf{D}}^s$ respectively, we look for an eigentensor of $\underset{\sim}{\mathbf{D}}^s$ under the form

$$\underset{\sim}{\mathbf{x}} = \xi_1 \underset{\sim}{\mathbf{e}}_1 + \xi_2 \underset{\sim}{\mathbf{e}}_2 \tag{51}$$

The equation

$$\underset{\sim}{\mathbf{D}}^s \, \underset{\sim}{\mathbf{x}} = \omega \, \underset{\sim}{\mathbf{x}} \tag{52}$$

leads to an homogeneous system with two unknowns (ξ_1, ξ_2). The determinant of this system must be zero if non-trivial solutions are to be found. This condition gives a relation between the hardening modulus and ω. H^u is then obtained for $\omega = 0$.

The complete analysis has been carried out by Raniecki and Bruhns [1981] and Runesson and Mroz [1989]. They give the following sufficient condition for uniqueness

$$H > H^u = \frac{1}{2}(\sqrt{\underset{\sim}{\mathbf{N}} : \underset{\approx}{\mathbf{E}} : \underset{\sim}{\mathbf{N}}} \sqrt{\underset{\sim}{\mathbf{P}} : \underset{\approx}{\mathbf{E}} : \underset{\sim}{\mathbf{P}}} - \underset{\sim}{\mathbf{N}} : \underset{\approx}{\mathbf{E}} : \underset{\sim}{\mathbf{P}}) \tag{53}$$

The fundamental bifurcation mode is

$$\underset{\sim}{\mathbf{x}} = \frac{\underset{\sim}{\mathbf{P}}}{\sqrt{\underset{\sim}{\mathbf{P}} : \underset{\approx}{\mathbf{E}} : \underset{\sim}{\mathbf{P}}}} + \frac{\underset{\sim}{\mathbf{N}}}{\sqrt{\underset{\sim}{\mathbf{N}} : \underset{\approx}{\mathbf{E}} : \underset{\sim}{\mathbf{N}}}} \tag{54}$$

For associated plasticity $\underset{\sim}{\mathbf{P}} = \underset{\sim}{\mathbf{N}}$ and the critical hardening modulus is then

$$H^u = 0 \tag{55}$$

When uniqueness is lost, a necessary condition for the existence of solutions can be found in [Benallal, Billardon, Geymonat 1989].

2.3 Well-posedness of the rate boundary value problem for the linear comparison solid

The linear comparison solid introduced by Hill [1958] is obtained when unloading is excluded, so that

$$\underset{\approx}{\mathbf{L}} = \underset{\approx}{\mathbf{D}} \tag{56}$$

In that linear case, necessary and sufficient conditions can be worked out for the well-posedness of the rate problem. Following [Benallal, Billardon, Geymonat 1991], the rate boundary problem is said to be well-posed if it admits a finite number of linearly independent solutions which depend continuously on the data, and which constitute diffuse modes of deformation. Benallal, Billardon and Geymonat [1990] show that the linear rate problem for a solid with boundary and possible interfaces is then well-posed if and only if the following conditions are met:

(i) the ellipticity condition
(ii) the boundary complementing condition
(iii) the interfacial complementing condition

Condition (i) states that the rate equilibrium equation must remain elliptic in the closure of the body $\mathcal{B}$. It is equivalent to the following conditions:

$(i)'$ Det $\underline{\mathbf{n}}.\underset{\sim}{\mathbf{D}}.\underline{\mathbf{n}} \neq 0 \quad \forall \underline{\mathbf{n}} \neq 0 \quad$ and $\quad \forall M \in \overline{\mathcal{B}}$

$(i)''$ bifurcation modes involving jumps of the velocity gradient are precluded

$(i)'''$ stationary acceleration waves are precluded

The meaning of conditions $(i)'$, $(i)''$ and $(i)'''$ will be given in the next section. The equivalence between $(i)'$ and $(i)''$ is established for instance in [Ottosen, Runesson 1991a]. The link between the existence of discontinuous bifurcation modes and of stationary acceleration waves has been seen by Mandel [1966] (see section 2.6) and is summarized in [Ottosen, Runesson 1991b].

The boundary value problem written for finite bodies can become ill-posed while the incremental field equations remain elliptic, as a consequence of the failure of the complementary condition at the boundaries or interfaces. The failure of the boundary complementing condition is equivalent to the existence of *Rayleigh surface waves.* This can be investigated by looking for wave solutions:

$$\underline{\mathbf{v}} = \underline{\mathbf{w}} \exp i\underline{\mathbf{k}}.\underline{\mathbf{x}} \tag{57}$$

Body waves correspond to solutions with real components of $\underline{k}$. If the solid extends over the half-space $x_1 \geq 0$, the boundary beeing free of traction, Needleman and Ortiz [1991] show that solutions with k_1 complex leading to Rayleigh free surface waves, will decay exponentially into the body if:

$$\Im m\ k_1 \geq 0 \tag{58}$$

Similar conditions exist for the existence of *Stoneley stationary interfacial waves*, that are deformation modes localized at each side of an interface. The interface can be perfect or described by a constitutive equation like in [Suo, Ortiz, Needleman 1992].

If no length scales are introduced in the constitutive equations, the wave length of body, surface or interfacial waves, remains arbitrary. The mismatch in mechanical properties at an interface can induce stress and strain concentration that may act as initiation sites for localization. Conversely, grain boundaries can act as barriers to localization that originates in the bulk of the material.

2.4 Existence of velocity gradient discontinuities

2.4.1 Acceleration waves; acoustic tensor; discontinuous bifurcation modes in the static case

Following [Mandel 1962] and [Ottosen, Runesson 1991b], we investigate the possibility of emergence of deformation modes involving jumps of the acceleration, of the velocity gradient and of the stress rate across a moving surface S with normal $\underline{\mathbf{n}}$

$$[\![\ddot{\underline{\mathbf{u}}}]\!] \neq 0, [\![\dot{\underline{\mathbf{u}}} \otimes \underline{\nabla}]\!] \neq 0 \text{ and } [\![\dot{\underset{\sim}{\sigma}}]\!] \neq 0 \tag{59}$$

But it is assumed that

$$[\![\underline{\mathbf{u}}]\!] = [\![\dot{\underline{\mathbf{u}}}]\!] = 0 \text{ and } [\![\underset{\sim}{\sigma}]\!] = 0 \tag{60}$$

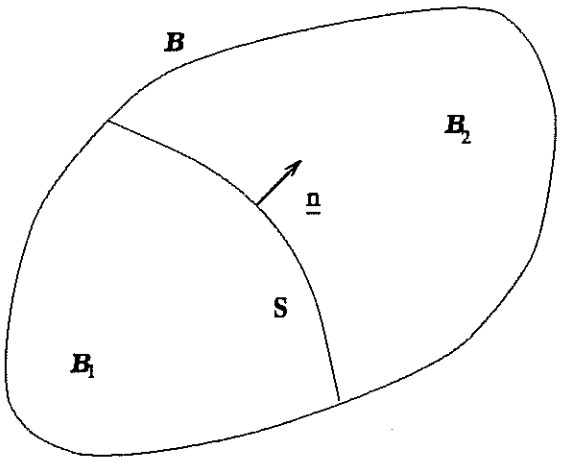

The discontinuity surface S propagates with the speed $U = \underline{x}.\underline{n}$ where $\underline{x} \in S$. According to Hadamard's compatibility conditions [Hadamard 1903], the jump of the velocity gradient at the interface must have the form

$$\exists \underline{g} / \ [\![\dot{\underline{u}} \otimes \underline{\nabla}]\!] \ = \ \underline{g} \otimes \underline{n} \tag{61}$$

A detailed description of singular surfaces can be found in [Truesdells, Toupin 1960] and [Thomas 1961]. Similarly

$$\exists \underset{\sim}{g} / \ [\![\underset{\sim}{\dot{\sigma}} \otimes \underline{\nabla}]\!] = \underline{g} \otimes \underline{n} \tag{62}$$

Furthermore the conditions 60 must hold at each time t, so that

$$[\![\underline{\ddot{u}}]\!] + U\underline{g} = 0 \tag{63}$$

$$[\![\underset{\sim}{\dot{\sigma}}]\!] + U\underset{\sim}{g} = 0 \tag{64}$$

Applying the previous relation to vector $\underline{n}$, one gets

$$[\![\underset{\sim}{\dot{\sigma}}]\!]\underline{n} + U[\![\underline{\text{div}}\ \underset{\sim}{\sigma}]\!] = 0 \tag{65}$$

On the other hand, continuing equilibrium implies

$$[\![\underline{\text{div}}\ \underset{\sim}{\sigma}]\!] = \rho[\![\underline{\ddot{u}}]\!] \tag{66}$$

provided that the body forces are the same on each side of S. Combining the two last equations gives

$$[\![\underset{\sim}{\dot{\sigma}}]\!]\ \underline{n} = \rho U^2 \underline{g} \tag{67}$$

If the constitutive equation have the linear incremental form 41, and assuming that $[\![\underset{\sim}{L}]\!] = 0$, one gets

$$\underset{\sim}{Q}\ \underline{g} \ = \ \rho U^2 \underline{g} \tag{68}$$

where

$$Q_{ij} = n_k D_{iklj} n_l \tag{69}$$

under plastic loading conditions on each side of S. $\underset{\sim}{Q}$ is called the acoustic tensor. The previous relation will be written

$$\underset{\sim}{Q} = \underline{n}.\underset{\approx}{D}.\underline{n} \tag{70}$$

in the sequel. As a result, the existence of discontinuity surfaces of the type 59 depends on the solutions of the eigenvalue problem 68.

Static case. We consider now the following jump conditions across a surface S which is not moving

$$[\![\dot{\underline{u}} \otimes \underline{\nabla}]\!] \neq 0 \text{ and } [\![\dot{\underline{u}}]\!] = C^{st} \tag{71}$$

Condition 61 must still hold and we make use of the linear incremental form 41. We investigate plastic/plastic bifurcations for which $[\![\underset{\sim}{L}]\!] = 0$. Elastic/plastic bifurcation modes will be considered in the next section. The equilibrium condition at the surface S reads in the static case

$$[\![\dot{\underset{\sim}{\sigma}}]\!]\, \underline{n} = 0 \tag{72}$$

Combining 61 and 72 leads to the condition

$$\underset{\sim}{Q}\, \underline{g} = 0 \tag{73}$$

where the acoustic tensor is still defined by 69. Non trivial solutions require the acoustic tensor to become singular. These discontinuous bifurcation modes can be regarded as stationary plastic waves in the dynamic case.

Hill and Hutchinson [1975] have investigated the general character of the governing partial differential equations and its dependence on the current value of the stress and tangent moduli. They have shown that ellipticity can be lost and that bifurcation modes may then develop. There is an equivalence between the *loss of ellipticity* of the governing equations and the existence of discontinuous bifurcation modes.

2.4.2 Conditions for plastic/plastic and elastic/plastic bifurcations

If plastic loading occurs on each side of S, the bifurcation modes are called plastic/plastic localization modes and necessary and sufficient conditions for such modes to become possible inside the body have been worked out by Rice [1976]:

$$\text{Det}\quad \underline{n}.\underset{\sim}{D}.\underline{n} = 0 \quad \text{and} \quad \underline{n}.\underset{\sim}{\underset{\sim}{E}} : \underset{\sim}{P} \neq 0 \tag{74}$$

If elastic unloading occurs on one side of S, the associated bifurcation modes are called elastic/plastic localization modes. Borré and Maier [1989] extended the results established by Rice and Rudnicki [1980] about a necessary and sufficient condition for the onset of elastic/plastic localization modes inside the body:

$$\text{Det}\quad \underline{n}.\underset{\sim}{D}.\underline{n} < 0 \quad \text{and} \quad \underline{n}.\underset{\sim}{\underset{\sim}{E}} : \underset{\sim}{P} \neq 0 \tag{75}$$

This result will be proved in section 2.5.1. It means that in the case of usual elastoplastic materials for which the work-hardening rate decreases with strain, an elastic/plastic localization mode involving elastic unloading cannot occur before the condition for plastic/plastic bifurcation modes 74 is fulfilled. However it does not exclude the fact that elastic unloading occurs on one side just after plastic/plastic bifurcation.

2.4.3 Bifurcation at the boundary or at an interface

Benallal, Billardon and Geymonat [1990] have searched necessary and sufficient conditions for a discontinuity surface S to appear at or to reach the boundary of a solid. To conditions 71 and 72, the following boundary conditions must be added:

$$\dot{\underset{\sim}{\sigma}}_2\, \underline{m} = \dot{\underset{\sim}{\sigma}}_1\, \underline{m} = \dot{\underline{F}} \tag{76}$$

where unit vector $\underline{\mathbf{m}}$ is normal to the boundary.
For a plastic/plastic bifurcation mode, this implies:

$$\left(\underline{\mathbf{m}}.\underset{\sim}{\mathbf{D}}.\underline{\mathbf{n}}\right)\ \underline{\mathbf{g}} = 0 \tag{77}$$

Combining 44, 82 and 83 (see next section) with this last condition, we obtain:

$$\left(\underline{\mathbf{m}}.\underset{\sim}{\mathbf{E}}.\underline{\mathbf{n}}\right)\ \left(\underline{\mathbf{n}}.\underset{\sim}{\mathbf{E}}.\underline{\mathbf{n}}\right)^{-1}\ \left(\underline{\mathbf{n}}.\underset{\sim}{\mathbf{E}} : \underset{\sim}{\mathbf{P}}\right) = \underline{\mathbf{m}}.\underset{\sim}{\mathbf{E}} : \underset{\sim}{\mathbf{P}} \tag{78}$$

Thus necessary and sufficient conditions for plastic/plastic localization to become possible are:

(i) $\exists \dot{\underset{\sim}{\varepsilon}}_0$ such that $\underline{\mathbf{m}}.\underset{\sim}{\mathbf{D}} : \dot{\underset{\sim}{\varepsilon}}_0 = \dot{\underline{\mathbf{F}}}$
(ii) Det $\underline{\mathbf{n}}.\underset{\sim}{\mathbf{D}}.\underline{\mathbf{n}} = 0$
(iii) $(\underline{\mathbf{m}}.\underset{\sim}{\mathbf{E}}.\underline{\mathbf{n}})(\underline{\mathbf{n}}.\underset{\sim}{\mathbf{E}}.\underline{\mathbf{n}})^{-1}(\underline{\mathbf{n}}.\underset{\sim}{\mathbf{E}} : \underset{\sim}{\mathbf{P}}) = \underline{\mathbf{m}}.\underset{\sim}{\mathbf{E}} : \underset{\sim}{\mathbf{P}}$
(iv) $\underline{\mathbf{n}}.\underset{\sim}{\mathbf{E}} : \underset{\sim}{\mathbf{P}} \neq 0$

The case of elastic/plastic localization modes is obtained by replacing (i) and (ii) by:

$(i)'$ $\exists \dot{\underset{\sim}{\varepsilon}}_0$ such that $\underline{\mathbf{m}}.\underset{\sim}{\mathbf{D}} : \dot{\underset{\sim}{\varepsilon}}_0 = \dot{\underline{\mathbf{F}}}$ and $\underline{\mathbf{n}}.\underset{\sim}{\mathbf{E}} : \dot{\underset{\sim}{\varepsilon}}_0 > 0$
$(ii)'$ Det $\underline{\mathbf{n}}.\underset{\sim}{\mathbf{D}}.\underline{\mathbf{n}} < 0$

These results imply that bands in the bulk and bands at the boundary are usually misaligned. Bands of localized deformation may display a kink when approaching the free surface.

2.5 Bifurcation analysis in elastoplasticity

2.5.1 Critical hardening modulus for a given normal $\underline{\mathbf{n}}$

Rice [1976] has determined the critical hardening modulus for which a plastic/plastic bifurcation becomes possible across a surface S of given normal $\underline{\mathbf{n}}$. One starts from the equilibrium equation at the interface

$$\underset{\sim}{\mathbf{D}}\ [\![\ \dot{\underset{\sim}{\varepsilon}}\ ]\!]\ \underline{\mathbf{n}} = 0 \tag{79}$$

where the linear incremental form 41 has been used. Taking 61 and 44 into account, one obtains

$$\left(\underline{\mathbf{n}}.\underset{\sim}{\mathbf{E}}.\underline{\mathbf{n}} - \frac{1}{A}(\underline{\mathbf{n}}.\underset{\sim}{\mathbf{E}} : \underset{\sim}{\mathbf{P}})(\underset{\sim}{\mathbf{N}} : \underset{\sim}{\mathbf{E}}.\underline{\mathbf{n}})\right)\ \underline{\mathbf{g}} = 0 \tag{80}$$

$$A = H + \underset{\sim}{\mathbf{N}} : \underset{\sim}{\mathbf{E}} : \underset{\sim}{\mathbf{P}} \tag{81}$$

It can be checked that

$$H(\underline{\mathbf{n}}) = -\underset{\sim}{\mathbf{N}} : \underset{\sim}{\mathbf{E}} : \underset{\sim}{\mathbf{P}} + (\underset{\sim}{\mathbf{N}} : \underset{\sim}{\mathbf{E}}.\underline{\mathbf{n}})(\underline{\mathbf{n}}.\underset{\sim}{\mathbf{E}}.\underline{\mathbf{n}})^{-1}(\underline{\mathbf{n}}.\underset{\sim}{\mathbf{E}} : \underset{\sim}{\mathbf{P}}) \tag{82}$$

and

$$\underline{\mathbf{g}} \propto (\underline{\mathbf{n}}.\underset{\sim}{\mathbf{E}}.\underline{\mathbf{n}})^{-1}(\underline{\mathbf{n}}.\underset{\sim}{\mathbf{E}} : \underset{\sim}{\mathbf{P}}) \tag{83}$$

are solutions of the previous equations.

The uniqueness of this solution must be proved. For that purpose we follow [Ottosen, Runesson 1991a] who investigate both plastic/plastic and elastic/plastic bifurcation modes.

Plastic/plastic bifurcations

We consider the generalized eigenvalue problem for the acoustic tensor

$$\underset{\sim}{\mathbf{Q}}\,\underline{\mathbf{y}} \;=\; \lambda \underset{\sim}{\mathbf{Q}}^{e}\,\underline{\mathbf{y}} \tag{84}$$

where

$$\underset{\sim}{\mathbf{Q}}^{e} \;=\; \underline{\mathbf{n}}.\underset{\approx}{\mathbf{E}}.\underline{\mathbf{n}} \tag{85}$$

is positive definite. If $\underset{\sim}{\mathbf{P}}^{e} = \underset{\sim}{\mathbf{Q}}^{e-1}$, the equation to be solved can be written

$$\underset{\sim}{\mathbf{B}}\,\underline{\mathbf{y}} = \lambda\,\underline{\mathbf{y}} \tag{86}$$

with

$$\underset{\sim}{\mathbf{B}} = \underset{\sim}{\mathbf{1}} - \frac{1}{A}\underset{\sim}{\mathbf{P}}^{e}(\underline{\mathbf{b}} \otimes \underline{\mathbf{a}}),\;\; \underline{\mathbf{a}} = \underset{\sim}{\mathbf{N}} : \underset{\approx}{\mathbf{E}}.\underline{\mathbf{n}},\;\; \underline{\mathbf{b}} = \underline{\mathbf{n}}.\underset{\approx}{\mathbf{E}} : \underset{\sim}{\mathbf{P}} \tag{87}$$

$\lambda = 1$ is an eigenvalue of order 2. The associated eigenvectors are orthogonal to $\underline{\mathbf{a}}$. The remaining eigenvalue is obtained using the trace operator

$$\mathrm{Tr}\,\underset{\sim}{\mathbf{B}} = 2 + \lambda_3 = 3 - \frac{1}{A}\underline{\mathbf{a}}.\underset{\sim}{\mathbf{P}}^{e}.\underline{\mathbf{b}} \;\Rightarrow\; \lambda_3 = 1 - \frac{1}{A}\underline{\mathbf{a}}.\underset{\sim}{\mathbf{P}}^{e}.\underline{\mathbf{b}} \tag{88}$$

One checks that $\underline{\mathbf{y}}_3 = \underset{\sim}{\mathbf{P}}^{e}\underline{\mathbf{b}}$ is the associated eigenvector. The solution of the initial problem, i.e. the eigenvalues of the acoustic tensor, is obtained only for $\lambda_3 = 0$ which gives relation 82. The expression of $\underline{\mathbf{y}}_3$ is then identical to 83.

Elastic/plastic bifurcations

If elastic behaviour is assumed on the side 1 of S, the equilibrium condition becomes

$$(\underset{\approx}{\mathbf{D}}\dot{\underset{\approx}{\varepsilon}}_2 \;-\underset{\approx}{\mathbf{E}}\dot{\underset{\approx}{\varepsilon}}_1)\,\underline{\mathbf{n}} \;=\; 0 \tag{89}$$

where

$$\dot{\underset{\approx}{\varepsilon}}_2 - \dot{\underset{\approx}{\varepsilon}}_1 \;=\; {}^{\{}\underline{\mathbf{g}} \otimes \underline{\mathbf{n}}^{\}} \tag{90}$$

Hence, the equation to be solved is now

$$\underset{\sim}{\mathbf{Q}}\,\underline{\mathbf{g}} = \frac{1}{A}\left((\underset{\approx}{\mathbf{E}} : \underset{\sim}{\mathbf{P}}) \otimes (\underset{\sim}{\mathbf{N}} : \underset{\approx}{\mathbf{E}}) : \dot{\underset{\approx}{\varepsilon}}_1\right)\,\underline{\mathbf{n}} \tag{91}$$

Eliminating $\dot{\underset{\approx}{\varepsilon}}_2$ gives

$$\underset{\sim}{\mathbf{Q}}\,\underline{\mathbf{g}} \;=\; \frac{\alpha}{A}\,\underline{\mathbf{b}} \quad \text{where} \quad \alpha = \underset{\sim}{\mathbf{N}} : \underset{\approx}{\mathbf{E}} : \dot{\underset{\approx}{\varepsilon}}_1 \leq 0 \tag{92}$$

(elastic unloading).
Eliminating $\dot{\underset{\approx}{\varepsilon}}_1$ gives

$$\underset{\sim}{\mathbf{Q}}^{e}\underline{\mathbf{g}} \;=\; \frac{\beta}{A}\,\underline{\mathbf{b}} \quad \text{where} \quad \beta = \underset{\sim}{\mathbf{N}} : \underset{\approx}{\mathbf{E}} : \dot{\underset{\approx}{\varepsilon}}_2 > 0 \tag{93}$$

(plastic loading).
The solution is then

$$\underline{\mathbf{g}} = \frac{\underline{\mathbf{n}} : \underset{\sim}{\mathbf{E}} : \dot{\underset{\sim}{\varepsilon}}_2}{A} \underset{\sim}{\mathbf{P}}^e \underline{\mathbf{b}} \tag{94}$$

In this case the amplitude of the discontinuity is not arbitrary any more. Furthermore it can be noticed that

$$\underset{\sim}{\mathbf{Q}}\,\underline{\mathbf{g}} = \frac{\alpha}{\beta}\,\underset{\sim}{\mathbf{Q}}^e \underline{\mathbf{g}} \tag{95}$$

It means that an elastic/plastic bifurcation is possible only if α/β is an eigenvalue of the previous $\underset{\sim}{\mathbf{B}}$. But $\alpha/\beta < 0$, so that the only possibility is $\lambda_3 = \alpha/\beta$. This is the proof of the result given in section 2.4.2: an elastic/plastic bifurcation cannot occur before the condition for plastic/plastic bifurcations is fulfilled.

2.5.2 Critical hardening modulus and orientation of the first possible shear band

For materials with decreasing hardening modulus, the critical hardening modulus for which the first discontinuous bifurcation mode becomes possible is

$$H^{cr} = \sup_{\|\underline{\mathbf{n}}\|=1} H(\underline{\mathbf{n}}) \tag{96}$$

where $H(\underline{\mathbf{n}})$ is given by equation 82.

The orientation of the first possible band of localized deformation is given by the values of $\underline{\mathbf{n}}$ for which H^{cr} is reached.

Three-dimensional case

The problem reduces to maximizing the Lagrangian function:

$$L(\underline{\mathbf{n}}, \lambda) = H(\underline{\mathbf{n}}) - \lambda(\|\underline{\mathbf{n}}\|^2 - 1). \tag{97}$$

For isotropic elasticity,

$$\begin{aligned} H(\underline{\mathbf{n}}) = 2\mu(2(\underline{\mathbf{n}}\underset{\sim}{\mathbf{P}}).(\underset{\sim}{\mathbf{N}}\underline{\mathbf{n}}) &- (\underline{\mathbf{n}}.\underset{\sim}{\mathbf{P}}.\underline{\mathbf{n}})(\underline{\mathbf{n}}.\underset{\sim}{\mathbf{N}}.\underline{\mathbf{n}}) - \underset{\sim}{\mathbf{P}} : \underset{\sim}{\mathbf{N}} \\ &- \frac{\nu}{1-\nu}(\underline{\mathbf{n}}.\underset{\sim}{\mathbf{P}}.\underline{\mathbf{n}} - \operatorname{Tr}\underset{\sim}{\mathbf{P}})(\underline{\mathbf{n}}.\underset{\sim}{\mathbf{N}}.\underline{\mathbf{n}} - \operatorname{Tr}\underset{\sim}{\mathbf{N}})) \end{aligned} \tag{98}$$

The associated vector $\underline{\mathbf{g}}$ is

$$\underline{\mathbf{g}} = 2\underset{\sim}{\mathbf{P}}\underline{\mathbf{n}} - \frac{1}{1-\nu}(\underline{\mathbf{n}}.\underset{\sim}{\mathbf{P}}.\underline{\mathbf{n}})(\underline{\mathbf{n}}.\underset{\sim}{\mathbf{N}}.\underline{\mathbf{n}})\ \underline{\mathbf{n}} + \frac{\nu}{1-\nu}(\operatorname{Tr}\underset{\sim}{\mathbf{P}})\ \underline{\mathbf{n}} \tag{99}$$

We refer to the method developed in [Bigoni, Hueckel, 1991] to solve this maximization problem for general non-associated elastoplasticity. But the present analysis is restricted to associated and incompressible plasticity

$$\underset{\sim}{\mathbf{P}} = \underset{\sim}{\mathbf{N}} \quad \text{and} \quad \operatorname{Tr}\underset{\sim}{\mathbf{P}} = 0 \tag{100}$$

Equation 97 combined with 82 and written in the principal axes of $\underset{\sim}{\mathbf{P}}$ then becomes:

$$L(\underline{\mathbf{n}}, \lambda) = 2\mu\left(2\,n_i^2 P_i^2 - \sum_{i=1}^{3} P_i^2 - \frac{1}{1-\nu}(n_i^2 P_i)^2\right) - \lambda(\sum_{i=1}^{3} n_i^2 - 1) \tag{101}$$

Writing $\dfrac{\partial L}{\partial \lambda} = \dfrac{\partial L}{\partial n_k} = 0$ makes the problem equivalent to the resolution of the system:

$$n_k \left(P_k^2 - \frac{1}{1-\nu} (n_i^2 P_i) P_k - \frac{\lambda}{4\mu} \right) = 0 \quad k \in \{1,2,3\} \text{ (no sum on } k) \tag{102}$$

If $n_1\ n_2\ n_3 \neq 0$, the system is indeterminate or impossible depending on P_1,P_2,P_3.
If $n_k = 0$ and $n_i\ n_j \neq 0$ (i, j, k distinct),
if $P_i = P_j$, the system is indeterminate;
if $P_i \neq P_j$,

$$n_i^2 = \frac{P_i + \nu P_k}{P_i - P_j} \quad \text{and} \quad n_j^2 = 1 - n_i^2 \tag{103}$$

The jump of the strain rate across the surface of normal $\underline{n}$ is also described by $\underline{g}$:

$$\begin{cases} g_i = (P_i - P_j)\ n_i \\ g_j = (P_j - P_i)\ n_j \\ g_k = 0 \end{cases} \tag{104}$$

$$\begin{cases} [\![\ \dot{\underset{\sim}{\varepsilon}}_i\ ]\!] = P_i + \nu P_k \\ [\![\ \dot{\underset{\sim}{\varepsilon}}_j\ ]\!] = P_j + \nu P_k \\ [\![\ \dot{\underset{\sim}{\varepsilon}}_k\ ]\!] = 0 \end{cases} \tag{105}$$

the corresponding critical hardening modulus being

$$H^{cr} = -E P_k^2 \tag{106}$$

where E is Young's modulus.
If $n_i^2 = 1$ and $n_j = n_k = 0$,

$$H^{cr} = -2\mu \left(\frac{(P_j + \nu P_k)^2}{1-\nu} + (1+\nu) P_k^2 \right) \tag{107}$$

The first possible band is given by the combination i, j, k for which H^{cr} has the highest value.

Two-dimensional case

The plane strain case can be solved using the three-dimensional analysis. If the deformation plane is normal to direction 3

$$\dot{\varepsilon}_{33} = \dot{\varepsilon}_{33}^e + \dot{\varepsilon}_{33}^p \tag{108}$$

If plastic flow is large enough and assuming that the elastic strain remains small enough, the contribution $\dot{\varepsilon}_{33}$ can be neglected. Furthermore the direction 3 is supposed to be a principal direction of $\underset{\sim}{\mathbf{P}}$. As a result, we have almost $P_3 = 0$ so that 106 becomes

$$H^{planestrain} = 0 \tag{109}$$

We have also $P_1 + P_2 = 0$, so that 103 gives

$$n_1^2 = n_2^2 = \frac{1}{2} \tag{110}$$

The orientation of shear bands under plane strain conditions is 45°.

The plane stress case must be reexamined ([Bigoni, Hueckel 1991], [Runesson, Ottosen, Perić 1991]). The solid is considered two-dimensional. This means for instance that the compatibility condition in the third direction will not be ensured. The condition $\varepsilon_{33,12} = 0$ holds only if ε_{33} is linear in x_1 and x_2. The vectors $\underline{\mathbf{g}}$ and $\underline{\mathbf{n}}$ are supposed to lie in the plane 1-2. Lastly the elasticity matrix in the isotropic case takes a special form

$$\begin{bmatrix} \sigma_{11} \\ \sigma_{22} \\ \sigma_{12} \end{bmatrix} = \frac{2\mu}{1-\nu} \begin{bmatrix} 1 & \nu & 0 \\ \nu & 1 & 0 \\ 0 & 0 & 1-\nu \end{bmatrix} \begin{bmatrix} \varepsilon^e_{11} \\ \varepsilon^e_{22} \\ \varepsilon^e_{12} \end{bmatrix} \tag{111}$$

In that conditions, the critical hardening modulus for a given orientation $\underline{\mathbf{n}}$ is ([Bigoni, Hueckel 1991])

$$H^{planestress}(\underline{\mathbf{n}}) = 2\mu(2(\underline{\mathbf{n}}\underset{\sim}{\mathbf{P}}).(\underset{\sim}{\mathbf{N}}\underline{\mathbf{n}}) - (\underline{\mathbf{n}}.\underset{\sim}{\mathbf{P}}.\underline{\mathbf{n}})(\underline{\mathbf{n}}.\underset{\sim}{\mathbf{N}}.\underline{\mathbf{n}}) \tag{112}$$

$$- \underset{\sim}{\mathbf{P}} : \underset{\sim}{\mathbf{N}} - \nu(\underline{\mathbf{n}}.\underset{\sim}{\mathbf{P}}.\underline{\mathbf{n}} - \mathrm{Tr}\,\underset{\sim}{\mathbf{P}})(\underline{\mathbf{n}}\underset{\sim}{\mathbf{N}}\underline{\mathbf{n}} - \mathrm{Tr}\,\underset{\sim}{\mathbf{N}})) \tag{113}$$

where $\underline{\mathbf{n}} = [n_1 \; n_2]^t$ and $\underset{\sim}{\mathbf{P}}$ and $\underset{\sim}{\mathbf{Q}}$ are also two-dimensional, and $\underline{\mathbf{g}}$ is given by

$$\underline{\mathbf{g}} = 2\underset{\sim}{\mathbf{P}}\underline{\mathbf{n}} - (1+\nu)(\underline{\mathbf{n}}.\underset{\sim}{\mathbf{P}}.\underline{\mathbf{n}})\;\underline{\mathbf{n}} + \nu(\mathrm{Tr}\,\underset{\sim}{\mathbf{P}})\underline{\mathbf{n}} \tag{114}$$

We consider now only the case of incompressible associated plasticity, but in the two-dimensional case $\mathrm{Tr}\,\underset{\sim}{\mathbf{P}} = P_1 + P_2 \neq 0$!

$$H(\underline{\mathbf{n}}) = 2\mu\left(2P_i^2 n_i^2 - (P_i n_i^2)^2 - \sum_{i=1}^{2} P_i^2 - \nu(n_i^2 P_i - \sum_{i=1}^{2} P_i)^2\right) \tag{115}$$

$$\frac{\partial H}{\partial n_1^2} = -4\mu(1+\nu)(P_1 - P_2)(n_1^2 P_1 + n_2^2 P_2 - P_1 - P_2) \tag{116}$$

If $P_1 = P_2, H^{cr} = -2\mu(1+\nu)P_1^2$ and $\underline{\mathbf{n}}$ is arbitrary,
If $P_1 \neq P_2$,

$$\begin{aligned} n_1^2 &= \frac{P_1}{P_1 - P_2} \\ n_2^2 &= 1 - n_1^2 \\ g_1 &= (P_1 - P_2)n_1 \\ g_2 &= -(P_1 - P_2)n_2 \end{aligned} \tag{117}$$

and

$$H^{planestress} = 0 \tag{118}$$

The jump is then proportional to $[\![\dot{\varepsilon}_1]\!] = P_1$ and $[\![\dot{\varepsilon}_2]\!] = P_2$. The calculation proves that for plane stress also the critical hardening modulus for discontinuous bifurcations generally is zero.

The two-dimensional solid is therefore more prone to localization than the real solid. The reason is that some bifurcation modes though incompatible (in the sense of Hadamard) in the direction 3 are compatible in the plane 1-2 and are then full discontinuous bifurcation modes for the 2D solid.

2.6 Stability

Concerning stability we present Mandel's approach [1966].

Let us consider a solid in a state of equilibrium. Perturbations of the equilibrium may be represented by plane waves

$$\underline{\mathbf{u}}^{\star} \;=\; f(\underline{\mathbf{n}}.\underline{\mathbf{x}} \pm Ut)\;\underline{\mathbf{c}} \tag{119}$$

One assumes that the initial equilibrium stress $\underset{\sim}{\sigma}$ is homogeneous. $\underset{\sim}{\sigma}^{\star}$ denotes then the stress variation due to the perturbation. It follows that

$$\underline{\mathrm{div}}\;\underset{\sim}{\sigma}^{\star} \;=\; \rho\;\underline{\ddot{\mathbf{u}}^{\star}} \tag{120}$$

Furthermore it is assumed that the constitutive equations take the linear incremental form 41 and that $\underset{\sim}{\mathbf{D}}$ is initially homogeneous and that it remains constant around the equilibrium state. In these conditions and taking 119 into account, the last equation becomes

$$\begin{aligned} D_{ijkl}\;u_{k,lj} &= \ddot{u}_i \\ n_i\;D_{ijkl}\;n_l c_k &= \rho U^2\;c_i \end{aligned} \tag{121}$$

that is

$$\underset{\sim}{\mathbf{Q}}\;\underline{\mathbf{c}} \;=\; \rho U^2\;\underline{\mathbf{c}} \tag{122}$$

As a result plane waves and acceleration waves are governed by the same equations (compare 68 and 122), even though they represent two distinct phenomena. The assumptions in the previous calculation correspond to the so-called "acoustic approximation" in fluid mechanics, which explains the denomination of tensor $\underset{\sim}{\mathbf{Q}}$. When the eigenvalues of the acoustic tensor are real and positive, equilibrium is said to be stable because plane waves can propagate without growing. If they are real but negative, equilibrium is unstable with divergence. Complex eigenvalues lead to a phenomenon called *flutter instability* in aerodynamics.

2.7 Localization criteria

2.7.1 Summary

The various bifurcation criteria that have been established in the previous sections are summed up on figure 7. Two critical hardening moduli have been defined: H^{u} corresponds to possible loss of uniqueness and H^{cr} is associated with the possible existence of discontinuous bifurcation modes. An additional critical hardening modulus can be determined for which general bifurcation modes become compatible, i.e. are of the form $[\![\,\dot{\underset{\sim}{\varepsilon}}\,]\!] = \{\,\underline{\mathbf{g}} \otimes \underline{\mathbf{n}}\,\}$

$$\dot{\underset{\sim}{\varepsilon}} : \underset{\sim}{\mathbf{D}} : \dot{\underset{\sim}{\varepsilon}} = 0 \;\Rightarrow\; \underline{\mathbf{g}}.\underset{\sim}{\mathbf{Q}}.\underline{\mathbf{g}} = \underline{\mathbf{g}}.\{\underset{\sim}{\mathbf{Q}}\}.\underline{\mathbf{g}} = 0 \tag{123}$$

which corresponds to the loss of positive definitiveness of the symmetrized acoustic tensor. This condition is called loss of strong ellipticity.

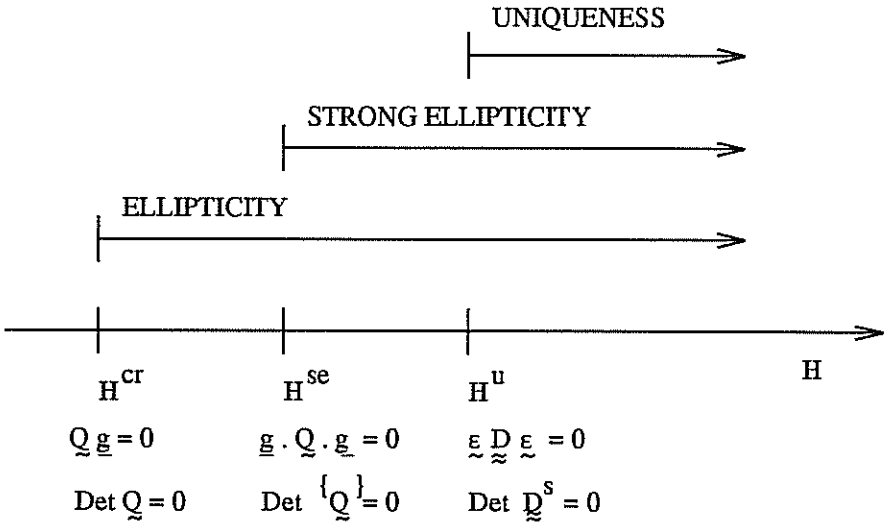

Figure A.7: Bifurcation criteria in non-associated plasticity.

A summary of the different criteria can also be found in [Benallal, Billardon, Geymonat 1991]. Furthermore Benallal [1991] analyses the implications of taking into account thermal effects and thermomechanical couplings on localization phenomena. This leads in particular to a description of adiabatic shear bands, studied in the case of single crystals by Duszek and Perzyna [1992, 1993].

In the general case, the sign of the three critical hardening moduli can be positive or negative. In particular bifurcation may occur while the material is hardening. In contrast, for associated plasticity at small strains, $H^u = 0$ so that bifurcations are possible only for ideal plastic or strain-softening materials. Furthermore $\underset{\sim}{\mathbf{D}}$ and $\underset{\sim}{\mathbf{Q}}$ are then symmetric tensors so that $H^{se} = H^{cr}$.

In general bifurcation may occur before the extremum $\dot{\underset{\sim}{\sigma}} = 0$ of the loading curve. The associated hardening modulus H^l for which $\mathrm{Det}\underset{\sim}{\mathbf{D}} = 0$ corresponds to a limit point.

General bifurcation modes may induce diffuse or localized deformation. It is difficult in practice to distinguish some localized general bifurcations and discontinuous ones (shear bands strictly speaking). However one can assume that a general bifurcation which is also compatible in the sense of Hadamard will induce localized rather than diffuse deformation. That is why Neilsen and Schreyer [1993] think of the strong ellipticity criterion as a good criterion for localization of deformation.

2.7.2 Examples: tension test

Bifurcation in the bulk

We consider the example of an elastoplastic model with the von Mises criterion

$$f = J_2(\underset{\sim}{\sigma}) - R \quad \text{with} \quad J_2(\underset{\sim}{\sigma}) = \sqrt{\frac{3}{2}\underset{\sim}{\sigma}^{dev} : \underset{\sim}{\sigma}^{dev}} \tag{124}$$

$\underset{\sim}{\sigma}^{dev}$ denoting the deviatoric part of $\underset{\sim}{\sigma}$. In that case,

$$\underset{\approx}{\mathbf{D}} = \underset{\approx}{\mathbf{E}} - \frac{2\mu^2}{H/3+\mu} \frac{\underset{\sim}{\sigma}^{dev} \otimes \underset{\sim}{\sigma}^{dev}}{\underset{\sim}{\sigma}^{dev} : \underset{\sim}{\sigma}^{dev}} \tag{125}$$

For isotropic elasticity, $\underset{\sim}{\mathbf{1}}$ is an eigentensor of $\underset{\approx}{\mathbf{D}}$ and the associated eigenvalue is $3k$

$$\underset{\sim}{\mathbf{d}}_1 = \frac{\underset{\sim}{\sigma}^{dev}}{\sqrt{\underset{\sim}{\sigma}^{dev} : \underset{\sim}{\sigma}^{dev}}} \tag{126}$$

is an eigentensor for the eigenvalue $\omega_1 = 2\mu H/(H+3\mu)$. The remaining eigentensors are in $\{\underset{\sim}{\mathbf{1}}, \underset{\sim}{\sigma}^{dev}\}^{\perp}$ and the eigenvalue is 2μ. Accordingly, only one eigenvalue depends on the hardening modulus. Uniqueness is lost for $\omega_1 = 0 = H$. For tensile straining

$$[\underset{\sim}{\mathbf{d}}_1] = \frac{1}{\sqrt{6}} \begin{bmatrix} -1 & 0 & 0 \\ 0 & 2 & 0 \\ 0 & 0 & -1 \end{bmatrix} \tag{127}$$

This is an incompatible diffuse mode that gives rise to the necking phenomenon.

We restrict ourselves to the tension of a plate to study the bifurcation modes in the plane 1-2. The mode 127 is assumed to occur within a band of normal $\underline{\mathbf{n}}$. The components of $\underset{\sim}{\mathbf{d}}_1$ in the basis $(\underline{\mathbf{m}}, \underline{\mathbf{n}})$ (see figure 8) read

$$[\underset{\sim}{\mathbf{d}}_1] = \frac{1}{\sqrt{6}} \begin{bmatrix} 2\sin^2\theta - \cos^2\theta & 3\cos\theta\sin\theta & 0 \\ 3\cos\theta\sin\theta & 2\cos^2\theta - \sin^2\theta & 0 \\ 0 & 0 & 1 \end{bmatrix} \tag{128}$$

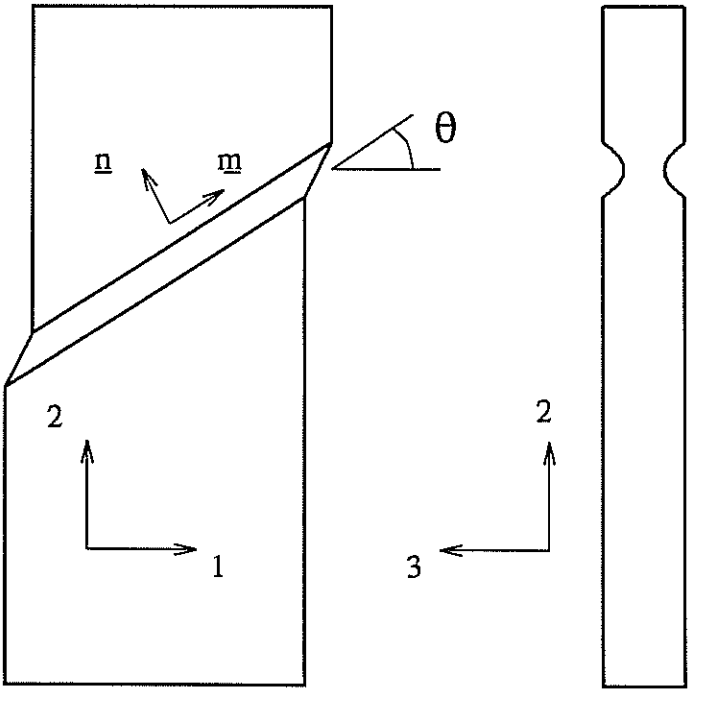

Figure A.8: Shear band in a plate under tensile loading.

The bifurcation mode becomes compatible in the sense of Hadamard in the 1-2 plane if $2\sin^2\theta - \cos^2\theta = 0$, i.e.

$$\tan^2\theta = \frac{1}{2}, \quad \theta = \pm 35.26^\circ \tag{129}$$

It means that deformation can localize within a band with the previous orientation. However, compatibility is not ensured in the third direction until the critical hardening modulus for discontinuous bifurcations is reached

$$H^{cr} = -E/4 \tag{130}$$

after equation 106. But the orientation of the band is then, according to equation 103

$$n_1^2 = \frac{1+\nu}{3} \tag{131}$$

which gives $\theta = 42^\circ$ for $\nu = 0.33$.

Bifurcation at the boundary

We provide now examples of application of condition (*iii*) of section 2.4.3 in the case of isotropic elasticity. The following expressions are useful:

$$\underset{\sim}{\underset{\sim}{\mathbf{E}}} : \underset{\sim}{\mathbf{P}}.\underline{\mathbf{n}} = \lambda\,(\mathrm{Tr}\,\underset{\sim}{\mathbf{P}})\;\underline{\mathbf{n}} + 2\mu\,\underset{\sim}{\mathbf{P}}\underline{\mathbf{n}} \tag{132}$$

$$\underline{\mathbf{m}}.\underset{\sim}{\underset{\sim}{\mathbf{E}}}.\underline{\mathbf{n}} = \lambda\;\underline{\mathbf{m}}\otimes\underline{\mathbf{n}} + \mu\;\underline{\mathbf{n}}\otimes\underline{\mathbf{m}} + \mu\,\underline{\mathbf{m}}.\underline{\mathbf{n}}\;\underset{\sim}{\mathbf{1}} \tag{133}$$

$$(\underline{\mathbf{n}}.\underset{\sim}{\underset{\sim}{\mathbf{E}}}.\underline{\mathbf{n}})^{-1} = -\frac{\lambda+\mu}{\mu(\lambda+2\mu)}\;\frac{\underline{\mathbf{n}}\otimes\underline{\mathbf{n}}}{\underline{\mathbf{n}}.\underline{\mathbf{n}}} + \frac{1}{\mu\;\underline{\mathbf{n}}.\underline{\mathbf{n}}}\;\underset{\sim}{\mathbf{1}}. \tag{134}$$

To permit a comparison with the results of Benallal, Billardon and Geymonat [1990], we do not assume, in this paragraph, that $\underline{\mathbf{m}}$ and $\underline{\mathbf{n}}$ are unit vectors. This leads to the following form of condition (*iii*) of section 2.4.3:

$$\begin{aligned}(\underline{\mathbf{n}}.\underline{\mathbf{n}})^2\;(\lambda\mathrm{Tr}\,\underset{\sim}{\mathbf{P}}\;\underline{\mathbf{m}} + 2\mu\underset{\sim}{\mathbf{P}}\underline{\mathbf{m}}) \;&=\; 2\mu\;(\underline{\mathbf{m}}.\underline{\mathbf{n}})\;(\underline{\mathbf{n}}.\underline{\mathbf{n}})\;\underset{\sim}{\mathbf{P}}\underline{\mathbf{n}} \\ &+\; \lambda\left(\frac{\lambda}{\lambda+2\mu}\,\mathrm{Tr}\,\underset{\sim}{\mathbf{P}}\;(\underline{\mathbf{n}}.\underline{\mathbf{n}})^2 + \frac{2\mu}{\lambda+2\mu}\;(\underline{\mathbf{n}}.\underset{\sim}{\mathbf{P}}.\underline{\mathbf{n}})\;(\underline{\mathbf{n}}.\underline{\mathbf{n}})\right)\;\underline{\mathbf{m}} \\ +\,2\mu\left(\frac{\lambda}{\lambda+2\mu}\,\mathrm{Tr}\,\underset{\sim}{\mathbf{P}}\;(\underline{\mathbf{m}}.\underline{\mathbf{n}})\;(\underline{\mathbf{n}}.\underline{\mathbf{n}}) - 2\frac{\lambda+\mu}{\lambda+2\mu}\;(\underline{\mathbf{n}}.\underset{\sim}{\mathbf{P}}.\underline{\mathbf{n}})\;(\underline{\mathbf{m}}.\underline{\mathbf{n}}) + (\underline{\mathbf{m}}.\underset{\sim}{\mathbf{P}}.\underline{\mathbf{n}})\;(\underline{\mathbf{n}}.\underline{\mathbf{n}})\right)\;&\underline{\mathbf{n}}\end{aligned} \tag{135}$$

(In [Benallal, Billardon, Geymonat 1990], we read $(\underline{\mathbf{n}}.\underline{\mathbf{n}})$ instead of $(\underline{\mathbf{n}}.\underline{\mathbf{n}})^2$ in the first term and $2(\underline{\mathbf{m}}.\underset{\sim}{\mathbf{P}}.\underline{\mathbf{n}})\;(\underline{\mathbf{n}}.\underline{\mathbf{n}})$ instead of $(\underline{\mathbf{m}}.\underset{\sim}{\mathbf{P}}.\underline{\mathbf{n}})\;(\underline{\mathbf{n}}.\underline{\mathbf{n}})$ in the last term).

For an incompressible plastic flow $\mathrm{Tr}\,\underset{\sim}{\mathbf{P}} = 0$, and for a tension test with

$$P = \begin{bmatrix} -a/2 & 0 & 0 \\ 0 & a & 0 \\ 0 & 0 & -a/2 \end{bmatrix} \tag{136}$$

the plane bifurcation modes are given by

$$\sin\theta = 0 \quad \text{or} \quad \tan^2\theta = \frac{3\lambda+4\mu}{3\lambda+2\mu} = \frac{2-\nu}{1+\nu} \tag{137}$$

where θ denotes the angle between the normal $\underline{\mathrm{n}}$ to the discontinuity surface and the normal $\underline{\mathrm{m}}$ to the boundary.

We can also apply the plane strain analysis of [Bigoni, Hueckel 1991] strain to the problem of bifurcation modes at the boundary. Elastic strains are neglected so that

$$P = \begin{bmatrix} -a & 0 & 0 \\ 0 & a & 0 \\ 0 & 0 & 0 \end{bmatrix} \tag{138}$$

Taking $m = \begin{bmatrix} 1 \\ 0 \\ 0 \end{bmatrix}$ as free boundary, condition (iii) yields

$$\theta = \pm 45° \tag{139}$$

This means that for plane strain, shear bands, regarded as bifurcation modes, undergo no deviation when approaching a free boundary.

2.8 Simulation of some bifurcation modes in elastoplasticity

2.8.1 Introductory example: slope localization

The first example in this work of simulation of localized deformation in elastoplastic materials is referred to in literature as *slope localization*. We consider a section of a soil with a slope and a rigid footing at the top. The vertical displacement of a node of the footing is prescribed. Finite elements calculations are performed at plane strain with a strain-softening elastoplastic behaviour. Slightly after the load reaches a maximum, strain localizes within a thin curved layer (figure 9). This coincides with an abrupt load drop. The slope localization problem has been studied by Yu, Perić and Owen [1991].

In the following we will focus on shear band formation triggered by the presence of geometrical or material defects.

2.8.2 Presentation of the calculations

We consider the tension of a plate with a geometrical imperfection. The mesh corresponds to one quarter of the entire plate and loading and boundary conditions are described in figure 10.

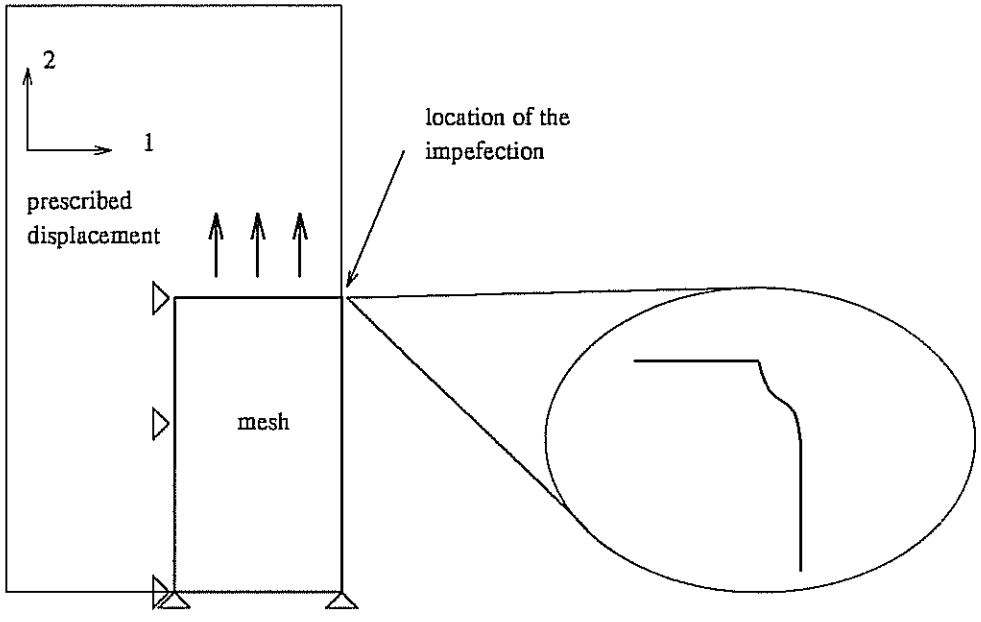

Figure A.10: 2D plate in tension with an initial flaw; boundary and loading conditions.

A thickness heterogeneity is introduced according to

$$x_1 = l(1 + a(\tanh \frac{m(x_2 - y_0)^2}{L^2} - 1)) \tag{140}$$

with $L = 2, l = 1, a = 0.002, m = 25$ and $y_0 = 2$ or 1.5. We have also used in some cases the form proposed by Peirce, Asaro and Needleman [1982]

$$x_1 = l(1 + a(\cos \frac{2\pi m x_2}{L})) \tag{141}$$

with $a = 0.0025$ and $m = 0.25$.

A classical phenomenological elastoplastic model has been chosen involving two hardening variables: isotropic hardening and kinematic hardening [Lemaitre, Chaboche 1985]. The constitutive equations are

$$f = J_2(\underset{\sim}{\sigma} - \underset{\sim}{\mathbf{X}}) - R(p) \tag{142}$$

$$\dot{\lambda} = \dot{p} = \sqrt{\frac{2}{3}\underset{\sim}{\dot{\varepsilon}}^p : \underset{\sim}{\dot{\varepsilon}}^p} \tag{143}$$

$$R(p) = R_0 + Q(1 - e^{-bp}) \tag{144}$$

$$\underset{\sim}{\mathbf{X}} = \frac{2}{3} C \underset{\sim}{\alpha} \tag{145}$$

$$\dot{\underset{\sim}{\alpha}} = \underset{\sim}{\dot{\varepsilon}}^p - D\dot{p}\underset{\sim}{\alpha} \tag{146}$$

the following parameters have been chosen so that the material first hardens and then softens. The maximum is reached after small deformation (figure 11).

$$E = 200000 \text{ MPa}, \ \nu = 0.3$$

$$R_0 = 102 \text{ MPa}, \ Q = -100 \text{ MPa}, \ b = 100$$

$$C = 91800 \text{ MPa}, \; D = 800$$

The FE calculations are performed with the code ZéBuLoN, developed at Ecole des Mines. In this work, we have used an explicit Runge-Kutta method or an implicit Newton method for the local integration of the constitutive equation. For the global resolution, we have used the BFGS method (see [Aazizou 1990] and [Culioli 1994]). The stiffness matrix at the beginning of the increment is the elastic matrix. In the two-dimensional case, we use quadratic elements with eight nodes and nine integration points. In the three-dimensional case, we use 20-node bricks with 27 Gauss points.

2.8.3 2D plane stress

In figure 12, the behaviour of the flawed plate in tension under plane stress conditions in elastoplasticity is compared with the homogeneous deformation of a plate without initial imperfection. Slightly after the maximum, the load-displacement curve displays an abrupt load drop and strain localizes within two narrow shear bands. Their orientation is that predicted in section 2.7.2, namely 54.7° with respect to the tensile axis.

2.8.4 Mesh dependence; regularization methods

The previous calculations have been carried out successively for 200, 800 and 1800 elements. The phenomenon exhibits a strong mesh-dependence. The load-displacement curves of figure 14 prove that the finer the mesh, the later the bifurcation occurs, the size of the defect being unchanged. The width of the band is always about the size of one element (figure 13).

The influence of rate-dependence on shear banding has been investigated. Two viscosity parameters are introduced in the previous model to give an elastoviscoplastic model

$$\underset{\sim}{\dot{\varepsilon}}^p = \frac{3}{2}\dot{p}\,\frac{\underset{\sim}{\sigma}^{\text{dev}} - \underset{\sim}{\mathbf{X}}}{J_2(\underset{\sim}{\sigma} - \underset{\sim}{\mathbf{X}})} \tag{147}$$

with

$$\dot{p} = < \frac{J_2(\underset{\sim}{\sigma} - \underset{\sim}{\mathbf{X}}) - R}{K} >^n \tag{148}$$

The problem of the plate in tension under plane stress conditions is reconsidered in viscoplasticity. The obtained shear bands are larger than for the plastic material and the strain reached in the band is lower. In figure 15 we see the initiation and growth of a large non-homogeneous deformation pattern. In contrast the profile of a shear band in a plastic material looks like a Dirac function. Figure 16 shows that for a slightly viscous material ($K = 10$ MPa $s^{1/n}$, $n = 5$), bifurcation is still possible (sharp load drop) but higher viscosity delays and damps the load drop ($K = 50$ MPa $s^{1/n}$). Viscoplasticity may even preclude shear band initiation. Moreover viscoplasticity significantly reduces mesh-dependence even for slightly viscous materials. Contrary to the elastoplastic case, a finer mesh does not delay band initiation in a viscoplastic material (figure 17a, $K = 10$ MPa $s^{1/n}$). The fact that the coarser mesh exhibits a somewhat less abrupt load drop has been mentionned in [Needleman, Asaro, Lemonds, Peirce 1985]. With higher viscosity the calculations become mesh-independent (figure 17b). Viscosity has also been used as a regularization method in [Peirce, Asaro, Needleman 1983]. However, since the regularizing

capability of vicoplasticity depends on the magnitude of the viscosity terms, we regard viscoplasticity only as a *pseudo-regularization method.*

The spurious mesh-dependence is due to the loss of ellipticity of the governing equilibrium equations in the static case and of hyperbolicity in the dynamic case. Harirêche and Loret [1992] have shown that hyperbolicity is preserved if viscoplasticity is used in the dynamic case. De Borst [1993] proposes three regularizing methods in the static case:

- non-locality (already used in damage mechanics)
- introduction of higher gradients (non simple materials)
- Cosserat theory

The last method will be investigated in the case of single crystals in part B (see section B.4.1).

2.8.5 2D plane strain; dissipative structures

We consider the problem of the tension of a plate under plane strain conditions. The geometrical imperfection is now located at three quarters of the height. The material is only slightly viscous ($K = 10$ MPa $s^{1/n}$, $n = 5$) so that a bifurcation with a sharp load drop can be expected. Shortly after the maximum load but before the load drop, we observe several reflecting and intersecting bands of intense deformation (figure 18a). This may be interpreted as a resonance between shear band orientation (45° as expected in section 2.5.2) and specimen geometry. This deformation mode can be regarded as a *dissipative structure* according to the terminology introduced by Prigogine (see for instance [Prigogine, Stengers 1984]). After the load drop only three shear bands remain and deformation strongly localizes within them (figure 18b). Thus the initial imperfection has first induced a symmetric non-homogeneous deformation pattern and then triggered a *symmetry-breaking* bifurcation. Such dissipative structures are observed in dry sand (see the references in [Chambon 1986]).

2.8.6 3D tensile test

The plate is now a three-dimensional solid and has a one-element thickness. Elements are 20-nod bricks with 27 Gauss points. Once again shear bands appear in a softening material with the same orientation but the bands are much larger and strain in them much lower than for the 2D plate (figure 19). The reason is that the observed bifurcation mode is only partially compatible as explained in section 2.7.2. It is compatible in the plane 1-3 but the incompatibility in direction 2 results in necking. That is why we obtain a more diffuse strain field.

2.8.7 Axisymmetric bar in tension

For a cylindrical bar in tension, bifurcation theory predicts no possible discontinuous bifurcations [Neilsen, Schreyer 1994]. Instead, 2D axisymmetric calculations on a flawed plate show that a necking zone forms (figure A.20).

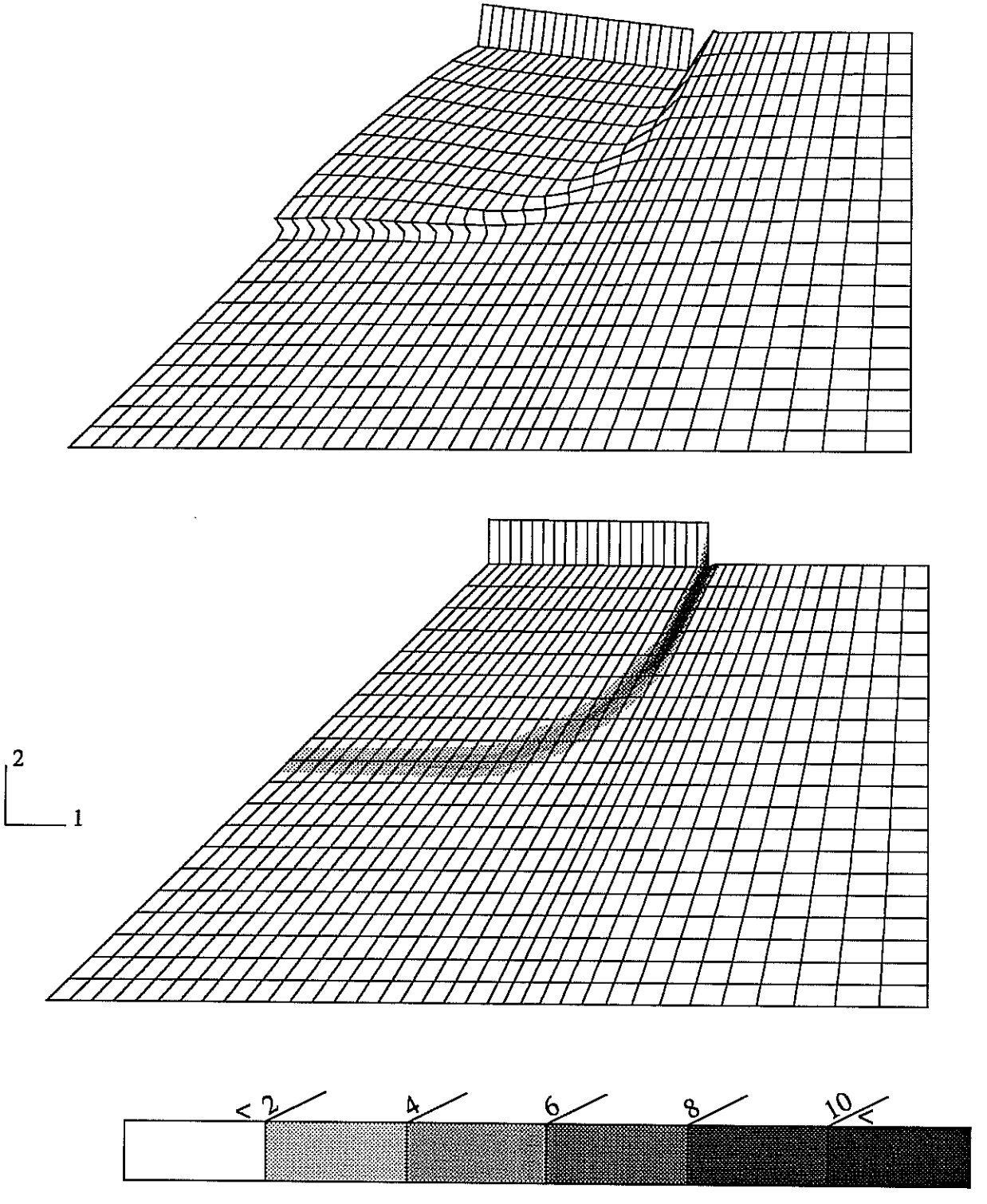

Figure A.9: Slope localization (rigid footing and elastoplastic softening soil); on the deformed state, displacements have been magnified by 15.

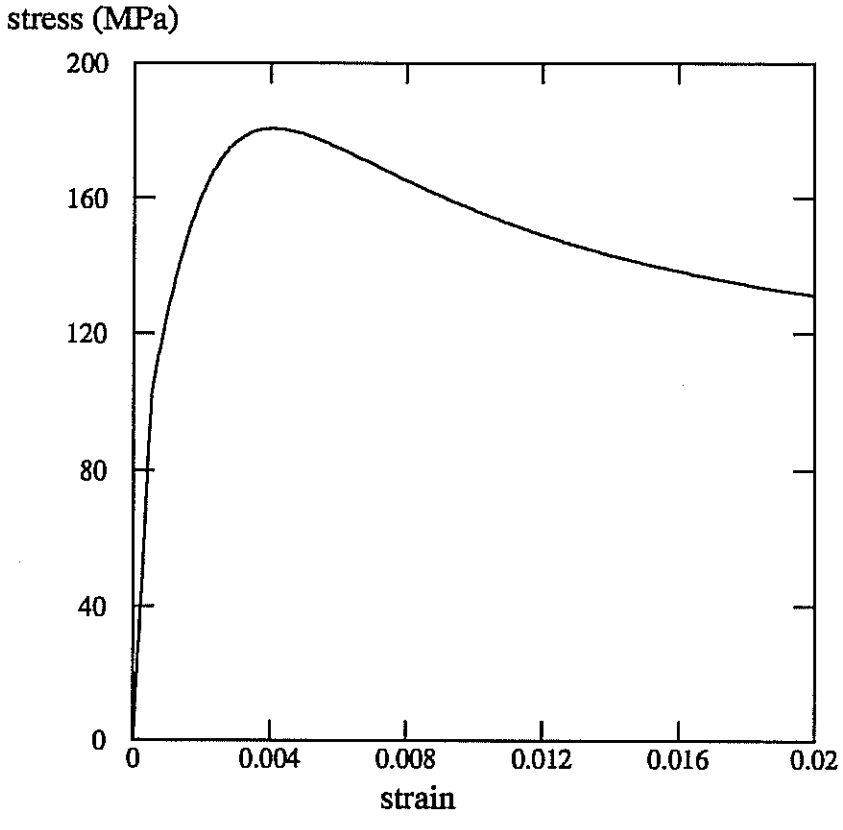

Figure A.11: Tensile behaviour corresponding to the set of parameters given in section A-2.8.2.

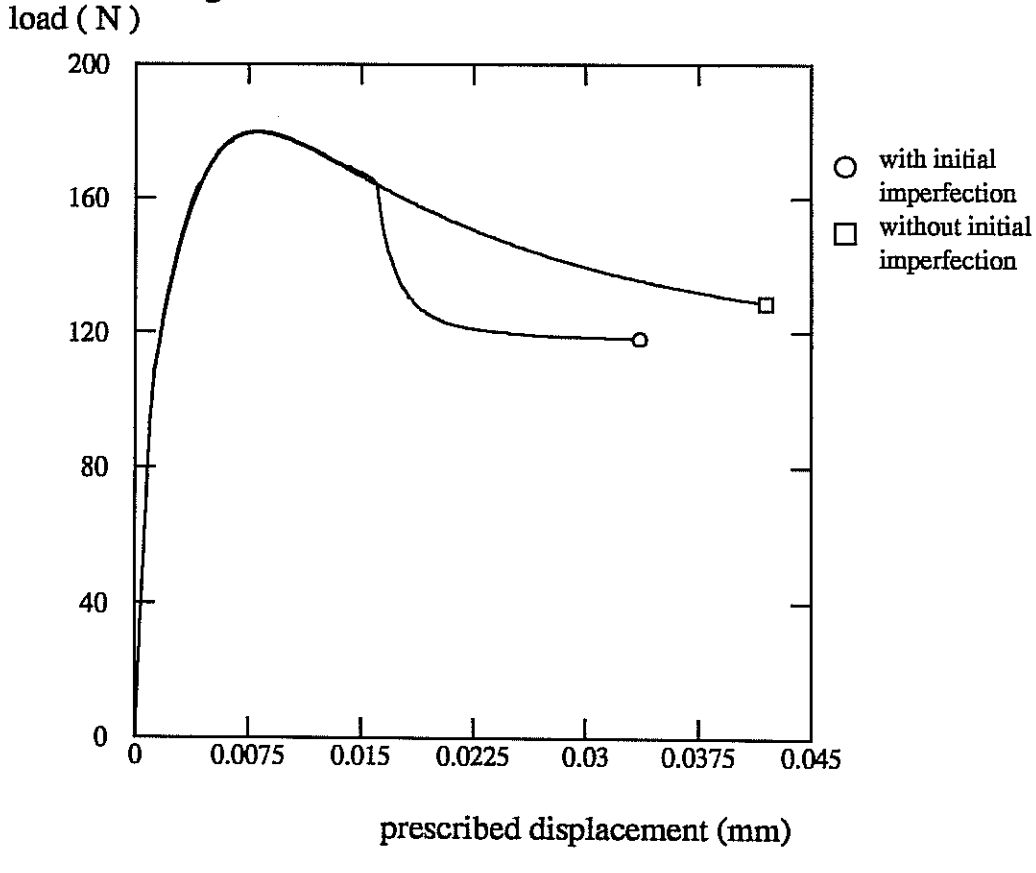

Figure A.12: Bifurcation of the load-displacement curve for a flawed plate in tension (elastoplasticity, plane stress).

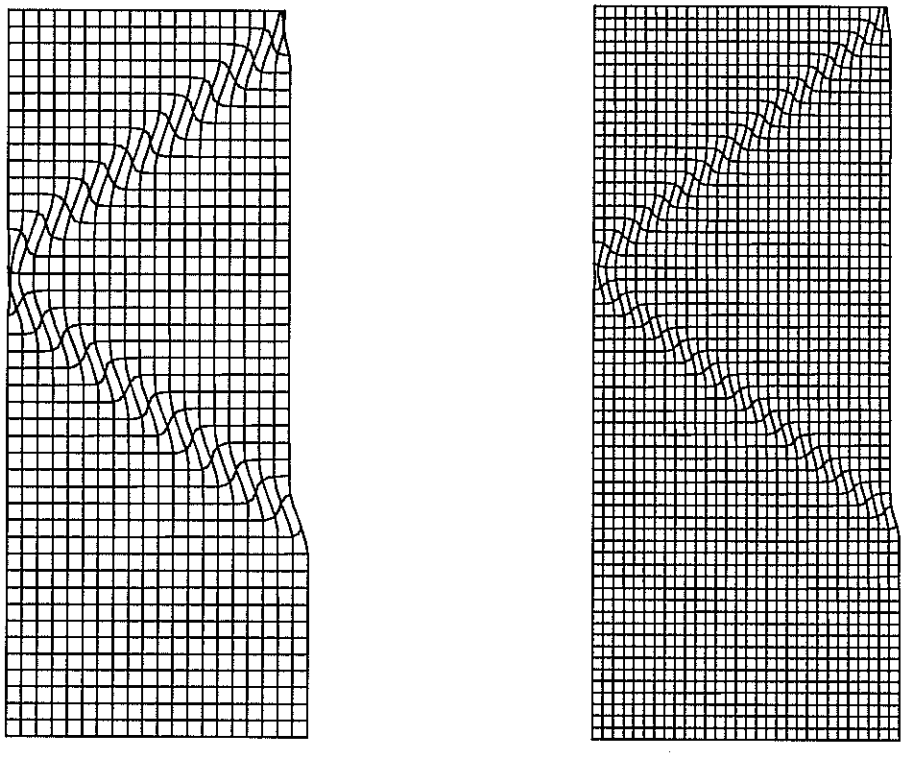

Figure A.13: Simulation of shear bands with a coarse and a fine mesh (tension, plane stress).

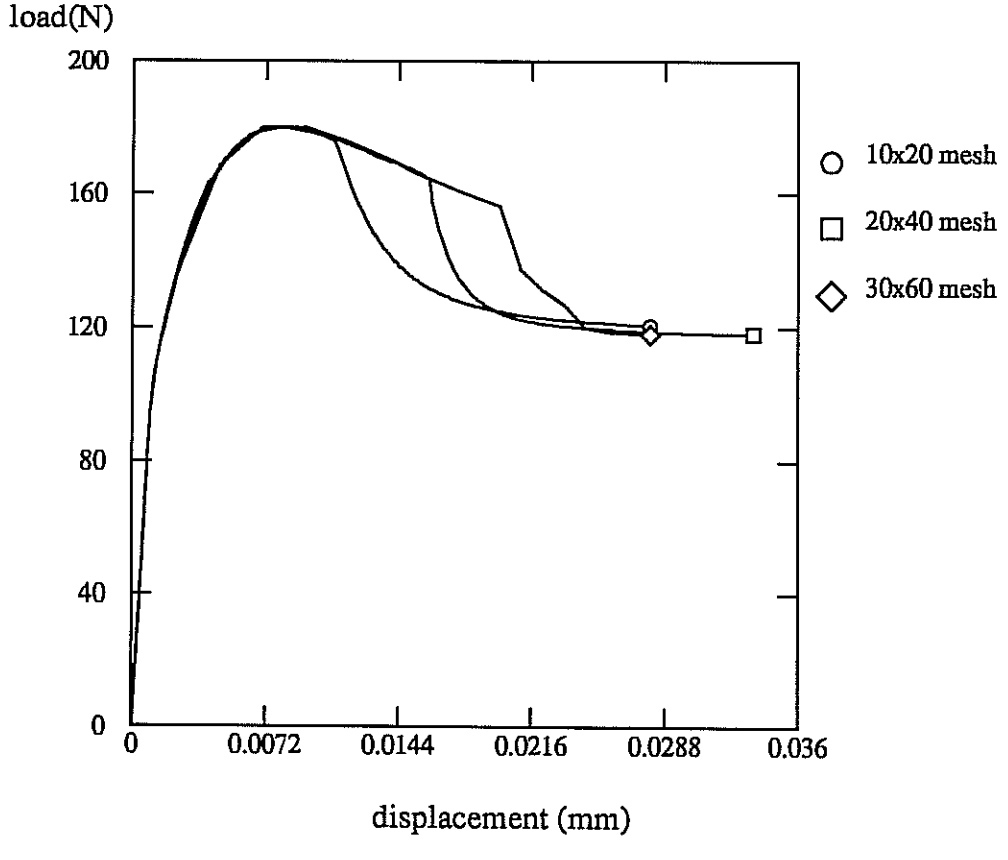

Figure A.14: Tension of a flawed plate at plane stress in elastoplasticity; load-displacement curves for 10x20, 20x40, 30x60 element meshes.

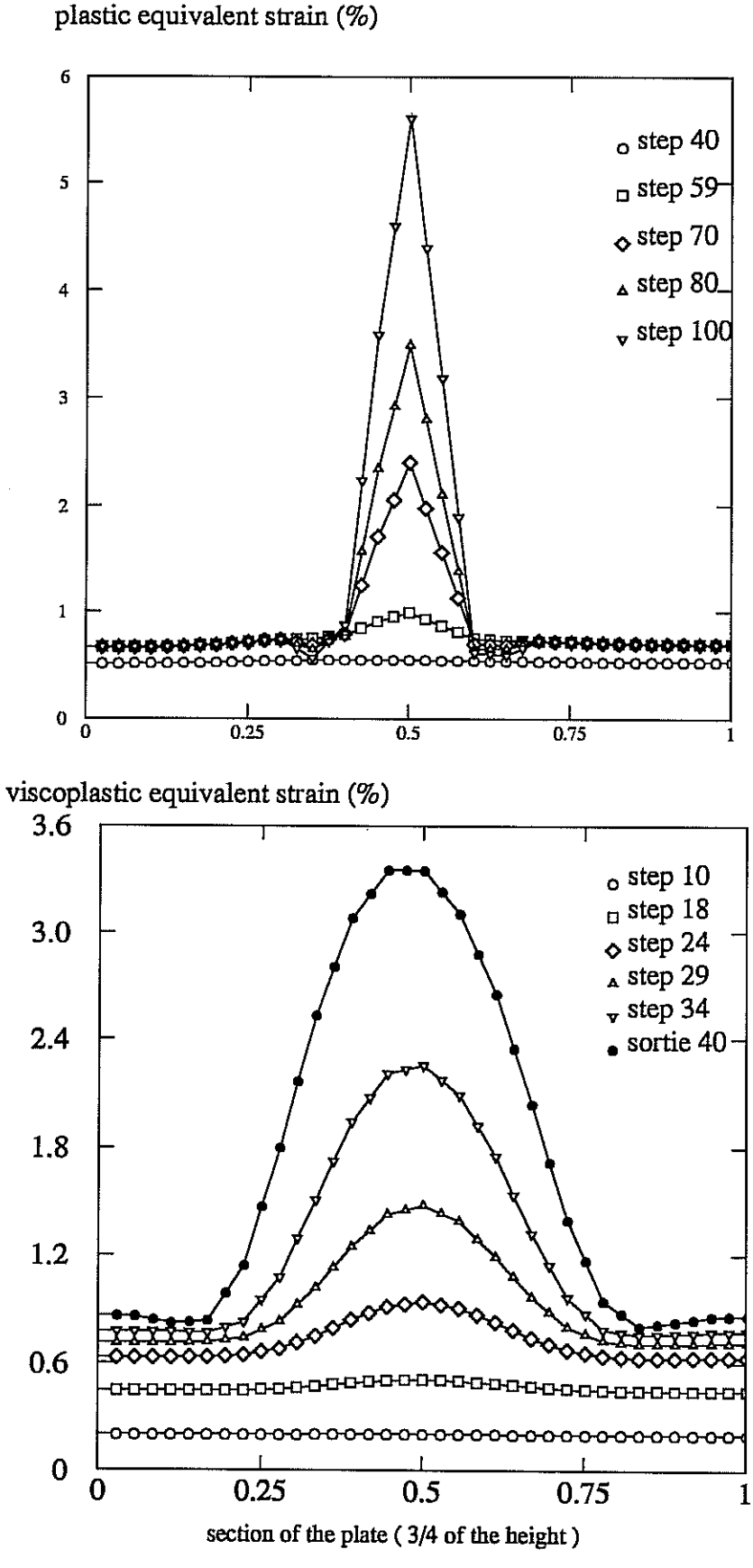

Figure A.15: Initiation and growth of a shear band in elastoplasticity (above) and elastoviscoplasticity (below).

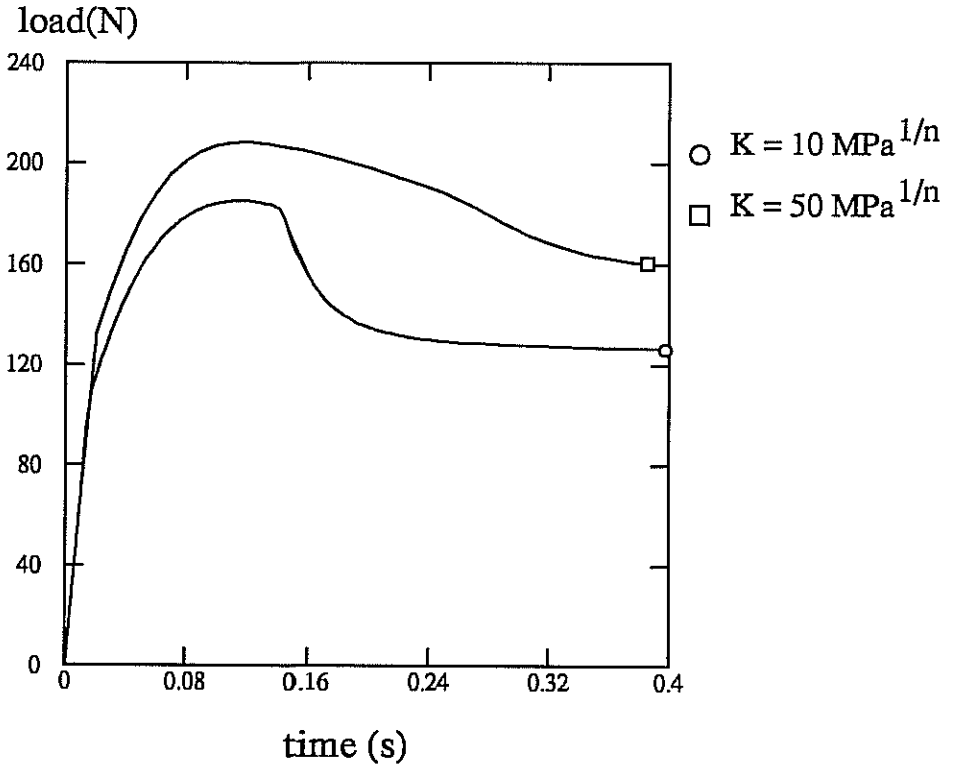

Figure A.16: Tension of a flawed plate at plane stress in viscoplasticity; load-displacement curves for a slightly viscous material and for a more viscous one.

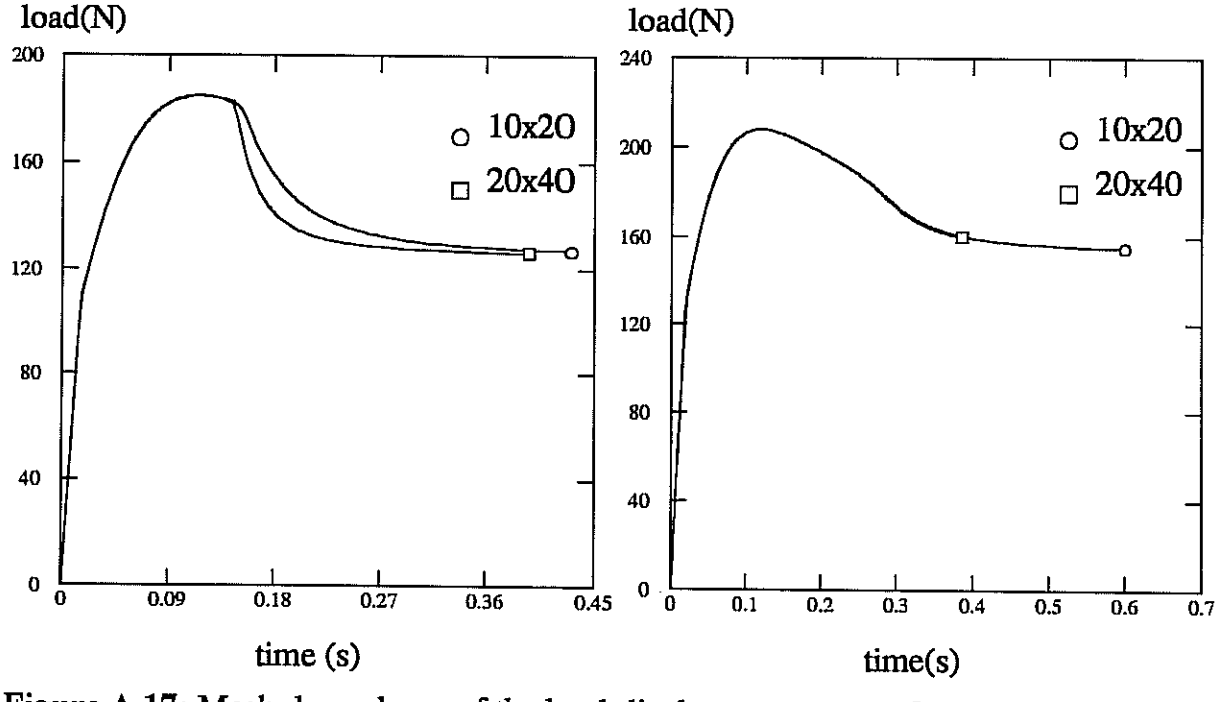

Figure A.17: Mesh-dependence of the load-displacement curves for a slightly viscous material (K=10, left) and a more viscous material (K=50, right)

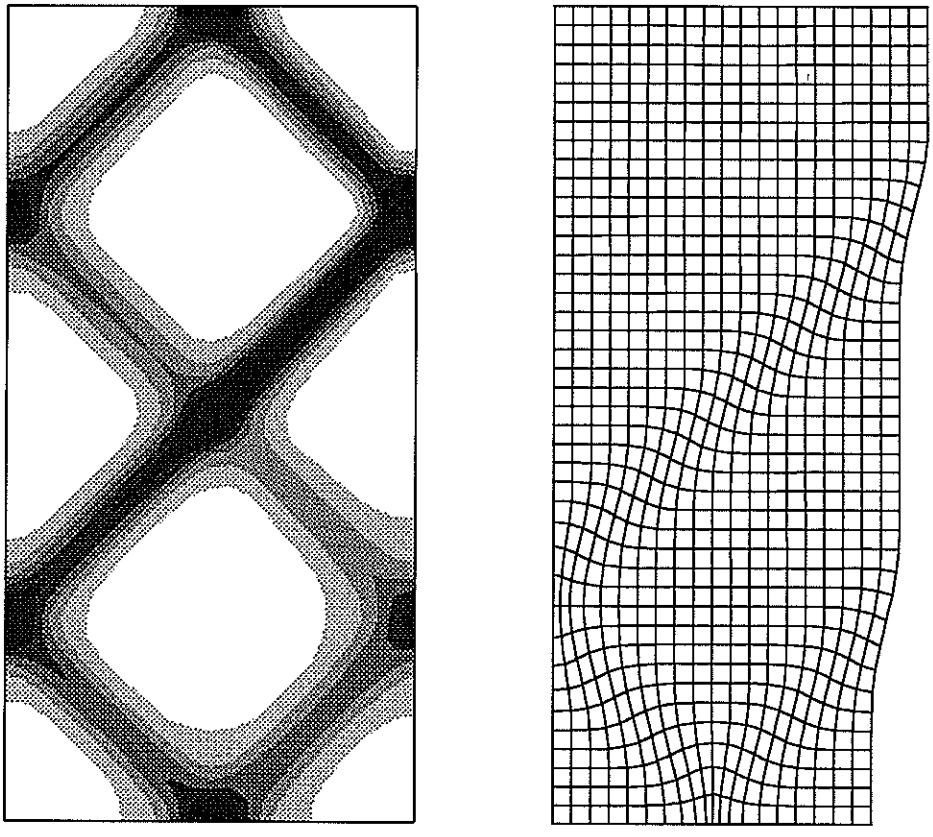

Figure A.18: Tension of a flawed plate at plane strain; the geometrical imperfection is located at 3/4 of the height; several reflecting bands form shortly after the maximum load (left); only three shear bands remain after the load drop (right, displacements have been magnified).

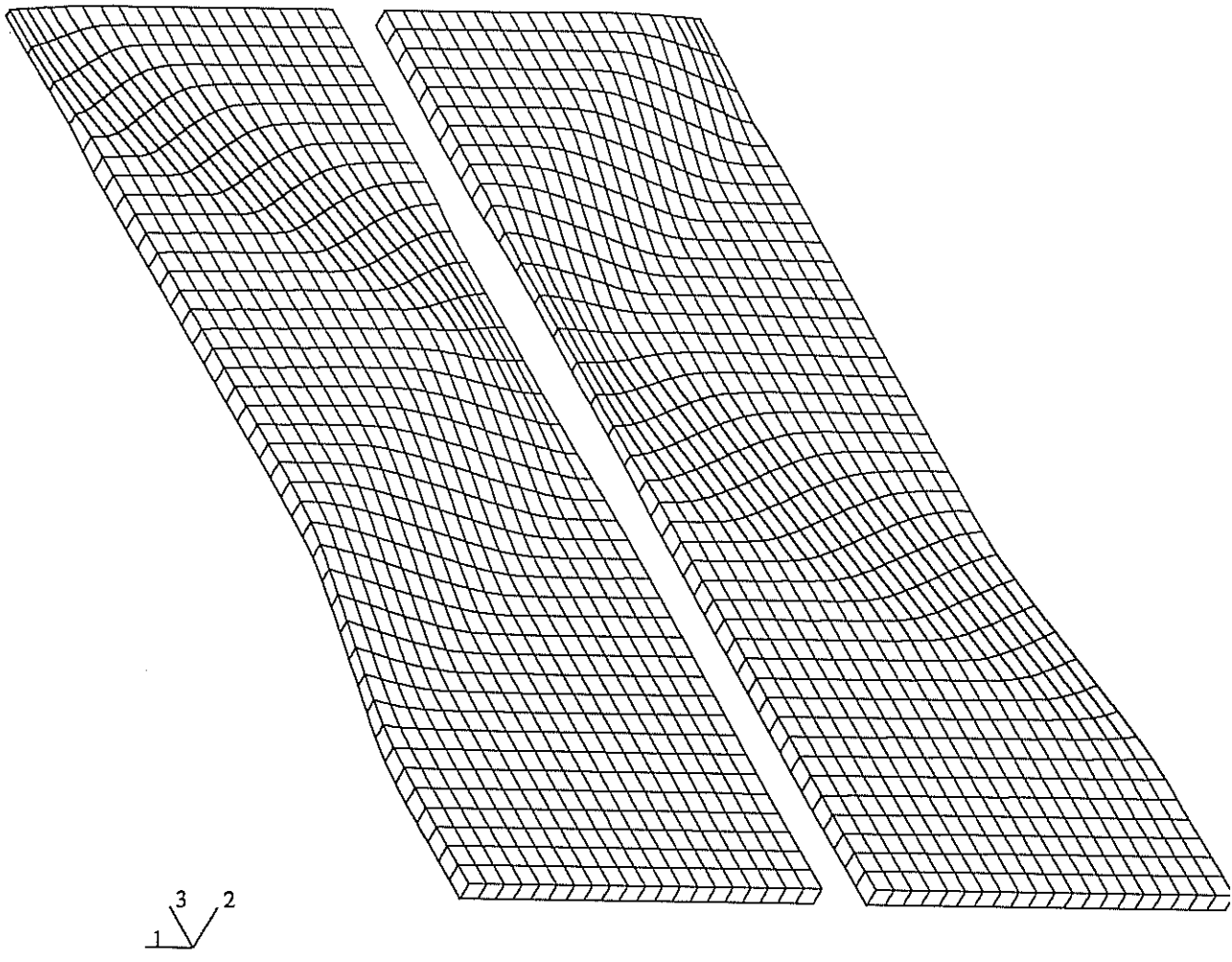

Figure A.19: Tension of a 3D flawed plate (elastoplasticity); two quarters of the entire plate are represented; displacements have been magnified by 15.

Figure A.20: Necking of a cylindrical bar (axisymmetric case).

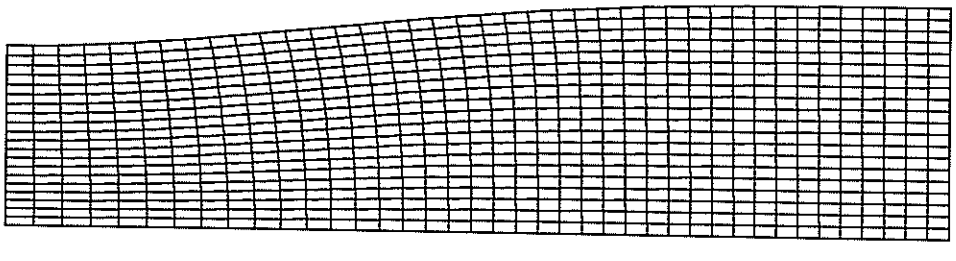

3 Constitutive equations for elastoviscoplastic single crystals at small strains

3.1 Presentation of the model

The model considered in this work to describe the elastoviscoplastic behaviour of f.c.c. single crystals has been proposed in [Cailletaud 1987] and [Méric, Poubanne, Cailletaud 1991]. It is based on crystal plasticity theory at small strain. The viscoplastic deformation results from the cooperative motion of dislocations on N slip systems

$$\underset{\sim}{\dot{\varepsilon}}^p = \sum_{g=1}^{N} \dot{\gamma}^g \ \{\underline{\mathbf{m}}^g \otimes \underline{\mathbf{z}}^g\} \tag{149}$$

where $\underline{\mathbf{m}}^g$ and $\underline{\mathbf{z}}^g$ denote the glide direction and the normal to the slip plane for slip system g. γ^g is the amount of slip for the slip system g. Slip systems are activated according to Schmid's law and internal variables are introduced for each slip system to describe the hardening of the material. The constitutive equations are
local flow rule

$$\dot{\gamma}^g = < \frac{\mid \tau^g - x^g \mid - r^g}{k} >^n \ \text{sign}\ (\tau^g - x^g) \tag{150}$$

$$\dot{v}^g = \mid \dot{\gamma}^g \mid \tag{151}$$

local kinematic hardening

$$x^g \ = \ c\ \alpha^g \tag{152}$$

$$\dot{\alpha}^g = \dot{\gamma}^g - d\,\dot{v}^g \alpha^g \tag{153}$$

local isotropic hardening

$$r^g = r_0 + q \sum_{r=1}^{N} h^{gr}(1 - \exp(-bv^r)) \tag{154}$$

$\tau^g = \underset{\sim}{\sigma} : (\underline{\mathbf{m}}^g \otimes \underline{\mathbf{z}}^g)$ is the resolved shear stress on slip system g. The evolution rules of the internal hardening variables are non-linear. The initial value of α^g must be given (zero, in this work).

The model is part of viscoplasticity theory with several mechanisms that are not independent (because of the interaction matrix h^{rs}). The framework of this theory has been established by Mandel [1965].

3.2 Thermodynamical formulation

Within the framework of continuum thermodynamics, *the local accompanying state model* assumes that the material state at point M and time t is entirely described by a set of state variables depending only on M and t (see [Germain, Nguyen, Suquet 1983]). The state variables include the observable variables $\underset{\sim}{\varepsilon}$ and T, total strain and temperature, and internal variables accounting for internal dissipative mechanisms. In this model, the derivatives of the state variables cannot enter the description of the local state of the material. Since these internal variables can generally not be directly related to the

underlying physical mechanisms, the expression of the free energy cannot be uniquely derived in the case of dissipative processes. Looking at the constitutive equations 150 to 154 it is then of the utmost importance to choose the set of independent variables on which the free energy will depend. In the first section we try to give a precise physical meaning to some of these variables. We then check that the derived thermodynamical formulation is compatible with the entropy principle. In particular the dissipation rate is evaluated in the case of strain softening crystals.

3.2.1 A link between physical microscopic quantities and thermodynamical variables; expression of the free energy

In order to find physically relevant variables, we go back to the evolution equations of dislocation populations presented in part 1. At the microscopic level, pertinent quantities are the total density ρ^s of dislocations belonging to system s, and the density ρ^s_m of mobile dislocations on system s. We adopt the balance equations proposed by Teodosiu and Raphanel [1993]. The density of mobile dislocations changes according to:

$$\dot{\rho}^s_m = r^s_p - \rho^s_m / t^s \tag{155}$$

where r^s_p is the production rate of dislocations and $t^s = \dfrac{L^s}{v^s}$ the average life time of mobile dislocations (L^s being their mean free path and v^s their mean velocity). When t^s is small with respect to the characteristic time of variation of $\mid \dot{\gamma}^s \mid$, the dislocation motion is almost stationary and the density of mobile dislocations is practically constant. As a result,

$$\mid \dot{\gamma}^s \mid = \rho^s_m b v^s = b r^s_p L^s \tag{156}$$

On the other hand, we assume that the evolution of the total dislocation density is given by:

$$\dot{\rho}^s = r^s_p - \frac{2 y_c \rho^s}{b} \mid \dot{\gamma}^s \mid \tag{157}$$

where the last term accounts for dynamic recovery and y_c denotes a characteristic length associated with the annihilation process of dislocation dipoles (the values $y_c = 1.5$ nm for edge dislocations and $y_c = 50$ nm for screw dislocations are taken by Canova, Kubin and Brechet [1993]). The elimination of r^s_p in 156 and 157 yields the evolution equation:

$$\dot{\rho}^s = \frac{1}{b}\left(\frac{1}{L_s} - 2 y_c \rho^s\right) \mid \dot{\gamma}^s \mid \tag{158}$$

Looking now at the constitutive model 150 to 154, we define the variables

$$\varrho^s = 1 - e^{-b v^s} \tag{159}$$

where the cumulative slip v^s is given by equation 151. The associated evolution rules

$$\dot{\varrho}^s = b(1 - \varrho^s) \mid \dot{\gamma}^s \mid \tag{160}$$

are very similar to equation 158. It means that these variables, which intervene in the expression of isotropic hardening can be interpreted as dislocation densities. That is why we will use ϱ^s rather than v^s in the following. Regarding kinematic hardening, the variables α^s are retained for the thermodynamical formulation.

The free energy ψ and the entropy η per unit volume are now regarded as functions of the elastic strain $\underset{\sim}{\varepsilon}^e$, temperature T and the internal variables $\{\varrho^s, \alpha^s\}_{s\in S}$. The following form of the free energy is postulated

$$\begin{aligned}\rho\psi(\underset{\sim}{\varepsilon}^e, T, \varrho^s, \alpha^s) &= \frac{1}{2}\,\underset{\sim}{\varepsilon}^e : \underset{\approx}{\mathbf{E}} : \varepsilon^e + \frac{1}{2}\sum_{s\in S} c\alpha^{s2} \\ &+ \frac{r_0}{b}\sum_{s\in S}\varrho^s + \frac{1}{2}\,\frac{q}{b}\sum_{r,s\in S} h^{sr}\varrho^s\varrho^r + f(T) \end{aligned} \tag{161}$$

under small strain conditions. The last term $f(T)$ denotes the thermal part of the free energy but the parameters appearing in the mechanical part are also temperature-dependent. 161 is a quadratic form in $\underset{\sim}{\varepsilon}^e$, ϱ^s and α^s as soon as the interaction matrix h^{sr} is assumed to be symmetric.

The Clausius-Duhem inequality reads

$$-\rho(\eta + \frac{\partial\psi}{\partial T})\,\dot{T} - (\rho\frac{\partial\psi}{\partial\underset{\sim}{\varepsilon}^e} - \underset{\sim}{\sigma}) : \dot{\underset{\sim}{\varepsilon}}^e + \underset{\sim}{\sigma} : \dot{\underset{\sim}{\varepsilon}}^p - \rho\frac{\partial\psi}{\partial\varrho^s}\dot{\varrho}^s - \rho\frac{\partial\psi}{\partial\alpha^s}\dot{\alpha}^s - \frac{1}{T}\underline{\mathbf{q}}.T\underline{\nabla} \geq 0 \tag{162}$$

Considering firstly only thermoelastic processes, the linearity of the previous expression in $\dot{T}$ and $\dot{\underset{\sim}{\varepsilon}}^e$ entails

$$\eta = -\frac{\partial\psi}{\partial T} \tag{163}$$

$$\underset{\sim}{\sigma} = \rho\frac{\partial\psi}{\partial\underset{\sim}{\varepsilon}^e} \tag{164}$$

The thermodynamical generalized forces associated with the internal variables are then

$$x^s = \rho\frac{\partial\psi}{\partial\alpha^s} = c\,\alpha^s \tag{165}$$

$$\frac{r^s}{b} = \rho\frac{\partial\psi}{\partial\varrho^s} = \frac{1}{b}\,(r_0 + q\sum_{s\in S} h^{sr}\varrho^r) \tag{166}$$

3.2.2 Intrinsic dissipation

The yield criterion and the evolution equations are recalled using the previous set of internal variables

$$\dot{\underset{\sim}{\varepsilon}}^p = \sum_{s\in S}\dot{\gamma}^s\,\{\underline{\mathbf{m}}^s \otimes \underline{\mathbf{z}}^s\} \tag{167}$$

$$\dot{\gamma}^s = <\frac{\mid \tau^s - x^s \mid - r^s}{k}>^n \ \mathrm{sign}(\tau^s - x^s) \tag{168}$$

$$\dot{\alpha}^s = \dot{\gamma}^s - d \mid \dot{\gamma}^s \mid \alpha^s \tag{169}$$

$$\dot{\varrho}^s = b(1-\varrho^s) \mid \dot{\gamma}^s \mid \tag{170}$$

The intrinsic dissipation rate D is now computed as follows

$$D = \underset{\sim}{\sigma} : \dot{\underset{\sim}{\varepsilon}}^p - \sum_{s\in S}\rho\frac{\partial\psi}{\partial\varrho^s}\dot{\varrho}^s - \sum_{s\in S}\rho\frac{\partial\psi}{\partial\alpha^s}\dot{\alpha}^s$$

$$
\begin{aligned}
&= \underset{\sim}{\sigma} : \dot{\underset{\sim}{\varepsilon}}^p - \sum_{s\in S}\left(\frac{r^s}{b}\dot{\varrho}^s - x^s\dot{\alpha}^s\right) \\
&= \sum_{s\in S}(\tau^s\dot{\gamma}^s - r^s(1-\varrho^s)\mid\dot{\gamma}^s\mid - c\alpha^s(\dot{\gamma}^s - d\mid\dot{\gamma}^s\mid\alpha^s) \\
&= \sum_{s\in S}\left(\tau^s - x^s)\dot{\gamma}^s - r^s\mid\dot{\gamma}^s\mid + r^s\varrho^s\mid\dot{\gamma}^s\mid + cd\alpha^{s2}\mid\dot{\gamma}^s\mid\right) \\
&= \sum_{s\in S}\left((\mid\tau^s - x^s\mid - r^s)\mid\dot{\gamma}^s\mid + r^s\varrho^s\mid\dot{\gamma}^s\mid + cd\alpha^{s2}\mid\dot{\gamma}^s\mid\right) \qquad (171)
\end{aligned}
$$

In the first term one may recognize the expression of the yield criterion for each slip system s so that it is always positive or vanishes. The definition of the critical shear stresses r^s requires that it is positive or zero. The parameters r_0, q and b must therefore be such that $r^s \geq 0$ at every step and for every loading path. A sufficient condition for the intrinsic dissipation rate to be positive is then

$$cd \geq 0 \qquad (172)$$

In this work we will take $c \geq 0$ and $d \geq 0$.

Accordingly, softening behaviour can be described by

$$q \leq 0 \quad \text{and} \quad r_0 + q \geq 0 \qquad (173)$$

and is compatible with the entropy principle. Such a material behaviour will be considered in the sequel of part A in order to trigger strain localization phenomena.

It must be noted that the present formulation does not correspond to a standard model in the sense of [Halphen, Nguyen 1975]. A pseudo-potential of dissipation could not be worked out, mainly because of the presence of the interaction matrix h^{rs} (see [Forest, Cailletaud 1994]). A classical result of convexity analysis is that the existence of a pseudo-potential of dissipation ensures the positiveness of the intrinsic dissipation. Nevertheless, in the proposed formulation, the positiveness of the intrinsic dissipation could be proved straightforwardly, after an appropriate choice of the internal variables and a simple plausible expression of the free energy.

4 Bifurcation analysis for single crystals at small strains; simulation of the predicted modes

4.1 Bifurcation analysis for single crystals undergoing single or multiple slip

4.1.1 Linear incremental formulation

In single crystals, the plastic strain rate is the sum of the contributions of each slip system. We take the twelve slip systems of f.c.c. single crystals into account:

$$\underset{\sim}{\dot{\varepsilon}}^p = \sum_{g=1}^{12} \dot{\gamma}^g \ \{\underline{\mathbf{m}}^g \otimes \underline{\mathbf{z}}^g\} \tag{174}$$

Schmid's law written for each slip system gives a yield surface with vertexes:

$$\tau^g - \tau_c^g \leq 0 \tag{175}$$

where τ^g is the resolved shear stress on the slip system g. Mandel's hardening rule involves an interaction matrix to describe latent hardening:

$$\dot{\tau}_c^s = \sum_{g=1}^{12} h^{sg} \ |\dot{\gamma}^g| \tag{176}$$

In the particular case of single crystals in tension undergoing symmetric multiple slip on n systems, the previous expressions simplify, providing that we take a very simple form for the interaction matrix:

$$\underset{\sim}{\dot{\varepsilon}}^p = \dot{\gamma} \ \underset{\sim}{\mathbf{P}} \quad \text{with} \quad \dot{\gamma} > 0 \quad \text{and} \quad \underset{\sim}{\mathbf{P}} = \sum_{g=1}^{n} \{\underline{\mathbf{m}}^g \otimes \underline{\mathbf{z}}^g\} \tag{177}$$

$$\dot{\tau} = \dot{\tau}_c = kh\dot{\gamma} \tag{178}$$

where

$$\begin{aligned} k = n \ \text{ if } \ h^{ij} &= h \qquad (\text{Taylor, isotropic hardening}) \\ k = 1 \ \text{ if } \ h^{ij} &= h\,\delta_{ij} \quad (\text{self} - \text{hardening}) \end{aligned}$$

It is then possible to give a linear incremental formulation of the elastoplastic constitutive equations:

$$\underset{\sim}{\dot{\sigma}} = \left(\underset{\sim}{\mathbf{E}} - \frac{(\underset{\sim}{\mathbf{E}} : \underset{\sim}{\mathbf{P}}) \otimes (\underset{\sim}{\mathbf{P}} : \underset{\sim}{\mathbf{E}})}{kh + \underset{\sim}{\mathbf{P}} : \underset{\sim}{\mathbf{E}} : \underset{\sim}{\mathbf{P}}} \right) : \underset{\sim}{\dot{\varepsilon}} \tag{179}$$

under plastic loading. Equation 179 is then a particular case of equation 44 with

$$\underset{\sim}{\mathbf{P}} = \underset{\sim}{\mathbf{n}} = \sum_{g=1}^{N} \{\underline{\mathbf{m}}^g \otimes \underline{\mathbf{z}}^g\} \tag{180}$$

4.1.2 Application of the bifurcation analysis to f.c.c. single srystals undergoing single or multiple slip

The linear incremental formulation of the constitutive equations given in 4.1.1 allows us to apply the bifurcation analysis presented in section 2.4.2 to the following situations:

Single slip

If the tensile direction is [123] for instance, the slip system $B4$ is active (see figure 21) so that, in the crystallographic axes:

$$P = \frac{1}{\sqrt{6}} \begin{bmatrix} -1 & -1/2 & 0 \\ -1/2 & 0 & 1/2 \\ 0 & 1/2 & 1 \end{bmatrix} \tag{181}$$

The eigenvectors are

$$a_1 = \frac{1}{\sqrt{6}} \begin{bmatrix} 1 \\ -2 \\ 1 \end{bmatrix} \tag{182}$$

$$a_2 = \frac{1}{2\sqrt{3}\sqrt{5-2\sqrt{6}}} \begin{bmatrix} -5+2\sqrt{6} \\ \sqrt{6}-2 \\ 1 \end{bmatrix} \tag{183}$$

$$a_3 = \frac{1}{2\sqrt{3}\sqrt{5+2\sqrt{6}}} \begin{bmatrix} -5-2\sqrt{6} \\ -\sqrt{6}-2 \\ 1 \end{bmatrix} \tag{184}$$

The eigenvalues are respectively $0, 1/2, -1/2$. In the reference system $(\underline{\mathbf{a}}_1, \underline{\mathbf{a}}_2, \underline{\mathbf{a}}_3)$, the components of $\underline{\mathbf{g}}$ and $\underline{\mathbf{n}}$ characterizing the bifurcation modes are, according to 103:

$$\begin{cases} n_1 = 0 \\ n_2 = \frac{1}{\sqrt{2}} \\ n_3 = \pm\frac{1}{\sqrt{2}} \end{cases}$$

$$\begin{cases} g_1 = 0 \\ g_2 = n_2 \\ g_3 = -n_3 \end{cases}$$

In the crystallographic reference system, this gives

$$n = \frac{1}{\sqrt{3}} \begin{bmatrix} 1 \\ 1 \\ 1 \end{bmatrix} \quad \text{or} \quad \frac{1}{\sqrt{2}} \begin{bmatrix} -1 \\ 0 \\ 1 \end{bmatrix} \tag{185}$$

Thus deformation can localize on the slip plane and on the plane normal to the slip direction which is referred to as *kink plane* in literature (see section 1.3.2). We have also recalled in 1.3.1 the existence of kink bands of Piobert-Lüders. The bifurcation modes are possible as soon as

$$h = h^{cr} = 0 \tag{186}$$

An analysis at finite strain does not essentially affect these results [Asaro, Rice 1977].

Double slip

If the tensile direction is [012], the slip systems $B4$ and $A3$ are simultaneously activated so that:

$$P = \frac{1}{\sqrt{6}} \begin{bmatrix} -2 & 0 & 0 \\ 0 & 0 & 1 \\ 0 & 1 & 2 \end{bmatrix} \tag{187}$$

The eigenvectors are

$$a_1 = \begin{bmatrix} 1 \\ 0 \\ 0 \end{bmatrix}$$

$$a_2 = \frac{1}{\sqrt{2}\sqrt{2-\sqrt{2}}} \begin{bmatrix} 0 \\ 1 \\ 1-\sqrt{2} \end{bmatrix}$$

$$a_2 = \frac{1}{\sqrt{2}\sqrt{2+\sqrt{2}}} \begin{bmatrix} 0 \\ 1 \\ 1+\sqrt{2} \end{bmatrix}. \tag{188}$$

The eigenvalues are respectively $-\sqrt{2/3}, \sqrt{1/6}-\sqrt{1/3}, \sqrt{1/6}+\sqrt{1/3}$. In the reference system $(\underline{\mathbf{a}}_1, \underline{\mathbf{a}}_2, \underline{\mathbf{a}}_3)$, the components of $\underline{\mathbf{n}}$ characterizing the bifurcation modes are:

$$\begin{cases} n_1^2 = \dfrac{1+\sqrt{2}+\nu(1-\sqrt{2})}{3+\sqrt{2}} \\ n_2^2 = 0 \\ n_3^2 = 1-n_1^2 \end{cases} \tag{189}$$

$$h^{cr} = -\frac{1}{k} E(\sqrt{1/6}-\sqrt{1/3})^2 \tag{190}$$

A very low value of the hardening modulus must be reached for compatible bifurcation modes to become possible. Furthermore the bifurcation planes are non-crystallographic and depend on Poisson's modulus.

The situation of symmetric double slip has been extensively studied for large strains by Asaro [1979] and Peirce, Asaro and Needleman [1982], though in the case of a planar model of single crystals that corresponds exactly to no physical situation. These authors found also non-crystallographic bifurcation planes. Peirce [1983] considered the actual 3D geometry of a single crystal undergoing symmetric double slip. He found bifurcation modes for which one system is under plastic loading whereas the other is under neutral loading. Instead in the previous analysis, we investigate modes for which the two systems are equally active. The solution proposed by Peirce gives bifurcation planes close to the slip or kink planes and, since large straining is taken into account, the critical hardening modulus is close to zero but positive.

Four slip systems

If the tensile direction is [011], the slip systems $B4$, $A3$, $B5$ and $A6$ are simultaneously activated so that:

$$P = \frac{4}{\sqrt{6}} \begin{bmatrix} -1 & 0 & 0 \\ 0 & 1/2 & 1/2 \\ 0 & 1/2 & 1/2 \end{bmatrix} \tag{191}$$

The eigenvectors are

$$a_1 = \begin{bmatrix} 1 \\ 0 \\ 0 \end{bmatrix} \tag{192}$$

$$a_2 = \frac{1}{\sqrt{2}} \begin{bmatrix} 0 \\ 1 \\ -1 \end{bmatrix} \tag{193}$$

$$a_3 = \frac{1}{\sqrt{2}} \begin{bmatrix} 0 \\ 1 \\ 1 \end{bmatrix}. \tag{194}$$

The eigenvalues are respectively $-\frac{4}{\sqrt{6}}, 0, \frac{4}{\sqrt{6}}$. In the reference system $(\underline{\mathbf{a}}_1, \underline{\mathbf{a}}_2, \underline{\mathbf{a}}_3)$, the components of $\underline{\mathbf{n}}$ characterizing the bifurcation modes are:

$$\begin{cases} n_1^2 = 1/2 \\ n_2^2 = 0 \\ n_3^2 = 1/2 \end{cases} \tag{195}$$

In the crystallographic reference system, this gives

$$n = \begin{bmatrix} 1/\sqrt{2} \\ 1/2 \\ 1/2 \end{bmatrix} \quad \text{or} \quad n = \begin{bmatrix} -1/\sqrt{2} \\ 1/2 \\ 1/2 \end{bmatrix} \tag{196}$$

and

$$h^{cr} = 0 \tag{197}$$

Once more the bifurcation planes are non-crystallographic but independent on ν. The critical hardening modulus is zero. This slip configuration is therefore prone to localization.

Six slip systems

If the tensile direction is [111], the slip systems $A3$, $A6$, $C1$, $C3$, $D1$, and $D6$ are theoretically simultaneously activated so that:

$$P = \frac{2}{\sqrt{6}} \begin{bmatrix} 0 & 1 & 1 \\ 1 & 0 & 1 \\ 1 & 1 & 0 \end{bmatrix} \tag{198}$$

The eigenvectors are

$$a_1 = \frac{1}{\sqrt{3}} \begin{bmatrix} 1 \\ 1 \\ 1 \end{bmatrix} \tag{199}$$

$$a_2 = \frac{1}{\sqrt{2}} \begin{bmatrix} 0 \\ 1 \\ -1 \end{bmatrix} \tag{200}$$

$$a_3 = \frac{1}{\sqrt{6}} \begin{bmatrix} -2 \\ 1 \\ 1 \end{bmatrix}. \tag{201}$$

The eigenvalues are respectively $\frac{4}{\sqrt{6}}, \frac{-2}{\sqrt{6}}, \frac{-2}{\sqrt{6}}$. In the reference system $(\underline{\mathbf{a}}_1, \underline{\mathbf{a}}_2, \underline{\mathbf{a}}_3)$, the components of $\underline{\mathbf{n}}$ characterizing the bifurcation modes are:

$$\begin{cases} n_1^2 = \dfrac{2-\nu}{3} \\ n_2^2 = \dfrac{1+\nu}{3} \\ n_3^2 = 0 \end{cases} \tag{202}$$

$$h^{cr} = -\frac{2}{3k}E \tag{203}$$

The critical hardening modulus is very low and the bifurcation planes are non-crystallographic.

Eight slip systems

If the tensile direction is [001], the slip systems $A2$, $A3$, $B2$, $B4$, $C1$, $C3$, $D1$, and $D4$ are theoretically simultaneously activated so that:

$$P = \frac{8}{\sqrt{6}} \begin{bmatrix} -1/2 & 0 & 0 \\ 0 & -1/2 & 0 \\ 0 & 0 & 1 \end{bmatrix} \tag{204}$$

The components of $\underline{\mathbf{n}}$ characterizing the bifurcation modes are:

$$\begin{cases} n_1^2 = \dfrac{1+\nu}{3} \\ n_2^2 = 0 \\ n_3^2 = \dfrac{2-\nu}{3} \end{cases} \tag{205}$$

$$h^{cr} = -\frac{8}{3k}E \tag{206}$$

It is clear that if $h^{cr} \ll 0$, diffuse bifurcation modes or modes for which slip does not remain identical on all active systems, are likely to develop earlier.

4.2 Simulation of slip bands, kink bands and shear bands

We consider again the problem of tension of flawed plates tackled in section 2.8. The material is now a single crystal and we focus on three-dimensional situations. The material parameters have been chosen so that the competition between the two non-linear hardening variables leads to an initial hardening followed by a softening behaviour. The interaction matrix is taken diagonal. For all orientations of the single crystals, an initial rather homogeneous deformation pattern gives way after the peak of the load-displacement curve to localization in narrow bands. The calculations have been performed with very low viscosity so that localization of deformation is accompanied with a sharp load drop (figure 22). The orientations of the bands found for several single and multislip configurations are confronted to the predicted ones in Table 1.

Single Slip

The material parameters used for this simulation are the following:

E = 200000 MPa
ν = 0.3
r_0 = 50 MPa
q = -45 MPa
b = 210
c = 20000 MPa
d = 900
k = 5 MPa $s^{1/n}$
n = 2

The length direction of the plate coincides with the [123] crystallographic direction and the perpendicular direction in the plane of the plate with $[6\,\overline{3}\,4]$. On figure 23a two bands of intense deformation have formed intersecting at the location of the initial geometrical flaw. One lies on the slip plane (below) the other one on the kink plane (above), as predicted by the bifurcation analysis for single slip. Given that in the model at small strain the slip direction and the normal to the slip plane play exactly the same role, these bands can be regarded as slip bands. The postbifurcation behaviour shows that deformation strongly localizes on the kink plane (figure 23b). On the deformed state shown on figure 23c, displacements have been significantly magnified. Since the single crystal is misoriented the strain field is really three-dimensional, which can be seen on figure 25a. It is also interesting to notice that the material undergoes plastic loading within the band (figure 24a) whereas it unloads elastically outside the band (figure 24b).

Double Slip

The materials parameters for the simulation are:

E = 200000 MPa
ν = 0.3
r_0 = 50 MPa
q = -45 MPa
b = 210
c = 40000 MPa
d = 1800
k = 5 MPa $s^{1/n}$
n = 2

In this case, the planes of localized deformation are not crystallographic as expected. The orientations given by formula 189 change only by 2 or 3° when ν varies between 0 and 0.5, so that this dependence on ν could not be precisely detected using finite element calculations. The bifurcation analysis for symmetric double slip states that the localized bifurcation modes are compatible only for a very low negative value of the hardening modulus (see formula 190). In contrast the bands of figure 26 and 27 appeared shortly after the peak of the load-displacement curve. They are therefore not strictly compatible modes but can develop in a slightly more diffuse manner.

Four Slip Systems

The materials parameters for the simulation are:

E = 200000 MPa

$\nu = 0.3$
$\tau_0 = 50$ MPa
q = -45 MPa
b = 1500
c = 200000 MPa
d = 9000
k = 5 MPa $s^{1/n}$
n = 2

In the configuration of figure 28, the plane $(0\,\bar{1}\,1)$ satisfies the plane strain condition. That is why bands of localized deformation are expected to develop at 45°. But when the plane of the plate does not coincide with this plane strain plane like for figure 29, the situation is more complex. An unexpected band pertains at 45° whereas two weaker bands with orientations close to predicted ones tend to appear. It is not clear whether this is an artefact of the mesh but calculations should be performed again for two or more element thick plate, which would cost much more computation time.

Eight Slip Systems

The materials parameters for the simulation are:

E = 200000 MPa
$\nu = 0.3$
$\tau_0 = 41.6$ MPa
q = -41 MPa
b = 1959
c = 108000 MPa
d = 6532
k = 5 MPa $s^{1/n}$
n = 2

This multislip configuration gives the same macroscopic deformation field as for isotropic polycrystals in tension. The expected compatible bifurcation modes correspond to localization bands oriented at θ from the tensile direction [001]:

$$\tan^2 \theta = \frac{2-\nu}{1+\nu} \tag{207}$$

after formula 205. θ ranges from 54.7° to 45° when ν varies between 0 and 0.5. For $\nu = 0.3$, $\theta \simeq 49°$. This deformation mode is compatible only for a very low negative hardening modulus.

Instead, figure 30 shows that two bands formed at about 53° from the tensile axis and this happened slightly after the peak of the load-displacement curve. In fact this deformation mode is close to the shear bands at 54.7° that are classical in plasticity of isotropic polycrystals. This is a diffuse bifurcation mode that can appear as soon as the hardening modulus vanishes as discussed in section 2.2.2.

As a conclusion, it has been shown for various single and multiple slip configurations of softening viscoplastic single crystals that the initial geometrical imperfection triggers the localization of deformation in narrow bands the orientations of which have been correctly predicted by the bifurcation analysis in elastoplasticity (these results are summarized in

[Forest, Cailletaud 1995]). The observed localization modes do not always correspond to compatible discontinuous bifurcation modes since some of them appear much earlier than expected. In these cases they are rather diffuse modes that are possible as soon as the hardening modulus vanishes. They may have the same orientation as the first compatible modes (like for two slip systems) or not (like for eight slip systems).

Mesh dependence The elements used in the 3D finite element calculations are 20-node bricks with 27 Gauss points. The previous calculations prove that they permit capturing bands of intense deformation with various orientations different from 45°. The previous calculations were performed for very low viscosity so as to obtain sharp effects. In spite of the *pseudo-regularization* role of viscoplasticity, the width of the bands and the instant of their apparition are clearly mesh-dependent but their orientation is not. This confirms some results obtained by Zbib and Jubran [1992] also in the three-dimensional case.

4.3 Material imperfections

The stability analysis performed at the level of the material volume element by Estrin and Kubin [1986] and presented in 1.2. has shown that there are two domains of instability in plasticity of single crystals, associated with negative values of the hardening modulus. The first domain characterizes the very beginning of plastic flow, so that plastic deformation will necessarily start in a more or less non-uniform manner. This domain is rapidly followed by stable plastic deformation and after large straining by a second instability domain that corresponds to the formation of non-uniform deformation patterns leading to the fracture of the specimen. The formation of *shear bands* as a precursor of rupture has been extensively studied experimentally by Chang and Asaro [1981] and more recently by Dubois [1988], Yang [1990], Gaspérini and Rey [1993]. Shear band initiation is associated with the attainment of a critical small positive value of the hardening modulus. According to [Chang, Asaro 1981], local intense deformation leads to geometrical softening within the shear band, so that shear bands are globally misaligned by several degrees with the active slip planes outside the bands. Although the details of these localization processes are affected by the microstructure (single phase, coherent zone or precipitation hardened single crystals ...), the generality of the phenomenon suggests that the underlying causes may result from more general mechanical characteristics of crytstalline deformation. This explains why, since Asaro [1979] until Yang and Rey [1993], the occurrence of shear bands has been described by a bifurcation analysis of the set of constitutive equations for single crystals at large strains. The bifurcation analysis in the case of Asaro's planar model for double slip yields small but positive values of the critical hardening modulus.

However the formation of shear bands is often preceded by the presence of *coarse slip bands* which may then serve as imperfections in which macroscopic localized shear sets in. Contrary to shear bands, coarse slip bands are strictly parallel to slip planes. To model the formation of coarse slip bands, Dao and Asaro [1994] are forced to introduce non-Schmid effects in the constitutive equations of their planar model. With this model coarse slip bands are interpreted as bifurcation modes in the case of single slip, for which the authors find a slight misorientation. The case of double slip yields greater misorientations of the bands with respect to the outside crystal and is supposed to account for shear bands. Only scarce experimental data favour the hypothesis of the existence of non-Schmid effects in

Al or Cu single crystals but Dao and Asaro claim that the magnitude of the non-Schmid effects introduced in their model is so small that it could not be experimentally observed.

In contrast, experimental evidence collected in 1.3. shows that macroscopic slip bands similar to Asaro's coarse slip bands can be observed in single crystals as early as the beginning of plastic flow. That is why we propose here that the formation of macroscopic slip bands or thick slip band bundles (until 0.1 mm) can be attributed to the initial domain of plastic instability defined by Estrin and Kubin [1986]. It means that we allow initial local softening of the single crystal, that results in local plastic instability and non-homogeneous deformation. In the following and in section 5, we will see that localized deformation caused by such local instabilities can propagate through the entire cross-section of the specimen. These macroscopic slip bands may then play an important role in fatigue. Introducing local softening at the beginning of plastic flow allows us to make use of the bifurcation analysis at small strain presented in section 4.1.2 and we will lay the stress on the case of single slip that leads to bifurcation on planes parallel to slip or kink planes. Since the slip direction and the normal to the slip plane play exactly the same role in the model of single crystals at small strain, we will not further distinguish kink bands from slip bands and refer to them indifferently as slip bands.

To trigger the formation of localization bands in finite element calculations, it has been made use in the literature of initial geometrical imperfections, as we did in 2.7. Su and Lu [1991] as for them introduced thin layers of multiple slip to model shear banding in single crystals oriented for single slip. In contrast we introduce in the following calculations material imperfections considered as non-uniformities of the material parameters involved in the constitutive equations. More specifically we introduce locally slightly different values of the elasticity limit. For the calculations presented on figure 32, one element in the bulk of the single crystal plate oriented for single slip ($x_2 \parallel [2\,3\,8], x_1 \parallel [\overline{1}9\,10\,1]$) deforms plastically slightly earlier than the surrounding crystal. We chose the following material parameters of the viscoplastic model for single crystals in the unflawed part of the mesh:

E = 200000 MPa
$\nu = 0.3$
r_0 = 50 MPa
q = -45 MPa
b = 210
c = 20000 MPa
d = 900
k = 5 MPa $s^{1/n}$
n = 2

and the following ones for the weaker element

E = 200000 MPa
$\nu = 0.3$
r_0 = 49 MPa
q = -48.9 MPa
b = 220
c = 20000 MPa
d = 900
k = 5 MPa $s^{1/n}$

n = 2

(see figure 31 for the corresponding behaviour in tension). Figure 32 shows that two orthogonal slip bands form starting from the material imperfection. Deformation localized actually between figure 32b and c when the load-displacement curve displays a load drop after the peak. Structural effects result then in the predominance of only one of them (figure 32c). Single crystal superalloys in tension at low temperature exhibit rather flat load-displacement curves (see section D.1). We have tested numerically this situation by introducing a local slightly softening behaviour within an overall perfectly plastic behaviour (figure 33). Once more slip bands are obtained as shown in figure 34. Figure 41 shows the initiation of the two slip bands and the progressive predominance of one of them.

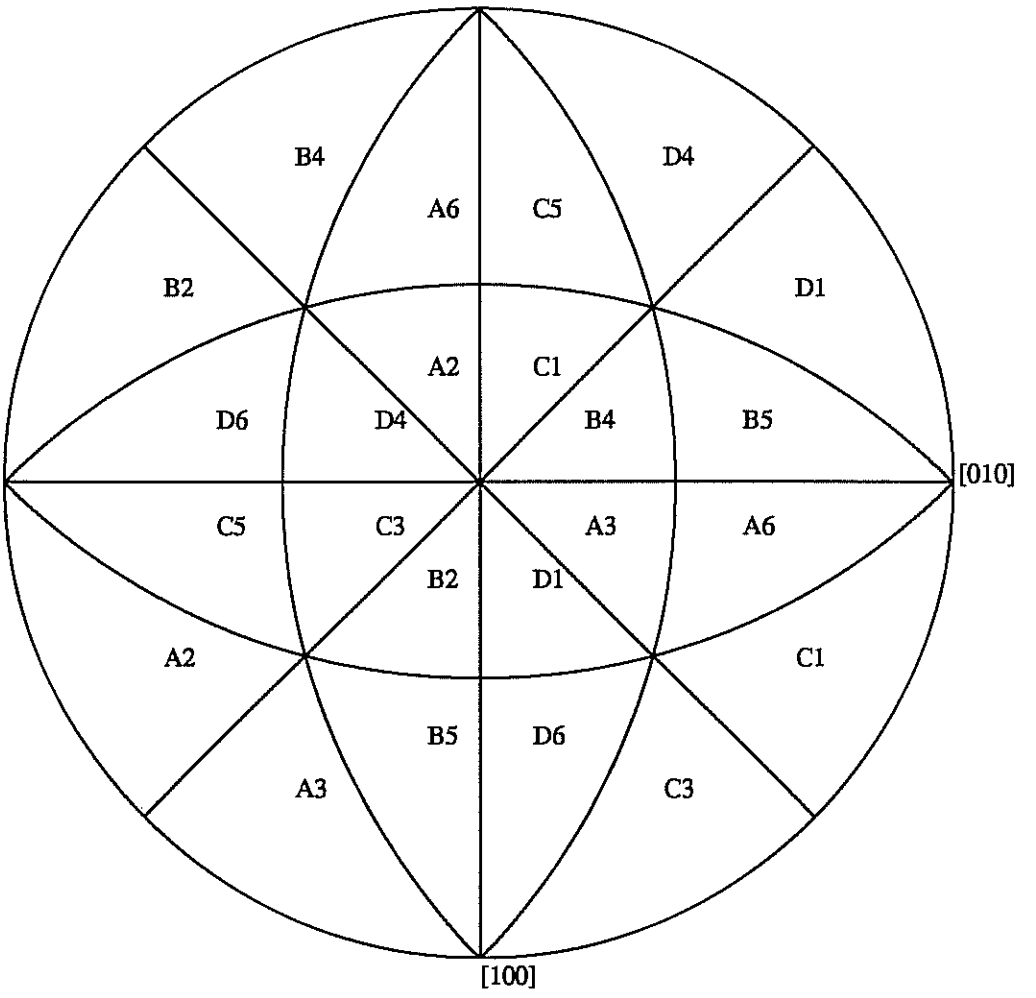

Figure A.21: First active slip systems in f.c.c. single crystals in tension, according to Schmid's law.

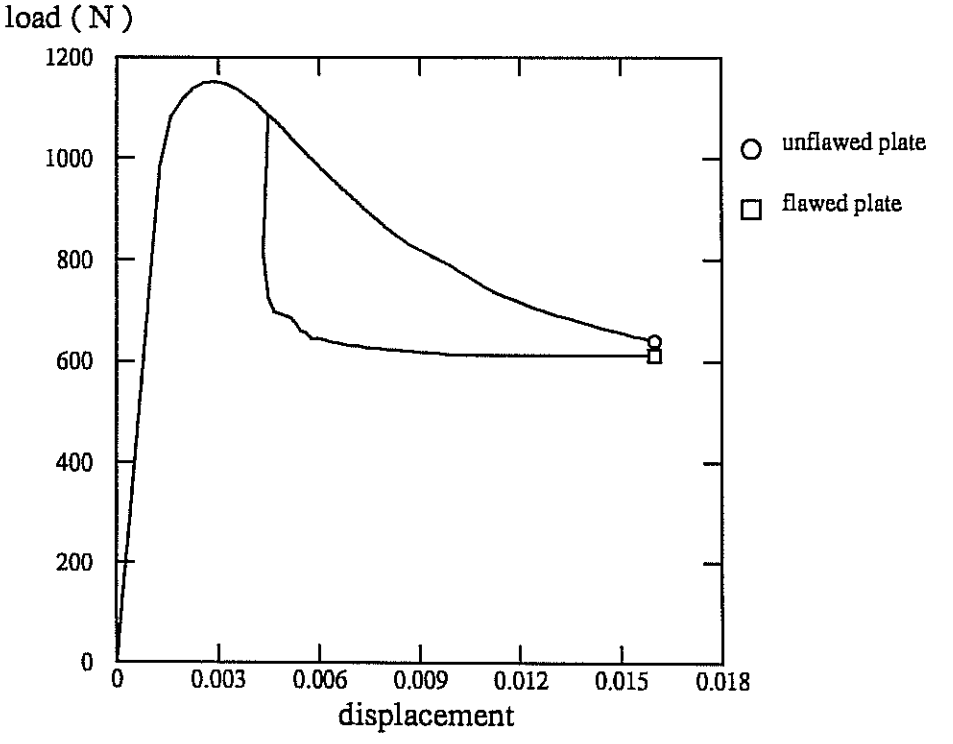

Figure A.22: Load-displacement curve of a flawed single crystal plate oriented for single slip in tension, compared with the reference one.

number of active slip systems; test name	crystal orientation $\underline{x}_3, \underline{x}_1$	slip planes orientation	predicted bifurcation orientation	observed bifurcation orientation	figures
1	[1 2 3]	A $\alpha = 50°$	$\alpha = 50°$	$\alpha = 50°$	23,25
plaque1	[6 3 $\bar{4}$]		$\beta = 77°$	$\beta = 76°$	24
2	[0 1 2]	B $\alpha = 50°$	$\alpha = 47°$	$\alpha = 49°$	25
plaque2	[5 2 $\bar{1}$]	A $\beta = 61°$	$\beta = 45°$	$\beta = 47°$	26
2	[0 1 2]	B $\alpha = 76°$	$\alpha = 53°$	$\alpha = 54°$	27
plaque2t	[2 $\bar{2}$ 1]	A $\beta = 53°$	$\beta = 57°$	$\beta = 58°$	
4	[0 1 1]	B $\alpha = 55°$	$\alpha = 45°$	$\alpha = 45°$	28
plaque4	[1 0 0]	A $\beta = 55°$	$\beta = 45°$	$\beta = 45°$	
4	[0 1 1]	B $\alpha = 68°$	$\alpha = 60°$	$\alpha = 45°$ and $60°$	29
plaque4b	[1 1 $\bar{1}$]	A $\beta = 68°$	$\beta = 60°$	$\beta = 60°$	
8	[0 0 1]	B,D $\alpha = 45°$	$\alpha = 55°$	$\alpha = 53°$	30
plaque8	[1 0 0]	A,C $\beta = 45°$	$\beta = 55°$	$\beta = 53°$	

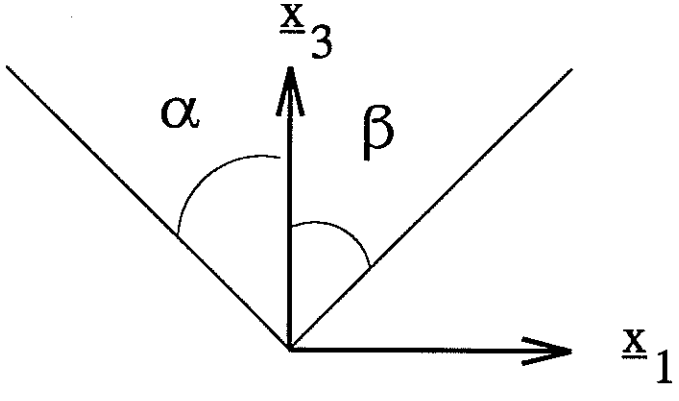

Table A.1: Comparison between slip plane traces in the plane of the plate, predicted bifurcation band traces in elastoplasticity and bifurcation band traces obtained by the FE analysis using the viscoplastic model for single crystals, for various multislip configurations.

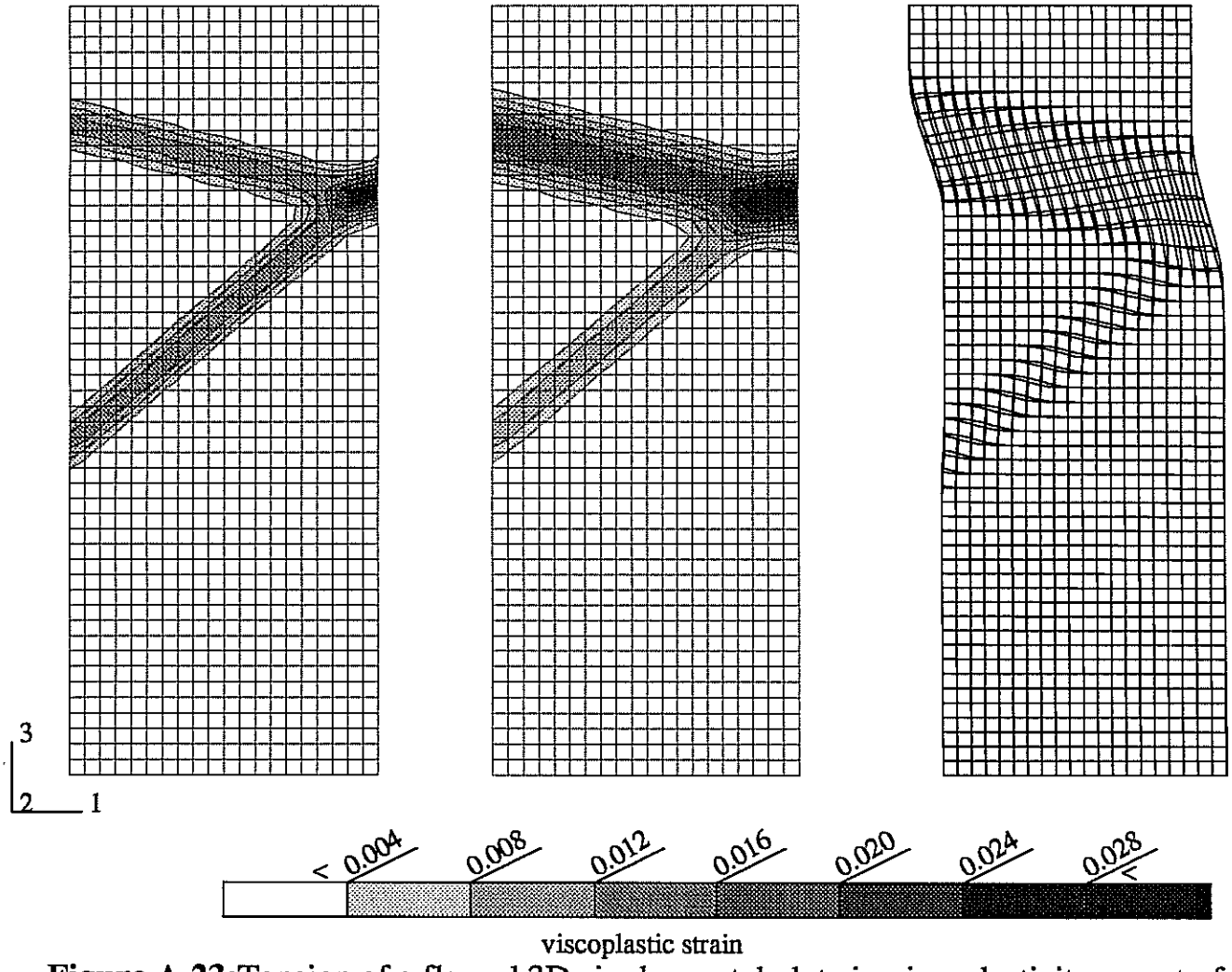

Figure A.23: Tension of a flawed 3D single crystal plate in viscoplasticity: onset of two slip bands, post-bifurcation behaviour, and final deformed state (magnification 15).

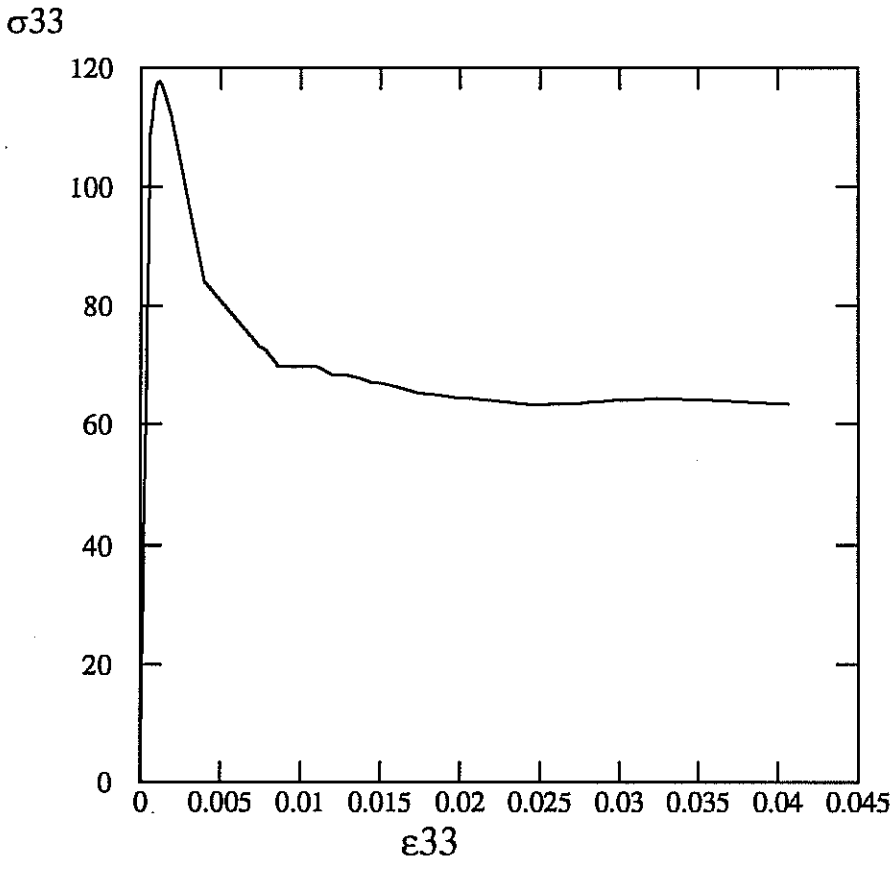

Figure A.24a: Continued plastic loading inside an intense slip band.

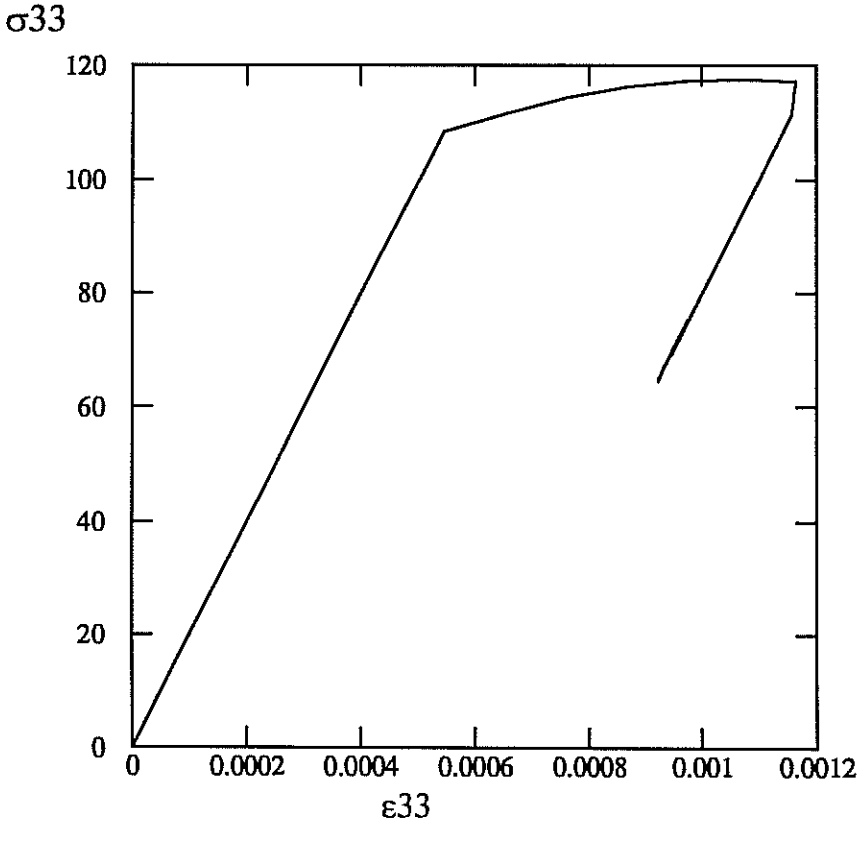

Figure A.24b: Elastic unloading outside an intense slip band.

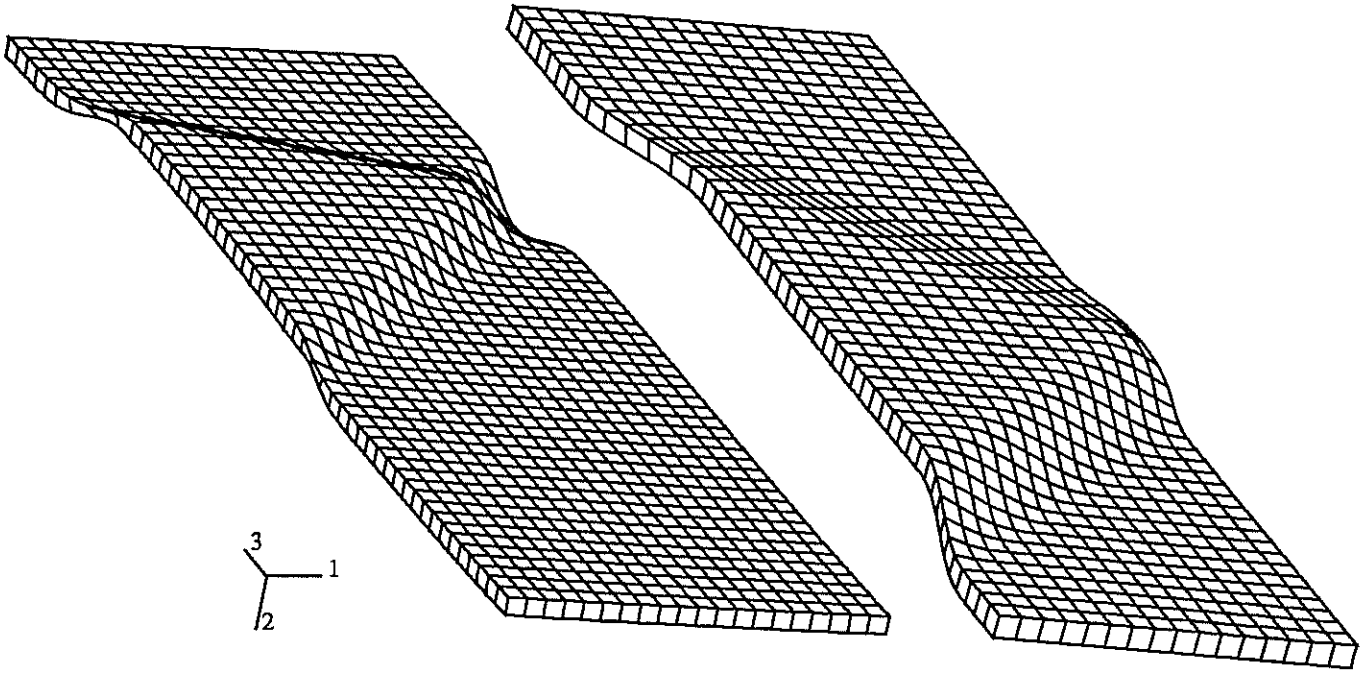

Figure A.25: Deformed state of two single crystal plates in tension oriented for single slip (left) and symmetric double slip (right) (magnification 25, tests 'plaque1' and 'plaque2' in table 1).

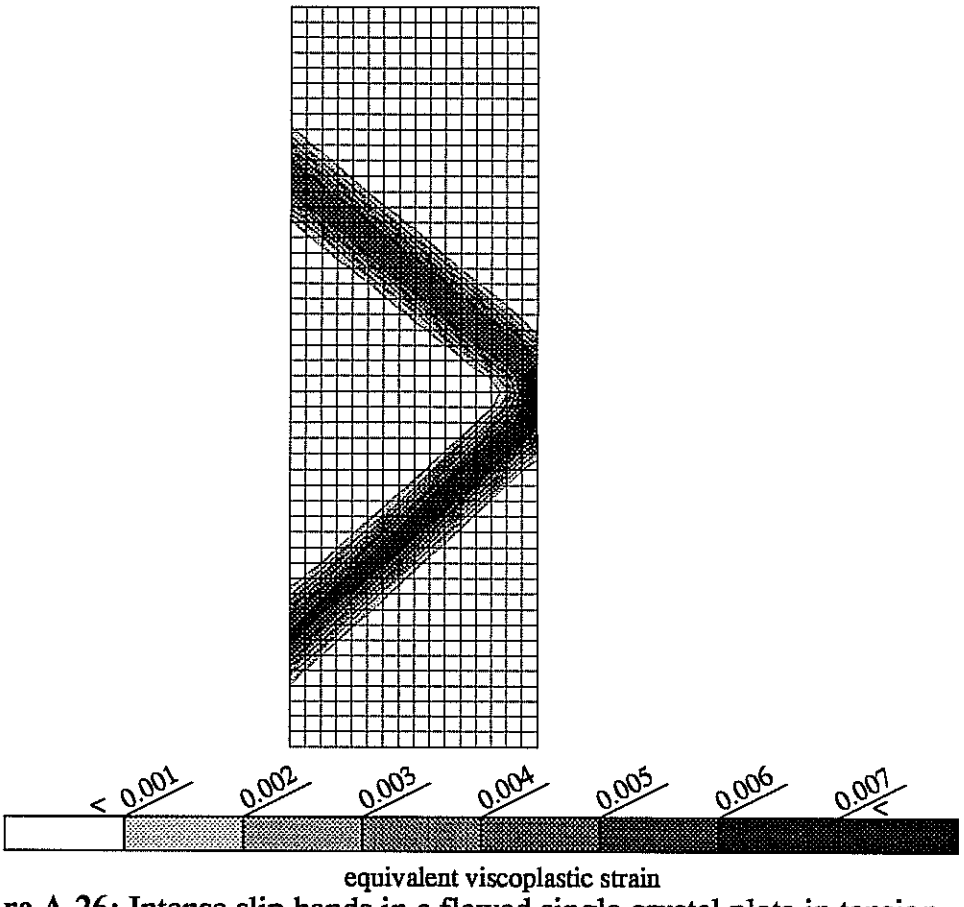

Figure A.26: Intense slip bands in a flawed single crystal plate in tension oriented for symmetric double slip (test 'plaque2' in table 1).

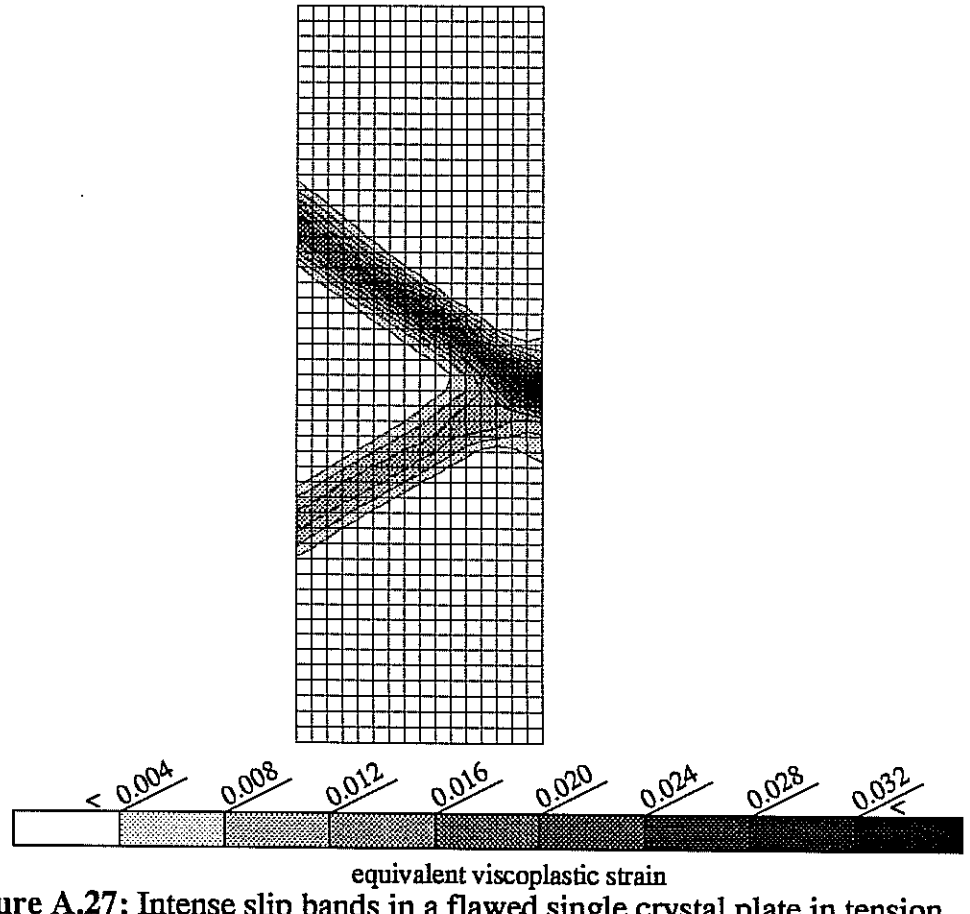

Figure A.27: Intense slip bands in a flawed single crystal plate in tension oriented for symmetric double slip (test 'plaque2t' in table 1).

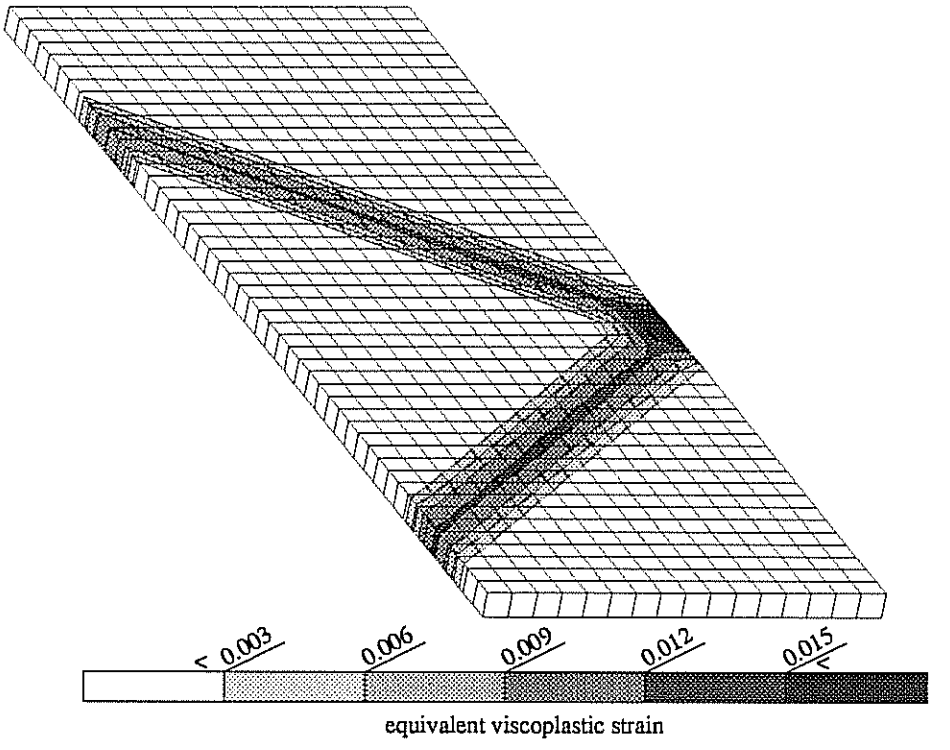

Figure A.28: Intense slip bands in a flawed single crystal plate in tension oriented for symmetric multiple slip (test 'plaque4' in table 1).

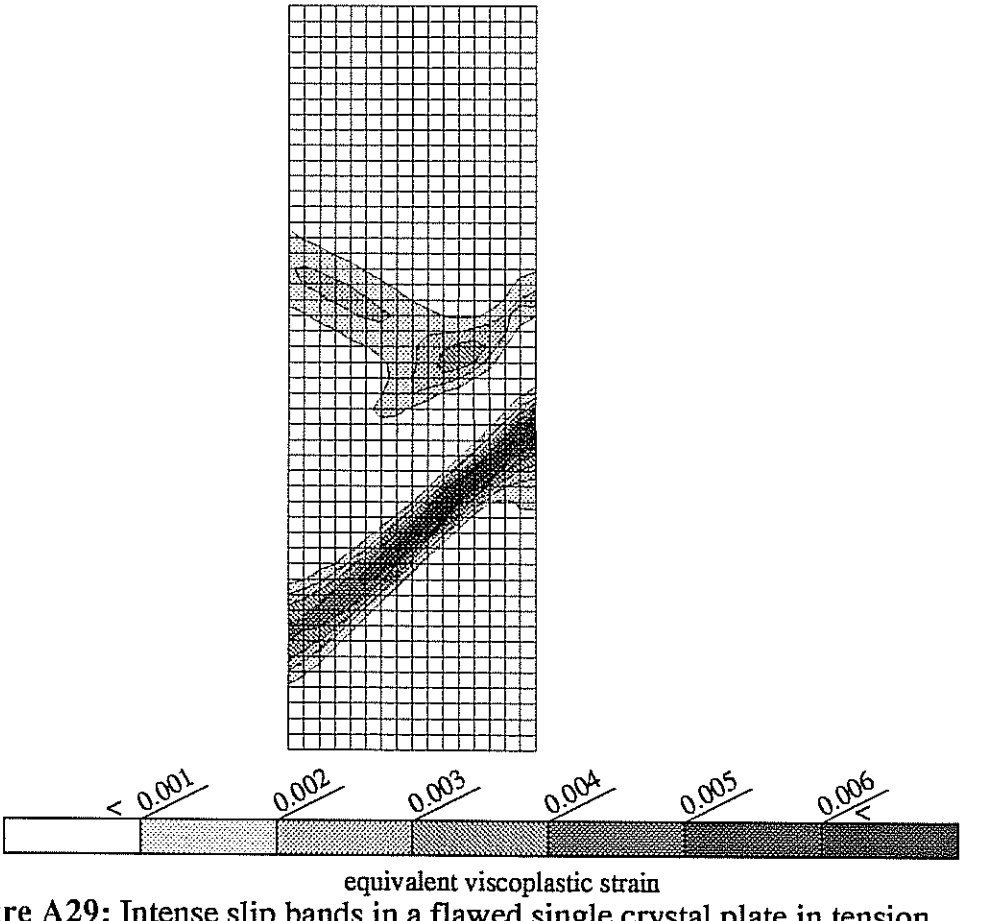

Figure A29: Intense slip bands in a flawed single crystal plate in tension with four active symmetric slip systems (test 'plaque4b' in table 1).

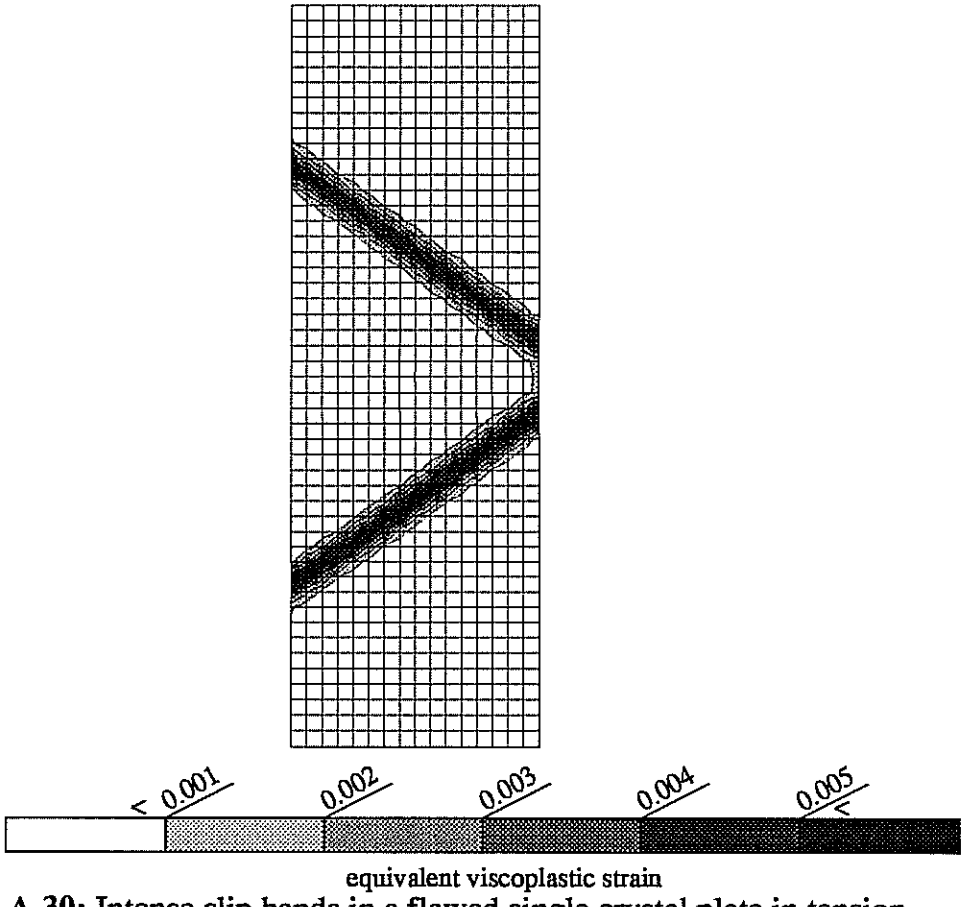

Figure A.30: Intense slip bands in a flawed single crystal plate in tension with eight active symmetric slip systems (test 'plaque8' in table 1).

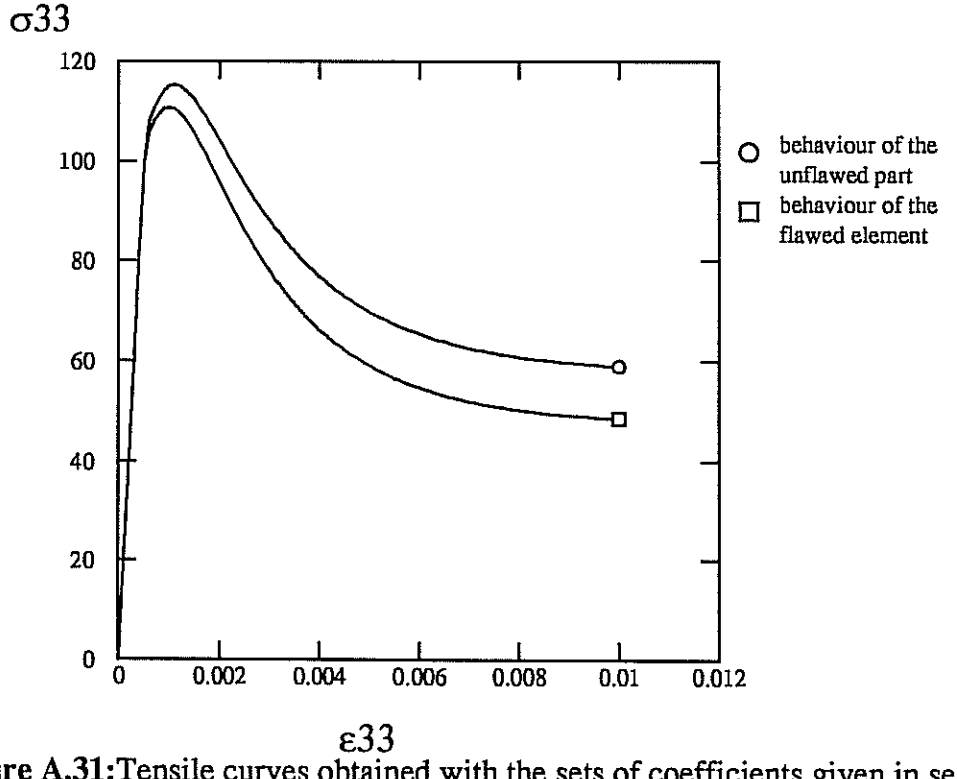

Figure A.31: Tensile curves obtained with the sets of coefficients given in section A.3.1, and used in the simulation of a single crystal plate with a material imperfection.

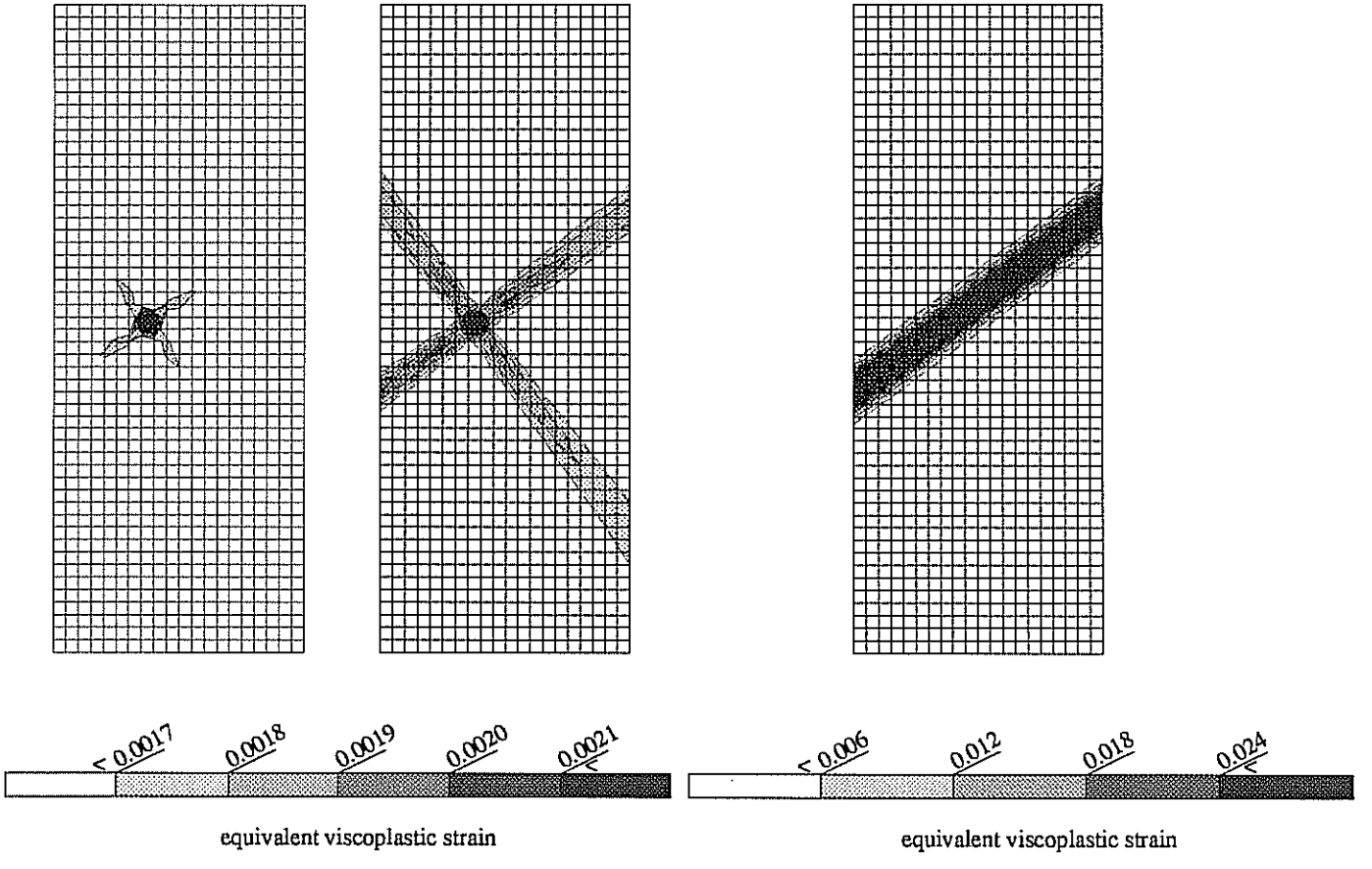

Figure A.32: Tension of a single crystal plate with a material flaw;
(a) and (b) two bands form starting from the element with a lower elasticity limit,
(c) only one of them remains at the end.

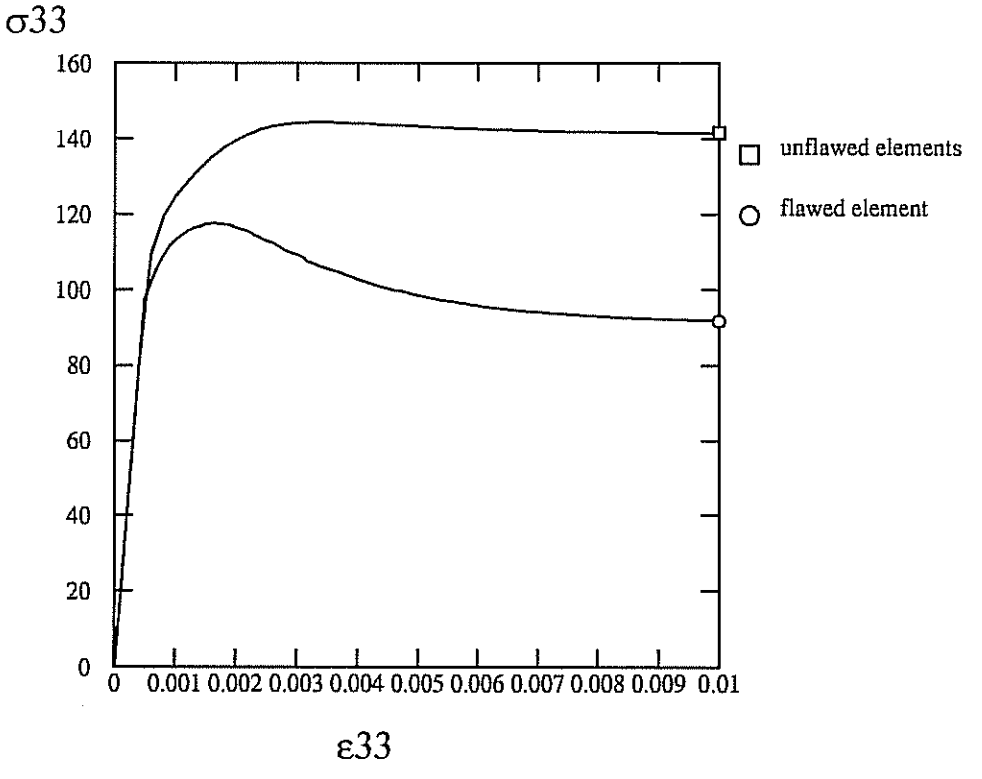

Figure A.33: Tensile curves obtained with parameters used for the study of a plate with a material imperfection; the unflawed part has only a slightly softening behaviour.

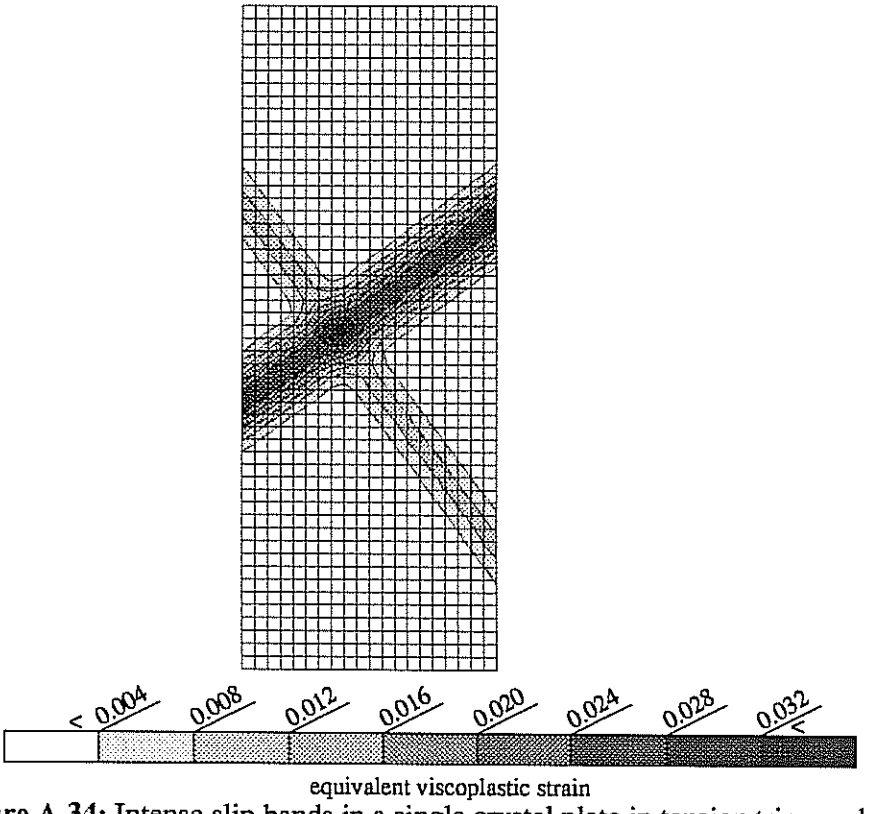

Figure A.34: Intense slip bands in a single crystal plate in tension triggered by the material imperfection.

5 Effect of boundaries and interfaces

5.1 Bifurcation analysis at the boundary and at an interface for single slip

Effect of boundaries

Contrary to shear bands in some cases, macroscopic slip bands do not deviate when approaching the free surface. Does the proposed model for describing macroscopic slip bands, that is regarded as discontinuous bifurcation modes in single slip, satisfy this requirement? To answer this question we go back to the localization condition at the boundary 78. $\underline{\mathbf{m}}$ is the unit vector normal to the boundary.

For a single crystal undergoing single slip at small strain:

$$\underset{\sim}{\mathbf{P}} = \frac{1}{2}\ (\underline{\mathbf{s}} \otimes \underline{\mathbf{z}} + \underline{\mathbf{z}} \otimes \underline{\mathbf{s}}) \tag{208}$$

where $\underline{\mathbf{z}}$ is the normal to the slip plane and $\underline{\mathbf{s}}$ the slip direction. We check successively whether the bifurcation solutions ($\underline{\mathbf{n}} = \underline{\mathbf{z}}$ and $\underline{\mathbf{g}} = \underline{\mathbf{s}}$) and ($\underline{\mathbf{n}} = \underline{\mathbf{s}}$ and $\underline{\mathbf{g}} = \underline{\mathbf{z}}$) satisfy the boundary condition 78.

If $\underline{\mathbf{n}} = \underline{\mathbf{z}}$, we calculate successively:

$$\underline{\mathbf{z}}.\underset{\approx}{\mathbf{E}} : \underset{\sim}{\mathbf{P}} = \mu\, \underline{\mathbf{s}} \tag{209}$$

for isotropic elasticity.

$$\left(\underline{\mathbf{z}}.\underset{\approx}{\mathbf{E}}.\underline{\mathbf{z}}\right)^{-1} = -\frac{\lambda+\mu}{\mu(\lambda+2\mu)}\ \underline{\mathbf{z}} \otimes \underline{\mathbf{z}} + \frac{1}{\mu}\ \underset{\sim}{\mathbf{1}} \tag{210}$$

then

$$\left(\underline{\mathbf{z}}.\underset{\approx}{\mathbf{E}}.\underline{\mathbf{z}}\right)^{-1}\ \left(\underline{\mathbf{z}}.\underset{\approx}{\mathbf{E}} : \underset{\sim}{\mathbf{P}}\right) = \underline{\mathbf{s}} \quad \text{since} \quad \underline{\mathbf{s}}.\underline{\mathbf{z}} = 0 \tag{211}$$

$$\left(\underline{\mathbf{m}}.\underset{\approx}{\mathbf{E}}.\underline{\mathbf{z}}\right) = \lambda\ \underline{\mathbf{m}} \otimes \underline{\mathbf{z}} + \mu\ \underline{\mathbf{z}} \otimes \underline{\mathbf{m}} + \mu \underline{\mathbf{m}}.\underline{\mathbf{z}}\ \underset{\sim}{\mathbf{1}} \tag{212}$$

$$\left(\underline{\mathbf{m}}.\underset{\approx}{\mathbf{E}}.\underline{\mathbf{z}}\right)\ \left(\underline{\mathbf{z}}.\underset{\approx}{\mathbf{E}}.\underline{\mathbf{z}}\right)^{-1}\ \left(\underline{\mathbf{z}}.\underset{\approx}{\mathbf{E}}.\underset{\sim}{\mathbf{P}}\right) = \mu\ (\underline{\mathbf{m}}.\underline{\mathbf{s}}\ \ \underline{\mathbf{z}} + \underline{\mathbf{m}}.\underline{\mathbf{z}}\ \ \underline{\mathbf{s}})\,. \tag{213}$$

On the other hand

$$\begin{aligned} \underline{\mathbf{m}}.\underset{\approx}{\mathbf{E}} : \underset{\sim}{\mathbf{P}} &= \mu\ (\underline{\mathbf{s}} \otimes \underline{\mathbf{z}}\ \underline{\mathbf{m}} + \underline{\mathbf{z}} \otimes \underline{\mathbf{s}}\ \underline{\mathbf{m}}) \\ &= \mu\ (\underline{\mathbf{m}}.\underline{\mathbf{s}}\ \ \underline{\mathbf{z}} + \underline{\mathbf{m}}.\underline{\mathbf{z}}\ \ \underline{\mathbf{s}}) \end{aligned} \tag{214}$$

so that condition

$$(\underline{\mathbf{m}}.\underset{\approx}{\mathbf{E}}.\underline{\mathbf{n}})(\underline{\mathbf{n}}.\underset{\approx}{\mathbf{E}}.\underline{\mathbf{n}})^{-1}(\underline{\mathbf{n}}.\underset{\approx}{\mathbf{E}} : \underset{\sim}{\mathbf{P}}) = \underline{\mathbf{m}}.\underset{\approx}{\mathbf{E}} : \underset{\sim}{\mathbf{P}} \tag{215}$$

is automatically satisfied. A similar proof is available for $\underline{\mathbf{n}} = \underline{\mathbf{s}}$. This establishes that slip bands and kink bands do not bend when approaching the surface or, conversely, slip bands nucleated at the boundary do no deviate when propagating through the bulk of the single crystal. This may not be the case for the more complicated bifurcation modes associated with continuing multislip within the band and calculated in 4.1.

Note that a more direct proof of the previous result can be provided, that holds also for anisotropic elasticity. Setting $\underline{n} = \underline{z}$ and $\underline{g} = \underline{s} = (\underline{n}.\underset{\sim}{\underline{E}}.\underline{n})^{-1}(\underline{n}.\underset{\sim}{\underline{E}}.\underset{\sim}{\underline{P}})$ (cf. equation 83), the first term of equation 215 becomes

$$\begin{aligned}(\underline{m}.\underset{\sim}{\underline{E}}.\underline{n})(\underline{n}.\underset{\sim}{\underline{E}}.\underline{n})^{-1}(\underline{n}.\underset{\sim}{\underline{E}} : \underset{\sim}{\underline{P}}) - \underline{m}.\underset{\sim}{\underline{E}} : \underset{\sim}{\underline{P}} &= (\underline{m}.\underset{\sim}{\underline{E}}.\underline{z})\underline{s} - \underline{m}.\underset{\sim}{\underline{E}} :^{\{}\, \underline{s} \otimes \underline{z}^{\}} \\ &= 0\end{aligned}$$

which again gives 215.

Effect of an interface

What happens now at an interface separating two single crystals with differing behaviours due to a slight misorientation (*subgrain boundary*), significant misorientation (*grains in a polycrystal*) or simply different material parameters?

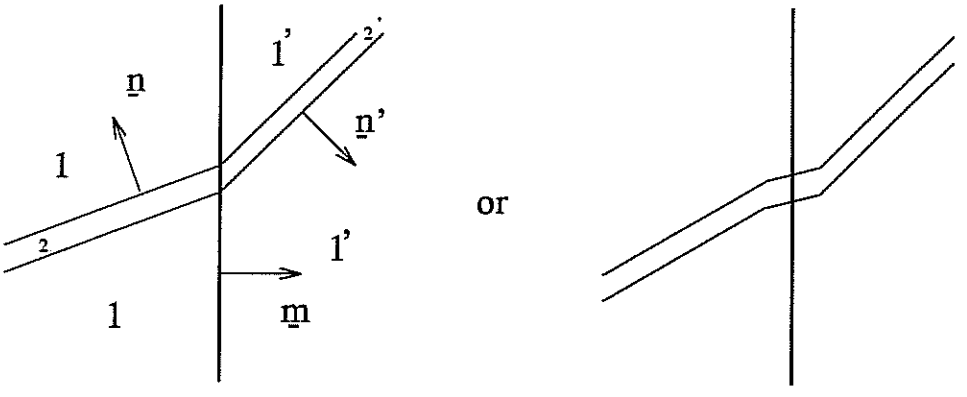

Bifurcation modes compatible on each side of the interface are of the form:

$$\dot{\underset{\sim}{\varepsilon}}_2 - \dot{\underset{\sim}{\varepsilon}}_1 = {}^{\{}\underline{g} \otimes \underline{n}^{\}} \tag{216}$$

$$\dot{\underset{\sim}{\varepsilon}}'_2 - \dot{\underset{\sim}{\varepsilon}}'_1 = {}^{\{}\underline{g}' \otimes \underline{n}'^{\}} \tag{217}$$

Continuing equilibrium implies:

$$\left(\dot{\underset{\sim}{\sigma}}_2 - \dot{\underset{\sim}{\sigma}}_1\right) \underline{n} = 0 \tag{218}$$

$$\left(\dot{\underset{\sim}{\sigma}}'_2 - \dot{\underset{\sim}{\sigma}}'_1\right) \underline{n}' = 0 \tag{219}$$

We know that the existence of continuous bifurcation modes (plastic/plastic bifurcations) give the upper bound of the critical hardening modulus for more general elastic/plastic bifurcation modes (see section 2.3.3). That is why we assume the same plastic behaviour inside and outside the localization band on each side of the interface:

$$\dot{\underset{\sim}{\sigma}}_i = \underset{\sim}{\underline{D}}\, \dot{\underset{\sim}{\varepsilon}}_i \qquad \text{for} \quad i \in \{1,2\} \tag{220}$$

$$\dot{\underset{\sim}{\sigma}}'_i = \underset{\sim}{\underline{D}}'\, \dot{\underset{\sim}{\varepsilon}}_i \qquad \text{for} \quad i \in \{1,2\} \tag{221}$$

Equilibrium conditions at the interface state that:

$$\dot{\underset{\sim}{\sigma}}_i\, \underline{m} = \dot{\underset{\sim}{\sigma}}'_i\, \underline{m} \quad \text{for} \quad i \in \{1,2\} \tag{222}$$

Equations 216 to 221 lead to the classical bifurcation condition in the bulk:

$$\left(\underline{n}.\underset{\sim}{D}.\underline{n}\right)\ \underline{g}\ = 0 \tag{223}$$

$$\left(\underline{n}'.\underset{\sim}{D}'.\underline{n}'\right)\ \underline{g}'\ = 0 \tag{224}$$

which becomes possible for critical values of the hardening modulus:

$$H = -\underset{\sim}{P} : \underset{\sim}{\underset{\sim}{E}} : \underset{\sim}{P} + (\underset{\sim}{P} : \underset{\sim}{\underset{\sim}{E}}.\underline{n})(\underline{n}.\underset{\sim}{\underset{\sim}{E}}.\underline{n})^{-1}(\underline{n}.\underset{\sim}{\underset{\sim}{E}} : \underset{\sim}{P}) \tag{225}$$

$$H' = -\underset{\sim}{P}' : \underset{\sim}{\underset{\sim}{E}}' : \underset{\sim}{P}' + (\underset{\sim}{P}' : \underset{\sim}{\underset{\sim}{E}}'.\underline{n}')(\underline{n}'.\underset{\sim}{\underset{\sim}{E}}'.\underline{n}')^{-1}(\underline{n}'.\underset{\sim}{\underset{\sim}{E}}' : \underset{\sim}{P}') \tag{226}$$

Interface condition 222 implies

$$\left(\dot{\underset{\sim}{\sigma}}_1 - \dot{\underset{\sim}{\sigma}}_2\right)\ \underline{m} = \left(\dot{\underset{\sim}{\sigma}}'_1 - \dot{\underset{\sim}{\sigma}}'_2\right) \underline{m} \tag{227}$$

and consequently

$$\left(\underline{m}.\underset{\sim}{D}.\underline{n}\right)\ \underline{g} = \left(\underline{m}.\underset{\sim}{D}'.\underline{n}'\right)\ \underline{g}' \tag{228}$$

Using equation 83 giving the direction of $\underline{g} \propto (\underline{n}.\underset{\sim}{\underset{\sim}{E}}.\underline{n})^{-1}(\underline{n}.\underset{\sim}{\underset{\sim}{E}} : \underset{\sim}{P})$ and the expression 44 of $\underset{\sim}{D}$, we find:

$$\begin{aligned}
\left(\underline{m}.\underset{\sim}{D}.\underline{n}\right)\ \underline{g} \quad &= \quad \left(\underline{m}.\underset{\sim}{\underset{\sim}{E}}.\underline{n}\right)\left(\underline{n}.\underset{\sim}{\underset{\sim}{E}}.\underline{n}\right)^{-1}\left(\underline{n}.\underset{\sim}{\underset{\sim}{E}} : \underset{\sim}{P}\right) \\
&\quad - \frac{\underline{m}.\left(\underset{\sim}{\underset{\sim}{E}} : \underset{\sim}{P}\right) \otimes \left(\underset{\sim}{P} : \underset{\sim}{\underset{\sim}{E}}\right).\underline{n}}{\left(\underset{\sim}{P} : \underset{\sim}{\underset{\sim}{E}}.\underline{n}\right)\left(\underline{n}.\underset{\sim}{\underset{\sim}{E}}.\underline{n}\right)^{-1}\left(\underline{n}.\underset{\sim}{\underset{\sim}{E}} : \underset{\sim}{P}\right)}\ \left(\underline{n}.\underset{\sim}{\underset{\sim}{E}}.\underline{n}\right)^{-1}\ \left(\underline{n}.\underset{\sim}{\underset{\sim}{E}} : \underset{\sim}{P}\right) \\
&= \quad \left(\underline{m}.\underset{\sim}{\underset{\sim}{E}}.\underline{n}\right)\left(\underline{n}.\underset{\sim}{\underset{\sim}{E}}.\underline{n}\right)^{-1}\left(\underline{n}.\underset{\sim}{\underset{\sim}{E}} : \underset{\sim}{P}\right) - \left(\underline{m}.\underset{\sim}{\underset{\sim}{E}} : \underset{\sim}{P}\right)
\end{aligned} \tag{229}$$

Since we are interested in the case of single slip, we set $\underset{\sim}{P} = \frac{1}{2}\ (\underline{s} \otimes \underline{z} + \underline{z} \otimes \underline{s})$ and $\underline{n} = \underline{z}$ (resp. $\underline{s}$) and $\underline{g} = \underline{s}$ (resp. $\underline{z}$), and in that conditions the previous investigation at the free boundary has yielded:

$$\left(\underline{m}.\underset{\sim}{\underset{\sim}{E}}.\underline{n}\right)\left(\underline{n}.\underset{\sim}{\underset{\sim}{E}}.\underline{n}\right)^{-1}\left(\underline{n}.\underset{\sim}{\underset{\sim}{E}} : \underset{\sim}{P}\right) = \left(\underline{m}.\underset{\sim}{\underset{\sim}{E}} : \underset{\sim}{P}\right) \tag{230}$$

The same is true on the other side.

This proves that interface condition for equilibrium 228 is automatically fulfilled in the case of single slip bifurcation. Thus, if single slip localization is possible on each side of the interface, equilibrium allows that slip bands do not bend when approaching the interface and that the abrupt change of orientation of the bands required by the possible misorientation of the two crystals takes place at the interface without violating local equilibrium.

Until now we have not addressed the problem of compatibility of deformation at the interface. Hadamard's compatibility conditions state that:

$$\exists\ \underline{g}_1 \quad \dot{\underline{u}}_1 \otimes \underline{\nabla} - \underset{\sim}{\nabla}\, \dot{\underline{u}}'_1 \otimes \underline{\nabla}\ = \underline{g}_1 \otimes \underline{m} \tag{231}$$

$$\exists\ \underline{g}_2 \quad \dot{\underline{u}}_2 \otimes \underline{\nabla} - \dot{\underline{u}}'_2 \otimes \underline{\nabla}\ = \underline{g}_2 \otimes \underline{m} \tag{232}$$

where $\underline{\mathbf{u}}$ denotes the displacement. Combining 216, 217 and 231, we have

$$\underline{\mathbf{g}} \otimes \underline{\mathbf{n}} - \underline{\mathbf{g}}' \otimes \underline{\mathbf{n}}' = \left(\underline{\mathbf{g}}_1 - \underline{\mathbf{g}}_2\right) \otimes \underline{\mathbf{m}}. \tag{233}$$

Compatibility equation 231 is usually not met even before localization. This induces non-homogeneous deformation at grain boundaries for instance. We have seen that equilibrium allows the crossing of the interface by slip bands with the necessary abrupt change in orientation but the question is whether strain incompatibilities impede the crossing or not. Only finite element calculations can answer the question and this is done in section 5.2. We may also imagine that strain incompatibilities may act as imperfections enhancing localization processes.

5.2 Bicrystals

Dève and Asaro [1989] studied both experimentally and numerically the development of shear bands in ductile f.c.c. polycrystals. They found that local lattice rotation tends to lower the misorientation between grain-scale shear band planes on each side of a grain boundary. Local geometrical softening occurs at certain grain boundaries leading to a partial alignment of shear bands. 2D calculations with randomly distributed grains deforming according to three planar slip systems confirmed that due to lattice rotations shear bands do not significantly deviate when crossing the grain boundaries.

Strain incompatibilities caused at small strain by the presence of a grain boundary have been observed experimentally and simulated numerically by Méric, Cailletaud and Gaspérini [1994] for copper bicrystals under cyclic loading. The bicrystals were highly misoriented so that a complex deformation field developped. Deformation modes were rather diffuse and no intense slip band could form.

In contrast, we study here the influence of plastic incompatibilities in bicrystals on the development of macroscopic slip bands and for that purpose once more a strain softening behaviour is introduced. Such a situation arises in the vicinity of a grain boundary where incipient plasticity can be accompanied with softening mechanisms.

The single crystal plate is now divided into two misoriented single crystals with the same material parameters. The single crystals are oriented for single slip and deform within the plane of the plate so that 2D FE calculations can be performed to reduce computation time. Such a slip configuration is obtained as follows:

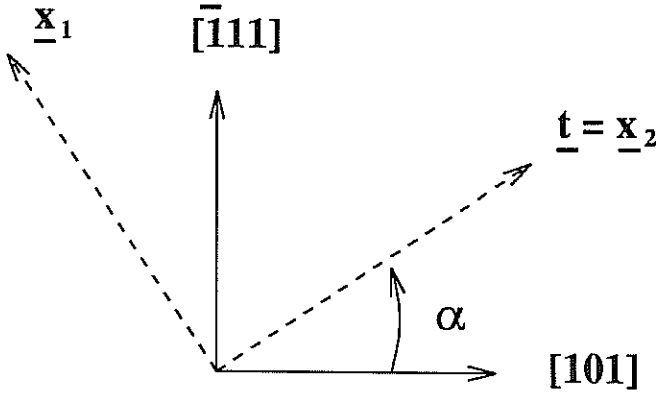

where $\underline{\mathbf{x}}_1, \underline{\mathbf{x}}_2$ defining the plate and slip direction [101] and the normal to the slip plane

$[\bar{1}11]$ are in the same plane. $\underline{x}_2 = \underline{t}$ is the tensile direction:

$$\underline{t} = \begin{bmatrix} \frac{\cos\alpha}{\sqrt{2}} - \frac{\sin\alpha}{\sqrt{3}} \\ \frac{\sin\alpha}{\sqrt{3}} \\ \frac{\cos\alpha}{\sqrt{2}} + \frac{\sin\alpha}{\sqrt{3}} \end{bmatrix}$$

We take $\underline{x}_2 = \underline{t} = [2\,3\,8], \underline{x}_1 = [\bar{1}9\,10\,1]$ for the left side, corresponding to $\alpha_{left} = 36.3°$ and we consider first a slight misorientation with $\alpha_{right} = 40°$, that is two subgrains rather than a bicrystal. The two sides exhibit a softening behaviour and the right upper corner has a slightly lower elasticity limit. A material imperfection is introduced to trigger the initiation of a slip band in one crystal. The misorientation results in non-homogeneous deformation shown in figure 35, that masks a bit the effect of the material imperfection. Nevertheless a slip band initiates at the location of the imperfection and refracts at the interface (figure 36). Later the refracted band reflects on the interface (figure 37).

Small local variations of the orientation of the single crystal leads to a so-called *"mosaic"* structure. Figure 40 shows in the case of a single crystal nickel-base superalloy that such subgrain boundaries can actually be crossed by slip bands.

For a large misorientation $\Delta\alpha = 20°$, the situation is comparable to that of two neighbouring grains. Incompatibility of plastic deformation results immediately in non-homogeneous deformation (figure 38) but does not prevent a slip band from initiating and propagating across the interface with the expected deviation (figure 39).

5.3 Propagation of a slip band through a hardening zone

We have seen that plastic flow can be at the very beginning an unstable process at the level of the material volume element. To model in a macroscopic way the collective behaviour of dislocations that leads to formation of macroscopic slip bands, we have introduced in our FE calculations local softening behaviour that results in the initiation of bands of localized deformation. We show in this section that these initiated bands can propagate through surrounding hardening zones. For that purpose we consider once again a rectangular single crystal plate divided in two parts with the same orientation, one displaying a softening behaviour, the other one a hardening behaviour. The upper right corner of the softening part has a slightly weaker behaviour so that the initiation of a slip band is expected at this point. The tensile curves corresponding to these different behaviours are given in figure 42. The respective material parameters are the following:

1

E = 200000 MPa
$\nu = 0.3$
$r_0 = 50$ MPa
q = 10 MPa
b = 150
c = 13640 MPa
d = 2300
k = 5 MPa $s^{1/n}$
n = 2

2

E = 200000 MPa
ν = 0.3
r_0 = 50 MPa
q = -45 MPa
b = 210
c = 20000 MPa
d = 900
k = 5 MPa $s^{1/n}$
n = 2

3

E = 200000MPa
ν = 0.3
r_0 = 49 MPa
q = -48.9 MPa
b = 210
c = 20000 MPa
d = 900
k = 5 MPa $s^{1/n}$
n = 2

Only single slip is taken into account ($x_2 \parallel [2\,3\,8], x_1 \parallel [\overline{1}9\,10\,1]$). Figure 43 shows that a zone of non-homogeneous deformation appears starting from the location of the imperfection and stopped at the interface. Between figures 43 and 44, the peak of the curve in the softening zone has been overcome and an intense slip band forms crossing the softening and the hardening zones. It is important to notice that conditions for localization considered as a bifurcation mode are not met in the hardening zone. The propagation of the band through the hardening zone results from structural effects: the material hardens inside the band on the strong side, whereas elastic unloading occurs outside (figure 45).

If we take an even harder behaviour on the left side, the slip band initiated at the upper right corner does not develop further (figure 46a). Instead, geometrical effects and stress redistribution lead to localization of deformation at the lower right part that results in another intense slip band once the peak of the tensile curve in the softening zone is overcome (figure 46b and 47a). Despite all that, figures 47b show that a band of localized deformation corresponding to the second possible bifurcation mode in single slip, forms and crosses the hardening zone.

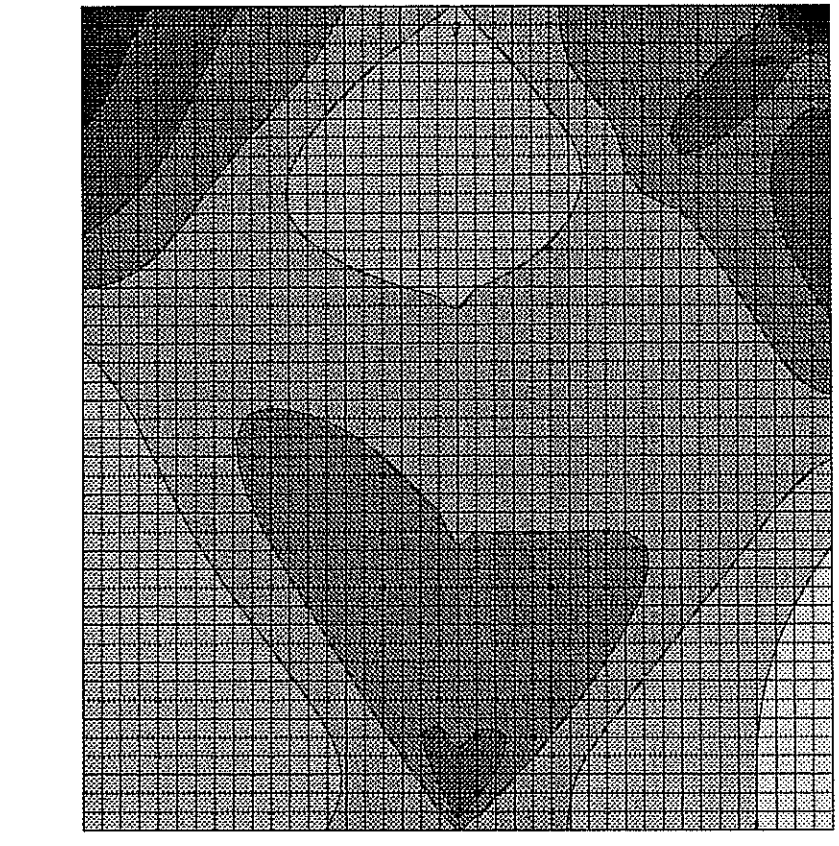

Figure A.35: Tension of a bicrystal with a slight misorientation; initial non homogeneous deformation due to strain incompatibity; the material defect is at the top right corner.

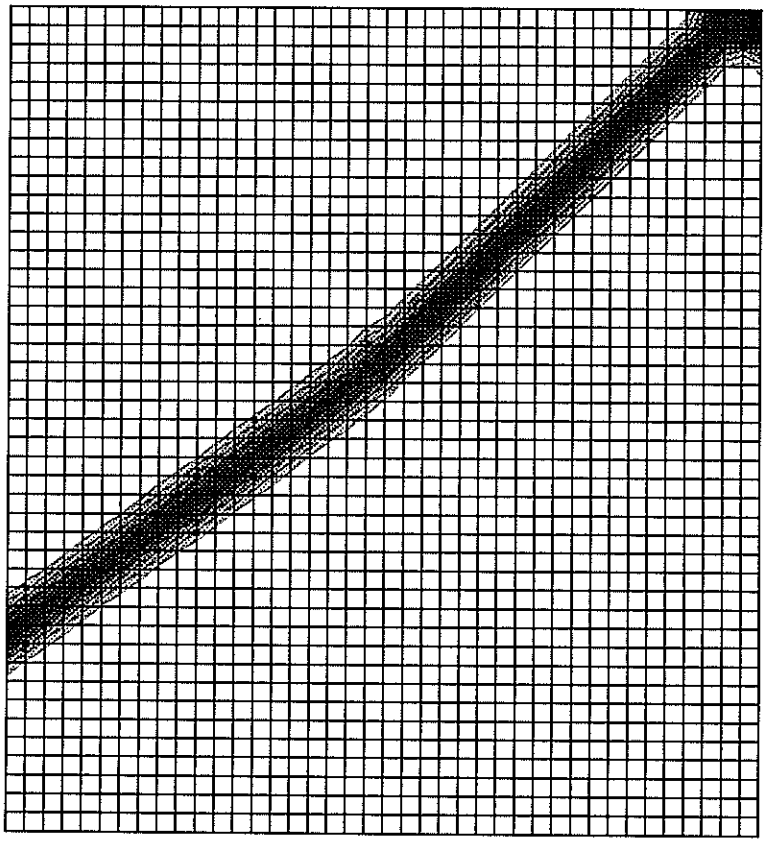

Figure A.36: Tension of a bicrystal with a slight misorientation; refraction of the slip band at the interface.

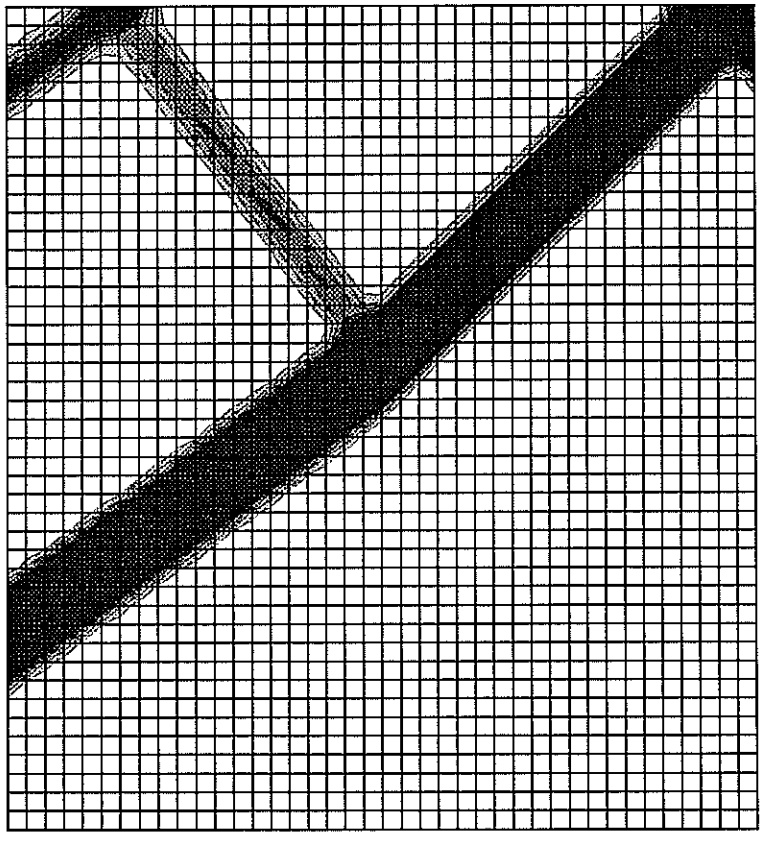

Figure 37: Tension of a bicrystal with a slight misorientation; reflexion of the refracted slip band at the interface.

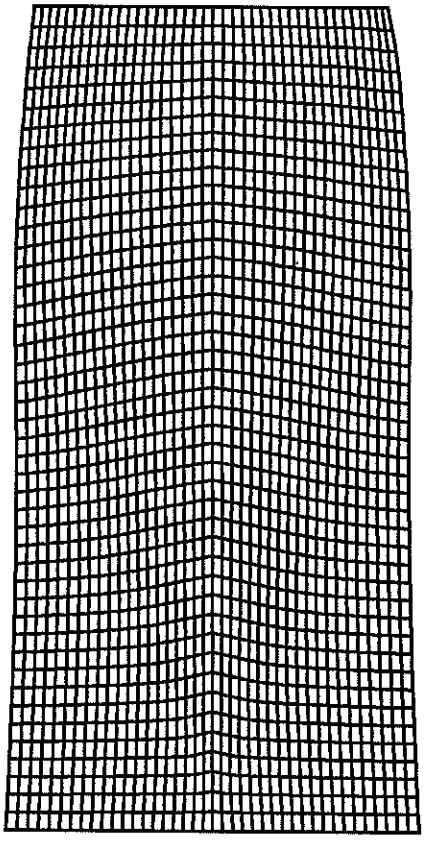

Figure A.38: Tension of a bicrystal with a misorientation of 20 ^{o}; initial strain incompatiblity (deformed state, magnification 300).

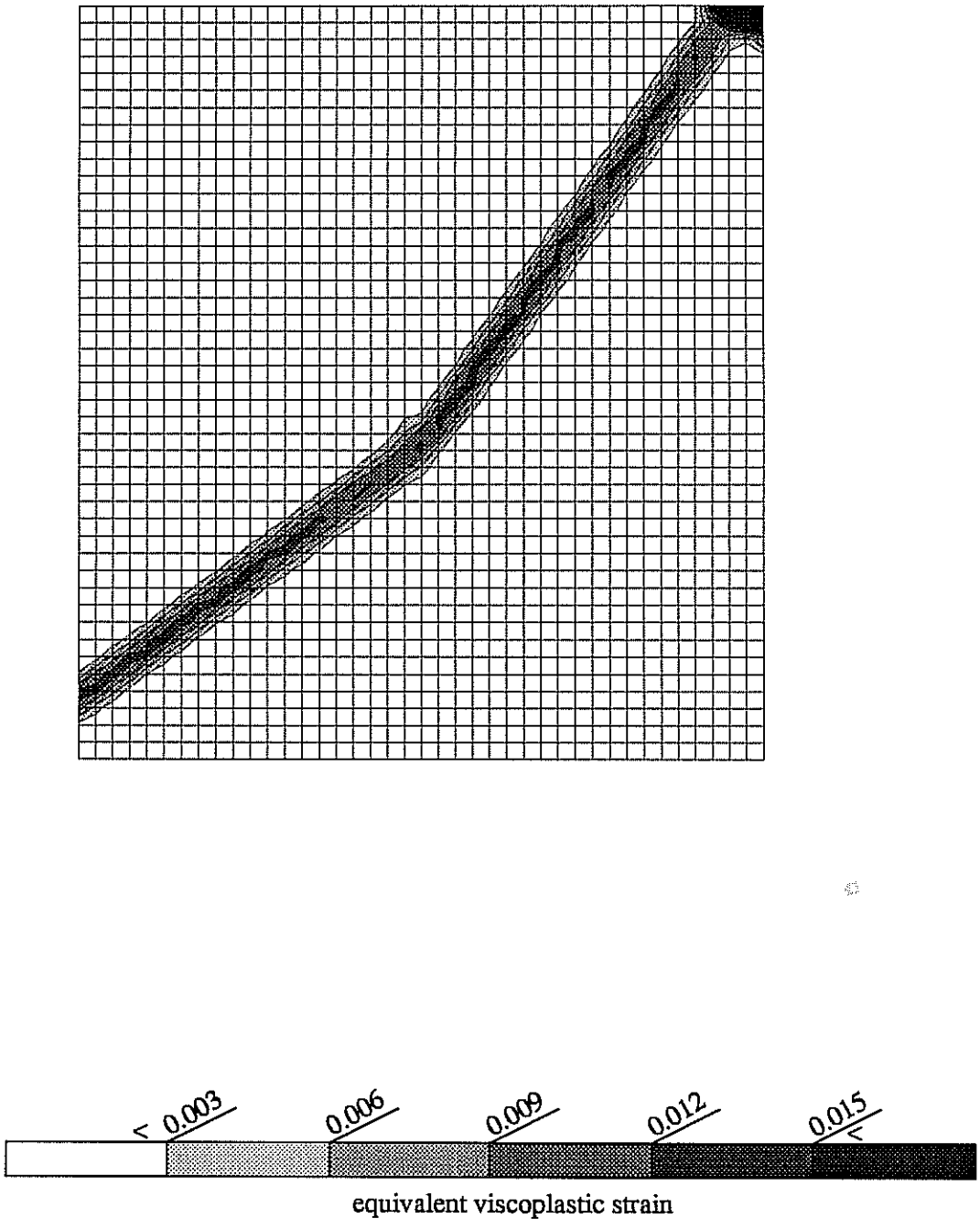

Figure A.39: Tension of a bicrystal with a misorientation of 20 ^{o}; propagation of a slip band in the two grains.

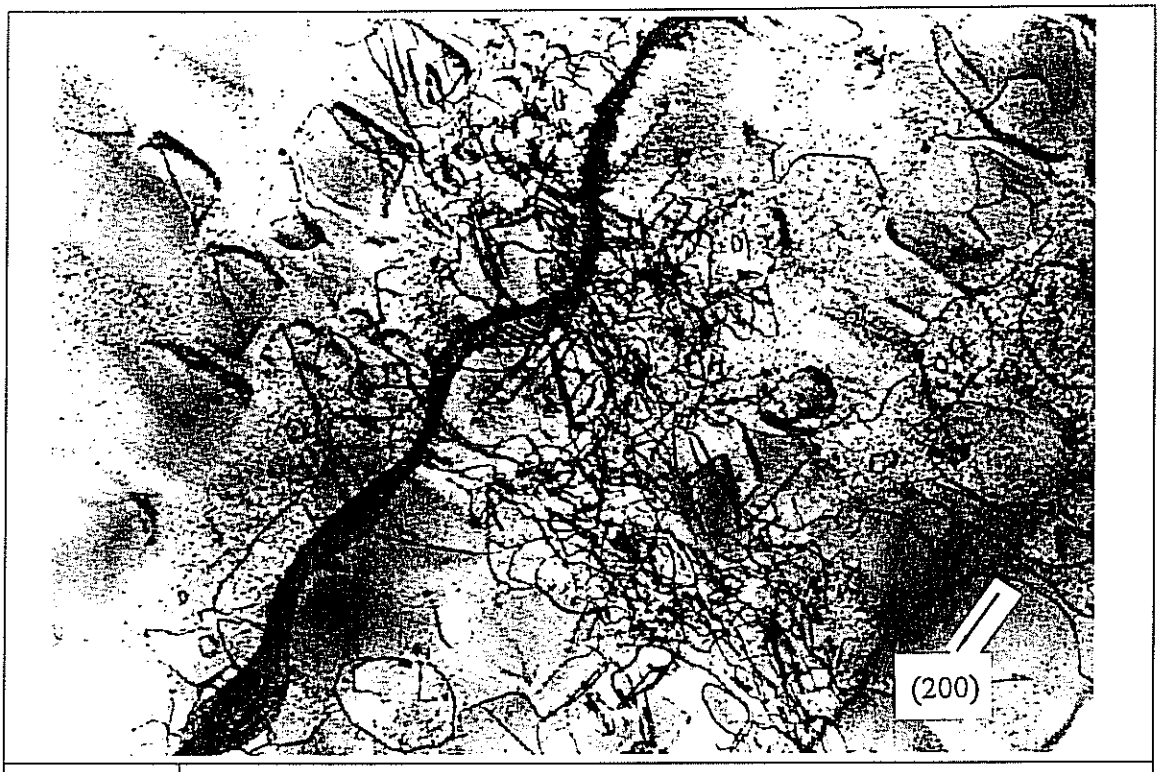

BAM
1.13
Sfb339, B7

SC16, Zugversuch, 750°C, 1E-3 1/s, 1%
Gleitband schneidet Subkorngrenze,
TEM, BF

D. Bettge, 16.11.94

Figure A.40: Propagation of a slip band through a subgrain boundary (photo D.Bettge, BAM 1.13).

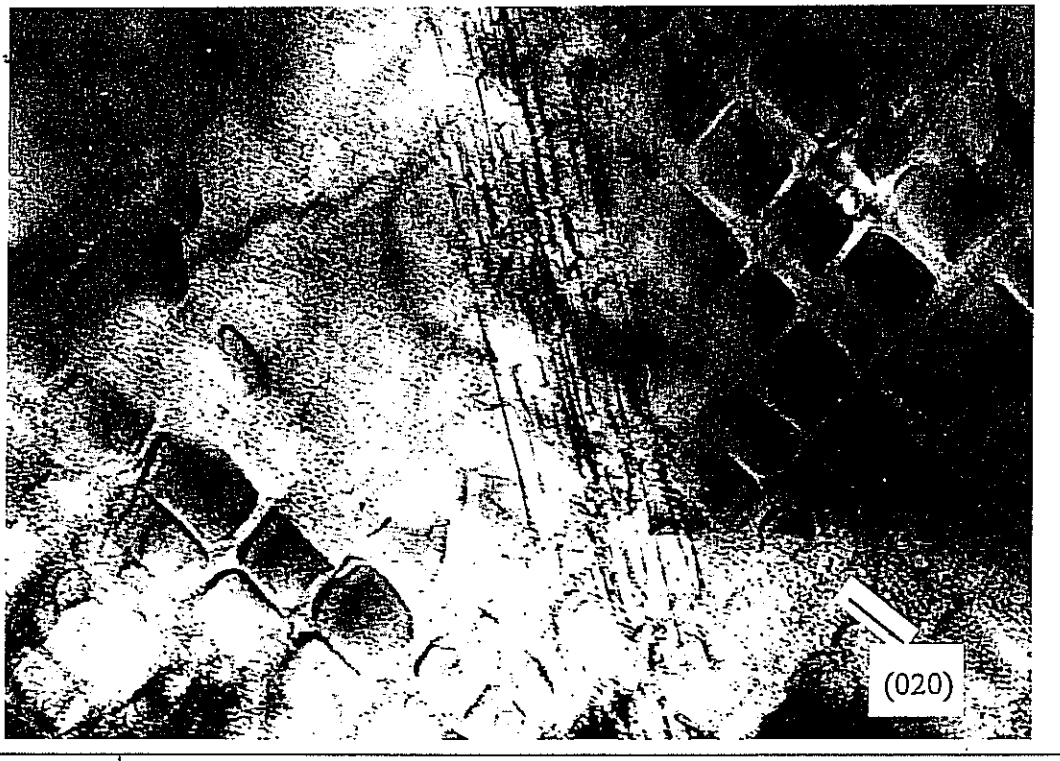

BAM
1.13
Sfb339, B7

SC16, Zugversuch, 750°C, 1E-3 1/s, 1%,
Gleitband edge-on gekippt zur Darstellung der Planarität,
TEM, BF

D. Bettge, 16.11.94

AB1224, 500nm=15mm

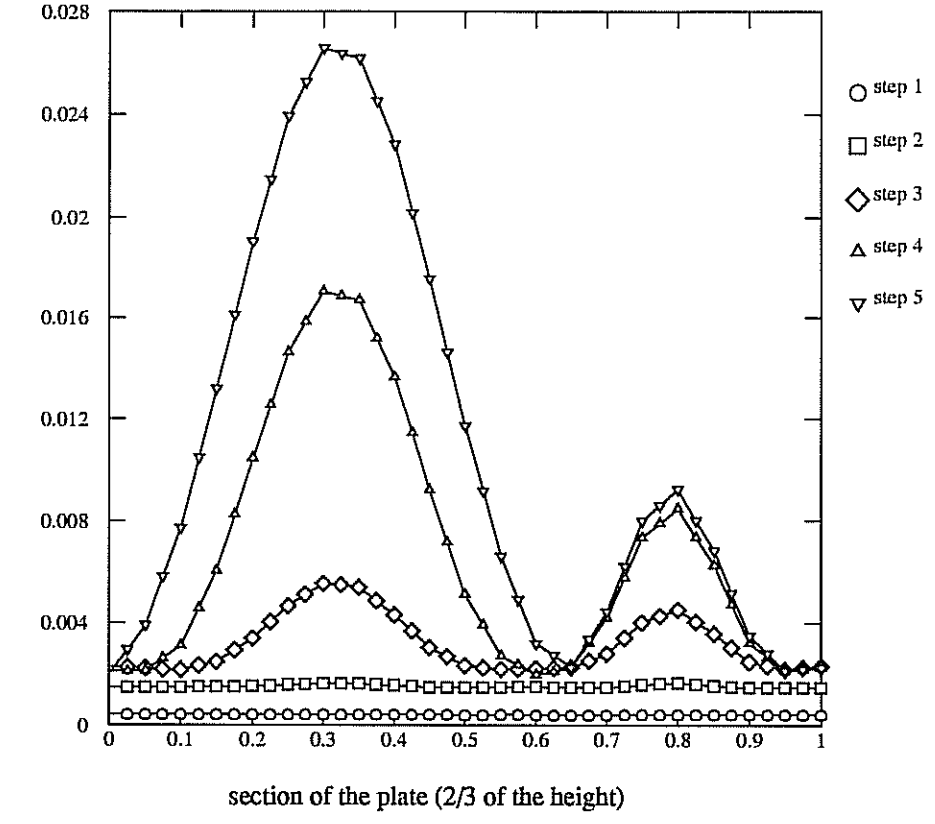

Figure A.41: Initiation and growth of two intense slip bands and progressive predominance of one of them.

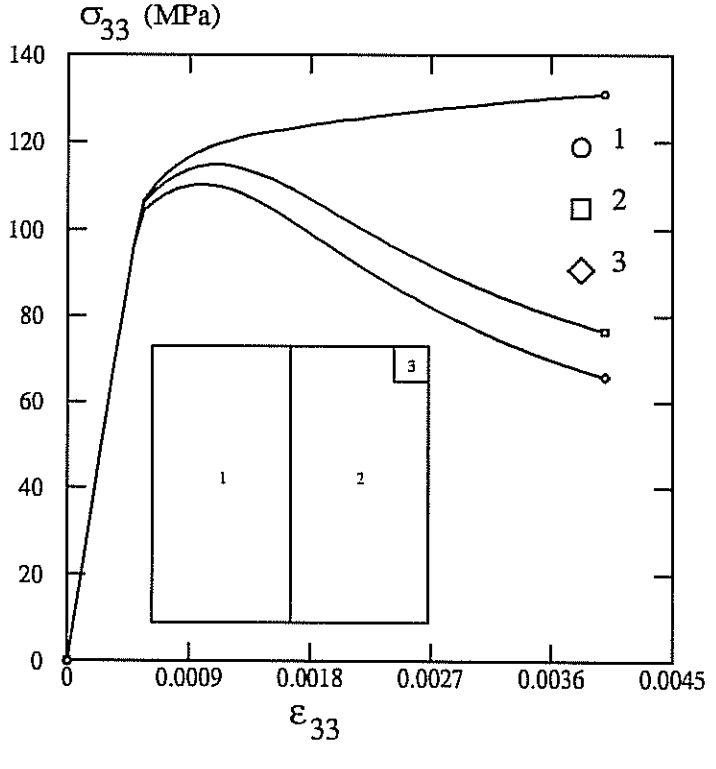

Figure A.42: Tension of a bicrystal composed of grains with the same orientation but different hardening behaviours: behaviour of each part of the mesh.

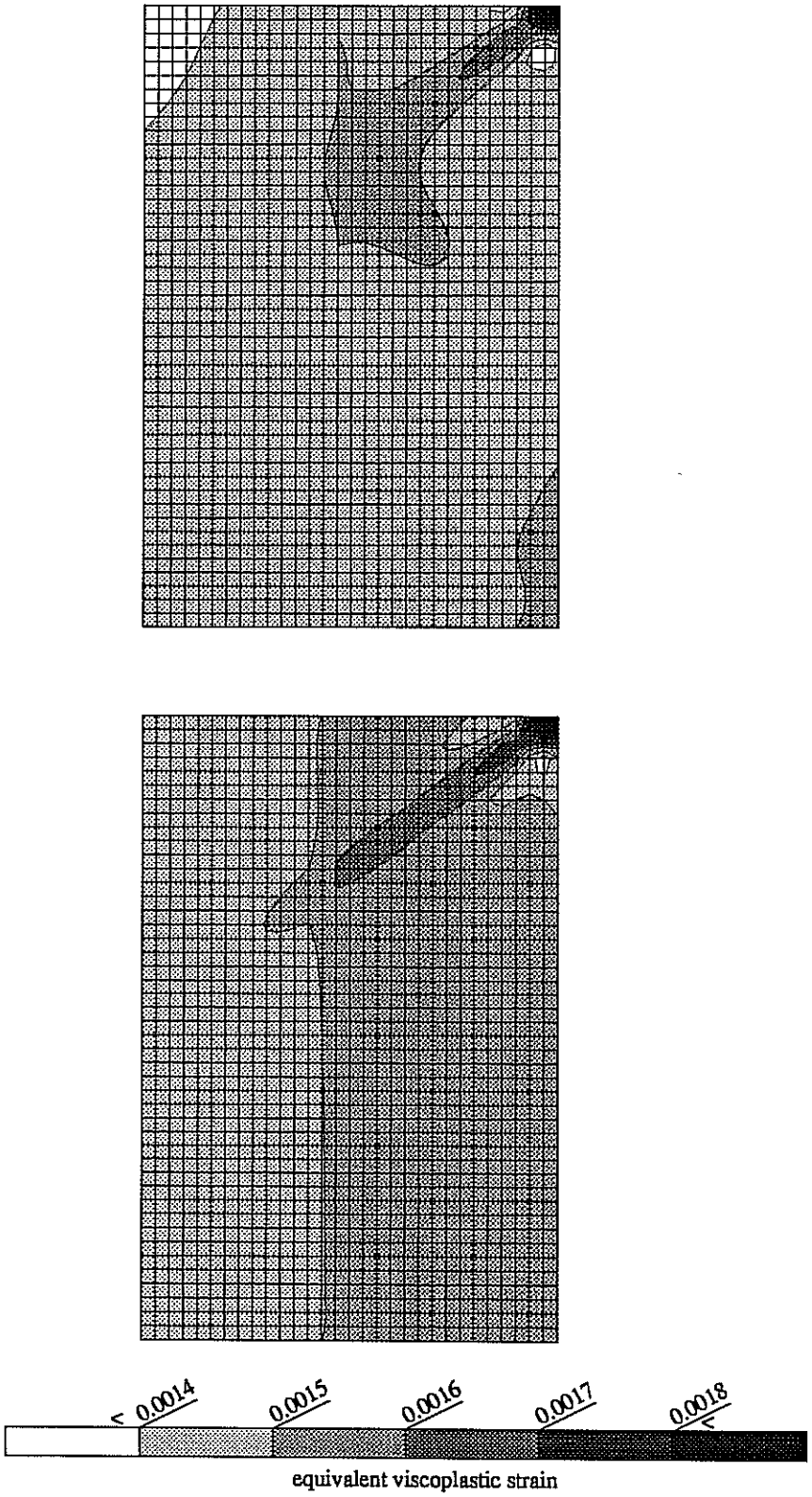

Figure A.43: Propagation of an intense slip band through a hardening zone; Initiation of the band in the softening zone.

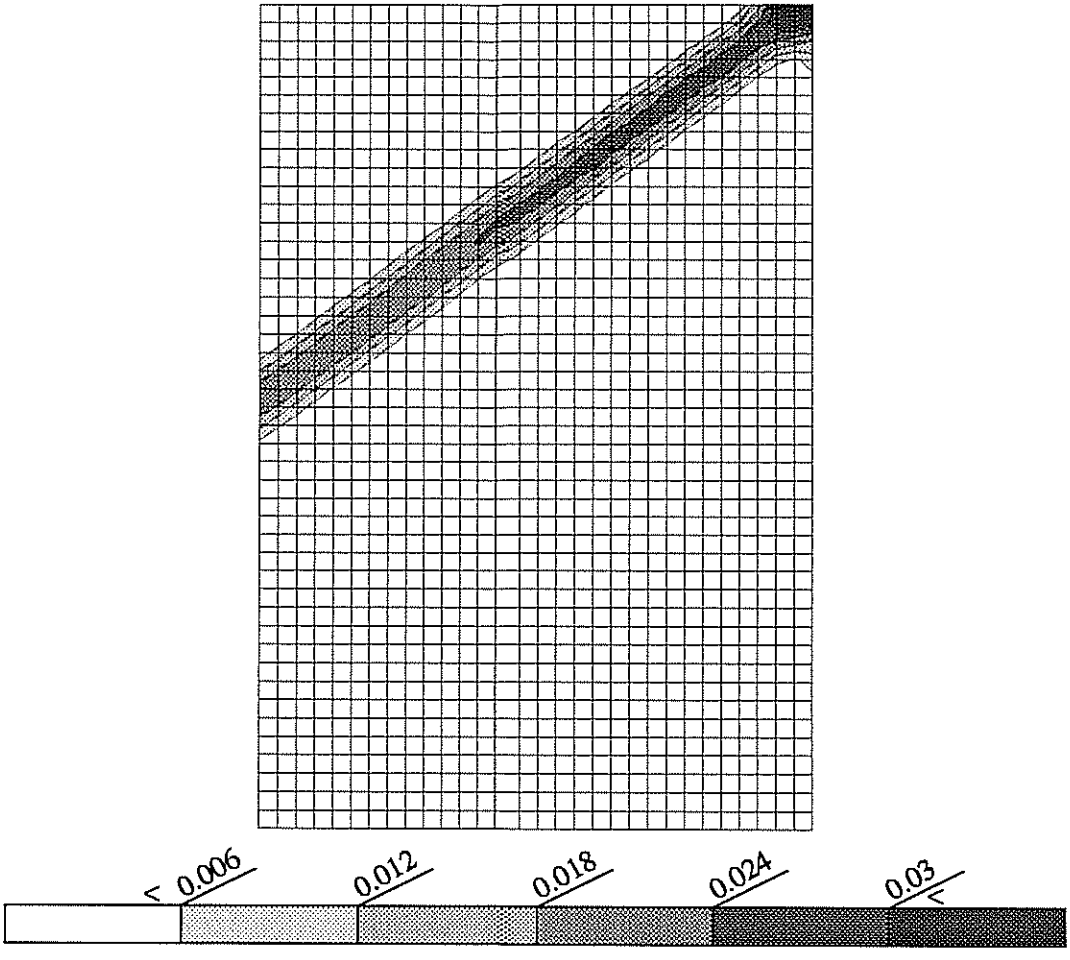

Figure A.44: Propagation of an intense slip band through a hardening zone; Crossing of the interface by the slip band.

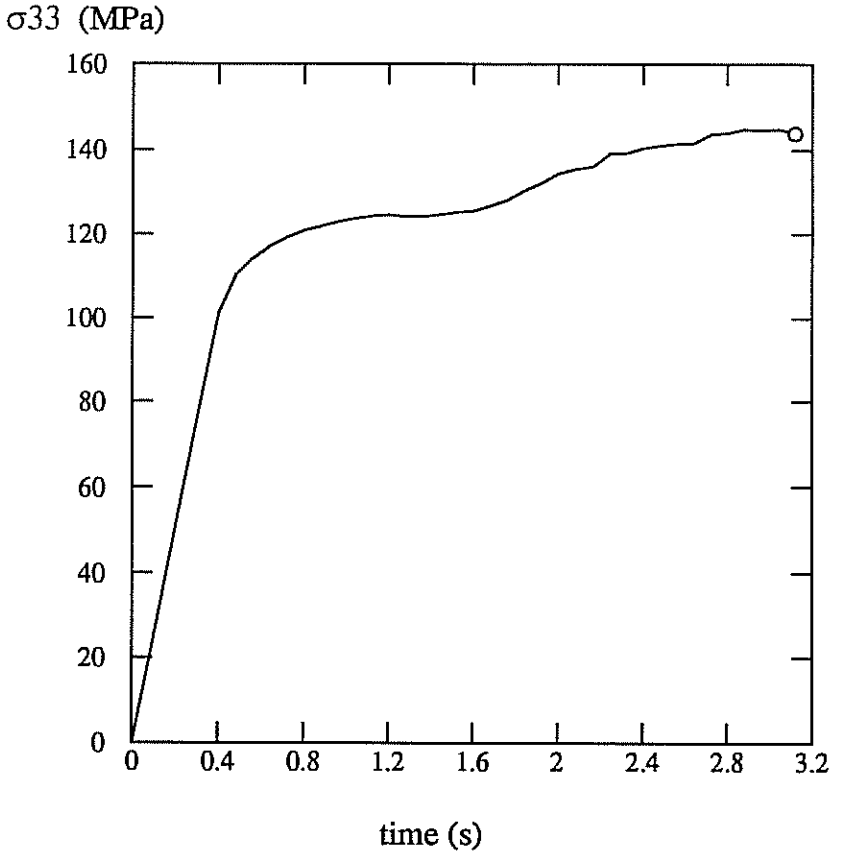

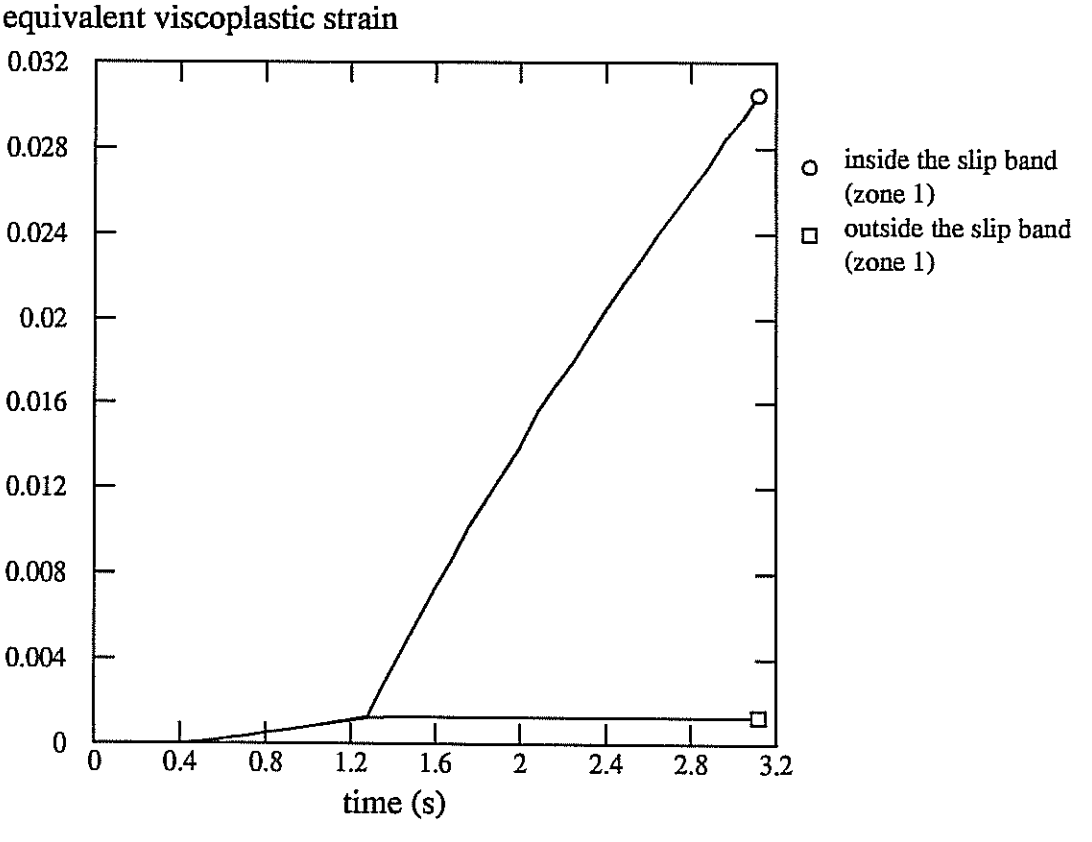

Figure A.45: Viscoplastic hardening inside the slip band (above) and elastic unloading outside the band (below) in the hardening zone of crystal, after crossing of the interface.

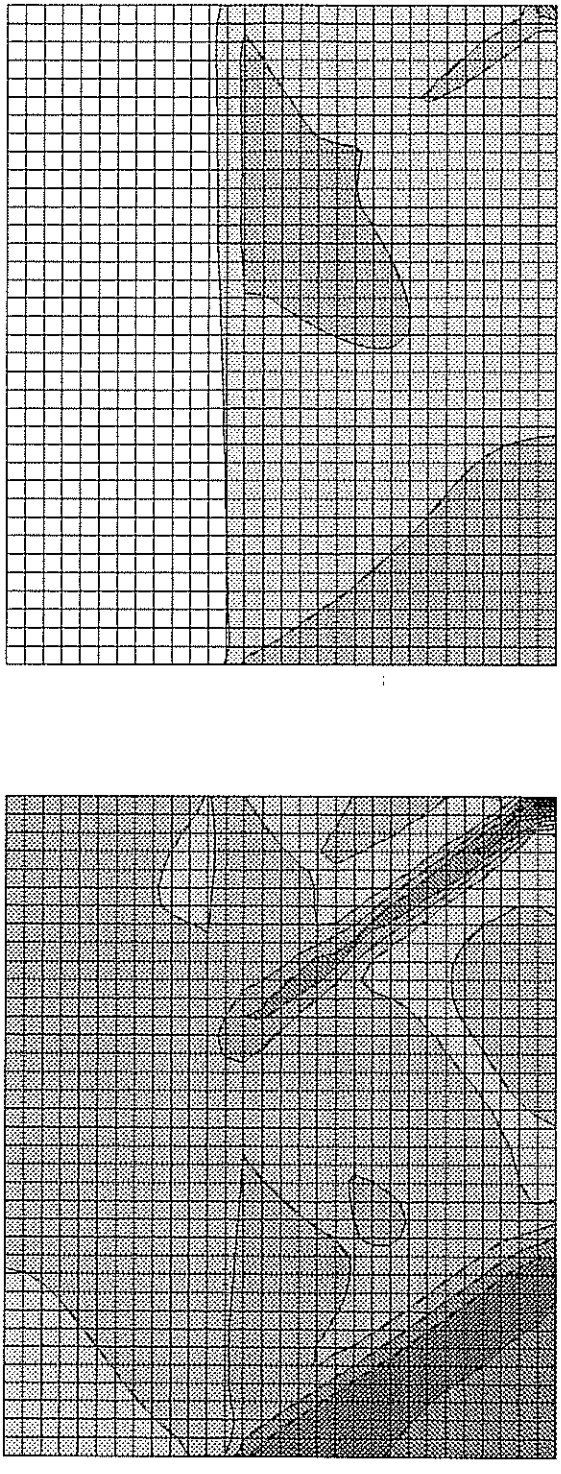

Figure A.46: The propagation of the slip band is stopped by the hardening zone; strain localizes at the lower left corner; for these calculations the mesh of the hardening zone is a bit narrower than the other one.

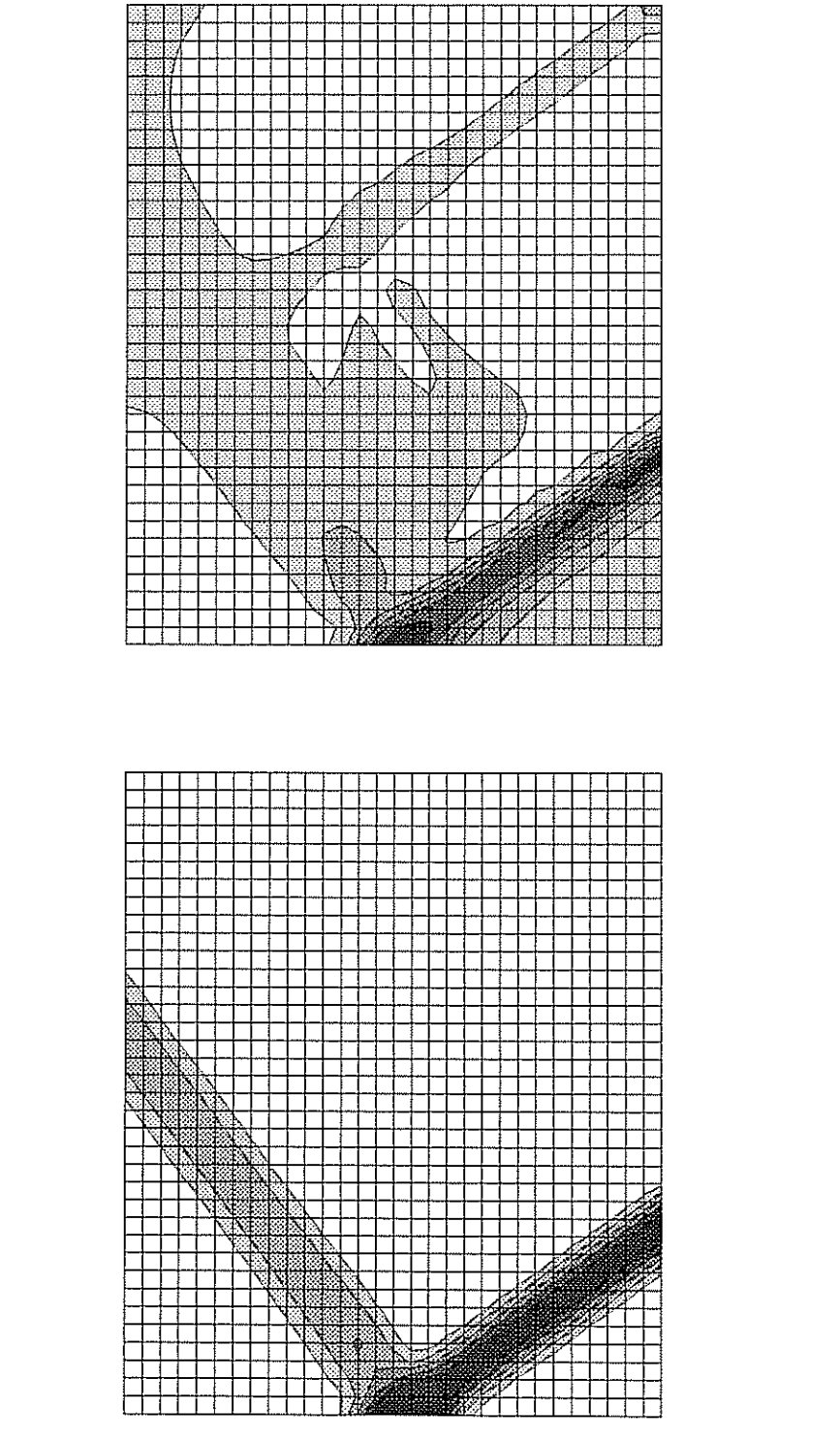

Figure A.47: Initiation of a slip band crossing the hardening zone.

6 Influence of latent hardening on localization for multiple slip

6.1 Polyslip in single crystals

In section 4.1.2, we have considered multislip configurations that are expected to be observed experimentally in tension along given directions, when the interaction matrix is isotropic or diagonal. But Franciosi, Berveiller and Zaoui [1980] have shown that pronounced latent hardening makes the simultaneous macroscopic activation of many slip systems locally very unlikely. For small strain and materials with low stacking-fault energy, experimental data reported in [Franciosi, Zaoui 1982] show that the initially preferred slip system combinations consist of sytems that are weakly interacting and do not form *junctions*. The predicted slip systems are observed later at larger strains. The interaction matrix cannot then be isotropic at the beginning of plastic flow. This recent studies have their roots in the work of Kocks [1960]. He investigated experimentally various different tests to trigger multislip in aluminum single crystals:

- tension in direction [100] (8 slip systems are expected);
- tension in direction [111] (6 slip systems are expected);
- (100)[010] shear test (8 slip systems are expected);
- [100] compression + (100)[011] shear (6 slip systems are expected).

In each case, the expected slip systems were not observed simultaneously. The suppression of one of two glide systems in critical relationship is due to dislocation interactions. This local instability propagates then throughout the specimen. In addition to the Lomer-Cottrell locks, Kocks proposes also a *"hedge"* mechanism to explain the exclusion of some slip system combinations.

6.2 Bifurcation with symmetry breaking

In the case of multiple slip we have investigated until now only constrained bifurcation modes for which one single amount of slip γ is calculated for symmetric slip systems. Regarding double slip for instance, we imposed $\gamma_1 = \gamma_2$. If this constraint is dropped, new bifurcation modes are possible. Figure 48 shows strain localization bands obtained for a single crystal oriented for double slip (tensile axis [012], secondary direction $[52\bar{1}]$) in the constrained and unconstrained case. In the former case, the orientation of the shear bands is not crystallographic and is that predicted in section 4.1.2. In the unconstrained case the bifurcation mode induces a symmetry breaking since the amounts of slip on the two systems are not identical any more (figure 49). The obtained shear bands are slip bands along the two slip planes. For these calculations we have used a diagonal interaction matrix. The existence of such crystallographic bifurcation modes is explained in the next section. The deformed state of the two single crystal plates is given on figure 50.

6.3 Influence of latent hardening on the stability of multiple slip configurations

The bifurcation analysis in section 4.2 for multislip has provided bifurcation modes for which symmetric slip still occurs inside the band, i.e. the amount of slip on the active slip systems remain equal after bifurcation. This usually leads to non-crystallographic shear band orientations. However some slip system may be desactivated in the band and other modes are then possible. We investigate here the influence of latent hardening on the

possible bifurcation modes. If two symmetric slip systems are active and assuming linear viscosity and hardening, we have

$$\begin{aligned} k\,\dot{\gamma}_1 &= \tau - \tau_0 - H_{11}\gamma_1 - H_{12}\gamma_2 \\ k\,\dot{\gamma}_2 &= \tau - \tau_0 - H_{12}\gamma_1 - H_{11}\gamma_2 \\ \Rightarrow k\,\Delta\dot{\gamma} &= -(H_{11} - H_{12})\,\Delta\gamma \end{aligned} \tag{234}$$

where $\Delta\gamma = \gamma_2 - \gamma_1$. If $H_{11} - H_{12} < 0$, symmetric slip may not be stable and one slip system may then accommodate the entire deformation.

The formation of slip and shear bands for double slip in tension (tensile direction [012], secondary direction $[52\bar{1}]$, the systems A3 and B4 are active) has been investigated for various latent hardening ratios. In the following, we denote $H_{11} = qh_{11}$ and $H_{12} = qh_{12}$, and the material parameters are those used in section 4.1.2 for double slip.

- $h_{11} = 1, h_{12} = 4$: symmetric slip is stable and we obtained the bifurcation modes predicted in section 4.1.2, with non-crystallographic shear band orientations. Figure 51 shows that the amounts of slip due to the two slip systems in the bands remain equal.
- $h_{11} = 1, h_{12} = 1$ (isotropic hardening): the results are very similar to the previous ones (figure 52).
- $h_{11} = 2, h_{12} = 1$: in this case, mixed modes are obtained. In one of the two bands the two systems remain equally active. The other one is a slip band for the system B4 (figure 53).
- $h_{11} = 4, h_{12} = 1$: in this case, two slip bands and a kink band are obtained (figure 54).
- $h_{11} = 1, h_{12} = 0$: the analysis has been performed at large strains (see next section). Two slip bands and one kink band formed (figure 55).

On figure 55b it can be seen once more that three-dimensional calculations are required to take the actual geometry of double slip into account, contrary to the plane study by Peirce, Asaro and Needleman [1983].

The obtained bifurcation modes are in accordance with the stability analysis of equation 234 (it must be noted that we have considered softening crystals so that H_{11} and H_{12} become negative and formula 234 can be used to study the stability of the bifurcation modes). For softening crystals and strong latent hardening, symmetric slip is stable and non-crystallographic bands may form. When the diagonal components are the biggest ones, slip and kink bands appear because symmetric slip becomes unstable.

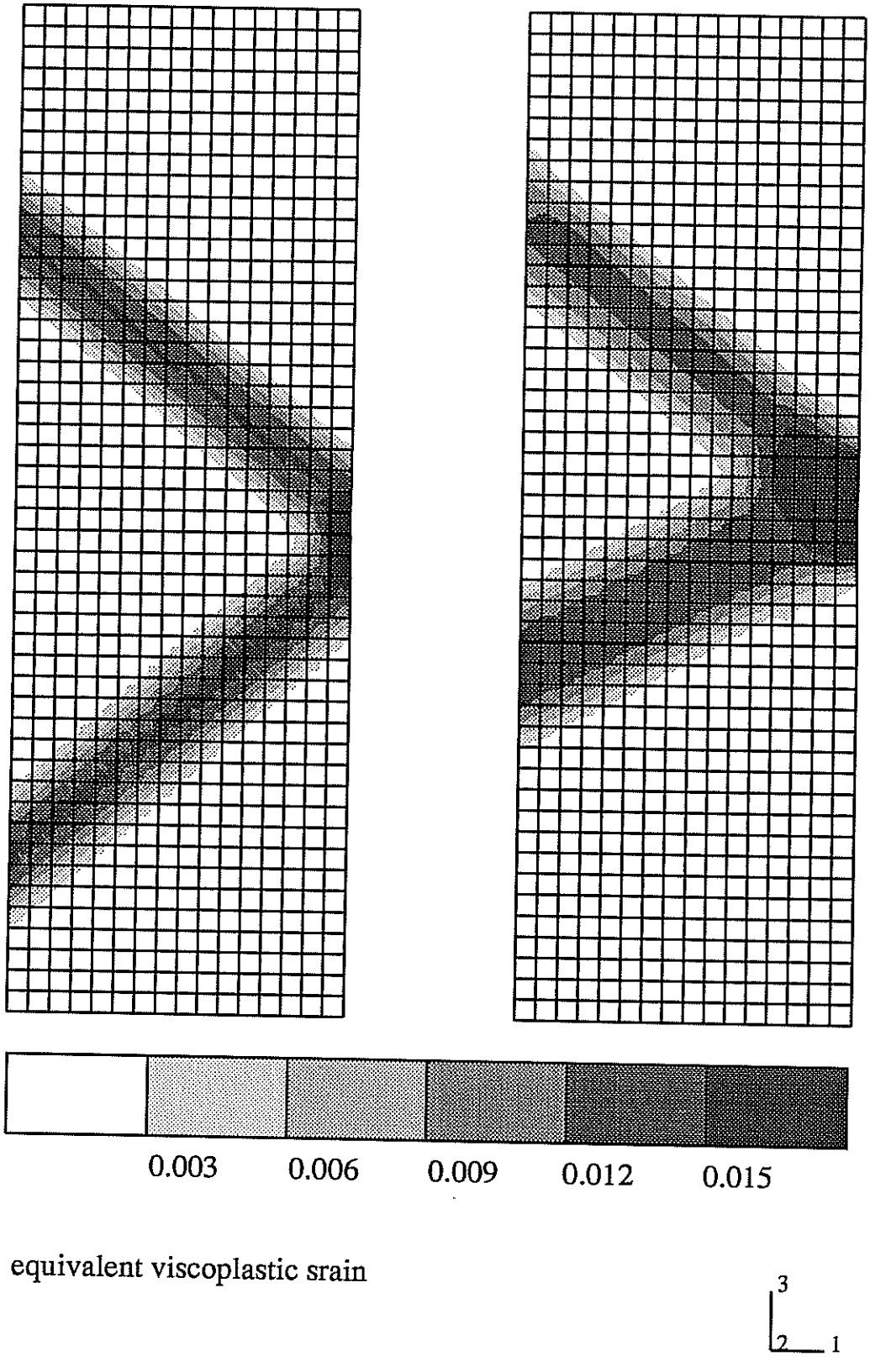

Figure A.48: Shear band patterns for a single crystal with constrained double slip (left) and unconstrained double slip (right).

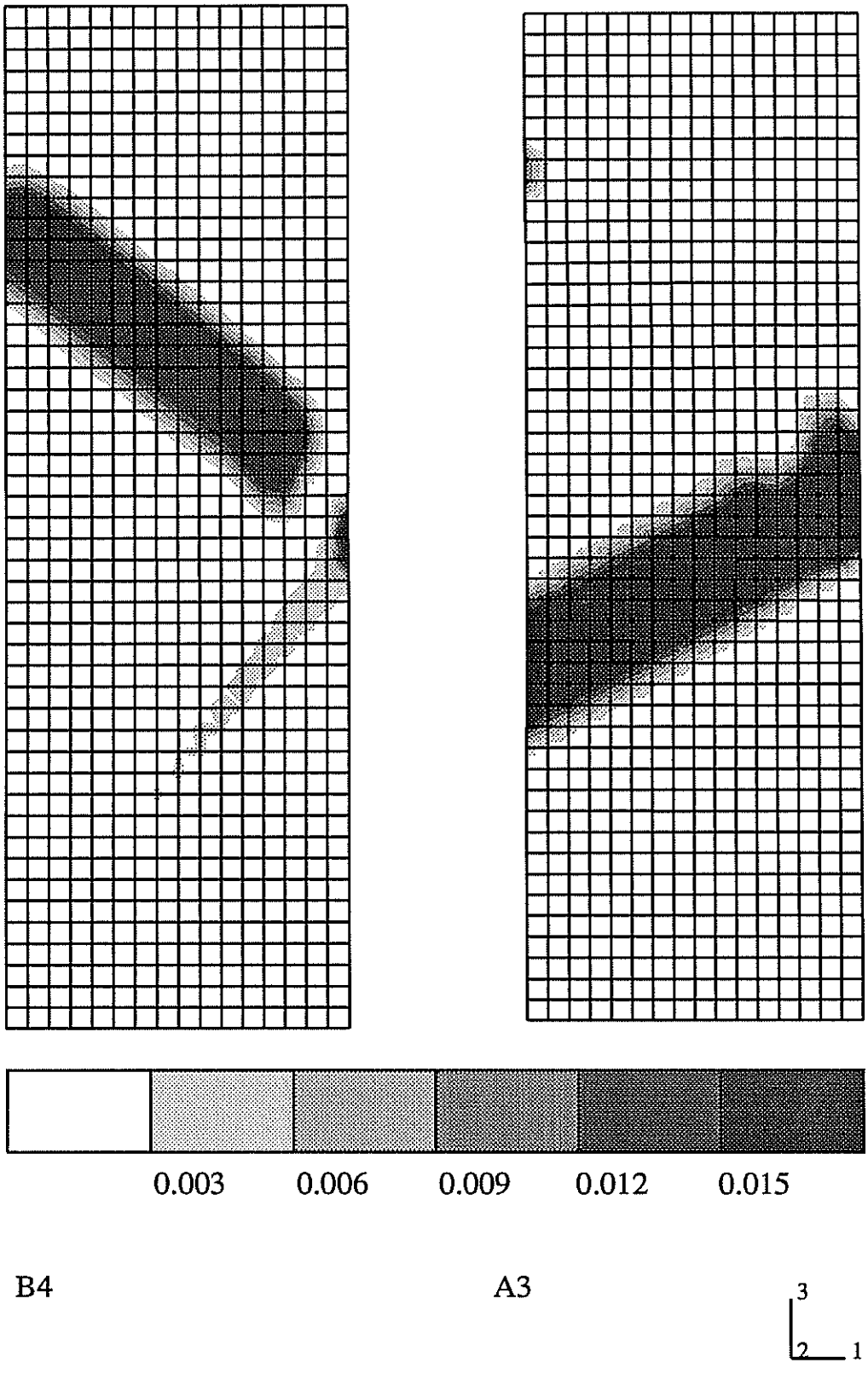

Figure A.49: Active slip systems in the slip bands after tension in a single crystal oriented for double slip (amount of slip γ^S).

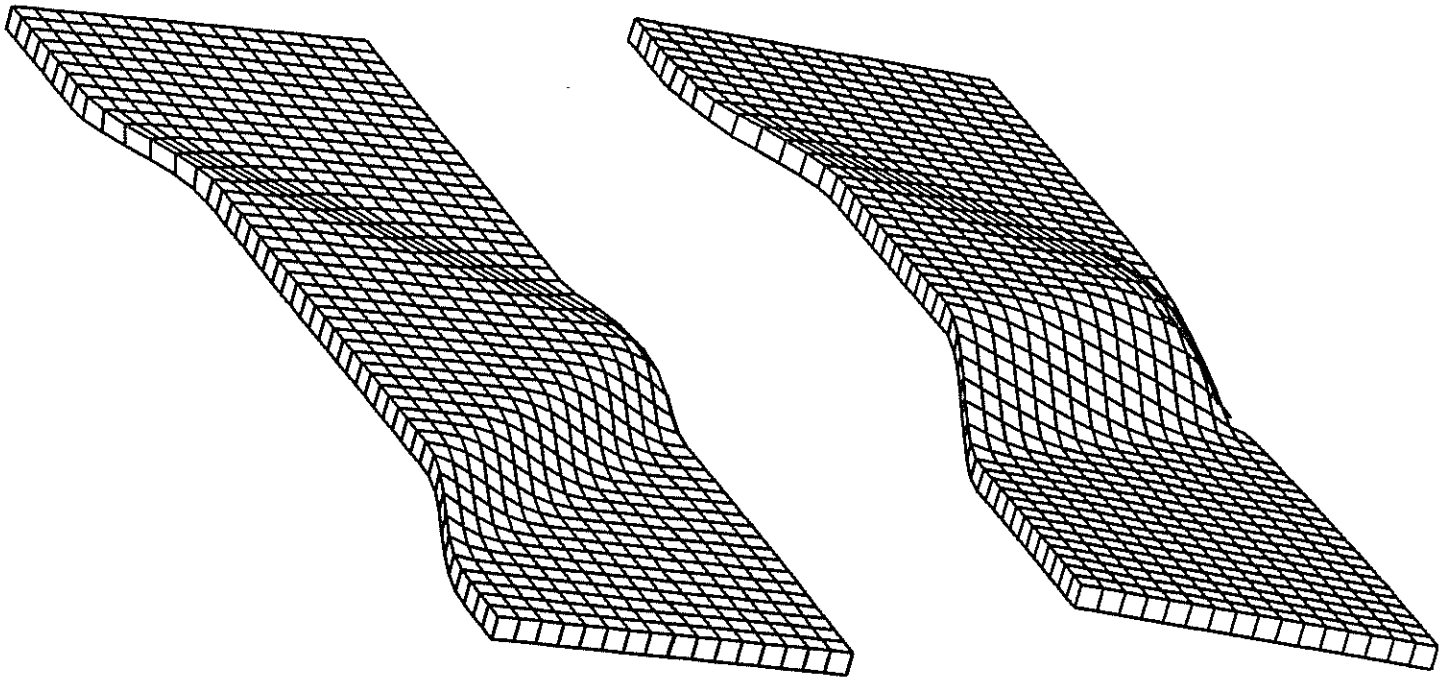

x 40

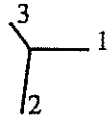

Figure A.50: Deformed states corresponding to figure A.48.

Figure A.51: Influence of latent hardening on localization (h11=1, h12=4). The pictures show the equivalent viscoplastic strain and the amounts of slip for each slip system.

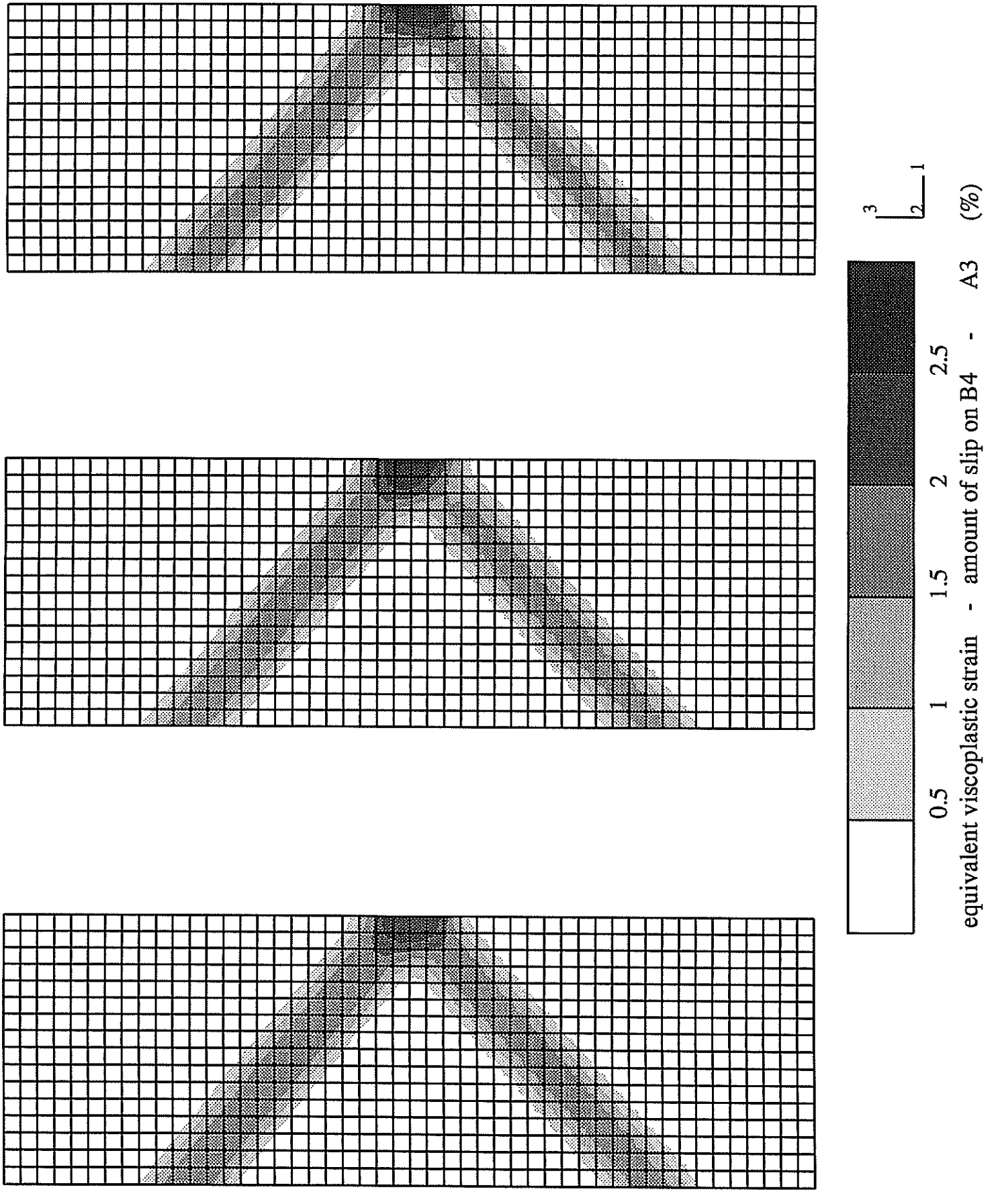

Figure A.52: Influence of latent hardening on localization (h11=1, h12=1)

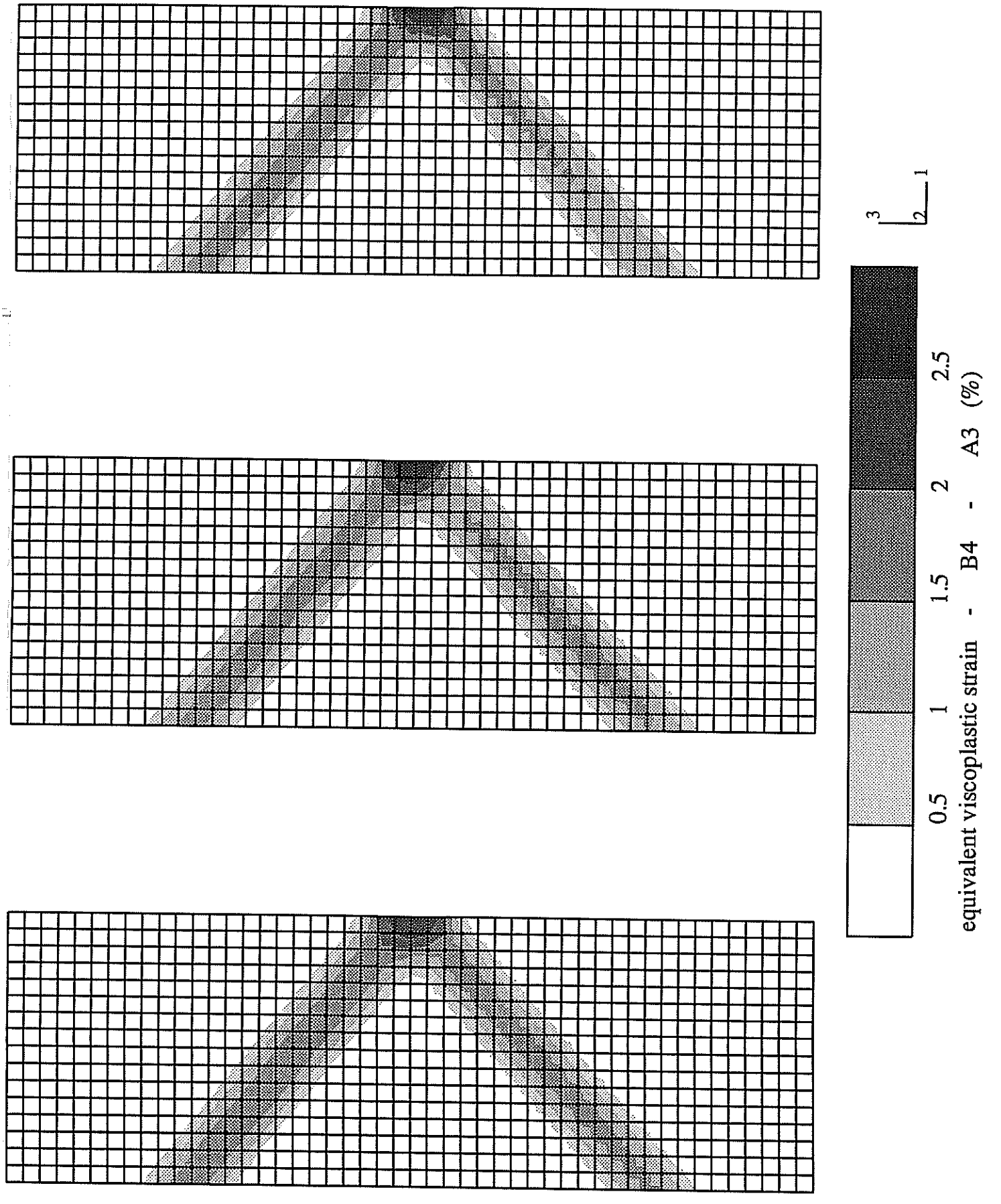

Figure A.53: Influence of latent hardening on localization (h11=2, h12=1)

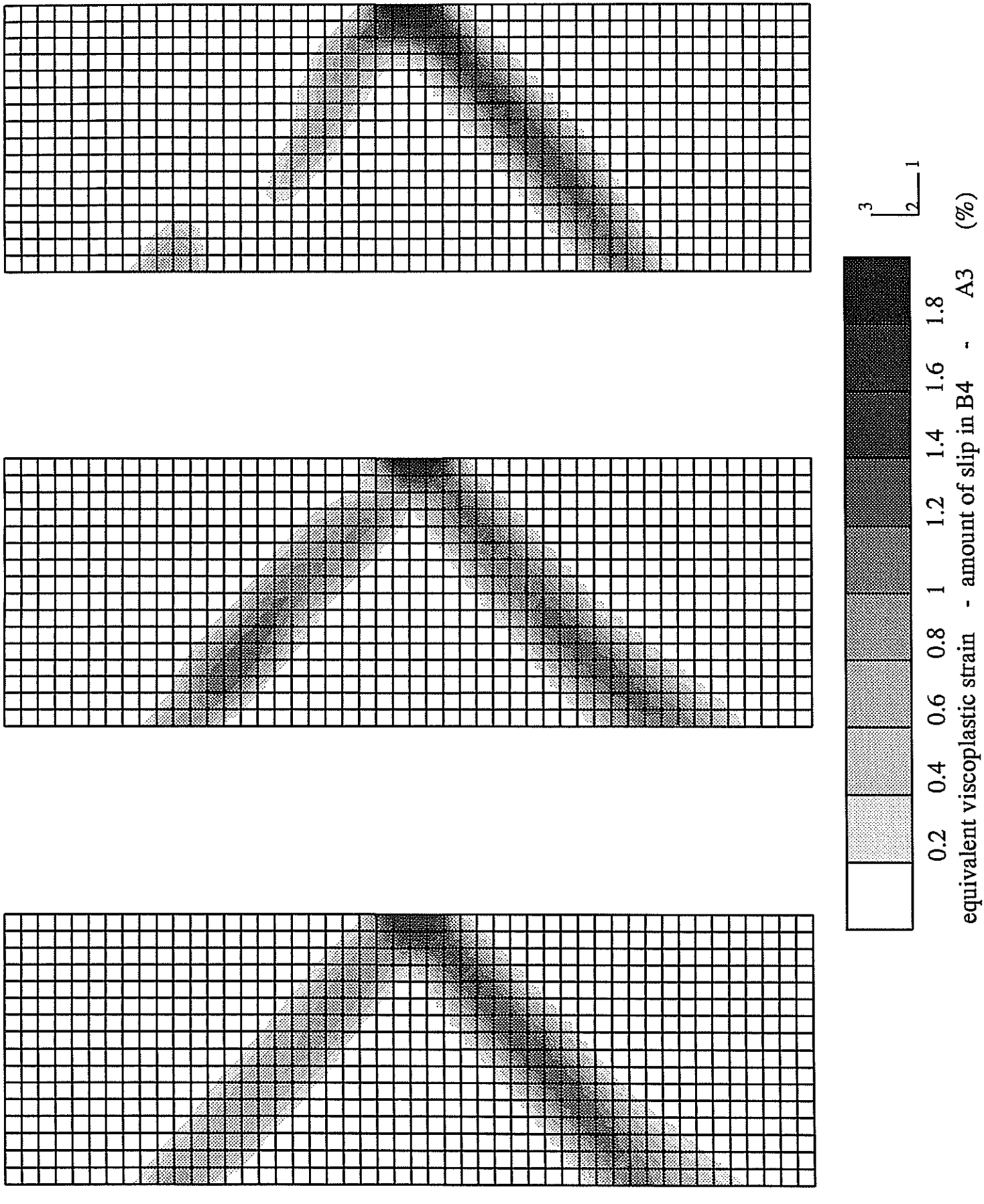

Figure A.54: Influence of latent hardening on localization (h11=4, h12=1)

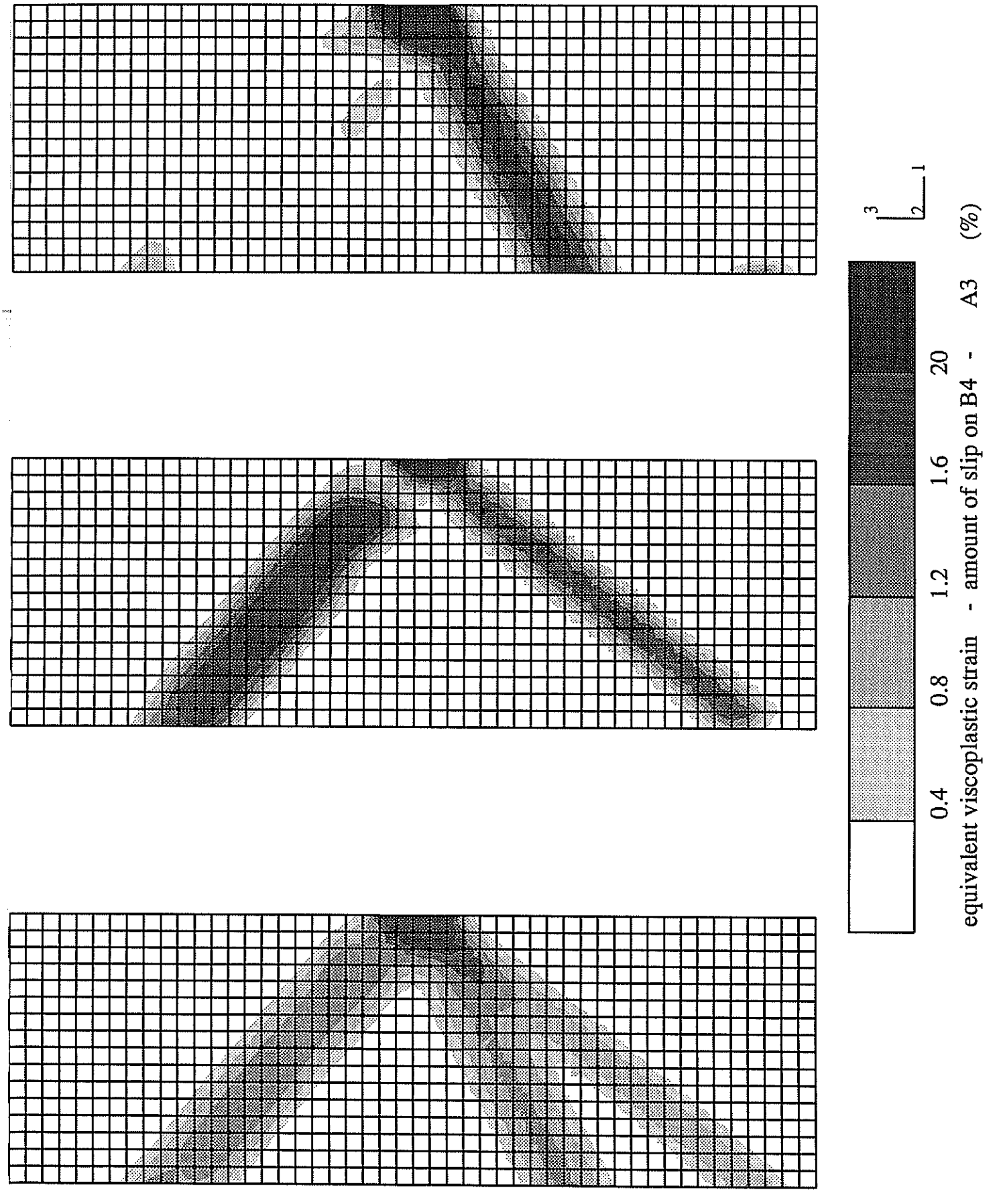

Figure A.55: Influence of latent hardening on localization (h11=1, h12=0)

7 Large strain formulation of the model

7.1 Formulations of constitutive equations at finite strains

7.1.1 Intrinsic description of material behaviour

The scope of this section is limited to the pure mechanical behaviour of simple materials (first-gradient theory). The so-called principle of objectivity states that the form of constitutive equations does not change under Euclidean transformations. Furthermore they cannot depend on a special placement at a given time taken as reference configuration and must also be invariant under superimposed rigid body motion. A now classical method to automatically fulfill the first two requirements has been suggested in [Noll 1972] and further developed in [Rougée 1980], [Krawietz 1986] and [Bertram 1989]. The necessary mathematical tools are those of differential geometry that can be found for instance in [Cartan 1977] and [Berger, Gostiaux 1987]. Within this framework a three-dimensional differential manifold $\mathcal{B}$ models the material body and can be embedded in a given affine Euclidean space frame $\mathcal{E}$ by a placement p:

$$p : \mathcal{B} \longrightarrow \mathcal{E}$$

Then a deformation process can be regarded as a mapping:

$$t \longrightarrow p_t \tag{235}$$

p_t is assumed to be a diffeomorphism. In the first gradient theory, the vicinity of a material point $X \in \mathcal{B}$ is described by the linear tangent space $T_X\mathcal{B}$. The differential or tangent mapping K of p in X is called local placement at X:

$$K : T_X\mathcal{B} \longrightarrow T_{p(X)}E \tag{236}$$

$$K \in L^{inv}(T_X\mathcal{B}, T_{p(X)}E) \tag{237}$$

E being the Euclidean linear space related to $\mathcal{E}$ with metric $g \in L_s^+(E, E^*)$, the set of positive definite symmetric linear mappings from E to its dual E^*. There is no natural internal product in $T_X\mathcal{B}$ but the placement p induces a pull-back of inner product g to the body:

$$u.v = < gKu, Kv >_E = < Gu, v >_{T_X\mathcal{B}} \quad \forall u, v \in T_X\mathcal{B} \tag{238}$$

where

$$G = K^* g K \in L_s^+(T_X\mathcal{B}, T_X\mathcal{B}^*) \tag{239}$$

is called local configuration of $p(X)$ at X or metric tensor at X. This can be summarized as follows:

$$\begin{array}{ccc} T_X\mathcal{B} & \xrightarrow{G} & T_X\mathcal{B}^* \\ {\scriptstyle K}\downarrow & & \uparrow{\scriptstyle K^*} \\ T_{p(X)}(E) \simeq E & \xrightarrow{g} & T_{p(X)}(E)^* \simeq E^* \end{array}$$

An intrinsic stress tensor, denoted S, can be obtained, either totally intrinsically like in [Rougée 1980], or as a pull-pack of the Kirchhoff stress tensor, $T \in L(T_X E^*, T_X E)$ being the Cauchy stress ([Noll 1972]):

$$S = K^{-1}\frac{T}{\rho}K^{-*} \in L(T_X \mathcal{B}^*, T_X \mathcal{B}) \tag{240}$$

ρ being the mass density in the actual placement K. The classical Lagrangian representation can be derived from the intrinsic one if one chooses a reference placement p_0:

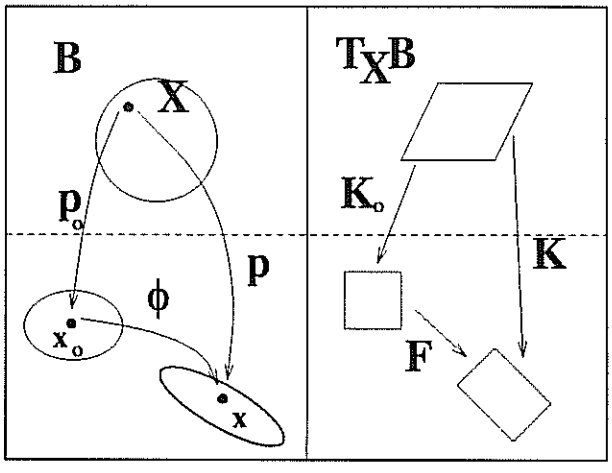

$$F = KK_o^{-1} \tag{241}$$

denotes a change of placement or the classical deformation gradient from the reference to the current configuration. The Eulerian velocity gradient L can be written:

$$L = \dot{F}F^{-1} = \dot{K}K^{-1} \in L(T_{p(X)}E \simeq E) \tag{242}$$

An intrinsic counterpart of the Eulerian stretching rate tensor D can be found:

$$D = \{ L \} = \frac{1}{2}K^{-*}\dot{G}K^{-1} \tag{243}$$

where the braces denote symmetrization.

The major interest of the intrinsic variables S, G and $\dot{G}$ is that they are invariant under change of observer, whereas T, $C = F^T F$ and D are objective tensors. The position of a space frame $\mathcal{E}'$ with respect to $\mathcal{E}$ is given by an isometry associated with a rotation $Q : E' \longrightarrow E$. If $K' = Q^T K$ then $G' = G$ whereas $D' = Q^T D Q$. It means that any relation like

$$S(t) = f(G(t)) \tag{244}$$

between the intrinsic variables automatically fulfills the principle of objectivity.

However the links between $\frac{T}{\rho}$, D and their intrinsic counterparts show that they are uncontested Eulerian tools for the formulation of constitutive equations.

Finally S and $\dot{G}$ are conjugate variables in the expression of the mechanical power per unit mass:

$$j = \frac{1}{2}\mathrm{Tr}\ (S\dot{G}) = \frac{T}{\rho} : D \tag{245}$$

7.1.2 Material derivatives

Relations between G, $\dot{G}$ and S like 244 are sufficient to formulate a large amount of constitutive equations at large strains: elasticity, hyperelasticty and even the behaviour of single crystals according to [Krawietz 1986], [Rougée 1992b] and [Bertram 1993], with of course some additional hidden variables. However most constitutive equations involve incremental evolution equations for the stress tensor (hypoelasticity) or internal variables. It is the case for instance if a tensorial kinematic hardening variable X is introduced. Let Y be an intrinsic variable for which we need an evolution equation (for instance S or X). Y is defined as a pull-back of some Eulerian variable y, like in equation 240:

$$Y = K^{-1}\ y\ g^{-1}\ K^{-*} \quad \text{for } y \in L(E) \tag{246}$$

An evolution equation for Y could have the form:

$$\dot{Y} = f(Y, G, \dot{G}, S) \tag{247}$$

Differentiation of 246 yields

$$K\ \dot{Y}\ K^*\ g\ =\ \dot{y} - Ly - y\ g^{-1}L^*g \tag{248}$$

so that the Eulerian formulation of 247 is

$$\overset{\nabla}{y} = g(y, D, C, T) \tag{249}$$

where

$$\overset{\nabla}{y} = \dot{y} - Ly - yL^T \tag{250}$$

is a classical convective derivative.

Instead of 246 we could have considered the following transport equations:

$$Y_2 = K^*g\ yK \tag{251}$$

$$Y_3 = K^*g\ y\ g^{-1}K^{-*} \tag{252}$$

$$Y_4 = K^{-1}\ y\ K \tag{253}$$

the differentiation of which would have provided the remaining convective derivatives.

The convective derivatives belong to the set of objective derivatives used in Eulerian formulations of constitutive equations at finite strains. Thus only a small class of behaviours can be reached by simply time-differentiating the intrinsic variables introduced in 7.1.1. Some combinations of previous derivatives yield the intrinsic counterparts of other usual objective derivatives, for instance the Jaumann derivative ([Bertram 1994b]):

$$\dot{Y} + (GYG)^{\cdot} = \dot{Y} + \dot{Y}_4 \quad \longrightarrow \quad \overset{\nabla}{y} = \dot{y} - Wy + yW \tag{254}$$

where W is the skew part of L.

Rougée ([1991],[1992],[1994]) enriches the intrinsic representation of materials to develop a more general description of material derivatives. He notices first that the usual identification of Euclidean linear space E with its dual E^* results in an unsymmetrical treatment of Euclidean vectors and tensors: first-order tensors reduce to vectors and second-order tensors to linear mappings on E. He argues that E and E^* should be treated in a rigorous symmetry since both vectors and covectors have a strong geometrical meaning. That is why a Euclidean first-order tensor will be represented by $u = (u_1, u_2) \in E \times E^*$ such that $u_2 = gu_1$ and second-order Euclidean tensors by

$$A = (A_1, A_2) \in (E^* \otimes E^*) \times (E \otimes E) \quad \text{with} \quad A_1 = gA_2g \tag{255}$$

where $E^* \otimes E^* \simeq L(E, E^*)$ and $E \otimes E \simeq L(E^*, E)$.

The four representatives of a Euclidean tensor reduce then to two (and not only one) after a symmetric identification of E and E^*. In that way we have to admit also that the vicinity of $X \in \mathcal{B}$ is described by both $T_X\mathcal{B}$ and $T_X\mathcal{B}^*$. The local metric at X is now equally characterized by

$$G = K^*gK \tag{256}$$

and

$$\check{G} = K^{-1}g^{-1}K^{-*} = G^{-1} \tag{257}$$

Likewise two intrinsic stress tensors are defined:

$$S = K^*g\frac{T}{\rho}K \tag{258}$$

$$\check{S} = K^{-1}\frac{T}{\rho}g^{-1}K^{-*} \tag{259}$$

where we consider $T \in L(E)$.

Let $\mathcal{M}$ be the set of all possible metric states for the vicinity of $X \in \mathcal{B}$ described by $T_X\mathcal{B}$:

$$\mathcal{M} = \{\mathbf{m} = (m, \check{m}) \mid m = \frac{1}{2}G, \check{m} = -\frac{1}{2}G^{-1}, G \in L_s^+(T_X\mathcal{B}, T_X\mathcal{B}^*)\} \tag{260}$$

$\mathcal{M}$ is a six-dimensional differentiable manifold. A deformation process can now be seen as a trajectory of the local metric $\mathbf{m}$ in $\mathcal{M}$. Tangent space $T_m\mathcal{M}$ at a $\mathbf{m} \in \mathcal{M}$ is then obtained by differentiating $m\ \check{m} = -\frac{1}{4}1_{T_X\mathcal{B}}$:

$$T_m\mathcal{M} = \{\mathbf{dm} = (dm, d\check{m}) \in L_s(T_X\mathcal{B}, T_X\mathcal{B}^*) \times L_s(T_X\mathcal{B}^*, T_X\mathcal{B}) \mid \tag{261}$$

$$dm\ \check{m} + m\ d\check{m} = 0 \Leftrightarrow dm\ = G\ d\check{m}\ G\} \tag{262}$$

According to equation 255 it appears that $T_m\mathcal{M}$ is the set of second-order symmetric Euclidean tensors on the Euclidean space $T_X^m\mathcal{B}$ obtained by endowing $T_X\mathcal{B}$ with the metric m ([Rougée 1994]). Consequently

$$\dot{\mathbf{m}} = (\frac{1}{2}\dot{G}, -\frac{1}{2}(G^{-1})^{\cdot}) \in T_m\mathcal{M} \tag{263}$$

and

$$\mathbf{S} = (S, \check{S}) \in T_m\mathcal{M} \tag{264}$$

Notice that

$$j = \mathbf{S} : \dot{\mathbf{m}} = tr\ (S\check{\dot{m}}) = tr\ (\check{S}\dot{m}) = \frac{T}{\rho} : D \tag{265}$$

At this point one can understand why problems arise when we want to derive for instance $\mathbf{S}$. For $T_m\mathcal{M}$ is time-dependent since m varies: the variation $\mathbf{S}(t+dt) - \mathbf{S}(t)$ has no sense because $T_{m(t)}\mathcal{M} \neq T_{m(t+dt)}\mathcal{M}$. $\mathbf{S}$ cannot be simply derived: there is not one unique derivative on $T_m\mathcal{M}$. It is necessary to define and choose a derivative law. In some cases the choice must be physically motivated.

A simple way to obtain derivative laws consists in following the motion of $T_m\mathcal{M}$ from a constant space frame using transport rules. Let us consider such a space frame $\mathcal{E}'$ and the mapping:

$$\mathcal{A} : \mathbf{m} \in \mathcal{M} \longrightarrow (K'^{-*}\ m\ K'^{-1}, K'\ \check{m}\ K'^{*}) \tag{266}$$

where K' is the local placement of X in $\mathcal{E}'$, and

$$A = \mathcal{A}'(\mathbf{m}) : T_mM \longrightarrow \left(E' \otimes E'\right) \times \left(E'^{*} \otimes E'^{*}\right) \tag{267}$$

$$(dm, d\check{m}) \longrightarrow (K'^{-*}\ dm\ K'^{-1}, K'\ d\check{m}\ K'^{*}) \tag{268}$$

A induces transport rules from $T_m\mathcal{M}$ into the set of Euclidean second-order tensors in E'. In particular, for $E' = E$,

$$A(\dot{\mathbf{m}}) = (gD, Dg^{-1}) = \mathbf{D} \tag{269}$$

$$A(\mathbf{S}) = (g\frac{T}{\rho}, \frac{T}{\rho}g^{-1}) = \frac{\mathbf{T}}{\rho} \tag{270}$$

It is interesting to notice that A is an isometry so that eigenelements are conserved: eigenvalues of $\mu \in T_m\mathcal{M}$ and $A(\mu)$ are equal and eigenvectors homologous ([Rougée 1991]). At each instant t we can define the transport A_t of $T_m\mathcal{M}$ in space frame $\mathcal{E}'$ and then a derivative law $\dfrac{\nabla}{dt}$ on $T_m\mathcal{M}$ with respect to this space frame:

$$\frac{\nabla}{dt}Y = \lim_{dt \to 0} \frac{(Y(t+dt) - A_{t+dt}^{-1}\ A_t\ Y(t))}{dt} \tag{271}$$

It seems that we have no other choice for a material derivative than the derivative relative to a chosen space frame. These derivatives are called rotational derivatives and are strongly recommended in [Dogui 1989].

7.1.3 Extension of models developed at small strains

Rotational derivatives provide a systematic method for the extension of constitutive equations developed at small strains to the framework of finite deformation. Let us consider for example the following set of constitutive equations in elastoplasticity or elastoviscoplasticity:

$$\begin{cases} \dot{\underset{\sim}{\varepsilon}} = \dot{\underset{\sim}{\varepsilon}}^e + \dot{\underset{\sim}{\varepsilon}}^p \\ \dot{\underset{\sim}{\varepsilon}}^p = f(\underset{\sim}{\sigma}, \underset{\sim}{\alpha}) \\ \underset{\sim}{\sigma} = \underset{\sim}{\mathbf{C}}\ \underset{\sim}{\varepsilon}^e \\ \dot{\underset{\sim}{\alpha}} = h(\alpha, \dot{\underset{\sim}{\varepsilon}}^p) \end{cases} \tag{272}$$

where $\underset{\sim}{\alpha}$ denotes internal variables. We have seen that at large strains the relevant Eulerian variables are $\underset{\sim}{\mathbf{D}}$ and $\frac{\underset{\sim}{\mathbf{T}}}{\rho}$ in space frame E. Considering now another space frame E',

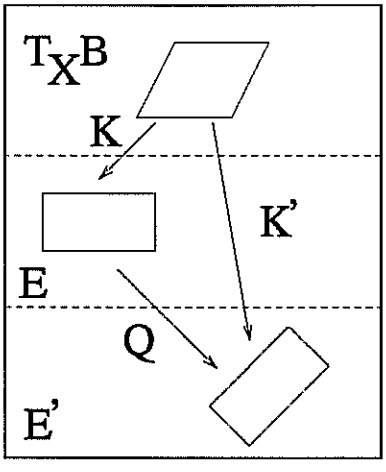

the position of which with respect to E is described by the time-dependent rotation $\underset{\sim}{\mathbf{Q}}$, the use of transport rules yields:

$$\dot{\underset{\sim}{\mathbf{e}}} = \underset{\sim}{\mathbf{Q}}^T\ \underset{\sim}{\mathbf{D}}\ \underset{\sim}{\mathbf{Q}} \tag{273}$$

$$\underset{\sim}{\mathbf{S}} = \underset{\sim}{\mathbf{Q}}^T\ \frac{\rho_0}{\rho}\underset{\sim}{\mathbf{T}}\ \underset{\sim}{\mathbf{Q}} \tag{274}$$

It appears that $\dot{\underset{\sim}{\mathbf{e}}}$ and $\underset{\sim}{\mathbf{S}}$ are invariant tensors under any further change of observer since $\underset{\sim}{\mathbf{D}}$ and $\underset{\sim}{\mathbf{T}}$ are objective, so that any relation between $\dot{\underset{\sim}{\mathbf{e}}}$ and $\underset{\sim}{\mathbf{S}}$ identically satisfies the principle of objectivity. The only prerequisite for the choice of this relation is the respect of material symmetries.

We may then extend the additive partition of elastic and viscoplastic strain rates:

$$\begin{cases} \dot{\underset{\sim}{\mathbf{e}}} = \dot{\underset{\sim}{\mathbf{e}}}^e + \dot{\underset{\sim}{\mathbf{e}}}^p \\ \dot{\underset{\sim}{\mathbf{e}}}^p = f(\underset{\sim}{\mathbf{S}}, \underset{\sim}{\alpha}) \\ \underset{\sim}{\mathbf{S}} = \underset{\sim}{\mathbf{C}}\ \underset{\sim}{\mathbf{e}}^e \\ \dot{\underset{\sim}{\alpha}} = h(\alpha, \dot{\underset{\sim}{\mathbf{e}}}^p) \end{cases} \tag{275}$$

The internal variables are here defined in the rotating frame and can then be pulled-back in E. This method has been proposed in [Ladevèze 1980].

7.1.4 Choice of the rotating frame

Rougée [1991] shows that a canonical material derivative can be derived from the structure of manifold $\mathcal{M}$ defined in 1.2. The scalar product in $T_m\mathcal{M}$ makes $\mathcal{M}$ a Riemannian manifold with metric tensor

$$ds^2 = \mathbf{dm} \ : \ \mathbf{dm} = \mathrm{Tr} \ (dm \ d\check{m}) \tag{276}$$

The length of the trajectory of $\mathbf{m}$ is equal to the classical cumulated strain $\int_{t1}^{t2} \|\underset{\sim}{\mathbf{D}}\| \ dt$ where $\|\underset{\sim}{\mathbf{D}}\| = \sqrt{\dot{\mathbf{m}} \ : \ \dot{\mathbf{m}}} = \sqrt{\underset{\sim}{\mathbf{D}} \ : \ \underset{\sim}{\mathbf{D}}}$.

Derivatives of tensor fields on a Riemannian manifold are then associated with parallel transports along a given curve on $\mathcal{M}$ ([Lehmann, Sacré 1982]). They are called covariant derivatives. The unique parallel transport without glide nor torsion gives the canonical Levi-Civita connexion. The scalar product is conserved during this transport. For $\mu \in T_m\mathcal{M}$ it yields $\nabla_{dm} \ \mu$ characterized by:

$$\nabla_{dm} \ \mu = \ d\mu \ + \ 2(dm \ \check{m}\mu \ + \ \mu \ \check{m} \ dm) \tag{277}$$

Using then the transport rule 268, one obtains

$$\underset{\sim}{\mu} = A(\mu) \Rightarrow A(\nabla_{dm} \ \mu) = \underset{\sim}{\mu}^J = \dot{\underset{\sim}{\mu}} \ + \ \underset{\sim}{\mu}\underset{\sim}{\mathbf{W}} \ - \underset{\sim}{\mathbf{W}}\underset{\sim}{\mu} \tag{278}$$

where $\underset{\sim}{\mathbf{W}}$ is the skew-symmetric part of the velocity gradient.

The Eulerian image of the canonical covariant derivative is thus the classical Jaumann derivative ([Rougée 1991]).

Furthermore the covariant derivative corresponds to the derivative with respect to a rotating frame called corotational frame. We introduce it still using intrinsic tools:

Proposition: $\forall X \in \mathcal{B}$, there is a unique space frame E_c and a unique local placement $K \in L_s(T_X\mathcal{B}, E_c)$ such that $L = \dot{K}K^{-1}$ is symmetric.

We want to call K corotational local placement or material placement K_c:

$$L_c = \dot{K}_c \ K_c^{-1} \in L_s(E_c) \tag{279}$$

It is not assumed that a global placement associated to local placements K_c should exist. Let K and K' be local placements of X respectively in space frame $(\mathcal{E}, E, g)$ and $(\mathcal{E}', E', g)$. E and E' are linked by rotation $Q(t)$ such that for instance $K' = Q^T K$. We have then:

$$L' = \dot{K}' \ K'^{-1} = \dot{Q}^T Q \ + \ Q^T L Q \tag{280}$$

so that,

$$L' \in L_s(E'_c) \Leftrightarrow \dot{Q}Q^T \ = \ W \tag{281}$$

Space frame E_c defined by Q_c solution of 281 with initial value $Q(0) = \underset{\sim}{1}$ for instance, is the corotational frame and $K_c = Q_c^T K$ the associated local placement. It can be shown that E_c and K_c do not depend on initial space frame E.

Considering now $\mu \in T_m\mathcal{M}$ and A_c the isomorphism between $T_m\mathcal{M}$ and $L_s(E_c)$, we have

$$\underset{\sim}{\mu} = A(\mu) \Rightarrow A_c(\frac{\nabla_{dm}\ \mu}{dt}) = \dot{\underset{\sim}{\mu}} \tag{282}$$

When convected into the corotational frame, the covariant derivative reduces to simple time-derivative, which makes the development of evolution equations much easier.

7.1.5 The corotational frame: the pros and the cons

Rotation of material fibers The physical meaning of the corotational frame becomes clear when one considers the simple shear test that has been extensively studied in [Dogui, Sidoroff 1986].

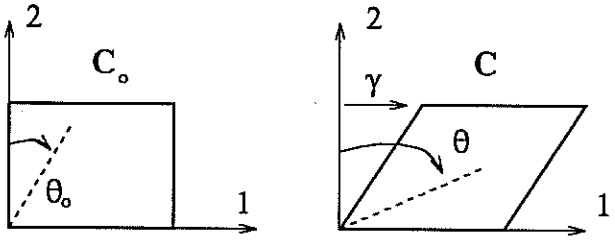

Let $\underline{dx}$ be a material segment drawn on the specimen, θ_0 and θ being respectively the initial and current orientations with respect to a fixed axis. The relation between θ_0, θ and the amount of shear γ is

$$\tan\theta = \tan\theta_0 + \gamma \tag{283}$$

and the rate of rotation of this material segment is

$$\dot{\theta} = \frac{\dot{\gamma}}{1 + (\tan\theta_0 + \gamma)^2} \tag{284}$$

It is of the utmost importance to notice that, whereas the deformation gradient

$$\underset{\sim}{\mathbf{F}} = \underset{\sim}{\mathbf{1}} + \gamma \underline{\mathbf{e}}_1 \otimes \underline{\mathbf{e}}_2 \tag{285}$$

is a homogeneous tensor field for simple shear, the rotation rates of material fibers are not homogeneous: $\underline{dx}_{|\theta_0=\pi/2}$ does not rotate whereas $\underline{dx}_{|\theta_0=0}$ undergoes the maximal rotation rate. Two mean values can be derived:

$$< \dot{\theta}_L >= \frac{\dot{\gamma}}{\pi} \int_{-\pi/2}^{\pi/2} \frac{1}{1 + (\tan\theta_0 + \gamma)^2}\, d\theta_0 = \frac{\dot{\gamma}}{2(1 + \frac{\gamma^2}{4})} \tag{286}$$

when C_0 is taken as reference configuration and

$$< \dot{\theta}_e >= \frac{\dot{\gamma}}{\pi} \int_{-\pi/2}^{\pi/2} \frac{1}{1 + \tan^2\theta}\, d\theta = \frac{\dot{\gamma}}{2} \tag{287}$$

when the current configuration is taken as reference configuration (updated Lagrangian, $\theta_0 \to \theta$ when $\gamma \to 0$). We will refer to these mean values respectively as Lagrangian and Eulerian mean rotation rates. At constant shear rate, the Lagrangian rotation rate vanishes with ever increasing shearing whereas the Eulerian one remains constant.

It can be shown that $< \dot{\theta}_L >$ is the rotation rate of the space frame associated with the rotation tensor in the polar decomposition of $\underset{\sim}{\mathbf{F}}$ for simple shear. The definition of this eigenrotational frame then requires the choice of a reference configuration. In contrast $< \dot{\theta}_e >$ is exactly the rotation rate of corotational frame E_c. θ_L reaches the limit $\pi/2$, while θ_e grows to infinity (figure 56).

Thus we can now say that the eigenrotational frame follows at best material fibers in a Lagrangian sense, that is with respect to a fixed reference configuration. In contrast, the corotational space frame follows at best material segments at each instant since its instantaneous rotation rate is exactly the mean value of all rotation rates in the specimen. Because of the non-homogeneous nature of rotations during a shear test, none of these space frames is entirely satisfactory. However its intrinsic definition (it depends on no reference configuration) and its physical meaning lead us to favour the corotational frame. We lay the stress on the fact that the corotational frame follows at best at a given time strain gauges that are laid on a specimen for testing. Consequently when such measurements are the only way to access to the material behaviour, we claim that an efficient and trustful inductive method for developing constitutive equations consists in infering them directly in the corotational frame.

Oscillations or not? One usually puts forward objections to the use of Jaumann rate or the corotational frame because it can induce an oscillatory behaviour. For, the endless rotation of E_c during a simple shear test makes a periodic mechanical response possible. We show here that oscillations can actually occur in elasticity, elastoplasticity and elastoviscoplasticity but that in the last two cases they disappear for usual values of hardening parameters for metals.

In figure 57 we compare stress-strain curves in the case of simple shear for the following elastic and hypoelastic formulations of isotropic elasticity:

Lagrangian formulation

$$\underset{\sim}{\mathbf{\Pi}} = 2\mu\ \underset{\sim}{\mathbf{E}} + \lambda \mathrm{Tr}\, \underset{\sim}{\mathbf{E}}\ \underset{\sim}{\mathbf{1}} \tag{288}$$

$\underset{\sim}{\mathbf{\Pi}}$ and $\underset{\sim}{\mathbf{E}}$ are the second Piola-Kirchhoff stress tensor and the Green-Lagrange strain tensor respectively. The intrinsic formulation 244 has the Lagrangian form $\underset{\sim}{\mathbf{\Pi}} = f(\underset{\sim}{\mathbf{C}})$.

Eulerian formulation

$$\underset{\sim}{\mathbf{T}} = 2\mu\ \ln \underset{\sim}{\mathbf{V}} + \lambda\ \mathrm{Tr}\,(\ln \underset{\sim}{\mathbf{V}})\ \underset{\sim}{\mathbf{1}} \tag{289}$$

$\underset{\sim}{\mathbf{V}}$ appears in the polar decomposition $\underset{\sim}{\mathbf{F}} = \underset{\sim}{\mathbf{V}}\underset{\sim}{\mathbf{R}}$.

Formulations within rotational frames

$$\underset{\sim}{\mathbf{S}} = 2\mu\ \underset{\sim}{\mathbf{e}} + \lambda \mathrm{Tr}\, \underset{\sim}{\mathbf{e}}\ \underset{\sim}{\mathbf{1}} \tag{290}$$

where $\underset{\sim}{\mathbf{S}}$ and $\underset{\sim}{\mathbf{e}}$ are given by equations 273 and 274; we take successively

$$\underset{\sim}{\mathbf{Q}} = \underset{\sim}{\mathbf{Q}}_c \quad \text{(corotational frame)} \tag{291}$$

$$\underset{\sim}{\mathbf{Q}} = \underset{\sim}{\mathbf{R}} \quad \text{(eigenrotational frame)} \tag{292}$$

The use of the corotational frame induces oscillations of the shear stress with period $\gamma = 2\pi$. We will not concentrate on this point since we are here interested only in metals with small elastic deformations.

In the rigid plastic case we consider isotropic and kinematical hardening variables, and the governing equations are written in the corotational frame:

yield function

$$f(\underset{\sim}{\mathbf{S}}, R, \underset{\sim}{\mathbf{X}}) = J_2(\underset{\sim}{\mathbf{S}} - \underset{\sim}{\mathbf{X}}) - R \tag{293}$$

where

$$\dot{p} = \sqrt{\frac{2}{3}\,\underset{\sim}{\mathbf{D}} : \underset{\sim}{\mathbf{D}}} \quad J_2(\underset{\sim}{\mathbf{S}} - \underset{\sim}{\mathbf{X}}) = \sqrt{\frac{3}{2}\,(\underset{\sim}{\mathbf{S}}^{dev} - \underset{\sim}{\mathbf{X}}) : (\underset{\sim}{\mathbf{S}}^{dev} - \underset{\sim}{\mathbf{X}})} \tag{294}$$

flow rule

$$\underset{\sim}{\mathbf{D}} = \dot{p}\,\frac{\partial f}{\partial \underset{\sim}{\mathbf{S}}} \tag{295}$$

evolution equation

$$\dot{\underset{\sim}{\mathbf{X}}} = \frac{2}{3}\,C\,\underset{\sim}{\mathbf{D}} - D\,\dot{p}\,\underset{\sim}{\mathbf{X}} \tag{296}$$

For simple shear we find

$$\begin{cases} T_{11} = -T_{22} = \dfrac{C}{D^2+3}(1 - \exp(-\dfrac{D}{\sqrt{3}}\gamma)(\cos\gamma + \dfrac{D}{\sqrt{3}}\sin\gamma)) \\ T_{12} = \dfrac{C}{3}\exp(-\dfrac{D}{\sqrt{3}}\gamma)\sin\gamma + \dfrac{DC}{\sqrt{3}(D^2+3)}(1 - \exp(-\dfrac{D}{\sqrt{3}}\gamma)(\cos\gamma + \dfrac{D}{\sqrt{3}}\sin\gamma)) + \dfrac{R}{\sqrt{3}} \end{cases} \tag{297}$$

It proves that isotropic hardening does not induce any oscillation. In contrast linear kinematical hardening is associated with oscillations of period $\gamma = 2\pi$, that are damped or even precluded (aperiodic response) as soon as a small non-linear component exists (figure 58). Other analytical results for simple shear using rotating frames can also be found in [Dafalias 1983].

When elasticity is introduced oscillations may occur for isotropic hardening the period of which decreases when H/μ increases (H hardening modulus, μ shear modulus). For usual values of H/μ they are unnoticeable (figure 59).

As a conclusion the modelling of elastoplastic or elastoviscoplastic behaviour of metals requires isotropic hardening and non-linear kinematical hardening, so that oscillations will simply not occur.

7.2 Description of finite inelastic deformation of single crystals

When the microstructure of the material can be taken into account in the formulation of constitutive equations, one could think that the previous framework is not relevant any more and that the corotational frame should be abandonned in order to take full advantage of available microstructural information. In some cases when for instance deformation proceeds according to a precise and limited physical mechanism, it may be true. In contrast we propose here that the corotational frame gives us an ideal point of view from which the microstructure evolution can be observed and measured. For that

purpose we consider two levels in the modelling: the material level represented by material fibers that can be followed within the corotational frame and the microstructural level the evolution of which is measured with respect to the first one. We apply first this program to single crystal modelling at large strains.

7.2.1 Description of finite inelastic deformation of single crystals using rotating frames

Body $\mathcal{B}$ has now at each material point X a microstructure represented by a trihedron of vectors $< 100 >$ in the tangent space $T_X\mathcal{B}$ corresponding to lattice directions. We introduce three local placements of $\mathcal{B}$ at X: the first in the space frame E of the current observer, the second in the corotational frame E_c and the third in the space frame $E_\sharp$ associated with the microstructure.

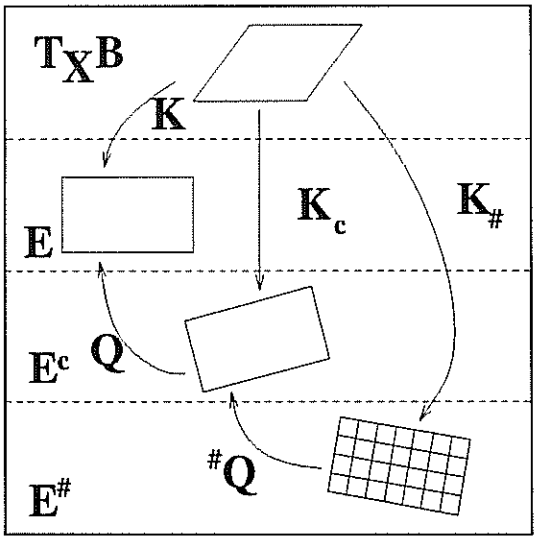

The position of $E^\sharp$ with respect to other space frames can be known at each instant by a physical experiment like X-ray diffraction. K, K_c and $K_\sharp$ are these respective placements in E, E^c and $E^\sharp$. Rotation ${}^c\underset{\sim}{Q}$ relates E^c to E, and ${}^\sharp\underset{\sim}{Q}$, $E^\sharp$ to E^c:

$$\underset{\sim}{L} = \underset{\sim}{D} + \underset{\sim}{W} \tag{298}$$

$${}^c\underset{\sim}{L} = {}^c\underset{\sim}{D} \tag{299}$$

$${}^c\dot{\underset{\sim}{Q}}\ {}^c\underset{\sim}{Q}^T = \underset{\sim}{W} \tag{300}$$

As a generalization of constitutive equations developed at small strains, we chose an additive decomposition of elastic and plastic strain rates:

$${}^c\underset{\sim}{D} = \dot{\underset{\sim}{e}}^e + \dot{\underset{\sim}{e}}^v \tag{301}$$

where $\dot{\underset{\sim}{e}}^v$ denotes the viscoplastic strain rate. Further justifications for this partition will be given in 7.2.2.

Assuming that viscoplastic deformation proceeds through collective glide of dislocations on particular slip planes, we have:

$$\dot{\underset{\sim}{e}}^v = \sum_s \dot{\gamma}^s \{ {}^c\underline{m}^s \otimes {}^c\underline{z}^s \} \tag{302}$$

where ${}^c\underline{\mathbf{m}}^s$ is the slip direction and ${}^c\underline{\mathbf{n}}^s$ the normal to the slip plane in E^c.

The corotational space frame is such that the instantaneous rotation rate vanishes:

$$ {}^c\underset{\sim}{\mathbf{W}} = {}^c\underset{\sim}{\mathbf{W}}^e + {}^c\underset{\sim}{\mathbf{W}}^v = 0 \tag{303} $$

where

$$ {}^c\underset{\sim}{\mathbf{W}}^v = \sum_s \dot{\gamma}^s \, \} \, {}^c\underline{\mathbf{m}}^s \otimes {}^c\underline{\mathbf{z}}^s \{ \tag{304} $$

and

$$ {}^c\underset{\sim}{\mathbf{W}}^e = {}^{\sharp}\dot{\underset{\sim}{\mathbf{Q}}} \, {}^{\sharp}\underset{\sim}{\mathbf{Q}}^T \tag{305} $$

being the lattice rotation rate. Crystallographic directions ${}^{\sharp}\underline{\mathbf{m}}^s$ and ${}^{\sharp}\underline{\mathbf{z}}^s$ are known and:

$$ {}^c\underline{\mathbf{m}}^s = {}^{\sharp}\underset{\sim}{\mathbf{Q}} \, {}^{\sharp}\underline{\mathbf{m}}^s \qquad {}^c\underline{\mathbf{z}}^s = {}^{\sharp}\underset{\sim}{\mathbf{Q}} \, {}^{\sharp}\underline{\mathbf{z}}^s \tag{306} $$

Finally we take the following linear elastic law:

$$ \underset{\sim}{\mathbf{S}} = \underset{\sim\sim}{\mathbf{C}} : \underset{\sim}{\mathbf{e}}^e \tag{307} $$

where the components of the elasticity tensor can be easily expressed with respect to material symmetry axes in $E^{\sharp}$.

This model can also be regarded as the extension of the model for single crystals at small strains and small lattice rotations. A similar approach in the case of polycrystals at finite deformation is proposed in Appendix 2.

7.2.2 Other formulations of crystal plasticity

Intrinsic formulations

Firstly we present the description of crystal kinematics developed in [Krawietz 1986] and [Rougée 1992] because it is the intrinsic counterpart of the classical model used in crystal plasticity during the two past decades. They introduce a lattice space T_s with lattice basis $\{g^s_\alpha\}$ and the mapping

$$ \aleph : \; T_X\mathcal{B} \longrightarrow T_s $$

such that $\aleph^{-1} g^s_\alpha$ gives the position of a lattice vector with respect to material directions on $\mathcal{B}$. Its position in Euclidean space is known as soon as a local placement K is introduced, through

$$ K_s = K\aleph^{-1} \in L^{inv}(T_s, E). $$

As in 7.1.2., we consider the metric $\mathbf{m} \in \mathcal{M}$ induced by the placement, a representation of which is

$$ m = \frac{1}{2} \, K^* \, g \, K \tag{308} $$

The mapping $\aleph$ induces also a metric m_s for the microstructure, an element of the space $\mathcal{M}_s$ of all possible metrics for the lattice:

$$ m_s = \aleph^{-*} \, m \, \aleph^{-1} = \frac{1}{2} \, K_s^* \, g \, K_s. \tag{309} $$

If m_{si} describes a released state of the lattice, we see that the motion of m_s on $\mathcal{M}_s$ represents the lattice distorsion and thus the elastic part of deformation. Relation $K = K_s \aleph$ can then be interpreted as a multiplicative decomposition of deformation in elastic and inelastic parts.

$$D^e = \dot{m}_s \tag{310}$$

denotes the elastic strain rate and

$$\dot{m}_s = \aleph^{-*} \dot{m} \aleph^{-1} - ((\dot{\aleph}\aleph^{-1})^* m_s + m_s \dot{\aleph}\aleph^{-1}) \tag{311}$$

i.e.

$$D^e = D - D^p \tag{312}$$

which yields an additive decomposition of deformation rates.

The kinematics of plastic deformation is given by

$$\dot{\aleph}\aleph^{-1} = \sum_g \dot{\gamma}^g m^g \otimes z^g \tag{313}$$

where $m^g \in T_s$ and $z^g \in T_s^*$. It must be noticed that $\dot{\aleph}$ is not a total differential as soon as more than one slip system is involved.

The norm of m^g and z^g are known only in an unloaded local configuration G_{si} (local placement K_{si}) whereby:

$$< m^g, G_{si}\, m^g > = \|m^g\|^2 = 1 \tag{314}$$

$$< z^g, G_{si}\, z^g > = \|z^g\|^2 = 1 \tag{315}$$

The introduction of an unloaded configuration G_{si} and of a reference local placement K_0 bridges the gap between this intrinsic formulation and the now classical description of crystal plasticity in [Mandel 1971] until [Asaro 1983], that involves a multiplicative decomposition of deformation according to

$$\underset{\sim}{\mathbf{F}} = \underset{\sim}{\mathbf{E}}\, \underset{\sim}{\mathbf{P}} \tag{316}$$

where

$$\underset{\sim}{\mathbf{F}} = K\, K_0^{-1} \tag{317}$$

$$\underset{\sim}{\mathbf{P}} = K_{si}\, \aleph\, K_0^{-1} \tag{318}$$

$$\underset{\sim}{\mathbf{E}} = K_s\, K_{si}^{-1} \tag{319}$$

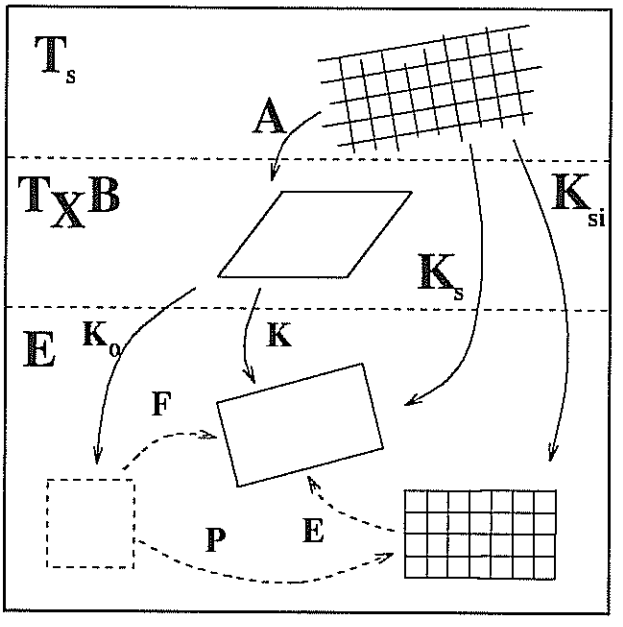

The model for single crystals proposed in [Bertram 1993] illuminates the role played by the unstressed configuration. It does not make use of a separate microstructure space T_s. Instead, an elastic range E_t, a set of local configurations, and an elastic law h_t are attached to each $X \in \mathcal{M}$ at each instant t, so that the stress is determined by

$$S = h_t(G) \quad \forall G \in E_t \tag{320}$$

The elastic ranges are linked together by a linear invertible mapping such that

$$\forall E_t, E_{t'} \quad \exists B \in L^{inv}(T_X B), \quad h_t(B^{-*} G_{t'} B^{-1}) = B h_{t'}(G_{t'}) B^* \quad \forall G_{t'} \in E_{t'} \tag{321}$$

B transforms the elastic behaviour from one elastic range to another and therefore corresponds to the inelastic deformation [Bertram 1992]. Now the elastic behaviour is entirely determined by an elastic law of one arbitrary elastic range E_0, and the material isomorphisms B between E_0 and the other elastic ranges. For a linear anisotropic elastic law,

$$S(t) = \underset{\approx}{C}_t (G_t - G_{0t}) \tag{322}$$

where G_{0t} is the stress-free configuration. $G_t - G_{0t}$ is the elastic deformation.

The use of an unstressed configuration is useful for two purposes: firstly, the expression of the elastic law and secondly, to fix a condition on the norms of the lattice directions. As pointed out by Mandel [1983], this configuration does not need to be stress-free, it must be an undistorted configuration (this expression is used by Bertram [1994a]) that respects all material symmetries.

The local unloaded configuration has two main characteristics. There is not necessarily a global placement associated with it: this released state may be obtained only locally. Furthermore G_{ot} does not necessarily belong to E_t. It means that the elastic law h_{0t} is extrapolated beyond the yield surface so that the released state may have no physical existence even locally, in case of a strong Bauschinger effect for instance. One assumes also that the stress-free state is reached so rapidly that no viscous effect occurs during the unloading of a viscoplastic material.

Equivalence between the various formulations

We have already considered that Krawietz's and Rougée's models are identical. That is why we have given a common presentation. The equivalence with Bertram's model can be seen if we consider the isomorphism B_{0t} between the two elastic ranges E_t and E_0. Let $\underline{t}_0$ be a crystallographic direction at instant 0:

$$\underline{t}_t = B_{0t}(\underline{t}_0) \tag{323}$$

is the same crystallographic direction at instant t. A similar relation exists in the first model:

$$\underline{t}_t = \aleph_t^{-1}\aleph_0(\underline{t}_0) \tag{324}$$

where $\aleph$ denotes the time-dependent mapping from $T_X\mathcal{B}$ into the lattice space. This establishes the equivalence of the two models and thus with Mandel's model also.

The formulation that we have proposed in 7.2.1. is also closely related to Mandel's model. The advantage that it shares with the intrinsic formulations is that no intermediate configuration is introduced. Instead we describe the current state of the crystal from three different points of view. For that purpose we are in fact using the concept of director frame presented in [Mandel 1971]. In the case of the single crystal the director frame coincides with $E_\sharp$. The director frame has also a thermodynamical meaning: in this space frame the states variables are a strain measure, the internal variables and temperature, any other geometrical variable being excluded [Mandel 1983]. It appears also that for us the configuration $G_\sharp = K_\sharp^* K_\sharp$ is an undistorted configuration in which all crystallographic symmetries are still respected. According to equations 298 to 305, we have on one hand

$$\begin{aligned}
\underset{\sim}{\mathbf{L}} &= {}^c\dot{\underset{\sim}{\mathbf{Q}}}\,{}^c\underset{\sim}{\mathbf{Q}}^T + {}^c\underset{\sim}{\mathbf{Q}}\dot{\underset{\sim}{\mathbf{e}}}\,{}^c\underset{\sim}{\mathbf{Q}}^T \\
&= \dot{\underset{\sim}{\mathbf{R}}}\underset{\sim}{\mathbf{R}}^T - {}^c\underset{\sim}{\mathbf{Q}}\,{}^\sharp\dot{\underset{\sim}{\mathbf{Q}}}\,{}^\sharp\underset{\sim}{\mathbf{Q}}^T\,{}^c\underset{\sim}{\mathbf{Q}}^T + {}^c\underset{\sim}{\mathbf{Q}}\dot{\underset{\sim}{\mathbf{e}}}^e\,{}^c\underset{\sim}{\mathbf{Q}}^T \\
&= \dot{\underset{\sim}{\mathbf{R}}}\underset{\sim}{\mathbf{R}}^T + {}^c\underset{\sim}{\mathbf{Q}}(\dot{\underset{\sim}{\mathbf{e}}}^v + {}^c\underset{\sim}{\mathbf{W}}^v)\,{}^c\underset{\sim}{\mathbf{Q}}^T + {}^c\underset{\sim}{\mathbf{Q}}\dot{\underset{\sim}{\mathbf{e}}}^e\,{}^c\underset{\sim}{\mathbf{Q}}^T \\
&= \dot{\underset{\sim}{\mathbf{R}}}\underset{\sim}{\mathbf{R}}^T + {}^c\underset{\sim}{\mathbf{Q}}(\sum_s \dot{\gamma}^s\ {}^c\underline{\mathbf{m}}^s \otimes {}^c\underline{\mathbf{z}}^s)\,{}^c\underset{\sim}{\mathbf{Q}}^T + {}^c\underset{\sim}{\mathbf{Q}}\dot{\underset{\sim}{\mathbf{e}}}^e\,{}^c\underset{\sim}{\mathbf{Q}}^T
\end{aligned} \tag{325}$$

hence

$$\underset{\sim}{\mathbf{L}} = \dot{\underset{\sim}{\mathbf{R}}}\underset{\sim}{\mathbf{R}}^T + \underset{\sim}{\mathbf{R}}(\sum_s \dot{\gamma}^s\ {}^\sharp\underline{\mathbf{m}}^s \otimes {}^\sharp\underline{\mathbf{z}}^s)\underset{\sim}{\mathbf{R}}^T + {}^c\underset{\sim}{\mathbf{Q}}\dot{\underset{\sim}{\mathbf{e}}}^e\,{}^c\underset{\sim}{\mathbf{Q}}^T \tag{326}$$

where

$$\underset{\sim}{\mathbf{R}} = {}^c\underset{\sim}{\mathbf{Q}}\,{}^\sharp\underset{\sim}{\mathbf{Q}} \tag{327}$$

Mandel's model yields on the other hand:

$$\underset{\sim}{\mathbf{L}} = \dot{\underset{\sim}{\mathbf{E}}}\underset{\sim}{\mathbf{E}}^{-1} + \underset{\sim}{\mathbf{E}}\dot{\underset{\sim}{\mathbf{P}}}\underset{\sim}{\mathbf{P}}^{-1}\underset{\sim}{\mathbf{E}}^{-1} \tag{328}$$

with

$$\dot{\underset{\sim}{\mathbf{P}}}\underset{\sim}{\mathbf{P}}^{-1} = \sum_s \dot{\gamma}^s\ {}^\sharp\underline{\mathbf{m}}^s \otimes {}^\sharp\underline{\mathbf{n}}^s \tag{329}$$

so that it appears that for small elastic strains the two models are equivalent.

At this point we have presented four different formulations that lead to the same kinematics of crystal plasticity. Each of them enhances some particular aspect of the mechanical modelling of materials with microstructure.

The next step consists in writing detailed constitutive equations, which inevitably leads to choices and variants of the models. Two intricate questions must be tackled: the elastic law and the computation of resolved shear stresses on slip systems. Mandel [1981] proposes a hyperelastic law on the intermediate configuration so that:

$$\underset{\sim}{\Delta}^e = \underset{\approx}{\mathbf{L}}^0 : \underset{\sim}{\Pi} \tag{330}$$

where

$$\underset{\sim}{\Pi} = \underset{\sim}{\mathbf{E}}^{-1} \underset{\sim}{\mathbf{T}} \underset{\sim}{\mathbf{E}}^{-T} \mathrm{Det}E \tag{331}$$

and

$$\underset{\sim}{\Delta}^e = \frac{1}{2} (\underset{\sim}{\mathbf{E}} \underset{\sim}{\mathbf{E}}^T - \underset{\sim}{1}) \tag{332}$$

It is assumed that the four-rank elasticity tensor does not depend on any internal variable. Derivation of 330 yields the elastic strain rate:

$$\underset{\sim}{\mathbf{D}}^e = \{ \dot{\underset{\sim}{\mathbf{E}}} \underset{\sim}{\mathbf{E}}^{-1} \} = \underset{\approx}{\mathbf{L}}^a : \overset{\circ}{\underset{\sim}{\mathbf{T}}} \tag{333}$$

where

$$\overset{\circ}{\underset{\sim}{\mathbf{T}}} = \dot{\underset{\sim}{\mathbf{T}}} - \dot{\underset{\sim}{\mathbf{E}}} \underset{\sim}{\mathbf{E}}^{-1} \underset{\sim}{\mathbf{T}} - \underset{\sim}{\mathbf{T}} \underset{\sim}{\mathbf{E}}^{-T} \dot{\underset{\sim}{\mathbf{E}}}^T + \mathrm{Tr} (\dot{\underset{\sim}{\mathbf{E}}} \underset{\sim}{\mathbf{E}}^{-1}) \underset{\sim}{\mathbf{T}} \tag{334}$$

is referred to as Truesdells derivative, and $\underset{\approx}{\mathbf{L}}^a$ has the following components

$$L^a_{ijkl} = E^{-1}_{\alpha i} E^{-1}_{\beta j} E^{-1}_{\gamma k} E^{-1}_{\delta l} \; L^0_{\alpha\beta\gamma\delta} \; \mathrm{Det}\underset{\sim}{\mathbf{E}} \tag{335}$$

The elastic law 307 that we have chosen leads to the following derivative

$$\underset{\sim}{\mathbf{D}}^e = {}^c\underset{\sim}{\mathbf{Q}} \dot{\underset{\sim}{\mathbf{e}}}^e \, {}^c\underset{\sim}{\mathbf{Q}}^T = \underset{\approx}{\mathbf{L}}^a : \overset{\nabla}{\underset{\sim}{\tau}} \tag{336}$$

whith

$$L^a_{ijkl} = R_{i\alpha} R_{j\beta} R_{k\gamma} R_{l\delta} \; L^0_{\alpha\beta\gamma\delta} \tag{337}$$

and

$$\overset{\nabla}{\underset{\sim}{\tau}} = \dot{\underset{\sim}{\tau}} + \underset{\sim}{\tau} \dot{\underset{\sim}{\mathbf{R}}} \underset{\sim}{\mathbf{R}}^{-1} - \dot{\underset{\sim}{\mathbf{R}}} \underset{\sim}{\mathbf{R}}^{-1} \underset{\sim}{\tau} \tag{338}$$

being the Jaumann derivative of $\dfrac{\underset{\sim}{\tau}}{\rho_0} = \dfrac{\underset{\sim}{\mathbf{T}}}{\rho}$ with respect to director frame $E_\sharp$. Equations 333 and 336 coincide for small elastic strain ([Mandel 1983]).

Some arbitrariness remains in the choice of intrinsic stress tensors S or $\dfrac{S}{\rho}$. Only experiments with subtle measurements that are perhaps out of reach could help choosing between these two possibilities. However the mass density is an intrinsic charateristic of body $\mathcal{B}$ and furthermore the model should lead to a symmetrical Eulerian variational formulation to allow an easier implementation in classical FE codes according to [Ladevèze 1980]. That is why we retained the stress $\underset{\sim}{\mathbf{S}}$ given by 274 with $\underset{\sim}{\mathbf{Q}} = {}^c\underset{\sim}{\mathbf{Q}}$.

Consequently, we compute the resolved shear stresses:

$$\tau^s = \underset{\sim}{\mathbf{S}} : ({}^c\underline{\mathbf{m}}^s \otimes {}^c\underline{\mathbf{n}}^s) = \frac{\rho_0}{\rho} \underset{\sim}{\mathbf{T}} : (\underline{\mathbf{m}}^s \otimes \underline{\mathbf{n}}^s) \tag{339}$$

According to Mandel [1971], this gives:

$$\tau^s = (\underset{\sim}{\mathbf{E}}^T \underset{\sim}{\mathbf{E}} : \underset{\sim}{\Pi}) : ({}^\sharp\underline{\mathbf{m}}^s \otimes {}^\sharp\underline{\mathbf{n}}^s) \tag{340}$$

Mandel justifies this choice by referring to the work of forces on a dislocation line.

7.2.3 Numerical analysis of the simple shear test

The simple shear test is of great interest for the evaluation of the modelling because it involves large strains as well as large rotations. Experimental results can be found in literature, mainly in the case of polycrystalline sheets ([Bacroix, Genevoix, Teodosiu 1992]). In the experiment described in [Wack, Tourabi 1994], the amount of shear $\gamma = 10$ could be reached. Local measurements are necessary because non-homogeneous deformation arises early at the boundary of the specimen.

The model presented in 7.2.1. has been implemented in the program SiDoLo developed at Ecole des Mines de Paris, so that any situation for which all components of deformation gradient $\underset{\sim}{\mathbf{F}}$ are imposed can be treated. This only requires a Runge-Kutta integration method for instance. An intrinsic treatment of rotations ${}^{c}\underset{\sim}{\mathbf{Q}}$ and ${}^{\sharp}\underset{\sim}{\mathbf{Q}}$ has been adopted and is presented in Appendix 1. The variables to be integrated are the following:

- ${}^{c}\underline{\Psi}$, ${}^{\sharp}\underline{\Psi}$ two vectors describing rotations ${}^{c}\underset{\sim}{\mathbf{Q}}$ and ${}^{\sharp}\underset{\sim}{\mathbf{Q}}$,
- the elastic deformation $\underset{\sim}{\mathbf{e}}^{e}$,
- the amounts of slip γ^s,
- the hardening variables α^s.

We consider an elastoviscoplastic behaviour with linear or non-linear isotropic and kinematic hardening variables on each octahedral slip system of f.c.c. single crystals:

$$\dot{\gamma}^s = < \frac{\mid \tau^s - x^s \mid - r^s}{k} >^n \ \text{sign}\ (\tau^s - x^s) \tag{341}$$

$$r^s = r_0 + q \sum_{r=1}^{N} h^{sr}(1 - \exp(-bv^s)) \tag{342}$$

$$\dot{v}^s = \mid \dot{\gamma}^s \mid \tag{343}$$

$$x^s = c\ \alpha^s \tag{344}$$

$$\dot{\alpha}^s = \dot{\gamma}^s - d\dot{v}^s \alpha^s \tag{345}$$

where k, n, r_0, q, b, h^{rs}, c and d are material parameters. Kraska [1993] also proposes the introduction of an interaction matrix for linear kinematical hardening. Various orientations of the single crystal with respect to loading axes will be studied successively. We will lay the stress on the particular role played by the corotational frame E^c and the microstructural frame $E^{\sharp}$ in each case.

$\underline{\mathbf{e}}_1 = [100] / \underline{\mathbf{e}}_2 = [001]$.

$\underline{\mathbf{e}}_1$ and $\underline{\mathbf{e}}_2$ refer to the figure of section 7.1.5 and initially coincide respectively with crystallographic directions [100] and [001]. Figure 60 shows the response of the single crystal when no hardening is introduced (material parameters $E = 200000$ MPa, $\nu = 0.33$, $r_0 = 150$ MPa, $k = 150$ MPa $s^{1/n}$, $n = 10$, $h^{ij} = \delta_{ij}$). A periodic behaviour is obtained with period $\gamma = 2\pi$. The calculations give

$${}^{\sharp}\underset{\sim}{\mathbf{Q}} = \underset{\approx}{\mathbf{1}} \tag{346}$$

so that the lattice does not rotate with respect to the corotational frame. The endless rotation of the corotational frame in the case of simple shear has been described in 1.5.: it

rotates around axis $\underline{e}_3$ with rotation rate $\dot{\gamma}/2$. It means that for this initial orientation the lattice rotates at the same rate as the corotational frame. This is not an artefact of our formulation since we have obtained the same response with Mandel's model. Although the corotational frame has no explicit meaning in Mandel's model, the same periodic response is obtained and our formulation shows that the lattice accompanies the corotational frame.

This result has been mentioned in [Canova, Molinari, Fressengeas 1986] for purely linear viscous single crystals and also in [Boukadia, Chenaoui, Sidoroff 1993] for rigid plastic single crystals.

The lattice rotation proceeds without end so that some slip systems are successively activated and inactivated (figure 61). Always three slip systems remain simultaneously active during shearing. The introduction of linear isotropic hardening breaks the periodicity and is associated with an increase of the maximal stress in each pseudo-period (figure 62). Linear kinematic hardening induces more complex responses (figure 63). Similar results are presented in [Bertram, Kraska 1995].

$\underline{e}_1 = [\bar{1}10]/\underline{e}_2 = [111]$.

The fact that the corotational frame displays an endless rotation in the case of simple shear does not necessarily entail that the crystal orientation cannot stabilize. This paragraph and the following give two examples.

The shearing direction coincides with a slip direction $< 110 >$ and shearing proceeds within a slip plane $\{111\}$. The calculations prove that only one system $([\bar{1}10](111))$ contributes to the whole deformation of the specimen (figure 64a). The component T_{12} remains then constant (figure 64b). This means that the lattice does not rotate with respect to the loading axes. Since the corotational frame is in endless motion, rotation ${}^{\sharp}\underset{\sim}{Q}$ must compensate it (figure 65):

$$ {}^{c}\underset{\sim}{Q}\,{}^{\sharp}\underset{\sim}{Q} = \underset{\sim}{1} \tag{347} $$

$\underline{e}_1 = [\bar{2}10]/\underline{e}_2 = [123]$.

For this orientation, four main slip systems are activated (figure 66a). The stress softens and then stabilizes (figure 66b). A representation of the motion of axis $\underline{e}_2$ in the standard triangle of the f.c.c. crystal shows that the crystal undergoes a three-dimensional rotation with respect to the loading axes (figure 67). $\underline{e}_2$ tends to reach crystallographic direction $[\bar{1}11]$. Boukadia and Sidoroff [1988] have worked out analytically in the rigid plastic case the limit orientations that are reached depending on the starting orientation.

The previous examples have underlined the interest of studying deformation processes from the point of view of different observers. The corotational frame plays a key role for the first studied orientation, and combining corotation and lattice rotation can lead to stationary or stabilized behaviours like in the last two paragraphs. The equivalence between Mandel's formulation and ours for small elastic strains has been confirmed numerically.

7.3 Localization phenomena in single crystals at large strains

7.3.1 Necking

Mandel's model has been implemented in the FE code ZeBuLoN by Méric [1991]. We have also implemented our formulation, although no significant deviation from Mandel's model is expected. The major interest of the new formulation is that the extension of models developed at small strain to the case of large strain is automatic, once the general variational formulation for finite deformation is available. For the single crystal we have extended the model developed in [Méric, Poubanne, Cailletaud 1991]. It means that the small strain constitutive equations are now written within the corotational frame. The existence of the microstructure made it necessary to add the lattice rotation $^{\sharp}\underset{\sim}{\mathbf{Q}}$ as seen in 7.2.1. We still use the intrinsic representation of rotations (see Appendix 1).

Large strain effects in crystal plasticity appear during the tension of a single crystal plate oriented for single slip. For the FE simulations of figure 68 and 69, boundary conditions are such that a vertical displacement is imposed at one end, whereas it remains constrained in the vertical direction at the other end. Other boundary conditions just aim at impeding rigid body motion. The beginning of plastic flow results in incompatibility at the ends of the specimen, which produces a 'S'-shape (figure 68). No hardening is introduced (material parameters $r_0 = 150$ MPa, $k = 150$ MPa $s^{1/n}$, $n = 10$, $h^{ij} = \delta_{ij}$). Lattice rotation takes place mainly in the middle of the specimen and induces geometrical softening. This inevitably results in localization of deformation within a diffuse necking zone (figure 69).

7.3.2 Influence of lattice rotation on slip band formation

The influence of lattice rotation on localization could be investigated in the case of single slip. Although strain-softening has been introduced at the very beginning of plastic flow, i.e. for small strains, very small amounts of lattice rotation may play a role when the behaviour becomes instable. The same 2D problem has been studied using the small strain model and the large strain model successively. The plate is oriented for single slip (tensile axis [238], secondary direction [$\overline{1}9$ 10 1]). Figure 70 shows that the macroscopic load-displacement curves are almost identical after the peak. In the two cases two shear bands tend to form at the peak of the curve even though the boundary conditions induce more non-homogeneous deformation when lattice rotations are considered (figure 71). However the final state obtained after bifurcation is very different in the two cases: with the small strain model a kink band forms whereas a slip band forms with the large strain model (figure 72). The same result has been obtained for a 3D single slip configuration (figure 73). Figure 74 proves that the formation of the slip band induces no further lattice rotations. It does not mean that kink bands cannot form with the large strain model: for the calculation of figure 75 the position of the defect is such that only a kink band may form if starting from the defect. A kink band is indeed observed and a large amount of lattice rotation takes place inside the band (4°, figure 76).

The bifurcation analysis for single slip at small strain (section 4.1.2) and at large strain ([Asaro, Rice 1977]) predicts both slip and kink bands for the same critical hardening modulus. *Although the two modes cannot be distinguished when lattice rotation is excluded, the two modes turn out to be very different when lattice rotation is taken into account. A slip band does not induce any local relative lattice rotation if the grips*

are laterally free during testing, whereas a kink band is accompanied with strong lattice rotation gradients.

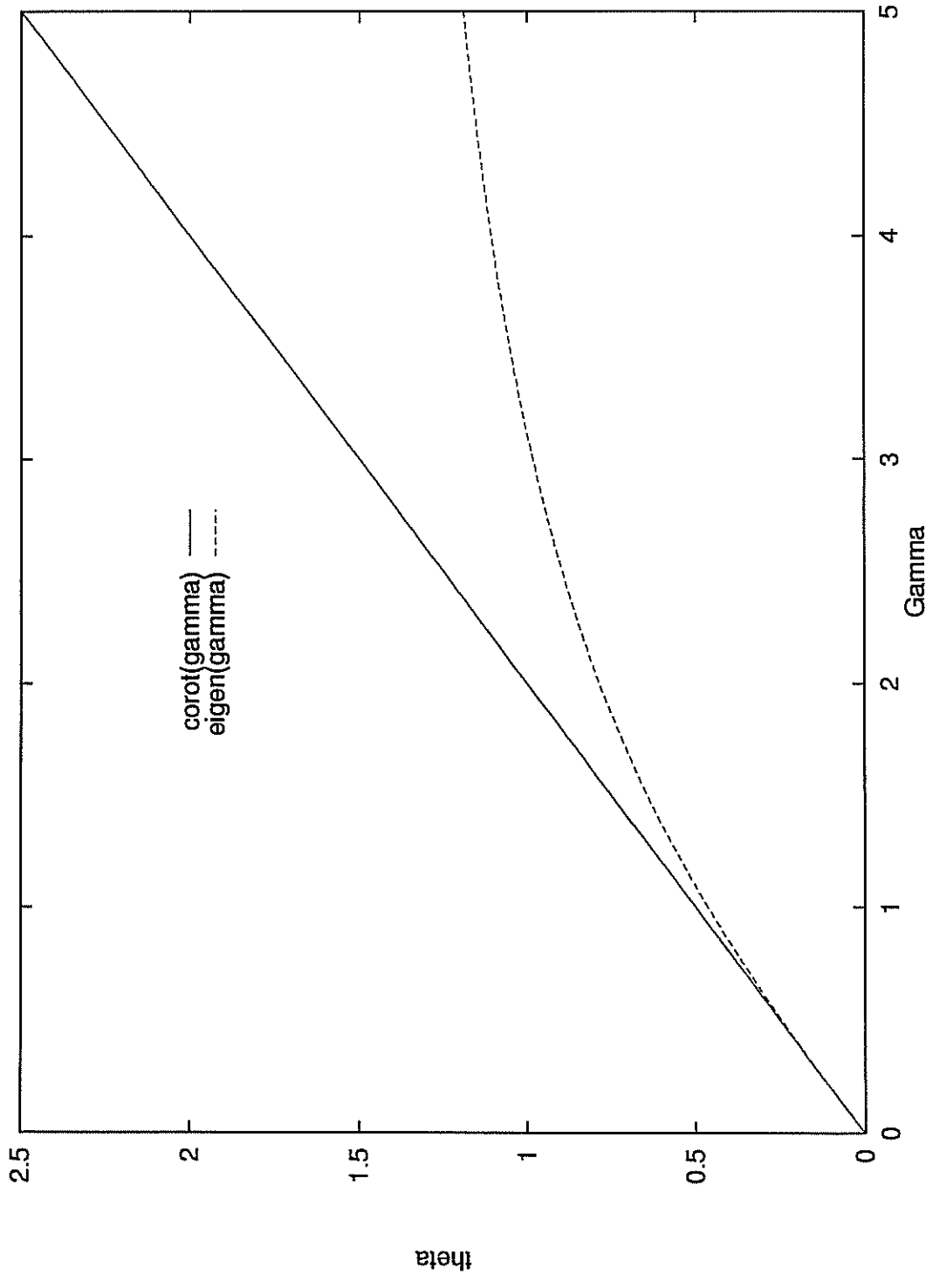

Figure A.56: Rotation of the corotational and eigenrotational frames during simple shear.

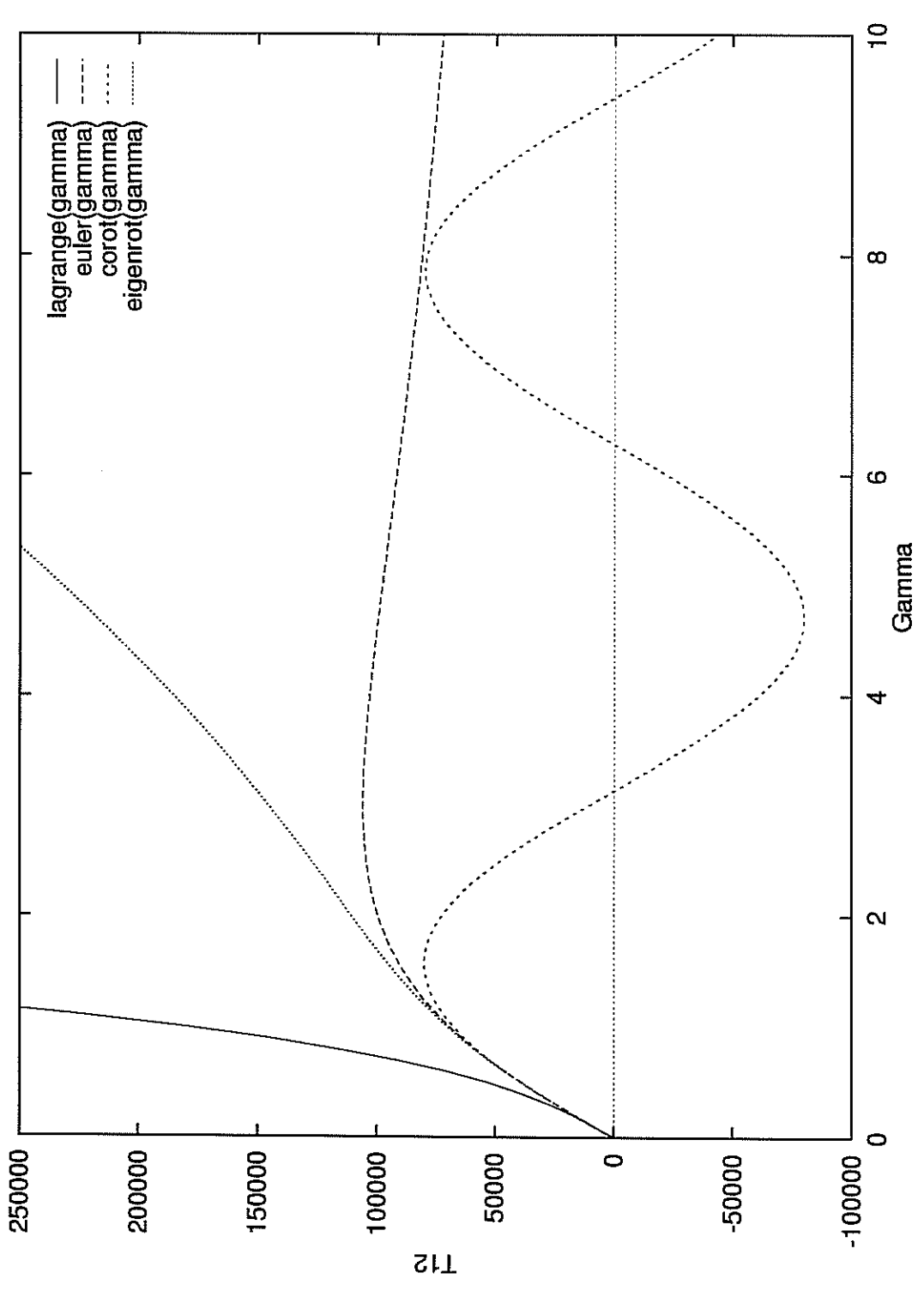

Figure A.57: Comparison between various formulations of isotropic elasticity at large strains for the simple shear test (T_{12} is the component 12 of the Cauchy stress).

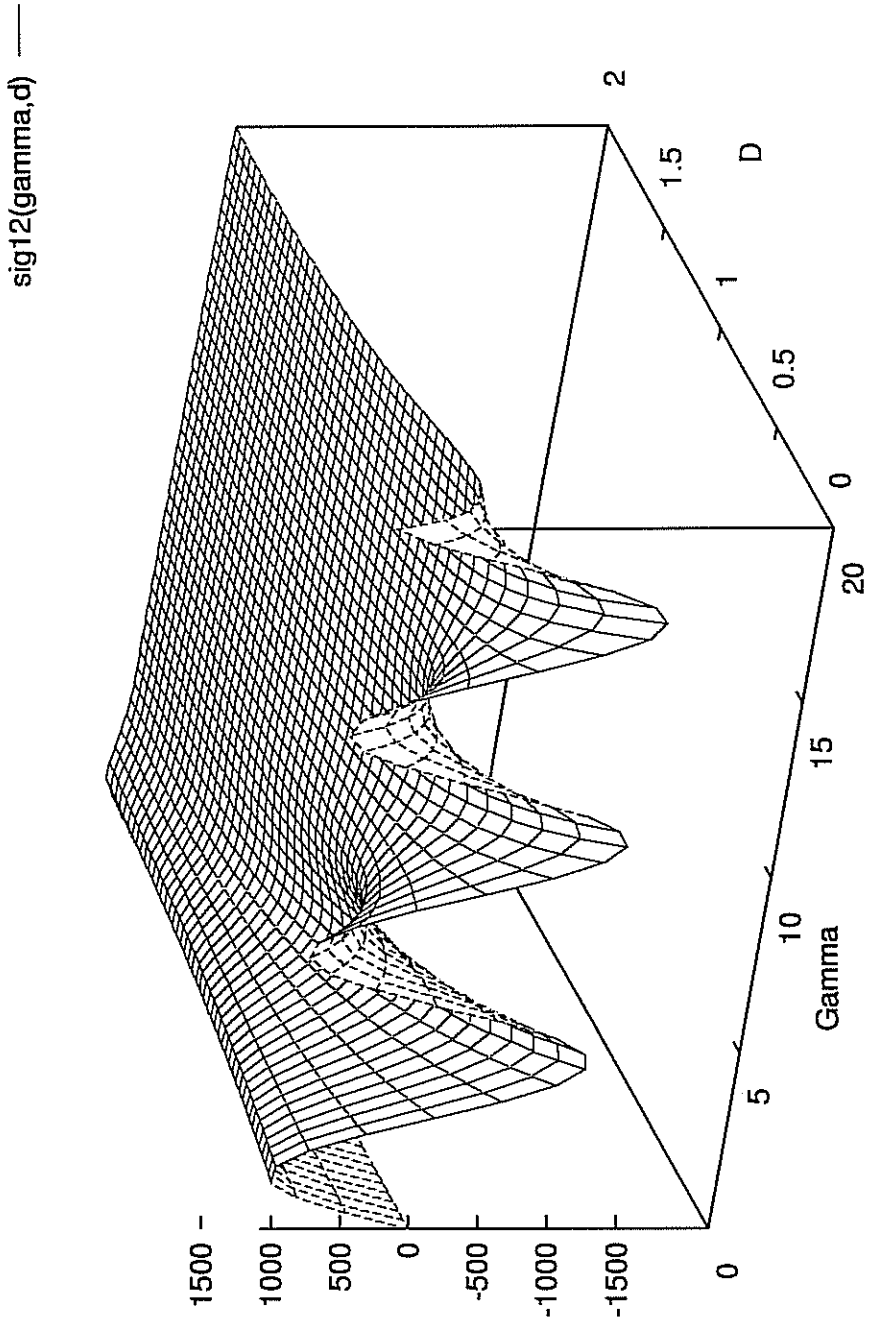

Figure A.58: Disparition of the oscillations of the stress during simple shear when a non-linear term is introduced in kinematical hardening.

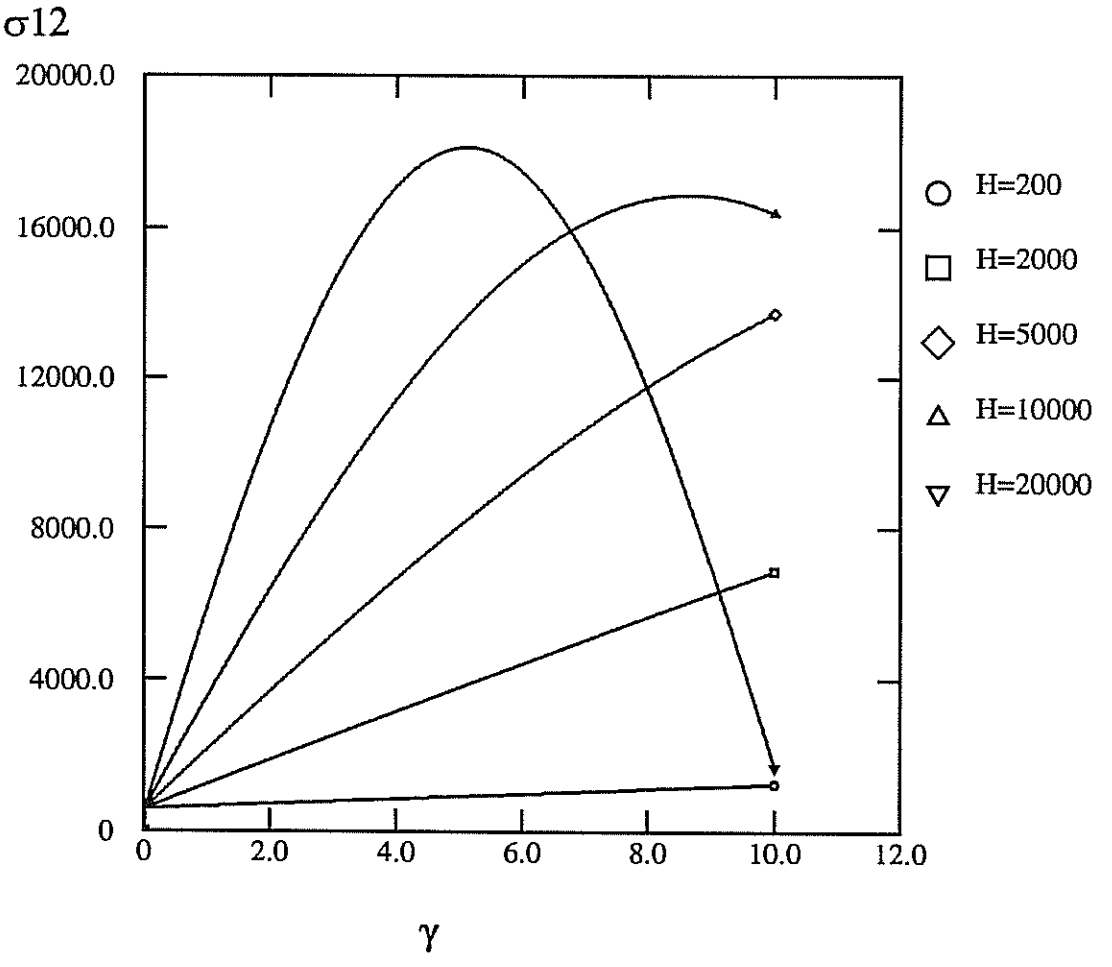

Figure A.59: Apparition of oscillations during simple shear when the hardening modulus has the order of magnitude of the elastic constants (elastoviscoplasticity, linear isotropic hardening, E=200000MPa, ν=0.33).

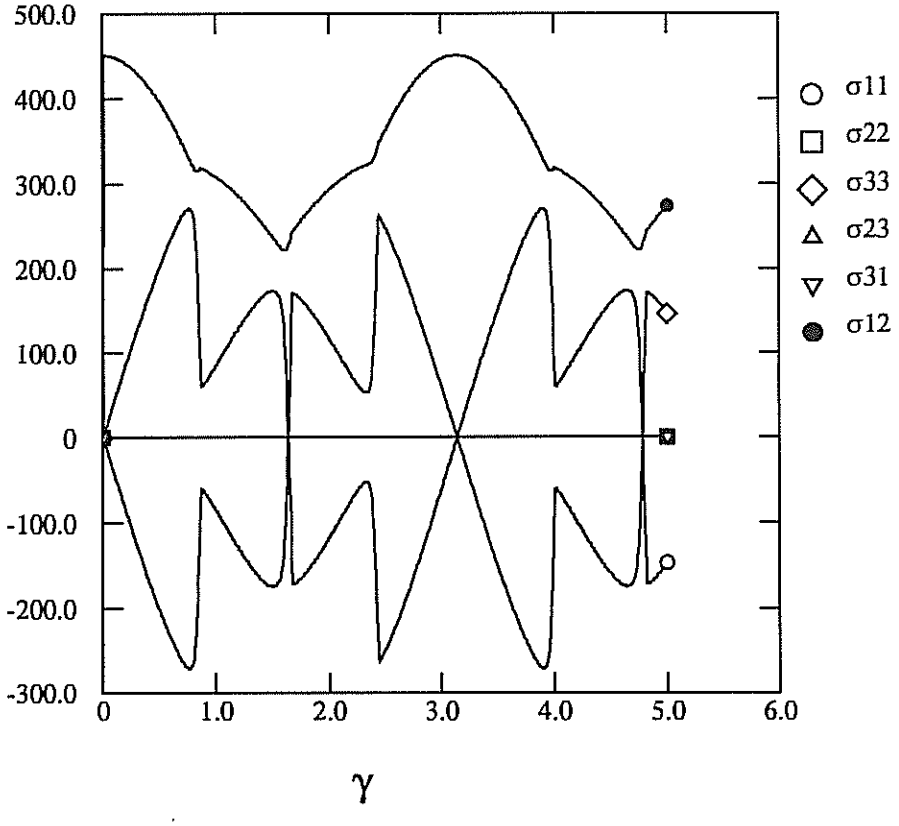

Figure A.60: Simple shear of a single crystal with initial orientation [100],[001] (Cauchy stress, elastoviscoplasticity, no hardening).

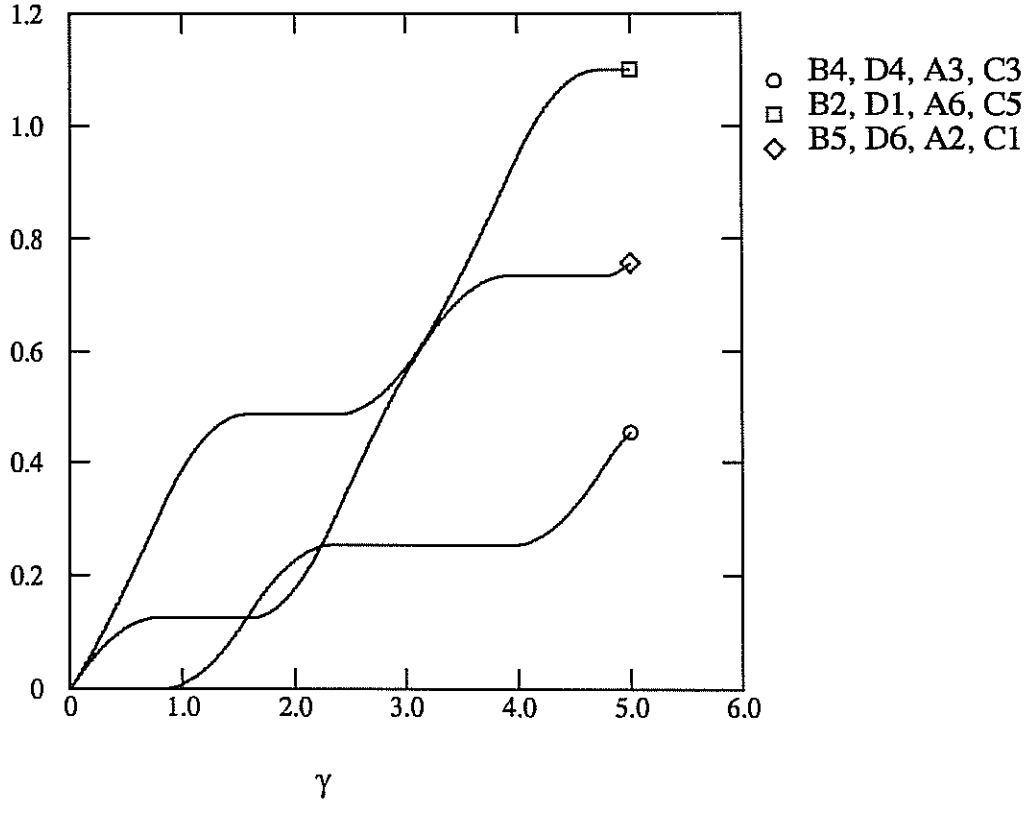

Figure A.61: Active slip systems during simple shear (cumulated strain, initial orientation [100][001]).

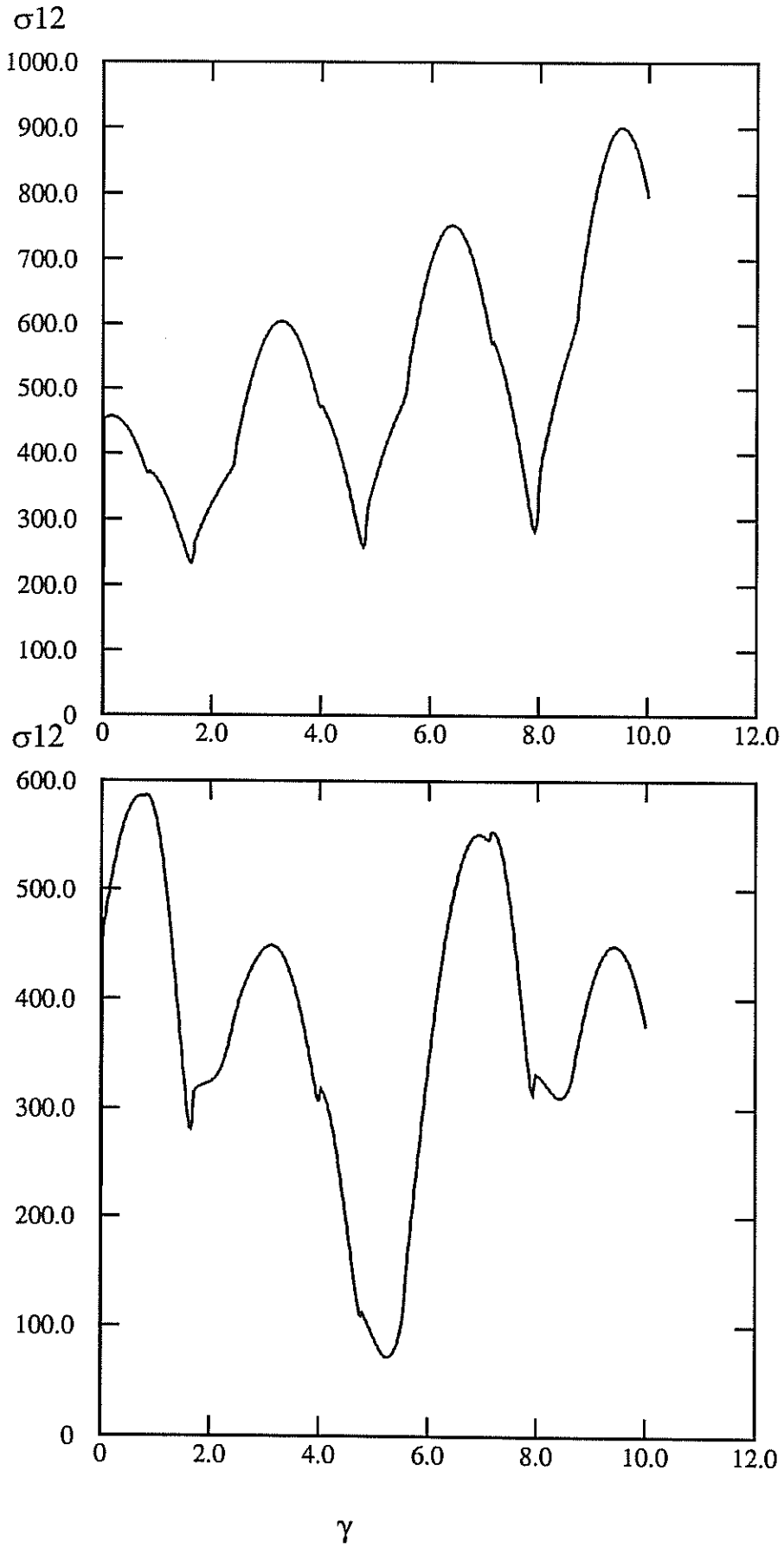

Figures A.62 and A.63: Effect of linear isotropic hardening (above) and linear kinematic hardening (below) on the shearing of a single crystal.

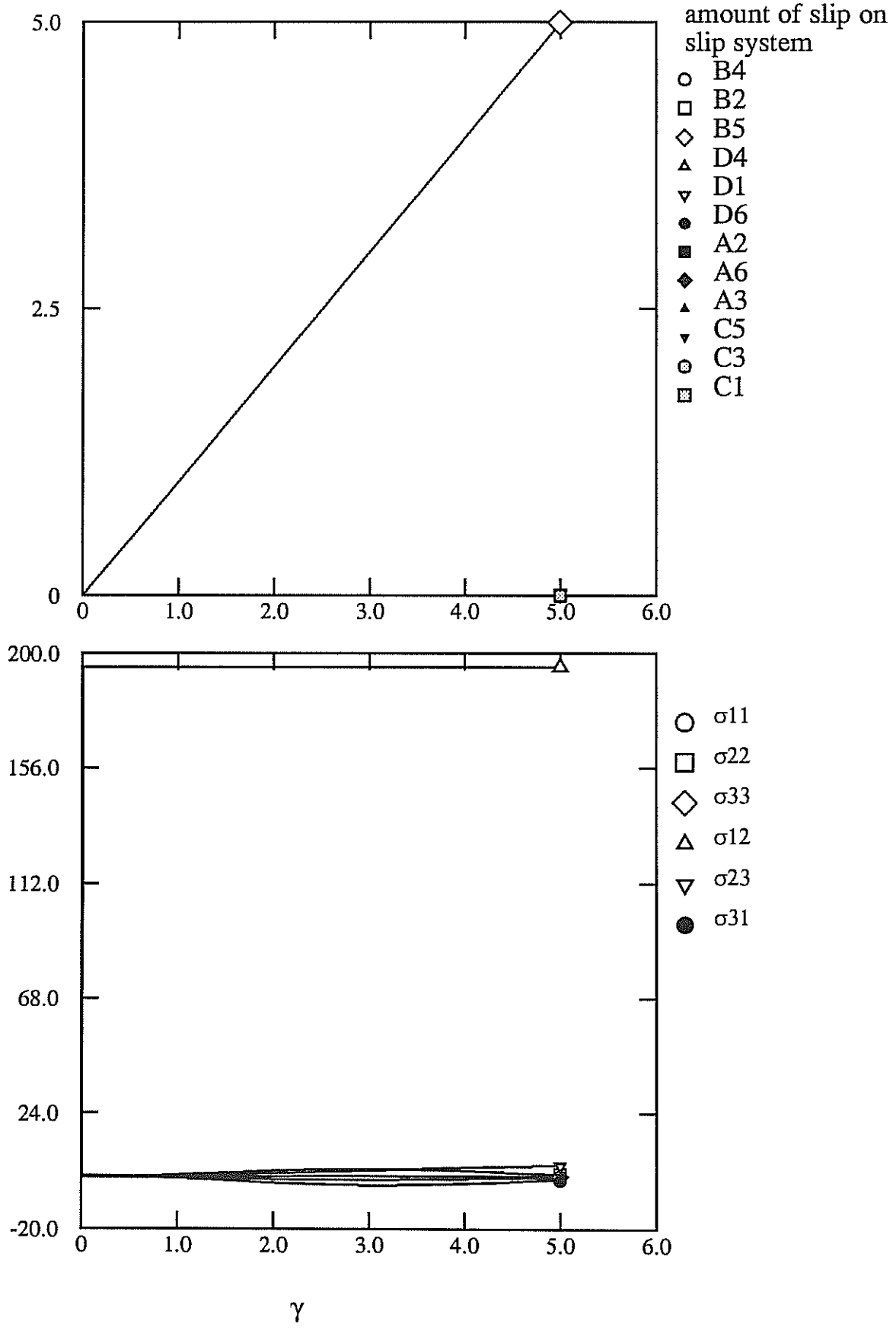

Figure A.64: Simple shear of a single crystal with initial orientation [-110][111]: only one active slip system (above), and constant stress (below).

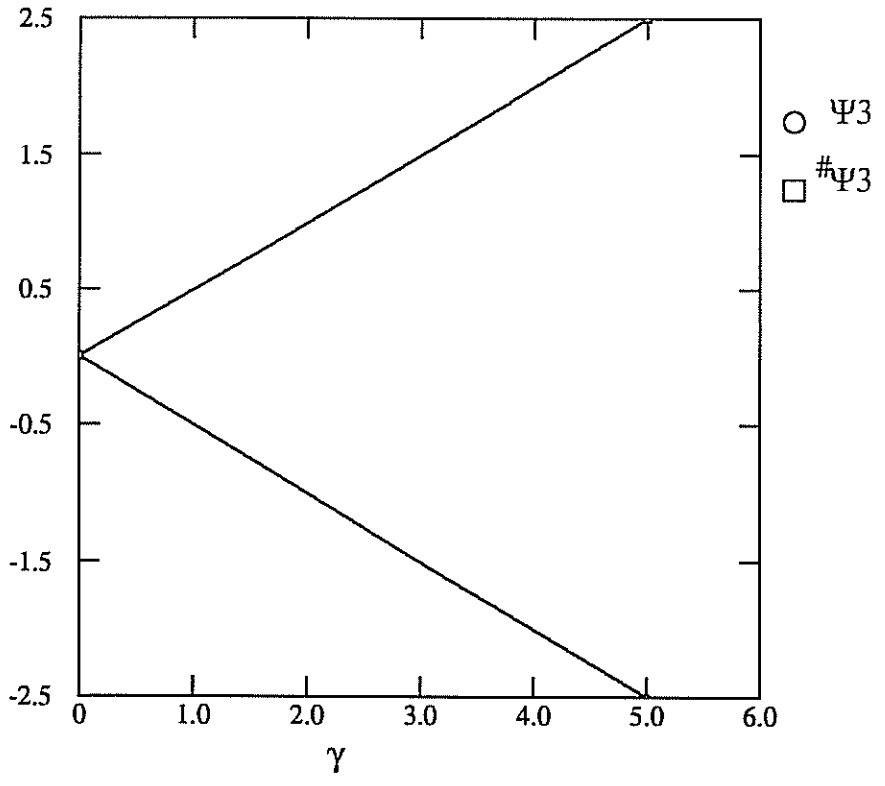

Figure A.65: Simple shear of a single crystal with initial orientation [-110],[111]: material and lattice rotations compensate each other so that the lattice does not rotate with respect to the loading axes.

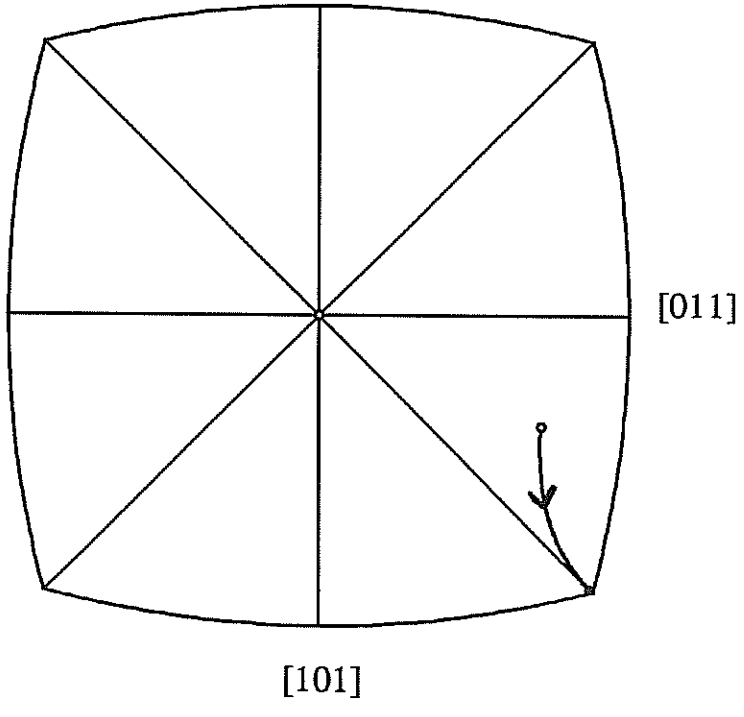

Figure A.67: Simple shear of a single crystal with initial orientation [-210],[123]; rotation of loading axis 2 with respect to the lattice.

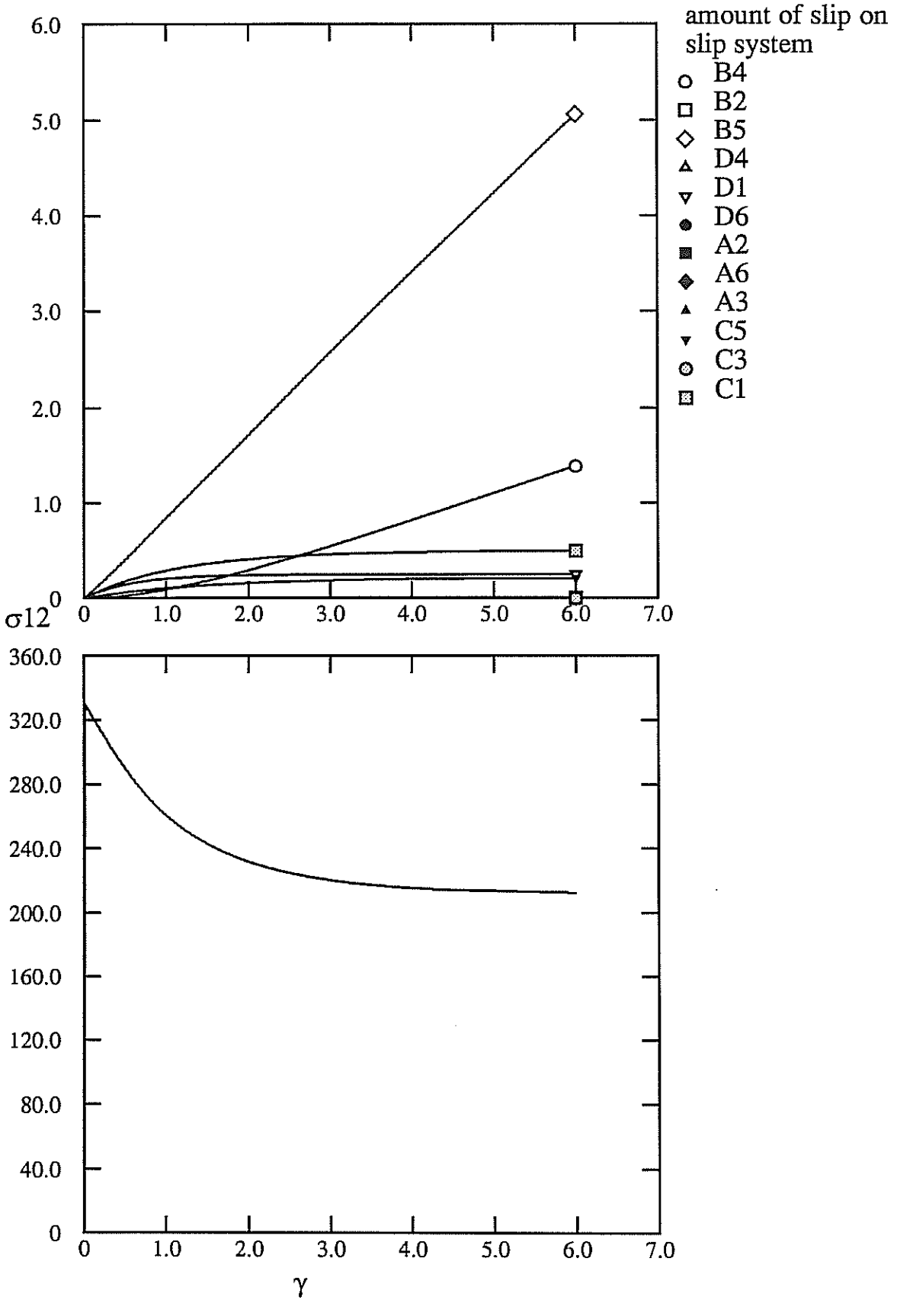

Figure A66: Simple shear of a single crystal with initial orientation [-210][123].

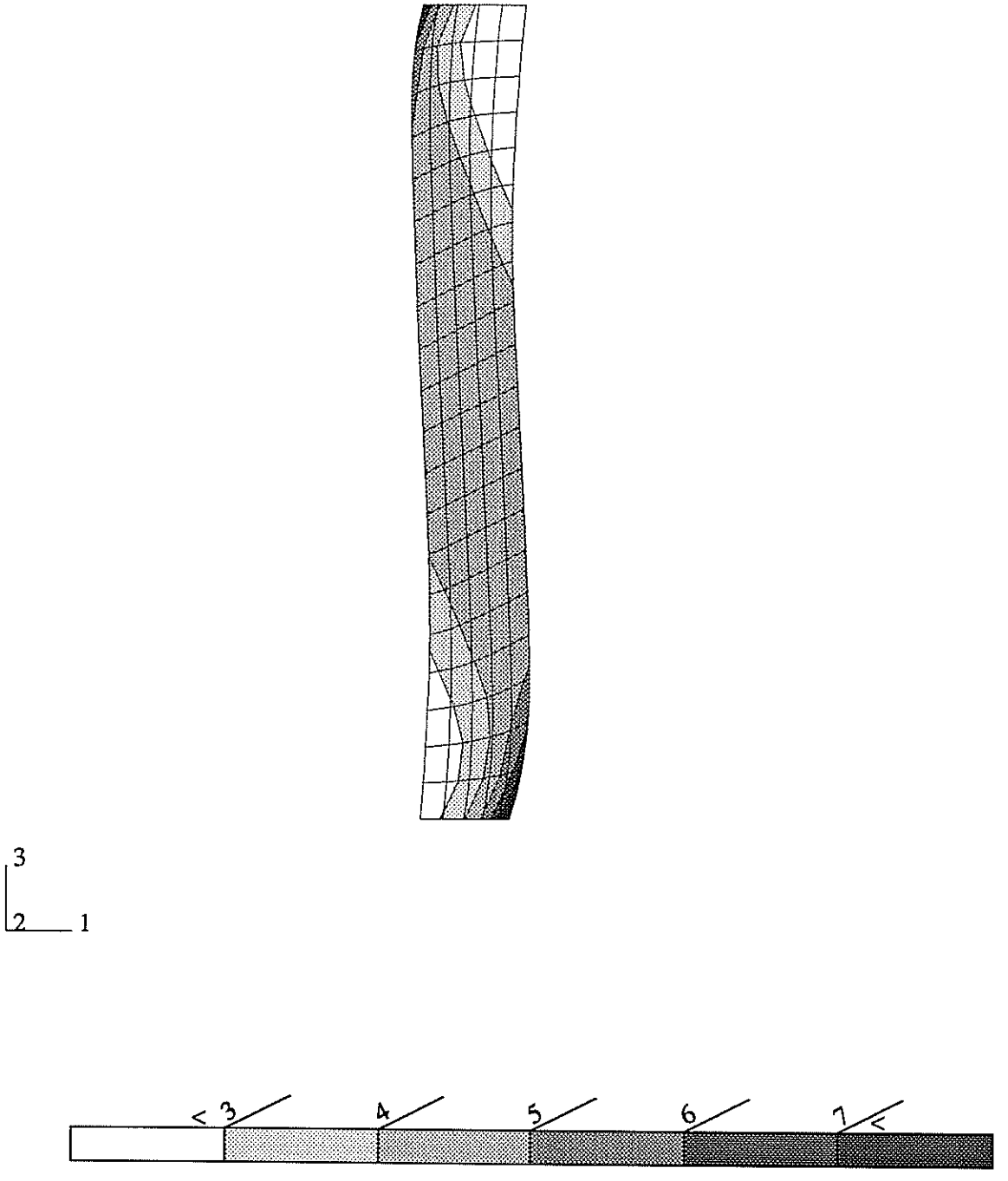

Figure A.68: Tension of a misoriented single crystal: 'S' form at incipient plasticity.

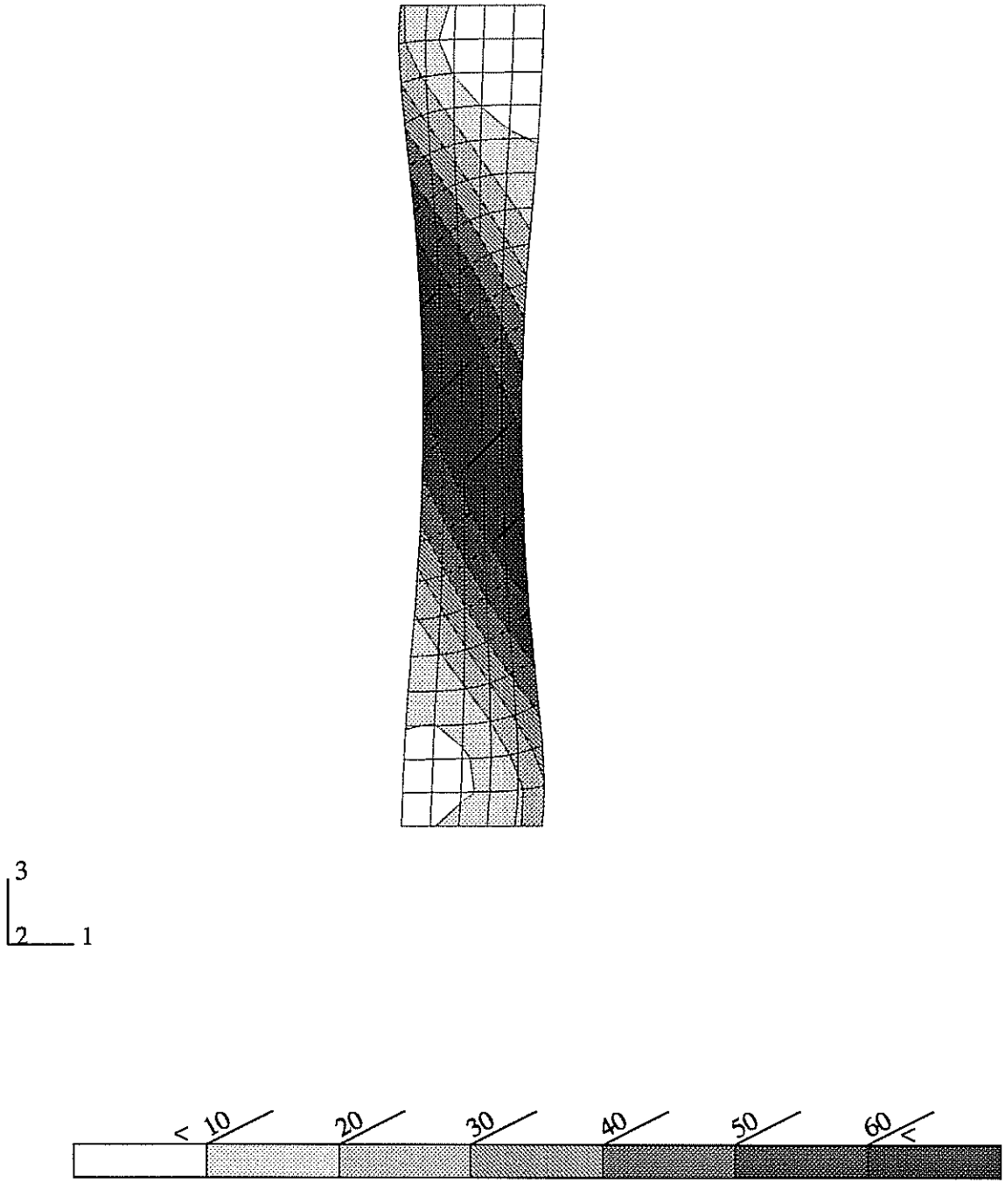

Figure A.69: Tension of a misoriented single crystal: development of a necking zone.

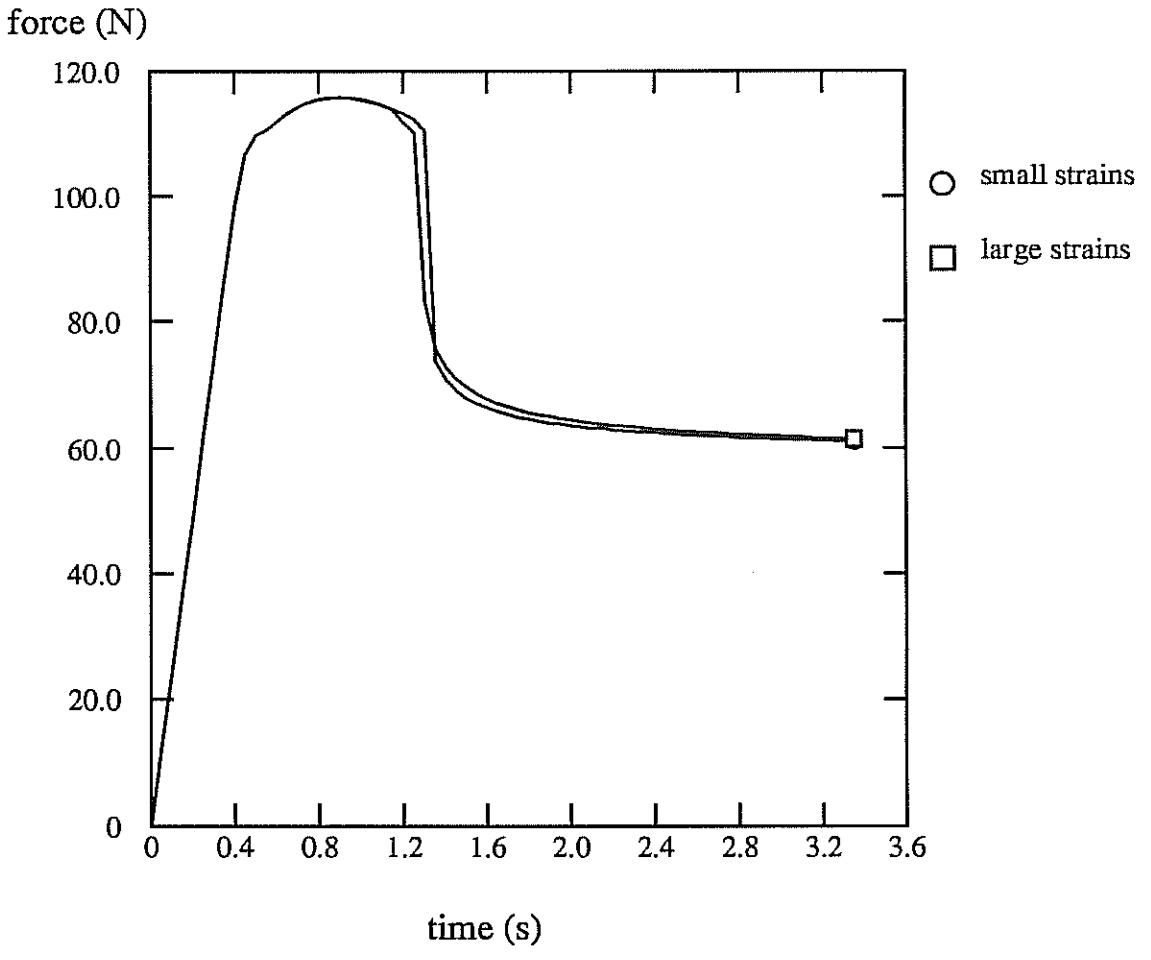

Figure A.70: Load-displacement curves for the tension of a single crystal plate with the small strain and large strain formulations of the model.

Figure A.71: Amount of slip on the active slip system before bifurcation with the small (left) and large (right) strain formulations of the model.

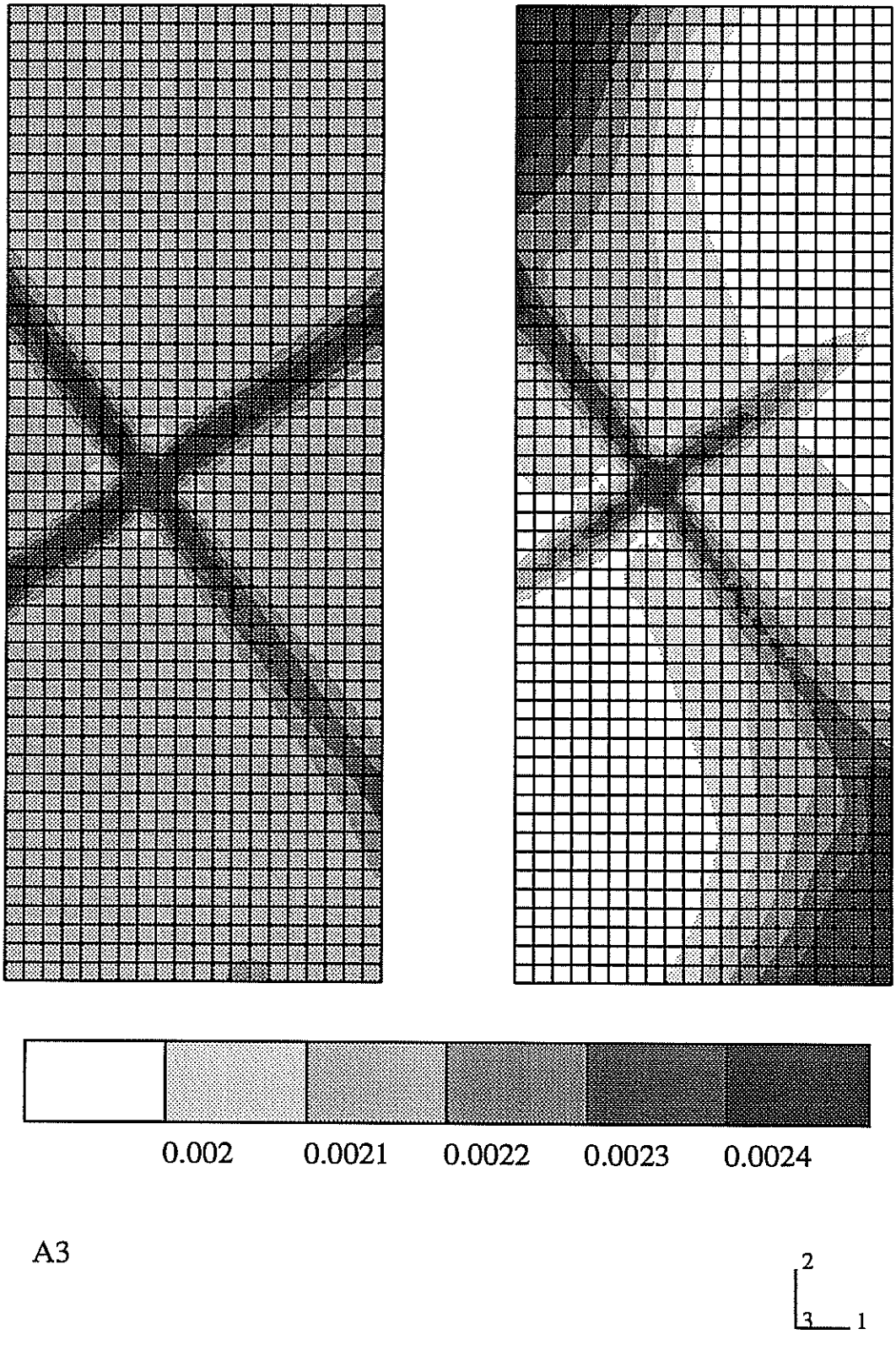

Figure A.72: Bifurcation modes obtained with the small (left) and large (right) formulations of the model.

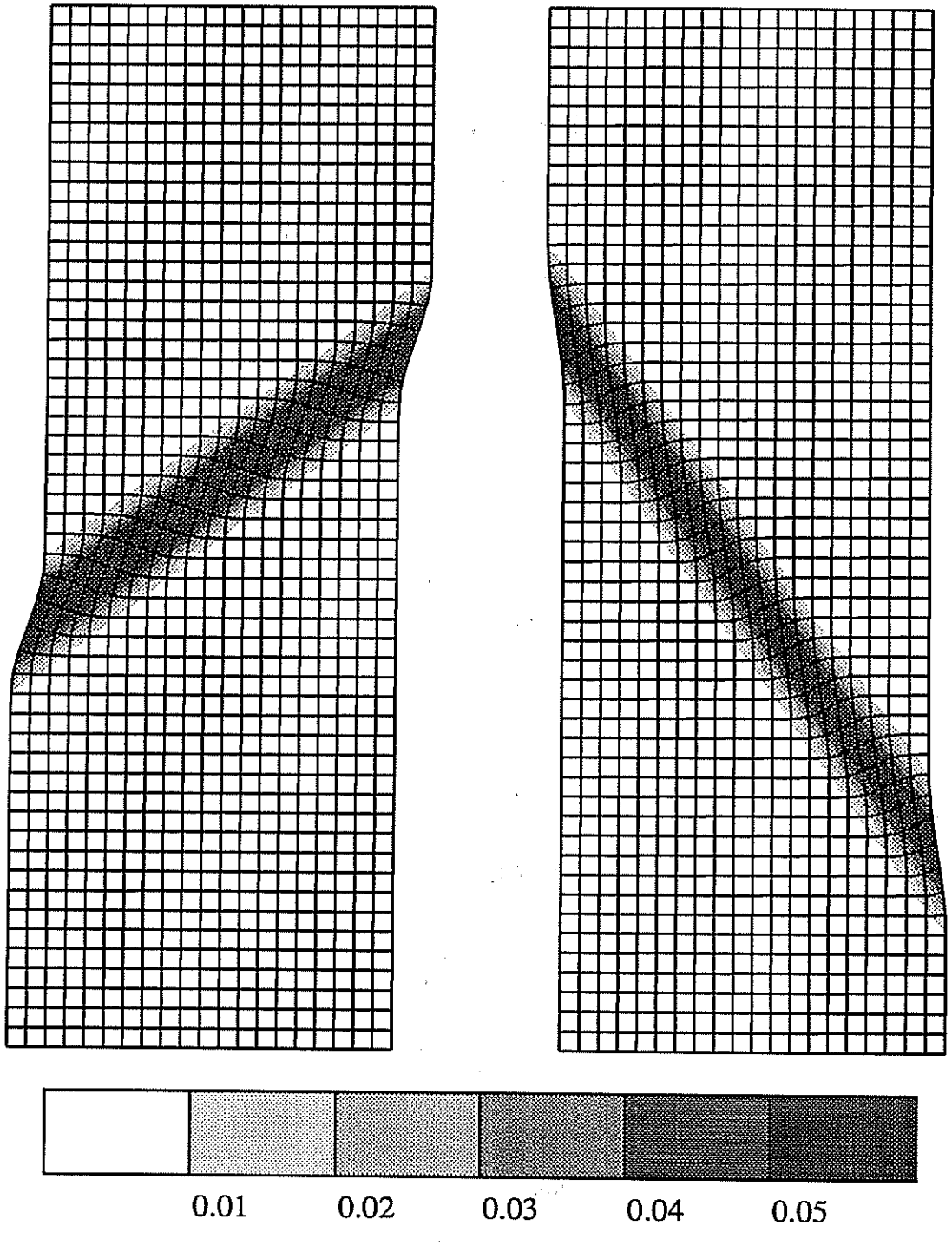

Figure A.73: Bifurcation modes obtained with the small (left) and large (right) strain formulations of the model.

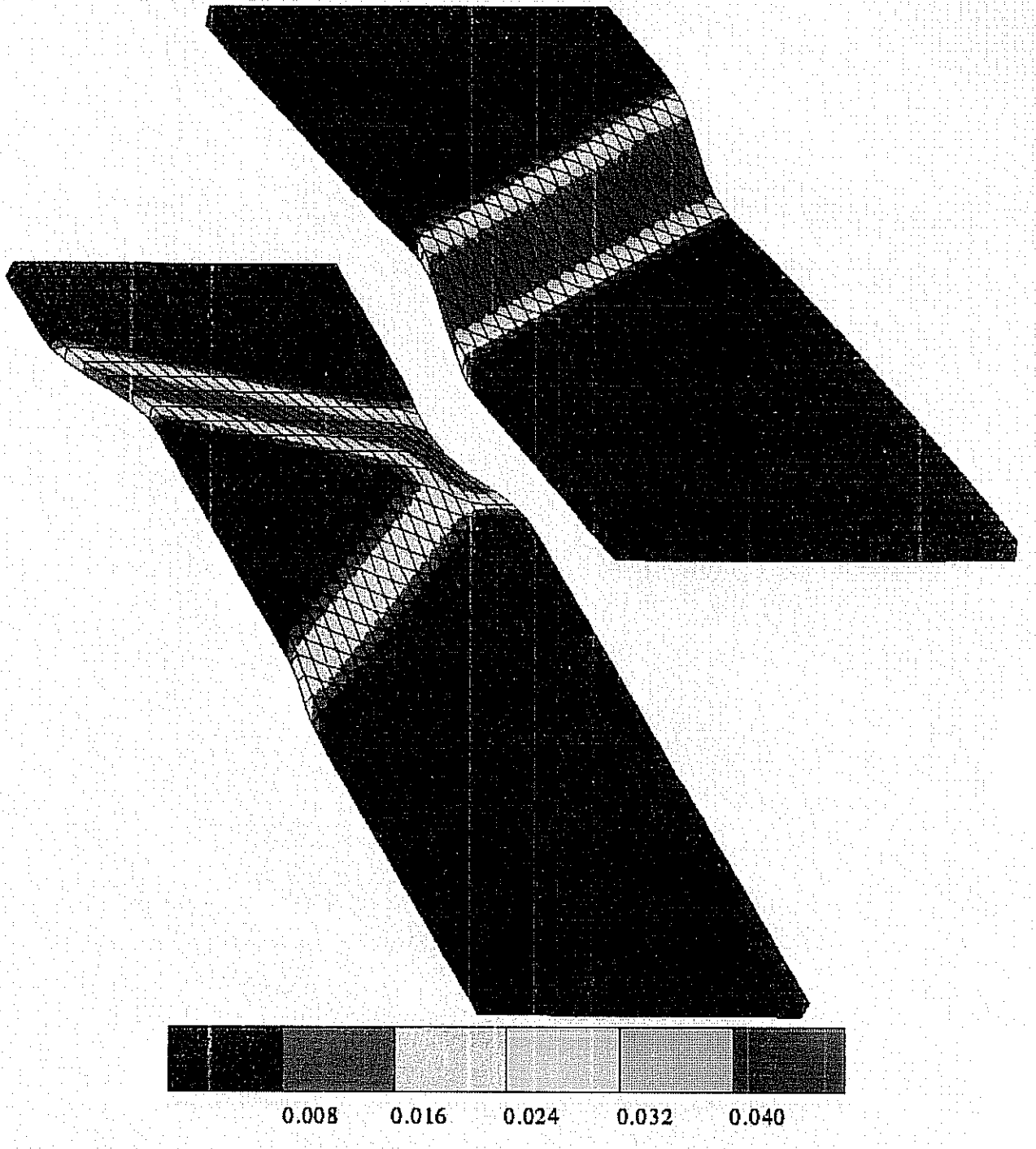

Figure A.74: Lattice rotation about the axis 3 before (left) and after bifurcation (right).

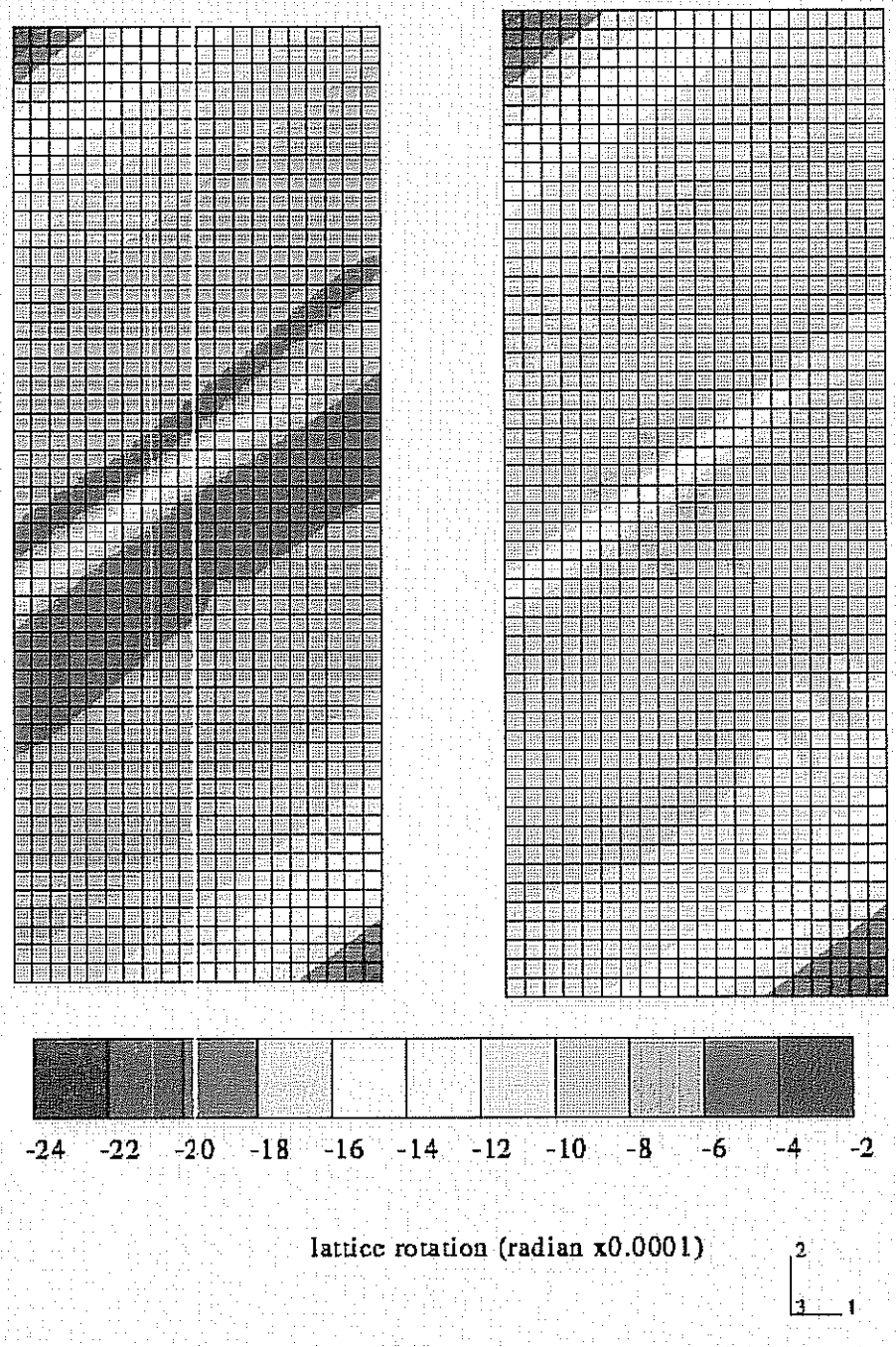

Figure A.75: Formation of a kink band using the large strain formulation of the model.

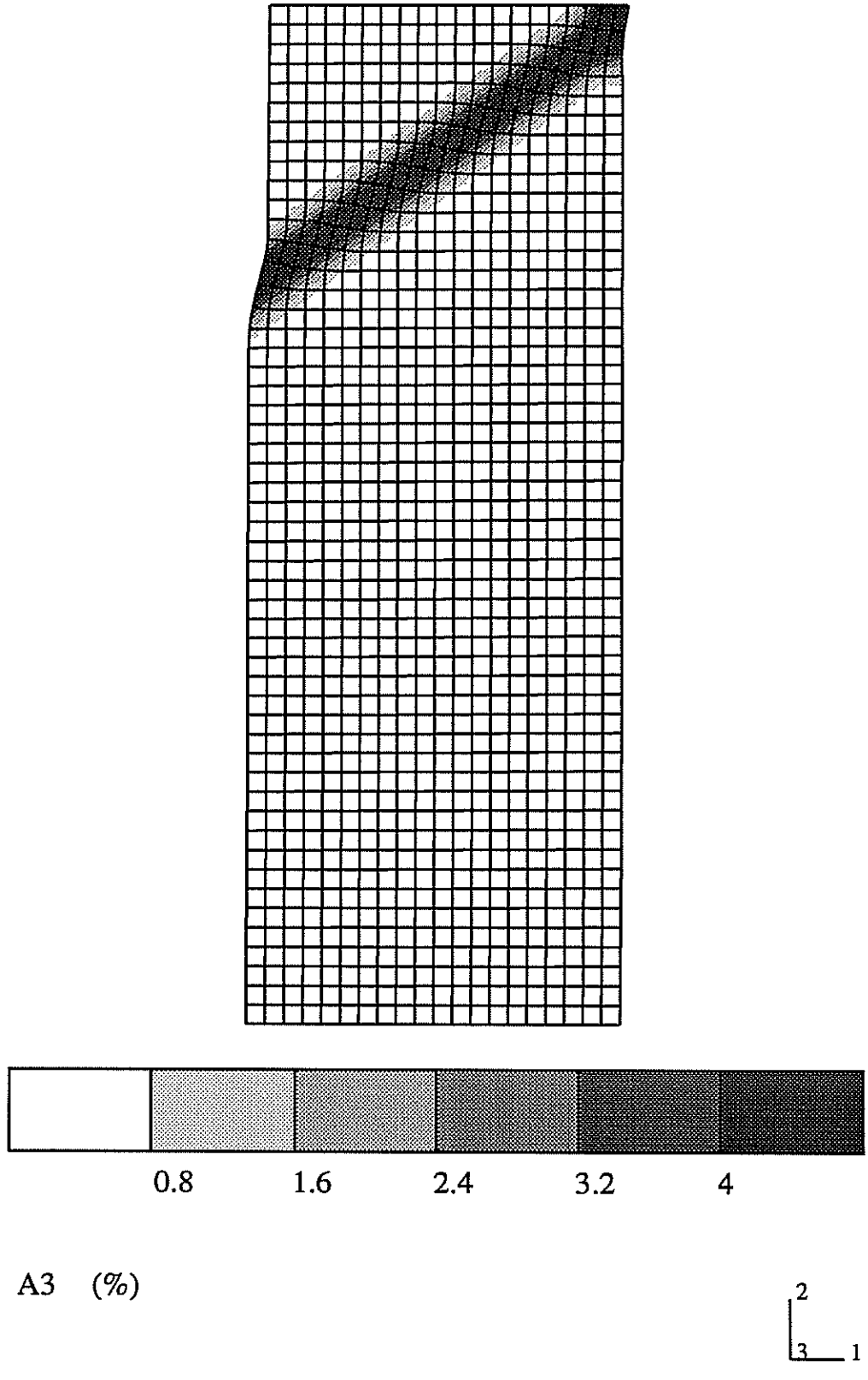

Figure A.76: Lattice rotation with respect to axis 3, due to the kink band.

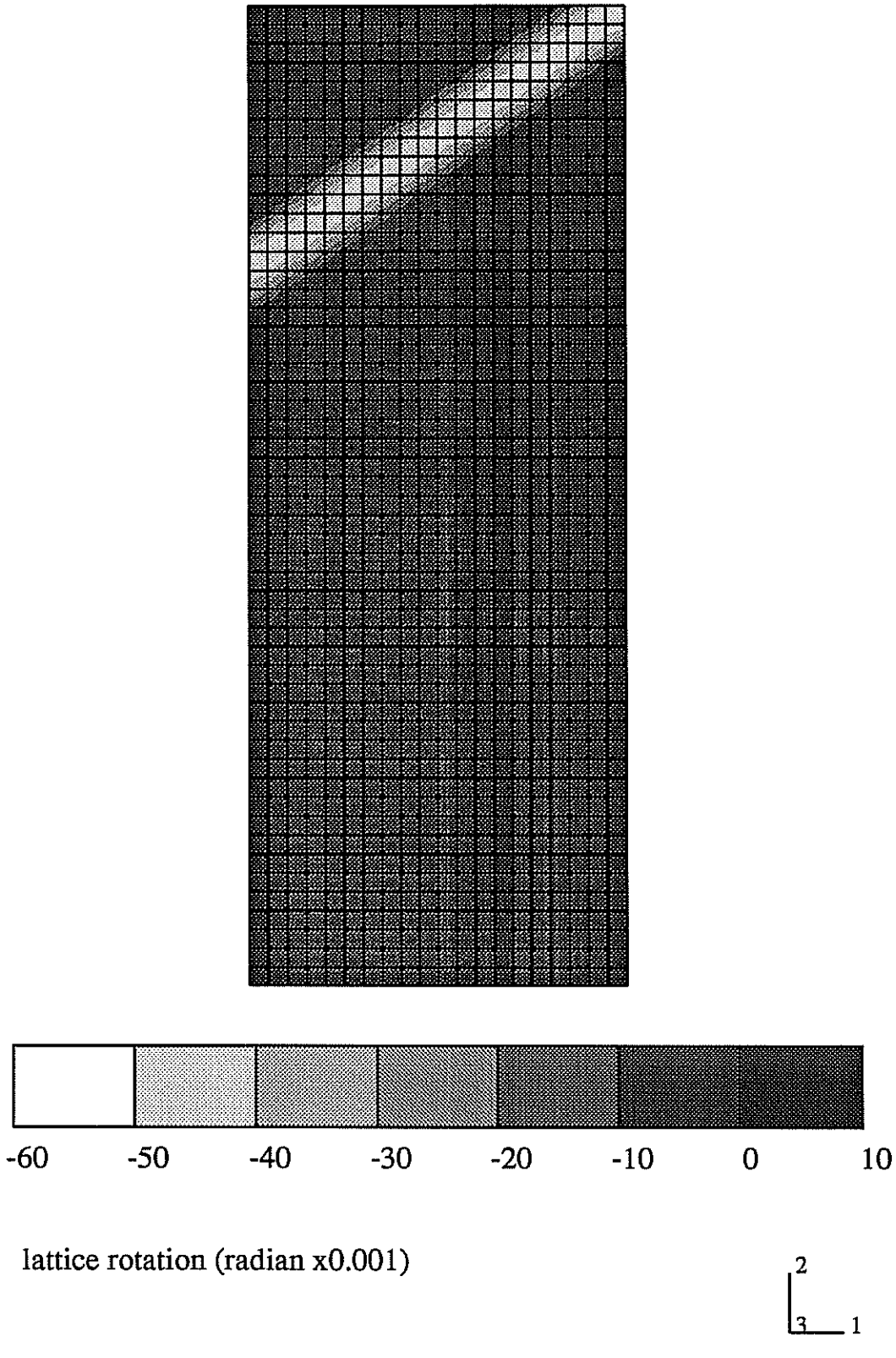

Part B

A COSSERAT THEORY FOR SINGLE CRYSTALS

1 A Cosserat theory for single crystals

1.1 Motivations

Mandel [1973] introduced the notion of oriented microelements characterized by some hidden directors into the theory of elastoviscoplasticity. The epoch-making expression "trièdre directeur" is directly taken from the Cosserat brothers' well-known work [Cosserat, Cosserat 1896,1909]. At this place Mandel's words must be quoted:

"Ces vecteurs ne subissent pas ([...]) la même transformation que les lignes matérielles qui joignent les centres des microéléments. C'est en cela que le milieu plastique diffère du milieu continu classique. On doit le concevoir un peu comme un milieu de Cosserat, dans lequel les microéléments ont une rotation différente de la rotation globale du macroélément."

The relative rotation of neighbouring microelements may induce local couple stresses. To a first approximation Mandel neglects them and regards the single crystal and the polycrystal as a classical continuum. We propose here the strict treatment of the single crystal as a Cosserat continuum.

Nye [1953] noticed that after bending or torsion a crystal contains excess dislocations of a definite sign that give rise to lattice curvature. In a modelling of single crystals with more reference to dislocations, this additional deformation possibility should be taken into account. Furthermore Kröner [1963] claimed that the macroscopic response of a medium to inner lattice curvature is the existence of actual Cosserat couple stresses:

"Die spezifische Reaktion eines Mediums gegen Anwesenheit einer Versetzungsdichte bzw. gegen die hiermit äquivalenten Nyeschen Gitterkrümmungen sind echte Kosseratsche Momentenspannungen."([Kröner 1966])

The couple-stresses may be of the same order of magnitude as force-stresses under some circumstances ([Hehl, Kröner 1965], [McClintock 1958, 1960]). In these early works Kröner regards the dislocated crystal as a Cosserat medium. However, his theory deals with symmetric force-stresses and he suggests later that there may be fundamental differences between dislocation theory and Cosserat theory [Kröner 1967].

The reason for such a misunderstanding stems from the frequent use in literature of the Cosserat continuum as the medium in which single dislocations may be embedded. Kessel [1970] computes the force and couple stress fields around a screw and an edge dislocation in a Cosserat continuum. In the present work we claim that the continuum containing a large number of dislocations in the sense of the continuum theory of dislocations [Nye 1953], can be modelled as a Cosserat continuum. Kröner [1993] argues that the rotation of the crystal lattice with dislocations is not the eigenrotation of physical particles but the rotation of a structure. This pleads against the constrained Cosserat theory that is usually used in the continuum theory of dislocations (see section 2.4). As a result, in the Cosserat theory presented here, the rotational degrees of freedom are independent of the displacement field and are linked only at the constitutive level. Whereas the definition of the Cosserat directors involved in the continuum theory of dislocation is left unspecified,

the "trièdre directeur" in this work is clearly made of three orthogonal lattice vectors attached to each volume element. The volume element must contain a large number of dislocations and its characteristic size must be such that a mean crystal orientation can be unambiguously defined at each time.

1.2 Kinematics of the Cosserat continuum

A material point $M \in$ B at time t_0 is described by its position $\underline{\mathbf{X}}$ and its inner state $\underset{\sim}{\mathbf{R}}$, for an arbitrary initial placement, chosen as the reference configuration. At time t, its position is $\underline{\mathbf{x}}(\underline{\mathbf{X}}, t)$ and its inner state $\underset{\sim}{\mathbf{R}}(\underline{\mathbf{X}}, t)$, in a given reference frame E. If $(\underline{\mathbf{d}}_i)_{i=1,3}$ are three orthogonal lattice vectors at t and $(\underline{\mathbf{d}}_i^0)_{i=1,3}$ their initial position in E, then the rotation $\underline{\mathbf{R}}$ is defined through

$$\underline{\mathbf{d}}_i \;=\; \underset{\sim}{\mathbf{R}}\;\underline{\mathbf{d}}_i^0 \tag{1}$$

with

$$\underset{\sim}{\mathbf{R}}(\underline{\mathbf{X}}, t_0) \;=\; \underset{\sim}{\mathbf{1}} \;\text{ and }\; \mathrm{Det}\;\underset{\sim}{\mathbf{R}} \;=\; 1 \tag{2}$$

A rotating frame $E^\sharp(M)$ is attached to the lattice structure at each point $M \in$ B and each tensor variable y considered with respect to $E^\sharp$ will be denoted ${}^\sharp y$.

The rotation field $\underline{\mathbf{R}}(\underline{\mathbf{X}}, t)$ can be replaced by the vector field $\underline{\mathbf{\Phi}}(\underline{\mathbf{X}}, t)$ given by equation Appendix1-15. The three components of $\underline{\mathbf{\Phi}}$ are three degrees of freedom of the continuum in addition to the three components of the displacement field

$$\underline{\mathbf{u}}(\underline{\mathbf{X}}, t) \;=\; \underline{\mathbf{x}}(\underline{\mathbf{X}}, t) \;-\; \underline{\mathbf{X}} \tag{3}$$

For $\underline{\mathbf{u}}$ and $\underline{\mathbf{\Phi}}$ are regarded as independent kinematic variables which can be connected only at the constitutive level or by some constraint.

The deformation gradient classically links a current infinitesimal material segment $d\underline{\mathbf{x}}$ with its initial position $d\underline{\mathbf{X}}$

$$d\underline{\mathbf{x}} \;=\; \underset{\sim}{\mathbf{F}}\; d\underline{\mathbf{X}} \tag{4}$$

so that

$$\underset{\sim}{\mathbf{F}} \;=\; \underline{\mathbf{u}} \otimes \underline{\nabla} \;=\; u_{i,j}\; \underline{\mathbf{e}}_i \otimes \underline{\mathbf{e}}_j \tag{5}$$

(in the absence of other indication, partial derivatives are taken with respect to the X_j).

Similarly and following [Sievert 1992], the variation $d\underset{\sim}{\mathbf{R}}$ of microrotation can be related to an infinitesimal displacement $d\underline{\mathbf{X}}$ in the reference configuration. The equation 15 of Appendix 1 implies

$$(d\underset{\sim}{\mathbf{R}})\;\underset{\sim}{\mathbf{R}}^T \;=\; \underset{\sim}{\mathbf{1}} \times \delta\underline{\mathbf{\Phi}} \;=\; \underset{\approx}{\epsilon}\;\delta\underline{\mathbf{\Phi}} \tag{6}$$

Hence

$$\begin{aligned}
\delta\underline{\mathbf{\Phi}} \;&=\; -\frac{1}{2}\,\underline{\underline{\epsilon}}(d\underset{\sim}{\mathbf{R}}\;\underline{\mathbf{R}}^T) \\
&=\; -\frac{1}{2}\,\epsilon_{ijk}\;dR_{jm}\;R^T_{mk}\;\underline{\mathbf{e}}_i \\
&=\; \frac{1}{2}\,\epsilon_{ikj}\;R_{km}\;R_{jm,n}\;dX_n\;\underline{\mathbf{e}}_i \\
&=\; \underset{\sim}{\mathbf{\Gamma}}\;d\underline{\mathbf{X}}
\end{aligned} \tag{7}$$

with

$$\underset{\sim}{\mathbf{\Gamma}} \;=\; \frac{1}{2}\,\underline{\underline{\epsilon}} : (\underset{\sim}{\mathbf{R}}\;(\underline{\mathbf{R}}^T \otimes \underline{\nabla})) \tag{8}$$

Contrary to $\underset{\sim}{\mathbf{F}}$, $\underset{\sim}{\Gamma}$ generally is not invertible. With respect to the local space frame $E^\sharp$,

$$ {}^\sharp d\underline{\mathbf{x}} = {}^\sharp\underset{\sim}{\mathbf{F}}\, d\underline{\mathbf{X}} \tag{9} $$

$$ {}^\sharp\delta\underline{\Phi} = {}^\sharp\underset{\sim}{\Gamma}\, d\underline{\mathbf{X}} \tag{10} $$

where ${}^\sharp d\underline{\mathbf{x}} = \underset{\sim}{\mathbf{R}}^T\, d\underline{\mathbf{x}}$ and ${}^\sharp d\underline{\Phi} = \underset{\sim}{\mathbf{R}}^T\, d\underline{\Phi}$ and

$$ {}^\sharp\underset{\sim}{\mathbf{F}} = \underset{\sim}{\mathbf{R}}^T\, \underset{\sim}{\mathbf{F}} \tag{11} $$

$$ {}^\sharp\underset{\sim}{\Gamma} = \underset{\sim}{\mathbf{R}}^T\, \underset{\sim}{\Gamma} \tag{12} $$

It can be seen that ${}^\sharp\underset{\sim}{\mathbf{F}}$ and ${}^\sharp\underset{\sim}{\Gamma}$ are invariant under any Euclidean transformation [Kafadar, Eringen 1971]. A Euclidean transformation is a space frame change with the form:

$$ \begin{aligned} \underline{\mathbf{x}}' &= \underset{\sim}{\mathbf{Q}}(t)\, \underline{\mathbf{x}}(\underline{\mathbf{X}}, t) + \underline{\mathbf{c}}(t) \\ \underset{\sim}{\mathbf{R}}' &= \underset{\sim}{\mathbf{Q}}(t)\, \underset{\sim}{\mathbf{R}}(\underline{\mathbf{X}}, t) \end{aligned} \tag{13} $$

where $\underset{\sim}{\mathbf{Q}}$ belongs to the orthogonal group and $\underset{\sim}{\mathbf{Q}}(t_0) = \underset{\sim}{\mathbf{1}}$. Accordingly they are natural Cosserat strains for the development of constitutive equations. They are called respectively the Cosserat deformation tensor and the wryness (or bend-twist, or curvature) tensor. Using 7 and 8 of Appendix 1, expression 8 can be transformed into

$$ \begin{aligned} {}^\sharp\underset{\sim}{\Gamma}\, d\underline{\mathbf{X}} &= -\frac{1}{2}\, \underline{\underline{\epsilon}}(d\underset{\sim}{\mathbf{R}}\, \underset{\sim}{\mathbf{R}}^T) \\ &= -\frac{1}{2}\, \underline{\underline{\epsilon}}(\underset{\sim}{\mathbf{R}}\, (\underset{\sim}{\mathbf{R}}^T\, d\underset{\sim}{\mathbf{R}})\, \underset{\sim}{\mathbf{R}}^T) \\ &= -\frac{1}{2}\, \underline{\underline{\epsilon}}(\underset{\sim}{\mathbf{R}}^T\, d\underset{\sim}{\mathbf{R}}) \end{aligned} $$

so that

$$ {}^\sharp\underset{\sim}{\Gamma} = -\frac{1}{2}\, \underline{\underline{\epsilon}} : (\underset{\sim}{\mathbf{R}}^T\, (\underset{\sim}{\mathbf{R}} \otimes \underline{\nabla})) \tag{14} $$

One defines next the velocity

$$ \underline{\mathbf{v}} = \dot{\underline{\mathbf{u}}} = \dot{u}_i\, \underline{\mathbf{e}}_i \tag{15} $$

and the gyration tensor [Eringen 1976]

$$ \underset{\sim}{v} = \dot{\underset{\sim}{\mathbf{R}}}\, \underset{\sim}{\mathbf{R}}^T \tag{16} $$

which can be replaced by the associated gyration vector

$$ \overset{\times}{\underline{v}} = -\frac{1}{2}\, \underline{\underline{\epsilon}}\, \underset{\sim}{v} \tag{17} $$

since it is antisymmetric. The time derivative of the Cosserat strains can be related to the gradient of the latter quantities:

$$ \begin{aligned} {}^\sharp\dot{\underset{\sim}{\mathbf{F}}}\ {}^\sharp\underset{\sim}{\mathbf{F}}^{-1} &= \underset{\sim}{\mathbf{R}}^T\, (\dot{\underset{\sim}{\mathbf{F}}}\, \underset{\sim}{\mathbf{F}}^{-1} - \dot{\underset{\sim}{\mathbf{R}}}\, \underset{\sim}{\mathbf{R}}^T)\, \underset{\sim}{\mathbf{R}} \\ &= \underset{\sim}{\mathbf{R}}^T\, (\underline{\mathbf{v}} \otimes \underline{\nabla}^c - \underset{\sim}{v})\, \underset{\sim}{\mathbf{R}} \\ &= \underset{\sim}{\mathbf{R}}^T\, (\underline{\mathbf{v}} \otimes \underline{\nabla}^c - \underset{\sim}{\mathbf{1}} \times \overset{\times}{\underline{v}})\, \underset{\sim}{\mathbf{R}} \end{aligned} \tag{18} $$

where $\underset{\sim}{\nabla}^c = \dfrac{\partial}{\partial x_i}\,\underline{\mathbf{e}}_i = \underset{\sim}{\mathbf{F}}^{-T}\,\underset{\sim}{\nabla}$ (Euclidean representation, c stands for current).
$\underline{\mathbf{v}}\otimes\underline{\nabla}^c - \underset{\sim}{v}$ is the relative velocity gradient and describes the local motion of the particle with respect to the microstructure. Taking the time derivative of equation 10, we get in a way similar to [Sievert 1992]

$$\begin{aligned}
(\,{}^{\sharp}d\underline{\mathbf{\Phi}}\,)^{\cdot} &= {}^{\sharp}\dot{\underset{\sim}{\mathbf{\Gamma}}}\; d\underline{\mathbf{X}} \\
&= -\frac{1}{2}\,\underline{\underline{\epsilon}}(\underset{\sim}{\mathbf{R}}^T\, d\underset{\sim}{\mathbf{R}})^{\cdot} \\
&= -\frac{1}{2}\,\underline{\underline{\epsilon}}(\dot{\underset{\sim}{\mathbf{R}}}^T\, d\underset{\sim}{\mathbf{R}} + \underset{\sim}{\mathbf{R}}^T\, d\dot{\underset{\sim}{\mathbf{R}}}) \\
&= -\frac{1}{2}\,\underline{\underline{\epsilon}}(\underset{\sim}{\mathbf{R}}^T\,(\underset{\sim}{\mathbf{R}}\,\dot{\underset{\sim}{\mathbf{R}}}^T\, d\underset{\sim}{\mathbf{R}}\,\underset{\sim}{\mathbf{R}}^T + d\dot{\underset{\sim}{\mathbf{R}}}\,\underset{\sim}{\mathbf{R}}^T)\,\underset{\sim}{\mathbf{R}}) \\
&= -\frac{1}{2}\,\underset{\sim}{\mathbf{R}}^T\,\underline{\underline{\epsilon}}(\underset{\sim}{\mathbf{R}}\,\dot{\underset{\sim}{\mathbf{R}}}\, d\underset{\sim}{\mathbf{R}}\,\underset{\sim}{\mathbf{R}}^T + d\dot{\underset{\sim}{\mathbf{R}}}\,\underset{\sim}{\mathbf{R}}^T) \\
&= -\frac{1}{2}\,\underset{\sim}{\mathbf{R}}^T\,\underline{\underline{\epsilon}}(\dot{\underset{\sim}{\mathbf{R}}}\,\underset{\sim}{\mathbf{R}}^T\,\underset{\sim}{\mathbf{R}}\, d\underset{\sim}{\mathbf{R}}^T + d\dot{\underset{\sim}{\mathbf{R}}}\,\underset{\sim}{\mathbf{R}}^T) \\
&= -\frac{1}{2}\,\underset{\sim}{\mathbf{R}}^T\,\underline{\underline{\epsilon}}\, d\underset{\sim}{v} \\
&= \underset{\sim}{\mathbf{R}}^T\, d\overset{\times}{\underline{v}} \\
&= \underset{\sim}{\mathbf{R}}^T\,\overset{\times}{\underline{v}}\otimes\underline{\nabla}\, d\underline{\mathbf{X}}
\end{aligned} \tag{19}$$

Hence

$${}^{\sharp}\dot{\underset{\sim}{\mathbf{\Gamma}}} = \underset{\sim}{\mathbf{R}}^T\,\overset{\times}{\underline{v}}\otimes\underline{\nabla} \tag{20}$$

or using the Eulerian representation,

$${}^{\sharp}\dot{\underset{\sim}{\mathbf{\Gamma}}}\;{}^{\sharp}\underset{\sim}{\mathbf{F}}^{-1} = \underset{\sim}{\mathbf{R}}^T\,\overset{\times}{\underline{v}}\otimes\underline{\nabla}^c\,\underset{\sim}{\mathbf{R}} \tag{21}$$

1.3 Sthenics

In order to introduce forces and stresses and to deduce the equilibrium equations, we resort to the method of virtual power developed by Germain [1973] in the case of micromorphic media. The method is readily adapted to the case of a Cosserat continuum.

The virtual motions are the velocity $\underline{\mathbf{v}}$ and the gyration $\overset{\times}{\underline{v}}$ (or microrotation rate vector). The next step is to choose the form of the virtual power of a system of forces. Within the framework of a first gradient theory, the virtual power of the internal forces is a linear form of the virtual motions and their gradients. The principle of material frame indifference requires that this linear form should be invariant under any Euclidean transformation. That is why we will work with the objective quantities $\underline{\mathbf{v}}\otimes\underline{\nabla}^c - \underset{\sim}{v}$ and $\overset{\times}{\underline{v}}\otimes\underline{\nabla}^c$. The dual quantities involved in the linear form of the virtual power of the internal forces are denoted $\underset{\sim}{\sigma}$ and $\underset{\sim}{\mu}$ respectively and are assumed to be objective tensors. For objectivity reasons the dual variable associated with $\underline{\mathbf{v}}$ is zero. For any subdomain $\mathcal{D}\subset\mathcal{B}$

$$\mathcal{P}_{(i)} = -\int_{\mathcal{D}} \left(\underset{\sim}{\sigma} : (\underline{\mathbf{v}}\otimes\underline{\nabla}^c - \underset{\sim}{v}) + \underset{\sim}{\mu} : (\overset{\times}{\underline{v}}\otimes\underline{\nabla}^c)\right) dV$$

$$
\begin{aligned}
&= -\int_{\mathcal{D}} \left(\sigma_{ij}\, v_{i,j} + \mu_{ij}\, \overset{\times}{v}_{i,j} - \sigma_{ij}\, v_{ij}\right) dV \\
&= -\int_{\mathcal{D}} \left(\sigma_{ij}\, v_i + \mu_{ij}\overset{\times}{v}_i\right)_{,j} dV + \int_{\mathcal{D}} \left(\sigma_{ij,j}\, v_i + (\mu_{ij,j} - \epsilon_{ikl}\, \sigma_{kl})\, \overset{\times}{v}_i\right) dV \\
&= -\int_{\partial\mathcal{D}} \left(\sigma_{ij}\, v_i + \mu_{ij}\overset{\times}{v}_i\right) n_j\, dS + \int_{\mathcal{D}} \left(\sigma_{ij,j}\, v_i + (\mu_{ij,j} - \epsilon_{ikl}\, \sigma_{kl})\, \overset{\times}{v}_i\right) dV \\
&= -\int_{\partial\mathcal{D}} \left(\underline{\mathbf{v}}\, \underset{\sim}{\sigma} + \overset{\times}{\underline{v}}\, \underset{\sim}{\mu}\right).\underline{\mathbf{n}}\, dS + \int_{\mathcal{D}} \left(\underline{\mathbf{v}}.\underline{\mathrm{div}}\, \underset{\sim}{\sigma} + \overset{\times}{\underline{v}}.(\underline{\mathrm{div}}\, \underset{\sim}{\mu} + 2\overset{\times}{\underline{\sigma}})\right) dV \qquad (22)
\end{aligned}
$$

(in this section the partial derivatives are taken with respect to the current configuration). The virtual power of external forces reads

$$\mathcal{P}_{(e)} = \int_{\mathcal{D}} \left(\underline{\mathbf{f}}.\underline{\mathbf{v}} + \underline{\mathbf{c}}.\overset{\times}{\underline{v}}\right) dS \qquad (23)$$

The virtual power of contact forces must then be defined

$$\mathcal{P}_{(c)} = \int_{\partial\mathcal{D}} \left(\underline{\mathbf{t}}.\underline{\mathbf{v}} + \underline{\mathbf{m}}.\overset{\times}{\underline{v}}\right) dS \qquad (24)$$

The dual quantities of the velocity and microrotation rate in $\mathcal{P}_{(e)}$ and $\mathcal{P}_{(i)}$ have the dimensions of force and moment respectively. The principle of virtual power then states that

$$\forall \mathcal{D} \subset \mathcal{B}, \forall (\underline{\mathbf{v}}, \overset{\times}{\underline{v}}) \quad \mathcal{P}_{(i)} + \mathcal{P}_{(e)} + \mathcal{P}_{(c)} = 0 \qquad (25)$$

In particular

$$
\begin{gathered}
\forall \mathcal{D} \subset \mathcal{B}, \forall (\underline{\mathbf{v}}, \overset{\times}{\underline{v}}) \;/\; \underline{\mathbf{v}} = \overset{\times}{\underline{v}} = 0 \text{ on } \partial\mathcal{D}, \\
\int_{\mathcal{D}} \left(\underline{\mathbf{v}}.(\underline{\mathrm{div}}\, \underset{\sim}{\sigma} + \underline{\mathbf{f}}) + \overset{\times}{\underline{v}}.(\underline{\mathrm{div}}\, \underset{\sim}{\mu} + 2\overset{\times}{\underline{\sigma}} + \underline{\mathbf{c}})\right) dV = 0 \qquad (26)
\end{gathered}
$$

Assuming that the quantities are continuous on $\mathcal{B}$, the local equilibrium equations follow from 26

$$\begin{cases} \underline{\mathrm{div}}\, \underset{\sim}{\sigma} + \underline{\mathbf{f}} = 0 \\ \underline{\mathrm{div}}\, \underset{\sim}{\mu} + 2\overset{\times}{\underline{\sigma}} + \underline{\mathbf{c}} = 0 \end{cases} \qquad (27)$$

As a result, the principle of virtual power becomes

$$\forall \mathcal{D} \subset \mathcal{B}, \forall (\underline{\mathbf{v}}, \overset{\times}{\underline{v}}) \quad \int_{\partial\mathcal{D}} \left((\underset{\sim}{\sigma}\, \underline{\mathbf{n}} - \underline{\mathbf{t}}).\underline{\mathbf{v}} + (\underset{\sim}{\mu}\, \underline{\mathbf{n}} - \underline{\mathbf{m}}).\overset{\times}{\underline{v}}\right) dV = 0 \qquad (28)$$

from which the boundary conditions are deduced

$$\begin{cases} \underset{\sim}{\sigma}\, \underline{\mathbf{n}} = \underline{\mathbf{t}} \\ \underset{\sim}{\mu}\, \underline{\mathbf{n}} = \underline{\mathbf{m}} \end{cases} \qquad (29)$$

$\underset{\sim}{\sigma}$ is called the Cauchy force stress tensor and $\underset{\sim}{\mu}$ the couple-stress tensor. They are generally not symmetric.

1.4 Hyperelasticity

1.4.1 Energy balance

Let ε be the internal energy per unit mass, $\underline{\mathbf{q}}$ the heat flux vector, ρ the current density. The energy balance equation reads then

$$\rho\, \dot{\varepsilon} = \underset{\sim}{\sigma} : (\underline{\mathbf{v}} \otimes \underline{\nabla}^c - \underset{\sim}{v}) + \underset{\sim}{\mu} : (\overset{\times}{\underline{v}} \otimes \underline{\nabla}^c) - \mathrm{div}\, \underline{\mathbf{q}} \qquad (30)$$

(any other inner heat supply is excluded).

According to the thermodynamics of irreversible processes, the entropy principle is written

$$\rho\,\dot{\eta} \;+\; \mathrm{div}\,(\frac{\underline{\underline{\mathbf{q}}}}{T}) \;\geq\; 0 \tag{31}$$

where T denotes the temperature and η the entropy per unit mass.

Introducing the free energy $\psi \;=\; \varepsilon \;-\; \eta\,T$ and combining the energy and entropy equations, one derives the Clausius-Duhem inequality

$$-\,\rho\,(\dot{\psi} \;+\; \eta\,T) \;+\; \underset{\sim}{\sigma} : (\underline{\mathbf{v}} \otimes \underline{\nabla}^c \;-\; \underline{\underline{v}}) \;+\; \underset{\sim}{\mu} : (\overset{\times}{\underline{\underline{v}}} \otimes \underline{\nabla}^c) \;-\; \frac{1}{T}\,\underline{\mathbf{q}}.T\underline{\nabla}^c \;\geq\; 0 \tag{32}$$

or equivalently,

$$-\,\rho\,(\dot{\psi} \;+\; \eta\,T) \;+\; {}^{\sharp}\underset{\sim}{\sigma} : (\,{}^{\sharp}\dot{\underset{\sim}{\mathbf{F}}}\;\,{}^{\sharp}\underset{\sim}{\mathbf{F}}^{-1}) \;+\; {}^{\sharp}\underset{\sim}{\mu} : (\,{}^{\sharp}\dot{\underset{\sim}{\Gamma}}\;\,{}^{\sharp}\underset{\sim}{\mathbf{F}}^{-1}) \;-\; \frac{1}{T}\,\underline{\mathbf{q}}.T\underline{\nabla}^c \;\geq\; 0 \tag{33}$$

where

$$\left\{\begin{array}{l} {}^{\sharp}\underset{\sim}{\sigma} \;=\; \underset{\sim}{\mathbf{R}}^T\,\underset{\sim}{\sigma}\,\underset{\sim}{\mathbf{R}} \\ {}^{\sharp}\underset{\sim}{\mu} \;=\; \underset{\sim}{\mathbf{R}}^T\,\underset{\sim}{\mu}\,\underset{\sim}{\mathbf{R}} \end{array}\right. \tag{34}$$

are rotated stress tensors with respect to the space frame $E^{\sharp}$ attached to the microstructure.

A material is said to be hyperelastic if its free energy and entropy are function of ${}^{\sharp}\underset{\sim}{\mathbf{F}}$ and ${}^{\sharp}\underset{\sim}{\Gamma}$ only. The Clausius-Duhem inequality 33 becomes

$$\begin{aligned} -\left(\rho\,\frac{\partial\psi}{\partial\,{}^{\sharp}\underset{\sim}{\mathbf{F}}} \;-\; {}^{\sharp}\underset{\sim}{\sigma}\;{}^{\sharp}\underset{\sim}{\mathbf{F}}^{-T}\right) \;:\; {}^{\sharp}\dot{\underset{\sim}{\mathbf{F}}} \qquad & -\left(\rho\,\frac{\partial\psi}{\partial\,{}^{\sharp}\underset{\sim}{\Gamma}} \;-\; {}^{\sharp}\underset{\sim}{\mu}\;{}^{\sharp}\underset{\sim}{\mathbf{F}}^{-T}\right) \;:\; {}^{\sharp}\dot{\underset{\sim}{\Gamma}} \\ & -\left(\rho\,\eta \;+\; \rho\,\frac{\partial\psi}{\partial T}\right)\,\dot{T} \;-\; \frac{1}{T}\,\underline{\mathbf{q}}.T\underline{\nabla}^c \;\geq\; 0 \end{aligned} \tag{35}$$

Since this expression is linear in ${}^{\sharp}\underset{\sim}{\mathbf{F}}^{-T}$, ${}^{\sharp}\dot{\underset{\sim}{\Gamma}}$ and $\dot{T}$, the last inequality implies

$$\eta \;=\; -\frac{\partial\psi}{\partial T} \tag{36}$$

and

$$\left\{\begin{array}{l} {}^{\sharp}\underset{\sim}{\sigma} \;=\; \rho\,\dfrac{\partial\psi}{\partial\,{}^{\sharp}\underset{\sim}{\mathbf{F}}}\;{}^{\sharp}\underset{\sim}{\mathbf{F}}^T \\ {}^{\sharp}\underset{\sim}{\mu} \;=\; \rho\,\dfrac{\partial\psi}{\partial\,{}^{\sharp}\underset{\sim}{\Gamma}}\;{}^{\sharp}\underset{\sim}{\mathbf{F}}^T \end{array}\right. \tag{37}$$

or

$$\left\{\begin{array}{l} \underset{\sim}{\sigma} \;=\; \rho\,\underset{\sim}{\mathbf{R}}\,\dfrac{\partial\psi}{\partial\,{}^{\sharp}\underset{\sim}{\mathbf{F}}}\;\underset{\sim}{\mathbf{F}}^T \\ \underset{\sim}{\mu} \;=\; \rho\,\underset{\sim}{\mathbf{R}}\,\dfrac{\partial\psi}{\partial\,{}^{\sharp}\underset{\sim}{\Gamma}}\;\underset{\sim}{\mathbf{F}}^T \end{array}\right. \tag{38}$$

1.4.2 Linear case; isotropic elasticity

Deformation and curvature are small if $\| {}^{\natural}\underset{\sim}{\mathbf{F}} - \underset{\sim}{\mathbf{1}} \| \ll 1$ and $\| {}^{\natural}\underset{\sim}{\Gamma} \| \; l \ll 1$, where l is a characteristic length. If, in addition, microrotations remain small, i.e. if $\|\underline{\mathbf{\Phi}}\| \ll 1$, then

$$\underset{\sim}{\mathbf{R}} \simeq \underset{\sim}{\mathbf{1}} + \underset{\sim}{\mathbf{1}} \times \underline{\mathbf{\Phi}} = \underset{\sim}{\mathbf{1}} - \underset{\sim}{\epsilon}\, \underline{\mathbf{\Phi}} \tag{39}$$

$$\|\underline{\mathbf{u}} \otimes \underline{\nabla}\| \ll 1 \text{ and } \| \underline{\mathbf{\Phi}} \otimes \underline{\nabla}\| \; l \ll 1 \tag{40}$$

$${}^{\natural}\underset{\sim}{\mathbf{F}} \simeq \underset{\sim}{\mathbf{1}} + \underline{\mathbf{u}} \otimes \underline{\nabla} + \underset{\sim}{\epsilon}\, \underline{\mathbf{\Phi}} = \underset{\sim}{\mathbf{1}} + \underset{\sim}{\mathbf{e}} \tag{41}$$

$${}^{\natural}\underset{\sim}{\Gamma} \simeq \underline{\mathbf{\Phi}} \otimes \underline{\nabla} = \underset{\sim}{\kappa} \tag{42}$$

Furthermore, ${}^{\natural}\underset{\sim}{\sigma} \simeq \underset{\sim}{\sigma}$ and ${}^{\natural}\underset{\sim}{\mu} \simeq \underset{\sim}{\mu}$. Accordingly, for linear elasticity, two four-rank elasticity tensors are introduced

$$\underset{\sim}{\sigma} = \underset{\approx}{\mathbf{E}} : \underset{\sim}{\mathbf{e}} \tag{43}$$

$$\underset{\sim}{\mu} = \underset{\approx}{\mathbf{C}} : \underset{\sim}{\kappa} \tag{44}$$

(No coupling between deformation and curvature is possible as soon as point symmetry is assumed even for the less symmetric solid [Kessel 1964]). Some symmetry properties of these tensors are derived from the hyperelasticity conditions 37

$$E_{ijkl} = E_{klij} \text{ and } C_{ijkl} = C_{klij} \tag{45}$$

Further symmetry conditions can be gained if material symmetries are taken into account. The form of the Cosserat elasticity tensors for all symmetry classes has been established by [Kessel 1964] and can be found in [Ilcewicz, Narasimhan, Wilson 1986]. For a triclinic solid, 90 independent constants are necessary instead of 21 in the classical case (for a solid without point symmetry, Kessel found 171 constants!). For cubic symmetry, 10 constants instead of 3. We now lay the stress on the isotropic case, which will be used in part 5. The two classical Lamé constants λ, μ are complemented by 4 additional parameters according to

$$\underset{\sim}{\sigma} = \lambda\, \underset{\sim}{\mathbf{1}}\, \mathrm{Tr}\, \underset{\sim}{\mathbf{e}} + 2\mu\, \{\underset{\sim}{\mathbf{e}}\} + 2\mu_c\, \}\underset{\sim}{\mathbf{e}}\{ \tag{46}$$

$$\underset{\sim}{\mu} = \alpha\, \underset{\sim}{\mathbf{1}}\, \mathrm{Tr}\, \underset{\sim}{\kappa} + 2\beta\, \{\underset{\sim}{\kappa}\} + 2\gamma\, \}\underset{\sim}{\kappa}\{ \tag{47}$$

Relation 46 can be inverted in

$$\underset{\sim}{\mathbf{e}} = \frac{1}{2\mu}\, \{\underset{\sim}{\sigma}\} - \frac{\lambda}{2\mu(3\lambda + 2\mu)}\, \underset{\sim}{\mathbf{1}}\, (\mathrm{Tr}\, \underset{\sim}{\sigma}) + \frac{1}{2\mu_c}\, \}\underset{\sim}{\sigma}\{ \tag{48}$$

The expression of the free energy is

$$\begin{aligned} \psi(\underset{\sim}{\mathbf{e}}, \underset{\sim}{\kappa}) &= \frac{1}{2}\, \underset{\sim}{\mathbf{e}} : \underset{\approx}{\mathbf{E}} : \underset{\sim}{\mathbf{e}} + \frac{1}{2}\, \underset{\sim}{\kappa} : \underset{\approx}{\mathbf{C}} : \underset{\sim}{\kappa} \\ &= \frac{1}{2}\, e_{ij}\, E_{ijkl}\, e_{kl} + \frac{1}{2}\, \kappa_{ij}\, C_{ijkl}\, \kappa_{kl} \end{aligned} \tag{49}$$

Stability conditions are derived by [Eringen 1976] and require the non-negativeness of the elastic work, so that

$$\begin{cases} 3\lambda + 2\mu \geq 0 \\ \mu \geq 0 \\ \mu_c \geq 0 \end{cases} \tag{50}$$

and similar relations hold for α, β, γ.

1.4.3 Example: simple bending in the linear case

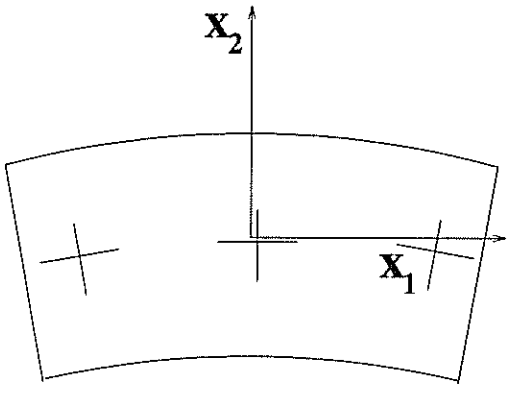

We consider the simple bending of an isotropic elastic material under plane strain conditions (see the figure for the definition of the axes). We postulate the form of the stress tensor

$$\underset{\sim}{\sigma} = Ax_2\ \underline{\mathbf{e}}_1 \otimes \underline{\mathbf{e}}_1 + \sigma_3\ \underline{\mathbf{e}}_3 \otimes \underline{\mathbf{e}}_3 \tag{51}$$

We first give the solution in the classical case for which no microstructure is considered:

$$\sigma_3 = \nu A x_2 \text{ and } A = -\frac{\mathcal{M}}{\mathrm{I}} \tag{52}$$

where M is the applied bending moment. The displacement field is

$$\begin{cases} u_1 = \dfrac{A}{E}(1-\nu^2)\, x_1 x_2 \\ u_2 = -\dfrac{\nu A}{2E}(1+\nu)\, x_2^2 - \dfrac{A(1-\nu^2)}{2E}\, x_1^2 \\ u_3 = 0 \end{cases} \tag{53}$$

We can compute the material curvature tensor $\underset{\sim}{\chi}$ (curvature of the material fibres)

$$\underset{\sim}{\chi} = \overset{\times}{\underline{\mathbf{F}}} \otimes \underline{\nabla} = -\frac{A}{E}(1-\nu^2)\ \underline{\mathbf{e}}_3 \otimes \underline{\mathbf{e}}_1 \tag{54}$$

For the Cosserat continuum the material is, for instance, an elastic single crystal. We investigate the existence of a solution with the same form of stress tensor as 51 and the following form of rotation field

$$\underline{\mathbf{\Phi}} = Bx_1\ \underline{\mathbf{e}}_3 \tag{55}$$

From the elastic relations 48 we get

$$\sigma_3 = \nu A x_2$$

and

$$\begin{aligned} \underset{\sim}{\mathbf{e}} &= \frac{A}{E}x_2(1-\nu^2)\ \underline{\mathbf{e}}_1 \otimes \underline{\mathbf{e}}_1 - \frac{\nu A}{E}x_2(1+\nu)\ \underline{\mathbf{e}}_2 \otimes \underline{\mathbf{e}}_2 \\ &= \underline{\mathbf{u}} \otimes \underline{\nabla} + \underset{\sim}{\epsilon}\, \underline{\mathbf{\Phi}} \end{aligned}$$

We must then solve the partial differential equations

$$\begin{aligned} u_{1,1} &= \tfrac{A}{E} x_2 (1-\nu^2) \\ u_{2,2} &= -\tfrac{\nu A}{E} x_2 (1+\nu) \\ u_{1,2} + Bx_1 &= 0 \\ u_{2,1} - Bx_1 &= 0 \end{aligned}$$

The proposed form is a solution if and only if

$$B = -\frac{A}{E}(1-\nu^2) \tag{56}$$

In that case the displacement field is also given by 53. Then we compute the curvature tensor and the associated couple-stress

$$\underset{\sim}{\kappa} = B\, \underline{\mathbf{e}}_3 \otimes \underline{\mathbf{e}}_1 \tag{57}$$

$$\underset{\sim}{\mu} = B\,(\beta+\gamma)\, \underline{\mathbf{e}}_3 \otimes \underline{\mathbf{e}}_1 + (\beta-\gamma)\, \underline{\mathbf{e}}_1 \otimes \underline{\mathbf{e}}_3 \tag{58}$$

The condition 56 implies $\underset{\sim}{\kappa} = \underset{\sim}{\chi}$, which means that the lattice vectors move with the material lines. If this constraint is abandonned, a more complicated form of the solution must be worked out.

1.5 Elastoplastic Cosserat single crystals

The works of Sawczuk [1967], Lippmann [1969] and Besdo [1974] are the first milestones in the plasticity theory of Cosserat continua at small strains. In the case of single crystals we resort to recent results in Cosserat theory at large strains [Sievert 1992].

1.5.1 Strain decomposition

In single crystals non-homogeneous plastic deformations induce non-homogeneous permanent lattice rotations, which are associated with plastic lattice curvature. That is why elastic and plastic Cosserat deformations and curvatures are introduced: ${}^{\sharp}\underset{\sim}{\mathbf{F}}^e$, ${}^{\sharp}\underset{\sim}{\mathbf{F}}^p$, ${}^{\sharp}\underset{\sim}{\Gamma}^e$ and ${}^{\sharp}\underset{\sim}{\Gamma}^p$. Strain partition rules must then be proposed.

The multiplicative decomposition proposed in [Mandel 1971] is adopted here but only for the Cosserat deformation gradient

$${}^{\sharp}\underset{\sim}{\mathbf{F}} = {}^{\sharp}\underset{\sim}{\mathbf{F}}^e \; {}^{\sharp}\underset{\sim}{\mathbf{F}}^p \tag{59}$$

The expression

$${}^{\sharp}\dot{\underset{\sim}{\mathbf{F}}} \; {}^{\sharp}\underset{\sim}{\mathbf{F}}^{-1} = {}^{\sharp}\dot{\underset{\sim}{\mathbf{F}}}^e \; {}^{\sharp}\underset{\sim}{\mathbf{F}}^{e-1} + {}^{\sharp}\underset{\sim}{\mathbf{F}}^e \; {}^{\sharp}\dot{\underset{\sim}{\mathbf{F}}}^p \; {}^{\sharp}\underset{\sim}{\mathbf{F}}^{p-1} \; {}^{\sharp}\underset{\sim}{\mathbf{F}}^{e-1} \tag{60}$$

is to be substituted in the Clausius-Duhem inequality 33. The most natural assumption is that the hyperelastic relations still have the form

$$\left\{ \begin{aligned} {}^{\sharp}\underset{\sim}{\sigma} &= \rho \frac{\partial \psi}{\partial\, {}^{\sharp}\underset{\sim}{\mathbf{F}}^e} \; {}^{\sharp}\underset{\sim}{\mathbf{F}}^{eT} \\ {}^{\sharp}\underset{\sim}{\mu} &= \rho \frac{\partial \psi}{\partial\, {}^{\sharp}\underset{\sim}{\Gamma}^e} \; {}^{\sharp}\underset{\sim}{\mathbf{F}}^{eT} \end{aligned} \right. \tag{61}$$

Sievert [1992] has proved that the multiplicative decomposition 59 results from the hyperelastic relation 61a. Similarly, for the relations 61 to hold the form of the decomposition of the overall curvature tensor cannot be arbitrary. We must have (see [Sievert 1995] for the complete formulation of the theorem):

$$ {}^{\sharp}\underset{\sim}{\Gamma} = {}^{\sharp}\underset{\sim}{\Gamma}^{e} \; {}^{\sharp}\underset{\sim}{F}^{p} + {}^{\sharp}\underset{\sim}{\Gamma}^{p} \tag{62} $$

This decomposition has also been proposed by Dluzewski [1991]. Sansour [1994] also proposes an additive but different decomposition of the wryness tensor. We do not retain the decomposition rule by Steinmann [1994] because the author proposes a partition of the rotation $\underset{\sim}{R}$ itself and not of its gradient. This raises many questions since a similar partition of the displacement field turns out to be irrelevant.

1.5.2 Kinematics of elastoplastic Cosserat single crystals

The plastic deformation of single crystals is the result of slip processes on slip systems. For each slip system s, we define

$$ \underline{m}^{s} = \underline{b}^{s} / \|\underline{b}^{s}\| \tag{63} $$

where $\underline{b}^{s}$ is the Burgers vector. $\underline{z}^{s}$ is the unit vector normal to the slip plane. As a result, the plastic strain rate takes the form

$$ {}^{\sharp}\dot{\underset{\sim}{F}}^{p} \; {}^{\sharp}\underset{\sim}{F}^{p-1} = \sum_{s \in S} \dot{\gamma}^{s} \; {}^{\sharp}\underset{\sim}{P}^{s} \tag{64} $$

γ^{s} is the amount of slip for the system s. ${}^{\sharp}\underset{\sim}{P}^{s}$ is given by the kinematics of slip

$$ {}^{\sharp}\underset{\sim}{P}^{s} = {}^{\sharp}\underline{m}^{s} \otimes {}^{\sharp}\underline{z}^{s} \tag{65} $$

If we go back to the Eulerian representation

$$ \underline{v} \otimes \underline{\nabla}^{c} = \dot{\underset{\sim}{F}} \, \underset{\sim}{F}^{-1} = \dot{\underset{\sim}{R}} \, \underset{\sim}{R}^{T} + \underset{\sim}{R} \; {}^{\sharp}\dot{\underset{\sim}{F}}^{e} \; {}^{\sharp}\underset{\sim}{F}^{e-1} \, \underset{\sim}{R}^{T} + \underset{\sim}{R} \; {}^{\sharp}\underset{\sim}{F}^{e} \; {}^{\sharp}\dot{\underset{\sim}{F}}^{p} \; {}^{\sharp}\underset{\sim}{F}^{p-1} \; {}^{\sharp}\underset{\sim}{F}^{e-1} \, \underset{\sim}{R}^{T} \tag{66} $$

We can split the last expression into its symmetric and antisymmetric parts:

$$ \{\underline{v} \otimes \nabla^{c}\} = \{\underset{\sim}{R} \; {}^{\sharp}\dot{\underset{\sim}{F}}^{e} \; {}^{\sharp}\underset{\sim}{F}^{e-1} \, \underset{\sim}{R}^{T}\} + \sum_{s \in S} \dot{\gamma}^{s} \, \{ {}^{*}\underline{m}^{s} \otimes {}^{*}\underline{z}^{s}\} \tag{67} $$

and

$$ \}\underline{v} \otimes \underline{\nabla}^{c}\{ - \dot{\underset{\sim}{R}} \, \underset{\sim}{R}^{T} = \}\underset{\sim}{R} \; {}^{\sharp}\dot{\underset{\sim}{F}}^{e} \; {}^{\sharp}\underset{\sim}{F}^{e-1} \, \underset{\sim}{R}^{T}\{ + \sum_{s \in S} \dot{\gamma}^{s} \, \} {}^{*}\underline{m}^{s} \otimes {}^{*}\underline{z}^{s}\{ \tag{68} $$

where we have noted

$$ {}^{*}\underline{m}^{s} = \underset{\sim}{R} \; {}^{\sharp}\underset{\sim}{F}^{e} \; {}^{\sharp}\underline{m}^{s} \text{ and } {}^{*}\underline{z}^{s} = \underset{\sim}{R} \; {}^{\sharp}\underset{\sim}{F}^{e-T} \; {}^{\sharp}\underline{z}^{s} \tag{69} $$

Equation 68 clearly shows that the relative rotation rate of material lines with respect to the microstructure is due to the lattice rotation associated with slip processes, if elastic contributions are neglected.

We would like to compare the proposed formulation with Mandel's work. We are working with invariant tensors written in the microstructure space frame in order to get

rid of undetermined rotations. An equivalent method is to deal with the so-called isoclinic configuration introduced by Mandel [1971]. His description reads

$$\underset{\sim}{\mathbf{F}} = \underset{\sim}{\mathbf{E}}\,\underset{\sim}{\mathbf{P}} \tag{70}$$

where the rotation $\underset{\sim}{\mathbf{R}}^{isoclinic}$ appearing in the polar decomposition of $\underset{\sim}{\mathbf{E}}$ links the isoclinic reference frame to the working space frame. As a result comparing 59 and 70 one can think of the equivalence

$$\underset{\sim}{\mathbf{E}} = \underset{\sim}{\mathbf{R}}\ {}^{\sharp}\underset{\sim}{\mathbf{F}}^{e} \tag{71}$$

However, considering the respective polar decompositions

$$\underset{\sim}{\mathbf{E}} = \underset{\sim}{\mathbf{R}}^{isoclinic}\ \underset{\sim}{\mathbf{U}}^{e} \quad \text{and} \quad {}^{\sharp}\underset{\sim}{\mathbf{F}}^{e} = \underset{\sim}{\mathbf{R}}^{e}\ \underset{\sim}{\mathbf{U}}^{e} \tag{72}$$

we must then have

$$\underset{\sim}{\mathbf{R}}^{isoclinic} = \underset{\sim}{\mathbf{R}}\,\underset{\sim}{\mathbf{R}}^{e} \tag{73}$$

Regarding the elastic behaviour in the classical case, lattice vectors are material vectors with respect to the intermediate configuration. Within the proposed framework this is not exactly true any more. There is an additional rotation $\underset{\sim}{\mathbf{R}}^{e}$ of material fibres that could be attributed to the presence of heterogeneities. Nevertheless the constitutive theory must be such that $\underset{\sim}{\mathbf{R}}^{e}$ remains a corrective term. The equivalence of the two theories is established if ${}^{\sharp}\underset{\sim}{\mathbf{F}}^{e}$ is symmetric. A difficulty arises from the fact that the directors of a Cosserat theory are rigid. A more general theory for which directors can deform is called micromorphic [Eringen 1976]. A more suitable theory for single crystals would be a micromorphic one with constrained elastic deformation of the microstructure. Within this framework a complete second-rank tensor is attached to each point and not only a rotation. In the polar decomposition of this tensor, the rotation would have the same meaning as $\underset{\sim}{\mathbf{R}}$ or $\underset{\sim}{\mathbf{R}}\,\underset{\sim}{\mathbf{R}}^{e}$ but the stretching part should be related to $\underset{\sim}{\mathbf{U}}^{e}$. For simplicity and observing that the stress connected with $\underset{\sim}{\mathbf{U}}^{e}$, i.e. the classical one, is already taken into account, we restrict ourselves to the first approximation, the Cosserat theory.

The plastic lattice curvature and torsion are due to the presence of dislocations with a non-vanishing resulting Burgers vector (see section 2). The curvature planes and torsion axes are therefore related to crystallographic directions. They can be represented by the effect of continuous edge and screw dislocations for each slip system. That is why we propose the following kinematics for the plastic wryness

$${}^{\sharp}\dot{\underset{\sim}{\mathbf{\Gamma}}}^{p}\ {}^{\sharp}\underset{\sim}{\mathbf{F}}^{p-1} = \sum_{s\in S} \frac{\dot{\theta}^{s}}{l}\ {}^{\sharp}\underset{\sim}{\mathbf{Q}}^{s} \tag{74}$$

The θ^{s} are angles that measure the plastic curvature and torsion over a characteristic length l. Explicit forms for ${}^{\sharp}\underset{\sim}{\mathbf{Q}}^{s}$ are given in section 3.1. In section 2.4.2 an alternative more simple treatment for the plastic curvature is proposed.

1.6 Dissipation

In the Clausius-Duhem inequality 33, a contribution to the overall entropy production is due to the development of rotation gradients. The intrinsic dissipation rate is

$$\dot{D} = \underset{\sim}{\sigma} : \underset{\sim}{\mathbf{R}}\ {}^{\sharp}\underset{\sim}{\mathbf{F}}^{e}\ {}^{\sharp}\dot{\underset{\sim}{\mathbf{F}}}^{p}\ {}^{\sharp}\underset{\sim}{\mathbf{F}}^{p-1}\ {}^{\sharp}\underset{\sim}{\mathbf{F}}^{e-1}\ \underset{\sim}{\mathbf{R}}^{T}$$

$$
\begin{aligned}
&+ \ \underset{\sim}{\mu} \ : \ \underset{\sim}{\mathrm{R}} \ {}^{\natural}\underset{\sim}{\Gamma}^{e} \ {}^{\natural}\dot{\underset{\sim}{\mathrm{F}}}^{p} \ {}^{\natural}\underset{\sim}{\mathrm{F}}^{p-1} \ {}^{\natural}\underset{\sim}{\mathrm{F}}^{e-1} \ \underset{\sim}{\mathrm{R}}^{T} \\
&+ \ \underset{\sim}{\mu} \ : \ \underset{\sim}{\mathrm{R}} \ {}^{\natural}\dot{\underset{\sim}{\Gamma}}^{p} \ {}^{\natural}\underset{\sim}{\mathrm{F}}^{-1} \ \underset{\sim}{\mathrm{R}}^{T}
\end{aligned}
\tag{75}
$$

Taking 64 and 74 into account,

$$
\begin{aligned}
\dot{D} \ &= \ \sum_{s \in S} \dot{\gamma}^{s} \ \underset{\sim}{\alpha} \ : \ {}^{\star}\underset{\sim}{\mathrm{P}}^{s} \\
&+ \ \sum_{s \in S} \dot{\gamma}^{s} \ \underset{\sim}{\mu} \ : \ {}^{\star}\underset{\sim}{\mathrm{Q}}^{s} \\
&+ \ \underset{\sim}{\mu} \ : \ \underset{\sim}{\mathrm{R}} \ {}^{\natural}\underset{\sim}{\Gamma}^{e} \ {}^{\natural}\dot{\underset{\sim}{\mathrm{F}}}^{p} \ {}^{\natural}\underset{\sim}{\mathrm{F}}^{p-1} \ {}^{\natural}\underset{\sim}{\mathrm{F}}^{e-1} \ \underset{\sim}{\mathrm{R}}^{T}
\end{aligned}
\tag{76}
$$

where

$$
\left\{
\begin{array}{l}
{}^{\star}\underset{\sim}{\mathrm{P}}^{s} \ = \ \underset{\sim}{\mathrm{R}} \ {}^{\natural}\underset{\sim}{\mathrm{F}}^{e} \ {}^{\natural}\underset{\sim}{\mathrm{P}}^{s} \ {}^{\natural}\underset{\sim}{\mathrm{F}}^{e-1} \ \underset{\sim}{\mathrm{R}}^{T} \\
{}^{\star}\underset{\sim}{\mathrm{Q}}^{s} \ = \ \underset{\sim}{\mathrm{R}} \ {}^{\natural}\underset{\sim}{\mathrm{F}}^{e} \ {}^{\natural}\underset{\sim}{\mathrm{Q}}^{s} \ {}^{\natural}\underset{\sim}{\mathrm{F}}^{e-1} \ \underset{\sim}{\mathrm{R}}^{T}
\end{array}
\right.
\tag{77}
$$

Three terms appear in the dissipation. The first one is the classical one: slip processes due to irreversible dislocation motion are dissipative. The second one is due to the evolution of plastic curvature. It is clear that homogeneous lattice rotation is definitely not a dissipative process but plastic curvature due to non-homogeneous lattice rotation is related to the existence of accommodation dislocations and therefore must be associated with dissipation. This will be investigated in section 2.3. The last term which is of the second order when compared to the two other ones (in terms of elastic deformation and curvature), reveals a coupling between plastic flow and elastic curvature.

2 Closure of the continuum theory of dislocations

2.1 Closure problem of the continuum theory of dislocations

The origin of the continuum theory of dislocations goes back to Nye's epoch-making work on *"Some geometrical relations in dislocated crystals"* [1953]. He introduced the dislocation density tensor $\underset{\sim}{\alpha}$ which will be presented in section 2.2 and he established a link between $\underset{\sim}{\alpha}$ and the lattice curvature. Kröner and Rieder [1956] and Kröner [1958] proposed a general presentation of the theory and gave the set of partial differential equations to be solved in the linear static case for a given distribution of dislocations and here for an infinite body

$$
\left\{
\begin{array}{l}
\underset{\sim}{\mathrm{f}} \ = \ \underset{\sim}{\mathrm{f}}^{e} \ + \ \underset{\sim}{\mathrm{f}}^{p} \\
\underset{\sim}{\sigma} \ = \ \underset{\sim}{\mathrm{E}} \ \underset{\sim}{\mathrm{f}}^{e} \\
\underline{\mathrm{div}} \ \underset{\sim}{\sigma} \ = \ 0 \\
\mathrm{curl} \ \underset{\sim}{\mathrm{f}}^{e} \ = \ \underset{\sim}{\alpha}
\end{array}
\right.
\tag{78}
$$

where $\underset{\sim}{\mathrm{f}} \ = \ \underline{\mathrm{u}} \otimes \underline{\nabla} \ = \ u_{i,j} \ \underline{\mathrm{e}}_{i} \otimes \underline{\mathrm{e}}_{j}$. The continuum theory of dislocations is a way to think of dislocation theory as a physical field theory. Despite the fact that the system 78 enables us to find the stress strain field around dislocations in some given arrangement, such a theory cannot bridge the gap between dislocation theory and plasticity theory since it does not predict the motion of dislocations: the dislocation distribution must be known at each step. In the dynamic theory of continuous distributions of dislocations, Kröner

[1958] and Mura [1963a,b] introduce the dislocation velocity tensor $\underset{\sim}{\underline{V}}$ which is related to the plastic deformation rate $\dot{\underset{\sim}{f}}^p$ by

$$\dot{\underset{\sim}{f}}^p = -\left(\underline{\underline{\varepsilon}}\ \underset{\sim}{\underline{V}}\right)^T \tag{79}$$

and we still have

$$\dot{\underset{\sim}{\alpha}} = -\underset{\sim}{\text{curl}}\ \dot{\underset{\sim}{f}}^p \tag{80}$$

For a single dislocation

$$\underset{\sim}{\underline{\underline{V}}} = \underline{v} \otimes \underline{\xi} \otimes \underline{b} \tag{81}$$

$\underline{v}$ is the dislocation velocity vector, $\underline{\xi}$ is the dislocation line vector (notation of [Hirth, Lothe 1982]) and $\underline{b}$ the Burgers vector. In this case stress and strain can be obtained provided that $\underset{\sim}{\alpha}$ and $\underset{\sim}{\underline{V}}$ are given at each time, which is of no help to derive a plasticity theory. For, the continuum theory of dislocations, even in more recent review articles like [Kossecka, De Wit 1977], does not provide constitutive equations. As pointed out by Hahn and Jaunzemis [1973], in a complete theory of dislocations, the density and motion of dislocations should be derivable from the knowledge of initial conditions (and boundary conditions) only. This is what we call the closure problem of the continuum theory of dislocations.

Two attempts to derive the missing constitutive equations must be mentioned. On the one hand Mura [1965a] showed how the v. Mises yield criterion and Prandtl-Reuss relations can be explained in terms of the dislocation velocity tensor and a so-called "gliding force". The underlying constitutive assumption is a linear relation between $\underset{\sim}{\underline{V}}$ and the gliding force. The derivation of similar results in the anisotropic case is given in [Mura 1965b]. According to [Lardner 1969] and [Eisenberg 1970] the constitutive equations are also necessary to link plasticity and dislocation theories. On the other hand Hahn and Jaunzemis [1973] distinguish mobile dislocations (M) from immobile ones (I) with common line and Burgers vectors. $A^{ab} = A_I^{ab} + A_M^{ab}$ is the number of dislocations of Burgers vector $\underline{b}^a$ and line vector $\underline{\xi}^b$. Using a large strain formulation, 79 combined with 81 yields

$$\begin{aligned} \dot{\underset{\sim}{F}}^p\ \underset{\sim}{F}^{p-1} &= \sum_{a,b} \underline{b}^a \otimes (\underline{\xi}^b \times \underline{v}^{ab})\ A_M^{ab} \\ &= \sum_a A^a V^a\ \underline{b}^a \otimes \underline{z}^a \end{aligned} \tag{82}$$

where $A^a V^a\ \underline{z}^a = \sum_b A_M^{ab}\ \underline{\xi}^b \times \underline{v}^{ab}$ is normal to the slip plane. Evolution equations are proposed for A_I^a and A_M^a. Isotropic and kinematic hardening and a viscous stress are also introduced in the modelling.

2.2 Statistical description of dislocation distribution

The dislocation network and dislocation sources distribution within a considered single crystal volume element often is or becomes so intricate that an exact description of all dislocation lines and Burgers vectors must be abandoned. Instead some overall and statistical information about the distribution may be sufficient for the modelling of the plastic behaviour of the element. The only known attempt to develop a complete

statistical theory of dislocations goes back to Zorski [1968]. The systematic approach comes up against tremendous difficulties which are still not overcome. Some researchers try also to derive kinetic theories of continuously distributed dislocations [Mescheryakov, Prockuratova 1995]. This explains why the concepts reviewed in this section are only rudimentory tools which do not exhaust the complexity of dislocation structures.

2.2.1 Dislocation density tensor and the continuum theory of dislocations

Within the framework of the continuum theory of dislocations, the characteristic size l of the volume element is taken large enough for the effects of the dislocations within it to be averaged. The distribution of dislocations is made continuous by letting $b = \|\underline{\mathbf{b}}\|$ approach zero and increasing the number n of dislocations of each kind so as to keep nb constant [Nye 1953]. The definition of the Burgers vector can be extended to continuous distributions of dislocations [Teodosiu 1982]. For that purpose one refers to the kinematic description proposed by Mandel [1971] making use of the isoclinic configuration and of the strain partition given by 70. In 70, $\underset{\sim}{\mathbf{E}}$ relates the infinitesimal vectors $d\underline{\zeta}$ and $d\underline{\mathbf{x}}$, where $d\underline{\zeta}$ results from the cutting and releasing operations from the infinitesimal current lattice vector $d\underline{\mathbf{x}}$

$$d\underline{\zeta} \;=\; \underset{\sim}{\mathbf{E}}^{-1}\, d\underline{\mathbf{x}} \tag{83}$$

It can be seen that the decomposition 70 actually goes back to [Bilby, Bullough, Gardner, Smith 1957].

Accordingly, if S is a smooth surface containing $\underline{\mathbf{x}}$ in the current configuration and bounded by the closed line c, the true Burgers vector is defined as in [Teodosiu 1982]

$$\underline{\mathbf{b}} \;=\; \oint_c \underset{\sim}{\mathbf{E}}^{-1}\, d\underline{\mathbf{x}} \tag{84}$$

The application of Stokes' formula 24 (Appendix 1) leads to the definition of the so-called true dislocation density tensor

$$\underset{\sim}{\alpha} \;=\; -\mathrm{curl}^{\mathrm{c}}\, \underset{\sim}{\mathbf{E}}^{-1} \;=\; \underset{\sim}{\mathbf{E}}^{-1} \times \underline{\nabla}^{c} \;=\; -\epsilon_{jkl}\, E^{-1}_{ik,l}\, \underline{\mathbf{e}}_i \otimes \underline{\mathbf{e}}_j \tag{85}$$

such that

$$\underline{\mathbf{b}} \;=\; \int_S \underset{\sim}{\alpha}\, \underline{\mathbf{n}}\, dS \tag{86}$$

If the surface is infinitesimal of normal $\underline{\mathbf{n}}$, $d\underline{\mathbf{b}} \;=\; \underset{\sim}{\alpha}\, \underline{\mathbf{n}}\, dS$ is the resulting true Burgers vector of dislocations crossing the surface dS. It is convenient to associate each component α_{ij} of the dislocation density tensor with a (super)dislocation characterized by its line vector $\underline{\mathbf{e}}_j$ and its Burgers vector $b_i\, \underline{\mathbf{e}}_i$ (no summation). As a result, the diagonal components of $\underset{\sim}{\alpha}$ represent screw dislocations and the out-of-diagonal ones edge dislocations. For n dislocations of Burgers vector $\underline{\mathbf{b}}$ and line vector $\underline{\xi}$, we have

$$\underset{\sim}{\alpha} \;=\; n\, \underline{\mathbf{b}} \otimes \underline{\xi} \tag{87}$$

2.2.2 Scalar dislocation densities and crystal plasticity

In the classical continuum theory of dislocations, say [Nye 1953] to [Mura 1967], the description of the dislocation distribution is restricted to the dislocation density tensor. It enables one to compute stress-strain fields for special distributions and even discrete

dislocations for which $\underset{\sim}{\alpha}$ becomes the sum of Dirac's functions [Kröner 1958]. We do not tackle here the problem of the description of distributions of point defects (see [Kröner 1958], [Kluge 1969]) or disclinations (see [Anthony, Essmann, Seeger, Träuble 1967] and [Kossecka, De Wit 1977]). However the classical continuum theory of dislocations has failed to describe the elastoplastic behaviour of single crystals. The main reason is that the dislocation density tensor is not the relevant variable to explain the hardening processes. In Hahn and Jaunzemis [1973], the kinematics of plastic deformation are derived from the dislocation velocity tensor and corresponds exactly to the purely mechanical description of slip processes proposed by Mandel [1971]. The next step is the introduction of hardening variables as in the classical macroscopic plasticity theory. They are related to usual scalar dislocation densities that are commonly used by metal phycisists and which represent the total length of dislocation lines within a volume element. The multiplication and interaction of dislocations is responsible for the hardening of single crystals and the scalar densities are reliable measures for it. This type of description culminates with the work of Mandel [1971], Zarka [1972] and Teodosiu and Sidoroff [1976]. In these theories the dislocation density tensor is not even mentioned since it is not the relevant quantity any more. Constitutive equations for hardening variables are proposed in a more or less phenomenological way and several elementary dislocation interaction processes are taken into account.

The main successes of these theories are the modelling of the tensile behaviour of single crystals, the lattice rotations [Fortunier 1987] and the cyclic behaviour of single and polycrystals [Cailletaud 1992].

2.2.3 Proposed description

In this work we claim that both types of descriptions are required for the modelling of non-homogeneous deformation of single crystals. That is why the statistical description of dislocation distribution must contain at least:

- the dislocation density tensor $\underset{\sim}{\alpha}$ which accounts for the resulting Burgers vector across any infinitesimal surface,

and

- scalar dislocation densities ρ^{is} or the associated hardening variables, for instance r^s and x^s already used in [Méric, Poubanne, Cailletaud 1991]. Additional variables (densities of mobile and immobile dislocations...) may also be necessary.

The scalar dislocation densities are necessary to account for the hardening or softening behaviour of the material whereas the dislocation density tensor may play a significant role when strong lattice incompatibilities are present.

2.3 Link between the dislocation density tensor and the lattice torsion-curvature tensor

2.3.1 Analysis at small strains and small rotations

Nye [1953] introduces the rotation vector $\underline{\Phi}$ of the lattice and the curvature tensor

$$\underset{\sim}{\kappa} = \underline{\Phi} \otimes \underline{\nabla} \tag{88}$$

Using Nye's terminology, the components of $d\underline{\Phi} = \underset{\sim}{\kappa}\, d\underline{X}$ are small rotations about the three axes associated with the infinitesimal displacement $d\underline{X}$. At small strains and small

rotations, the strain and rotation rate decomposition into elastic and plastic parts reads

$$\begin{aligned} \dot{\underset{\sim}{f}} &= \dot{\underset{\sim}{f}}^{e} + \dot{\underset{\sim}{f}}^{p} \\ &= \dot{\underset{\sim}{\varepsilon}} + \underset{\sim}{\omega} \\ &= \dot{\underset{\sim}{\varepsilon}}^{e} + \underset{\sim}{\omega}^{e} + \dot{\underset{\sim}{\varepsilon}}^{p} + \underset{\sim}{\omega}^{p} \end{aligned} \tag{89}$$

$\underset{\sim}{\omega}^{p} = \underset{\sim}{\omega} - \underset{\sim}{\omega}^{e} = \underset{\sim}{1} \times \dot{\underline{\Phi}} = -\underset{\sim}{\varepsilon}\,\dot{\underline{\Phi}}$ represents the relative rotation of material lines with respect to the lattice. As a result, relation 80 becomes

$$\begin{aligned} \dot{\underset{\sim}{\alpha}} &= \underset{\sim}{\mathrm{curl}}\, \dot{\underset{\sim}{f}}^{e} \\ &= \underset{\sim}{\mathrm{curl}}\, \dot{\underset{\sim}{\varepsilon}}^{e} + \underset{\sim}{\mathrm{curl}}\, \underset{\sim}{\omega}^{e} \end{aligned} \tag{90}$$

In a way similar to Kröner [1958], we derive

$$\begin{aligned} \underset{\sim}{\mathrm{curl}}\, \underset{\sim}{\omega}^{e} &= \epsilon_{jkl}\, \omega_{ik,l}\, \underline{e}_i \otimes \underline{e}_j \\ &= -\epsilon_{jkl}\, \epsilon_{ikm}\, \dot{\Phi}_{m,l}\, \underline{e}_i \otimes \underline{e}_j \\ &= -\epsilon_{klj}\epsilon_{kmi}\, \dot{\kappa}_{ml}\, \underline{e}_i \otimes \underline{e}_j \\ &= -(\delta_{ml}\delta_{ij} - \delta_{il}\delta_{mj})\, \dot{\kappa}_{ml} \underline{e}_i \otimes \underline{e}_j \\ &= \dot{\underset{\sim}{\kappa}}^{T} - \mathrm{Tr}\, \dot{\underset{\sim}{\kappa}}\, \underset{\sim}{1} \end{aligned} \tag{91}$$

where equation 4 (Appendix 1) has been used. Neglecting the elastic strain, one obtains the expression proposed by Nye [1953] and which appears in [Seeger 1955] with somewhat different conventions

$$\underset{\sim}{\alpha} = \underset{\sim}{\kappa}^{T} - \mathrm{Tr}\, \underset{\sim}{\kappa}\, \underset{\sim}{1} \tag{92}$$

and its reverse form

$$\underset{\sim}{\kappa} = \underset{\sim}{\alpha}^{T} - \frac{1}{2}\, \mathrm{Tr}\, \underset{\sim}{\alpha}\, \underset{\sim}{1} \tag{93}$$

Keeping the elastic term

$$\underset{\sim}{\alpha} = \underset{\sim}{\mathrm{curl}}\, \underset{\sim}{\varepsilon}^{e} + \underset{\sim}{\kappa}^{T} - \mathrm{Tr}\, \underset{\sim}{\kappa}\, \underset{\sim}{1} \tag{94}$$

(see also [Weng, Phillips 1976]).

2.3.2 Analysis at finite deformation for the classical crystal plasticity theory

At finite strains, in the classical case, the definition of a lattice torsion-curvature tensor should be based on the polar decomposition 72 as follows

$$\begin{aligned} \underset{\sim}{\alpha} &= -(\underset{\sim}{\mathbb{U}}^{-1}\, \underset{\sim}{\mathbb{R}}^{isoclinicT}) \times \underline{\nabla}^{c} \\ &= -\epsilon_{jkl}\, (U^{-1}_{im}\, R^{isoclinic}_{km})_{,l}\, \underline{e}_i \otimes \underline{e}_j \\ &= -\left(\epsilon_{jkl}\, U^{-1}_{im,l}\, R^{isoclinic}_{km} + U^{-1}_{im}\, \epsilon_{jkl}\, R^{isoclinic}_{km,l}\right)\, \underline{e}_i \otimes \underline{e}_j \end{aligned} \tag{95}$$

(partial derivatives are taken here with respect to the current configuration). The tensor $\epsilon_{jkl}\, R^{isoclinic}_{km,l}\, \underline{e}_i \otimes \underline{e}_j$ enters in the definition of a lattice curvature tensor. An explicit expression is derived in the next section and can be applied here.

2.3.3 Analysis for the Cosserat theory

Within the framework of the Cosserat theory for single crystals presented in part 2, we propose the following definition for the true dislocation density tensor

$$\underset{\sim}{\alpha} \;=\; \underset{\sim}{\mathrm{curl}}\,(\,{}^{\sharp}\underset{\sim}{\mathbf{F}}^{e-1}\,\underset{\sim}{\mathbf{R}}^{T}) \tag{96}$$

Since a Cosserat theory enables us to take the rotations of the directors into account but not their deformations, the expression ${}^{\sharp}\underset{\sim}{\mathbf{F}}^{e-1}\,\underset{\sim}{\mathbf{R}}^{T}\,d\underline{\mathbf{x}}$ is not exactly the result of cutting and releasing $d\underline{\mathbf{x}}$. However the definition is such that

$$\left({}^{\sharp}\underset{\sim}{\mathbf{F}}^{p} \;=\; \underset{\sim}{1}\right) \;\Longrightarrow\; (\underset{\sim}{\alpha} \;=\; 0) \tag{97}$$

since $\underset{\sim}{\mathbf{F}}$ is a compatible deformation field. We try now to link the dislocation density tensor and the wryness tensor. As in the last section, 96 becomes

$$\underset{\sim}{\alpha} \;=\; -\left(\epsilon_{jkl}\,\frac{\partial\,{}^{\sharp}F^{e-1}_{im}}{\partial x_l}\,R_{km} \;+\; {}^{\sharp}F^{e-1}_{im}\,\epsilon_{jkl}\,R^{T}_{mk,L}\,F^{-1}_{Ll}\right)\,\underline{\mathbf{e}}_i\otimes\underline{\mathbf{e}}_j \tag{98}$$

(the comma denotes again a derivative with respect to the reference configuration). Using the result 5 of Appendix 1,

$$\underset{\sim}{\Gamma} \;=\; \frac{1}{2}\,\underline{\underline{\epsilon}}:(\underset{\sim}{\mathbf{R}}\,(\underset{\sim}{\mathbf{R}}^{T}\otimes\underline{\nabla})) \;\Longrightarrow\; \underset{\sim}{\mathbf{R}}\,(\underset{\sim}{\mathbf{R}}^{T}\otimes\underline{\nabla}) \;=\; \underline{\underline{\epsilon}}\,\underset{\sim}{\Gamma} \tag{99}$$

(we have checked that the condition $R_{il}\,R_{jl,k} \;=-R_{jl}\,R_{il,k}$ is fulfilled) or, in components,

$$R^{T}_{mk,l} \;=\; -R^{T}_{mu}\,\epsilon_{ukv}\,\Gamma_{vl} \tag{100}$$

As a result 96 can now be written

$$\begin{aligned}
\underset{\sim}{\alpha} \;&=\; \underset{\sim}{\mathbf{A}}^{el} \;-\; {}^{\sharp}F^{e-1}_{im}\,R^{T}_{mu}\,\epsilon_{klj}\,\epsilon_{kvu}\,\Gamma_{vL}\,F^{-1}_{Ll}\,\underline{\mathbf{e}}_i\otimes\underline{\mathbf{e}}_j \\
&=\; \underset{\sim}{\mathbf{A}}^{el} \;+\; {}^{\sharp}\underset{\sim}{\mathbf{F}}^{e-1}\,\underset{\sim}{\mathbf{R}}^{T}\,\left((\underset{\sim}{\Gamma}\,\underset{\sim}{\mathbf{F}}^{-1})^{T} \;-\; \mathrm{Tr}\,(\underset{\sim}{\Gamma}\,\underset{\sim}{\mathbf{F}}^{-1})\,\underset{\sim}{1}\right) \\
&=\; \underset{\sim}{\mathbf{A}}^{el} \;+\; {}^{\sharp}\underset{\sim}{\mathbf{F}}^{e-1}\,\left(({}^{\sharp}\underset{\sim}{\Gamma}\;{}^{\sharp}\underset{\sim}{\mathbf{F}}^{-1})^{T} \;-\; \mathrm{Tr}\,({}^{\sharp}\underset{\sim}{\Gamma}\;{}^{\sharp}\underset{\sim}{\mathbf{F}}^{-1})\,\underset{\sim}{1}\right)
\end{aligned} \tag{101}$$

where $\underset{\sim}{\mathbf{A}}^{el} \;=\; \epsilon_{jkl}\,\dfrac{\partial\,{}^{\sharp}F^{e-1}_{im}}{\partial x_l}\,R_{km}\,\underline{\mathbf{e}}_i\otimes\underline{\mathbf{e}}_j$. It can be checked that equation 94 is retrieved for small strains and rotations. We define

$${}^{\sharp}\underset{\sim}{\alpha} \;=\; \underset{\sim}{\alpha}\,\underset{\sim}{\mathbf{R}} \tag{102}$$

and $\underset{\sim}{\mathbf{R}}\;{}^{\sharp}\underset{\sim}{\mathbf{F}}^{e}\;\underset{\sim}{\alpha}$ can be interpreted as Cosserat counterpart of the local dislocation density tensor introduced in the classical continuum theory of dislocations.

2.4 Constrained Cosserat theories

2.4.1 Dislocation theory and Cosserat continuum

The work of the Cosserat brothers was almost forgotten until Günther rediscovered it in 1958. Furthermore Günther has revealed the close link between the Cosserat theory and the continuum theory of dislocations which has been thriving since the early fifties:

"Das kinematische Modell der Versetzungstheorie ist das eines inkompatiblen Cosseratschen Kontinuums."

This explained why the continuum theory of dislocations has often been further developed within the framework of a Cosserat continuum, for instance in [Schäfer 1967, 1969]. In [Kessel 1970] discrete screw and edge dislocations are embedded in the Cosserat continuum. However the physical meaning of the directors remains unclear in these works: are they independent lattice vectors or material vectors? How do they rotate? In many cases the resulting framework is that of a constrained Cosserat theory like in [Sawczuk 1967]. The rotation rate of the directors is then given by the skew-symmetric part of the overall deformation gradient

$$\dot{\underline{\underline{\Phi}}} = -\frac{1}{2}\,\underline{\underline{\epsilon}}\,(\dot{\underline{u}} \otimes \underline{\nabla}) \tag{103}$$

The bend-twist tensor that we denote $\underset{\sim}{\chi}$ in the constrained case then becomes

$$\dot{\underset{\sim}{\chi}} = \dot{\underline{\underline{\Phi}}} \otimes \underline{\nabla} = -\frac{1}{2}\,\epsilon_{imn}\,u_{m,nj}\,\underline{e}_i \otimes \underline{e}_j \tag{104}$$

It is clear that because of this constraint the directors generally are not lattice vectors. Besides the microrotations are entirely determined by the displacement field, which is not the case in the theory presented in section 1. Considering the decomposition of the deformation and bend-twist tensors into elastic and plastic parts, many authors write

$$\begin{aligned} \underset{\sim}{f} &= \underset{\sim}{f}^e + \underset{\sim}{f}^p \\ \underset{\sim}{\chi} &= \underset{\sim}{\chi}^e + \underset{\sim}{\chi}^p \end{aligned}$$

Mura [1965] defines

$$\begin{aligned} \dot{\underline{\underline{\Phi}}}^e &= -\frac{1}{2}\,\underline{\underline{\epsilon}}\,\dot{\underset{\sim}{f}}^e \\ \dot{\underline{\underline{\Phi}}}^p &= -\frac{1}{2}\,\underline{\underline{\epsilon}}\,\dot{\underset{\sim}{f}}^p \end{aligned} \tag{105}$$

such that

$$\dot{\underline{\underline{\Phi}}}^e \otimes \underline{\nabla} + \dot{\underline{\underline{\Phi}}}^p \otimes \underline{\nabla} = \dot{\underset{\sim}{\chi}} \tag{106}$$

which also implies the constraint 103. As for them, Kossecka and De Wit [1977] define

$$\begin{aligned} \underset{\sim}{\alpha}^T &= \epsilon_{pkm}\left(f^p_{lk,m} + \epsilon_{klq}\,\chi^p_{qm}\right)\underline{e}_p \otimes \underline{e}_l \\ &= \operatorname{curl}\{\underset{\sim}{f}^p\} + \underset{\sim}{\chi}^{pT} - \operatorname{Tr}\underset{\sim}{\chi}^p\,\underset{\sim}{1} \end{aligned} \tag{107}$$

Finally they interpret $(\operatorname{curl}\{\underset{\sim}{\chi}^p\})^T$ as the disclination density tensor. However these formula are not derived from a precise definition of the Burgers vector like in 84 or 96 and are therefore difficult to assess.

2.4.2 A Cosserat theory for single crystals with constrained elastic curvature

The main advantage of the previous restricted Cosserat theories is that no constitutive equations are required for the plastic curvature. But it must be noted that the expression of the dislocation density tensor 94 or 101 involves the total torsion-curvature tensor.

As a result nothing is known *a priori* about the elastic and plastic relative contributions, so that constitutive equations with a yield criterion for the plastic curvature may be necessary.

However looking at equation 101 may lead us to propose a constraint on the elastic part of the wryness tensor. For that purpose we use the decomposition of the total wryness given by equation 62. The expression of the dislocation density tensor becomes

$$\begin{aligned} \underset{\sim}{\alpha} \;=\; \underset{\sim}{A}^{el} \;+\; & {}^{\sharp}\underset{\sim}{F}^{e-1} \left(({}^{\sharp}\underset{\sim}{\Gamma}^{e} \; {}^{\sharp}\underset{\sim}{F}^{e-1})^{T} \;-\; \mathrm{Tr}({}^{\sharp}\underset{\sim}{\Gamma}^{e} \; {}^{\sharp}\underset{\sim}{F}^{e-1}) \, \underset{\sim}{1} \right) \underset{\sim}{R}^{T} \\ + \; & {}^{\sharp}\underset{\sim}{F}^{e-1} \left(({}^{\sharp}\underset{\sim}{\Gamma}^{p} \; {}^{\sharp}\underset{\sim}{F}^{-1})^{T} \;-\; \mathrm{Tr}({}^{\sharp}\underset{\sim}{\Gamma}^{p} \; {}^{\sharp}\underset{\sim}{F}^{-1}) \, \underset{\sim}{1} \right) \underset{\sim}{R}^{T} \end{aligned} \tag{108}$$

so that we may impose the constraint

$$({}^{\sharp}\underset{\sim}{\Gamma}^{e} \; {}^{\sharp}\underset{\sim}{F}^{e-1})^{T} \;-\; \mathrm{Tr}({}^{\sharp}\underset{\sim}{\Gamma}^{e} \; {}^{\sharp}\underset{\sim}{F}^{e-1}) \, \underset{\sim}{1} \;=\; -\, {}^{\sharp}\underset{\sim}{F}^{e} \; \underset{\sim}{A}^{el} \; \underset{\sim}{R} \tag{109}$$

which defines ${}^{\sharp}\underset{\sim}{\Gamma}^{e}$ without ambiguity and ${}^{\sharp}\underset{\sim}{\Gamma}^{p}$ is deduced from 62. One can check that $\underset{\sim}{\alpha} = 0$ if ${}^{\sharp}\underset{\sim}{F}^{p} = \underset{\sim}{1}$. At small strains and small rotations,

$$\underset{\sim}{\alpha} \;=\; \underset{\sim}{\mathrm{curl}} \; \underset{\sim}{\varepsilon}^{e} \;+\; (\underset{\sim}{\kappa}^{eT} \;-\; \mathrm{Tr} \, \underset{\sim}{\kappa}^{e} \, \underset{\sim}{1}) \;+\; (\underset{\sim}{\kappa}^{pT} \;-\; \mathrm{Tr} \, \underset{\sim}{\kappa}^{p} \, \underset{\sim}{1}) \tag{110}$$

so that the constraint reads

$$\underset{\sim}{\kappa}^{eT} \;-\; \mathrm{Tr} \, \underset{\sim}{\kappa}^{e} \, \underset{\sim}{1} \;=\; -\underset{\sim}{\mathrm{curl}} \; \underset{\sim}{\varepsilon}^{e} \tag{111}$$

This Cosserat theory with constraint seems to be a natural way to avoid writing constitutive equations for the evolution of plastic curvature without dropping the couple-stresses which are still computed using an hyperelastic law. But to model the influence of plastic curvature on the hardening of the material, it seems necessary to develop additional constitutive equations. This is done in part 3.

2.5 Non-Euclidean geometry and the continuum theory of dislocations

The links between dislocation theory and non-Euclidean geometry was first recognized by Kondo (see [Kondo 1964] for a review) and by Bilby, Bullough and Smith [1955, 1956, 1957]. The results of the well-developed mathematical theories of differential geometry and manifold analysis find a beautiful new application. The dislocated crystal turns out to have a non-Riemannian geometry. Kröner [1958] introduced also a geometrical description of dilute atoms and proposed a general non-linear analysis ([Kröner, Seeger 1959], [Kröner 1960]). He is still working in this field [Kröner 1992]. Günther [1967] applied the efficient tools coming from general relativity theory to the non-linear continuum theory of moving dislocations. We review here very briefly the main features of the geometric field theory of dislocations.

The inner lattice structure of a macroscopic crystal enables one to define a parallel-transfer on the body: two vectors $\underline{e}(P)$ and $\underline{e}(Q)$ at points P and Q will be said to be parallel if they represent the same crystallographic direction $\underline{c}$ in the intermediate isoclinic configuration.

$$\underline{e}(P) \;-\; \underline{e}(Q) \;=\; (\underset{\sim}{E}(P) \;-\; \underset{\sim}{E}(Q)) \; \underline{c} \tag{112}$$

Calling $d\underline{e}$ this difference when P and Q are very closed, one derives in a way similar to [Bilby, Bullough, Smith 1955]

$$de_i \;=\; E_{ij,\gamma} \; c_j \; dx_\gamma$$

$$
\begin{aligned}
&= E_{ij,\gamma}\, E^{-1}_{jk}\, e_k\, dx_\gamma \\
&= -L_{ik\gamma}\, e_k\, dx_\gamma
\end{aligned} \tag{113}
$$

which defines the crystal connection

$$
L_{ik\gamma} = -E_{ij,\gamma}\, E^{-1}_{jk} = E_{ij}\, E^{-1}_{jk,\gamma} \tag{114}
$$

If now dislocations are present, one considers the resulting local and true Burgers vectors for an infinitesimal surface of normal $\underline{\mathrm{n}}$ as in section 3.2.1

$$
\begin{aligned}
d\underline{\mathrm{b}}^{local} &= \underset{\sim}{\mathrm{E}}\, d\underline{\mathrm{b}}^{true} \\
&= \underset{\sim}{\mathrm{E}}\, (\mathrm{curl}^{\mathrm{c}}\, \underset{\sim}{\mathrm{E}}^{-1})\, \underline{\mathrm{n}}\, dS
\end{aligned} \tag{115}
$$

In components, it reads

$$
\begin{aligned}
db_i &= E_{ij}\, \epsilon_{akl}\, E^{-1}_{jk,l}\, n_a\, dS \\
&= \frac{1}{2}\, E_{ij}\, (E^{-1}_{jk,l} - E^{-1}_{jl,k}) \epsilon_{kla}\, n_a\, dS \\
&= L_{i\}kl\{}\, dS_{kl}
\end{aligned} \tag{116}
$$

where $dS_{kl} = \epsilon_{kla}\, n_a\, dS$. Whereas the linear connection is not a tensor, the $L_{i\}kl\{}$ are the components of a tensor, the so-called torsion or Cartan tensor. One can check that the Riemann tensor or curvature tensor associated with the linear connection vanishes. This corresponds to the assumption that the lattice structure can be defined uniquely everywhere. The dislocated crystal therefore has a geometric structure with vanishing curvature and non-zero torsion. A four-rank contorsion tensor can be defined and related to the usual curvature tensor used in the previous sections [De Wit 1981].

A modern presentation of the relationships between differential geometry and continuum theory of dislocations can be found in [Le, Stumpf 1994]. These authors regard the intermediate state as an anholonomic global placement.

2.6 Geometrically necessary dislocations and statistically stored dislocations

According to Ashby [1971] (see section A.1.3.1), dislocations become stored in a plastically non-homogeneous solid for two reasons: dislocations are either required for the compatible deformation of various parts of the specimen or they accumulate by trapping each other in a random way. This gives rise on the one hand to the density ρ_G of so-called geometrically necessary dislocations and on the other hand to the density ρ_S of statistically stored dislocations. The density ρ_G can be computed approximately in some situations like plastic bending, studied by [Nye 1953] and [Read 1957] or punching. This variable comes directly from the continuum theory of dislocations and corresponds to the components of the dislocation density tensor $\underset{\sim}{\alpha}$. This can be clearly seen on figure 1 taken from Ashby [1971] and Kröner [1958]. In section 4 we will introduce additional inner variables which are directly related to the density ρ_G of geometrically necessary dislocations for each slip system.

In contrast, the density ρ_S belongs to the second group of variables that have been listed in section 2.3, namely the hardening variables. However, as shown by Ashby in the case of two-phase alloys, geometrically necessary dislocations may lead to additional

hardening. In section 3 we will try to model this coupling effect between the two types of variables that describe the dislocation distribution.

The relative importance of ρ_G and ρ_S depends on the amount of overall plastic deformation (see Ashby's map, figure A.5) and on the type of sollicitation. Clearly ρ_G can dominate in the case of strong deformation gradients.

These considerations have led Fleck, Müller, Ashby and Hutchinson [1994] to apply a so-called strain-gradient plasticity theory to the tension and torsion of copper wires with various diameters. The model is in fact a constrained Cosserat theory first proposed by [Sawczuk 1967]. The J_2-theory is extended to couple stresses in a way similar to [De Borst 1993]. However the modelling becomes questionable when applied to wires with diameters comparable to the grain size. For in that case the constrained rotations of the model have nothing to do with local lattice rotations, as explained in section 2.4 and the associated curvature is not a relevant variable.

3 Explicit constitutive equations

We propose a set of constitutive equations for the elastoviscoplastic deformation and intrinsic curvature of metal single crystals.

3.1 Kinematics of plastic deformation and curvature

The plastic flow due to slip on various slip systems has been studied in section 1.5.2 (equation 64):

$$ {}^{\natural}\dot{\underset{\sim}{\mathbf{F}}}^{p} \; {}^{\natural}\underset{\sim}{\mathbf{F}}^{p-1} = \sum_{s\in S} \dot{\gamma}^{s} \; {}^{\natural}\underline{\mathbf{m}}^{s} \otimes {}^{\natural}\underline{\mathbf{z}}^{s} $$

Similarly an expression of the plastic curvature evolution has been proposed (equation 74)

$$ {}^{\natural}\dot{\underset{\sim}{\mathbf{\Gamma}}}^{p} \; {}^{\natural}\underset{\sim}{\mathbf{F}}^{p-1} = \sum_{s\in S} \frac{\dot{\theta}^{s}}{l} \; {}^{\natural}\underset{\sim}{\mathbf{Q}}^{s} $$

An expression of ${}^{\natural}\underset{\sim}{\mathbf{Q}}^{s}$ is now derived from the analysis of the dislocation density tensor in section 2.3.3. The scalar γ^s represent the amount of slip due to the passage of dislocations of type s through the volume element. As for them the scalars θ^s represent the plastic curvature due to dislocations trapped in the volume element of characteristic length l. In equation 108 we will assume that the curvature axes or say the expression ${}^{\natural}\underset{\sim}{\mathbf{F}}^{e-1}\left(({}^{\natural}\underset{\sim}{\mathbf{\Gamma}}^{p}\,{}^{\natural}\underset{\sim}{\mathbf{F}}^{-1})^{T} - \mathrm{Tr}({}^{\natural}\underset{\sim}{\mathbf{\Gamma}}^{p}\,{}^{\natural}\underset{\sim}{\mathbf{F}}^{-1})\,\underset{\sim}{\mathbf{1}}\right)$ are given by the dislocation density tensor ${}^{\natural}\underset{\sim}{\alpha}$. Conversely, the curvature axes ${}^{\natural}\underset{\sim}{\mathbf{\Gamma}}^{p}\;{}^{\natural}\underset{\sim}{\mathbf{F}}^{p-1}$ are then given by $\left(({}^{\natural}\underset{\sim}{\mathbf{F}}^{e}\,{}^{\natural}\underset{\sim}{\alpha})^{T} - \frac{1}{2}\mathrm{Tr}({}^{\natural}\underset{\sim}{\mathbf{F}}^{e}\,{}^{\natural}\underset{\sim}{\alpha})\,\underset{\sim}{\mathbf{1}}\right){}^{\natural}\underset{\sim}{\mathbf{F}}^{e}$ for each type of dislocation. The amount of curvature θ^s will be computed using constitutive equations proposed in the next section. Furthermore we drop the factors ${}^{\natural}\underset{\sim}{\mathbf{F}}^{e}$ since our Cosserat theory cannot account for the deformation of the directors.

Curvature due to edge dislocations ($\perp$)

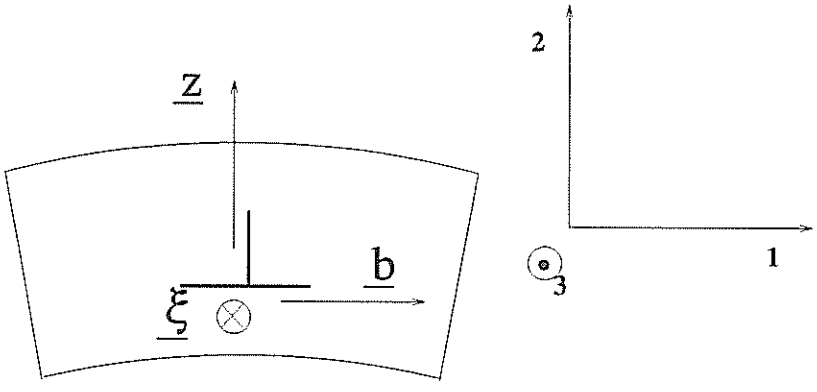

For edge dislocations, ${}^{\natural}\underset{\sim}{\alpha} = b\ {}^{\natural}\underline{\mathrm{m}} \otimes {}^{\natural}\underline{\xi}$.
$\underline{\xi}$ is the dislocation line vector and the normal to the glide plane is defined as

$$\underline{\mathrm{z}} = \underline{\mathrm{m}} \times \underline{\xi} \tag{117}$$

is the vector normal to the slip plane. The associated curvature is then

$${}^{\natural}\underset{\sim}{\Gamma}^{p}\ {}^{\natural}\underset{\sim}{\mathrm{F}}^{p-1} = b\ {}^{\natural}\underline{\xi} \otimes {}^{\natural}\underline{\mathrm{m}} \tag{118}$$

so that we take

$${}^{\natural}\underset{\sim}{\mathrm{Q}}_{\perp} = {}^{\natural}\underline{\xi} \otimes {}^{\natural}\underline{\mathrm{m}} \tag{119}$$

Arrays of edge dislocations of the same type give rise to lattice curvature in the plane $(\underline{\mathrm{m}}, \underline{\mathrm{b}})$. The rotation vector $\underline{\Phi}$ has the same direction as the dislocation line vector.

Torsion due to screw dislocations ($\odot$)

For a screw dislocation, ${}^{\natural}\underset{\sim}{\alpha} = b\ {}^{\natural}\underline{\mathrm{m}} \otimes {}^{\natural}\underline{\mathrm{m}}$
The associated curvature is then

$${}^{\natural}\underset{\sim}{\Gamma}^{p}\ {}^{\natural}\underset{\sim}{\mathrm{F}}^{p-1} = b\,({}^{\natural}\underline{\mathrm{m}} \otimes {}^{\natural}\underline{\mathrm{m}} - \frac{1}{2}\,\underset{\sim}{1}) \tag{120}$$

so that we take

$${}^{\natural}\underset{\sim}{\mathrm{Q}}_{\odot} = {}^{\natural}\underline{\mathrm{m}} \otimes {}^{\natural}\underline{\mathrm{m}} - \frac{1}{2}\,\underset{\sim}{1} \tag{121}$$

As a result screw dislocations cause lattice torsion about the three reference axes. This can be seen on figure 2 that shows a screw dislocation when the couple at its end is released [Friedel 1964]. Kröner [1958] noticed that a planar array of crossed screw dislocations with perpendicular Burgers vectors produces a twist of the lattice about the third direction. This is equivalent to a grain boundary of the second kind. Grain boundaries of the first kind are generated by an array of edge dislocations with parallel Burgers and line vectors. Note that the result 120 is different from that proposed in [Dluzewski 1992]

$$\underset{\sim}{\Gamma}^{Dluzewski} = b\,({}^{\natural}\underline{\mathrm{m}} \otimes {}^{\natural}\underline{\mathrm{m}} - \underset{\sim}{1}) \tag{122}$$

which gives no torsion with respect to the dislocation line axis. This seems to hold only when the couple that can be derived from the classical stress field around a screw

dislocation is not released (see [Friedel 1964], [Hirth, Lothe 1982]). Dzulewski gives also a definition of a dislocation density tensor $\underset{\sim}{\mathbf{a}}$ which is different from that derived in 3.4.2

$$\underset{\sim}{\mathbf{a}} = \underset{\sim}{\mathbf{R}}\ \underset{\sim}{\Gamma}^{p}\ \underset{\sim}{\mathbf{F}}^{-1} \tag{123}$$

which is similar to our local dislocation density tensor $\underset{\sim}{\mathbf{R}}\ {}^{\sharp}\underset{\sim}{\mathbf{F}}^{e}\ \underset{\sim}{\alpha}$ if we abandon the transposition and the term with the trace. Our expression 108 is derived from an extension of the definition of the Burgers vector for continuously distributed dislocations.

At last we give the proposed kinematics of the plastic lattice torsion-curvature

$${}^{\sharp}\dot{\underset{\sim}{\Gamma}}^{p}\ {}^{\sharp}\underset{\sim}{\mathbf{F}}^{p-1} = \sum_{s\in S}\left(\frac{\dot{\theta}^{s}_{\perp}}{l}\ {}^{\sharp}\underline{\xi}^{s}\otimes{}^{\sharp}\underline{\mathbf{m}}^{s} + \frac{\dot{\theta}^{s}_{\odot}}{l}\left({}^{\sharp}\underline{\mathbf{m}}^{s}\otimes{}^{\sharp}\underline{\mathbf{m}}^{s} - \frac{1}{2}\,\underset{\sim}{\mathbf{1}}\right)\right) \tag{124}$$

3.2 Generalized Schmid's law

3.2.1 Peach and Koehler's force

Kröner [1956] shows that Peach and Koehler's formula giving the force on a dislocation $(\underline{\mathbf{b}},\underline{\xi})$ due to a stress field $\underset{\sim}{\sigma}$ applies also for non-symmetric stress tensor. But it is important to derive again the formula taking care of any transposition. Following Kröner in [Sommerfeld 1978] the force $\underline{\mathbf{f}}$ per unit length of dislocation is defined through

$$\underline{\mathbf{f}}.d\underline{\mathbf{x}} = \underline{\mathbf{b}}.(\underset{\sim}{\sigma}\ \underline{\mathbf{n}})\ dS \tag{125}$$

where

$$\underline{\mathbf{n}}\ dS = \underline{\xi}\times d\underline{\mathbf{x}} \tag{126}$$

Hence,

$$\begin{aligned}\underline{\mathbf{f}}.d\underline{\mathbf{x}} &= b_i\ \sigma_{ij}\ \epsilon_{jkl}\ \xi_k\ dx_l\\ &= \epsilon_{ljk}\ b_i\ \sigma_{ij}\ \xi_k\ dx_l\\ &= ((\underline{\mathbf{b}}\ \underset{\sim}{\sigma})\times\underline{\xi}).d\underline{\mathbf{x}}\end{aligned} \tag{127}$$

The dislocation can move in its plane only if the component of the force in the glide plane

$$\begin{aligned}b\tau &= \underline{\mathbf{f}}.(\underline{\mathbf{n}}\times\underline{\xi})\\ &= \left((\underline{\mathbf{b}}\ \underset{\sim}{\sigma})\times\underline{\xi}\right).(\underline{\mathbf{n}}\times\underline{\xi})\\ &= (\underline{\mathbf{b}}\ \underset{\sim}{\sigma}).(\underline{\xi}\times(\underline{\mathbf{n}}\times\underline{\xi}))\\ &= \underline{\mathbf{b}}\ \underset{\sim}{\sigma}\ \underline{\mathbf{n}}\\ &= \underset{\sim}{\sigma} : (\underline{\mathbf{b}}\otimes\underline{\mathbf{n}})\end{aligned} \tag{128}$$

reaches a threshold. This is the physical meaning of Schmid's criterion already used in part A. We will still use this criterion to compute the slip rate on slip system s

$$\dot{\gamma}^{s} = <\frac{|\ \tau^{s} - x^{s}\ | - r^{s}}{k^{s}}>^{n^{s}}\ \text{sign}\ (\tau^{s} - x^{s}) \tag{129}$$

The cumulative slip is defined as

$$\dot{v}^{s} = |\ \dot{\gamma}^{s}\ | \tag{130}$$

where $\tau^s = {}^{\sharp}\underset{\sim}{\sigma} : {}^{\sharp}\underset{\sim}{\mathbf{P}}^s$ according to 128, and x^s and r^s are internal kinematic and isotopic hardening variables. x^s and r^s represent respectively a back-stress and the yield threshold. The associated variables α^s and ϱ^s (see the thermodynamical formulation in section A.3.2) are supposed to describe with sufficient accuracy the dislocation structure with a view to modelling the hardening behaviour. Their meaning within the framework of a statistical description of dislocation distributions has been explained in 2.1.2

3.2.2 Evolution law for the viscoplastic torsion-curvature variables

We consider an array of edge dislocations with $\underline{\mathbf{b}} = b\,\underline{\mathbf{e}}_1$, the normal to the glide plane $\underline{\mathbf{z}} = \underline{\mathbf{e}}_2$ and $\underline{\xi} = -\underline{\mathbf{e}}_3$ (see figure section 4.1). At small strains they produce a curvature

$$\underset{\sim}{\kappa}^p = -nb\,\underline{\mathbf{e}}_3 \otimes \underline{\mathbf{e}}_1 = \kappa^p_{31}\,\underline{\mathbf{e}}_3 \otimes \underline{\mathbf{e}}_1 \tag{131}$$

We will assume that such geometrically necessary dislocations are produced by local dislocation sources if the local moment $\underset{\sim}{\mu} = m\,\underline{\mathbf{e}}_3 \otimes \underline{\mathbf{e}}_1$ ($m < 0$ here) is so high that the imposed curvature cannot be accommodated elastically any longer.

Generalizing the previous example, we propose the following expression of the viscoplastic curvature rate

$$\dot{\theta}^s = < \frac{|\ {}^{\sharp}\underset{\sim}{\mu} : {}^{\sharp}\underset{\sim}{\mathbf{Q}}^s\ | - l\,r^s_c}{l\,k^s_c} >^{n^s_c} \text{sign}\,(\underset{\sim}{\mu} : {}^{\sharp}\underset{\sim}{\mathbf{Q}}^s) \tag{132}$$

where r^s_c denotes the threshold and k^s_c and n^s_c are viscosity parameters. The formula is to be applied successively for edge and screw dislocations belonging to the same system. Equations 129 and 132 and the hardening rules of the next section close the theory based on multicriteria and associated flow rules. Accordingly this theory is part of associated generalized plasticity.

3.3 Deformation-curvature constitutive coupling

3.3.1 hardening rules

Evolution rules for the hardening variables must be proposed:

kinematic hardening

$$x^s = c^s\,\alpha^s \tag{133}$$

$$\dot{\alpha}^s = \dot{\gamma}^s - d\,\dot{v}^s\,\alpha^s \tag{134}$$

as in part A.

isotropic hardening

We think that additional hardening due to the plastic lattice curvature must be introduced. Assuming linear hardening for simplicity,

$$r^s = r^s_0 + \sum_{r \in S} (h^{sr}\ |\gamma^r| + h^{sr}_{\perp}\ |\theta^r_{\perp}| + h^{sr}_{\odot}\ |\theta^r_{\odot}|) \tag{135}$$

where h^{sr}, $h^{sr}_{\perp}$, $h^{sr}_{\odot}$ are three interaction matrices in the spirit of [Mandel 1965]. Regarding the evolution of the plastic curvature threshold, we do not introduce any coupling effect

$$r^s_c = r^s_{c0} + \sum_{r \in S} h^{sr}_c \mid \theta^r \mid \tag{136}$$

which must be written for edge and screw dislocations. The existence of additional hardening due to plastic curvature must be investigated experimentally. Available experimental data and some recommended experiments are given in the final discussion.

3.3.2 Coupled yield criterion

Lattice curvature may have even more influence on slip activity if couple stresses are directly introduced in the yield criterion according to

$$\begin{aligned} \dot{v}^s &= < \frac{\mid {}^{\sharp}\underset{\sim}{\sigma} : {}^{\sharp}\underset{\sim}{\mathbf{P}}^s + \frac{1}{l}\ {}^{\sharp}\underset{\sim}{\mu} : {}^{\sharp}\underset{\sim}{\mathbf{Q}}^s - x^s \mid - r^s}{k^s} >^{n^s} \\ \dot{\gamma}^s &= \dot{v}^s \operatorname{sign}\left({}^{\sharp}\underset{\sim}{\sigma} : {}^{\sharp}\underset{\sim}{\mathbf{P}}^s + \frac{1}{l}\ {}^{\sharp}\underset{\sim}{\mu} : {}^{\sharp}\underset{\sim}{\mathbf{Q}}^s - x^s \right) \end{aligned} \tag{137}$$

This extension is very similar to the extension of the von Mises criterion proposed by [Mühlhaus, Vardoulakis 1987] and [De Borst 1993], but is based on a multicriterion formulation.

3.4 Dissipation

We go back to the expression of the intrinsic dissipation rate derived in 1.6 and we write it for small strains and rotations

$$\dot{D} = \sum_{r \in S} \left(\tau^s \dot{\gamma}^s + \nu^s_{\perp} \dot{\theta}^s_{\perp} + \nu^s_{\odot} \dot{\theta}^s_{\odot} \right) \tag{138}$$

where

$$\nu^s_{\perp} = \frac{1}{l} \underset{\sim}{\mu} : \underset{\sim}{\mathbf{Q}}^s{}_{\perp} \quad \text{and} \quad \nu^s_{\odot} = \frac{1}{l} \underset{\sim}{\mu} : \underset{\sim}{\mathbf{Q}}^s{}_{\odot} \tag{139}$$

The multiplication and motion of dislocation are dissipative processes. The first term in 138 accounts for dissipation due to slip activity whereas the two last terms account for multiplication of geometrically necessary dislocations. In many cases the two last terms can be neglected. But when strong lattice rotation gradients develop, they may well be the leading terms.

4 Application to localization phenomena in single crystals

4.1 Cosserat continuum and regularization

4.1.1 Towards "mesh-objectivity"

The recent second renewal of interest in the Cosserat continuum has its roots in the spurious mesh-dependence of many FE analyses of localization failure modes when materials are strain-softening ([De Borst 1991], [Perić, Owen 1992]). To ged rid of such unwanted effects due to the ill-posedness of the boundary value problem in the case of

strain-softening, it has been proposed to enrich the continuum in several ways: non-locality, higher-order gradients or additional degrees of freedom should be introduced according to [De Borst, Sluys, Mühlhaus, Pamin 1993]. Some localization modes in the case of anisotropic materials have been investigated by Steinmann, Miehe and Stein [1994] and the width of the simulated shear band in a classical continuum is shown to be mesh-dependent. The rush for so-called "mesh-objective" continua (the word has been coined at this occasion) began in the late eighties. Batra [1987] compared single and dipolar materials to study adiabatic shear bands. Needleman [1988] investigated the regularization role played by viscosity in an one-dimensional case. Because of its relatively easy implementation in FE programs when compared with non-local or grade-n continua, the Cosserat theory displays many advantages according to [Yu, Perić, Owen 1991]. Nevertheless it must be noted that no special attention has been paid on the physical meaning of the use of a Cosserat medium. It is often considered as an *ad hoc* regularization method. The precise physical meaning of the directors is often not even mentioned ([De Borst, Sluys 1991], [De Borst, Mühlhaus 1992], [Fleck, Müller, Ashby, Hutchinson 1994]). An exception is the modelling of granular materials as a Cosserat continuum where the introduced characteristic length has a clear signification with respect to the grain size ([Mühlhaus, Vardoulakis 1987], [Mühlhaus 1989]). Furthermore the enriched continua are not the panacea since some bifurcation modes remain possible or new ones may appear. A bifurcation analysis must also be carried out using the new continua (see [Leblond, Perrin, Devaux 1994] in the non-local case). As noted by [Dietsche 1993] and [De Borst, Mühlhaus 1991], the Cosserat continuum actually plays a regularizing role only if the rotational degrees of freedom are activated by the loading conditions. If gradients of curvatures and couple stresses are almost absent, no regularization is achieved (see section 4.3).

4.1.2 The bifurcation analysis of Steinmann and Willam for an elastic ideal plastic Cosserat continuum

Steinmann and Willam [1991] performed the bifurcation analysis for elastoplastic materials with rotational degrees of freedom at small strains and rotations. The analysis is very similar to the classical one presented in part A.2. The yield criterion is taken as a function $F(\underset{\sim}{\sigma}, \underset{\sim}{\mu})$ of both force stress and couple stress tensors. For associated plasticity the authors take

$$\begin{aligned} \dot{\underset{\sim}{e}}^p &= \dot{\lambda}\, \frac{\partial F}{\partial \underset{\sim}{\sigma}} = \dot{\lambda}\, \underset{\sim}{P} \\ \dot{\underset{\sim}{\kappa}}^p &= \dot{\lambda}\, \frac{\partial F}{\partial \underset{\sim}{\mu}} = \dot{\lambda}\, \underset{\sim}{Q} \end{aligned} \tag{140}$$

The constitutive equations take the following form

$$\begin{aligned} \dot{\underset{\sim}{\sigma}} &= \underset{\approx}{D} : \dot{\underset{\sim}{e}} + \underset{\approx}{D}^1 : \dot{\underset{\sim}{\kappa}} \\ \dot{\underset{\sim}{\mu}} &= \underset{\approx}{D}^{1T} : \dot{\underset{\sim}{e}} + \underset{\approx}{D}^c : \dot{\underset{\sim}{\kappa}} \end{aligned} \tag{141}$$

where for perfect plasticity and plastic loading conditions

$$\underset{\approx}{D} = \underset{\approx}{E} - \frac{(\underset{\approx}{E} : \underset{\sim}{P}) \otimes (\underset{\sim}{P} : \underset{\approx}{E})}{\underset{\sim}{P} : \underset{\approx}{E} : \underset{\sim}{P} + \underset{\sim}{Q} : \underset{\approx}{C} : \underset{\sim}{Q}}$$

$$\begin{aligned} \underset{\approx\approx}{\mathbf{D}}^1 &= -\frac{(\underset{\approx\approx}{\mathbf{E}} : \underset{\sim}{\mathbf{P}}) \otimes (\underset{\sim}{\mathbf{Q}} : \underset{\approx\approx}{\mathbf{C}})}{\underset{\sim}{\mathbf{P}} : \underset{\approx\approx}{\mathbf{E}} : \underset{\sim}{\mathbf{P}} + \underset{\sim}{\mathbf{Q}} : \underset{\approx\approx}{\mathbf{C}} : \underset{\sim}{\mathbf{Q}}} \\ \underset{\approx\approx}{\mathbf{D}}^c &= \underset{\approx\approx}{\mathbf{C}} - \frac{(\underset{\approx\approx}{\mathbf{C}} : \underset{\sim}{\mathbf{Q}}) \otimes (\underset{\sim}{\mathbf{Q}} : \underset{\approx\approx}{\mathbf{C}})}{\underset{\sim}{\mathbf{P}} : \underset{\approx\approx}{\mathbf{E}} : \underset{\sim}{\mathbf{P}} + \underset{\sim}{\mathbf{Q}} : \underset{\approx\approx}{\mathbf{C}} : \underset{\sim}{\mathbf{Q}}} \end{aligned} \tag{142}$$

$\underset{\approx\approx}{\mathbf{E}}$ and $\underset{\approx\approx}{\mathbf{C}}$ are the Cosserat elasticity tensor seen in section 1.4.2. The choice of a yield criterion involving both force and couple stress tensors leads to a strong coupling between plastic strain and curvature rates. This has significant effects on the regularization capabilities of the model.

Steinman and Willam investigate the existence of discontinuities of both the total strain and curvature across a given surface S of normal $\underline{\mathbf{n}}$:

$$[\![\dot{\underline{\mathbf{u}}}]\!] = 0 \text{ and } [\![\dot{\underset{\sim}{\Phi}}]\!] = 0 \tag{143}$$

but

$$[\![\dot{\underset{\approx}{\mathbf{e}}}]\!] \neq 0 \text{ and } [\![\dot{\underset{\sim}{\Phi}} \otimes \underline{\nabla}]\!] = [\![\dot{\underset{\approx}{\kappa}}]\!] \neq 0 \tag{144}$$

Hadamard's compatibility conditions imply that these jumps must have the following form

$$\exists (\underline{\mathbf{g}}, \underline{\mathbf{g}}^c) \;/\; [\![\dot{\underset{\approx}{\mathbf{e}}}]\!] = \underline{\mathbf{g}} \otimes \underline{\mathbf{n}} \text{ and } [\![\dot{\underset{\approx}{\kappa}}]\!] = \underline{\mathbf{g}}^c \otimes \underline{\mathbf{n}} \tag{145}$$

Continuing equilibrium at the interface is assumed

$$[\![\dot{\underset{\sim}{\sigma}}]\!]\, \underline{\mathbf{n}} = 0 \text{ and } [\![\dot{\underset{\sim}{\mu}}]\!]\, \underline{\mathbf{n}} = 0 \tag{146}$$

Plastic/plastic bifurcation modes like 145 can occur only if

$$\begin{cases} \underset{\sim}{\mathbf{A}}\, \underline{\mathbf{g}} & + \underset{\sim}{\mathbf{A}}^1\, \underline{\mathbf{g}}^c = 0 \\ \underset{\sim}{\mathbf{A}}^2\, \underline{\mathbf{g}} & + \underset{\sim}{\mathbf{A}}^c\, \underline{\mathbf{g}}^c = 0 \end{cases} \tag{147}$$

where

$$\begin{aligned} \underset{\sim}{\mathbf{A}} &= \underline{\mathbf{n}}.\underset{\approx\approx}{\mathbf{D}}.\underline{\mathbf{n}} \\ \underset{\sim}{\mathbf{A}}^1 &= \underline{\mathbf{n}}.\underset{\approx\approx}{\mathbf{D}}^1.\underline{\mathbf{n}} \\ \underset{\sim}{\mathbf{A}}^2 &= \underline{\mathbf{n}}.\underset{\approx\approx}{\mathbf{D}}^{1T}.\underline{\mathbf{n}} \\ \underset{\sim}{\mathbf{A}}^c &= \underline{\mathbf{n}}.\underset{\approx\approx}{\mathbf{L}}^c.\underline{\mathbf{n}} \end{aligned} \tag{148}$$

Within the framework of a Cosserat theory, the localization criterion is given by the determinant of system 147. $\underset{\sim}{\mathbf{A}}$ is similar to the classical acoustic tensor. Dietsche [1993] shows that contrary to the classical case, this condition generally does not coincide with the existence of stationary waves any more (compare with section A.2.6).

According to [Steinmann, Willam 1991] an additional localization condition can be derived from the equilibrium conditions on both sides (+/−) of the discontinuity surface

$$\begin{cases} \underline{\mathrm{div}}\, \dot{\underset{\sim}{\sigma}}^+ = 0 \\ \underline{\mathrm{div}}\, \dot{\underset{\sim}{\sigma}}^- = 0 \end{cases} \Longrightarrow \underline{\mathrm{div}}\, [\![\dot{\underset{\sim}{\sigma}}]\!] = 0 \tag{149}$$

(see [Truesdells, Toupin 1960]) and on the other hand,

$$\left\{\begin{array}{lll} \underset{\sim}{\mathrm{div}}\,\dot{\underset{\sim}{\mu}}^{+} & +2\overset{\times}{\dot{\underset{\sim}{\sigma}}}^{+} & = 0 \\ \underset{\sim}{\mathrm{div}}\,\dot{\underset{\sim}{\mu}}^{-} & +2\overset{\times}{\dot{\underset{\sim}{\sigma}}}^{-} & = 0 \end{array}\right. \Longrightarrow \underset{\sim}{\mathrm{div}}\,[\![\dot{\underset{\sim}{\mu}}]\!] + 2[\![\overset{\times}{\dot{\underset{\sim}{\sigma}}}]\!] = 0 \tag{150}$$

Steinmann and Willam look for bifurcation modes with constant jump along the interface and eliminate the divergence term in 150. They get therefore an additional localization condition

$$[\![\overset{\times}{\dot{\underset{\sim}{\sigma}}}]\!] = 0 \tag{151}$$

which means that the stress rate jump must be symmetric.

Dietsche, Steinman and Willam [1991, 1993] investigate the possible resulting localization modes for several yield criteria (extension of von Mises, Rankine criteria) and show some regularization effects mainly due to their second localization condition 151.

4.2 Loss of uniqueness for an elastoplastic Cosserat continuum with hardening variables

4.2.1 Linear incremental form of the constitutive equations

We consider a very general form of Cosserat elastoplasticity (but not the most general) with two coupled yield criteria $F(\underset{\sim}{\sigma}, \underset{\sim}{\mu}, \underset{\sim}{\alpha}, \underset{\sim}{\alpha}^c)$ and $F^c(\underset{\sim}{\sigma}, \underset{\sim}{\mu}, \underset{\sim}{\alpha}, \underset{\sim}{\alpha}^c)$ for plastic deformation and curvature flows:

$$\dot{\underset{\sim}{e}}^p = \dot{\gamma}\,\underset{\sim}{P} \tag{152}$$

$$\dot{\underset{\sim}{\kappa}}^p = \frac{\dot{\theta}}{l}\,\underset{\sim}{Q} \tag{153}$$

The $\underset{\sim}{\alpha}$ and $\underset{\sim}{\alpha}^c$ denote hardening variables. Under plastic loading conditions,

$$\dot{F} = \underset{\sim}{N} : \dot{\underset{\sim}{\sigma}} + \frac{1}{l}\,\underset{\sim}{M} : \dot{\underset{\sim}{\mu}} - \dot{\gamma}\,H - \dot{\theta}\,H' = 0 \tag{154}$$

$$\dot{F}^c = \underset{\sim}{N}^c : \dot{\underset{\sim}{\sigma}} + \frac{1}{l}\,\underset{\sim}{M}^c : \dot{\underset{\sim}{\mu}} - \dot{\gamma}\,H'' - \dot{\theta}\,H_c = 0 \tag{155}$$

where

$$\underset{\sim}{N} = \frac{\partial F}{\partial \underset{\sim}{\sigma}} \tag{156}$$

$$\underset{\sim}{M} = l\frac{\partial F}{\partial \underset{\sim}{\mu}} \tag{157}$$

$$\underset{\sim}{N}^c = \frac{\partial F^c}{\partial \underset{\sim}{\sigma}} \tag{158}$$

$$\underset{\sim}{M}^c = l\frac{\partial F^c}{\partial \underset{\sim}{\mu}} \tag{159}$$

$$\dot{\gamma}\,H = -\frac{\partial F}{\partial \underset{\sim}{\alpha}} : \dot{\underset{\sim}{\alpha}} \tag{160}$$

$$\dot{\theta}\, H' \;=\; -\frac{\partial F}{\partial \underset{\sim}{\alpha}^c} : \dot{\underset{\sim}{\alpha}}^c \tag{161}$$

$$\dot{\gamma}\, H'' \;=\; -\frac{\partial F^c}{\partial \underset{\sim}{\alpha}} : \dot{\underset{\sim}{\alpha}} \tag{162}$$

$$\dot{\theta}\, H_c \;=\; -\frac{\partial F^c}{\partial \underset{\sim}{\alpha}^c} : \dot{\underset{\sim}{\alpha}}^c \tag{163}$$

In a way similar to that of the last section, a linear incremental form of the constitutive equations can be derived

$$\dot{\underset{\sim}{\sigma}} \;=\; \underset{\approx}{\mathrm{D}} : \dot{\underset{\sim}{\mathrm{e}}} + \underset{\approx}{\mathrm{D}}' : \dot{\underset{\sim}{\kappa}} \tag{164}$$

$$\dot{\underset{\sim}{\mu}} \;=\; \underset{\approx}{\mathrm{D}}'' : \dot{\underset{\sim}{\mathrm{e}}} + \underset{\approx}{\mathrm{D}}^c : \dot{\underset{\sim}{\kappa}} \tag{165}$$

with

$$\underset{\approx}{\mathrm{D}} \;=\; \underset{\approx}{\mathrm{E}} \;-\; \frac{1}{\Delta}\,(\underset{\approx}{\mathrm{E}} : \underset{\sim}{\mathrm{P}}) \otimes (A_c \underset{\sim}{\mathrm{N}} - A' \underset{\sim}{\mathrm{N}}^c) : \underset{\approx}{\mathrm{E}} \tag{166}$$

$$\underset{\approx}{\mathrm{D}}' \;=\; -\frac{1}{l\Delta}\,(\underset{\approx}{\mathrm{E}} : \underset{\sim}{\mathrm{P}}) \otimes (A_c \underset{\sim}{\mathrm{M}} - A' \underset{\sim}{\mathrm{M}}^c) : \underset{\approx}{\mathrm{C}} \tag{167}$$

$$\underset{\approx}{\mathrm{D}}'' \;=\; -\frac{1}{l\Delta}\,(\underset{\approx}{\mathrm{C}} : \underset{\sim}{\mathrm{Q}}) \otimes (A \underset{\sim}{\mathrm{N}}^c - A'' \underset{\sim}{\mathrm{N}}) : \underset{\approx}{\mathrm{E}} \tag{168}$$

$$\underset{\approx}{\mathrm{D}}^c \;=\; \underset{\approx}{\mathrm{C}} \;-\; \frac{1}{l^2\Delta}\,(\underset{\approx}{\mathrm{C}} : \underset{\sim}{\mathrm{Q}}) \otimes (A \underset{\sim}{\mathrm{M}}^c - A'' \underset{\sim}{\mathrm{M}}) : \underset{\approx}{\mathrm{C}} \tag{169}$$

and

$$A \;=\; H \;+\; \underset{\sim}{\mathrm{N}} : \underset{\approx}{\mathrm{E}} : \underset{\sim}{\mathrm{P}} \tag{170}$$

$$A' \;=\; H' \;+\; \frac{1}{l^2}\, \underset{\sim}{\mathrm{M}} : \underset{\approx}{\mathrm{C}} : \underset{\sim}{\mathrm{Q}} \tag{171}$$

$$A'' \;=\; H'' \;+\; \underset{\sim}{\mathrm{N}}^c : \underset{\approx}{\mathrm{E}} : \underset{\sim}{\mathrm{P}} \tag{172}$$

$$A_c \;=\; H_c \;+\; \frac{1}{l^2}\, \underset{\sim}{\mathrm{M}}^c : \underset{\approx}{\mathrm{C}} : \underset{\sim}{\mathrm{Q}} \tag{173}$$

$$\Delta \;=\; A\, A_c \;-\; A'\, A'' \tag{174}$$

Note that in general and contrary to the case presented in the last section, $\underset{\approx}{\mathrm{D}}' \neq \underset{\approx}{\mathrm{D}}''^T$.

4.2.2 Sufficient condition for uniqueness; limit points

We try to extend Hill's sufficient condition for uniqueness to the Cosserat framework. If two solutions $(\underset{\sim}{\sigma}^A, \underset{\sim}{\mu}^A, \underset{\sim}{\mathrm{e}}^A, \underset{\sim}{\kappa}^A)$ and $(\underset{\sim}{\sigma}^B, \underset{\sim}{\mu}^B, \underset{\sim}{\mathrm{e}}^B, \underset{\sim}{\kappa}^B)$ of the same boundary value problem are available, the principle of virtual power (see section 1.3) implies

$$\int_{\mathcal{D}} (\Delta \underset{\sim}{\sigma} : \Delta \dot{\underset{\sim}{\mathrm{e}}} \;+\; \Delta \underset{\sim}{\mu} : \Delta \dot{\underset{\sim}{\kappa}})\, dV \;\geq\; 0 \tag{175}$$

As a result, a sufficient local condition for uniqueness is

$$\dot{\underset{\sim}{\sigma}} : \dot{\underset{\sim}{\mathrm{e}}} \;+\; \dot{\underset{\sim}{\mu}} : \dot{\underset{\sim}{\kappa}} \;>\; 0 \tag{176}$$

for all admissible fields $(\dot{\underset{\sim}{e}}, \dot{\underset{\sim}{\kappa}})$ that vanish on the boundary with prescribed velocity and gyration. Using the previous incremental formulation, this condition reads

$$[\dot{\underset{\sim}{e}} \quad \dot{\underset{\sim}{\kappa}}] \begin{bmatrix} \underset{\approx}{D} & \underset{\approx}{D}' \\ \underset{\approx}{D}'' & \underset{\approx}{D}^c \end{bmatrix} \begin{bmatrix} \dot{\underset{\sim}{e}} \\ \dot{\underset{\sim}{\kappa}} \end{bmatrix} > 0 \tag{177}$$

Limit points. We now look for the solution of the limit point problem:

$$\begin{bmatrix} \underset{\approx}{D} & \underset{\approx}{D}' \\ \underset{\approx}{D}'' & \underset{\approx}{D}^c \end{bmatrix} \begin{bmatrix} \dot{\underset{\sim}{e}} \\ \dot{\underset{\sim}{\kappa}} \end{bmatrix} = 0 \tag{178}$$

For simplicity we restrict ourselves to associated plasticity with uncoupled yield functions: $\underset{\sim}{P} = \underset{\sim}{N}$, $\underset{\sim}{Q} = \underset{\sim}{M}^c$, $\underset{\sim}{M} = \underset{\sim}{N}^c = 0$. But the coupling of the hardening variables is taken into account. Instead of directly working out the eigenvectors associated with the zero eigenvalue of the previous operator, we consider the following generalized eigenvalue problem

$$\begin{cases} \underset{\approx}{D}\,\underset{\sim}{x} + \underset{\approx}{D}'\,\underset{\sim}{y} &= \lambda\,\underset{\approx}{E}\,\underset{\sim}{x} \\ \underset{\approx}{D}''\,\underset{\sim}{x} + \underset{\approx}{D}^c\,\underset{\sim}{y} &= \lambda_c\,\underset{\approx}{C}\,\underset{\sim}{y} \end{cases} \tag{179}$$

We find

$$\underset{\sim}{x} \propto \underset{\sim}{P} \quad \text{and} \quad \underset{\sim}{y} \propto \underset{\sim}{Q}/l \tag{180}$$

and

$$\lambda = 1 - \frac{1}{\Delta}\left(A_c\,\underset{\sim}{P} : \underset{\approx}{E} : \underset{\sim}{P} - \frac{H'}{l^2}\,\underset{\sim}{Q} : \underset{\approx}{C} : \underset{\sim}{Q}\right) \tag{181}$$

$$\lambda_c = 1 + \frac{1}{\Delta}\left(H''\,\underset{\sim}{P} : \underset{\approx}{E} : \underset{\sim}{P} - \frac{A}{l^2}\,\underset{\sim}{Q} : \underset{\approx}{C} : \underset{\sim}{Q}\right) \tag{182}$$

The remaining eigentensors belong to $\{\underset{\sim}{P}\}^{\perp_E}$ (resp. $\{\underset{\sim}{Q}\}^{\perp_C}$) with the eigenvalue 1. The solution of the initial problem is obtained for $\lambda = \lambda_c = 0$ and the associated critical hardening moduli are

$$H = -H' \quad \text{and} \quad H_c = -H'' \tag{183}$$

and

$$H = -\underset{\sim}{P} : \underset{\approx}{E} : \underset{\sim}{P}\,(1 - \frac{H''l^2}{\underset{\sim}{Q} : \underset{\approx}{C} : \underset{\sim}{Q}}) \quad \text{and} \quad l^2 H_c = -\underset{\sim}{Q} : \underset{\approx}{C} : \underset{\sim}{Q}\,(1 - \frac{H'}{\underset{\sim}{P} : \underset{\approx}{E} : \underset{\sim}{P}}) \tag{184}$$

If the hardening rules are not coupled, the classical result saying that a limit point is reached for $H = 0$, is retrieved.

4.3 Bifurcation analysis for Cosserat crystals undergoing single slip

In this section we investigate the existence of plastic/plastic bifurcation modes for the model for single crystals undegoing single slip within the framework of a Cosserat continuum.

4.3.1 Bifurcation analysis in a simple case

We consider the case of single slip $\underset{\sim}{P} = \underline{m} \otimes \underline{z}$ without coupling terms and before plastic curvature appears and we ask whether the slip bands and kink bands studied in part A are still bifurcation modes for Cosserat crystals or not.

Slip band: $\underline{g} \propto \underline{m}$ *(glide direction)* $\underline{n} = \underline{z}$ *(slip plane)*

We investigate the existence of a discontinuity surface of normal $\underline{n} = \underline{z}$ with the jump

$$[\![\dot{\underset{\sim}{e}}]\!] \propto \underline{m} \otimes \underline{z} \tag{185}$$

The equilibrium condition at the interface reads

$$[\![\dot{\underset{\sim}{\sigma}}]\!]\, \underline{z} = 0 \tag{186}$$

Assuming plastic loading on each side, it follows

$$[\![\underset{\sim\sim}{D}\, \dot{\underset{\sim}{e}}]\!]\, \underline{z} = 0 \tag{187}$$

$$(\underset{\sim\sim}{D}\, \underset{\sim}{P})\, \underline{z} = 0 \tag{188}$$

that is

$$E_{ijkl}\, P_{kl}\, z_j - \frac{1}{H + P_{ab}\, E_{abcd}\, P_{cd}}\, E_{ijkl}\, P_{kl}\, P_{mn}\, E_{mnpq}\, P_{pq}\, z_j = 0 \tag{189}$$

It can be checked immediately that $H = 0$ is still a solution of the previous equation. It means that under the above hypotheses, slip bands are still possible and lead to the loss of ellipticity of the equations as soon as the hardening modulus vanishes.

Kink band: $\underline{g} \propto \underline{z}$, $\underline{n} = \underline{m}$

We must have now

$$(\underset{\sim\sim}{D}\, \underset{\sim}{P}^T)\, \underline{m} = 0 \tag{190}$$

This implies

$$\underline{z}.(\underset{\sim\sim}{D}\, \underset{\sim}{P}^T).\underline{m} = 0$$

and hence

$$\underset{\sim}{P}^T : \underset{\sim\sim}{E} : \underset{\sim}{P}^T - \frac{(\underset{\sim}{P}^T : \underset{\sim\sim}{E} : \underset{\sim}{P})(\underset{\sim}{P} : \underset{\sim\sim}{E} : \underset{\sim}{P}^T)}{H + \underset{\sim}{P} : \underset{\sim\sim}{E} : \underset{\sim}{P}} = 0 \tag{191}$$

One obtains the critical hardening modulus for which a kink band may appear

$$H^{kink} = \frac{(\underset{\sim}{P}^T : \underset{\sim\sim}{E} : \underset{\sim}{P})^2}{\underset{\sim}{P}^T : \underset{\sim\sim}{E} : \underset{\sim}{P}^T} - \underset{\sim}{P} : \underset{\sim\sim}{E} : \underset{\sim}{P} \tag{192}$$

For isotropic elasticity

$$\begin{aligned} \underset{\sim}{P} : \underset{\sim\sim}{E} : \underset{\sim}{P} &= \underset{\sim}{P}^T : \underset{\sim\sim}{E} : \underset{\sim}{P}^T = \mu + \mu_c \\ \underset{\sim}{P}^T : \underset{\sim\sim}{E} : \underset{\sim}{P} &= \underset{\sim}{P} : \underset{\sim\sim}{E} : \underset{\sim}{P}^T = \mu - \mu_c \end{aligned}$$

so that

$$H^{kink} = -\frac{4\,\mu\mu_c}{\mu + \mu_c} < 0 \tag{193}$$

One must check that 190 is fulfilled

$$(\underset{\sim}{\mathbf{E}}\underset{\sim}{\mathbf{P}}^T - \frac{\underset{\sim}{\mathbf{P}}^T : \underset{\sim}{\mathbf{E}} : \underset{\sim}{\mathbf{P}}^T}{\underset{\sim}{\mathbf{P}} : \underset{\sim}{\mathbf{E}} : \underset{\sim}{\mathbf{P}}^T}\,\underset{\sim}{\mathbf{E}}\underset{\sim}{\mathbf{P}})\,\underline{\mathbf{m}} = (\mu + \mu_c)\,\underline{\mathbf{m}} - \frac{\mu + \mu_c}{\mu - \mu_c}(\mu - \mu_c)\,\underline{\mathbf{m}} = 0 \tag{194}$$

As a result the occurrence of the kink band is delayed. The elastic Cosserat modulus μ_c is responsible for this regularizing effect. For $\mu_c = 0$ the classical result is retrieved.

4.3.2 General case

The constitutive equations under small strain and curvature assumptions are recalled in the case of single slip. Equations 152 and 153 hold with

$$\underset{\sim}{\mathbf{P}} = \underline{\mathbf{m}} \otimes \underline{\mathbf{z}} \tag{195}$$

and

$$\underset{\sim}{\mathbf{Q}} = \underline{\xi} \otimes \underline{\mathbf{m}} \tag{196}$$

The retained hardening rules are

$$\underset{\sim}{\mathbf{P}} : \dot{\underset{\sim}{\sigma}} = H\,\dot{\gamma} + H'\,\dot{\theta} \tag{197}$$

$$\underset{\sim}{\mathbf{Q}} : \dot{\underset{\sim}{\mu}} = lH_c\,\dot{\theta} \tag{198}$$

The linear incremental form of the constitutive equations can be derived

$$\dot{\underset{\sim}{\sigma}} = \underset{\sim}{\mathbf{D}} : \dot{\underset{\sim}{\mathbf{e}}} + \underset{\sim}{\mathbf{D}}' : \dot{\underset{\sim}{\kappa}} \tag{199}$$

$$\dot{\underset{\sim}{\mu}} = \underset{\sim}{\mathbf{D}}^c : \dot{\underset{\sim}{\kappa}} \tag{200}$$

with

$$\underset{\sim}{\mathbf{D}} = \underset{\sim}{\mathbf{E}} - \frac{1}{\Delta}(\underset{\sim}{\mathbf{E}} : \underset{\sim}{\mathbf{P}}) \otimes (\underset{\sim}{\mathbf{P}} : \underset{\sim}{\mathbf{E}}) \tag{201}$$

$$\underset{\sim}{\mathbf{D}}' = \frac{H'}{l\Delta\Delta_c}(\underset{\sim}{\mathbf{E}} : \underset{\sim}{\mathbf{P}}) \otimes (\underset{\sim}{\mathbf{Q}} : \underset{\sim}{\mathbf{C}}) \tag{202}$$

$$\underset{\sim}{\mathbf{D}}^c = \underset{\sim}{\mathbf{C}} - \frac{1}{l^2\Delta_c}(\underset{\sim}{\mathbf{C}} : \underset{\sim}{\mathbf{Q}}) \otimes (\underset{\sim}{\mathbf{Q}} : \underset{\sim}{\mathbf{C}}) \tag{203}$$

and

$$\Delta = H + \underset{\sim}{\mathbf{P}} : \underset{\sim}{\mathbf{E}} : \underset{\sim}{\mathbf{P}} \tag{204}$$

$$\Delta^c = H^c + \underset{\sim}{\mathbf{Q}} : \underset{\sim}{\mathbf{C}} : \underset{\sim}{\mathbf{Q}}/l^2 \tag{205}$$

We investigate the conditions for the existence of a surface S across which $\dot{\underset{\sim}{\mathbf{e}}}$ and $\dot{\underset{\sim}{\kappa}}$ are discontinuous. Let $\underline{\mathbf{n}}$ be the normal to the surface at $\underline{\mathbf{x}} \in S$. Hadamard compatibility conditions imply that the jumps are of the form 145. The equilibrium conditions are given by equation 146. They lead to the following conditions

$$\left(\underline{\mathbf{n}}.\underset{\sim}{\mathbf{E}}.\underline{\mathbf{n}} - \frac{1}{\Delta}(\underline{\mathbf{n}}.\underset{\sim}{\mathbf{E}} : \underset{\sim}{\mathbf{P}}) \otimes (\underset{\sim}{\mathbf{P}} : \underset{\sim}{\mathbf{E}}.\underline{\mathbf{n}})\right)\,\underline{\mathbf{g}} + \frac{H'}{l\Delta\Delta_c}\left((\underline{\mathbf{n}}.\underset{\sim}{\mathbf{E}} : \underset{\sim}{\mathbf{P}}) \otimes (\underset{\sim}{\mathbf{Q}} : \underset{\sim}{\mathbf{C}}.\underline{\mathbf{n}})\right)\underline{\mathbf{g}}^c = 0 \tag{206}$$

$$\left(\underline{\mathbf{n}}.\underset{\sim}{\mathbf{C}}.\underline{\mathbf{n}} - \frac{1}{l^2\Delta_c}(\underline{\mathbf{n}}.\underset{\sim}{\mathbf{C}} : \underset{\sim}{\mathbf{Q}}) \otimes (\underset{\sim}{\mathbf{Q}} : \underset{\sim}{\mathbf{C}}.\underline{\mathbf{n}})\right)\,\underline{\mathbf{g}}^c = 0 \tag{207}$$

Remark. We have adopted short notations but it must be noticed that by $\underline{n}.\underset{\sim}{\underset{\sim}{E}}.\underline{n}$ we mean here $n_j E_{ijkl} n_l$. This holds also for some other expressions that are not explicitely written in components (see section 4.3.1 for similar calculations).

Equation 207 has already been solved in section A.2.5.1 (equations A.82 and A.83):

$$\underline{g}^c \propto (\underline{n}.\underset{\sim}{\underset{\sim}{C}}.\underline{n})^{-1}(\underline{n}.\underset{\sim}{\underset{\sim}{C}} : \underset{\sim}{Q})/l \tag{208}$$

$$l^2 H^c = -\underset{\sim}{Q} : \underset{\sim}{\underset{\sim}{C}} : \underset{\sim}{Q} + (\underset{\sim}{Q} : \underset{\sim}{\underset{\sim}{C}}.\underline{n})(\underline{n}.\underset{\sim}{\underset{\sim}{C}}.\underline{n})^{-1}(\underline{n}.\underset{\sim}{\underset{\sim}{C}} : \underset{\sim}{Q}) \tag{209}$$

We now restrict ourselves to isotropic elasticity and for that purpose, in addition to the tensor $\underset{\sim}{\underset{\sim}{I}}$, $\underset{\sim}{\underset{\sim}{J}}$ and $\underset{\sim}{\underset{\sim}{K}}$ used in section C.3.2, we introduce the tensors $\underset{\sim}{\underset{\sim}{I}}^a$ and $\underset{\sim}{\underset{\sim}{J}}^a$, such that

$$\underset{\sim}{\underset{\sim}{I}}\,\underset{\sim}{e} = {}^{\{}\underset{\sim}{e}^{\}} \quad \text{and} \quad \underset{\sim}{\underset{\sim}{I}}^a\underset{\sim}{e} = {}^{\}}\underset{\sim}{e}^{\{} \tag{210}$$

and

$$\underset{\sim}{\underset{\sim}{K}} + \underset{\sim}{\underset{\sim}{J}} + \underset{\sim}{\underset{\sim}{J}}^a = \underset{\sim}{\underset{\sim}{1}} \tag{211}$$

where $\underset{\sim}{\underset{\sim}{1}}$ is the identity linear operator on non-symmetric second-rank tensors. As a result the isotropic elasticity tensors can be written

$$\underset{\sim}{\underset{\sim}{C}} = 3\alpha\underset{\sim}{\underset{\sim}{K}} + 2\beta\underset{\sim}{\underset{\sim}{I}} + 2\gamma\underset{\sim}{\underset{\sim}{I}}^a = (3\alpha+2\beta)\underset{\sim}{\underset{\sim}{K}} + 2\beta\underset{\sim}{\underset{\sim}{J}} + 2\gamma\underset{\sim}{\underset{\sim}{J}}^a \tag{212}$$

Similar relations hold for $\underset{\sim}{\underset{\sim}{E}}$. We have the very convenient property

$$\underset{\sim}{\underset{\sim}{C}}^{-1} = \frac{1}{3\alpha+2\beta}\,\underset{\sim}{\underset{\sim}{K}} + \frac{1}{2\beta}\,\underset{\sim}{\underset{\sim}{J}} + \frac{1}{2\gamma}\,\underset{\sim}{\underset{\sim}{J}}^a \tag{213}$$

As a result

$$\underline{n}.\underset{\sim}{\underset{\sim}{C}}.\underline{n} = (\beta+\gamma)\underline{1} + (\alpha+\beta-\gamma)\,\underline{n}\otimes\underline{n} \tag{214}$$

and

$$(\underline{n}.\underset{\sim}{\underset{\sim}{C}}.\underline{n})^{-1} = \frac{1}{\beta+\gamma}\,\underline{1} - \frac{\alpha+\beta-\gamma}{(\beta+\gamma)(\alpha+2\beta)}\,\underline{n}\otimes\underline{n} \tag{215}$$

We get

$$\underline{g}^c = g^c\left(\underline{n}.\underline{m}\,\underline{\xi} + \frac{\beta-\gamma}{\beta+\gamma}\,\underline{n}.\underline{\xi}\,\underline{m} - \frac{2\gamma(\alpha+\beta-\gamma)}{(\beta+\gamma)(\alpha+2\beta)}\,\underline{n}.\underline{m}\,\underline{n}.\underline{\xi}\,\underline{n}\right) \tag{216}$$

and

$$l^2\,H^c = (\beta+\gamma)((\underline{n}.\underline{m})^2-1) + \frac{(\beta-\gamma)^2}{\beta+\gamma}(\underline{n}.\underline{\xi})^2 - (\underline{n}.\underline{m})^2\,(\underline{n}.\underline{\xi})^2\,\frac{4\beta\gamma(\alpha+\beta-\gamma)}{(\alpha+2\beta)(\beta+\gamma)} \tag{217}$$

The two last expressions must now be substituted in equation 206. At this stage we resort to coordinates relative to the basis $(\underline{m}, \underline{z}, -\underline{\xi})$. This leads to the following system of equations

$$(\mu+\mu_c)\begin{bmatrix} g_1 \\ g_2 \\ g_3 \end{bmatrix} + (\lambda+\mu-\mu_c)(n_i g_i)\begin{bmatrix} n_1 \\ n_2 \\ n_3 \end{bmatrix}$$

$$-\frac{1}{\Delta}\left((\mu+\mu_c)n_2g_1+(\mu-\mu_c)n_1g_2\right)\left((\mu+\mu_c)n_2\begin{bmatrix}1\\0\\0\end{bmatrix}+(\mu-\mu_c)n_1\begin{bmatrix}0\\1\\0\end{bmatrix}\right)$$
$$+\frac{H'g^c}{l\Delta\Delta^c}\left((\beta+\gamma)n_1^2+\frac{(\beta-\gamma)^2}{\beta+\gamma}n_3^2-\frac{4\beta\gamma(\alpha+\beta-\gamma)}{(\alpha+2\beta)(\beta+\gamma)}n_1^2n_3^2\right)$$
$$\left((\mu+\mu_c)n_2\begin{bmatrix}1\\0\\0\end{bmatrix}+(\mu-\mu_c)n_1\begin{bmatrix}0\\1\\0\end{bmatrix}\right)=0$$

Two cases can be distinguished but the details of the calculation are not given.

- $n_3=0$

  then $g_3=0$ and

$$g_1 = -\frac{H'g^c}{\Delta\Delta^c}(\beta+\gamma)n_1^2n_2\left((\mu+\mu^c)((\mu+\mu_c)+(\lambda+\mu-\mu_c)n_2^2-\frac{1}{\Delta}(\mu-\mu_c)^2n_1^2\right.$$
$$\left.-(\mu-\mu_c)n_1^2((\lambda+\mu-\mu_c)-\frac{1}{\Delta}(\mu^2-\mu_c^2))\right)/D \tag{218}$$

$$g_2 = -\frac{H'g^c}{\Delta\Delta^c}(\beta+\gamma)n_1^3\left((\mu-\mu^c)((\mu+\mu_c)+(\lambda+\mu-\mu_c)n_2^2-\frac{1}{\Delta}(\mu+\mu_c)^2n_2^2\right.$$
$$\left.-(\mu+\mu_c)n_2^2((\lambda+\mu-\mu_c)-\frac{1}{\Delta}(\mu^2-\mu_c^2))\right)/D \tag{219}$$

where D is the determinant of the system.

- $n_3\neq 0$

  For the sake of simplicity, we do not give the expressions in this case.

Extrema of $H^c(\underline{\mathrm{n}})$. We now look for the critical hardening modulus for which the first plastic/plastic bifurcation becomes possible. Like in section A.2.5.2, we consider the Lagrangian function

$$L(\underline{\mathrm{n}},\lambda) = H^c(\underline{\mathrm{n}}) - \lambda(n_1^2+n_2^2+n_3^2-1) \tag{220}$$

When written in components, equation 209 becomes

$$H_c(\underline{\mathrm{n}})=(\beta+\gamma)(n_1^2-1)+\frac{(\beta-\gamma)^2}{\beta+\gamma}n_3^2-n_1^2n_3^2\frac{4\beta\gamma(\alpha+\beta-\gamma)}{(\alpha+2\beta)(\beta+\gamma)} \tag{221}$$

The maximization procedure leads to the three following cases

- $\underline{\mathrm{n}}=\underline{\xi}$

  but this implies $\underline{\mathrm{g}}^c=\underline{\mathrm{g}}=0$. No bifurcation is possible in that case.
- $\underline{\mathrm{n}}=\underline{\mathrm{m}}$ and $\underline{\mathrm{g}}^c=-g^c\underline{\xi}$

  Then

$$\underline{\mathrm{g}}=-g^c\frac{H'(\mu-\mu_c)}{l(H(\mu+\mu_c)+4\mu\mu_c)}\,\underline{\mathrm{z}} \tag{222}$$

This corresponds to a kink band. Contrary to the classic case, for a given amplitude of the curvature rate jump g^c at the surface, the amplitude of the strain rate jump is no longer arbitrary. The critical hardening modulus is

$$H_c = 0 \tag{223}$$

The case $g^c = 0$ has already been treated in section 4.3.1.

- $n_1 n_3 \neq 0$

In this case, $H^c < 0$.

Conclusion of the bifurcation analysis. If curvature and deformation are decoupled (no lattice rotation gradients), slip bands are still possible bifurcation modes (section 4.3.1). In the coupled case, the first possible mode is the kink band that can appear if the Cosserat hardening modulus H^c vanishes. The use of a positive H_c leads to the regularization of the kink band. If a coupling exists between slip and curvature in equation 198 the amplitudes of the deformation rate and curvature rate jumps are not arbitrary any more.

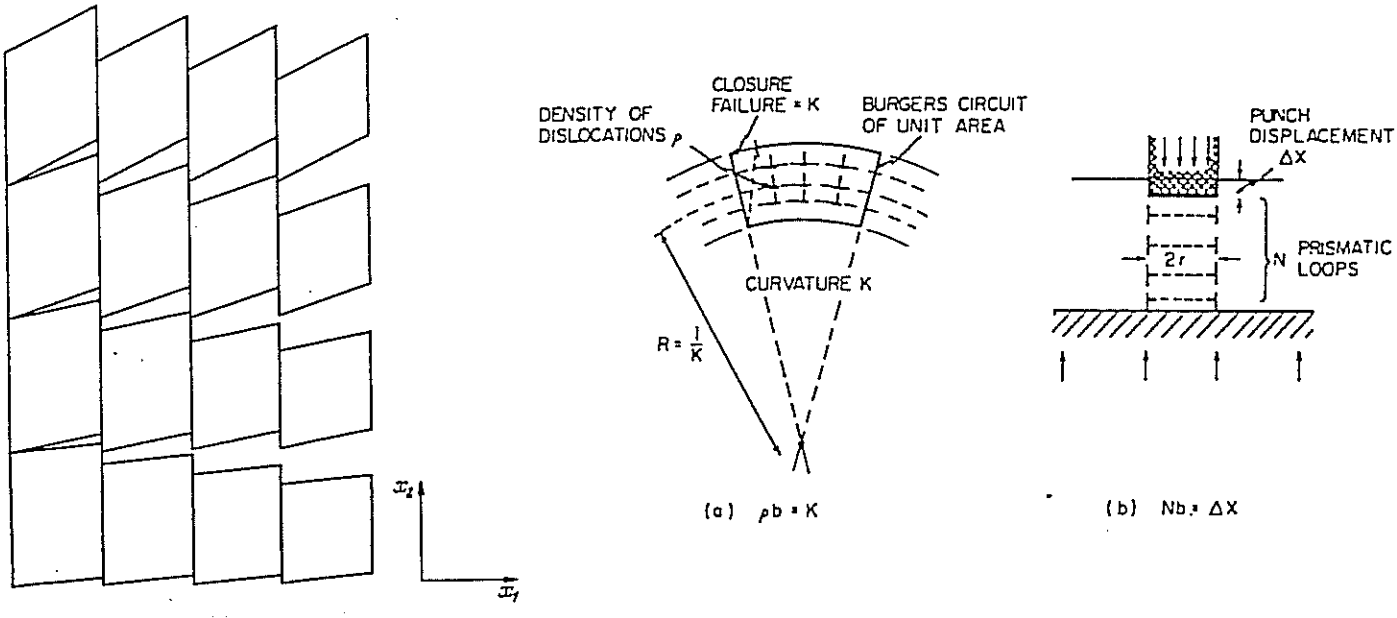

Figure B.1: Geometrically necessary dislocations in the case of non-homogeneous deformation of single crystals, after [Kröner 1958], [Ashby 1971].

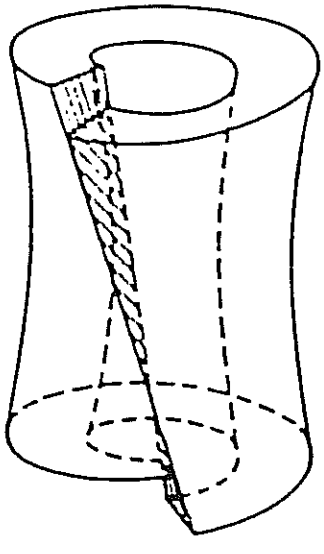

Figure B.2: Screw dislocation, when the couple at its ends is released, after [Friedel 1964].

Part C

NON-HOMOGENEOUS DEFORMATION OF TWO-PHASE SINGLE CRYSTALS

1 Statistical modelling of non-homogeneous materials

1.1 Integral equation of heterogeneous elasticity

We consider an elastically non-homogeneous body Ω the local behaviour of which is given by the random function $\underset{\sim}{\underset{\sim}{\mathbf{c}}}(\underline{\mathbf{r}})$ according to

$$\underset{\sim}{\sigma}(\underline{\mathbf{r}}) = \underset{\sim}{\underset{\sim}{\mathbf{c}}}(\underline{\mathbf{r}}) : \underset{\sim}{\varepsilon}(\underline{\mathbf{r}}) \tag{1}$$

at point $\underline{\mathbf{r}}$ (the treatment would apply for a non-local form $\underset{\sim}{\sigma}(\underline{\mathbf{r}}) = \int_\Omega \underset{\sim}{\underset{\sim}{\mathbf{c}}}(\underline{\mathbf{r}}, \underline{\mathbf{r}}') : \underset{\sim}{\varepsilon}(\underline{\mathbf{r}}')dr'$). We choose a homogeneous reference medium described by the elasticity tensor $\underset{\sim}{\underset{\sim}{\mathbf{C}}}^0$ and define

$$\delta\underset{\sim}{\underset{\sim}{\mathbf{c}}} = \underset{\sim}{\underset{\sim}{\mathbf{c}}} - \underset{\sim}{\underset{\sim}{\mathbf{C}}}^0 \tag{2}$$

The equilibrium equation reads then

$$\underline{\text{div}}\ \underset{\sim}{\underset{\sim}{\mathbf{C}}}^0 : \underset{\sim}{\varepsilon} + \underline{\text{div}}\ \delta\underset{\sim}{\underset{\sim}{\mathbf{c}}} : \underset{\sim}{\varepsilon} = 0 \tag{3}$$

Regarding $\delta\underset{\sim}{\underset{\sim}{\mathbf{c}}} : \underset{\sim}{\varepsilon}$ as a polarization function, i.e. div $\delta\underset{\sim}{\underset{\sim}{\mathbf{c}}} : \underset{\sim}{\varepsilon}$ as a body force, the displacement field solution of equation 3 is given by

$$u_i(\underline{\mathbf{r}}) = u_i^0(\underline{\mathbf{r}}) + \int_\Omega G_{ij}(\underline{\mathbf{r}}, \underline{\mathbf{r}}')(\delta\underset{\sim}{\underset{\sim}{\mathbf{c}}} : \underset{\sim}{\varepsilon})_{jk,k'}dr' \tag{4}$$

where $\underline{\mathbf{u}}_0$ is the solution of the homogeneous problem associated with $\underset{\sim}{\underset{\sim}{\mathbf{C}}}^0$ and the Green tensor $\underset{\sim}{\mathbf{G}}$ associated with the reference medium is defined by

$$C^0_{ijkl}G_{km,lj}(\underline{\mathbf{r}}, \underline{\mathbf{r}}') + \delta(\underline{\mathbf{r}}, \underline{\mathbf{r}}')\delta_{im} = 0 \qquad \forall \underline{\mathbf{r}}, \underline{\mathbf{r}}' \in \Omega \tag{5}$$

$$G_{im}(\underline{\mathbf{r}}, \underline{\mathbf{r}}') = 0 \qquad \forall \underline{\mathbf{r}} \in \partial\Omega, \forall \underline{\mathbf{r}}' \in \Omega \tag{6}$$

for prescribed displacements at $\partial\Omega$ (see [Kröner, Koch 1976] for surface forces). Equation 4 may be rewritten

$$u_i(\underline{\mathbf{r}}) = u_i^0(\underline{\mathbf{r}}) - \int_\Omega G_{ij,k'}(\underline{\mathbf{r}}, \underline{\mathbf{r}}')\delta c_{jkmn}(\underline{\mathbf{r}}')u_{m,n}(\underline{\mathbf{r}}')dr' \tag{7}$$

Defining the Green operator associated with the reference medium

$$\Gamma_{injk}(\underline{\mathbf{r}}, \underline{\mathbf{r}}') = G_{ij,k'n}(\underline{\mathbf{r}}, \underline{\mathbf{r}}')_{(in)(jk)} \tag{8}$$

the strain may be derived

$$\varepsilon_{in} = \varepsilon^0_{in} - \int_\Omega \Gamma_{injk} \delta c_{jkpq} \varepsilon_{pq} dr' \tag{9}$$

Using a symbolic notation, the previous integral equation becomes

$$\underset{\sim}{\varepsilon} + (\underset{\approx}{\Gamma} : \delta\underset{\approx}{\mathbf{c}}) * \underset{\sim}{\varepsilon} = \underset{\sim}{\varepsilon}^0 \tag{10}$$

(so-called Lippmann-Schwinger equation).

A discussion on the convergence of the integral and of the singularity of Green operator for the finite and infinite body can be found in [Zaoui 1993].

1.2 Equation of the effective moduli

The effective elastic moduli characterizing the homogeneous equivalent medium may be defined according to

$$< \underset{\sim}{\sigma} > = < \underset{\approx}{\mathbf{c}} : \underset{\sim}{\varepsilon} > = \underset{\approx}{\mathbf{C}}^{\text{eff}} : < \underset{\sim}{\varepsilon} > \tag{11}$$

$$< \underset{\sim}{\varepsilon} > = < \underset{\approx}{\mathbf{s}} : \underset{\sim}{\sigma} > = \underset{\approx}{\mathbf{S}}^{\text{eff}} : < \underset{\sim}{\sigma} > \tag{12}$$

The notation <> denotes strictly speaking the ensemble average for a random variable but, resorting to the ergodic hypothesis, it will be taken as the volume average. The energetic definition of the overall properties reads

$$< \underset{\sim}{\varepsilon} : \underset{\approx}{\mathbf{c}} : \underset{\sim}{\varepsilon} > = < \underset{\sim}{\varepsilon} > : \underset{\approx}{\mathbf{C}}^{\text{eff}} : < \underset{\sim}{\varepsilon} > \tag{13}$$

$$< \underset{\sim}{\sigma} : \underset{\approx}{\mathbf{s}} : \underset{\sim}{\sigma} > = < \underset{\sim}{\sigma} > : \underset{\approx}{\mathbf{S}}^{\text{eff}} : < \underset{\sim}{\sigma} > \tag{14}$$

The two definitions are mutually consistent if the so-called Hill-Mandel condition

$$< \underset{\sim}{\sigma} : \underset{\sim}{\varepsilon} > = < \underset{\sim}{\sigma} > : < \underset{\sim}{\varepsilon} > \tag{15}$$

holds. In particular 15 holds in the case of homogeneous boundary conditions

$$\underline{\mathbf{u}}^d = < \underset{\sim}{\varepsilon} > \underline{\mathbf{r}} \qquad \forall \underline{\mathbf{r}} \in \partial\Omega \tag{16}$$

or

$$\underline{\mathbf{T}}^d = < \underset{\sim}{\sigma} > \underline{\mathbf{n}} \qquad \forall \underline{\mathbf{r}} \in \partial\Omega \tag{17}$$

Equation 10 can be formally inverted

$$\underset{\sim}{\varepsilon} = (\underset{\approx}{\mathbf{I}} + \underset{\approx}{\Gamma} : \delta\underset{\approx}{\mathbf{c}})^{-1} * \underset{\sim}{\varepsilon}^0 \tag{18}$$

$$< \underset{\sim}{\varepsilon} > = < (\underset{\approx}{\mathbf{I}} + \underset{\approx}{\Gamma} : \delta\underset{\approx}{\mathbf{c}})^{-1} > * \underset{\sim}{\varepsilon}^0 \tag{19}$$

Hence

$$\underset{\sim}{\varepsilon} = (\underset{\approx}{\mathbf{I}} + \underset{\approx}{\Gamma} : \delta\underset{\approx}{\mathbf{c}})^{-1} * < (\underset{\approx}{\mathbf{I}} + \underset{\approx}{\Gamma} : \delta\underset{\approx}{\mathbf{c}})^{-1} >^{-1} : < \underset{\sim}{\varepsilon} > \tag{20}$$

It follows that

$$\underset{\approx}{\mathbf{C}}^{\text{eff}} = < \underset{\approx}{\mathbf{c}} : (\underset{\approx}{\mathbf{I}} + \underset{\approx}{\Gamma} : \delta\underset{\approx}{\mathbf{c}})^{-1} > * < (\underset{\approx}{\mathbf{I}} + \underset{\approx}{\Gamma} : \delta\underset{\approx}{\mathbf{c}})^{-1} >^{-1} \tag{21}$$

A similar analysis is done for the compliances in [Dederichs, Zeller 1973]. They introduce the four-rank tensor

$$\underset{\sim\sim}{\Delta} = \underset{\sim\sim}{C}^0 - \underset{\sim\sim}{C}^0 : \underset{\sim\sim}{\Gamma} : \underset{\sim\sim}{C}^0 \tag{22}$$

(since $\underset{\sim}{\sigma} = \underset{\sim}{\sigma}^0 + \underset{\sim\sim}{C}^0 : \int_\Omega \underset{\sim\sim}{\Gamma} : \underset{\sim\sim}{C}^0 : \delta\underset{\sim\sim}{s} : \underset{\sim}{\sigma} dr' - \underset{\sim\sim}{C}^0 : \delta\underset{\sim\sim}{s})$ and find

$$\underset{\sim\sim}{S}^{\text{eff}} = < \underset{\sim\sim}{s} : (\underset{\sim\sim}{I} + \underset{\sim\sim}{\Delta} : \delta\underset{\sim\sim}{s})^{-1} > * < (\underset{\sim\sim}{I} + \underset{\sim\sim}{\Delta} : \delta\underset{\sim\sim}{s})^{-1} >^{-1} \tag{23}$$

Setting $\underset{\sim\sim}{C}^0 = \underset{\sim\sim}{C}^{\text{eff}}$, an implicit integral equation is obtained

$$< \delta\underset{\sim\sim}{c} : (\underset{\sim\sim}{I} + \underset{\sim\sim}{\Gamma} : \delta\underset{\sim\sim}{c})^{-1} >= 0 \tag{24}$$

1.3 Upper and lower bounds

Kröner [1977] derives upper and lower bounds for the effective elastic properties of non-homogeneous materials. He introduces the projection operator P or 'prime operator'

$$Pf = f' = f - < f > \tag{25}$$

Applying it to equation 10

$$\underset{\sim}{\varepsilon}' + (P\underset{\sim\sim}{\Gamma} : \delta\underset{\sim\sim}{c}) * \underset{\sim}{\varepsilon}' + (P\underset{\sim\sim}{\Gamma} : \delta\underset{\sim\sim}{c}) * < \underset{\sim}{\varepsilon} >= 0 \tag{26}$$

and multiplying by $\delta\underset{\sim\sim}{c}$ and taking the ensemble average, Kröner obtains, dropping the stars,

$$< \delta\underset{\sim\sim}{c} : \underset{\sim}{\varepsilon} >= - < (\underset{\sim\sim}{I} + \delta\underset{\sim\sim}{c} : P\underset{\sim\sim}{\Gamma})^{-1} : \delta\underset{\sim\sim}{c} : P\underset{\sim\sim}{\Gamma} : \delta\underset{\sim\sim}{c} > : < \underset{\sim}{\varepsilon} > \tag{27}$$

On the other hand

$$< \delta\underset{\sim\sim}{c} : \underset{\sim}{\varepsilon}' >= \underset{\sim\sim}{C}^{\text{eff}} : < \underset{\sim}{\varepsilon} > - < \underset{\sim}{\sigma} > : < \underset{\sim}{\varepsilon} > \tag{28}$$

Hence

$$\underset{\sim\sim}{C}^{\text{eff}} = < \underset{\sim\sim}{c} > - < (\underset{\sim\sim}{I} + \delta c : P\underset{\sim\sim}{\Gamma})^{-1} : \delta\underset{\sim\sim}{c} : P\underset{\sim\sim}{\Gamma} : \delta\underset{\sim\sim}{c} > \tag{29}$$

Kröner gives the more convenient form

$$\underset{\sim\sim}{C}^{\text{eff}} = < \underset{\sim\sim}{c} : \underset{\sim\sim}{B} > \qquad \text{with} \qquad \underset{\sim\sim}{B} = (\underset{\sim\sim}{I} + P\underset{\sim\sim}{\Gamma} : \delta\underset{\sim\sim}{c})^{-1} \tag{30}$$

(the property $< \underset{\sim\sim}{C}^0 : P\underset{\sim\sim}{\Gamma} : \delta\underset{\sim\sim}{c} >= 0$ has been used). To obtain the previous form the series expansion has been used

$$\underset{\sim\sim}{B} = \underset{\sim\sim}{I} - P\underset{\sim\sim}{\Gamma} : \delta\underset{\sim\sim}{c} + P\underset{\sim\sim}{\Gamma} : \delta\underset{\sim\sim}{c} : P\underset{\sim\sim}{\Gamma} : \delta\underset{\sim\sim}{c} + ... \tag{31}$$

the convergence of which is ensured when for instance $< \underset{\sim\sim}{c} >^{-1} : \underset{\sim\sim}{c}' < 1$ (inequality in the sense of quadratic forms). It means that for very heterogeneous materials convergence is not ensured ([Kröner, Koch 1976], however in [Gambin, Kröner 1981] the convergence of the series is proved for any statistically homogeneous and isotropic finite medium without pores nor rigid inclusions).

The minimum energy principles yield

$$< \underset{\sim}{\varepsilon} >: \underset{\approx}{\mathbf{C}}^{\text{eff}} :< \underset{\sim}{\varepsilon} > \quad \leq \quad < \underset{\sim}{\varepsilon}^* : \underset{\approx}{\mathbf{c}} : \underset{\sim}{\varepsilon}^* > \tag{32}$$

$$< \underset{\sim}{\sigma} >: \underset{\approx}{\mathbf{S}}^{\text{eff}} :< \underset{\sim}{\sigma} > \quad \leq \quad < \underset{\sim}{\sigma}^* : \underset{\approx}{\mathbf{s}} : \underset{\sim}{\sigma}^* > \tag{33}$$

where $\underset{\sim}{\varepsilon}^*$ and $\underset{\sim}{\sigma}^*$ are admissible trial functions such that

$$< \varepsilon^* >=< \varepsilon > \qquad \text{and} \qquad < \underset{\sim}{\sigma}^* >=< \underset{\sim}{\sigma} > \tag{34}$$

The most general trial function admits the form $(\underset{\approx}{\mathbf{I}}+P\underset{\approx}{\Gamma} : \underset{\approx}{\tau}) :< \underset{\sim}{\varepsilon} >$ where $\underset{\approx}{\tau}$ is arbitrary (see [Kröner 1977]). A particularly useful set of trial functions $\underset{\approx}{\mathbf{B}}_m :< \underset{\sim}{\varepsilon} >$ is obtained by truncating the series 31 after the m$^{\text{th}}$ term (m=0,1,2,...):

$$\underset{\approx}{\mathbf{B}}_m = \underset{\approx}{\mathbf{I}} - P\underset{\approx}{\Gamma} : \delta\underset{\approx}{\mathbf{c}} + (P\underset{\approx}{\Gamma} : \delta\underset{\approx}{\mathbf{c}})^2 + ... + (-1)^m (P\underset{\approx}{\Gamma} : \delta\underset{\approx}{\mathbf{c}})^m \tag{35}$$

(i.e. $\underset{\approx}{\mathbf{B}}_m = \underset{\approx}{\mathbf{I}} - P\underset{\approx}{\Gamma} : \delta\underset{\approx}{\mathbf{c}} : B_{m-1}$). The trial function $\underset{\approx}{\mathbf{B}}_\infty :< \underset{\sim}{\varepsilon} >= \underset{\approx}{\mathbf{B}} :< \underset{\sim}{\varepsilon} >$ provides the exact solution $\underset{\approx}{\mathbf{C}}^{\text{eff}}$ if the $\underset{\approx}{\mathbf{B}}_m$ are formed with the same Green operator as $\underset{\approx}{\mathbf{B}}$.

Using the identity

$$< \underset{\approx}{\mathbf{B}}_m^T : \underset{\approx}{\mathbf{c}} : \underset{\approx}{\mathbf{B}}_m >=< \underset{\approx}{\mathbf{c}} : \underset{\approx}{\mathbf{B}}_{n-1} > \tag{36}$$

with $n = 2m + 1$, upper bounds are obtained

$$\underset{\approx}{\mathbf{C}}^{\text{eff}} \quad \leq \quad \underset{\approx}{\mathbf{C}}^0 + < \delta\underset{\approx}{\mathbf{c}} : \underset{\approx}{\mathbf{B}}_{n-1} >= \underset{\approx}{\mathbf{C}}^{(n)} \tag{37}$$

Equation 30 provides a series expansion for the effective moduli

$$\underset{\approx}{\mathbf{C}}^{\text{eff}} = \underset{\approx}{\mathbf{C}}^0 + < \delta\underset{\approx}{\mathbf{c}} > - < \underset{\approx}{\mathbf{c}}' : \underset{\approx}{\Gamma} : \underset{\approx}{\mathbf{c}}' > + < \underset{\approx}{\mathbf{c}}' : \underset{\approx}{\Gamma} : \delta\underset{\approx}{\mathbf{c}} : \underset{\approx}{\Gamma} : \underset{\approx}{\mathbf{c}}' >$$
$$- < (\underset{\approx}{\mathbf{c}}' : \underset{\approx}{\Gamma} : \delta\underset{\approx}{\mathbf{c}})' : \underset{\approx}{\Gamma} : (\delta\underset{\approx}{\mathbf{c}} : \underset{\approx}{\Gamma} : \underset{\approx}{\mathbf{c}}')' > + < (\underset{\approx}{\mathbf{c}}' : \underset{\approx}{\Gamma} : \delta\underset{\approx}{\mathbf{c}})' : \underset{\approx}{\Gamma} : \delta\underset{\approx}{\mathbf{c}} : \underset{\approx}{\Gamma}(\delta\underset{\approx}{\mathbf{c}} : \underset{\approx}{\Gamma} : \underset{\approx}{\mathbf{c}}')' > +... \tag{38}$$

so that the bounds $\underset{\approx}{\mathbf{C}}^{(n)}$ are obtained by truncating the series after $n = 2m + 1$ terms. The result pertains for any choice of the reference medium. That is why these bounds are called upper bounds of odd order. Kröner has shown that the $\underset{\approx}{\mathbf{C}}^{(n)}$ for n even are also upper bounds but only if $\underset{\approx}{\mathbf{C}}^0 \leq \underset{\approx}{\mathbf{C}}^{(0)}$, where the zeroth-order bound $\underset{\approx}{\mathbf{C}}^{(0)}$ is defined in the next section. Similarly lower bounds $\underset{\approx}{\mathbf{C}}^{(-n)}$ can be obtained using 33.

1.4 Optimum bounds and estimates of the effective parameters of disordered materials

The previous bounds $\underset{\approx}{\mathbf{C}}^{(\pm n)}$ are not always the optimum bounds calculable under the given statistical information about the structure of the material. If no statistical information at all is available, the zeroth-order bounds $\underset{\approx}{\mathbf{C}}^{(\pm 0)}$ are given by the largest and smallest microscopic elasticity tensors and are optimum. $\underset{\approx}{\mathbf{C}}^{(\pm 1)}$ are the Voigt and Reuss bounds and are optimum if the only available information is the volume fraction of each constituent. The statistical information can be given in terms of correlation functions of random

variable $\underset{\sim}{\underset{\sim}{c}}$ up to order n. The term $< \underset{\sim}{\underset{\sim}{c}}' : \underset{\sim}{\underset{\sim}{\Gamma}} : \underset{\sim}{\underset{\sim}{c}}' >$ in series 38 contains the two-point correlation function $< \underset{\sim}{\underset{\sim}{c}} : \underset{\sim}{\underset{\sim}{c}} >$ ([Kröner 1980]). Similarly the higher order terms involve correlation functions of increasing order. Optimum bounds of order $n \geq 2$ can be obtained assuming the knowledge of all correlation functions up to order n. Only the infinite set of correlation functions yields the exact value of $\underset{\sim}{\underset{\sim}{C}}^{\text{eff}}$.

$$\underset{\sim}{\underset{\sim}{C}}^{(2')} =< \underset{\sim}{\underset{\sim}{c}} > - < \underset{\sim}{\underset{\sim}{c}}' : \underset{\sim}{\underset{\sim}{\Gamma}} : \underset{\sim}{\underset{\sim}{c}}' > \tag{39}$$

is the optimum second-order bound provided that the Green operator is formed with $\underset{\sim}{\underset{\sim}{C}}^0 = \underset{\sim}{\underset{\sim}{C}}^{(0)}$. The optimum bound of order 3 is given by Kröner [1977]:

$$\underset{\sim}{\underset{\sim}{C}}^{(3')} =< \underset{\sim}{\underset{\sim}{c}} > - < \underset{\sim}{\underset{\sim}{c}}' : \underset{\sim}{\underset{\sim}{\Gamma}} : \underset{\sim}{\underset{\sim}{c}}' >:< \underset{\sim}{\underset{\sim}{c}}' : \underset{\sim}{\underset{\sim}{\Gamma}} : \underset{\sim}{\underset{\sim}{c}}' + \underset{\sim}{\underset{\sim}{c}}' : \underset{\sim}{\underset{\sim}{\Gamma}} : \delta\underset{\sim}{\underset{\sim}{c}} : \underset{\sim}{\underset{\sim}{\Gamma}} : \underset{\sim}{\underset{\sim}{c}}' >^{-1}:< \underset{\sim}{\underset{\sim}{c}}' : \underset{\sim}{\underset{\sim}{\Gamma}} : \underset{\sim}{\underset{\sim}{c}}' > \tag{40}$$

(this expression does not depend on the choice of the reference medium).

The statistical information must describe on the one hand the topology of the material, i.e. the distribution of geometric domains, and on the other hand how to "fill" them with the material parameters. If the two repartitions are uncorrelated, the medium is said to be statistically decoupled. This leads to an important simplification of the theory in so far as the correlation functions of $\underset{\sim}{\underset{\sim}{c}}'$ factorize into a part that contains only moments of the material parameters and a function describing the topology ([Kröner 1980]). If now the topological structure is uncorrelated in the sense that the shape and size of the domains are completely or partially irregular, the already statistically decoupled material is said to be statistically disordered. In that case it is sufficient to use the Green functions of the infinite medium and the Green operator can be split into two parts:

$$\underset{\sim}{\underset{\sim}{\Gamma}}(\underline{r}, \underline{r}') = \underset{\sim}{\underset{\sim}{E}} + \underset{\sim}{\underset{\sim}{F}} \tag{41}$$

with

$$\underset{\sim}{\underset{\sim}{E}} = \underset{\sim}{\underset{\sim}{\check{E}}}\, \delta(\underline{r}, \underline{r}') \tag{42}$$

and

$$\underset{\sim}{\underset{\sim}{F}} = \underset{\sim}{\underset{\sim}{\check{F}}}/\|\underline{r} - \underline{r}'\|^3 \tag{43}$$

where $\underset{\sim}{\underset{\sim}{\check{E}}}$ is constant and $\underset{\sim}{\underset{\sim}{\check{F}}}$ depends only on angles. Under the assumption of graded or perfect disorder, only part $\underset{\sim}{\underset{\sim}{E}}$ of the Green operator contributes to the effective parameters. Kröner [1980] proposes a more specific definition of a medium which is statistically disordered of grade n:

$$< \underset{\sim}{\underset{\sim}{c}}' : (\underset{\sim}{\underset{\sim}{F}} : \underset{\sim}{\underset{\sim}{c}}')^p >= 0 \qquad 0 < p < n \tag{44}$$

where the Green operator is formed with $\underset{\sim}{\underset{\sim}{C}}^0 = \underset{\sim}{\underset{\sim}{C}}^{\text{eff}}$.

These conditions imply for a perfectly disordered material

$$\underset{\sim}{\underset{\sim}{C}}^{\text{eff}} =< \underset{\sim}{\underset{\sim}{c}} : (\underset{\sim}{\underset{\sim}{I}} + \underset{\sim}{\underset{\sim}{E}} : \delta\underset{\sim}{\underset{\sim}{c}})^{-1} >:< (\underset{\sim}{\underset{\sim}{I}} + \underset{\sim}{\underset{\sim}{E}} : \delta\underset{\sim}{\underset{\sim}{c}})^{-1} >^{-1} \tag{45}$$

(the Green operator is formed with $\underset{\sim}{\underset{\sim}{C}}^0 = \underset{\sim}{\underset{\sim}{C}}^{\text{eff}}$).

Optimum bounds for the effective material parameters of disordered materials of grade 2 and 3 have been worked out by Kröner [1977]. When the material is homogeneous isotropic and disordered of grade 2

$$\underset{\sim}{\underset{\sim}{C}}^{(2')} = < \underset{\sim}{\underset{\sim}{c}} > - < \underset{\sim}{\underset{\sim}{c}}' : \underset{\sim}{\underset{\sim}{E}} : \underset{\sim}{\underset{\sim}{c}}' > \tag{46}$$

where $\underset{\sim}{\underset{\sim}{E}}$ must be formed with $\underset{\sim}{\underset{\sim}{C}}^0 = \underset{\sim}{\underset{\sim}{C}}^{(0)}$. When furthermore statistical homogeneity and isotropy of grade ∞ (but disorder of grade 2) are assumed, one gets the Hashin-Shtrikman bound

$$\underset{\sim}{\underset{\sim}{C}}^{H-S} = < \underset{\sim}{\underset{\sim}{c}} : (\underset{\sim}{\underset{\sim}{I}} + \underset{\sim}{\underset{\sim}{E}} : \delta\underset{\sim}{\underset{\sim}{c}})^{-1} > : < (\underset{\sim}{\underset{\sim}{I}} + \underset{\sim}{\underset{\sim}{E}} : \delta\underset{\sim}{\underset{\sim}{c}})^{-1} >^{-1} \tag{47}$$

(the Green operator is formed with $\underset{\sim}{\underset{\sim}{C}}^0 = \underset{\sim}{\underset{\sim}{C}}^{(0)}$).

For a material of overall grade 3 (homogeneity, isotropy, disorder),

$$\underset{\sim}{\underset{\sim}{C}}^{(3')} = < \underset{\sim}{\underset{\sim}{c}} > - < \underset{\sim}{\underset{\sim}{c}}' : \underset{\sim}{\underset{\sim}{E}} : \underset{\sim}{\underset{\sim}{c}}' > : < \underset{\sim}{\underset{\sim}{c}}' : \underset{\sim}{\underset{\sim}{E}} : \underset{\sim}{\underset{\sim}{c}}' + \underset{\sim}{\underset{\sim}{c}}' : \underset{\sim}{\underset{\sim}{E}} : \delta\underset{\sim}{\underset{\sim}{c}} : \underset{\sim}{\underset{\sim}{E}} : \underset{\sim}{\underset{\sim}{c}}' >^{-1} : < \underset{\sim}{\underset{\sim}{c}}' : \underset{\sim}{\underset{\sim}{E}} : \underset{\sim}{\underset{\sim}{c}}' > \tag{48}$$

(the Green operator is formed with $\underset{\sim}{\underset{\sim}{C}}^0 = \underset{\sim}{\underset{\sim}{C}}^{(1)}$).

1.5 Self-consistent scheme

In a polycrystalline medium Kröner [1958] calls phase Ω the set of all Körner which have the crystalline orientation $\Omega \pm d\Omega$. Let f_Ω be its volume fraction. The shape of the grains may be that of needles but if these needles are distributed isotropically, the geometry of the phase can be taken as a sphere. The state of the phase Ω may be that of a spherical inclusion of Ω in an infinite isotropic medium the characteristics of which are the unknowns of the problem, i.e. that of the homogeneous equivalent medium. The matrix can be homogeneously strained at infinity by

$$\underset{\sim}{E} = < \underset{\sim}{\varepsilon} > \tag{49}$$

where

$$< \underset{\sim}{\varepsilon} > = \sum_\Omega f_\Omega \, \underset{\sim}{\varepsilon}_\Omega \tag{50}$$

$\underset{\sim}{\varepsilon}_\Omega$ denotes the (uniform) strain in the spherical inclusion Ω.

This modelling has been referred to as self-consistent and is used in several fields of physics (quantum mechanics...). The stress in the heterogeneous inclusion can be found for instance in [François, Pineau, Zaoui 1991]:

$$\underset{\sim}{\sigma}_\Omega = \underset{\sim}{\Sigma} + \underset{\sim}{\underset{\sim}{C}}^{eff} : (\underset{\sim}{\underset{\sim}{I}} - \underset{\sim}{\underset{\sim}{S}}^{-1}) : (\underset{\sim}{\varepsilon}_\Omega - \underset{\sim}{E}) \tag{51}$$

$\underset{\sim}{\Sigma}$ is the stress at infinity and $\underset{\sim}{\underset{\sim}{S}}$ is Eshelby's tensor. It can be seen that

$$\underset{\sim}{\underset{\sim}{S}} : \underset{\sim}{\underset{\sim}{C}}^{eff-1} = \int_\Omega \underset{\sim}{\underset{\sim}{\Gamma}} dV' \tag{52}$$

$\underset{\sim}{\underset{\sim}{\Gamma}}$ being formed with $\underset{\sim}{\underset{\sim}{C}}^0 = \underset{\sim}{\underset{\sim}{C}}^{eff}$. Writing $\underset{\sim}{\sigma}_\Omega = \underset{\sim}{\underset{\sim}{c}}_\Omega : \underset{\sim}{\varepsilon}_\Omega$ and dropping indices Ω yields

$$\underset{\sim}{\varepsilon} = (\underset{\sim}{\underset{\sim}{I}} + \underset{\sim}{\underset{\sim}{S}} : \underset{\sim}{\underset{\sim}{C}}^{eff-1} : \delta\underset{\sim}{\underset{\sim}{c}})^{-1} : \underset{\sim}{E} \tag{53}$$

This result could have been obtained directly from Lippmann-Schwinger equation 10 for a spherical inclusion:

$$\underset{\sim}{\varepsilon} = (\underset{\sim}{\mathbf{I}} + \underset{\sim}{\mathbf{E}} : \delta\underset{\sim}{\mathbf{c}})^{-1} : \underset{\sim}{\mathbf{E}} \tag{54}$$

($\underset{\sim}{\mathbf{E}}$ formed with $\underset{\sim}{\mathbf{C}}^0 = \underset{\sim}{\mathbf{C}}^{\text{eff}}$).

From 54 and using $\underset{\sim}{\Sigma} =< \underset{\sim}{\sigma} >= \underset{\sim}{\mathbf{C}}^{\text{eff}} : \underset{\sim}{\mathbf{E}}$, we get

$$\underset{\sim}{\mathbf{C}}^{\text{SC}} = \underset{\sim}{\mathbf{C}}^{\text{eff}} =< \underset{\sim}{\mathbf{c}} : (\underset{\sim}{\mathbf{I}} + \underset{\sim}{\mathbf{E}} : \delta\underset{\sim}{\mathbf{c}})^{-1} > \tag{55}$$

Since 54 implies $< (\underset{\sim}{\mathbf{I}} + \underset{\sim}{\mathbf{E}} : \delta\underset{\sim}{\mathbf{c}})^{-1} >= \underset{\sim}{\mathbf{I}}$, it appears that 53 is identical to 45. *It means that the effective parameters obtained according to the self-consistent scheme are those of a perfectly disordered material.*

The self-consistent effective parameters can be calculated with an iterative procedure using relation 45. For the first step $\underset{\sim}{\mathbf{C}}^{\text{eff}}$ is replaced by $\underset{\sim}{\mathbf{C}}^{(0)}$ (or $\underset{\sim}{\mathbf{C}}^{(1)}$), the result is $\underset{\sim}{\mathbf{C}}_2$ (or $\underset{\sim}{\mathbf{C}}_3$) and we continue according to the recurrence formula

$$\underset{\sim}{\mathbf{C}}_n =< \underset{\sim}{\mathbf{c}} : (\underset{\sim}{\mathbf{I}} + \underset{\sim}{\mathbf{E}}_{n-2} : \delta\underset{\sim}{\mathbf{c}}_{n-2})^{-1} >:< (\underset{\sim}{\mathbf{I}} + \underset{\sim}{\mathbf{E}}_{n-2} : \delta\underset{\sim}{\mathbf{c}}_{n-2})^{-1} >^{-1} \tag{56}$$

where $\underset{\sim}{\mathbf{E}}_{n-2}$ is formed with $\underset{\sim}{\mathbf{C}}^0 = \underset{\sim}{\mathbf{C}}_{n-2}$.

Similarly bounds $\underset{\sim}{\mathbf{C}}_{-n}$ can be built. The $\underset{\sim}{\mathbf{C}}_{\pm n}$ are bounds for media which are disordered of grade n. They are optimum bounds for $n = 0, 1, 2, 3$ and likely to be optimum bounds also for $n > 3$. If the series $\underset{\sim}{\mathbf{C}}_n$ (resp. $\underset{\sim}{\mathbf{C}}_{-n}$) converge, they converge towards $\underset{\sim}{\mathbf{C}}^{\text{SC}}$ (resp. $\underset{\sim}{\mathbf{S}}^{\text{SC}-1} = \underset{\sim}{\mathbf{C}}^{\text{SC}}$) which are the effective moduli of the perfectly disordered material ([Kröner 1977]).

1.6 Generalized self-consistent scheme

The statistical theory developed by Kröner is well-adapted for the treatment of random materials with a cell structure ([Kröner, Koch 1976]). In contrast the effective parameters of random materials with a matrix-inclusion structure have been investigated only recently. Hervé and Zaoui [1990] propose a generalized self-consistent scheme for an inclusion-matrix configuration, also called three-phase model. Let us consider a composite sphere comprising a spherical core of material 1 and a concentric shell of material 2 (inner and outer radii are a and b respectively, $c = a^3/b^3$ is the inclusion volume fraction). The composite sphere is embedded in an infinite matrix which is the unknown homogeneous equivalent medium. The necessary additional requirement is that the average strain in the composite sphere must be the same as the strain $\underset{\sim}{\varepsilon}^0$ prescribed at infinity:

$$\underset{\sim}{\varepsilon}^0 = \underset{\sim}{\mathbf{E}} =< \underset{\sim}{\varepsilon} > \tag{57}$$

where the volume average refers only to the composite sphere.

Furthermore, Hervé, Stolz and Zaoui [1991] have shown that a statistical analysis like in 1.4 and 1.5 can be performed using composite spheres. They proved that the previous three-phase model provides the effective material parameters of a perfectly disordered assembly of composite spheres of any size. This justifies the denomination generalized self-consistent scheme.

2 An optimization procedure for the determination of the self-consistent effective material parameters

2.1 Presentation of the method

We consider the following scheme: an arbitrary finite multiphase composite assembly, the behaviour of each phase being known, is embedded in an infinite matrix with unknown material parameters. The composite assembly is assumed to be representative of the microstructure of the investigated material at least in a statistical sense. Its morphology can be quite intricate. The matrix represents the wanted homogeneous equivalent medium. The form of the constitutive equations describing its behaviour is fixed, but the involved material parameters are determined after an optimization procedure.

The stress and strain states of the assembly are computed using the finite element method. Homogeneous boundary conditions (strain $\underset{\sim}{\varepsilon}^0$) are prescribed at the boundary of the matrix which must be large enough to be considered infinite. We will say that the *self-consistency condition* is fulfilled at a given instant if:

$$\underset{\sim}{\varepsilon}^0 = \underset{\sim}{\mathbf{E}} = < \underset{\sim}{\varepsilon} > \tag{58}$$

where averaging has to be performed only on the composite assembly.

Since the parameters of the matrix are unknown, we will start with some initial set A of estimated material parameters (say Voigt or Reuss bounds for instance) and try to minimize the functional

$$\mathcal{L}(\mathrm{A}) = \sum_t \mathrm{N}(\underset{\sim}{\varepsilon}_t^0 - < \underset{\sim}{\varepsilon}_t >) \tag{59}$$

where N denotes a norm and t some instants of the performed test. The existence of the solution of the optimization problem will be assumed in the following calculations. Its uniqueness is generally not ensured so that the physical relevance of the result must be appreciated (comparison with known bounds for instance...).

The fact that the self-consistent effective parameters can be regarded as the result of an optimization process can be illustrated in the case of an elastic two-phase material. The material is assumed linear elastic and globally and locally isotropic. We consider successively each phase as a spherical inclusion embedded in an isotropic matrix. The strain prescribed at infinity can be decomposed into its spherical and deviatoric parts

$$\underset{\sim}{\varepsilon}^0 = \mathrm{Tr}\,\underset{\sim}{\varepsilon}^0/3\ \underset{\sim}{1} + \underset{\sim}{\varepsilon}^{0\,\mathrm{dev}} \tag{60}$$

The solution of the heterogeneous spherical inclusion problem is

$$\mathrm{Tr}\,\underset{\sim}{\varepsilon}^i = \frac{k_0}{(1-\alpha_0)k_0 + \alpha_0 k_i}\ \mathrm{Tr}\,\underset{\sim}{\varepsilon}^0 \qquad i \in \{1,2\} \tag{61}$$

$$\underset{\sim}{\varepsilon}^{i\,\mathrm{dev}} = \frac{\mu_0}{(1-\beta_0)\mu_0 + \beta_0 \mu_i}\ \underset{\sim}{\varepsilon}^{0\,\mathrm{dev}} \qquad i \in \{1,2\} \tag{62}$$

with

$$\alpha_0 = \frac{3k_0}{3k_0 + 4\mu_0} \tag{63}$$

$$\beta_0 = \frac{6(k_0 + 2\mu_0)}{5(3k_0 + 4\mu_0)} \tag{64}$$

k_0 and μ_0 (resp. k_i and μ_i) are the bulk and shear moduli of the matrix (resp. phase i). The strain is uniform in each inclusion. As a result

$$< \underset{\sim}{\varepsilon} > - \underset{\sim}{\varepsilon}^0 = f_1(\mu_0, k_0)\underline{\underline{1}} + f_2(\mu_0, k_0)\underset{\sim}{\varepsilon}^{0\,\mathrm{dev}} \tag{65}$$

where

$$f_1(\mu_0, k_0) = \frac{f_1 k_0}{(1-\alpha_0)k_0 + \alpha_0 k_1} + \frac{f_2 k_0}{(1-\alpha_0)k_0 + \alpha_0 k_2} - 1 \tag{66}$$

$$f_2(\mu_0, k_0) = \frac{f_1 \mu_0}{(1-\beta_0)\mu_0 + \beta_0 \mu_1} + \frac{f_2 \mu_0}{(1-\beta_0)\mu_0 + \beta_0 \mu_2} - 1 \tag{67}$$

f_i being the volume fraction of phase i in the investigated material. The solution (k, μ) of the problem is that of the non-linear system $\mathcal{S}$ of two algebraic equations $\{f_1(\mu, k) = 0, f_2(\mu, k) = 0\}$. It can be solved using a standard numerical method. Instead one can look at the surfaces $\mid f_1(\mu, k) \mid$ and $\mid f_2(\mu, k) \mid$ (figures 1 and 2) or the surface $\sqrt{f_1^2 + f_2^2}/\sqrt{2}$ (figure 3). The solution in the case of incompressibility can be read at the end of the valley of figure 2. Similarly the basin of the surface of figure 3 contains the solution of the previous system. The status of extremum can be better seen if the surface $0.1/(0.1 + \sqrt{f_1^2 + f_2^2}/\sqrt{2})$ is plotted (figure 4). Note that the surface is not differentiable at the peak.

2.2 Test of the method

The method requires a finite element code, here the code ZéBuLoN, and an optimization code, here SiDoLo developed at Ecole des Mines de Paris ([Pilvin 1988], [Cailletaud, Pilvin 1993]). The entire procedure is explained in figure 5. Initial values of the material parameters of the "infinite" matrix are necessary for the first computation of N tests (tension, extension...). The average strain over the different phases is then calculated in order to evaluate the merit function

$$\mathcal{L}(\mathrm{A}) = \sum_j^N \omega_j \sum_t \| \underset{\sim}{\varepsilon}^0_{jt} - < \underset{\sim}{\varepsilon}_{jt} > \|^2 \tag{68}$$

where ω_j is a weight associated with each test. If the value of the merit function can be lowered, the optimization code proposes a new set of material parameters for the homogeneous equivalent medium, according to the Levenberg-Marquardt method combined with a steepest descent method.

2.2.1 Self-consistent estimates of a globally and locally isotropic two-phase medium

We consider again the problem tackled at the end of 2.1 but, instead of solving numerically the non-linear system $\mathcal{S}$, we resort to our optimization procedure. The geometry of the problem is that of a spherical inclusion embedded in a matrix large enough to be considered infinite (the ratio 1/4 of characteristic lengths is adopted here). A perfect interface is

assumed. Preliminary calculations show that a coarse mesh is sufficient for the analysis. Table 1 gives the comparison of results obtained with a coarse (figure 6) and a fine (figure 7) mesh for a tension test.

$< \sigma_{22} >$ at $\varepsilon^0_{22} = 0.001$ MPa	2D 44 elements 161 nodes	2D 940 elements 2945 nodes	3D 176 elements 1041 nodes
2 phases	113.6	113.4	113.8
3 phases			
inclusion	164.2	163.7	164.2
shell	98.7	98.5	98.7

Table 1: Finite element results obtained with coarse and fine meshes for two configurations: one inclusion ($E_1 = 355000$ MPa, $\nu_1 = 0.1986$) in a quasi-infinite matrix ($E_2 = 70000$ MPa, $\nu_2 = 0.33$), and the same inclusion (volume fraction 39.75%) in a shell ($E_2 = 70000$ MPa, $\nu_2 = 0.33$) and a quasi-infinite matrix ($E_3 = 124731$ MPa, $\nu_3 = 0.281$).

The problem can be treated in the axisymmetric 2D case but 3D calculations (figure 10) have also been performed to test the method with a view to dealing with more complex situations. We have chosen the following material parameters of the two phases:

$$E_1 = 355000\text{MPa} \qquad \nu_1 = 0.1986$$

$$E_2 = 70000\text{MPa} \qquad \nu_2 = 0.33$$

(glass and aluminium). The volume fraction of phase 1 is $f = 40\%$. The two phases take successively the position of the inclusion in the "infinite" matrix and two tests (tension and simple extension) are performed. This means that 4 calculations are performed for each new set of material parameters of the homogeneous equivalent medium.

Figure 12 shows that the moduli of the matrix converge towards a single set starting from different initial values. The reached moduli are indeed solutions of system $\mathcal{S}$ (see table 2). The number of iterations can vary between 20 and 100. The convergence can be bettered if one looks for parameters k and μ instead of E and ν, because the non-linearity is a bit different. It would also be much more efficient to choose a different norm for the merit function. Figure C.3 shows that the basin associated with the retained norm is rather flat. The quality of the solution is bettered if a finer mesh is used.

	(semi-) analytical results	optimization method
self-consistent scheme		
E (MPa)	132974	133064
ν	0.2811	0.2810
generalized self-consistent scheme		
E (MPa)	124731	124781
ν	0.2874	0.2873

Table 2: Self-consistent and generalized self-consistent estimates of the elastic moduli for a locally and globally isotropic two-phase material ($E_1 = 355000$ MPa, $\nu_1 = 0.1986$, $E_2 = 70000$ MPa, $\nu_2 = 0.33$, $f_1 = 39.75\%$): analytical results and values obtained after the optimization procedure.

2.2.2 Generalized self-consistent estimates of a globally and locally isotropic two-phase medium

Phases 1 and 2 are now limited by two concentric spheres, phase 1 being the inclusion and phase 2 filling the shell. One recognizes the configuration of the three-phase model described in 1.6. Once more a coarse mesh is sufficient (figures 8 and 9 and table 1). The advantage of the generalized self-consistent scheme (that accounts for a random inclusion-matrix microstructure) is that the tests are simulated only once instead of twice in the last section. This is extremely valuable in the 3D case. Two finite element calculations are thus performed (tension and extension) for each new set of material parameters of the homogeneous equivalent medium. The explicit solution for globally and locally isotropic materials is given in [Hervé, Zaoui 1990] and is used to check the validity of our method. Figure 13 shows that a single solution is obtained after the optimization procedure starting from very different initial parameters. Note that the self-consistent and generalized self-consistent estimates are not very different (see table 2). The same procedure has been applied in the 3D case using the mesh of figure 11.

2.2.3 Self-consistent and generalized self-consistent estimates of a globally and locally cubic two-phase medium.

We consider an elastic material made of two coherent cubic phases. The crystallographic symmetry axes coincide for both phases so that the global behaviour can be assumed cubic with the same symmetry axes as the individual phases. This situation is met in the case of single crystal superalloys. We want to determine the self-consistent and the generalized self-consistent estimates of the overall elastic properties of this material. For that purpose we compute successively

- a tension test in direction [001]

- a tension test in direction [011]
- an extension test along the crystallographic axes < 001 >

for each iteration of the optimization procedure. The 3D meshes of figure 10 and 11 are used for the self-consistent and generalized self-consistent estimates respectively.

The material parameters $C_{1111}, C_{1122}, C_{1212}$ of the "infinite" matrix are optimized to fulfill the self-consistency condition 58. We deal here with an optimization problem with constraint since the definite-positiveness of the elasticity tensor must be ensured at each step. Table 3 gives the obtained values for the self-consistent and generalized self-consistent schemes for a special choice of phases 1 and 2. Once more it can be noticed that the two estimates are very close although we have chosen an illustrative example with two very different phases (tungsten and aluminium). The second one is closer to Reuss bound.

(MPa)	C_{1111}	C_{1122}	C_{1212}
1	502000	198000	151400
2	108200	61300	28500
Voigt	264338	115638	77353
Reuss	156246	85616	42077
self-consistent (spheres)	189771	90174	55178
generalized self-consistent (spheres)	178097	86715	51470
self-consistent (cubes)	187766	87515	52337
self-consistent (cuboides)	190437	88927	54384

Table 3: Estimates of the effective elastic moduli for a globally and locally cubic coherent two-phase material (phases 1 and 2, volume fraction $f_1 = 39.75\%$). The self-consistent and generalized self-consistent estimates have been obtained using the optimization method.

2.3 Further applications of the method

2.3.1 Representative morphological pattern-based modelling

The description of the representative volume element in the homogenization theory for a given material is usually incomplete because of the huge amounts of statistical data that would be necessary. Only some essential features are retained for the definition of each phase. They can be of mechanical nature (elastic properties), crystallographic nature (orientation of a grain) but also of geometric nature (grain shape). The concept of representative morphological pattern-based modelling has been introduced by Hervé,

Stolz, Zaoui [1993] in the case of multilayered composite spheres. The generalized self-consistent scheme can be regarded as a first step in that direction.

The main advantage of the proposed optimization method is that it involves finite element calculations that can account for every inclusion morphology. Up to now we have considered spheres but the influence of the inclusion morphology on the overall properties can be investigated. Looking at the microstructure of single crystal nickel-base superalloys it can be seen that the morphology of the γ' precipitates varies from a sphere to a cube depending on the volume fraction. The possible geometries of γ/γ' interfaces is shown in figure 14. In order to represent them and to build a finite element mesh, we have retained the following parametrical description:

$$(\mathcal{P}) \quad \begin{cases} x = r\sqrt{1-e^{-b\cos^2 2u}}\sqrt{1-e^{-b\cos^2 2v}} \\ y = r\sqrt{1-e^{-b\sin^2 2u}}\sqrt{1-e^{-b\cos^2 2v}} \\ z = r\sqrt{1-e^{-b\sin^2 2v}}/\sqrt{b} \end{cases}$$

where r and b are *morphological parameters* which can describe rather spherical or parallepipedic precipitates. The effective self-consistent elastic moduli of a coherent agregate of cuboidal precipitates have been determined using the optimization method. Figure 15 shows the coarse meshes for cuboidal inclusions in the directions [001] and [011]. The obtained values are compared with that for cubes and spheres in table 3. It can be seen that these morphologies do not play a significant role in the overall elastic behaviour.

2.3.2 Multisite self-consistent modelling

The previous analysis does not take the influence of the spatial distribution of the phases in the direct neighbourhood of one phase on the overall properties into account. The interaction of neighbouring γ' precipitates may play a significant role for large volume fractions. That is why 6 or more neighbouring inclusions separated by γ channels should be considered, and the entire pattern should be embedded in the homogeneous equivalent medium. This corresponds to the so-called multisite self-consistent scheme introduced by Berveiller and Zaoui [1984].

2.3.3 Inverse approach

We want here to emphasize the fact that the present method can also be used to determine the properties of one phase when the behaviour of the other ones and of the overall behaviour are known. This inverse approach has been used in [Nouailhas, Cailletaud 1994] within the periodic assumption for single crystal nickel-base superalloys. This would be possible for both the self-consistent and the generalized self-consistent schemes.

Figure C.1 and C.2: Functions $| f_1(\mu_0, k_0) |$ and $| f_2(\mu_0, k_0) |$ (see equations C.66 and C.67) give the "distance" between any (μ_0, k_0) and the self-consistent estimate.

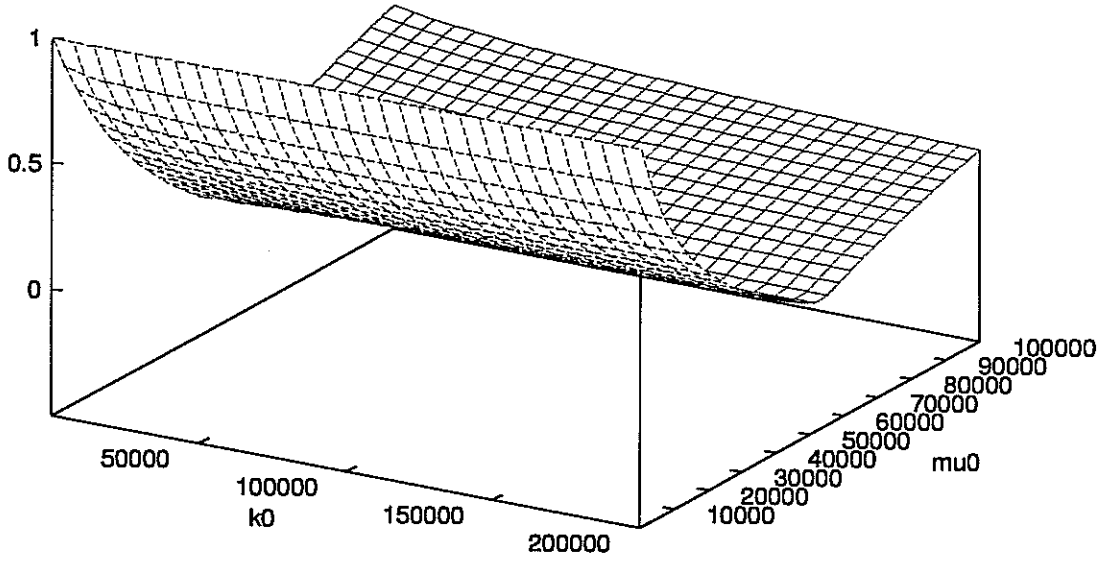

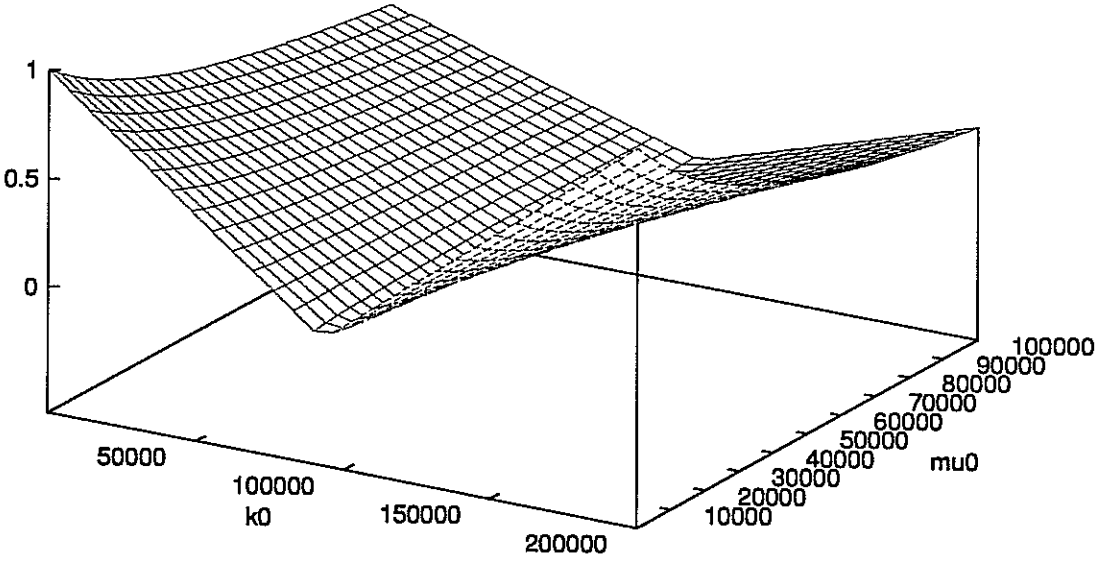

Figure C.3 and C.4: Surfaces $\sqrt{f_1^2 + f_2^2}/\sqrt{2}$ and $0.1/(0.1 + \sqrt{f_1^2 + f_2^2}/\sqrt{2})$. The minimum (resp. the maximum) gives the self-consistent estimate.

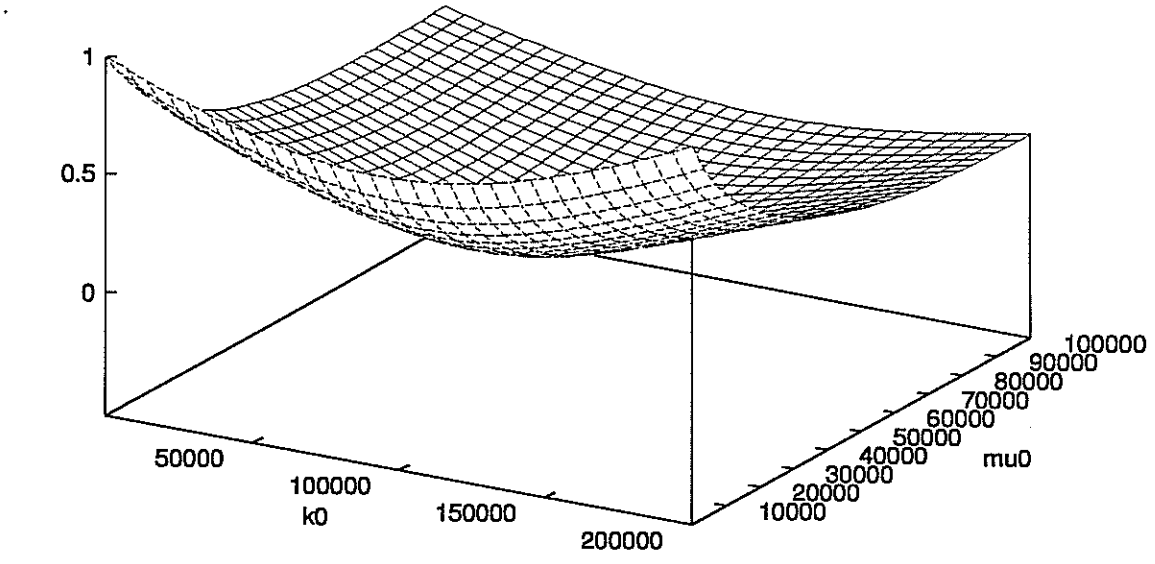

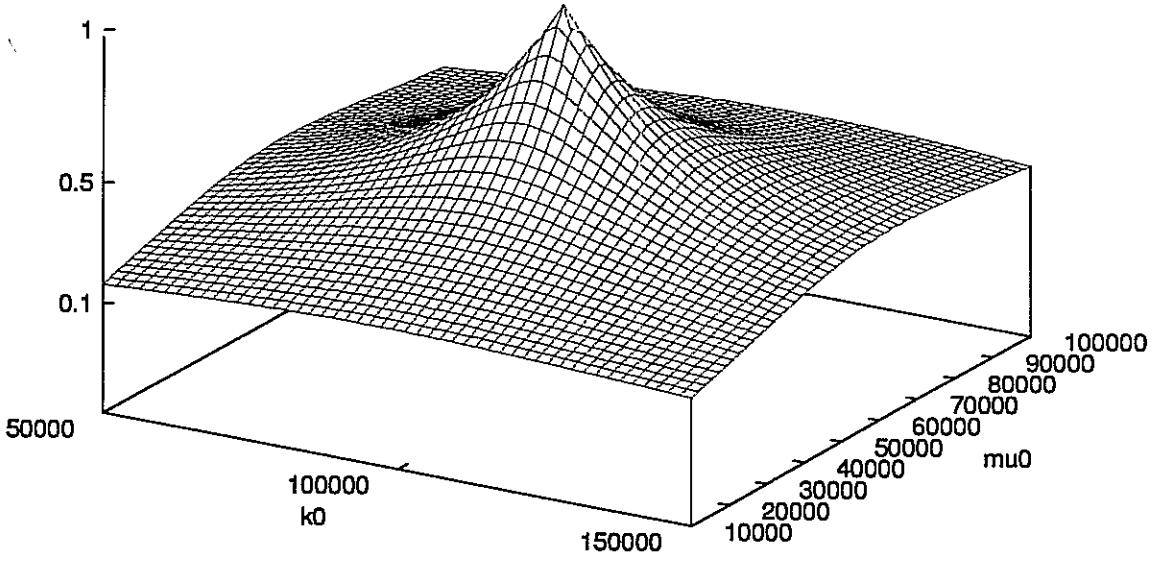

Figure C.5: Optimization process coupled with a finite element analysis to fulfill the self-consistency condition.

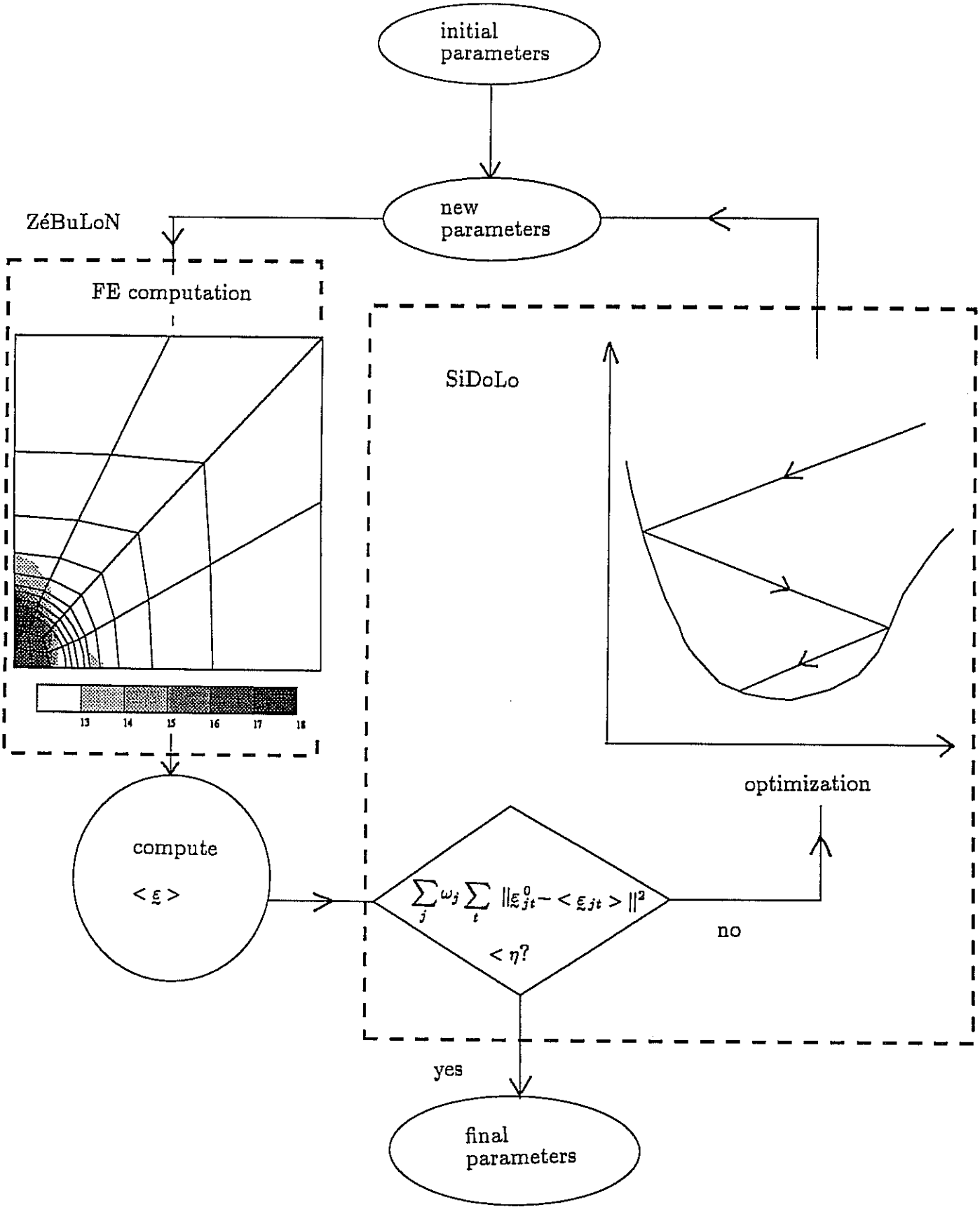

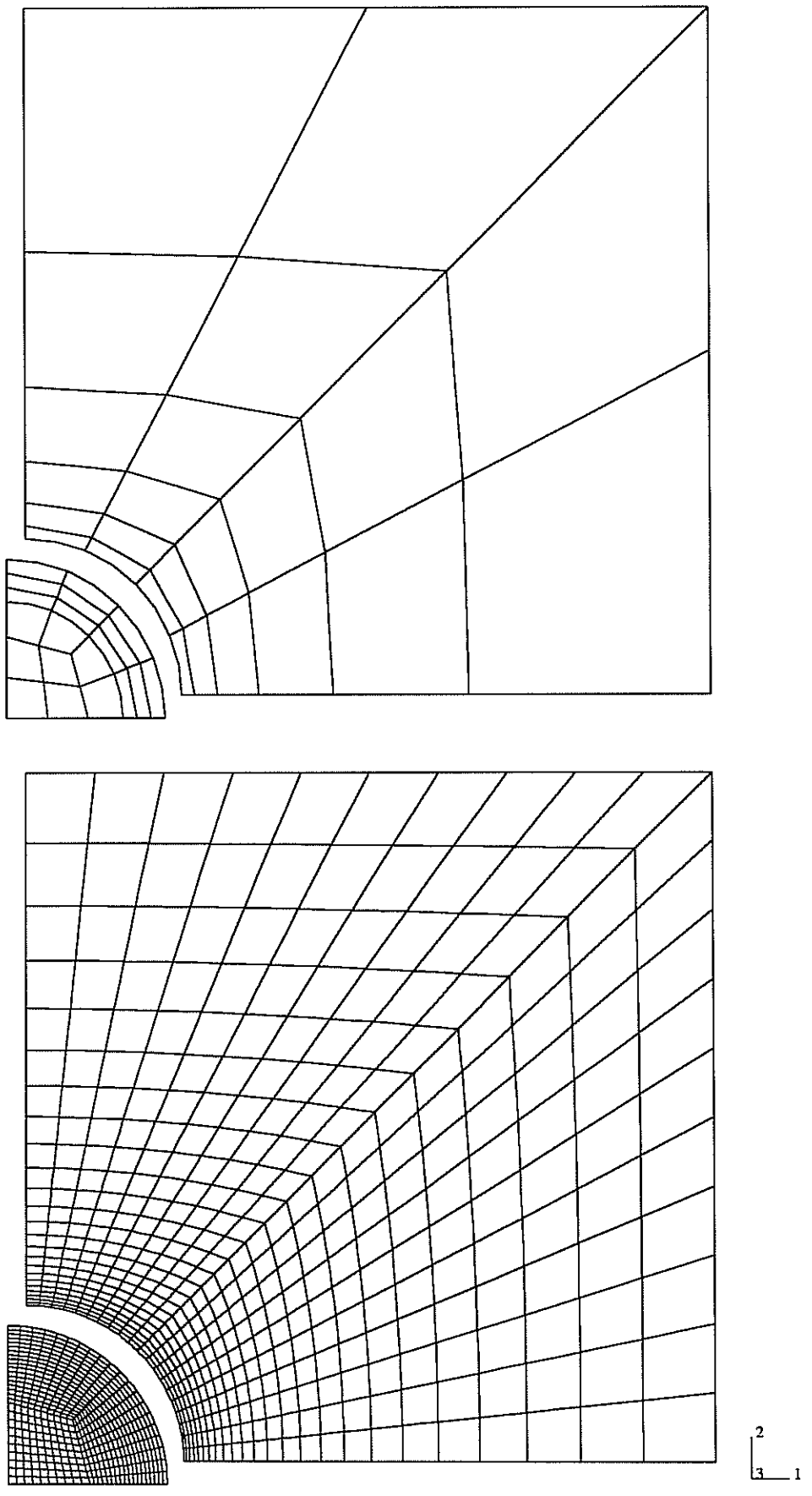

Figure C.6 and C.7: Coarse and fine 2D meshes for an inclusion in an "infinite" matrix; in the calculation the interface matrix-inclusion in assumed perfect.

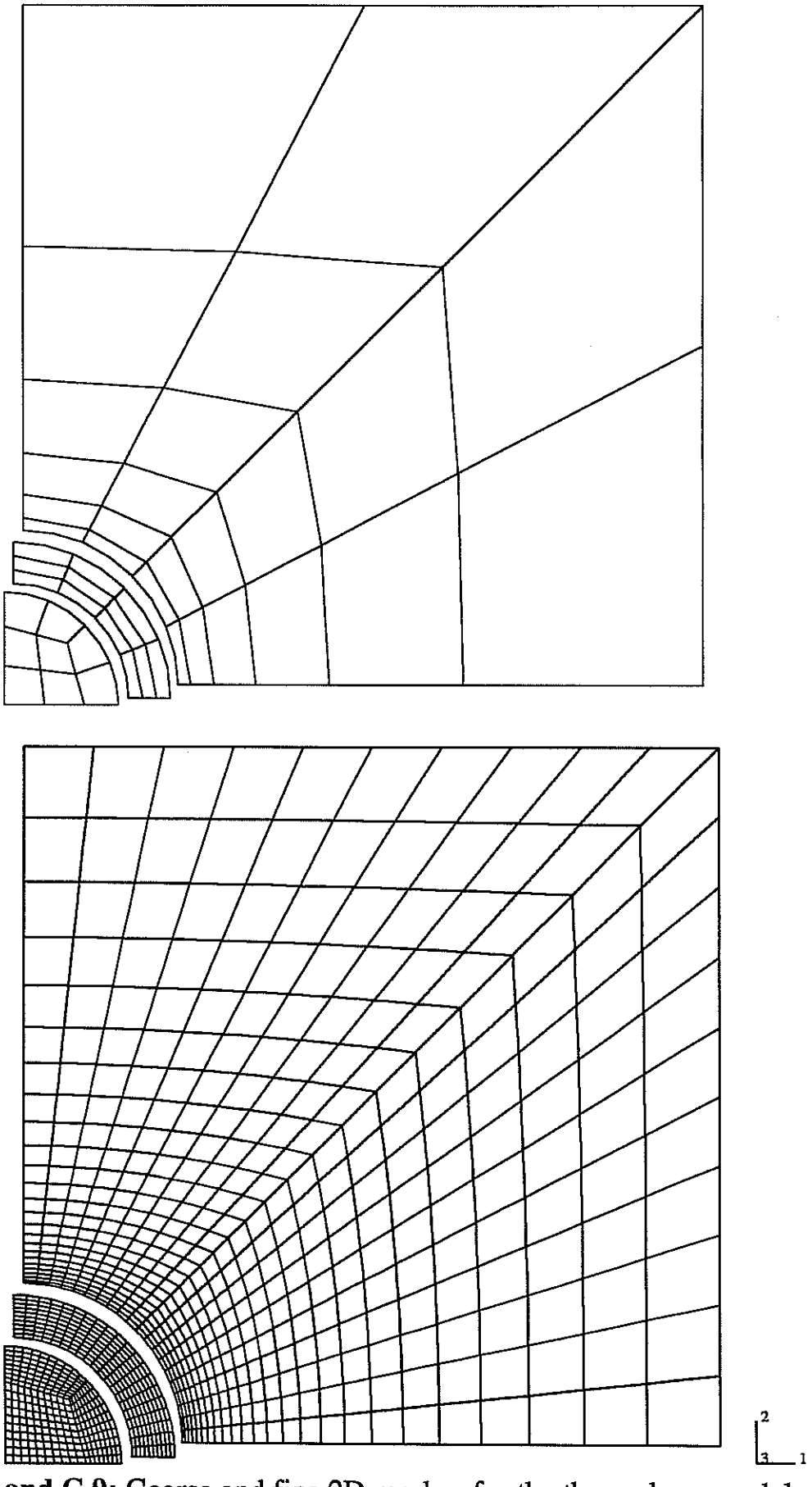

Figure C.8 and C.9: Coarse and fine 2D meshes for the three-phase model.

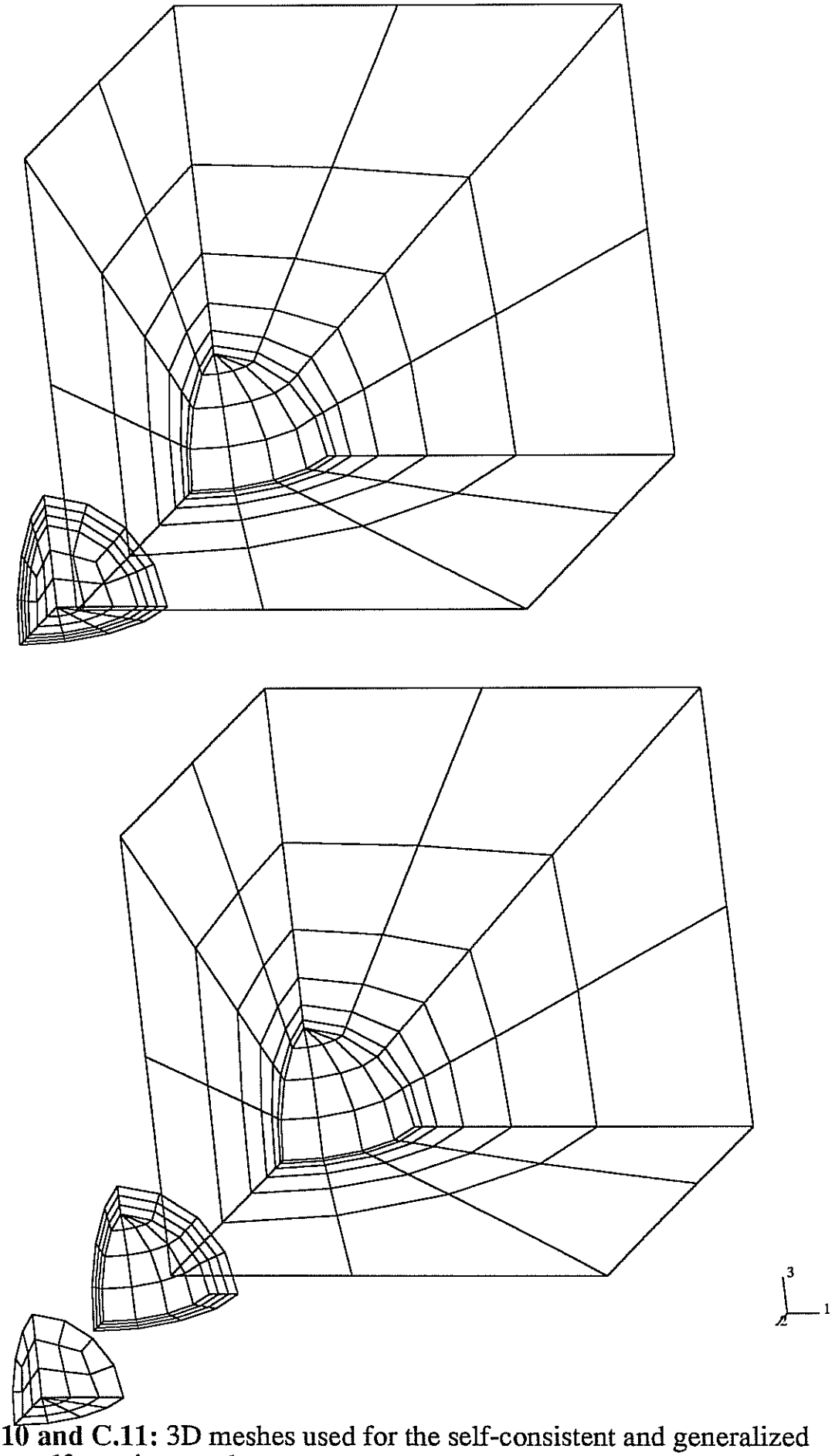

Figure C.10 and C.11: 3D meshes used for the self-consistent and generalized self-consistent schemes.

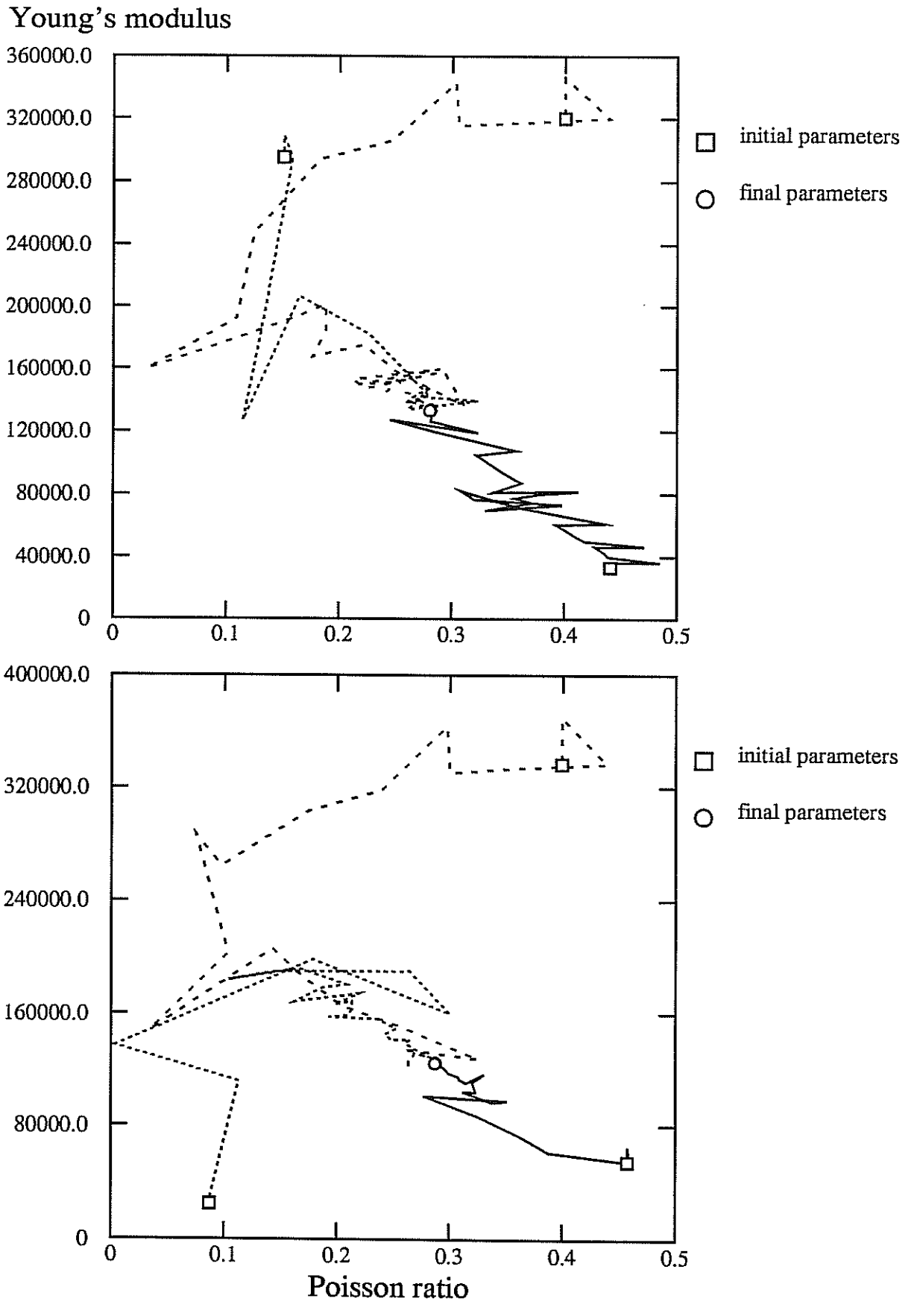

Figure C.12 and C.13: Determination of the self-consistent and generalized self-consistent effective parameters in the isotropic case using the optimization method.

Figure C.14: Possible morphologies of the γ/γ' interface in single crystal nickel-base superalloys from spheres to cubes.

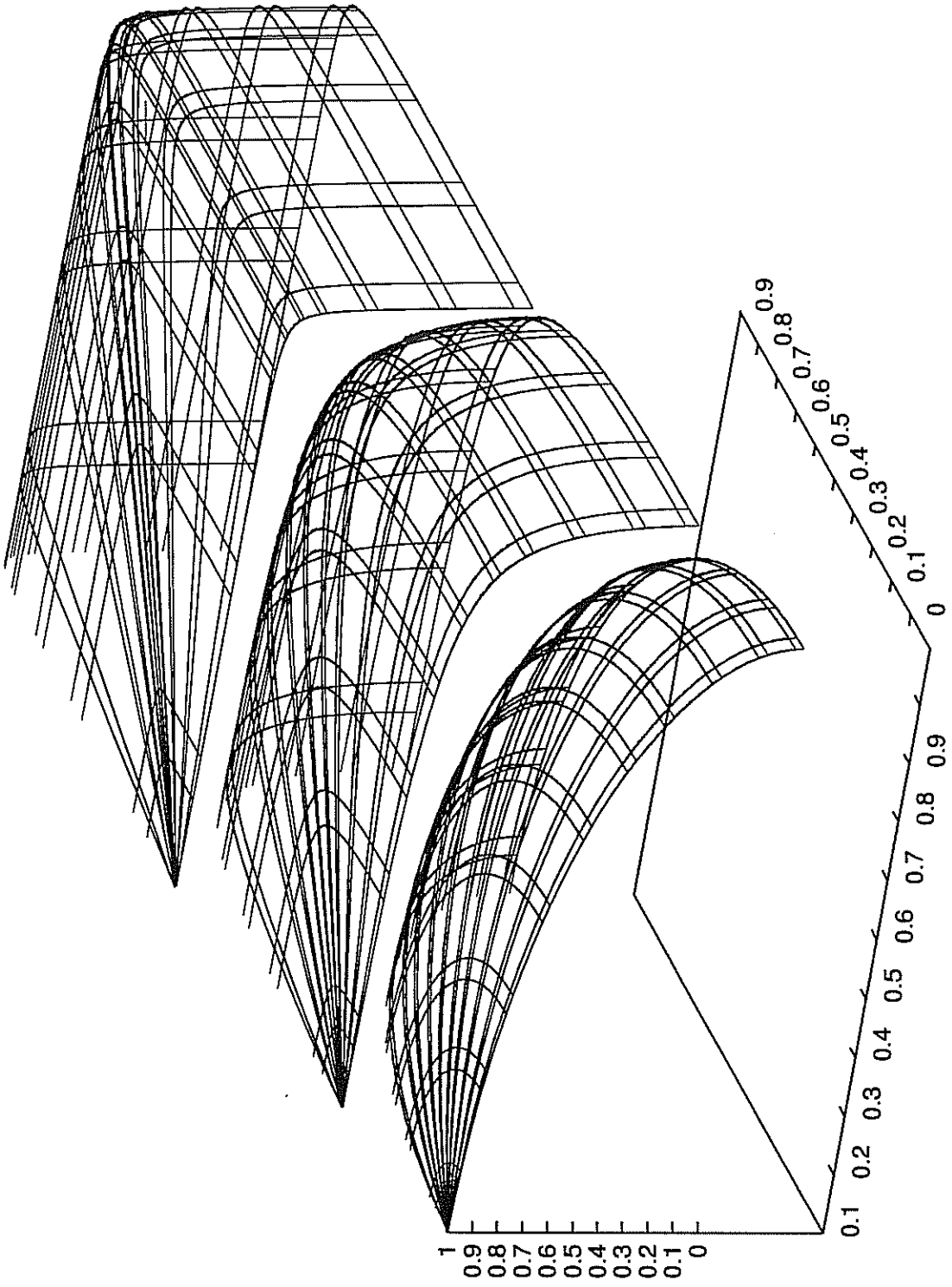

Figure C.15: Cuboidal γ' precipitate coarse mesh for tension tests in directions [001] (a) and [011] (b) (next page).

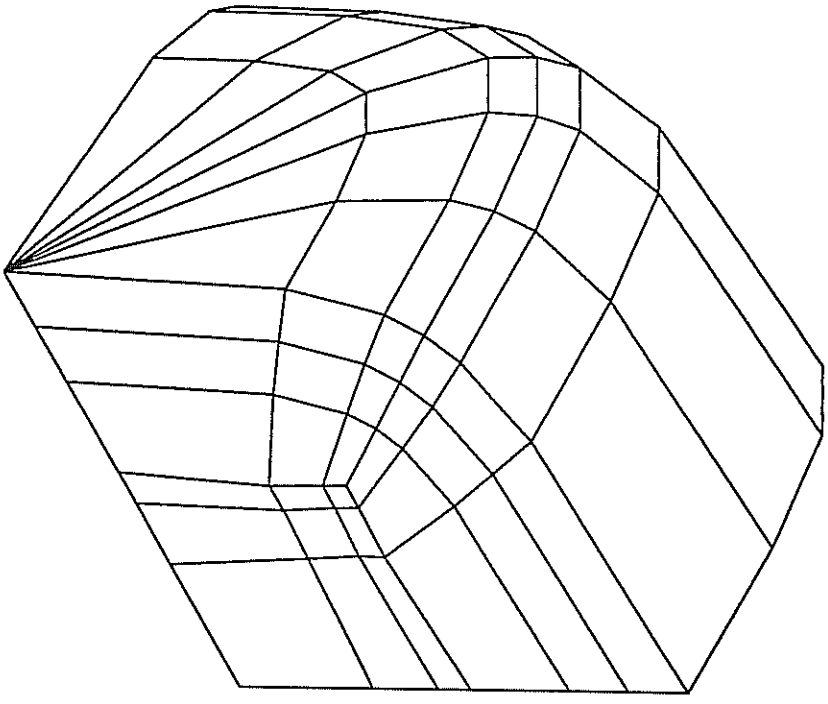

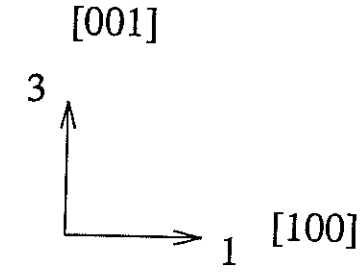

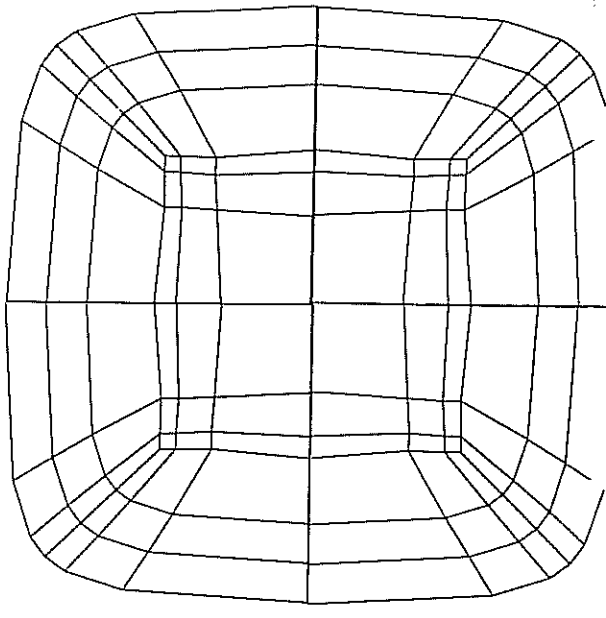

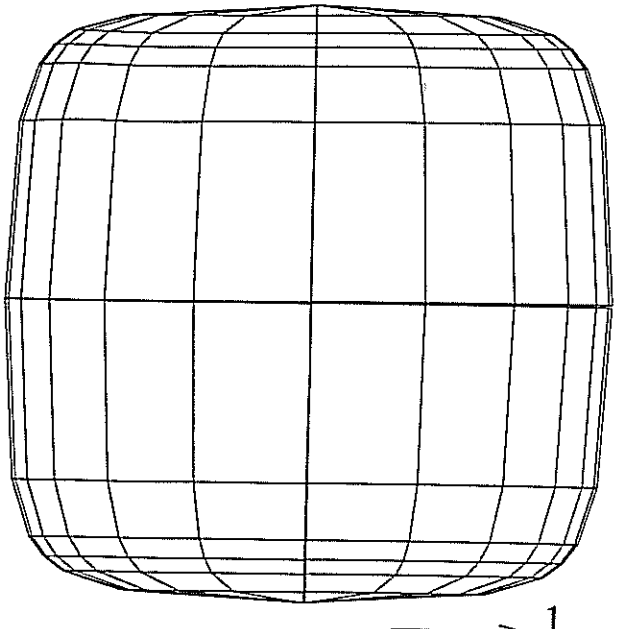

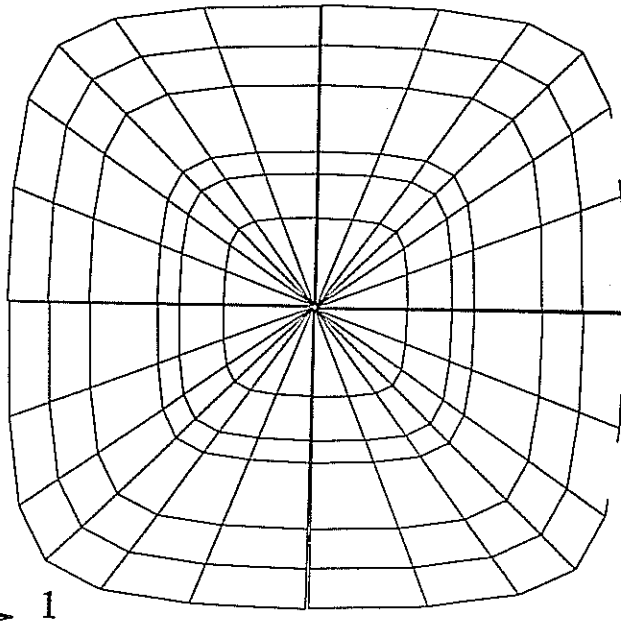

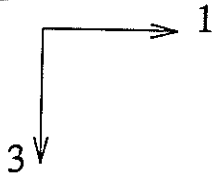

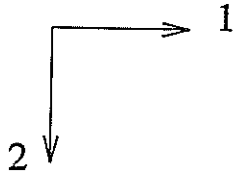

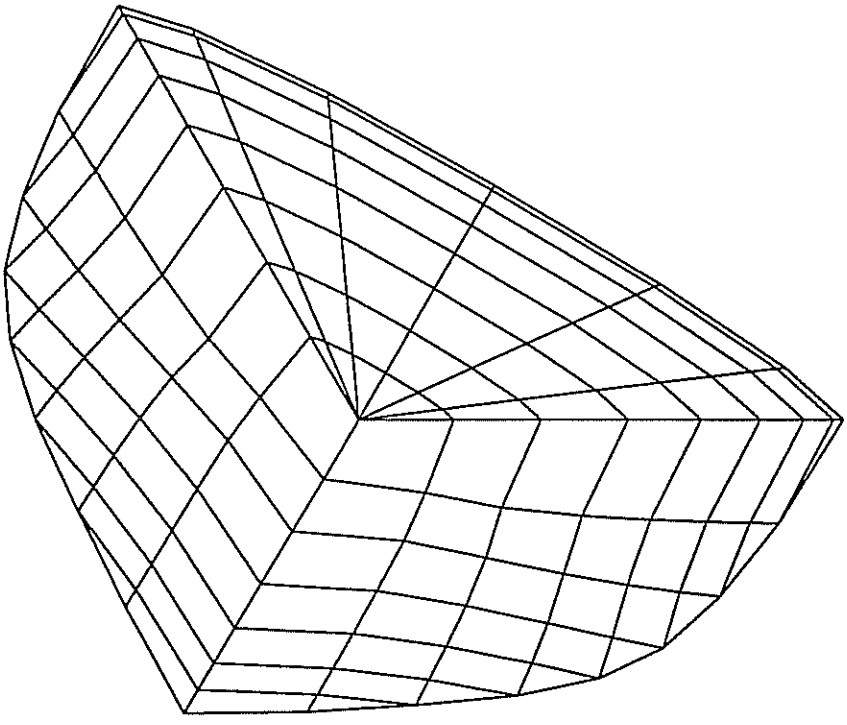

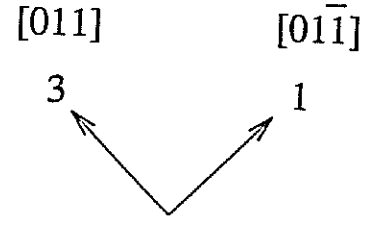
[011]
[01$\bar{1}$]
3
1

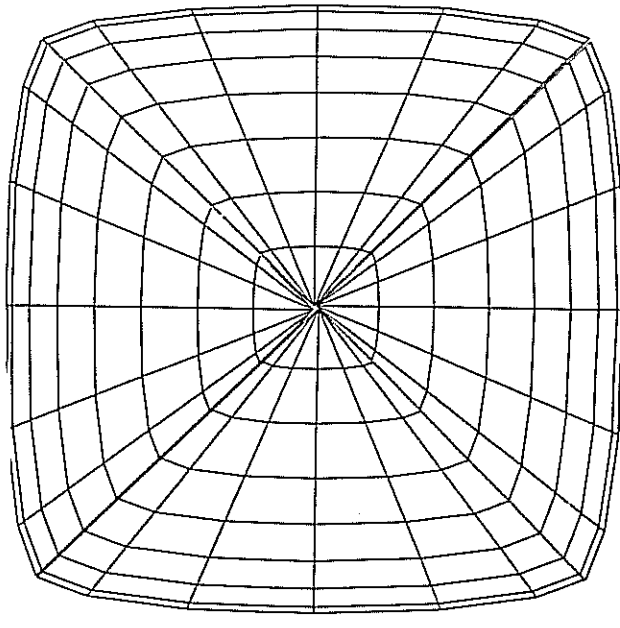

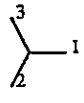
3
1
2

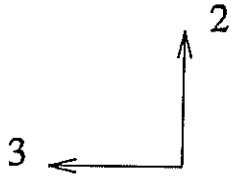
2
3

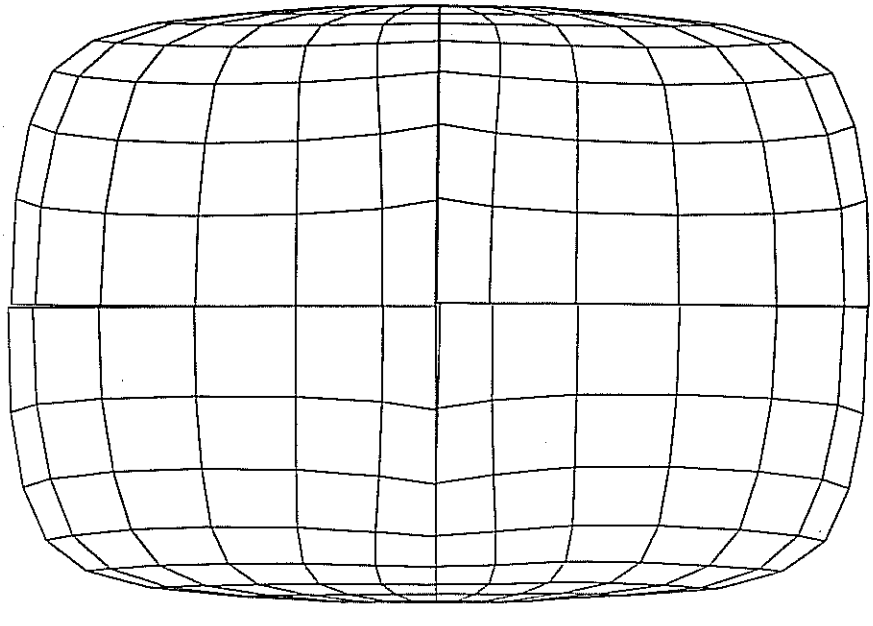

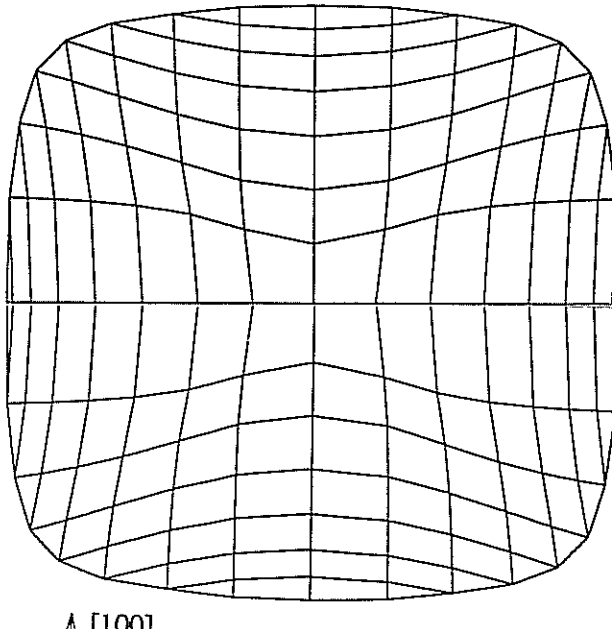

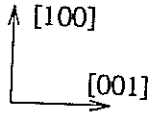
[100]
[001]

3 Quasi-self-consistent modelling in the non-linear case

3.1 Hill's treatment and related ones

Hill [1965] worked out a self-consistent scheme for elastoplastic polycrystalline (or more generally multiphase) materials. For each phase he considered the problem of an elastoplastic ellipsoidal inclusion embedded in an unbounded elastoplastic matrix representing the unknown homogeneous equivalent medium. The local behaviour of each elastoplastic phase takes the form

$$\dot{\underset{\sim}{\sigma}} = \underset{\sim}{\underset{\sim}{L}} : \dot{\underset{\sim}{\varepsilon}} \tag{69}$$

where the linear tangent operator is multi-branched.

In order to keep applying Green's techniques, Hill neglects the perturbations of the tangent operator in the neighbourhood of the inclusion and considers that the elastoplastic behaviour of the matrix is described by the uniform tensor of instantaneous moduli $\underset{\sim}{\underset{\sim}{L}}^{\text{eff}}$ that relates stress and strain rates at infinity

$$\dot{\underset{\sim}{\Sigma}} = \underset{\sim}{\underset{\sim}{L}}^{\text{eff}} : \dot{\underset{\sim}{E}} \tag{70}$$

The solution of the problem is then formally identical to that presented in 1.1 and 1.2 in the elastic case and involves Green's operator. In particular the stress rate in the inclusion is homogeneous and

$$\dot{\underset{\sim}{\sigma}} = \dot{\underset{\sim}{\Sigma}} + \underset{\sim}{\underset{\sim}{L}}^{*} : (\dot{\underset{\sim}{E}} - \dot{\underset{\sim}{\varepsilon}}) \tag{71}$$

where

$$\underset{\sim}{\underset{\sim}{L}}^{*} = \underset{\sim}{\underset{\sim}{L}}^{\text{eff}} : (\underset{\sim}{\underset{\sim}{S}}^{-1} - \underset{\sim}{\underset{\sim}{I}}) \tag{72}$$

is called the "constraint tensor". Eshelby's tensor is computed using $\underset{\sim}{\underset{\sim}{L}}^{\text{eff}}$ according to 52. It follows

$$(\underset{\sim}{\underset{\sim}{L}} + \underset{\sim}{\underset{\sim}{L}}^{*}) : \dot{\underset{\sim}{\varepsilon}} = (\underset{\sim}{\underset{\sim}{L}}^{\text{eff}} + \underset{\sim}{\underset{\sim}{L}}^{*}) : \dot{\underset{\sim}{E}} \tag{73}$$

and

$$\dot{\underset{\sim}{\sigma}} = \underset{\sim}{\underset{\sim}{L}} : (\underset{\sim}{\underset{\sim}{L}} + \underset{\sim}{\underset{\sim}{L}}^{*})^{-1} : (\underset{\sim}{\underset{\sim}{L}}^{\text{eff}} + \underset{\sim}{\underset{\sim}{L}}^{*}) : \dot{\underset{\sim}{E}} \tag{74}$$

Accordingly

$$\underset{\sim}{\underset{\sim}{L}}^{\text{eff}} = < \underset{\sim}{\underset{\sim}{L}} : (\underset{\sim}{\underset{\sim}{L}} + \underset{\sim}{\underset{\sim}{L}}^{*})^{-1} : (\underset{\sim}{\underset{\sim}{L}}^{\text{eff}} + \underset{\sim}{\underset{\sim}{L}}^{*}) > \tag{75}$$

is the solution of an implicit integral equation which must be solved for each step of the loading path. Setting $\delta\underset{\sim}{\underset{\sim}{L}} = \underset{\sim}{\underset{\sim}{L}} - \underset{\sim}{\underset{\sim}{L}}^{\text{eff}}$ and $\underset{\sim}{\underset{\sim}{\Gamma}} = \underset{\sim}{\underset{\sim}{S}} : \underset{\sim}{\underset{\sim}{L}}^{-1}$, it can be seen that 75 is identical to 55.

Following Hill's work, self-consistent schemes have been established for aggregates of viscoplastic and linear viscoelastic materials. A truly self-consistent scheme for elastoviscoplastic materials has been worked out recently in [Rougier, Stolz, Zaoui 1994] and involves a tangent linearization which makes it close to a numerical solution of the problem.

The use of the previous results requires tedious numerical operations that still prevent any implementation in a finite element code for 3D structural calculations. That

is why further simplifications are welcome provided that the nature (elastoplastic or elastoviscoplastic...) of the interphase accommodation is not violated (for that concern see [Zaoui, Raphanel 1993]). Furthermore the consequences of the assumption of uniform tangent operator in the matrix must be assessed.

3.2 Approximations of the self-consistent scheme

We still consider the elastoplastic case treated by Hill, but we now assume that the elastic behaviour is homogeneous and described by the moduli $\underset{\sim}{\underset{\sim}{C}}$ so that

$$\dot{\underset{\sim}{E}}^p = < \dot{\underset{\sim}{\varepsilon}}^p > \tag{76}$$

holds. We have taken the decomposition of the macroscopic strain into its elastic and plastic parts

$$\dot{\underset{\sim}{E}} = \dot{\underset{\sim}{E}}^e + \dot{\underset{\sim}{E}}^p \tag{77}$$

As a result concentration rule 71 can be written

$$\dot{\underset{\sim}{\sigma}} - \dot{\underset{\sim}{\Sigma}} = \underset{\sim}{\underset{\sim}{L}}^{\text{eff}} : (\underset{\sim}{\underset{\sim}{S}}^{-1} - \underset{\sim}{\underset{\sim}{I}}) : \underset{\sim}{\underset{\sim}{C}}^{-1} : (\dot{\underset{\sim}{\Sigma}} - \dot{\underset{\sim}{\sigma}}) + \underset{\sim}{\underset{\sim}{L}}^{\text{eff}} : (\underset{\sim}{\underset{\sim}{S}}^{-1} - \underset{\sim}{\underset{\sim}{I}})(\dot{\underset{\sim}{E}}^p - \dot{\underset{\sim}{\varepsilon}}^p) \tag{78}$$

which yields

$$\dot{\underset{\sim}{\sigma}} = \dot{\underset{\sim}{\Sigma}} + (\underset{\sim}{\underset{\sim}{I}} + \underset{\sim}{\underset{\sim}{L}}^{\text{eff}} : (\underset{\sim}{\underset{\sim}{S}}^{-1} - \underset{\sim}{\underset{\sim}{I}}) : \underset{\sim}{\underset{\sim}{C}}^{-1})^{-1} : \underset{\sim}{\underset{\sim}{L}}^{\text{eff}} : (\underset{\sim}{\underset{\sim}{S}}^{-1} - \underset{\sim}{\underset{\sim}{I}}) : (\dot{\underset{\sim}{E}}^p - \dot{\underset{\sim}{\varepsilon}}^p) \tag{79}$$

Some approximations are now possible. The simplest one would be to take

$$\underset{\sim}{\underset{\sim}{L}}^{\text{eff}} = \underset{\sim}{\underset{\sim}{C}} \tag{80}$$

which means that only elastic accommodation is allowed. That is why we will call the tensor

$$\underset{\sim}{\underset{\sim}{L}}^{\dagger} = \underset{\sim}{\underset{\sim}{C}} : (\underset{\sim}{\underset{\sim}{I}} - \underset{\sim}{\underset{\sim}{S}}) \tag{81}$$

the *elastic accommodation tensor*. Within this approximation the concentration rule becomes

$$\dot{\underset{\sim}{\sigma}} = \dot{\underset{\sim}{\Sigma}} + \underset{\sim}{\underset{\sim}{L}}^{\dagger} : (\dot{\underset{\sim}{E}}^p - \dot{\underset{\sim}{\varepsilon}}^p) \tag{82}$$

This approximation has been developed by Kröner [1961] in the isotropic case for elastoplastic polycrystals. It has been shown in the case of polycrystals that this model does not significantly depart from the crude Taylor approximation which sets uniform deformation in the polycrystal [Zaoui 1985].

In contrast Berveiller and Zaoui [1979] introduce an isotropic approximation of the effective instantaneous moduli

$$\underset{\sim}{\underset{\sim}{L}}^{\text{eff}} = \underset{\sim}{\underset{\sim}{L}}' \tag{83}$$

with

$$\underset{\sim}{\underset{\sim}{L}}' = 3k'\underset{\sim}{\underset{\sim}{K}} + 2\mu'\underset{\sim}{\underset{\sim}{J}} \tag{84}$$

k' and μ' are approximate elastoplastic tangent moduli. The adopted notation is

$$\underset{\sim\sim}{\mathbf{I}} = \underset{\sim\sim}{\mathbf{J}} + \underset{\sim\sim}{\mathbf{K}} \tag{85}$$

$$K_{ijkl} = 1/3\ \delta_{ij}\delta_{kl} \tag{86}$$

We recall that

$$I_{ijkl} = 1/2\ (\delta_{ik}\delta_{jl} + \delta_{il}\delta_{jk}) \tag{87}$$

The associated Eshelby tensor is

$$\underset{\sim\sim}{\mathbf{S}} = \alpha' \underset{\sim\sim}{\mathbf{K}} + \beta' \underset{\sim\sim}{\mathbf{J}} \tag{88}$$

with

$$\alpha' = \frac{3k'}{3k' + 4\mu'} \tag{89}$$

$$\beta' = \frac{6(k' + 2\mu')}{5(3k' + 4\mu')} \tag{90}$$

The previous decomposition of symmetric four-rank tensors has the tremendous advantage that for invertible tensors

$$\underset{\sim\sim}{\mathbf{A}} = a\underset{\sim\sim}{\mathbf{J}} + b\underset{\sim\sim}{\mathbf{K}} \quad \Rightarrow \quad \underset{\sim\sim}{\mathbf{A}}^{-1} = 1/a\underset{\sim\sim}{\mathbf{J}} + 1/b\underset{\sim\sim}{\mathbf{K}} \tag{91}$$

Using then the fact that $\dot{\underset{\sim}{\mathbf{E}}}^p$ and $\dot{\underset{\sim}{\xi}}^p$ are traceless, we get

$$\dot{\underset{\sim}{\sigma}} = \dot{\underset{\sim}{\Sigma}} + 2\mu \frac{\mu'(1-\beta')}{\beta'\mu + (1-\beta')\mu'} (\dot{\underset{\sim}{\mathbf{E}}}^p - \dot{\underset{\sim}{\xi}}^p) \tag{92}$$

The result is identical to that obtained by Berveiller and Zaoui [1979]

$$\dot{\underset{\sim}{\sigma}} = \dot{\underset{\sim}{\Sigma}} + 2\mu \frac{\mu'(7-5\nu')}{\mu'(7-5\nu') + 2\mu(4-5\nu')} (\dot{\underset{\sim}{\mathbf{E}}}^p - \dot{\underset{\sim}{\xi}}^p) \tag{93}$$

after noting that

$$\beta' = \frac{2(4-5\nu')}{15(1-\nu')} \tag{94}$$

Setting $\mu' = \mu$ and $\beta' = \beta$, Kröner's result [1961], here written in rate form, is recovered

$$\dot{\underset{\sim}{\sigma}} = \dot{\underset{\sim}{\Sigma}} + 2\mu(1-\beta)(\dot{\underset{\sim}{\mathbf{E}}}^p - \dot{\underset{\sim}{\xi}}^p) \tag{95}$$

3.3 Influence of non-homogeneous inelastic deformation around the inclusion on the self-consistent treatment of a two-phase Mises-type material with linear isotropic hardening

We propose here to check the validity of the approximate concentration rule 92 using a finite element analysis in a very simple case. We consider a two-phase isotropic elastoplastic material, the behaviour of each phase being given by

yield criterion

$$F(\underset{\sim}{\sigma}, R) = J_2(\underset{\sim}{\sigma}) - R \tag{96}$$

linear isotropic hardening

$$R = R_0 + Hp \tag{97}$$

flow rule

$$\dot{\underset{\sim}{\varepsilon}}^p = \dot{p}\frac{3}{2}\frac{\underset{\sim}{\sigma}^{\text{dev}}}{J_2(\underset{\sim}{\sigma})} \tag{98}$$

$$\dot{p} = \sqrt{\frac{2}{3}\dot{\underset{\sim}{\varepsilon}}^p : \dot{\underset{\sim}{\varepsilon}}^p} \tag{99}$$

($\dot{p}$ results from the consistency condition). The flow rule may be written

$$d\underset{\sim}{\varepsilon}^p = \frac{3}{2}\frac{dJ_2}{H}\frac{\underset{\sim}{\sigma}^{\text{dev}}}{J_2(\underset{\sim}{\sigma})} \tag{100}$$

For a radial and monotonous loading path, this gives

$$\underset{\sim}{\varepsilon}^p = h\underset{\sim}{\sigma}^{\text{dev}} \tag{101}$$

with

$$h = \frac{3}{2}\frac{p}{R_0 + Hp} \tag{102}$$

The secant operator can then be worked out as follows

$$\underset{\sim}{\sigma} = (3k\underset{\sim}{\mathbf{K}} + 2\mu\underset{\sim}{\mathbf{J}}) : \underset{\sim}{\varepsilon} - 2\mu h\underset{\sim}{\mathbf{J}} : \underset{\sim}{\sigma} \tag{103}$$

$$\underset{\sim}{\sigma} = (\underset{\sim}{\mathbf{K}} + (1 + 2\mu h)\underset{\sim}{\mathbf{J}})^{-1} : (3k\underset{\sim}{\mathbf{K}} + 2\mu\underset{\sim}{\mathbf{J}}) : \underset{\sim}{\varepsilon} \tag{104}$$

which has the form $\underset{\sim}{\sigma} = \underset{\sim}{\mathbf{L}}' : \underset{\sim}{\varepsilon}$ with

$$\underset{\sim}{\mathbf{L}}' = 3k'\underset{\sim}{\mathbf{K}} + 2\mu'\underset{\sim}{\mathbf{J}} \tag{105}$$

The secant elastoplastic moduli are then

$$k' = k \quad \text{and} \quad \mu' = \frac{2\mu}{1 + 2\mu h} \tag{106}$$

As an approximation of the behaviour of the homogeneous equivalent medium we use the previous secant operator $\underset{\sim}{\mathbf{L}}'$ computed with

$$h = 2J_2(\underset{\sim}{\mathbf{E}}^p)/3J_2(\underset{\sim}{\Sigma}) \tag{107}$$

Under the previous assumptions, the rate form of the concentration rule 92 can be replaced by

$$\underset{\sim}{\sigma} = \underset{\sim}{\Sigma} + 2\mu\frac{\mu'(1-\beta')}{\beta'\mu + (1-\beta')\mu'}(\underset{\sim}{\mathbf{E}}^p - \underset{\sim}{\varepsilon}^p) \tag{108}$$

It must be noted that an exact self-consistent treatment is possible in the case of n Mises-type phases. The constitutive form

$$\underset{\sim}{\mathbf{E}}^p = h^{eff}\underset{\sim}{\Sigma}^{\text{dev}} \tag{109}$$

may be assumed for the homogeneous equivalent medium . h^{eff} must then be root of equation

$$h^{eff} = \sum_{i=1}^{n} \frac{f_i h_i \mu_i'}{(1-\beta')\mu' + \beta'\mu_i'} \tag{110}$$

(note that β' depends on h^{eff} in this equation). However in this section we aim at testing the approximate localization rule 92 which will be used later for somewhat more complicated constitutive equations.

The complete set of constitutive equations that have been retained to describe the behaviour of the homogeneous equivalent medium are then

$$\left\{\begin{array}{l} \dot{\underset{\sim}{\sigma}}_i = \dot{\underset{\sim}{\Sigma}} + 2\mu\dfrac{\mu'(1-\beta')}{\beta'\mu + (1-\beta')\mu'}(\dot{\underset{\sim}{\mathbf{E}}}^p - \dot{\underset{\sim}{\varepsilon}}_i^p) \\ \dot{\underset{\sim}{\varepsilon}}_i^p = \dot{p}\dfrac{3}{2}\dfrac{\underset{\sim}{\sigma}_i^{\text{dev}}}{J_2(\underset{\sim}{\sigma}_i)} \\ F(\underset{\sim}{\sigma}_i, R_i) = J_2(\underset{\sim}{\sigma}_i) - R_i \\ \dot{\underset{\sim}{\mathbf{E}}}^p = \sum_i f_i\, \dot{\underset{\sim}{\varepsilon}}_i^p \\ \underset{\sim}{\mathbf{\Sigma}} = (3k\underset{\sim}{\mathbf{K}} + 2\mu\underset{\sim}{\mathbf{J}}) : \underset{\sim}{\mathbf{E}}^e \end{array}\right. \tag{$\mathcal{M}$}$$

We now want to appreciate whether the calculated $\underset{\sim}{\sigma}_i$ according to the previous constitutive equations actually is the stress in an inclusion of phase i embedded in the homogeneous equivalent medium obeying ($\mathcal{M}$). For that purpose a finite element analysis is performed using the 2D mesh of figure 6. The behaviour of the matrix is given by ($\mathcal{M}$) and that of the inclusion by equations 96 to 99. Two tension tests are succesfully performed, the value of the hardening modulus being successively

$$H_1 = 1000\,\text{MPa} \quad \text{and} \quad H_2 = 20000\,\text{MPa}$$

(furthermore, $E = 70000\,\text{MPa}$, $\nu = 0.33$ and $R_{01} = R_{02} = 130\,\text{MPa}$). After the finite element calulations, the stress and strain in the inclusion are compared with the direct prediction of equations ($\mathcal{M}$). We lay the stress on the fact that the direct application of equations ($\mathcal{M}$) involves a uniform h (see equation 107) at each step whereas f varies in the neighbourhood of the inclusion in the finite element calculations. We recall that these variations are neglected in Hill's treatment (see 3.1). Firstly it can be checked that the self-consistency condition is fulfilled during the finite element computation

$$\underset{\sim}{\mathbf{E}} = <\underset{\sim}{\varepsilon}> = f_1 \; <\underset{\sim}{\varepsilon}_1> + f_2 \; <\underset{\sim}{\varepsilon}_2> = \underset{\sim}{\varepsilon}_0 \tag{111}$$

Numerically the condition is actually satisfied up to 0.6% (after 3% straining). Figure 16 shows that the stress in each inclusion is given with a good approximation by the concentration rule of the approximate selfconsistent model ($\mathcal{M}$). *It proves that non-homogeneous plastic deformation around the inclusion can actually be neglected in order to work out a simplified self-consistent scheme.*

In contrast, Kröner's approximation, which accounts only for elastic accommodation, leads to underestimate the strain heterogenity. Figure 18 shows that the concentration

rule 95 does not give a good approximation of the mean stress in an inclusion of one phase surrounded by the fictitious equivalent medium. *It confirms that the use of only elastic accommodation does not provide a satisfactory approximation of the self-consistent scheme at all.*

3.4 Modification of the approximate concentration rule for a use out of its initial a priori validity range

The explicit concentration rule 108 has been established in the case of isotropic elastoplasticity and monotonous radial loading paths. But with some modification it is shown thereafter that it can still be used as a good approximation for more general cases.

3.4.1 Cyclic behaviour

Pilvin [1990] has modified the concentration rule 108 so that it could work for cyclic loading. For that purpose he introduces the so-called *interphase accommodation* variables $\underset{\sim}{\beta}_i$ following the non-linear evolution rule

$$\dot{\underset{\sim}{\beta}}_i = \dot{\underset{\sim}{\varepsilon}}_i^p - D\frac{2}{3}J_2(\dot{\underset{\sim}{\varepsilon}}_i^p)\ \underset{\sim}{\beta}_i \tag{112}$$

which will be called *interphase accommodation rule.* The concentration rule is then rewritten

$$\underset{\sim}{\sigma}_i = \underset{\sim}{\Sigma} + 2\mu(1-\beta)\ (\underset{\sim}{\mathbf{B}} - \underset{\sim}{\beta}_i) \tag{113}$$

where

$$\underset{\sim}{\mathbf{B}} = <\underset{\sim}{\beta}> = \sum_i f_i\ \underset{\sim}{\beta}_i \tag{114}$$

The rule 113 can be compared with Kröner's approximation 95.

Parameter D can be fitted such that the response of the model for a tensile test is almost identical to that of the approximate self-consistent model used in 3.3 ([Pilvin 1995]). But it can also be chosen such that it fulfills at best the self-consistency condition. It is clear that the two procedures should give very similar values for D. Our optimization technique has been applied to work out a value of D satisfying at best the self-consistency condition, with the set of material parameters used in the last section. The condition has been checked after 3% of overall tension and we have found

$$D = 55.$$

The validity of the concentration rule with this value is illustrated in figure 17. It can be seen that the response of the model is close to that of the approximate self-consistent model used in 3.3 (figure 16). But the major advantage of this formulation is that it accounts also for cyclic loading. Figure 19 shows the validity of the concentration rule for one cycle with imposed strain.

3.4.2 Elastoviscoplastic behaviour

In the viscoplastic case, the plastic multiplier in the model $(\mathcal{M})$ is replaced by

$$\dot{p}_i = < \frac{J_2(\underline{\sigma}_i) - R}{K_i} >^{n_i} \tag{115}$$

where K and n are the viscosity parameters. Concentration rules 92 and 113 can still be used, but their validity is not ensured by the analytical treatment of 3.2 any longer. That is why it is checked here numerically. We have chosen a very slightly viscous phase 1 and a strongly viscous phase 2:

$$K_1 = 10\,\mathrm{MPa}^{1/n} \quad \text{and} \quad K_2 = 400\,\mathrm{MPa}^{1/n}$$

$$n_1 = 5 \quad \text{and} \quad n_2 = 5$$

(the other parameters are the same as in 3.4.1, in particular $D = 55$, and the hardening moduli are given in 3.3).

Figures 20 and 21 show that the concentration rule 113 still describes the stress and strain state of the inclusion with good precision in the case of a tensile test ($E_{22}^{\max} = 3\%$ and $\dot{E}_{22} = 10^{-3}s^{-1}$). Figure 22 shows that it is satisfactory enough to describe a relaxation test.

3.4.3 Non-proportional loading

With the same set of parameters as in the last section we have performed numerically a cyclic test with non-proportional prescribed strain. The loading path is given in figure 23 for E_{11} and E_{22}. Plane strain and plane stress ($E_{33} = 0$ or $\Sigma_{33} = 0$) have been considered successively. We compare the response of the approximate self-consistent model with that of a finite element analysis requiring two 3D calculations (each phase as an inclusion successively; the boundary conditions concerning E_{11}, E_{22}, E_{33} or Σ_{33} are prescribed at "infinity"). Figure 23 also shows that the self-consistent condition is fulfilled with enough precision during the cycle. It can be seen on figures 24 and 25 that the complex deformation path undergone by the inclusion is correctly described by the concentration rule. However the prediction of the viscoplastic strain is not very precise.

3.5 Use of the approximate concentration rule for an inclusion-matrix assembly according to the generalized self-consistent scheme

We show here how far the concentration rule 113 can be used in an approximate three-phase model.

3.5.1 Non uniform deformation in the inclusion

In the elastoviscoplastic case the stress and strain states within the spherical inclusion turned out to be uniform. It is not the case any more if a layer of another material is introduced between the inclusion and the infinite matrix. Finite element calculations with various layer volume fractions have been performed to check this point. We have

considered an inclusion made of material 1, a shell made of material 2 and an "infinite" matrix of material 0. The respective material parameters are

$$H_1 = 40000\,\text{MPa} \quad H_2 = 1000\,\text{MPa} \quad H_0 = 10000\,\text{MPa}$$

$$K_0 = K_1 = K_2 = 40\,\text{MPa}^{1/n}$$

$$n_0 = n_1 = n_2 = 10$$

$$R_{00} = R_{01} = R_{02} = 130\,\text{MPa}$$

(note that the "infinite" matrix is not the homogeneous equivalent medium in this section).

The stress and strain gradients inside the inclusion are shown in figure 26 for a tensile test at $\dot{E}_{22} = 7.10^{-4}\text{s}^{-1}$ after 2% overall straining and for various layer volume fractions. Figure 27 shows the non-homogeneous stress field in the inclusion for a layer volume fraction of 60%.

Hervé and Zaoui [1990] propose to extend the generalized self-consistent scheme to the isotropic non-linear case and to replace the bulk and shear moduli by the tangent or secant elastoplastic moduli in the analytical expression of averaged strain and stress in the inclusion and shell. The authors mention the drawback of dealing with averaged quantities in the non-linear and non-uniform case.

3.5.2 Approximate generalized self-consistent modelling

We now consider a shell-inclusion assembly embedded in the homogeneous equivalent medium. The behaviour of the two materials are the same as in 3.4.2. We investigate here whether the homogenized equations used in 3.4 can be adapted in order to obtain an approximation of the generalized self-consistent scheme.

At first we take the same constitutive equations for the homogeneous equivalent medium as in 3.4 ($D = 55$) and we perform a tensile test with $\varepsilon_{22}^{0\max} = 3\%$ and $\dot{\varepsilon}_{22}^{0} = 10^{-3}s^{-1}$. We find that the self-consistency condition is not accurately satisfied any longer:

$$\text{at } \varepsilon_{22}^{0} = 0.03 \quad \text{we find} \quad < \varepsilon_{22} >_{\text{shell-inclusion}} = 0.0309.$$

Furthermore the concentration rule does not provide a good approximation of the mean stress in the inclusion any more as seen in figure 28. However figure 28 shows also that the stress state given by the concentration rule for phase 1 coincides with the state at the center of the inclusion.

Once more the optimization technique has been used to make the concentration rule work better for the fixed inclusion-matrix assembly (material 1 in the inclusion and material 2 in the shell). Parameter D has been determined such that the self-consistent condition is fulfilled up to 0.001%:

$$D = 85.$$

With this set of parameters the concentration rule gives accurately enough the averaged stress and strain in the shell and inclusion (figure 29), but of course not at the center of the inclusion any more. Nevertheless the concentration rule does not provide any information about the gradients in the inclusion and shell.

3.6 "Geometrical" nature of parameter D

It has been shown that the parameters entering the approximate concentration law (here only D but Pilvin [1994] introduces also the parameter δ in his concentration rule) can be determined to fulfill at best the self-consistency condition in the self-consistent and generalized self-consistent cases. "At best" must be understood "at best for the chosen form of the constitutive equations adopted for the homogeneous equivalent medium". It means that they do not belong to the set of material parameters but should rather be regarded as "geometrical" parameters. Note that concentration rules 92 or 113 do not depend directly on the behaviour of each phase but only on the approximate form of the constitutive equations of the homogeneous equivalent medium. However the explicit concentration rule 113 is only a numerical approximation of the actual self-consistent (or generalized self-consistent) concentration rule so that the value of D is valid only within a given range of material parameters. If new very different material parameters are used, the self-consistency condition will not be fulfilled any more and D must be determined anew thanks to the optimization procedure. Investigations in 3.4 have shown for instance that viscosity parameters can be significantly modified without changing D and without really violating the self-consistency condition.

That is why the following scheme can be proposed for an identification of material and geometrical parameters of the homogenized model for a given non-linear two-phase material:

- orders of magnitude of the material parameters (for each phase, hardening, viscosity...) must be found by looking at the experimental results;
- parameter D (and other ones if the concentration rule must be slightly modified) can be identified using the optimization procedure with fixed material parameters in order to fulfill the self-consistency condition;
- precise values of the material parameters can then be found following a classical inverse method, D being fixed;
- lastly it should be checked whether the self-consistency condition is still reasonably satisfied.

Another method consists in checking the self-consistency condition at each step of the identification procedure, i.e. D is identified with the other parameters. But it is presumably more time-demanding.

The methodology developed in this work is a tentative response to some difficulties mentionned in [Bornert, Hervé, Stolz, Zaoui 1993].

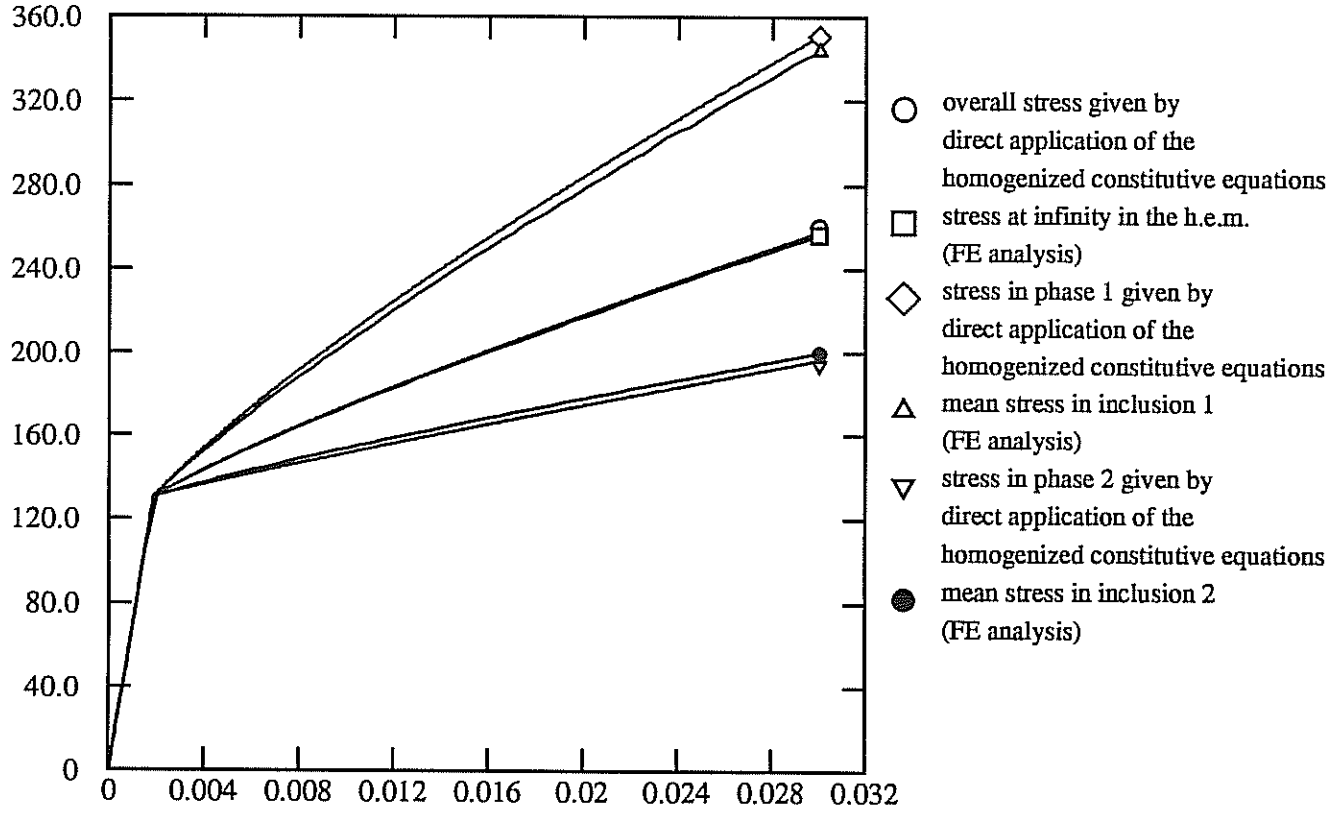

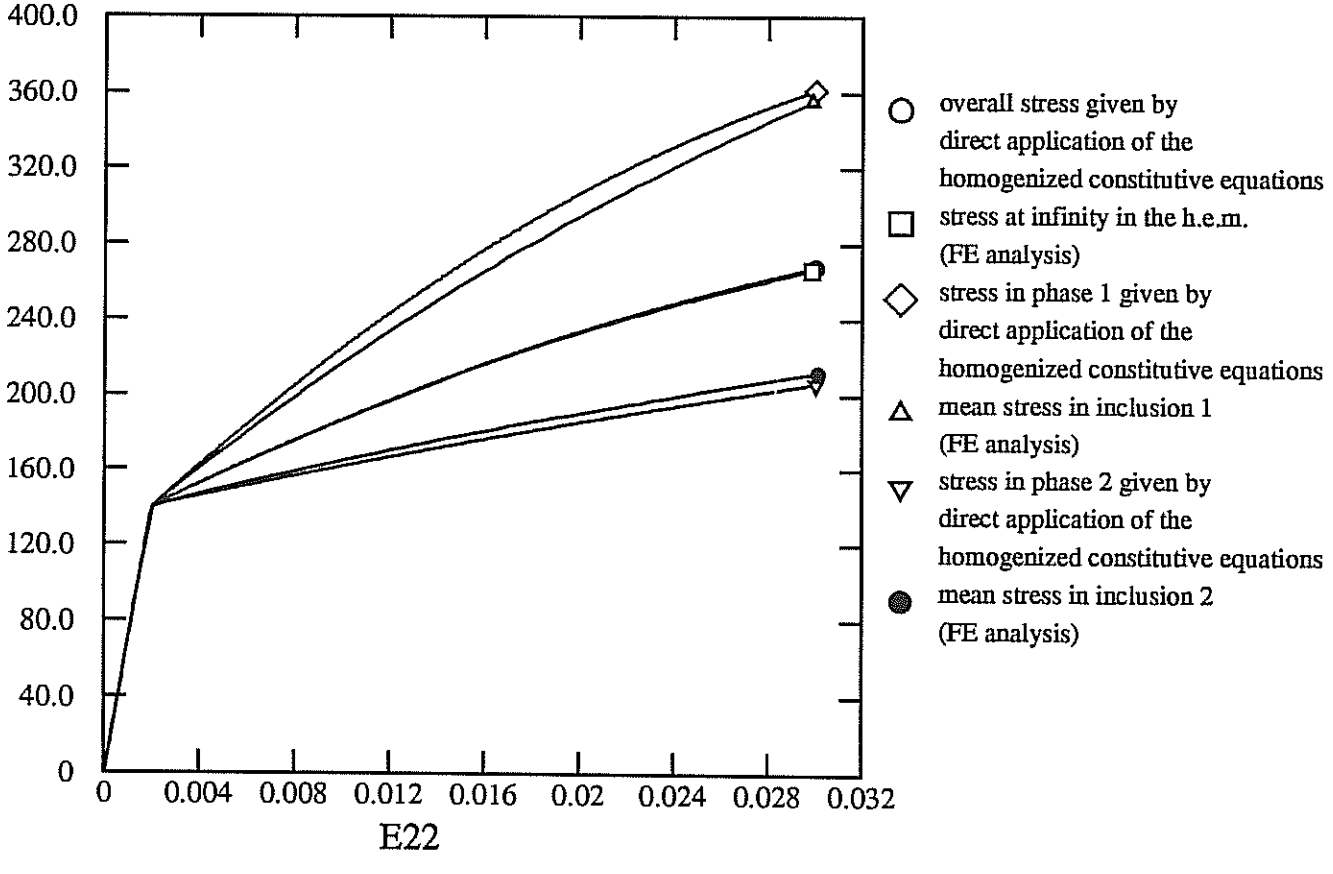

Figure C.16 and C.17: Comparison of Berveiller and Zaoui's (above) and Pilvin's (below) approximate self-consistent models applied to a two-phase material with the FE simulation of an inclusion in the homogeneous equivalent medium.

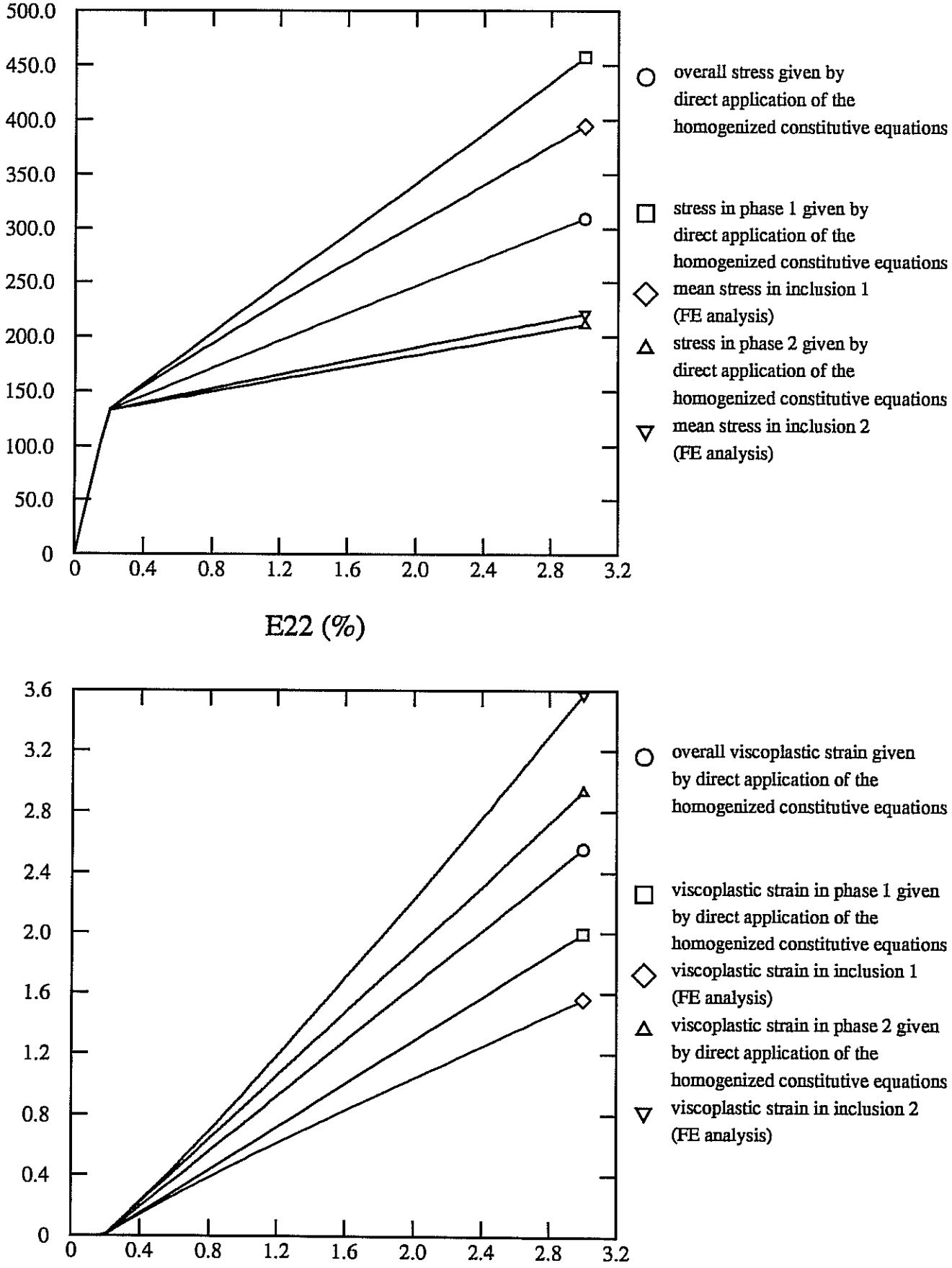

Figure C.18: Comparison of Kroener's approximate self-consistent model applied to a two-phase material with the finite element simulation of an inclusion in the fictitious homogeneous equivalent medium.

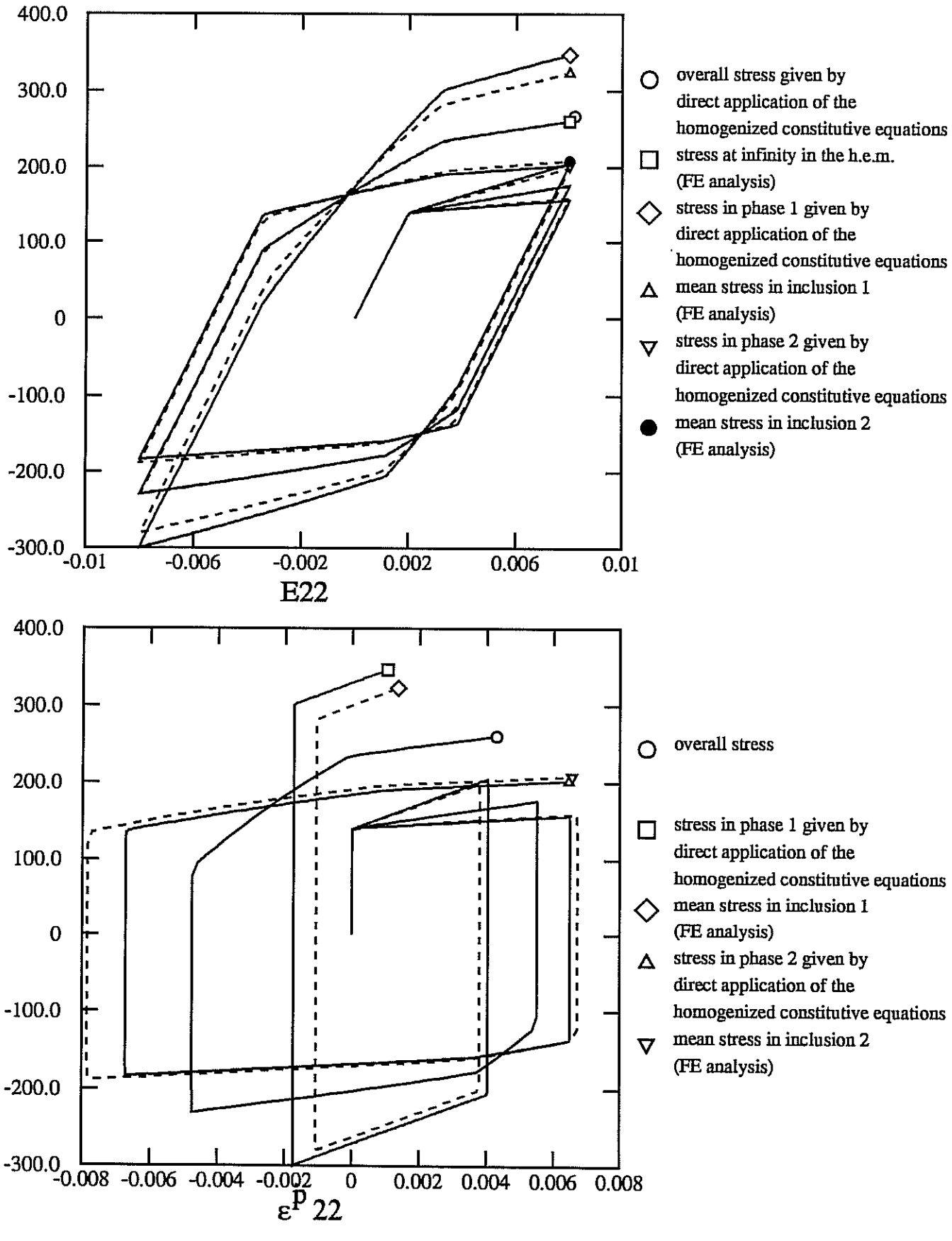

Figure C.19: Use of the approximate self-consistent model with interphase accommodation variables for cyclic loading.

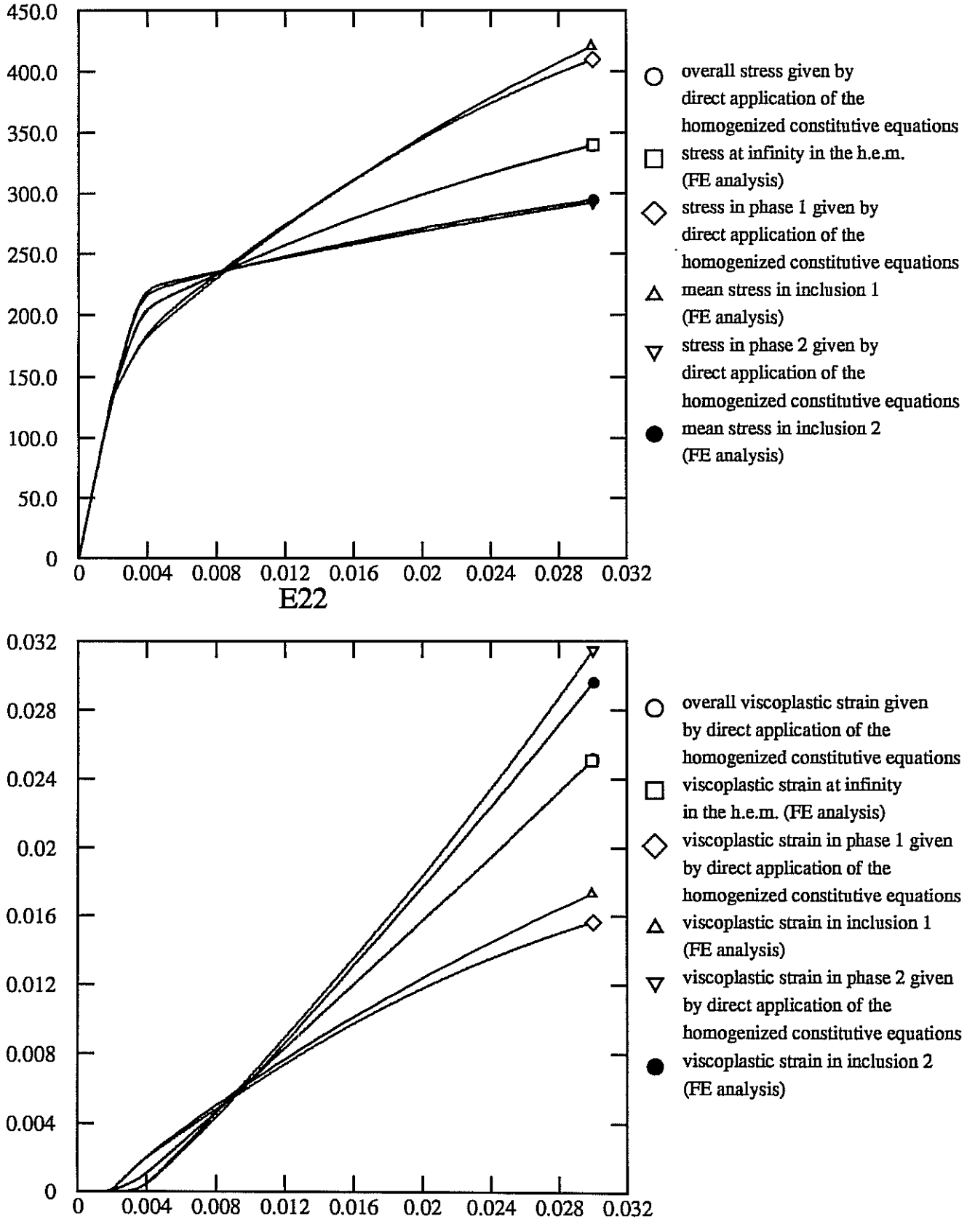

Figures C.20 and C.21: Use of the approximate self-consistent model with interphase accommodation variables in the case of elastoviscoplasticity (tensile test).

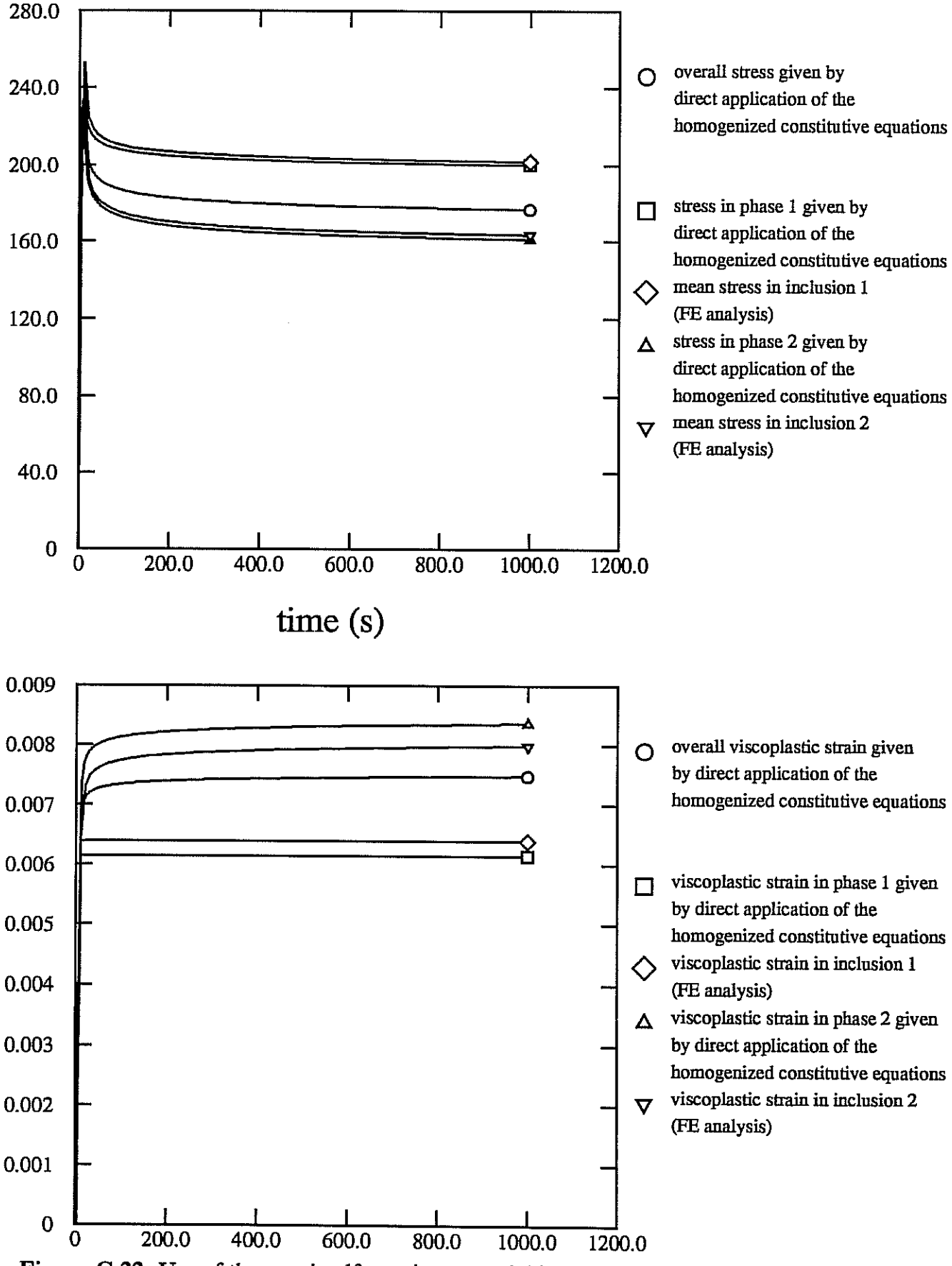

Figure C.22: Use of the quasi-self-consistent model in the case of elastoviscoplasticity (relaxation test).

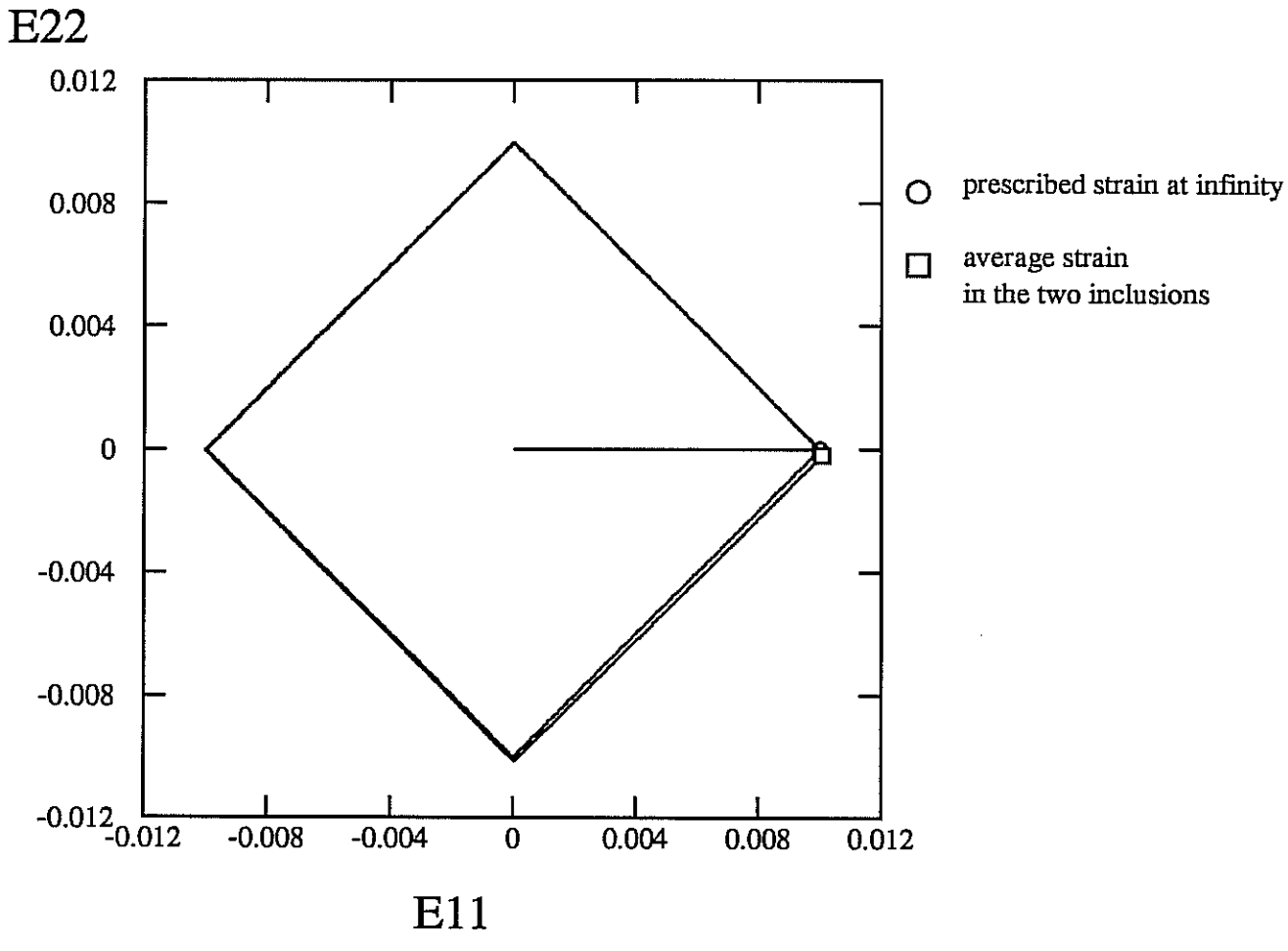

Figure C.23: Use of the quasi-self-consistent model in the case of non-proportional loading conditions: prescribed loading path and average strain in the inclusions during the test.

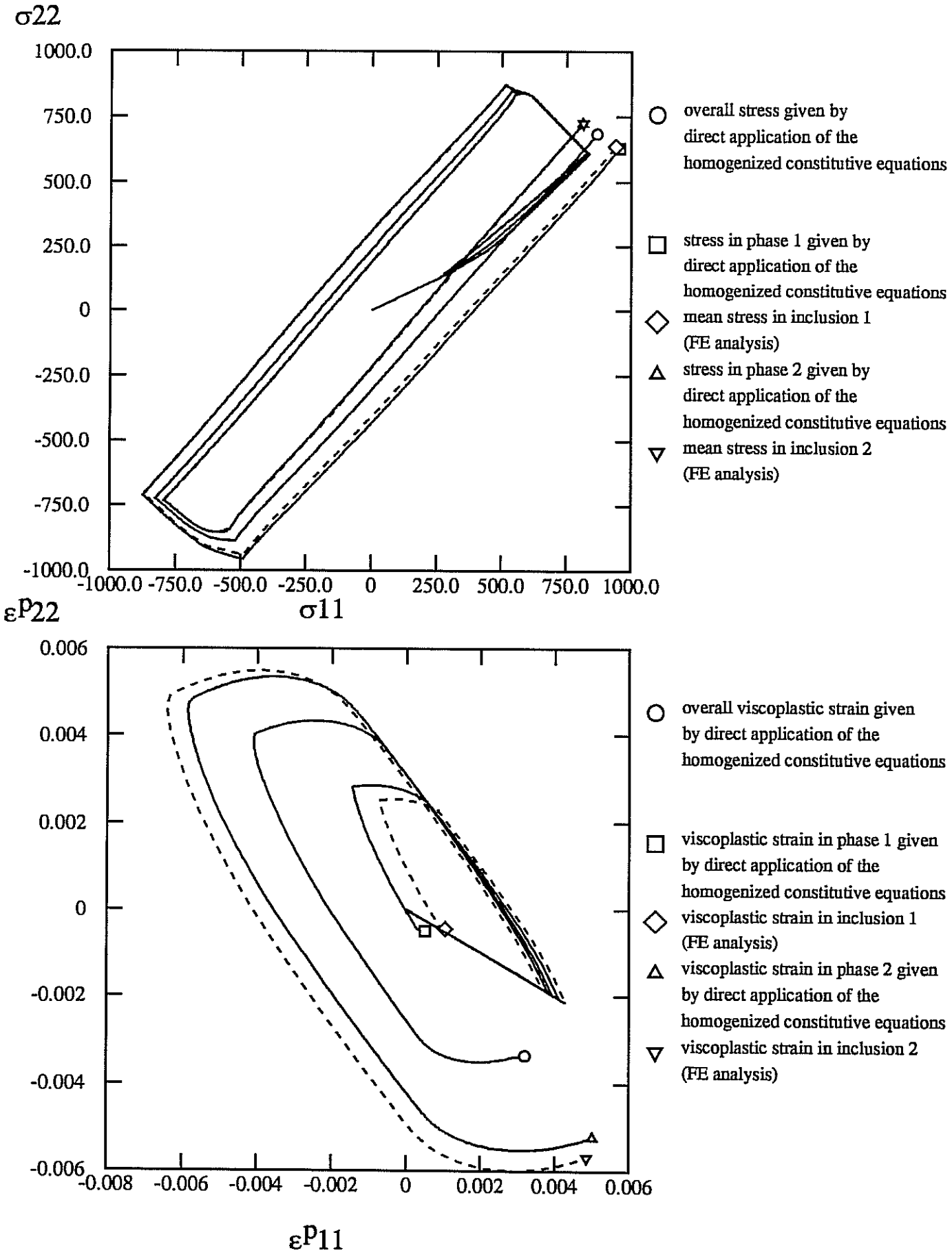

Figure C.24: Use of the quasi-self-consistent model in the case of non-proportional loading conditions: plane strain.

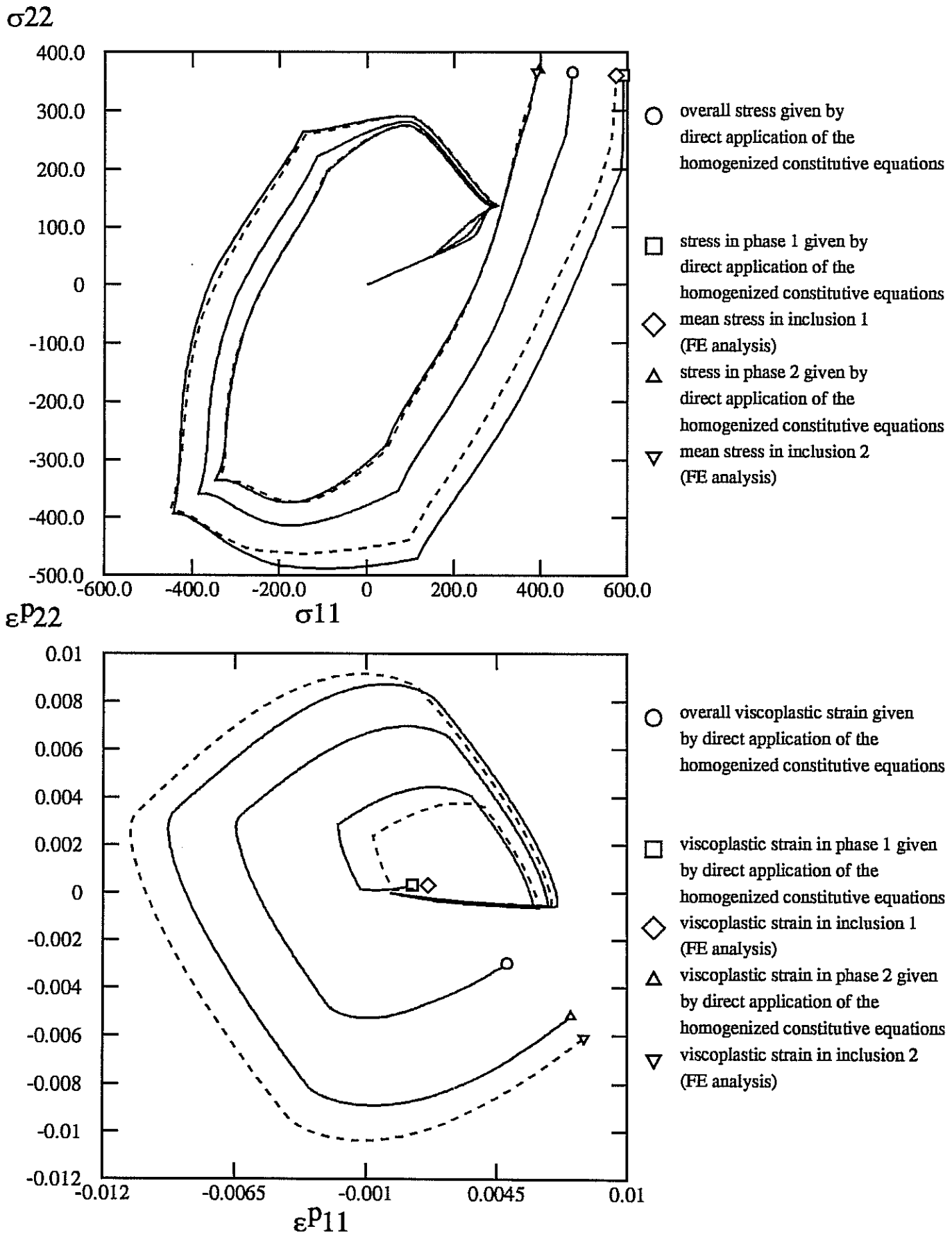

Figure C.25: Use of the quasi-self-consistent model in the case of non-proportional loading conditions: plane stress.

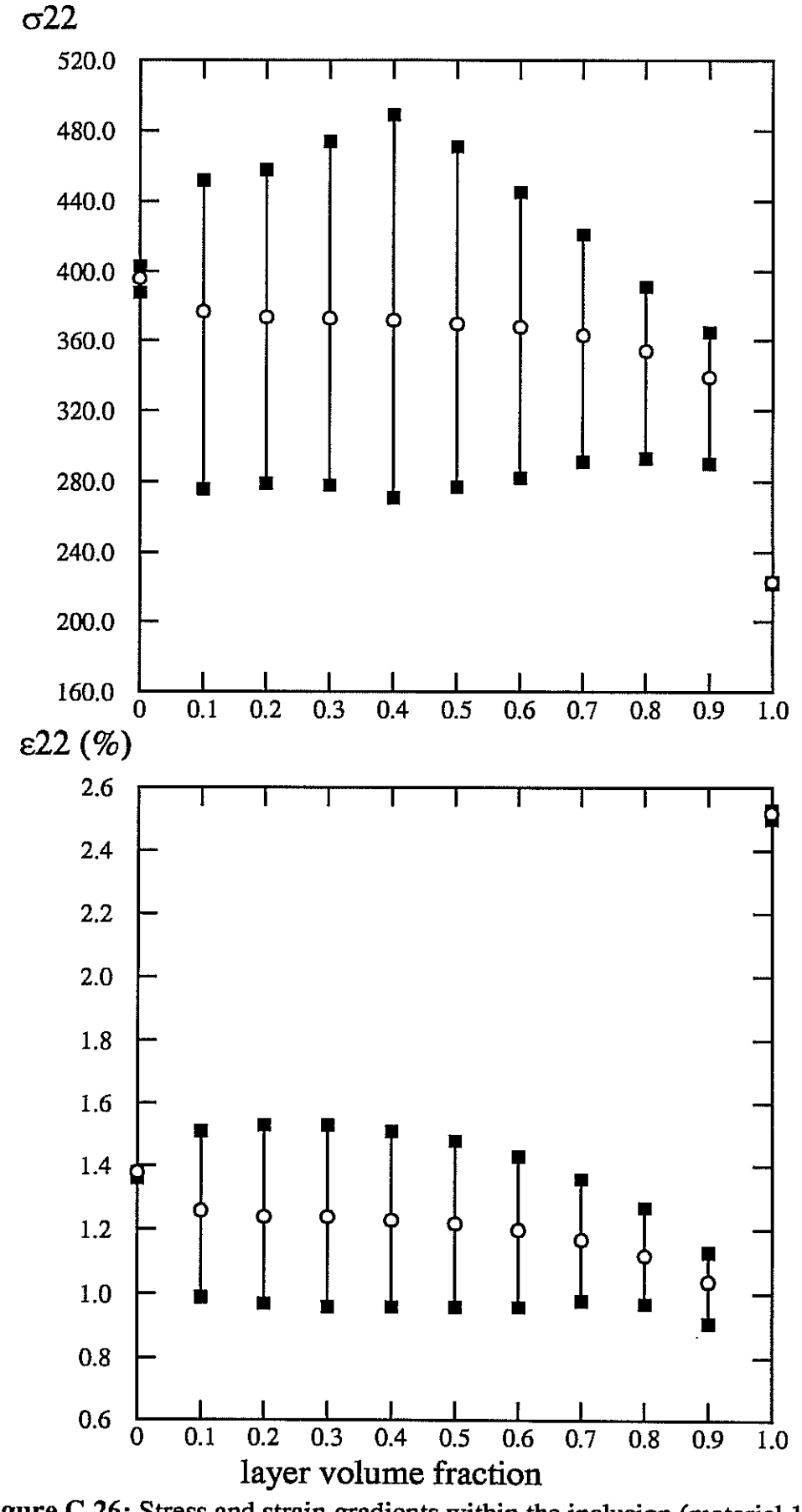

Figure C.26: Stress and strain gradients within the inclusion (material 1) according to the shell volume fraction (material 2); the inclusion-shell pattern is embbedded in an "infinite" matrix (material 3); each bar corresponds to a tensile test at 7.10e-4 per second and 2% strain.

Figure C.27: Stress state within the shell-inclusion pattern. The triangles show the interface.

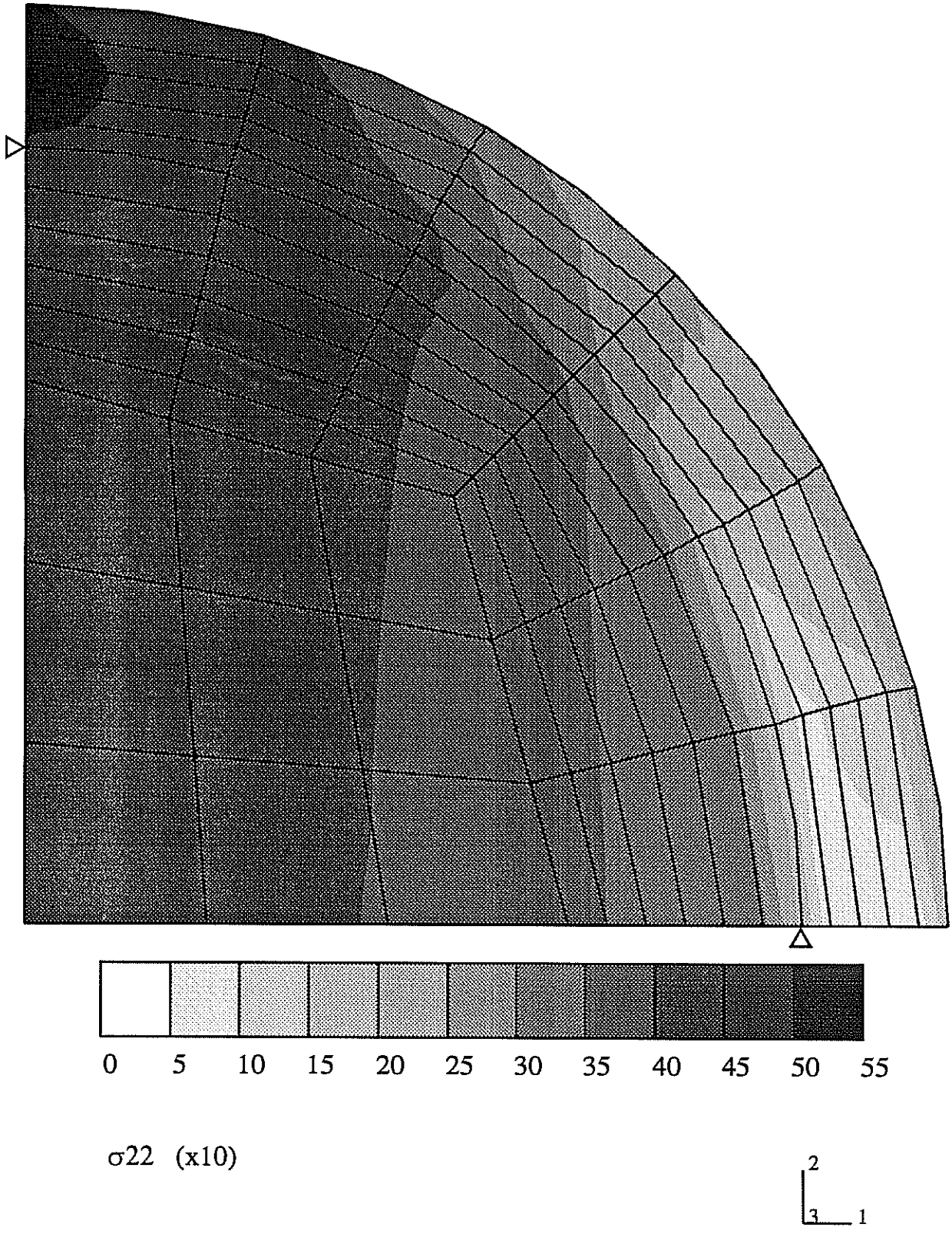

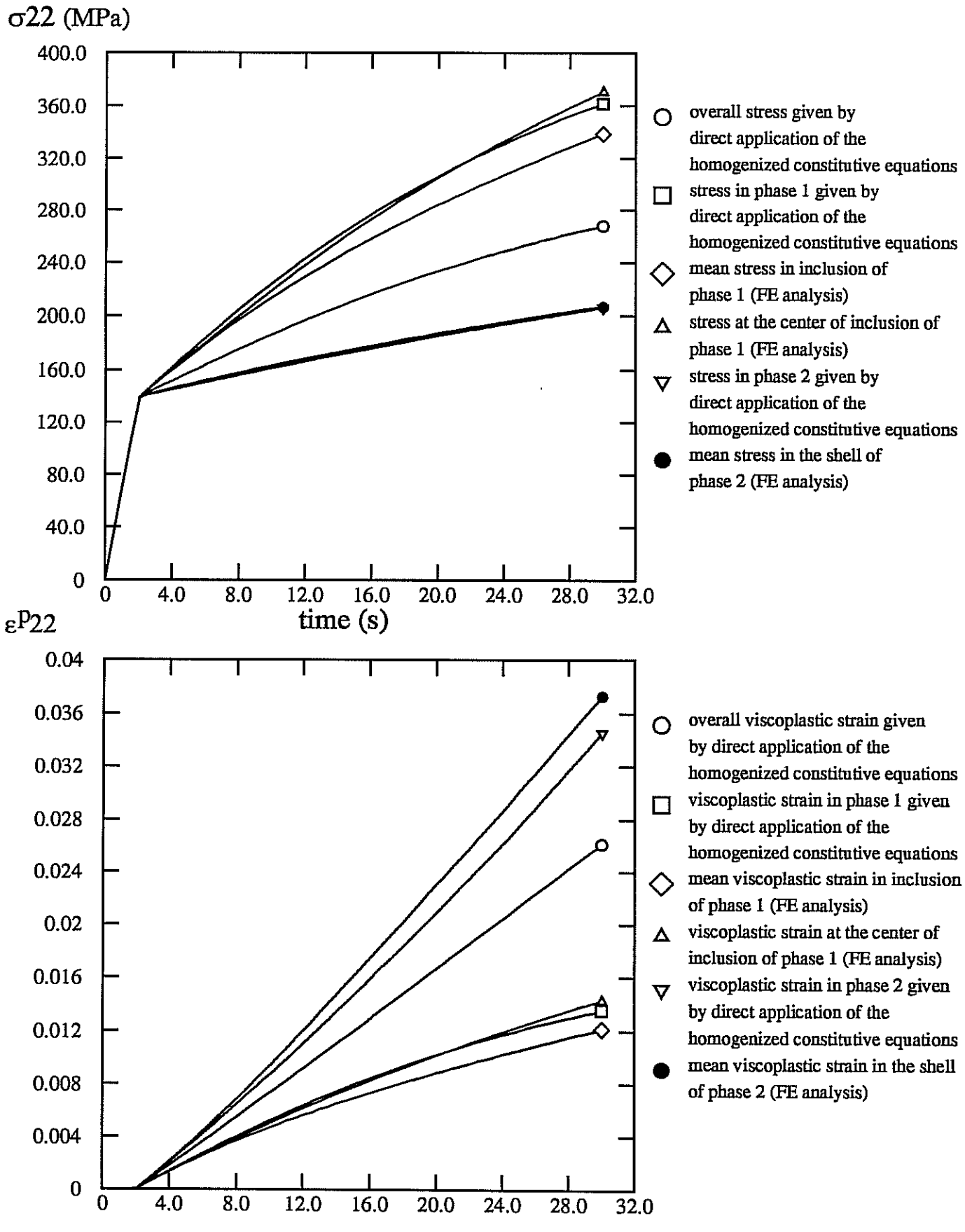

Figure C.28: Use of the quasi-self-consistent model in the three-phase model configuration.

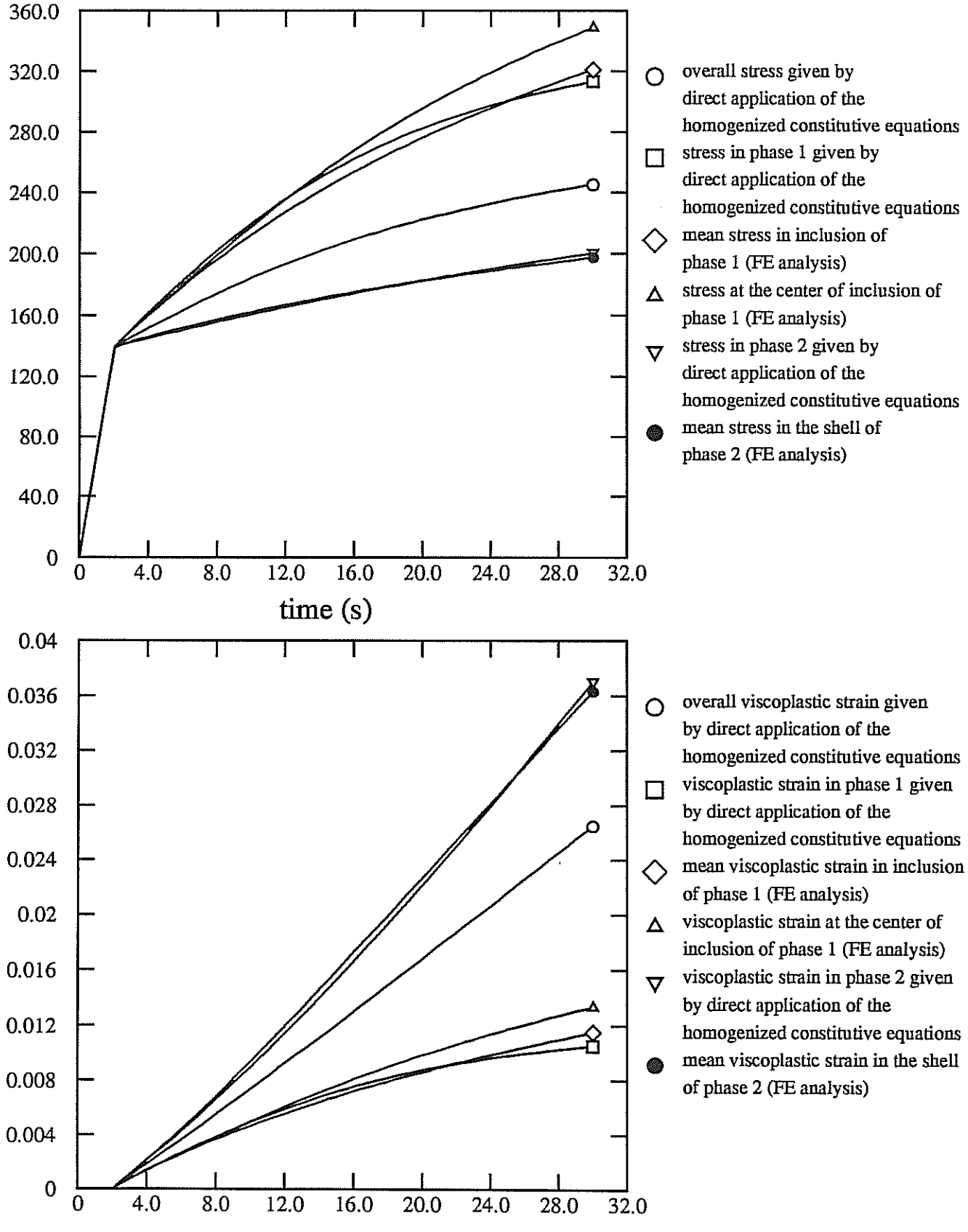

Figure C.29: Quasi-generalized-self-consistent model obtained using the optimization method.

4 Quasi-self-consistent modelling of two-phase single crystals

4.1 Description of the representative volume element

For a precise description of the inelastic behaviour of materials, the heterogeneous nature of materials at various scales should be included in mechanical modelling. Homogenization methods start from the assumption that the knowledge of the behaviour of constituents combined with suitable interaction laws should provide a description of the mechanical response of a macroscopic aggregate. For that purpose a relevant scale in the heterogeneous microstructure must be selected. This leads to the construction of a representative volume element, that is the classical volume element of continuum mechanics with an attached microstructure.

For the present model, we have retained only some features of the heterogeneous microstructure of single crystal superalloys that may influence significantly the macroscopic behaviour:

(*i*) the existence of two phases γ and γ' that exhibit very different behaviours at high temperatures;

(*ii*) the volume fraction of each phase $f_\gamma, f_{\gamma'}$;

(*iii*) the fact that matrix and precipitates are coherent.

Homogenization techniques require that the following inequalities are satisfied:

$$d_0 \ll d \ll l \ll L.$$

L is the typical size of the industrial component to be calculated, for instance about 10 cm for a hot section turbine blade in jet engines. l is the size of the continuum mechanics volume element, adopted for structural calculations, about 0.1 mm. d is the size of the heterogeneous unit of the microstructure that will be taken into account in the model: 0.5 μm for γ' precipitates. Lastly d_0 is the smallest scale at which continuum mechanics still work. Considering that stress and strain fields around a dislocation still have a meaning, we set $d_0 \sim$ 10nm. The condition $d \ll l$ can be removed if a complete geometrical description of the unit cell is available. In the present case, the retained microstructural information is incomplete, so that we will take advantage of the fact that $d \ll l$.

4.2 An approximate concentration rule for anisotropic multiphase materials

In the anisotropic non-linear case we propose the following approximate concentration rule

$$\underset{\sim}{\sigma} = \underset{\sim}{\Sigma} + \underset{\approx}{\mathbf{L}}^{\dagger} : (\underset{\sim}{\mathbf{B}} - \underset{\sim}{\beta}) \tag{116}$$

where the elastic accommodation tensor $\underset{\approx}{\mathbf{L}}^{\dagger}$ is computed with an anisotropic elasticity tensor $\underset{\approx}{\mathbf{C}}$, according to equation 81. We restrict ourselves to homogeneous elasticity. The interphase accommodation variables still obey to equations 112 and 114.

A simple form of the concentration rule can be derived in the cubic as follows. Regarding the algebra of cubic four-rank tensors we refer to [Walpole 1985]. If unit vectors $\underline{\mathbf{a}}$, $\underline{\mathbf{b}}$, $\underline{\mathbf{c}}$ lie on the edges of the cubic cell, one can define in a given orthonormal basis

$$N_{ijkl} = a_i a_j a_k a_l + b_i b_j b_k b_l + c_i c_j c_k c_l \tag{117}$$

It can be shown that these are the components of a four-rank tensor $\underset{\sim}{\underset{\sim}{\mathbf{N}}}$ with cubic symmetry. In the crystal axes the components of $\underset{\sim}{\underset{\sim}{\mathbf{N}}}$ read

$$N_{ijkl} = \delta_{ijkl} \tag{118}$$

using Mura's [1987] notation,

$$(\delta_{ijkl} \neq 0 \Rightarrow i = j = k = l) \quad \text{and} \quad \delta_{iiii} = 1 \quad \text{(no summation)} \tag{119}$$

The tensors

$$\underset{\sim}{\underset{\sim}{\mathbf{J}}}_1 = \underset{\sim}{\underset{\sim}{\mathbf{N}}} - \underset{\sim}{\underset{\sim}{\mathbf{K}}} \tag{120}$$

$$\underset{\sim}{\underset{\sim}{\mathbf{J}}}_2 = \underset{\sim}{\underset{\sim}{\mathbf{I}}} - \underset{\sim}{\underset{\sim}{\mathbf{N}}} \tag{121}$$

display the following properties

$$\underset{\sim}{\underset{\sim}{\mathbf{N}}} : \underset{\sim}{\underset{\sim}{\mathbf{N}}} = \underset{\sim}{\underset{\sim}{\mathbf{N}}}, \quad \underset{\sim}{\underset{\sim}{\mathbf{J}}}_1 : \underset{\sim}{\underset{\sim}{\mathbf{J}}}_1 = \underset{\sim}{\underset{\sim}{\mathbf{J}}}_1, \quad \underset{\sim}{\underset{\sim}{\mathbf{J}}}_2 : \underset{\sim}{\underset{\sim}{\mathbf{J}}}_2 = \underset{\sim}{\underset{\sim}{\mathbf{J}}}_2 \tag{122}$$

$$\underset{\sim}{\underset{\sim}{\mathbf{J}}}_1 : \underset{\sim}{\underset{\sim}{\mathbf{K}}} = \underset{\sim}{\underset{\sim}{\mathbf{K}}} : \underset{\sim}{\underset{\sim}{\mathbf{J}}}_1 = 0, \quad \underset{\sim}{\underset{\sim}{\mathbf{J}}}_2 : \underset{\sim}{\underset{\sim}{\mathbf{K}}} = \underset{\sim}{\underset{\sim}{\mathbf{K}}} : \underset{\sim}{\underset{\sim}{\mathbf{J}}}_2 = 0 \tag{123}$$

In that conditions tensor $\underset{\sim}{\underset{\sim}{\mathbf{C}}}$ can be written

$$\underset{\sim}{\underset{\sim}{\mathbf{C}}} = 3k\underset{\sim}{\underset{\sim}{\mathbf{K}}} + 2\mu_1 \underset{\sim}{\underset{\sim}{\mathbf{J}}}_1 + 2\mu_2 \underset{\sim}{\underset{\sim}{\mathbf{J}}}_2 \tag{124}$$

$$\underset{\sim}{\underset{\sim}{\mathbf{S}}} = 1/3k \ \underset{\sim}{\underset{\sim}{\mathbf{K}}} + 1/2\mu_1 \ \underset{\sim}{\underset{\sim}{\mathbf{J}}}_1 + 1/2\mu_2 \ \underset{\sim}{\underset{\sim}{\mathbf{J}}}_2 \tag{125}$$

If C_{ij} are the components of the Voigt matrix in the crystal axes,

$$3k = C_{11} + 2C_{12}, \quad 2\mu_1 = C_{11} - C_{12}, \quad \mu_2 = C_{44} \tag{126}$$

The associated Eshelby tensor reads then

$$\underset{\sim}{\underset{\sim}{\mathbf{S}}} = \alpha \underset{\sim}{\underset{\sim}{\mathbf{K}}} + \beta_1 \underset{\sim}{\underset{\sim}{\mathbf{J}}}_1 + \beta_2 \underset{\sim}{\underset{\sim}{\mathbf{J}}}_2 \tag{127}$$

As a result the elastic accommodation tensor becomes

$$\underset{\sim}{\underset{\sim}{\mathbf{L}}}^{\dagger} = 3k(1-\alpha)\underset{\sim}{\underset{\sim}{\mathbf{K}}} + 2\mu_1(1-\beta_1)\underset{\sim}{\underset{\sim}{\mathbf{J}}}_1 + 2\mu_2(1-\beta_2)\underset{\sim}{\underset{\sim}{\mathbf{J}}}_2 \tag{128}$$

It can be seen that

$$\operatorname{Tr} \underset{\sim}{\mathbf{a}} = 0 \quad \Rightarrow \quad \left[\underset{\sim}{\underset{\sim}{\mathbf{J}}}_1 : \underset{\sim}{\mathbf{a}}\right] = \begin{bmatrix} a_{11} & 0 & 0 \\ 0 & a_{22} & 0 \\ 0 & 0 & a_{33} \end{bmatrix} \quad \text{and} \quad \left[\underset{\sim}{\underset{\sim}{\mathbf{J}}}_2 : \underset{\sim}{\mathbf{a}}\right] = \begin{bmatrix} 0 & a_{12} & a_{13} \\ a_{12} & 0 & a_{23} \\ a_{13} & a_{23} & 0 \end{bmatrix} \tag{129}$$

in the crystallographic axes.

Finally we obtain the simple form

$$[\underset{\sim}{\sigma}] = [\underset{\sim}{\Sigma}] \quad +2\mu_1(1-\beta_1)\begin{bmatrix} B_{11}-\beta_{11} & 0 & 0 \\ 0 & B_{22}-\beta_{22} & 0 \\ 0 & 0 & B_{33}-\beta_{33} \end{bmatrix}$$
$$+2\mu_2(1-\beta_2)\begin{bmatrix} 0 & B_{12}-\beta_{12} & B_{13}-\beta_{13} \\ B_{12}-\beta_{12} & 0 & B_{23}-\beta_{23} \\ B_{13}-\beta_{13} & B_{23}-\beta_{23} & 0 \end{bmatrix} \tag{130}$$

for the concentration rule 116 when written in the crystallographic axes. For isotropic elasticity, $\mu_1 = \mu_2 = \mu$, $\beta_1 = \beta_2 = \beta$ and equation 113 is recovered. In the cubic case the components of Eshelby's tensor are given for spheroidal inclusions using irreductible integrals in [Mura 1987]. When spheres are considered Eshelby's tensor takes the form 127 and α, β_1, β_2 are computed numerically.

4.3 Complete set of constitutive equations

macroscopic strain partition

$$\underset{\sim}{\mathbf{E}} = \underset{\sim}{\mathbf{E}}^e + \underset{\sim}{\mathbf{E}}^p \tag{131}$$

elasticity law

$$\underset{\sim}{\Sigma} = \underset{\sim}{\mathbf{C}} : \underset{\sim}{\mathbf{E}}^e \tag{132}$$

concentration rule

$$\underset{\sim}{\sigma}_i = \underset{\sim}{\Sigma} + \underset{\sim}{\mathbf{L}}^{\dagger} : (\underset{\sim}{\mathbf{B}} - \underset{\sim}{\beta}_i) \tag{133}$$

local behaviour

$$\dot{\gamma}_i^s = < \frac{\mid \tau_i^s - x_i^s \mid - r_i^s}{k_i} >^{n_i} \ \text{sign}\ (\tau_i^s - x_i^s) \tag{134}$$

$$\dot{v}_i^s = \mid \dot{\gamma}_i^s \mid \tag{135}$$

$$r_i^s = r_{0i} + q_i \sum_{r=1}^{N_i} h_i^{sr}(1 - e^{(-b_i v_i^s)}) \tag{136}$$

$$x_i^s = c_i^s \ \alpha_i^s \tag{137}$$

$$\dot{\alpha}_i^s = \dot{\gamma}_i^s - d_i \dot{v}_i^s \alpha_i^s \tag{138}$$

$$\dot{\underset{\sim}{\varepsilon}}_i^p = \sum_{g=1}^{N_i} \dot{\gamma}_i^g \ \{\underline{\mathbf{l}}_i^g \otimes \underline{\mathbf{n}}_i^g\}. \tag{139}$$

local interphase accommodation rule

$$\dot{\underset{\sim}{\beta}}_i = \dot{\underset{\sim}{\varepsilon}}_i^p - \frac{2}{3} D J_2(\dot{\underset{\sim}{\varepsilon}}_i^p)\ (\underset{\sim}{\beta}_i - \delta \underset{\sim}{\varepsilon}_i^p) \tag{140}$$

homogenization

$$\dot{\underset{\sim}{\mathbf{E}}}^p = f_1 \dot{\underset{\sim}{\varepsilon}}^p{}_1 + f_2 \dot{\varepsilon}^p{}_2 \tag{141}$$

$$\dot{\underset{\sim}{\mathbf{B}}} = f_1 \dot{\underset{\sim}{\beta}}_1 + f_2 \dot{\underset{\sim}{\beta}}_2 \tag{142}$$

The N_i slip systems include 12 octahedral and 6 cubic slip systems. Geometrical parameters D and δ will be optimized in order to fulfill at best the self-consistency condition for a given morphology.

4.4 Identification process; influence of morphology

If the behaviour of the individual phases is known, the optimization procedure presented in section C-2 can be used to determine the parameters D and δ in order to best fulfill the self-consistency condition. For that purpose one or more FE simulations using the representative morphological pattern embedded in infinite homogeneous equivalent medium are necessary for each iteration.

But in many cases, the behaviour of specimen made of each phase alone is very different from the behaviour of each phase within the aggregate. An example is provided in section D.3. In that case, the material parameters of each phase are unknown as well as the "geometric" parameters. As a result, tensile and fatigue tests must also be simulated using the homogenized explicit constitutive equations and compared to experimental results. These additional simulations must be included in the optimization process shown in figure 5. They usually require no additional FE calculations but only the integration of the constitutive equation for each test. Any microstructural information can be taken into account as a constraint on the parameters in the identification process.

The influence of the morphology of the different phases can be studied using the appropriate representative morphological pattern for the FE calculations involved in the optimization process.

Part D

APPLICATION TO SINGLE CRYSTAL NICKEL-BASE SUPERALLOY SC16

1 Mechanical behaviour of single crystal Nickel-base superalloys

Two-phase nickel base superalloys are used in hot section components and especially in aircraft engines, because of the unusual temperature dependence of their flow stress: it increases with temperature until $700 - 800°C$ ($760°C$ for AM1). They still have good characteristics up to $1050 - 1100°C$. The microstructure of single crystal superalloys has been chosen for an optimal creep resistance in the [001] direction. It implies a high volume fraction of ordered phase γ', about 65 %. The γ' volume fraction slightly decreases from 65% at $20°C$ to 60% at $1050°C$, in the case of single crystal MarM200 studied by Fredholm [1987]. Freedholm showed also that the mismatch at the semi-coherent interface γ/γ',

$$\delta = \frac{a_{\gamma'} - a_{\gamma}}{a_{\gamma}} \tag{1}$$

is positive at room temperature and becomes negative at high temperature (about -0.5%). γ' cubes have a size of about $0.5\,\mu$m and matrix channels of $0.1\,\mu$m (figure 10). Because of the long range order they can be sheared only by pairs of $\frac{1}{2} < 110 >$ dislocations separated by an antiphase boundary. Each $\frac{1}{2} < 110 >$ dislocation may dissociate into partials separated by a complex stacking fault. The existence of a peak on the flow stress curve versus temperature can then be explained by thermally activated cross-slip followed by the activation of cubic slip systems but more details can be found in [Pope, Ezz 1984].

1.1 Behaviour at low temperature

Monotonic tensile curves of AM1 at $650°C$ are given on figure 1 for three orientations, after [Poubanne 1989]. They show a very unstable behaviour associated with perfect plasticity localization of deformation within some macroscopic slip bands. The slip band spacing may reach 0.5 mm but during the period of easy deformation on the curve, slip bands invade progressively the whole surface of the specimen [Poubanne 1989]. Cubic slip occurs at low temperature for $< 111 >$ specimens. An even more unstable behaviour has been observed in fatigue at $20°C$ by Hanriot [1992], which results in abrupt drops of the amplitude of plastic deformation on the stress-strain loops. An example of macroscopic slip bands is shown on figure 2. Similar plastic instabilities in fatigue have been noticed by Beaude [1988] for CMSX2 at room temperature. The presence of slip bands that cross the whole section of the specimen indicates that γ' precipitates are sheared by dislocations within this range of temperature. This can be seen on figure 3. Thus single crystal superalloys at low temperatures seem to behave much like single phase single crystals. Nevertheless deformation in the matrix remains predominant [Poubanne 1989].

Generally fatigue crack initiation in single crystal superalloys does not take place within intense slip bands but around some defects like carbides in the case of MarM200

[Chieragatti 1987], or porosities. Porosities, as big as 25 μm, may remain after solidification within interdendritic spaces. Bois [1985] has shown that the presence of dendrites introduces an important level of heterogeneity that plays a significant role in fatigue. Dendrites extend along the [001] direction, breaking the ideal cubic symmetry of the single crystal. Fatigue cracks usually propagate perpendiculary to the loading direction, no matter the crystallographic tensile direction. However propagation and fracture along crystallographic {111} or {001} planes are also observed.

1.2 Behaviour at high temperature

At the transition temperature 760°C, Ayrault [1989] observed that γ' precipitates can still be sheared but a greater number of slip systems are active in the matrix corridors.

Figure 4 shows the tensile behaviour of AM1 at 950°C after [Poubanne 1989]. The specimens deform homogeneously and no intense slip bands are observed after small deformation. Anisotropic hardening and high viscosity characterize the macroscopical behaviour of single crystal superalloys at high temperature. Both cubic and octahedral slip systems contribute to viscoplastic deformation.

On a microscale, deformation is concentrated in the matrix corridors and γ' precipitates are only occasionnally sheared by single dislocations causing stacking fault behind (see figures 5 and 6). The deformation mechanisms involve repeated cross-slip in matrix corridors on {111} planes globally in the $< 001 >$ direction, according to figure 7. This leads to a broadening of horizontal or vertical corridors during creep in the [001] direction. Quadratic, octogonal and hexagonal static dislocation networks develop during creep according to Fredholm [1987]. Precipitates can also be overcome by dislocations thanks to the mechanism of climb.

Under cyclic loading, deformation is also usually macroscopically homogeneous and microscopically localized in the matrix γ. However macroscopic slip bands cannot be excluded. Hanriot [1993] observed intense slip bands on specimens under cycling loading in the [001] and [111] direction at 950°C and for low strain rates (10^{-5} to 10^{-3} s^{-1}, figure 8). Crack initiation is due to the presence of porosities near the surface or to oxydation. Cyclic loading leads to the crackling of the oxyde film that forms on the surface at high temperature, which results in further oxydation of new parts of the crystal and possibly crack initiation. But crack initiation can also take place in an intense slip band as observed by [Fleury 1991]. Fleury has performed thermomechanical fatigue test combining cyclic mechanical and thermal loading, temperature varying between 600°C and 1100°C. On figure 9, the specimen loaded along a $< 111 >$ direction with amplitude of mechanical deformation of 1.2% , displays a macroscopic slip band, in which a crack initiated. Usually fatigue cracks propagate in a plane perpendicular to the loading direction but Fleury observed propagations along crystallographic planes for large imposed plastic amplitudes, at 950°C.

1.3 Microstructure of SC16

Single crystal nickel-base superalloy SC16 is a candidate for a use in stationary turbine blades. Its composition is given in table 1. The material is solution treated 3 hours at 1260°C in vacuum, followed by a cooling at 150°Cmin^{-1} under Argon (partial pressure

1 mbar). The wanted microstructure of the material is obtained after 4 hour aging at 1100°C in vacuum and 24 hours at 850°C.

C	Si	Mn	Cr	Mo	Ni	Ta
< 0.003	< 0.03	< 0.03	15.49	2.80	bal.	3.5
Ti	Al	Fe	W	Co	Cu	V
3.5	3.44	0.03	0.03	0.15	< 0.03	< 0.03
Nb	Zr	B	P	S	N	O
< 0.03	< 0.003	0.019	< 0.005	0.0003	3 ppm	5 ppm

Table 1: Composition of single crystal nickel-base superalloy SC16 (weight-%).

The microstructure is shown on figure 10 and displays a bimodal repartition of γ' precipitates: cuboidal 0.5 μm wide precipitates and smaller spherical ones. The last ones are only seldom located in the narrow matrix channels between large cuboidal precipitates. The volume fraction of the γ' phase is about 40%. The crystal structure is cubic face-centered and matrix and precipitates are coherent with a misfit of about -0.1% at room temperature.

The irregular and bimodal repartition of γ' precipitates prompts us to favour a statistical approach for disordered materials, say the general self-consistent scheme, rather than a model based on a periodicity hypothesis.

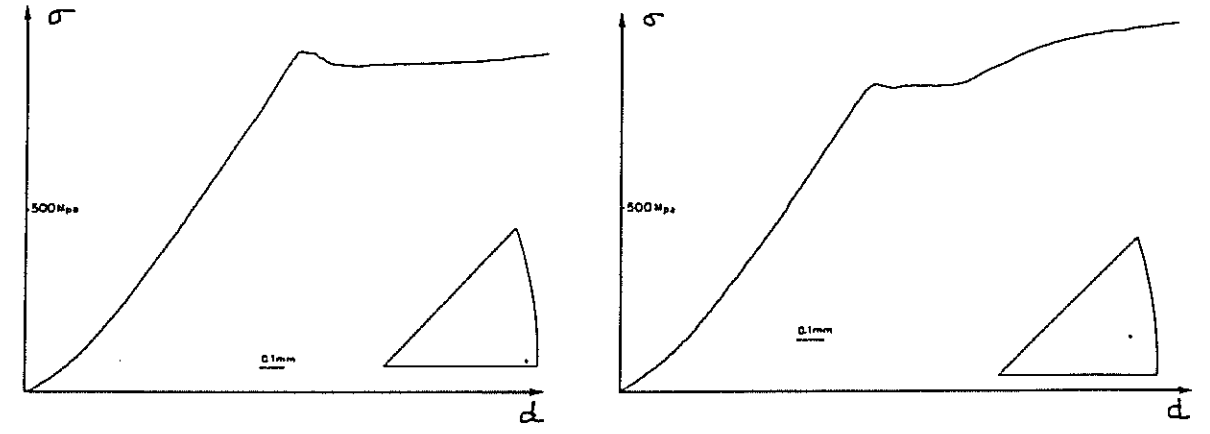

AM1 <011>, $T = 650°C$, $\dot{\varepsilon} \simeq 16\ 10^{-5}/s$ *AM1 <123>, $T = 650°C$, $\dot{\varepsilon} \simeq 16\ 10^{-5}/s$*

Figure D.1: Load-displacement curves of single crystal superalloy AM1 at 650°C (after [Poubanne 1989]).

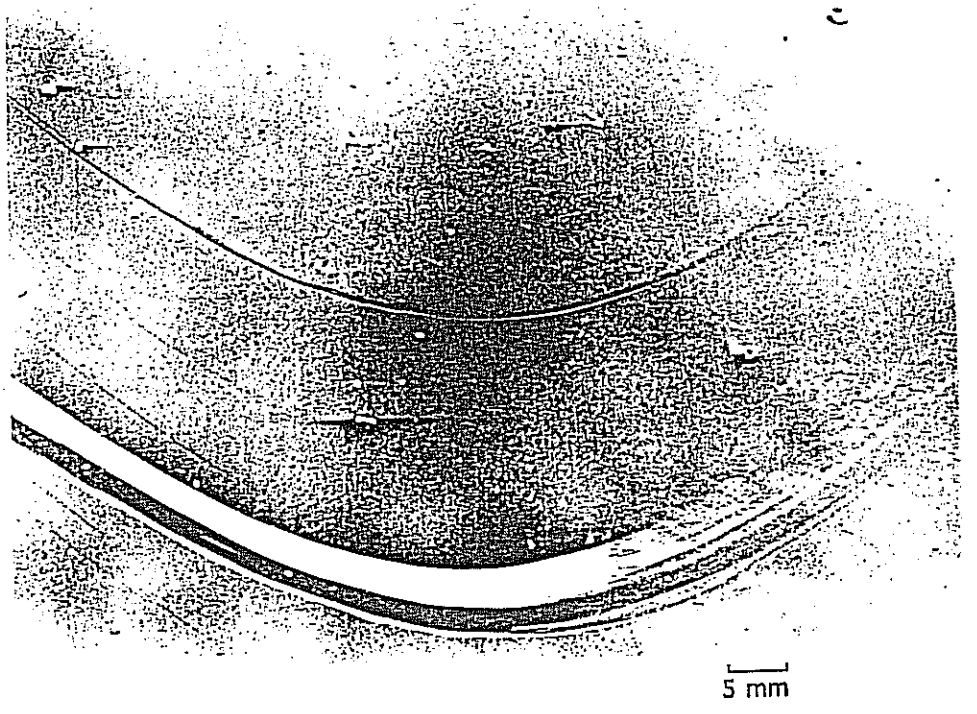

Figure D.2: Macroscopic slip band in AM1 at 20°C (developed replica of the surface of a cylindrical single crystal specimen in tension, after [Hanriot 1992]).

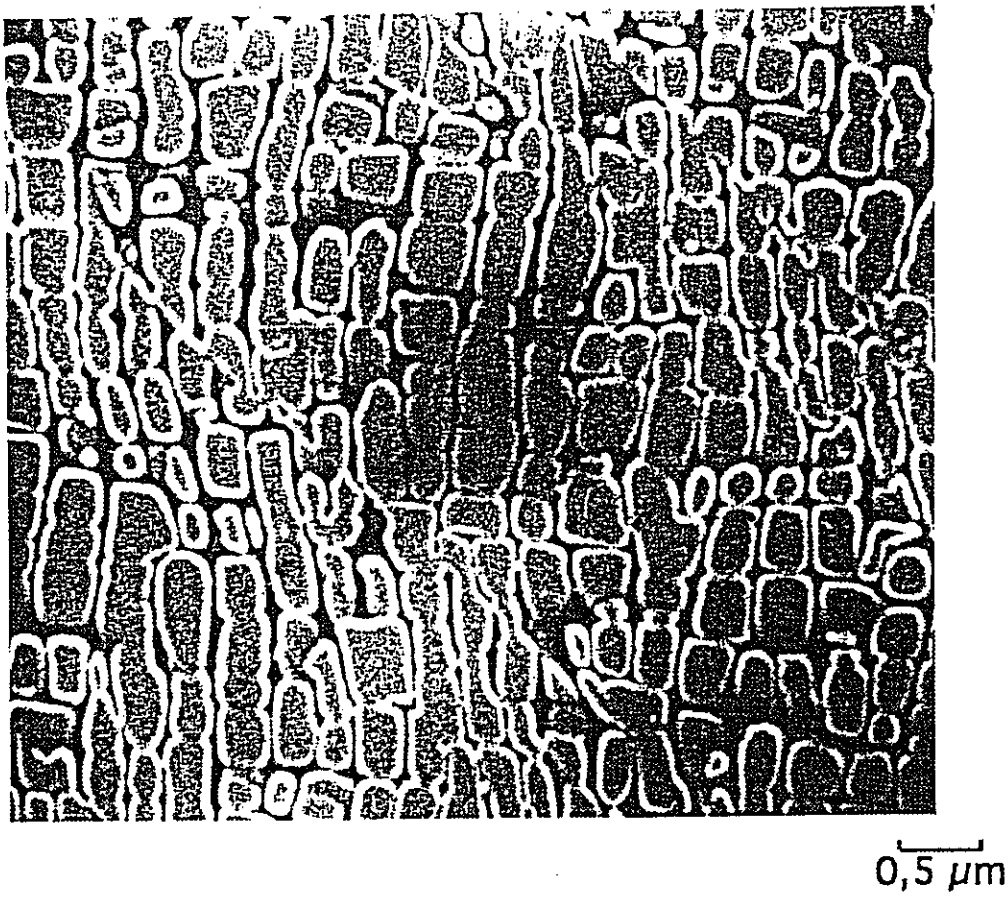

Figure D.3: Shearing of pricipitates in AM1 at 650°C (after [Hanriot 1992]).

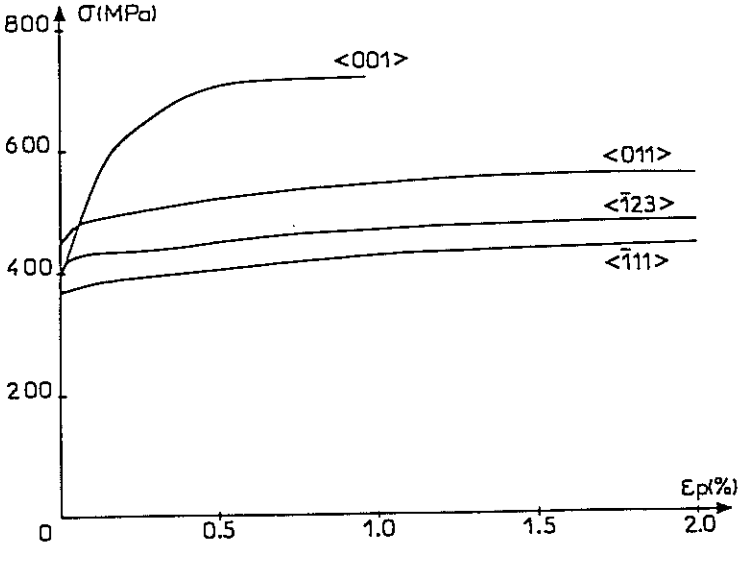

Figure D.4: Tensile curves of AM1 at 950°C (after [Poubanne 1989]).

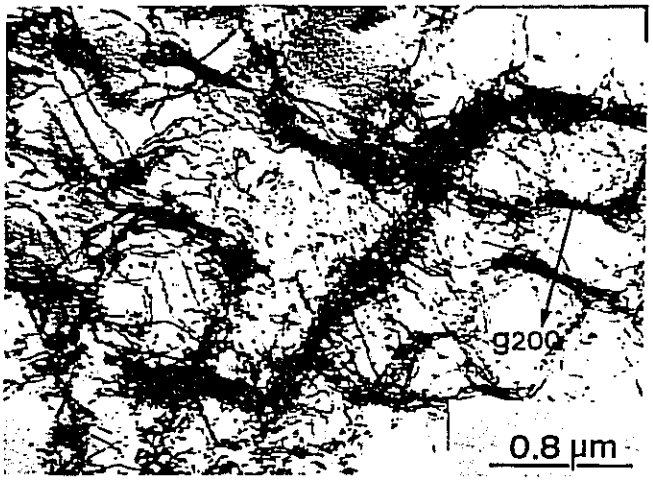

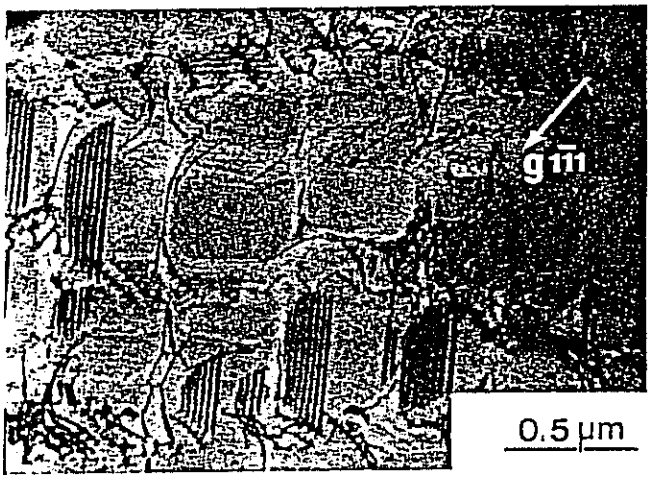

Figure D.5 and D.6: Localization of deformation in matrix channels of AM1 single crystals at 950°C (after [Poubanne 1989]).

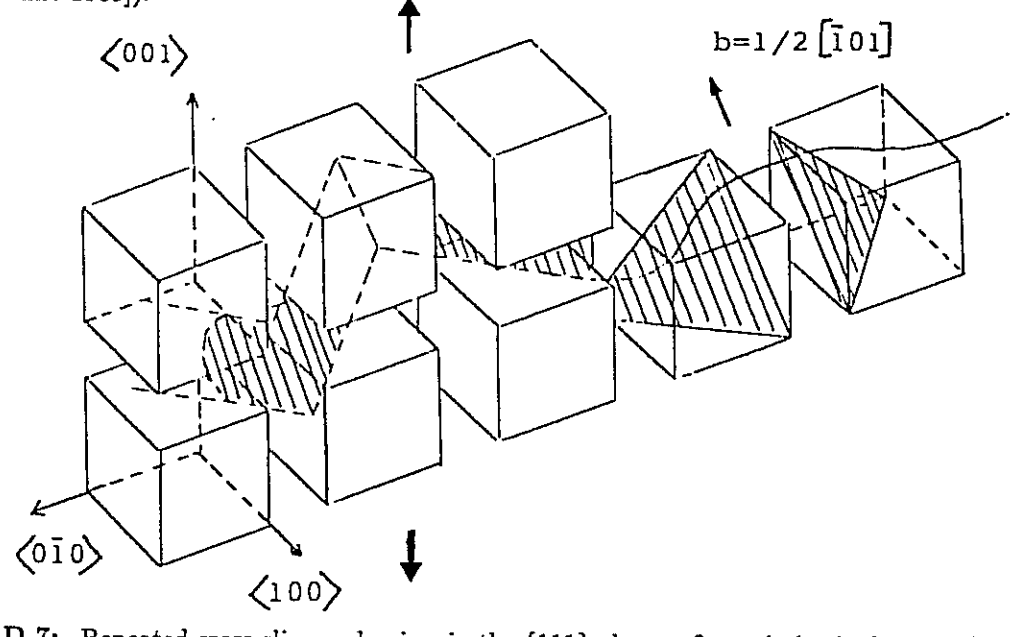

Figure D.7: Repeated cross-slip mechanism in the {111} planes of matrix in single crystal superalloys at high temperature (after [Ayrault 1989]).

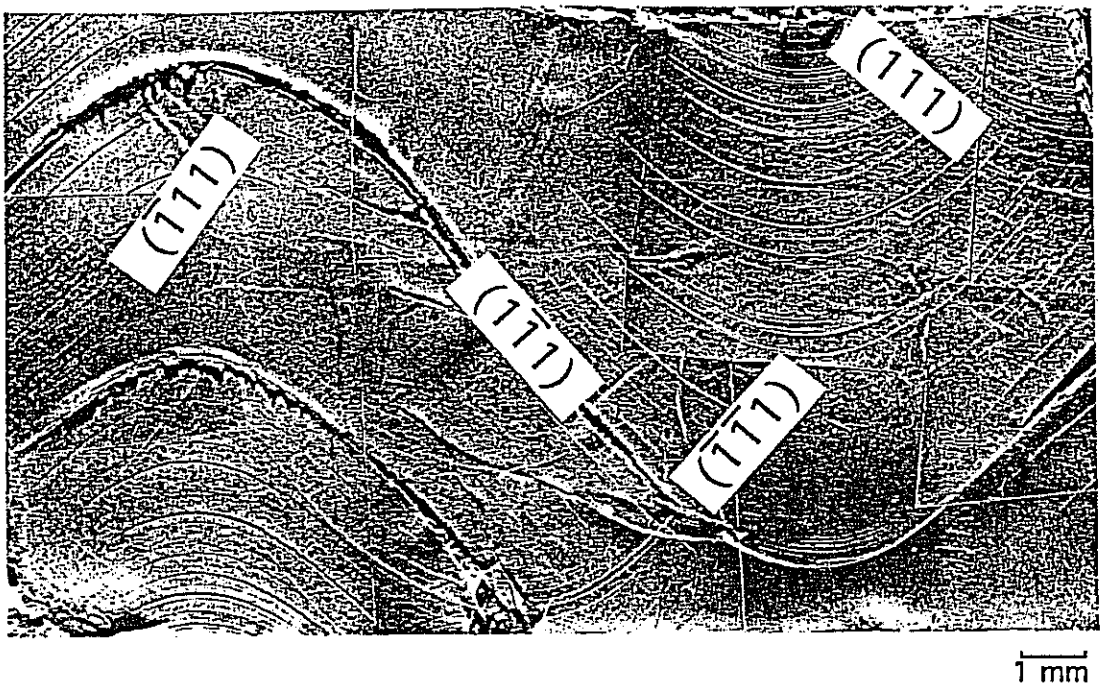

Figure D.8: Macroscopic slip bands in AM1 single crystals at 950°C (developped replica of the surface of a cylindrical specimen, after [Hanriot 1992]).

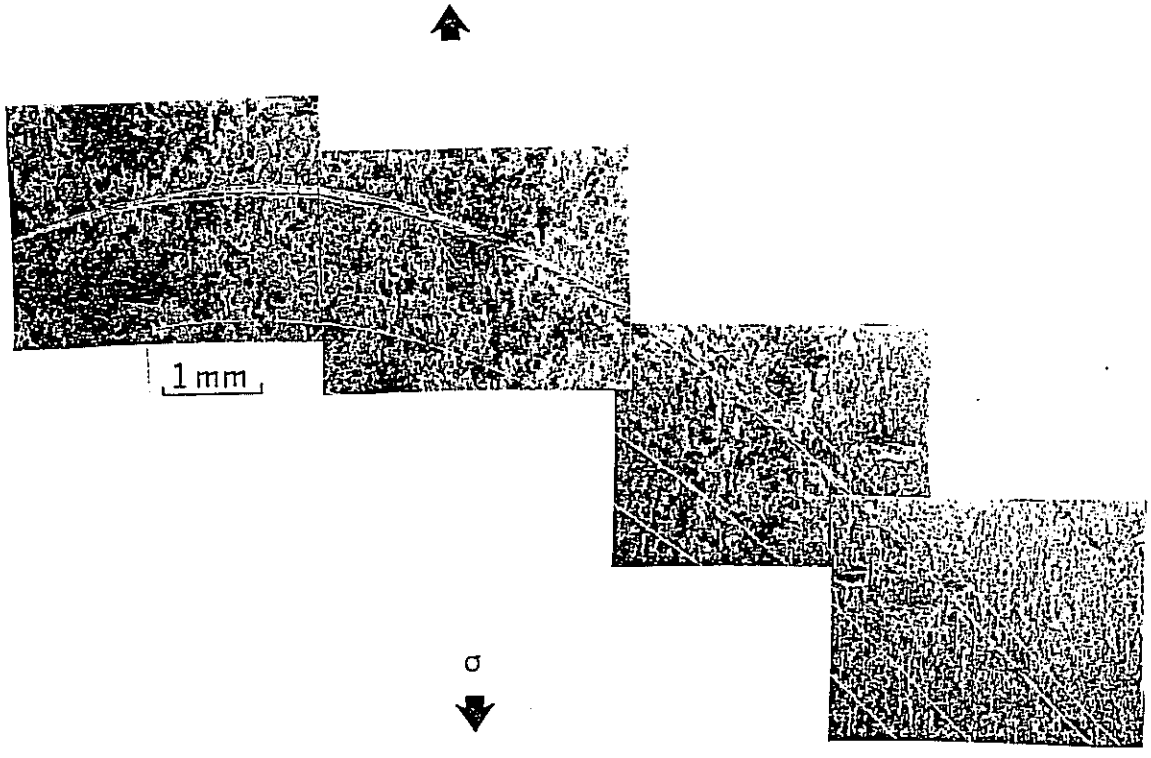

Figure D.9: Macroscopic slip band on the surface of a fatigued AM1 single crystal at 950°C, in which the final crack initiated (after [Fleury 1991]).

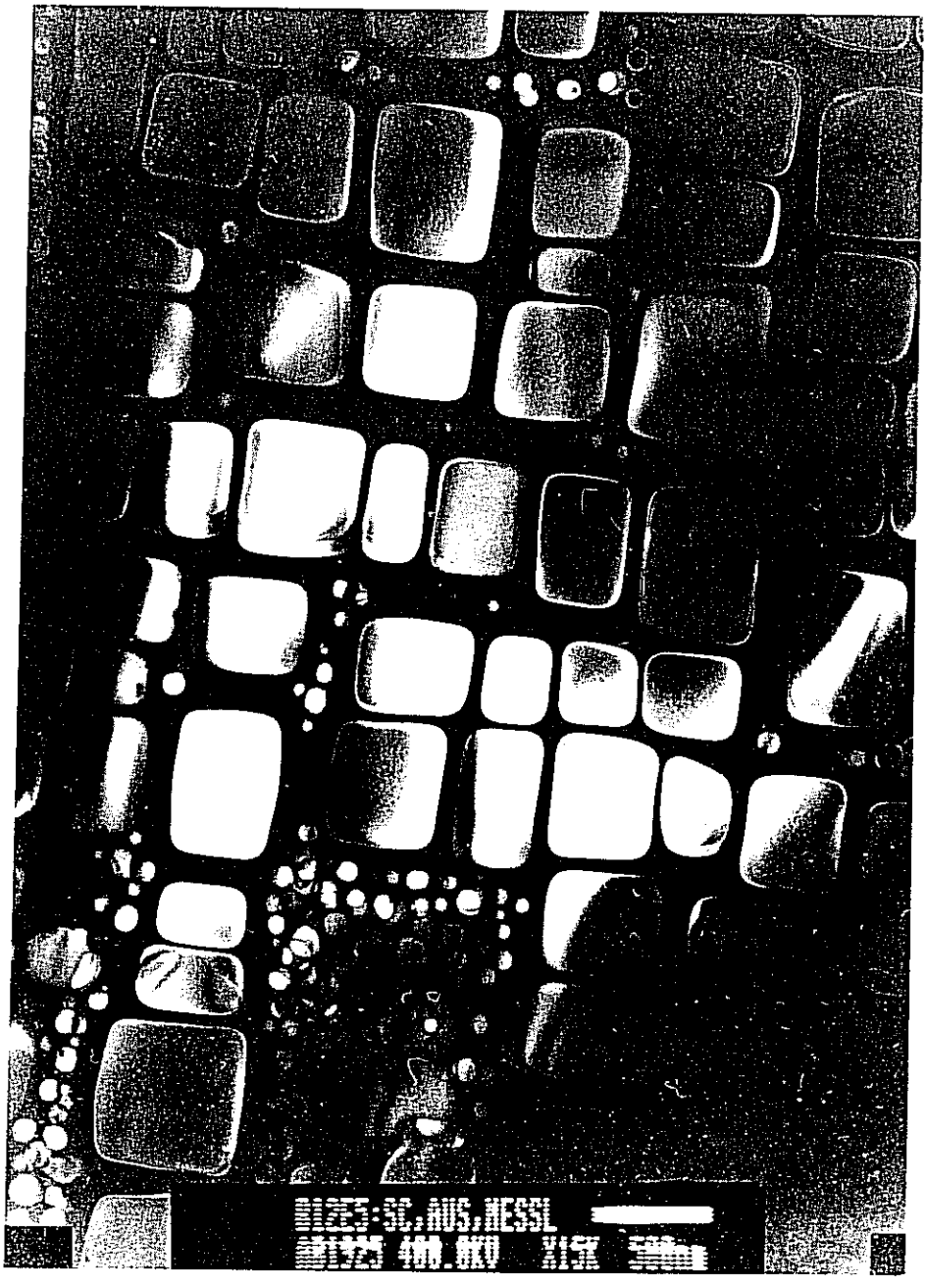

Figure D.10: Microstructure of single crystal nickel-base superalloy SC16 (after D.Bettge, BAM-Berlin).

2 Mechanical behaviour of SC16 at room temperature

2.1 Tensile behaviour: slip band propagation

2.1.1 Experimental evidence

The tensile curves of near-< 001 >, near-< 011 > and near-< 111 > SC16 specimens at room temperature are shown on figures 11 and 12. After the yield stress is reached, the load remains constant and for some tests the load increases again after further straining. We have not interpreted the curves in terms of stress and strain because there is some evidence that the deformation of the specimens is not homogeneous. In particular the tension test of the near-< 011 > specimen (specimen r1606005 of figure 12) has been filmed using a video-camera. The specimen was electro-polished before testing. The plastic behaviour began with the formation of a few isolated intense slip bands (figure 13). The localized deformation zone starts from the upper end of the specimen (rounded zone) and propagates slowly along the specimen. During the propagation of the band, the load remains constant. The test has been interrupted before the strongly deformed zone reached the lower end of the specimen. Figure 14 shows the zone where the localized deformation zone started from. Optical observations reported in [Martin 95] prove that only one octahedral slip system has been activated during the test.

In contrast the tension test with the near-< 111 > specimen (r1606104 in figure 12) did not reveal any non-homogeneous deformation at least using optical methods. No slip band has been observed. However the tensile curve is very similar to the previous one at the beginning but then the load increases tremendously.

In the following section we show how the propagation of slip bands can be modelled during a tensile test and that the obtained load-displacement curve is very similar to the reported experimental results.

2.1.2 Modelling slip band propagation

In part A we have postulated that a slip band forms when local softening occurs, that is when locally dislocations can move more easily because the way has been freed from obstacles by previous dislocations for instance. However with further straining fixed dislocations tend to accumulate in the band and the material hardens. That is why we have modified the hardening rule so that hardening occurs after softening until saturation:

$$r^s = r_0^s + q_1(1 - e^{-b_1 v^s}) + q_2(1 + \tanh(b_2 v^s - \frac{1}{b_3(\gamma_0 + v^s)})) \qquad (2)$$

Two defects have been introduced in a single crystal plate oriented for single slip. To the parameters used in section 4.1.2, the following parameters have been added

$$q_2 = 100 \quad b_2 = 100 \quad b_3 = 20 \quad \gamma_0 = 1.10^{-5}.$$

The corresponding stress-strain curve is shown on figure 15.

The abrupt fall on the load-displacement curve (figure 16) indicates that bifurcation occurred. The load remains then constant. At the same time slip bands spread over the entire specimen (figures 17 and 18). When the whole specimen is covered with slip bands, the load increases again. The calculation with the large strain model gives the same result

and figure 19 shows that no additional lattice rotation occurs with respect to the initial orientation.

The load-displacement curve of figure 16 can be compared with the tensile curves of figure 11 and 12. It must be noted that here we have used boundary conditions different from the experimental ones. In our calculations, the grips are laterally free of moving whereas they are fixed in the experiment. This may explain the complex situation observed on figure 14.

2.2 Tension-torsion tests: local strain measurements and confrontation with FE calculations

2.2.1 Torsion tests on < 001 > specimens

The specimens are 1.25 mm thin tubes with external diameter 26.5 mm. The crystal orientation of the tube axis is near < 001 >. Eight strain gauge rosettes have been stuck on the circumference of a cross-section and measure the strain at 0, 45 and 90° with respect to the axis. They correspond to crystallographical directions < 100 > and < 110 >. Each strain gauge is 3.5 mm long and 1.5 mm wide. The experimental devices are shown on figure 22bis.

Tension tests have been performed on the tube specimens in order to determine the material parameters involved in the model. In this work we are dealing with monotonous tests so that kinematical hardening will not be taken into account. Since no information is available about latent hardening in single crystal superalloys, the interaction matrix h^{sr} is taken diagonal like in [Méric, Poubanne, Cailletaud 1991].

Tension tests in direction < 001 > are used to determine the material parameters associated with octahedral slip (figure 20):

$$r_0 = 278 \text{ MPa}$$
$$q = 55 \text{ MPa}$$
$$b = 273$$
$$h^{ij} = \delta_{ij}$$
$$k = 100 \text{ MPa} s^{1/n}$$
$$n = 2.$$

Since no significant rate-dependence has been observed, fictitious material parameters related to viscosity have been chosen so that the previous set of parameters can be used only within a certain strain rate range.

For the determination of the elastic constants, we have used the results of the tensile tests on < 001 >, < 011 > and < 111 > specimens presented in section 2.1.1, and of the torsion tests

$$C_{11} = 275780 \text{ MPa}$$
$$C_{12} = 186730 \text{ MPa}$$
$$C_{44} = 110784 \text{ MPa}$$

Experimental results of the torsion tests

Torsion tests on tube specimens have been performed at room temperature. The local strain measurements prove that the deformation along the circumference is not homogeneous in the plastic regime. This fact has already been mentionned in [Nouailhas, Culié, Méric, Cailletaud 1992]. Figures 22 and 23 show that "soft" and "hard" zones form in the directions $< 110 >$ and $< 100 >$ respectively.

FE analysis

The interpretation of such a non-homogeneous test requires a finite element analysis as it has been done in [Méric, Cailletaud 1991] (see also [Nouailhas, Cailletaud 1995]). A simulation of the test with the previous model with only octahedral slip does not correctly describe the experiment. It has proved to be necessary to introduce cubic slip. Cubic slip in single crystal nickel-base superalloys has already been found predominent during torsion tests (see [Nouailhas, Cailletaud 1994]). As a result the plastic deformation has been assumed to start at the location $< 110 >$ with cubic slip. The critical shear stress associated with cubic slip has been derived from the angle-moment curve using the appropriate Schmid factor (figure 24):

$$r_0^{cub} = 335 \text{ MPa}$$

No hardening has been introduced for cubic slip and fictitious viscosity parameters $k^{cub} = 80$ MPa$s^{1/n}$ and $n^{cub} = 5$ are used.

The torsion angle is prescribed by a local extensometer with gauge length 25 mm. The exact location of the extensometer must be known with respect to the crystallographic axes. In our calculations we prescribe the global torsion angle at the grips in order to get the experimental values at the location of the extensometer.

The plastic strain distribution is shown on figure 26. With the set of parameters a good quantitative agreement is reached between the local strain measurements and the simulation (figure 25).

2.2.2 Tension-torsion test on a misoriented specimen

The multiaxial behaviour of SC16 at room temperature under proportional tension-torsion loadings with prescribed axial displacement and angle has been investigated. For each loading path the specimen has been unloaded at incipient plasticity and a new radial loading path in the stress space has been explored. The obtained force-moment curve is shown on figure 27 and compared with the FE simulation. It corresponds to branches oriented at 77, 55, 45, 32 and 20° in the $\sigma_{33} - \sigma_{31}$ space with respect to axis σ_{33}. These branches are called respectively "star 70-60-50-40-30" in the text and figures of this section.

The specimen axis displays a strong deviation θ from crystal orientation $< 001 >$:

$$\theta = 13°$$

$$\rho = 11°.$$

Non-homogeneous non-symmetrical deformation patterns

Eight strain gauge rosettes have been stuck along the circumference of a cross-section. One of them is located near a $< 100 >$ direction, the other ones are then regularly disposed like in 2.2.1. Figures 29 to 33 show the experimental results for the strain gauges in the

axial direction and at 45°. Once more the deformation is found to be non-uniform in the plastic regime but contrary to 2.2.1 the deformation patterns are not symmetrical (loading paths 70 and 60): there are two very soft regions and two other slightly deformed regions (figure 29 and 30). Between figures 30 and 31, the strain gauges have been accidentally reinitialized so that the residual plastic and elastic strains at the end of loading path 60 are lost. When tension becomes predominent, quasi-uniform straining is measured in the axial direction (figures 31 to 33).

FE analysis

The simulation takes the actual crystal orientation of the specimen into account. The resulting non-homogeneous and non-symmetrical deformation is shown on figure 38 at the end of the test. Figure 28 shows the calculated strain along the circumference of the cross-section where the strain gauges are located. In the elastic regime the deformation is almost homogeneous but at incipient plasticity non-symmetrical non-uniform deformation patterns form. Deformation localizes within two soft regions. The calculation proves that the non-symmetrical non-uniform deformation patterns are due to the significant deviation of the specimen axis with respect to crystal direction $< 001 >$. Both cubic and octahedral slip systems are activated but cubic slip is predominent for predominent torsion and octahedral slip for tension.

The local predictions agree with the local measurements for the loading paths 60-70 for both length and 45° strain gauges (figures 34 and 35). The simulation accounts also for the length strain gauge measurements for the loading paths 50, 40 and 30 (figures 36 and 37). However in this case the deformation of the 45° strain gauges seems to be overestimated (figure 36), but the strain is then small and essentially elastic because tensile straining becomes predominent.

The previous local measurements have shown that the plastic deformation of $< 001 >$ single crystal superalloys under torsion is not homogeneous. Qualitative and quantitative agreement has been obtained between experiment and FE simulation. Furthermore very complicated tests like a tension-torsion test on a misoriented specimen can be interpreted using finite element calculations.

2.3 Geometry effect on slip band formation; size effect in plasticity?

A great discrepancy between the response of tubes and full specimens under tension has been observed (figure 21). The geometry of the tubes has been described in section 2.2.1. As for them, the full specimens used in section 1 have a diameter of 9 mm. The tensile curves of full specimens seem to indicate an ideal plastic behaviour but in fact the deformation of the specimen is usually not homogeneous and slip bands progressively invade the whole specimen. In contrast the tube specimens display a hardening behaviour and plastic yielding occurs earlier. Slip band propagation could not be observed but intense slip lines are observed on some specimen. It must be noticed that the full and hollow specimens do not come from the same delivery and the caster Thyssen could not ensure that the tube specimens have been subjected to the standard heat treatments. That it is why new tests on new specimens should be performed before attributing the observed difference to a size effect or a geometry effect. Nevertheless a dependence of slip band formation on specimen geometry cannot be excluded and may provide a possible explanation for parts of the observed phenomenon. That is why we have investigated the influence of specimen geometry on slip band formation in single crystals.

For that purpose we consider the tension of a single crystal tube the behaviour of which is the same as in section A.4.2. The axis of the tube coincides with crystal direction [123]. The displacement of the ends of the specimen is imposed only in the direction 3 (initial axis). No further constraint is imposed. A material defect is introduced which results in strain localization on two planes as shown in figure 39. Figure 40 shows the developed surface of the cylinder and proves that the shear bands lie on the slip and kink planes as expected. A calculation with the large strain model shows that the kink band does not form (figure 41). Instead a more complex deformation pattern is induced at the ends of the specimen. The developed surface showing the slip band can be compared with the surface replica of figure 8.

However no sharp load drop is observed at bifurcation (see figure 42). It suggests that the tube geometry is much less prone to localization than the plate geometry studied in part A.

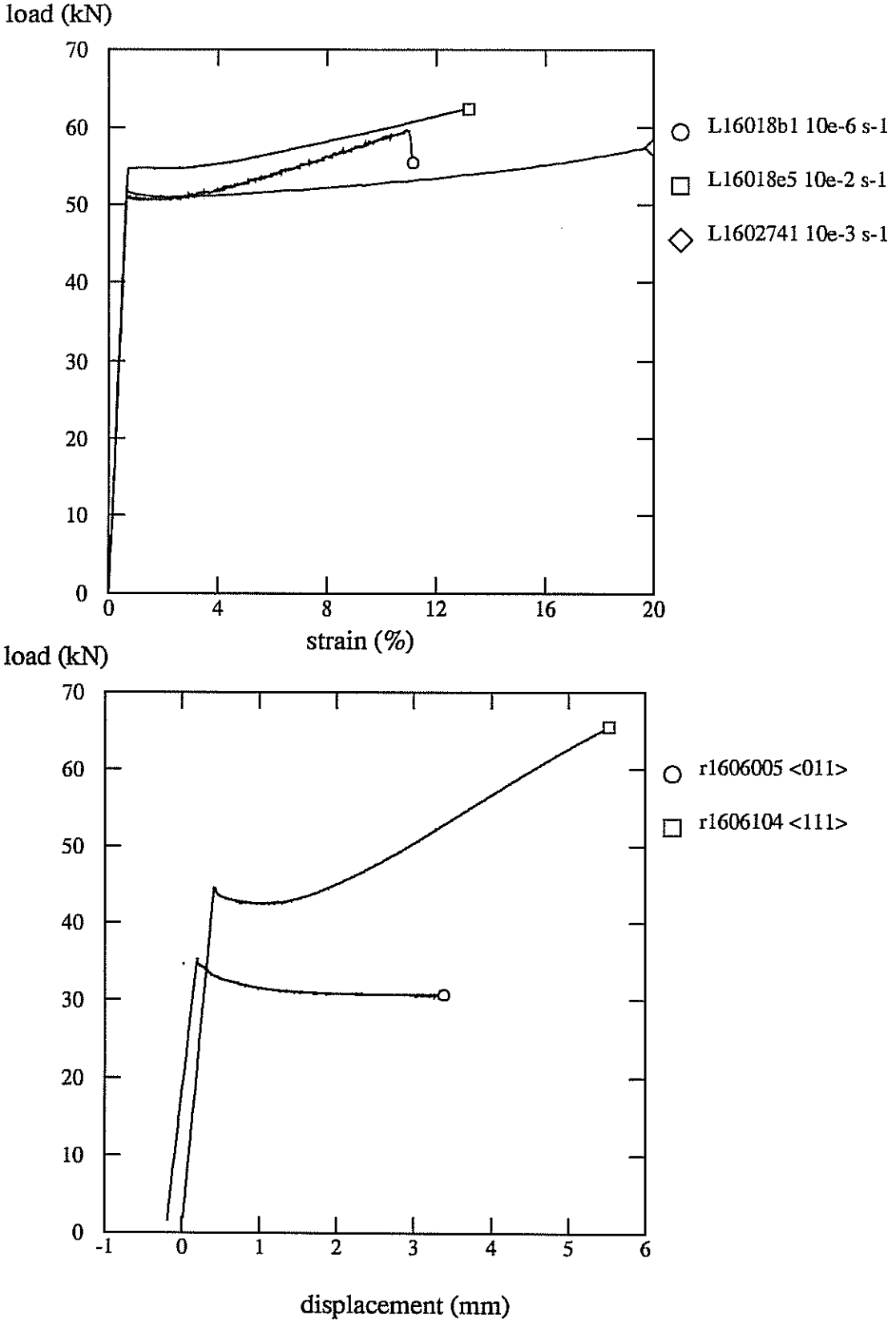

Figures D.11 and D.12: Tensile tests on <001> (above), near-<011> and near-<111> (below) SC15 specimens; the specimen diameters were 9 mm (above) and 8 mm (below).

Figure D.13: Slip bands on a near-< 011 > tensile specimen. The traces have been identified and belong to a single octahedral slip system.

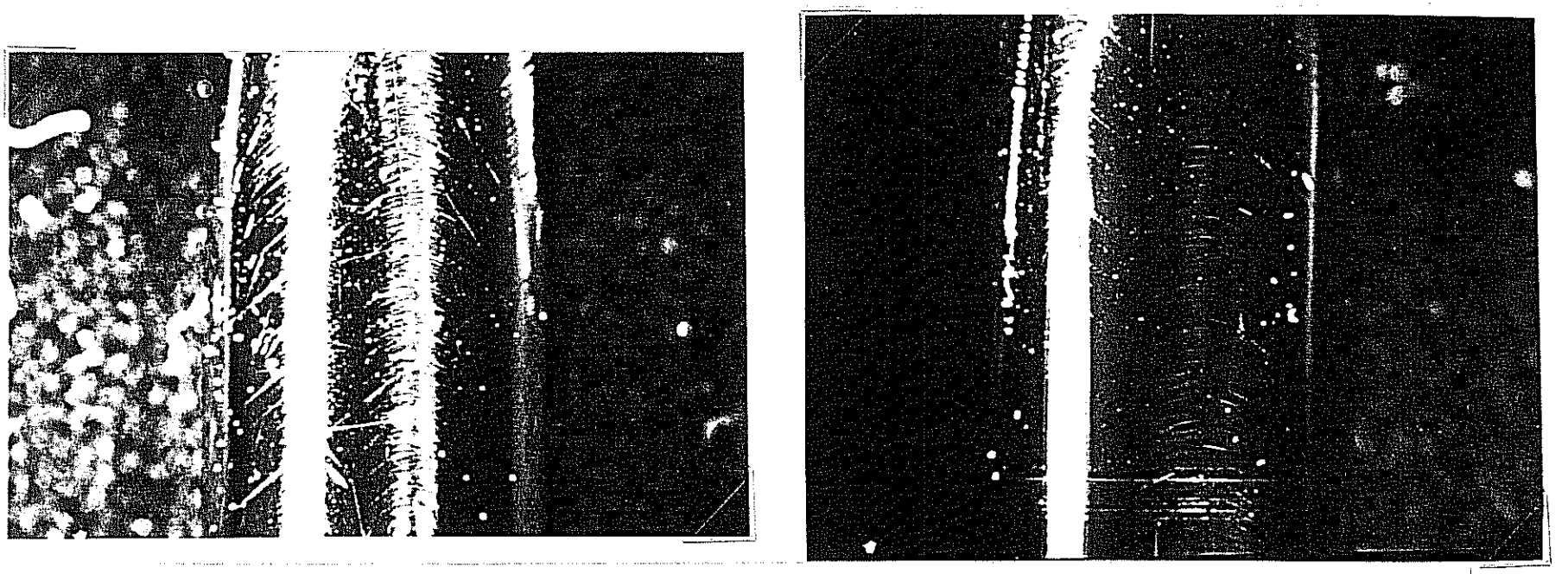

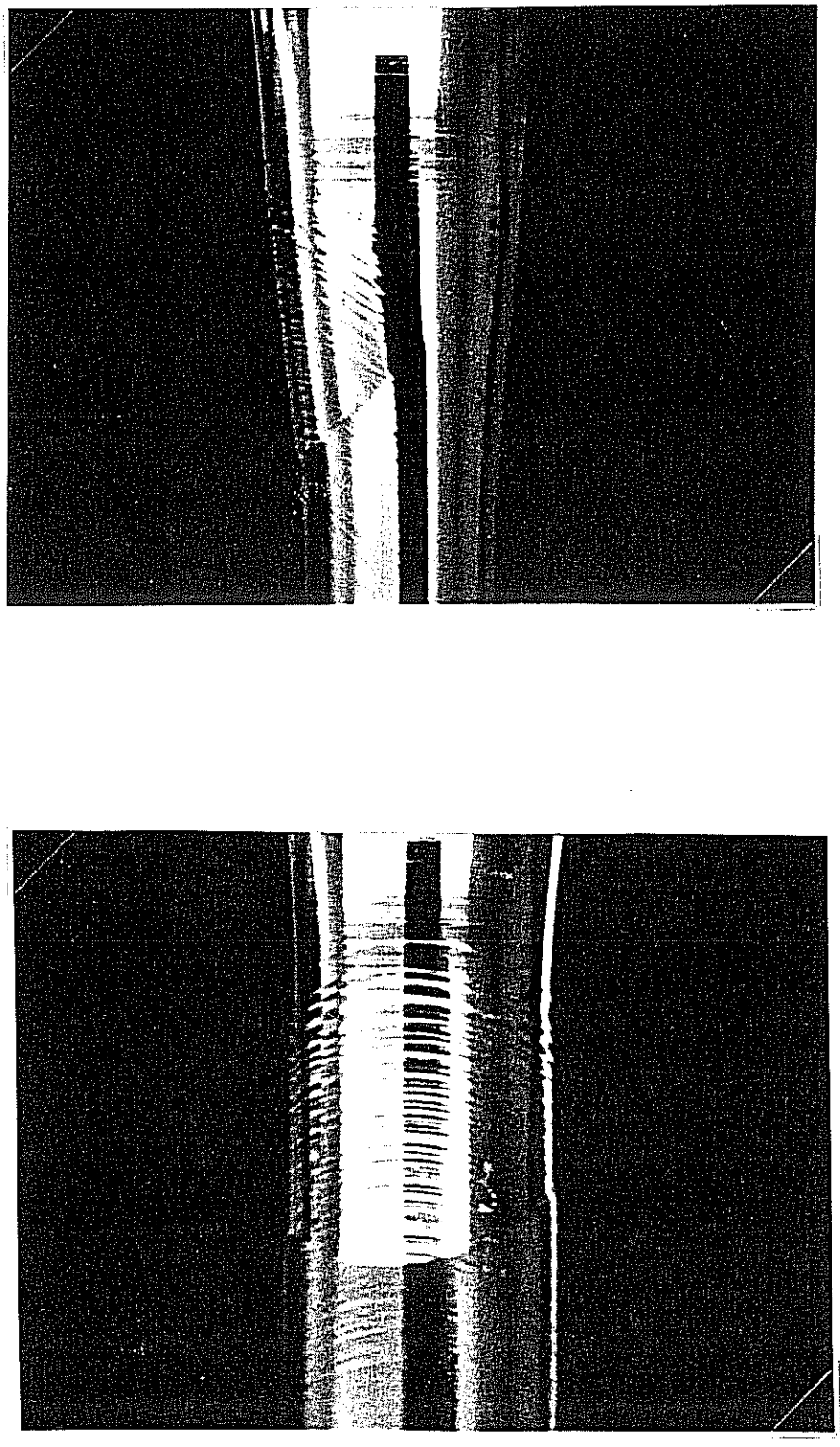

Figure D.14: Slip band propagation in a near-$< 011 >$ tensile specimen: two views of the initiation zone. Slip bands have propagated in the flattened zone.

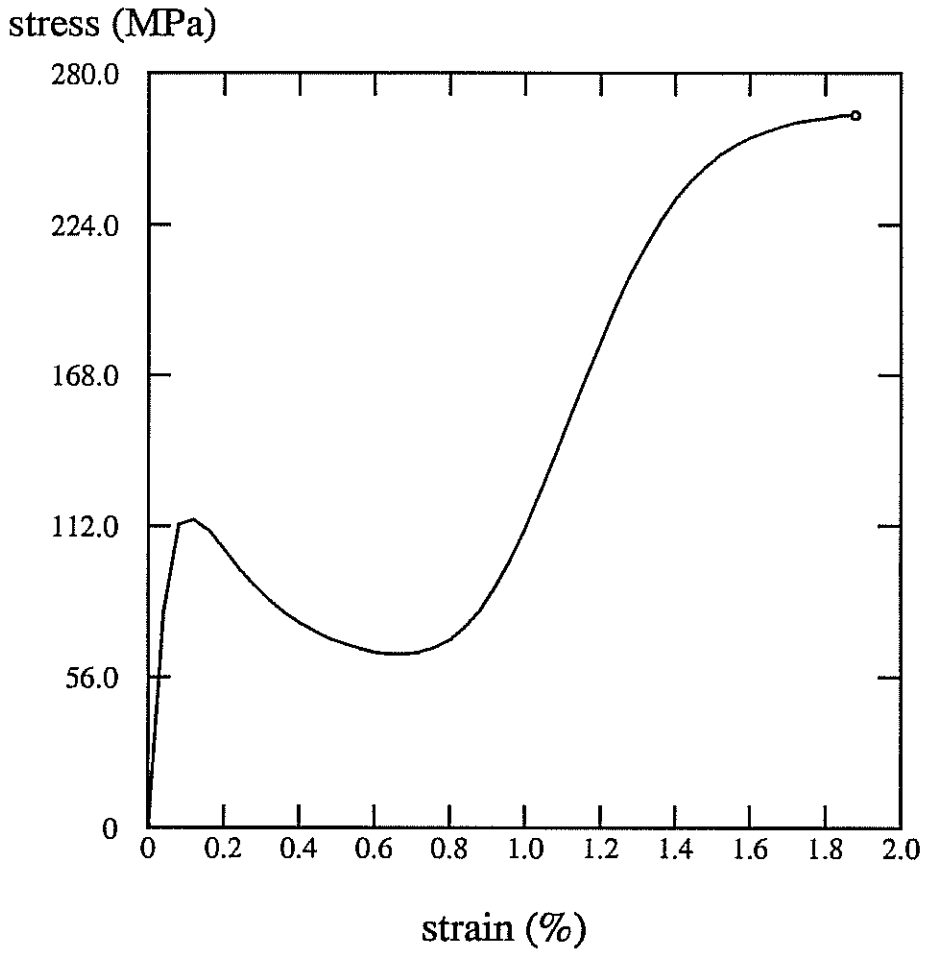

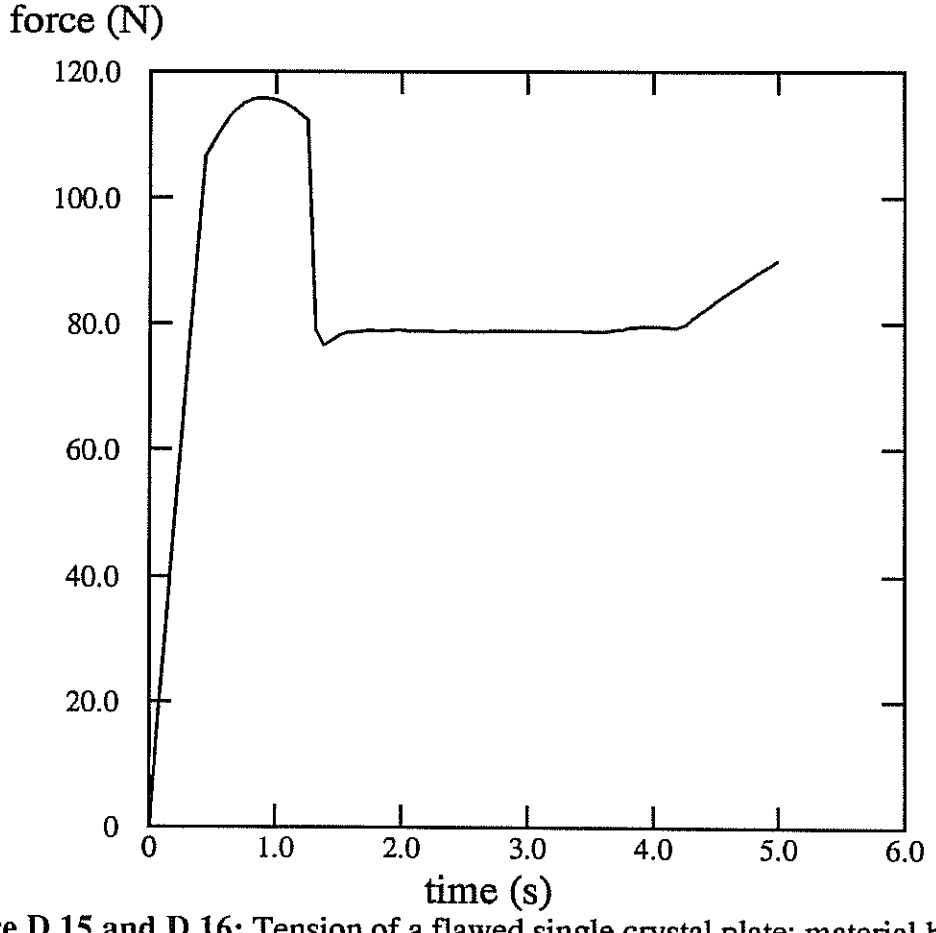

Figure D.15 and D.16: Tension of a flawed single crystal plate: material behaviour (above), load-displacement curve of the tension test (below).

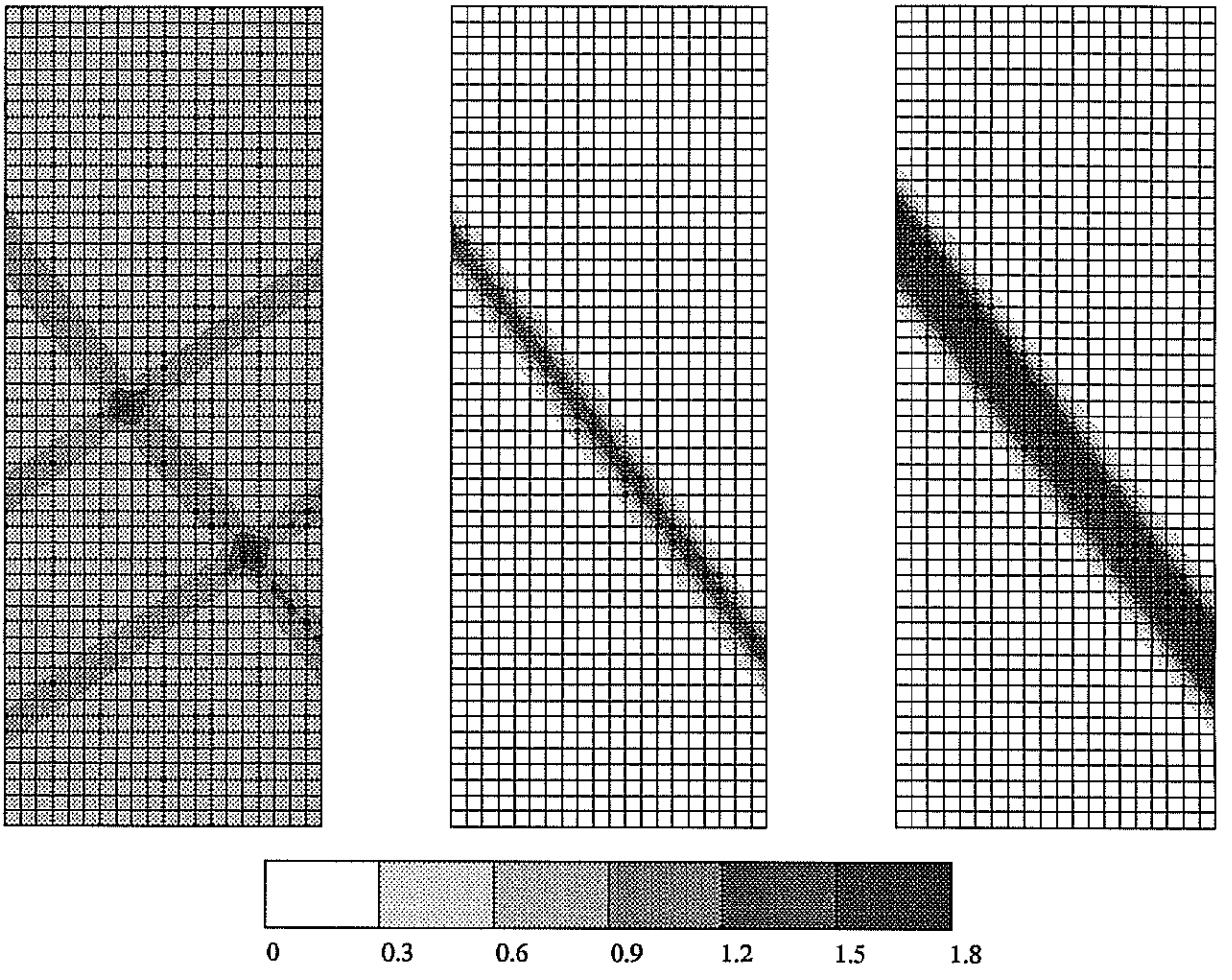

Figure D.17

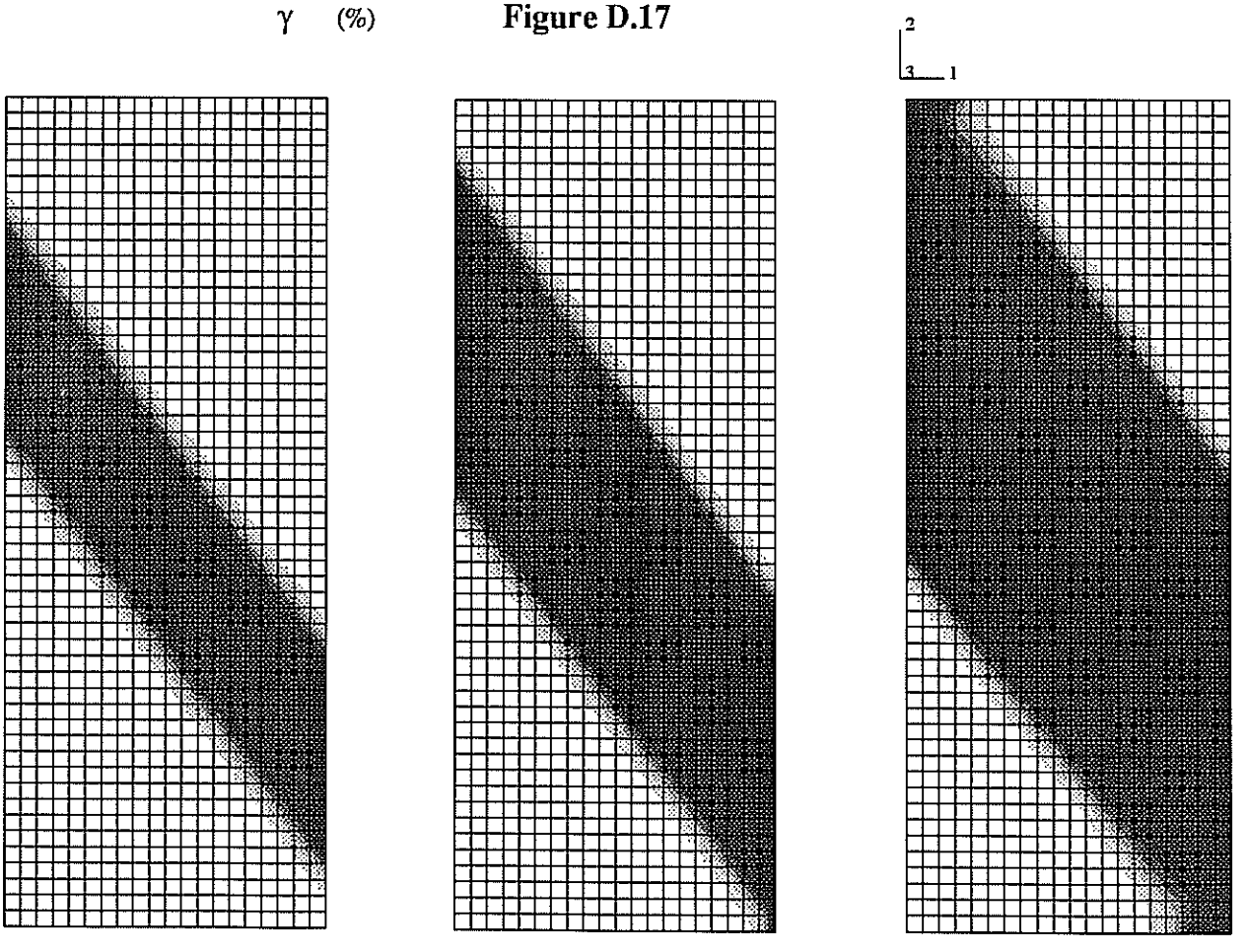

Figure D.18: Simulation of slip band propagation.

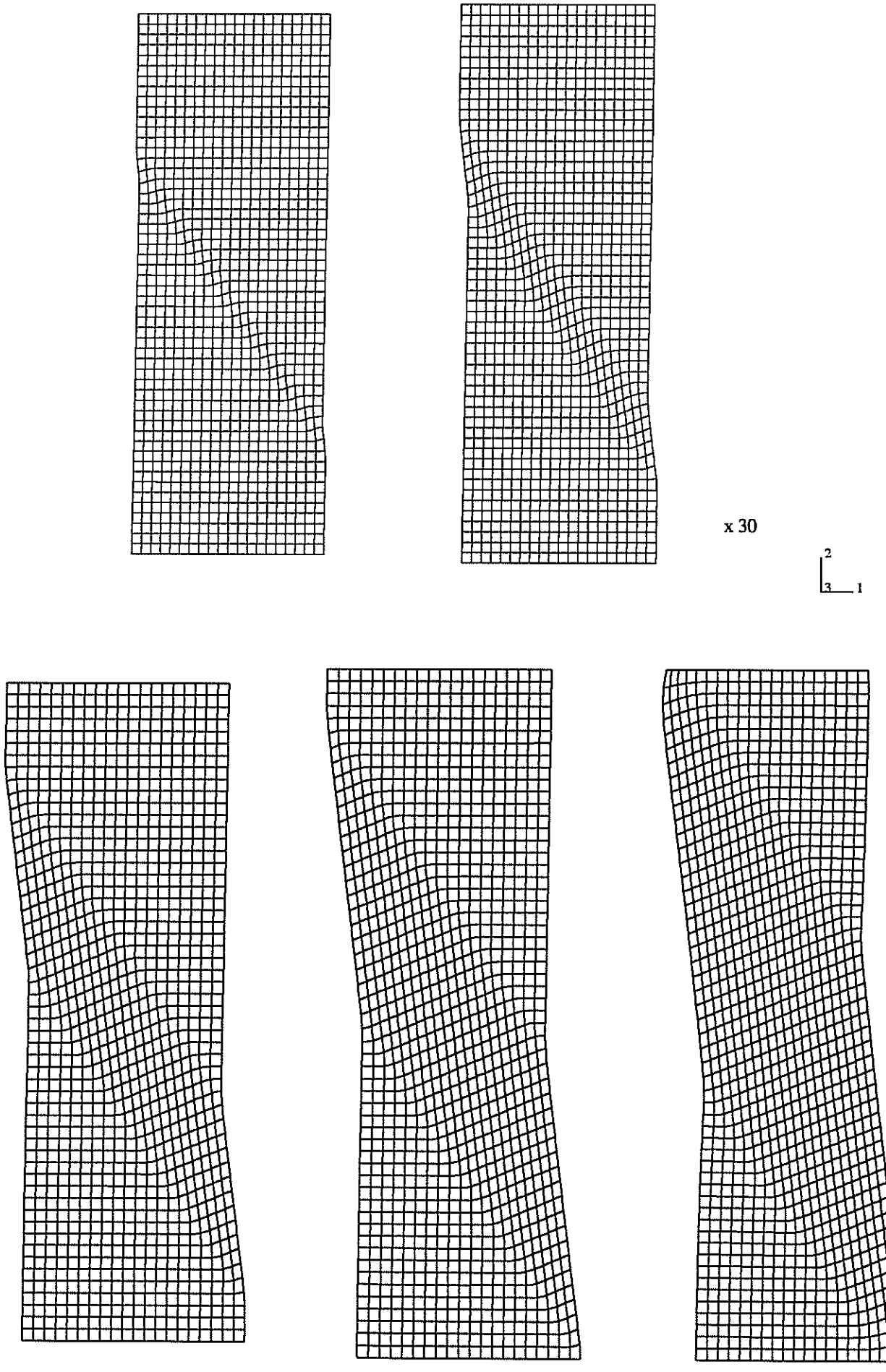

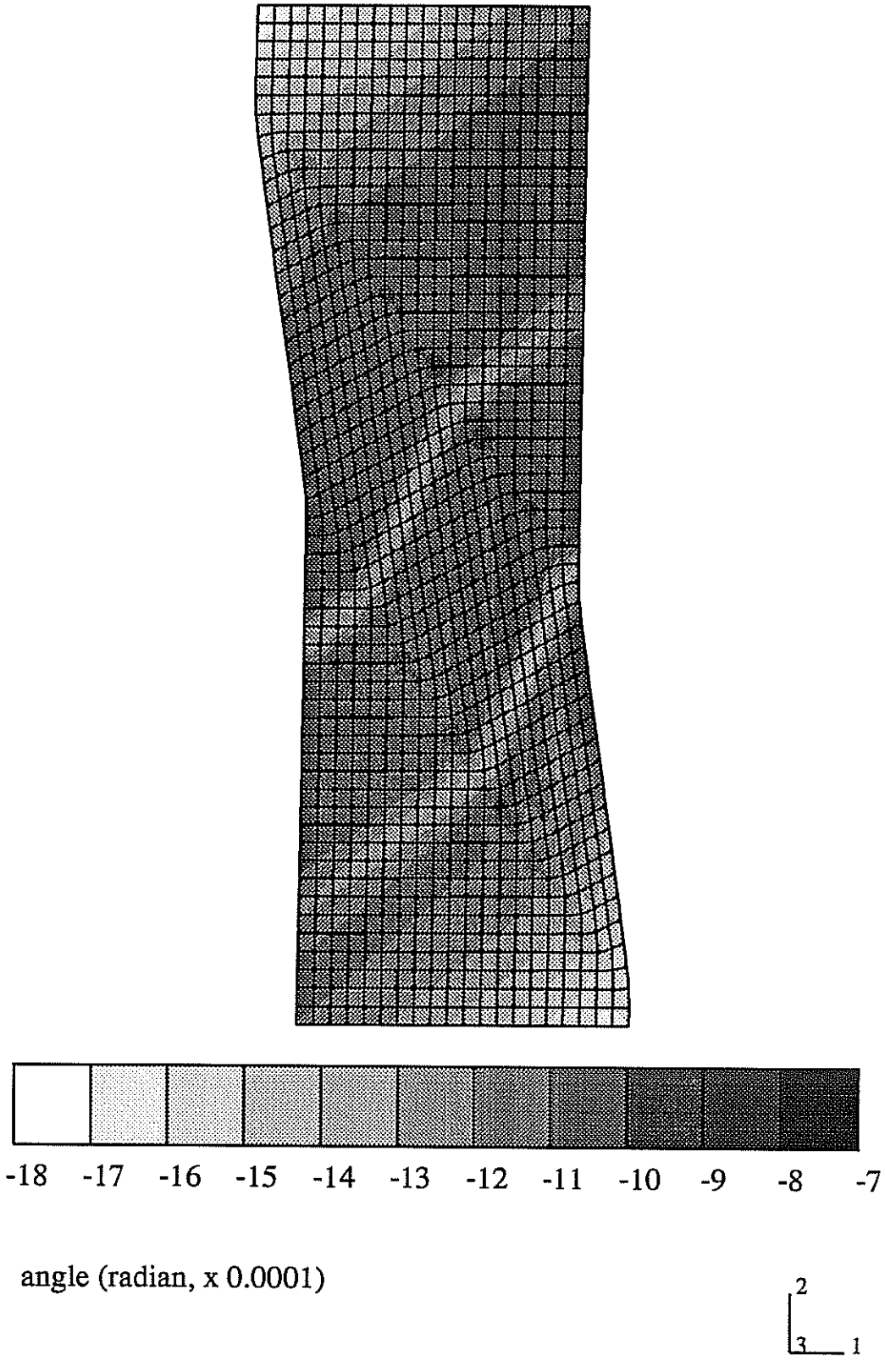

Figure D.19: Lattice rotation with respect to axis 3 during slip band propagation.

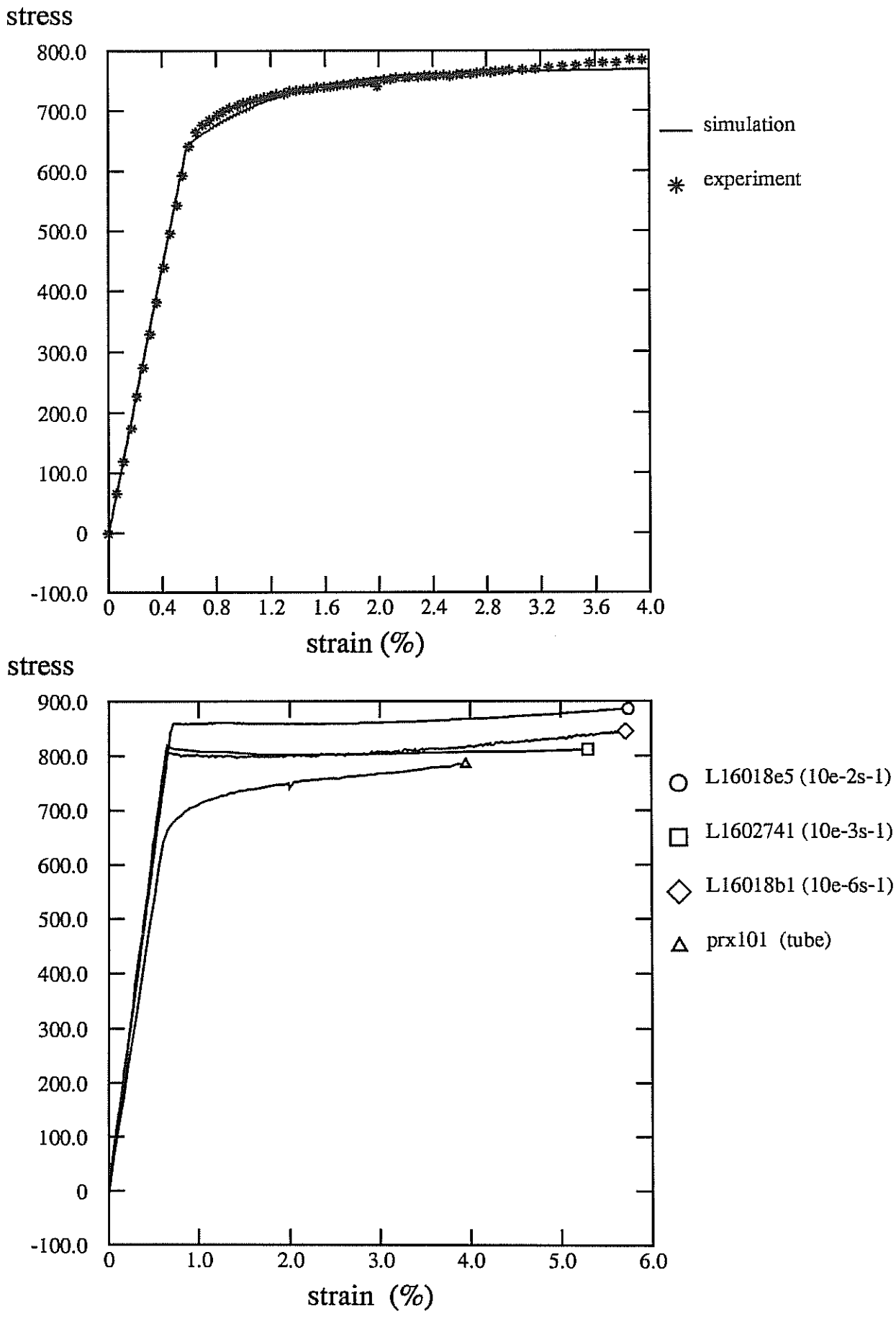

Figure D.20 and D.21: Identification of the material behaviour of <001> SC16 in tension at room temperature (above); comparison between the tensile behaviour of full specimens and tubes.

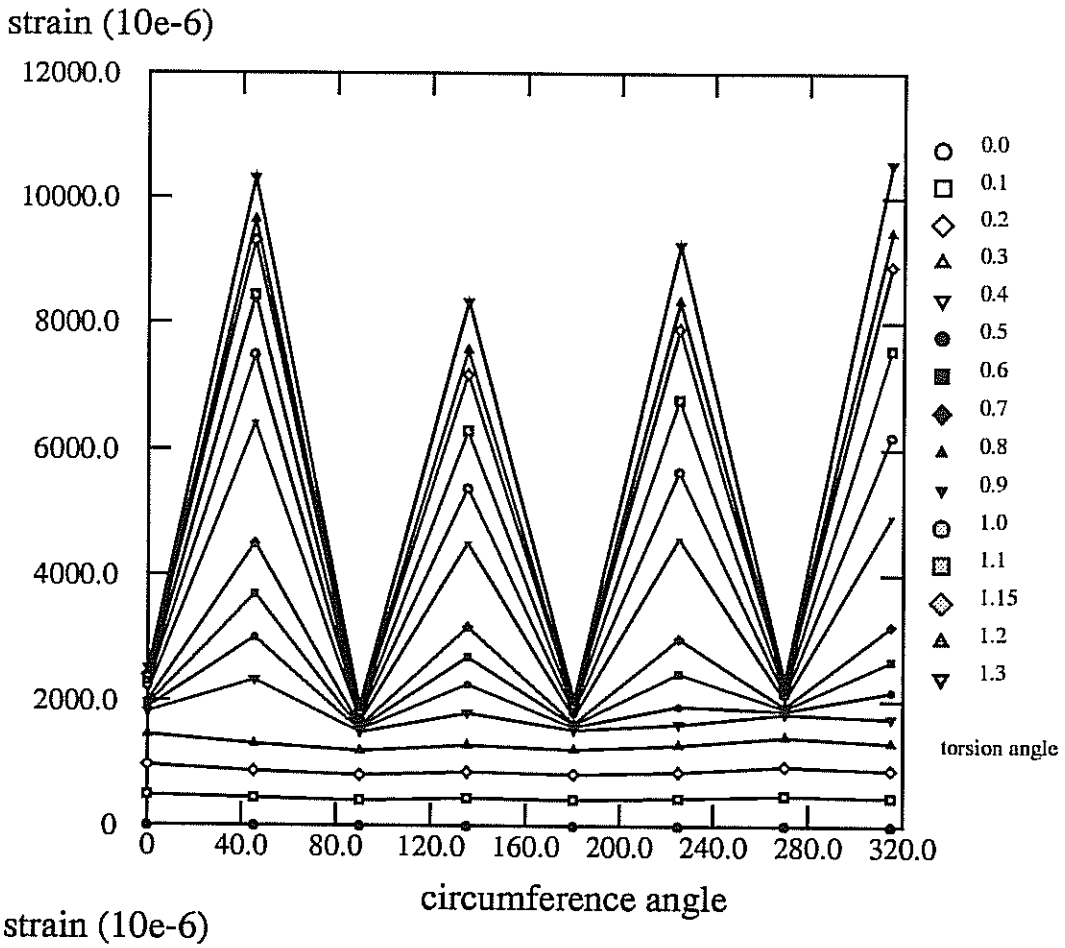

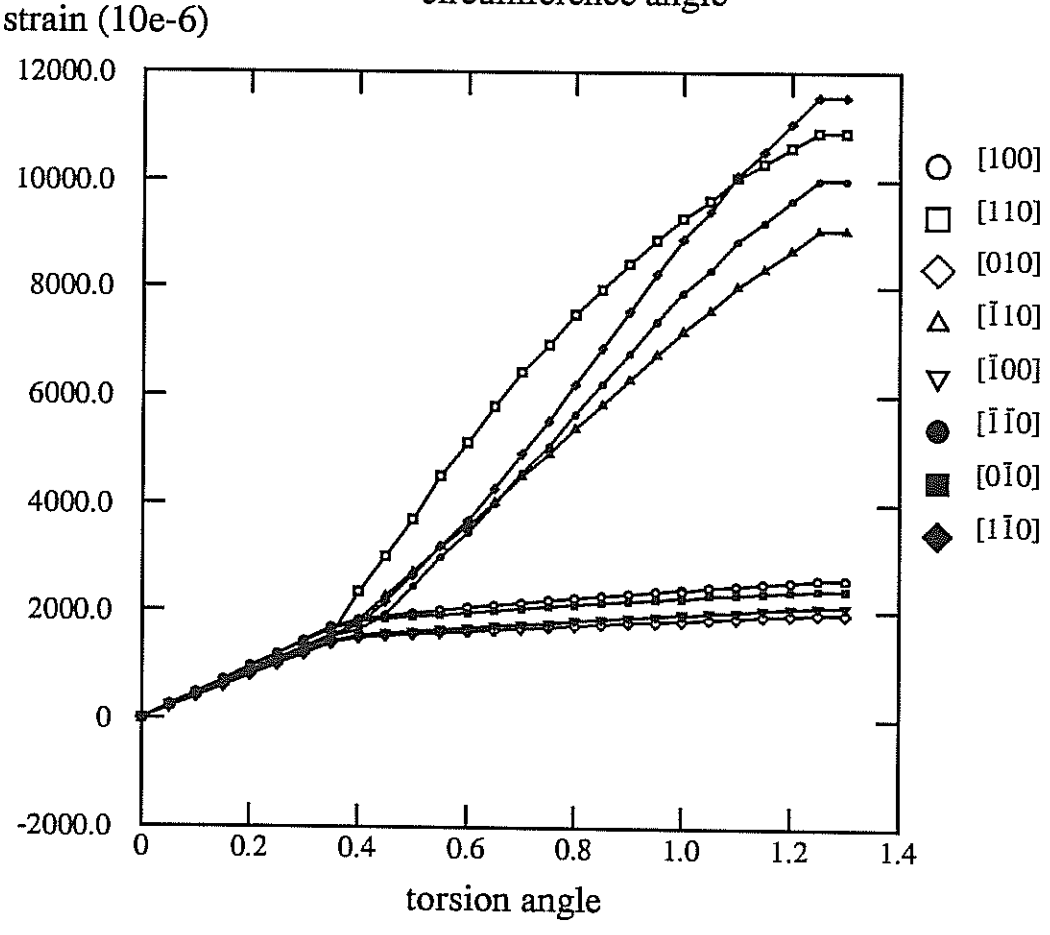

Figures D.22 and D.23: Local strain measurements for a torsion on a <001> SC16 specimen; load-displacement curve of the tension test (below).

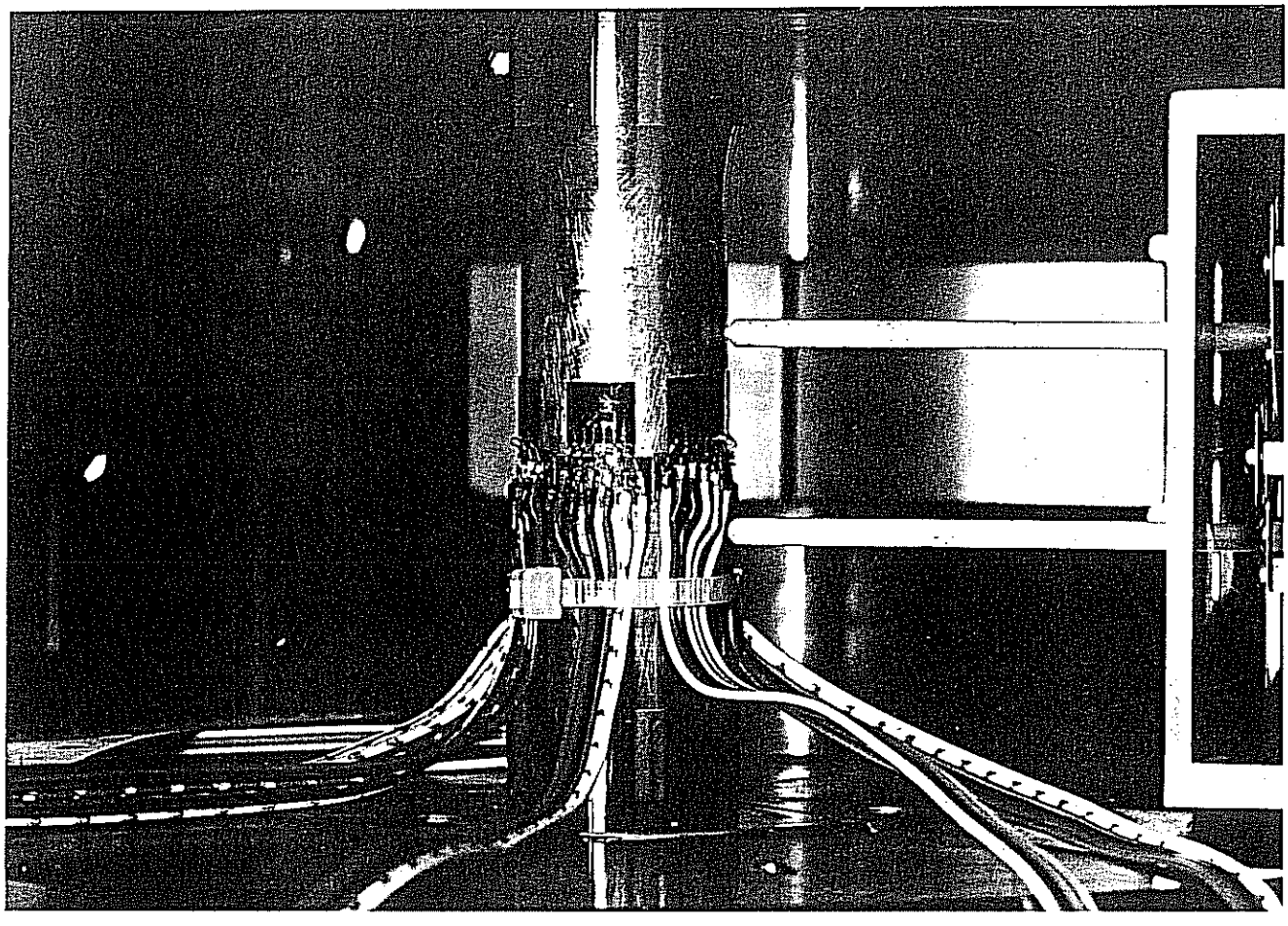

Figure D.22bis: Extensometer and rosettes for a torsion test on single crystal superalloy SC16 with local strain measurements.

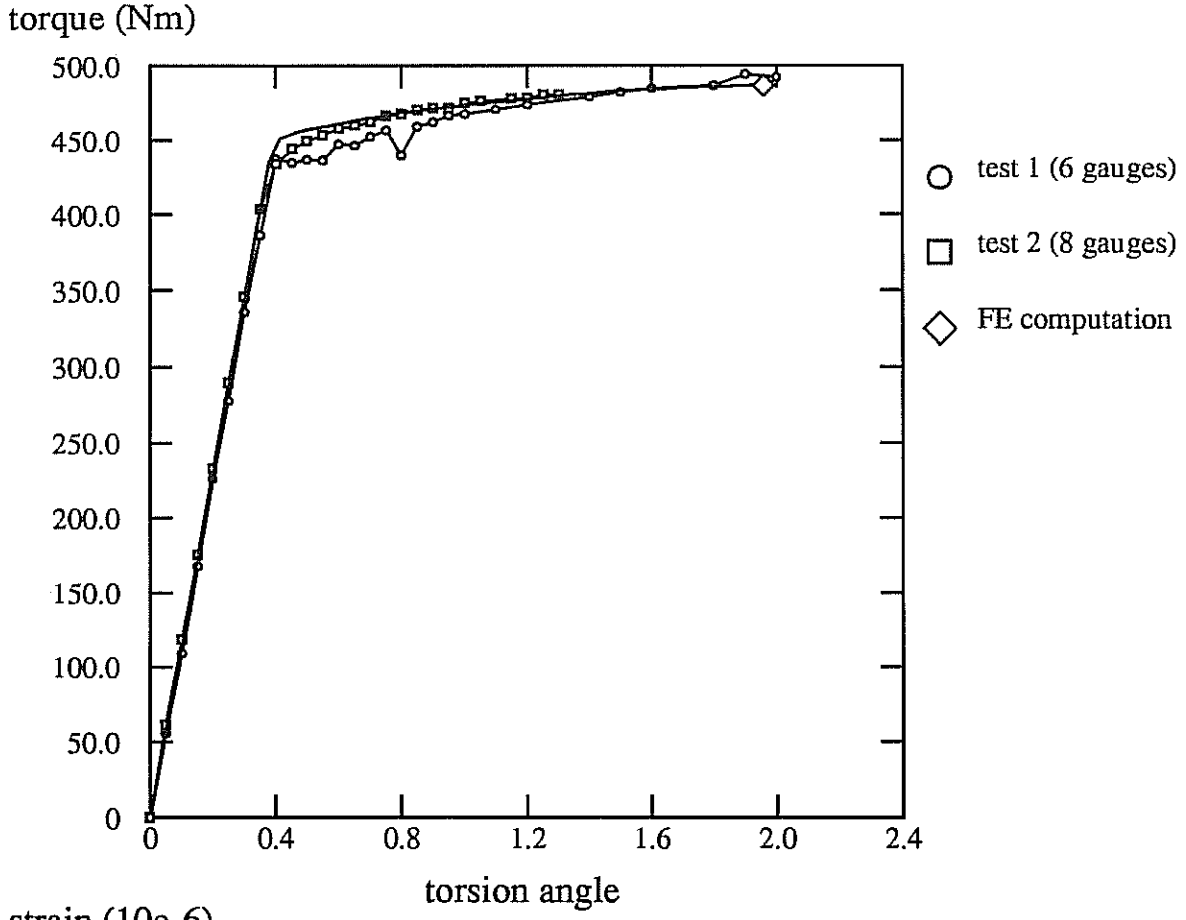

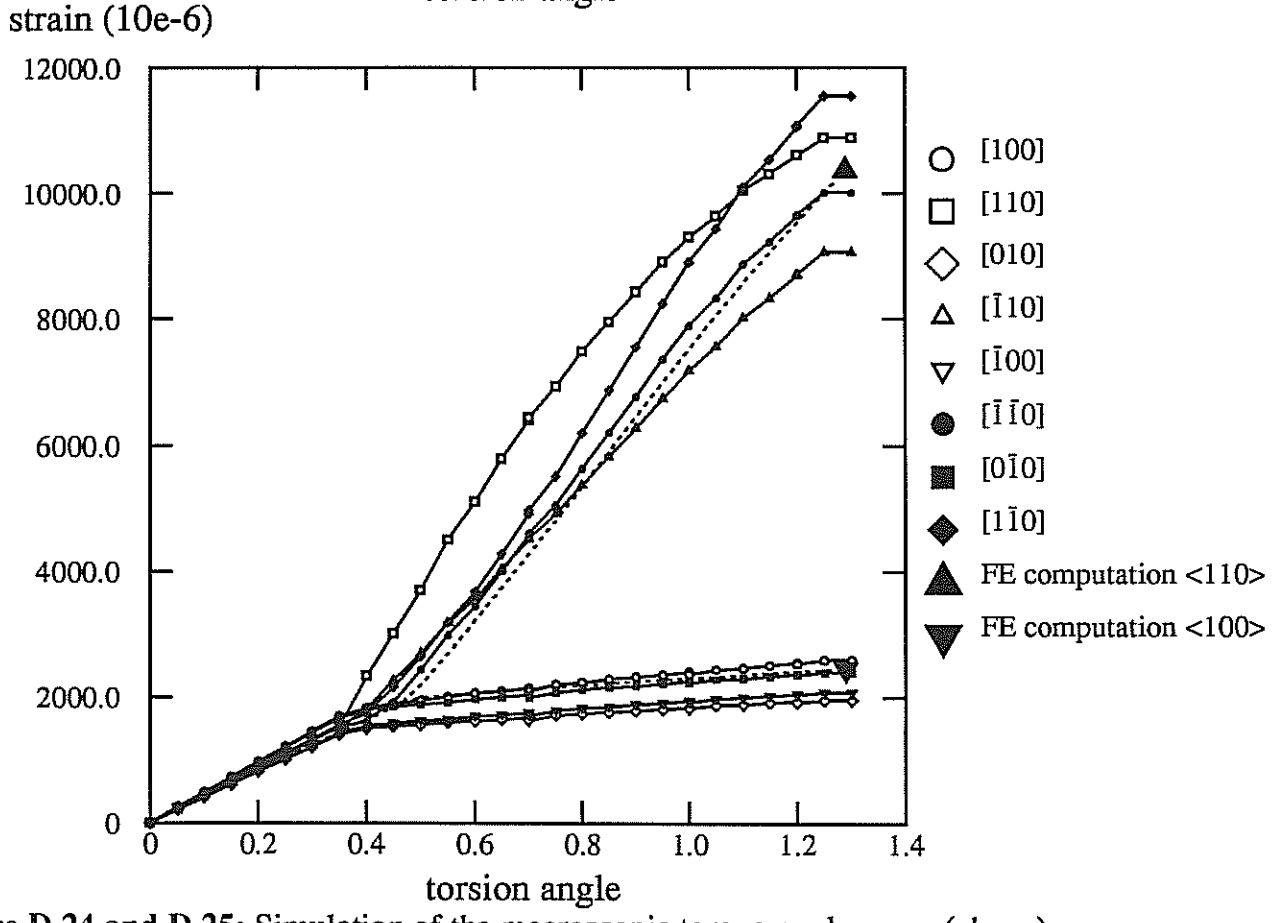

Figure D.24 and D.25: Simulation of the macroscopic torque-angle curve (above); local prediction of the model (below).

Figure D.26:
Torsion test on a <001> SC16 specimen.

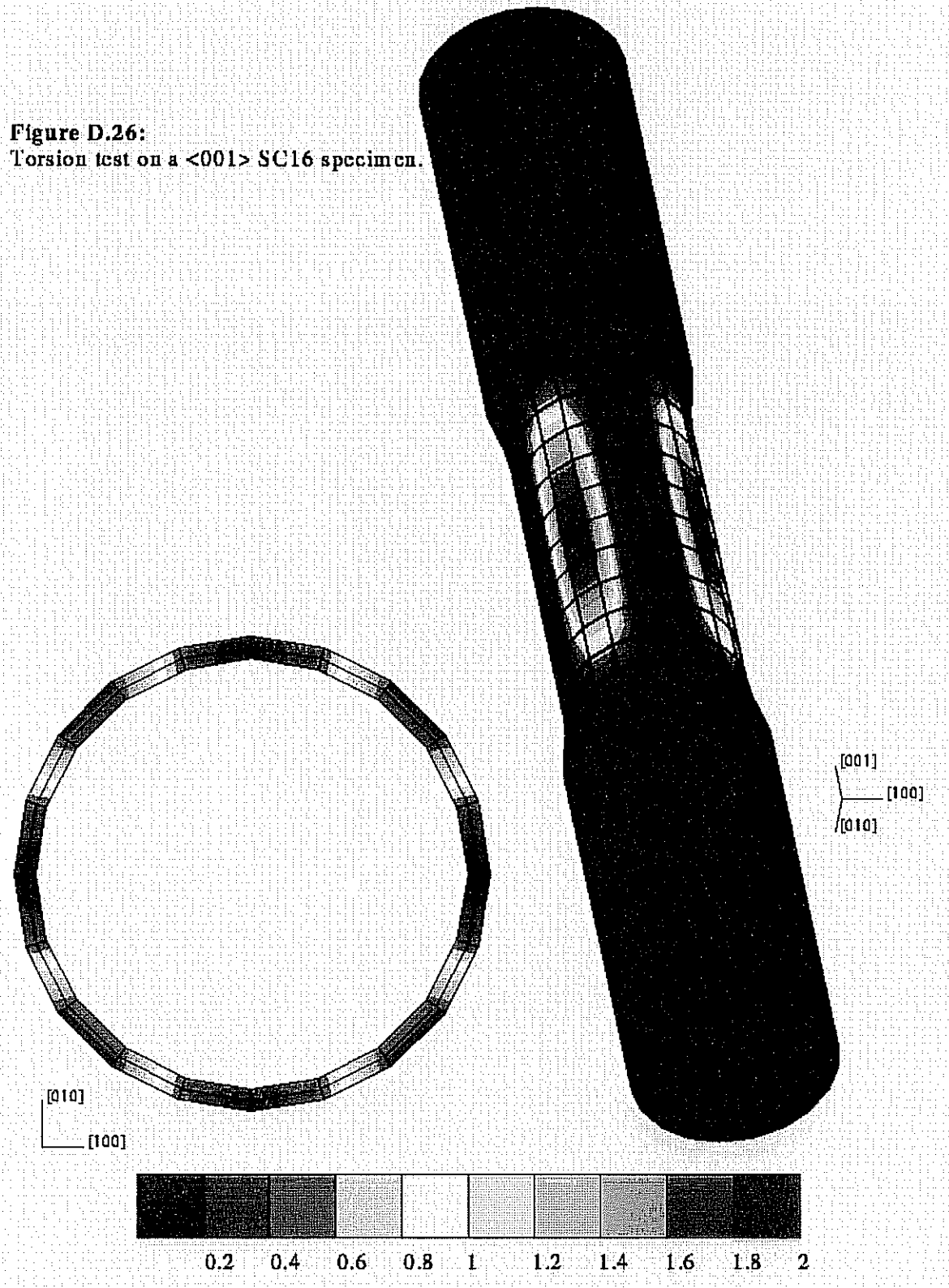

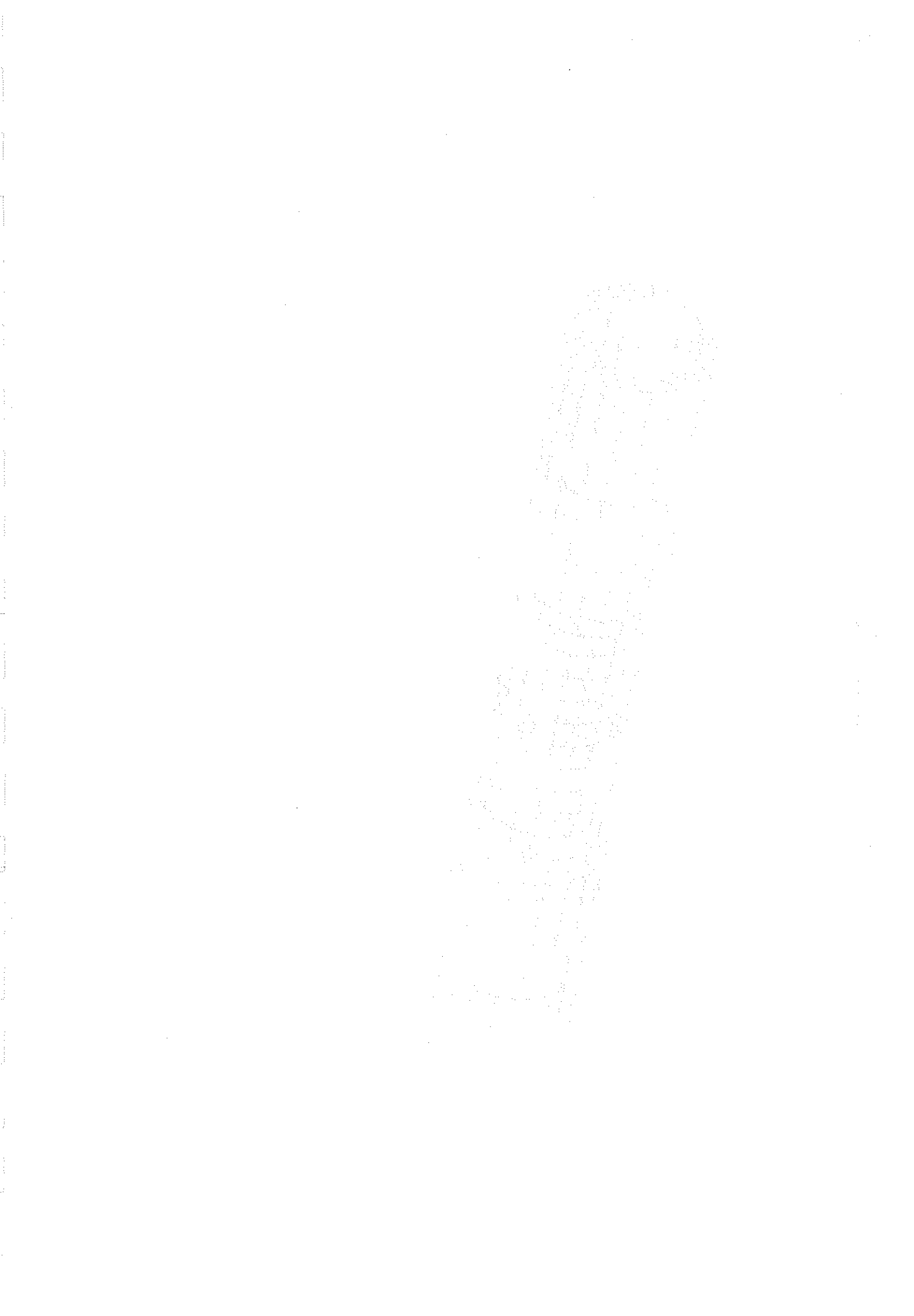

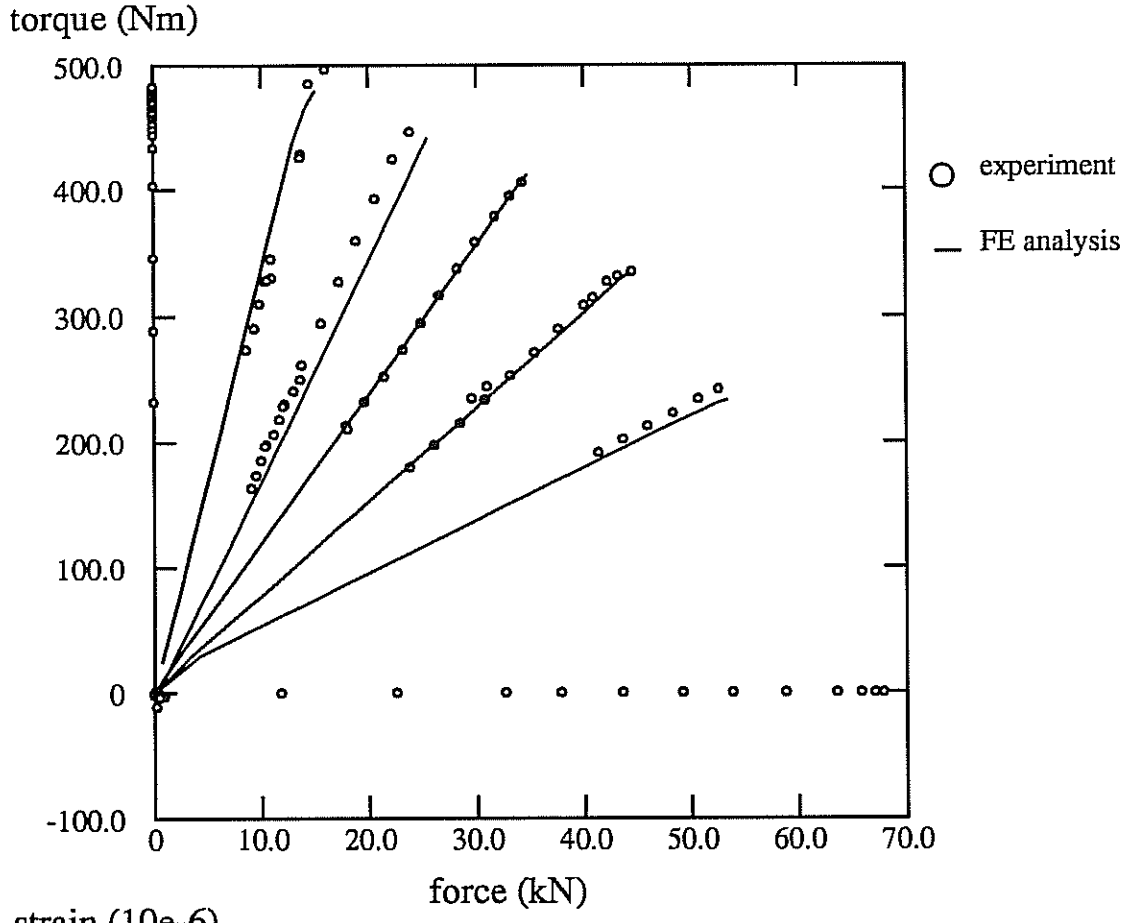

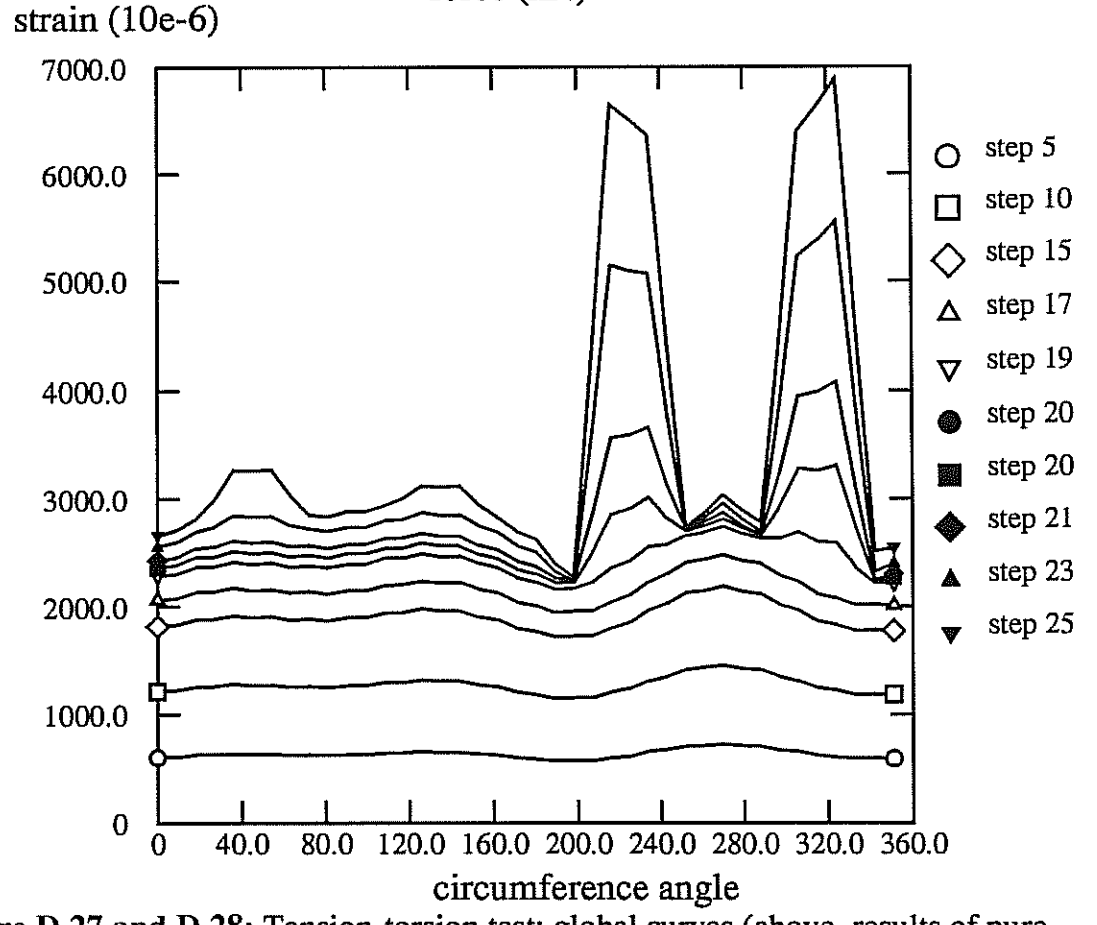

Figure D.27 and D.28: Tension-torsion test: global curves (above, results of pure tension and torsion have been plotted also); apparition of localized deformation zones during the simulation of the first loading path of the tension-torsion test (below, angle 0 corresponds to a near-[100] direction).

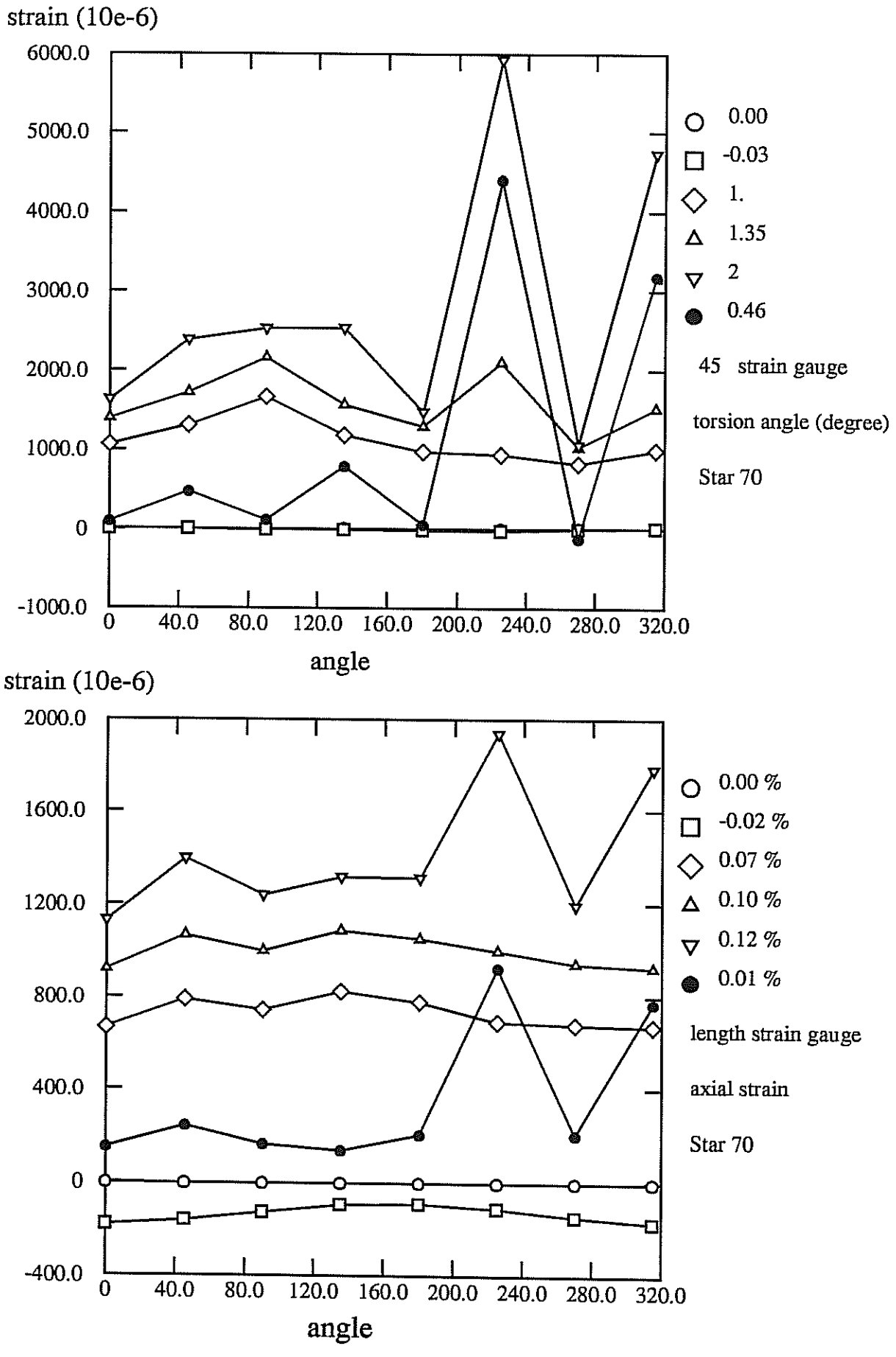

Figure D.29 : Tension-torsion test: local strain measurements (loading path at 70 deg.).

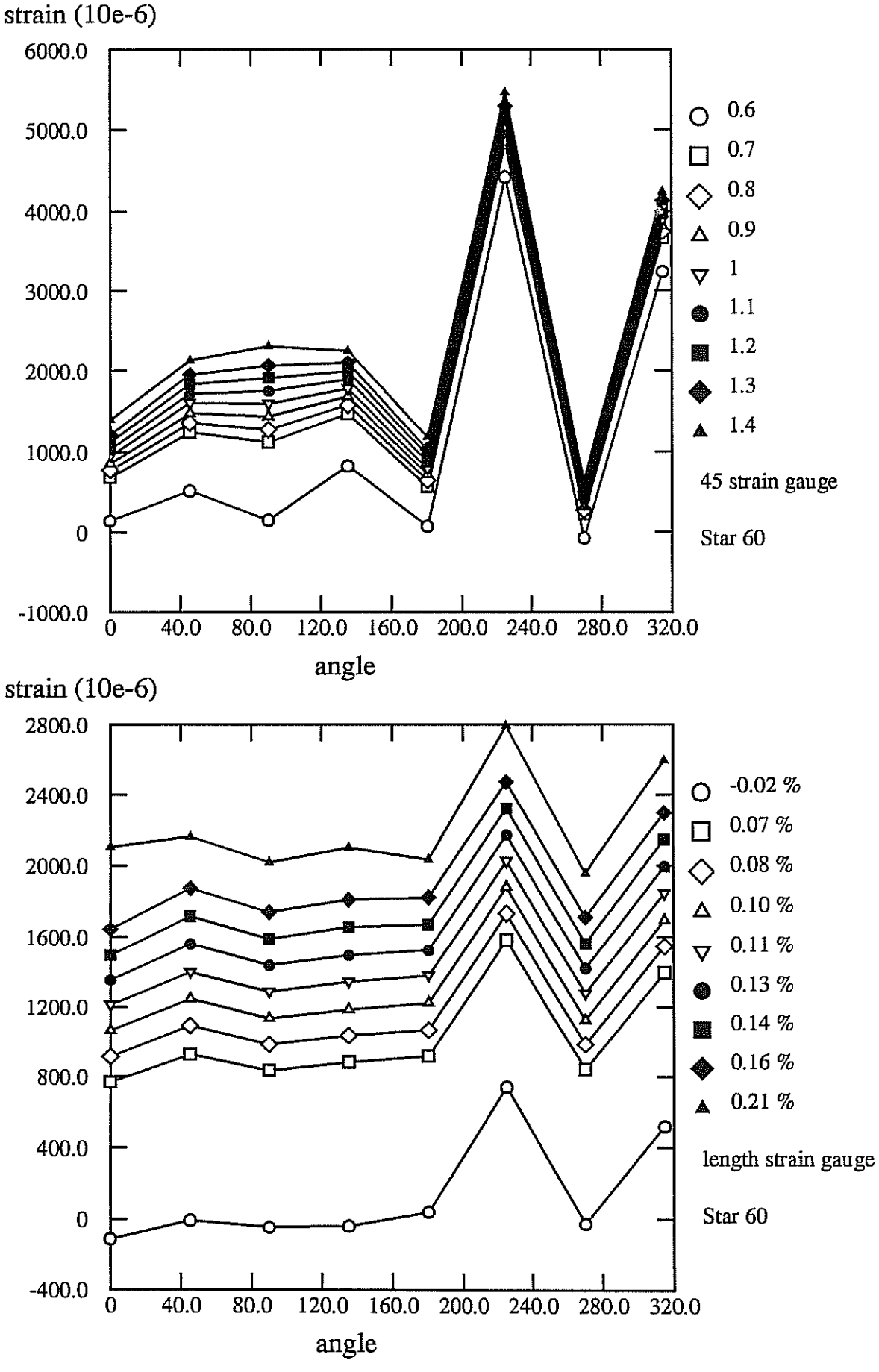

Figure D.30: Tension-torsion test: local strain measurements (loading path at 70 deg.) (loading path at 60 deg.).

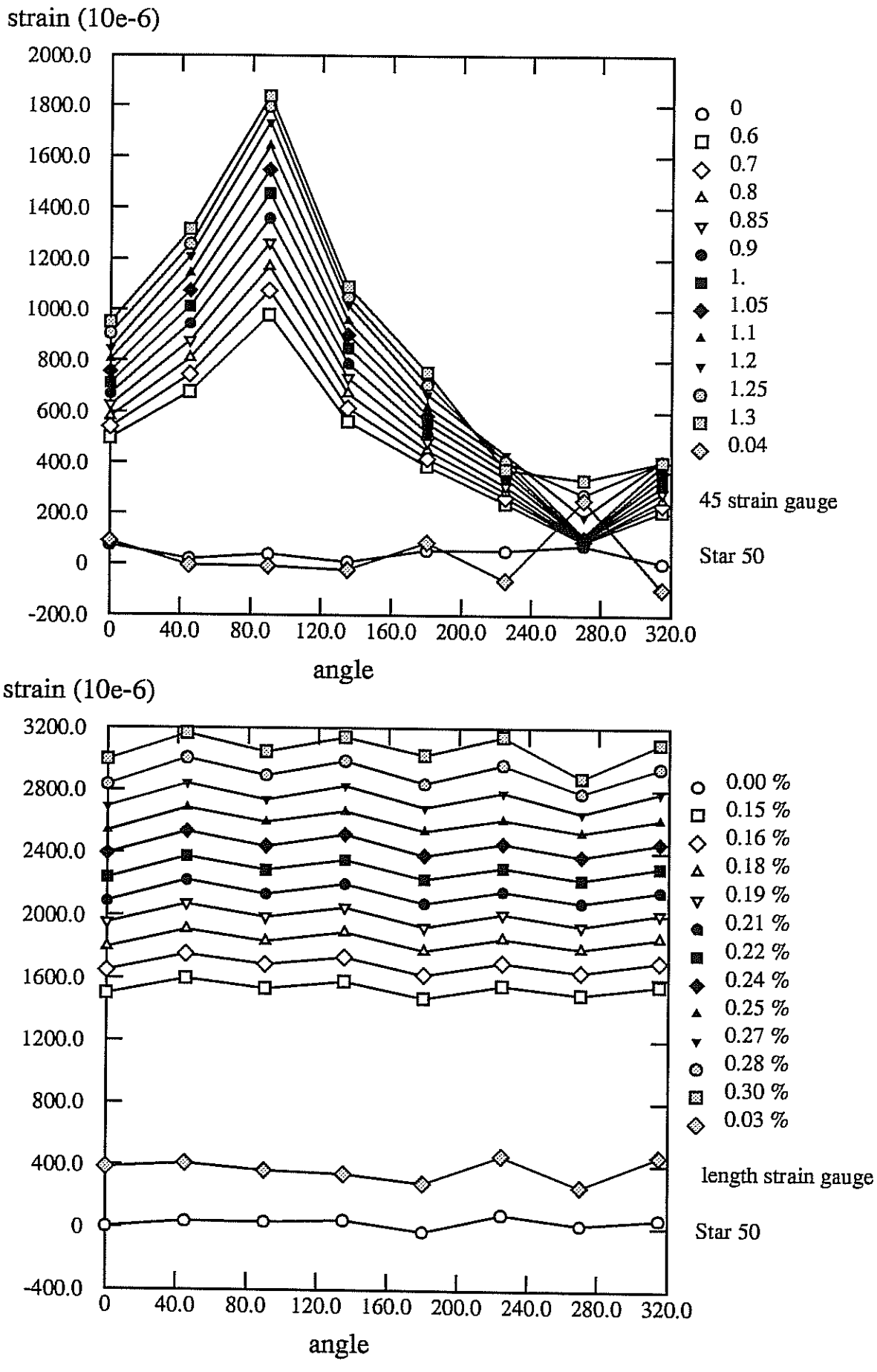

Figure D.31 : Tension-torsion test: local strain measurements (loading path at 50 deg.).

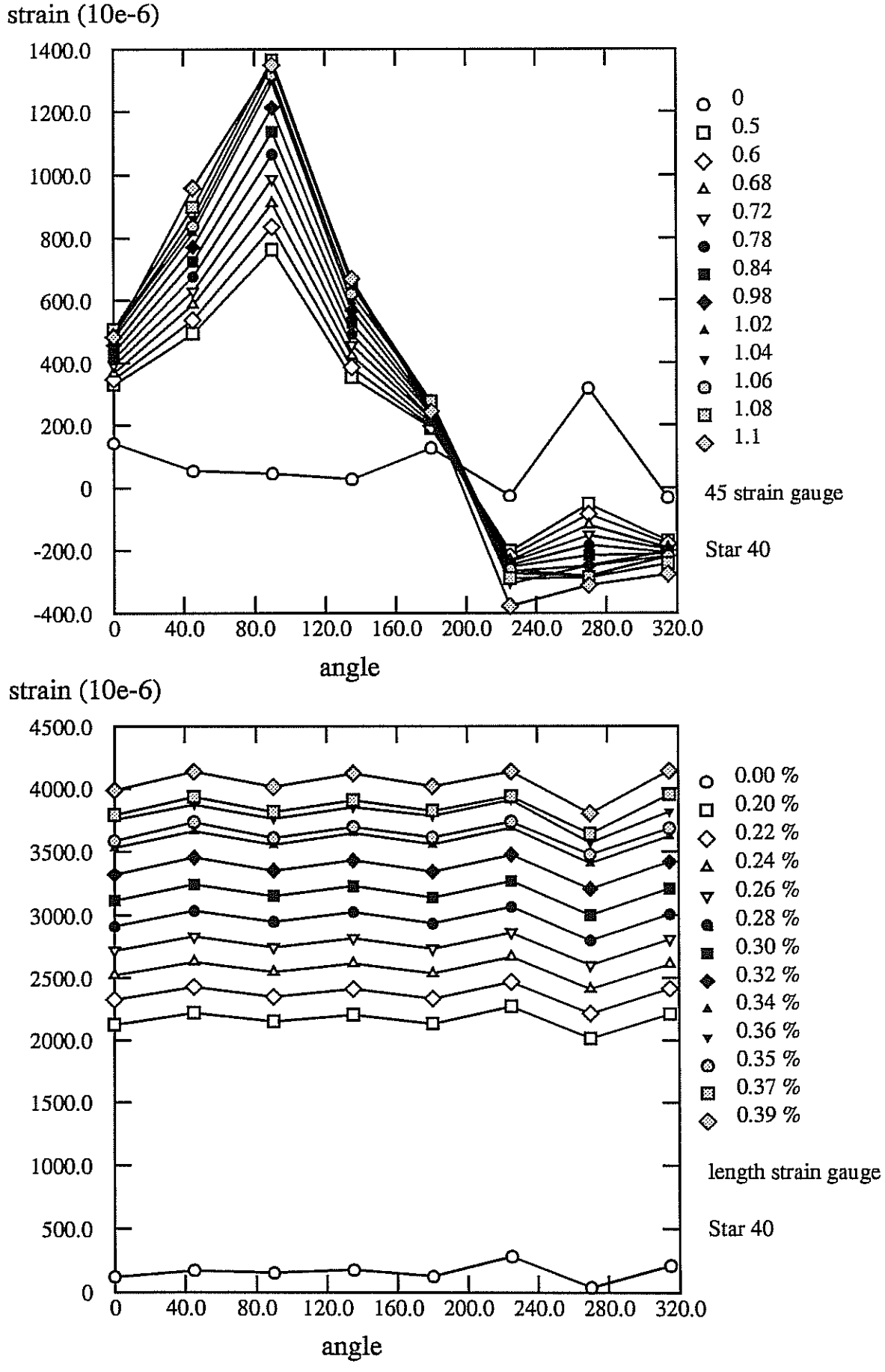

Figure D.32 : Tension-torsion test: local strain measurements (loading path at 40 deg.).

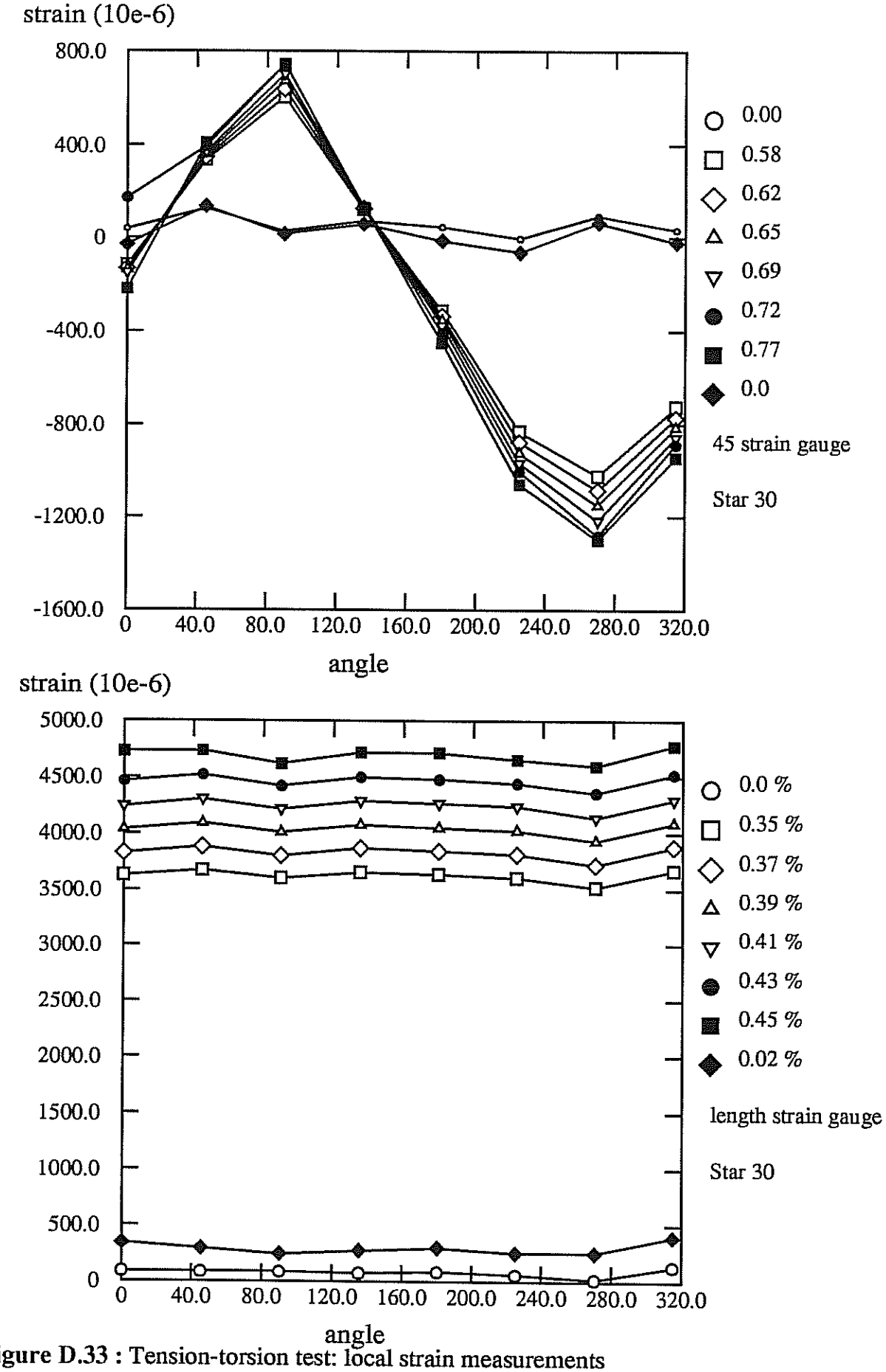

Figure D.33 : Tension-torsion test: local strain measurements (loading path at 30 deg.).

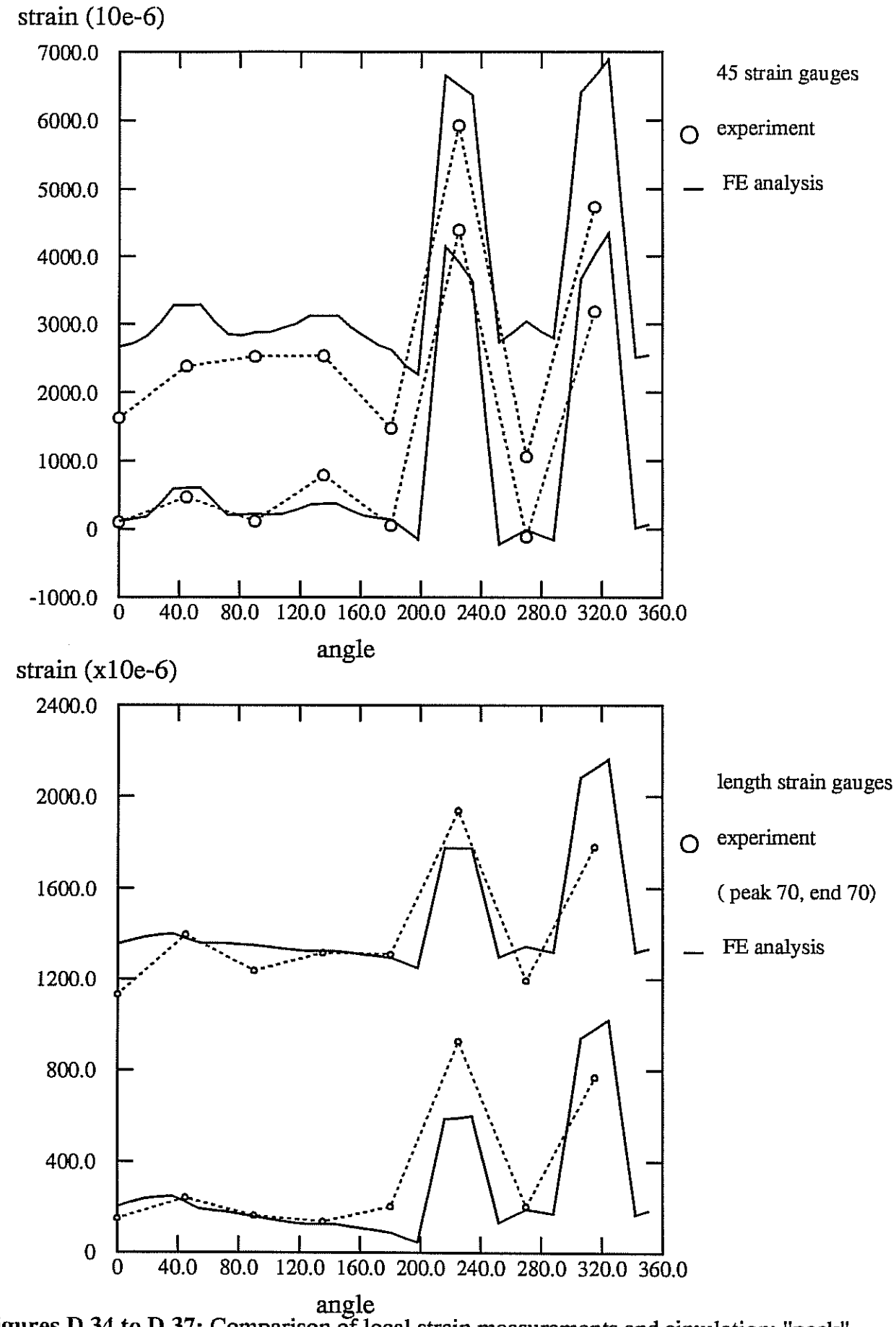

Figures D.34 to D.37: Comparison of local strain measurements and simulation; "peak" means the highest strain obtained for a given loading path and "end" means unloaded state after each loading branch.

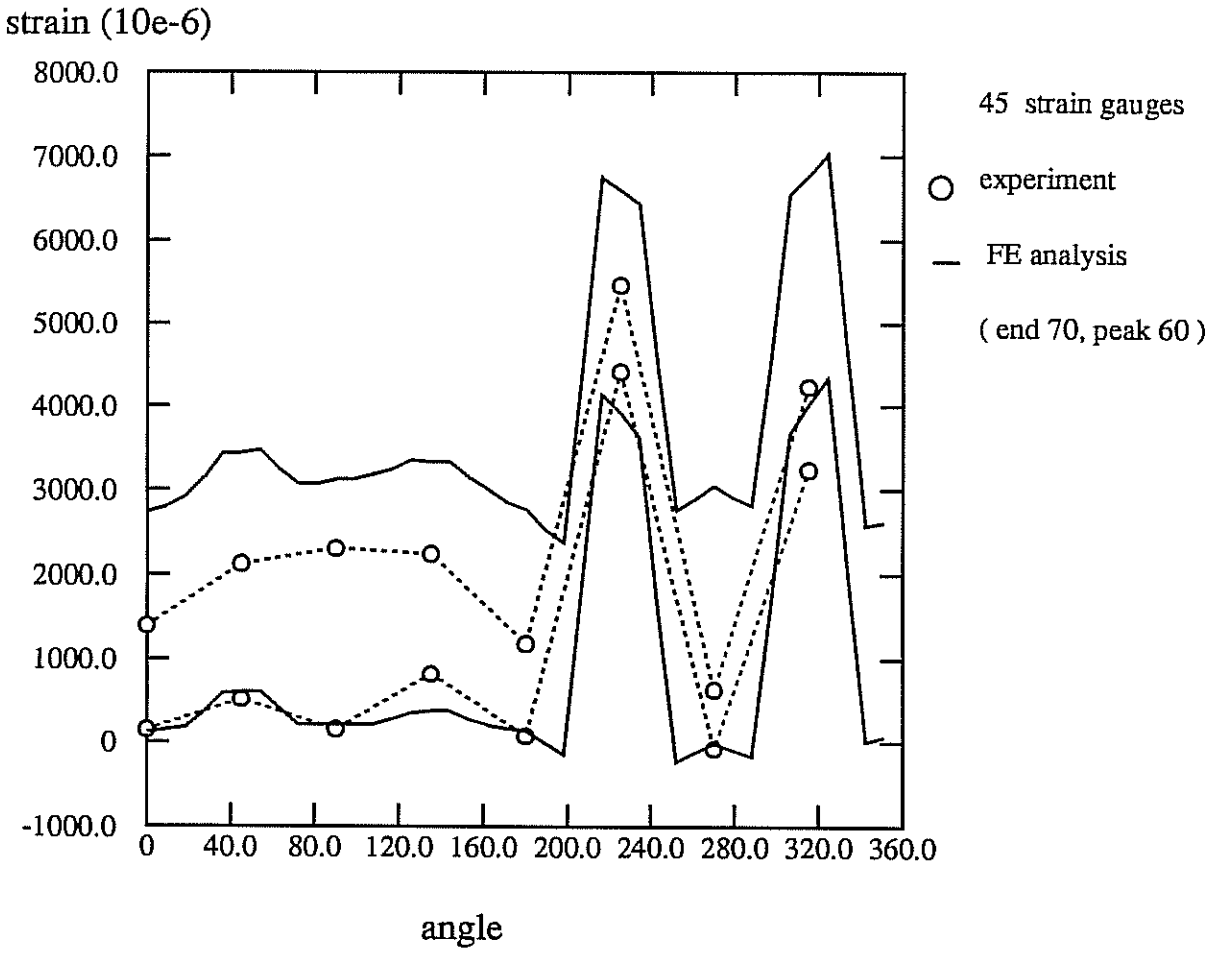
strain (10e-6)
8000.0
7000.0
6000.0
5000.0
4000.0
3000.0
2000.0
1000.0
0
-1000.0
0
40.0
80.0
120.0
160.0
200.0
240.0
280.0
320.0
360.0
angle
45 strain gauges
experiment
FE analysis
(end 70, peak 60)

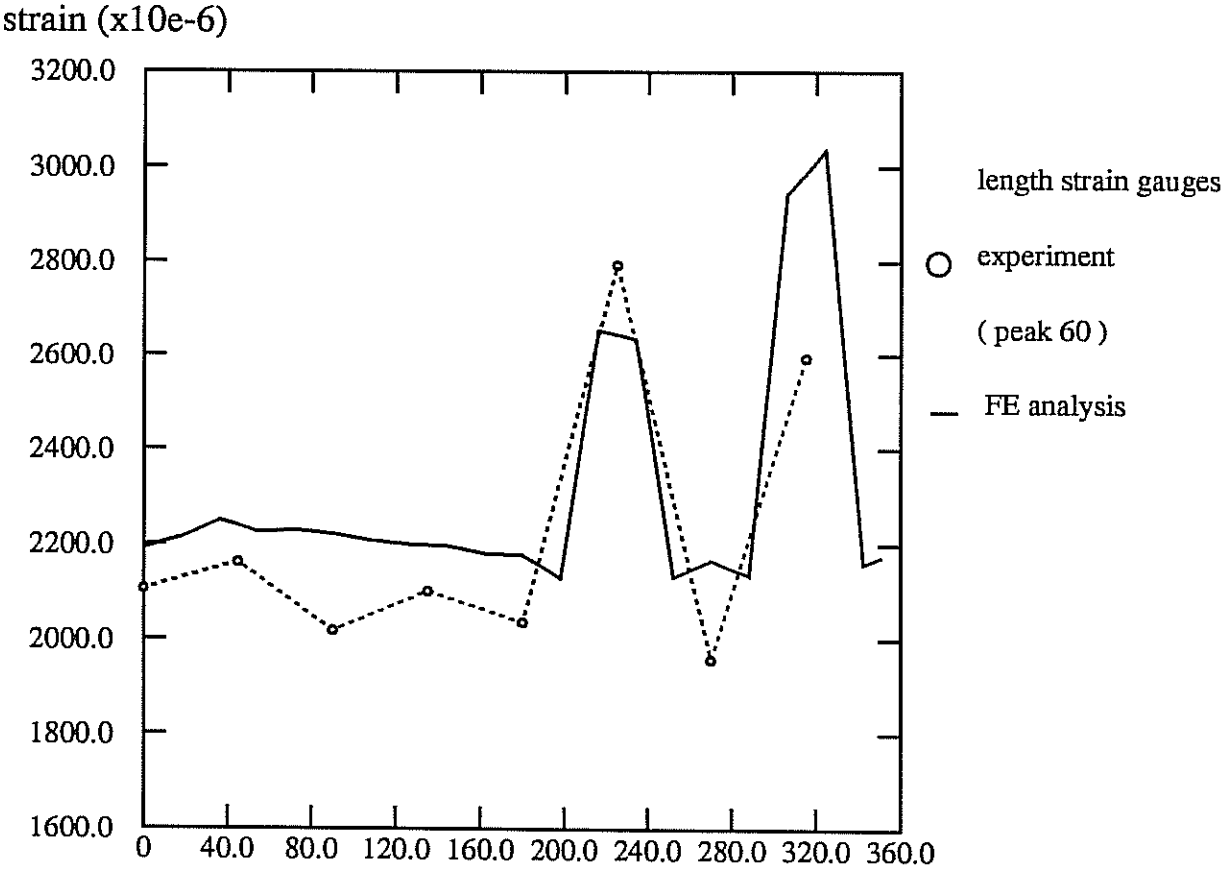
strain (x10e-6)
3200.0
3000.0
2800.0
2600.0
2400.0
2200.0
2000.0
1800.0
1600.0
0
40.0
80.0
120.0
160.0
200.0
240.0
280.0
320.0
360.0
angle
length strain gauges
experiment
(peak 60)
FE analysis

Figure D.35.

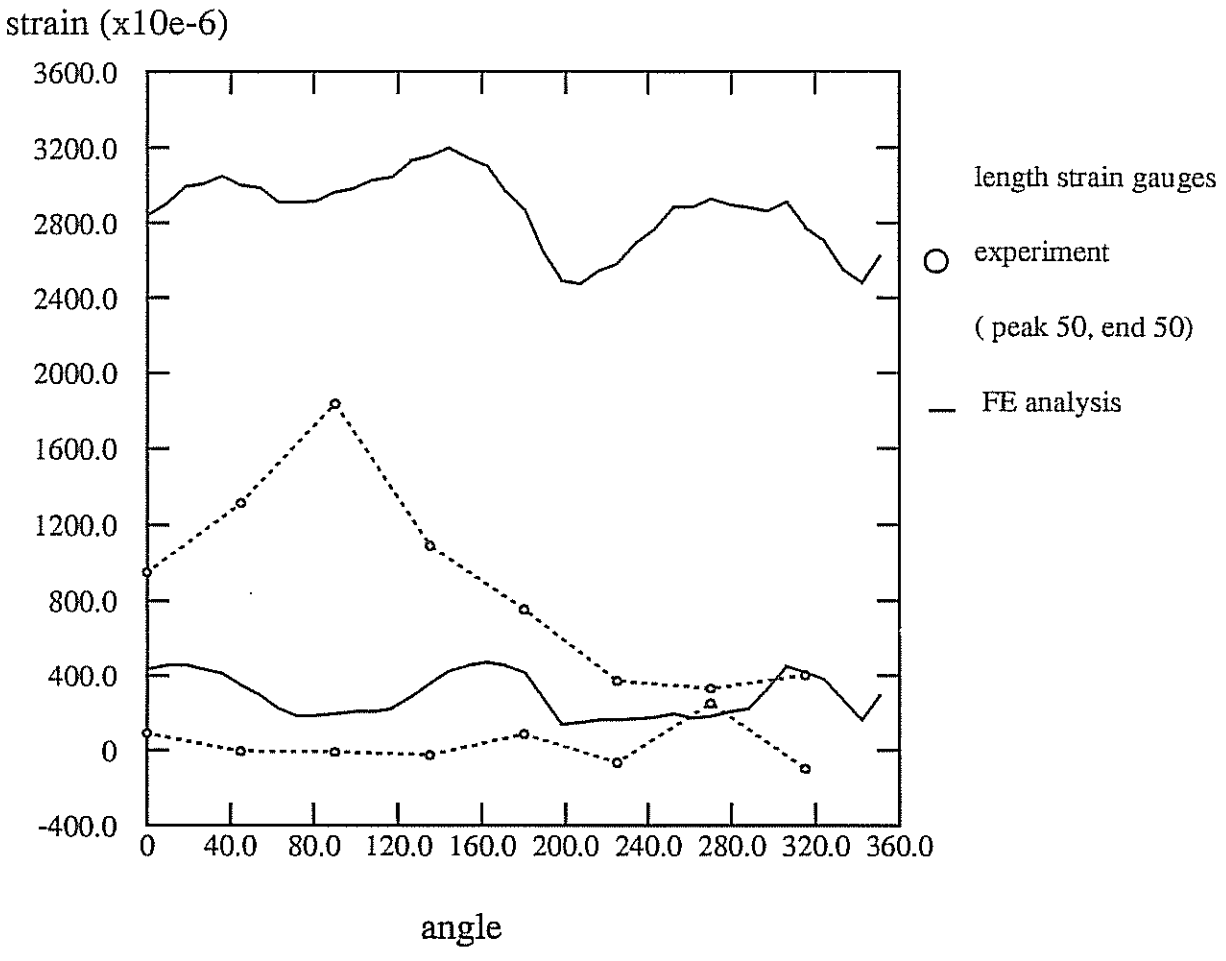
strain (x10e-6)
3600.0
3200.0
2800.0
2400.0
2000.0
1600.0
1200.0
800.0
400.0
0
-400.0
0
40.0
80.0
120.0
160.0
200.0
240.0
280.0
320.0
360.0
angle
length strain gauges
experiment
(peak 50, end 50)
FE analysis

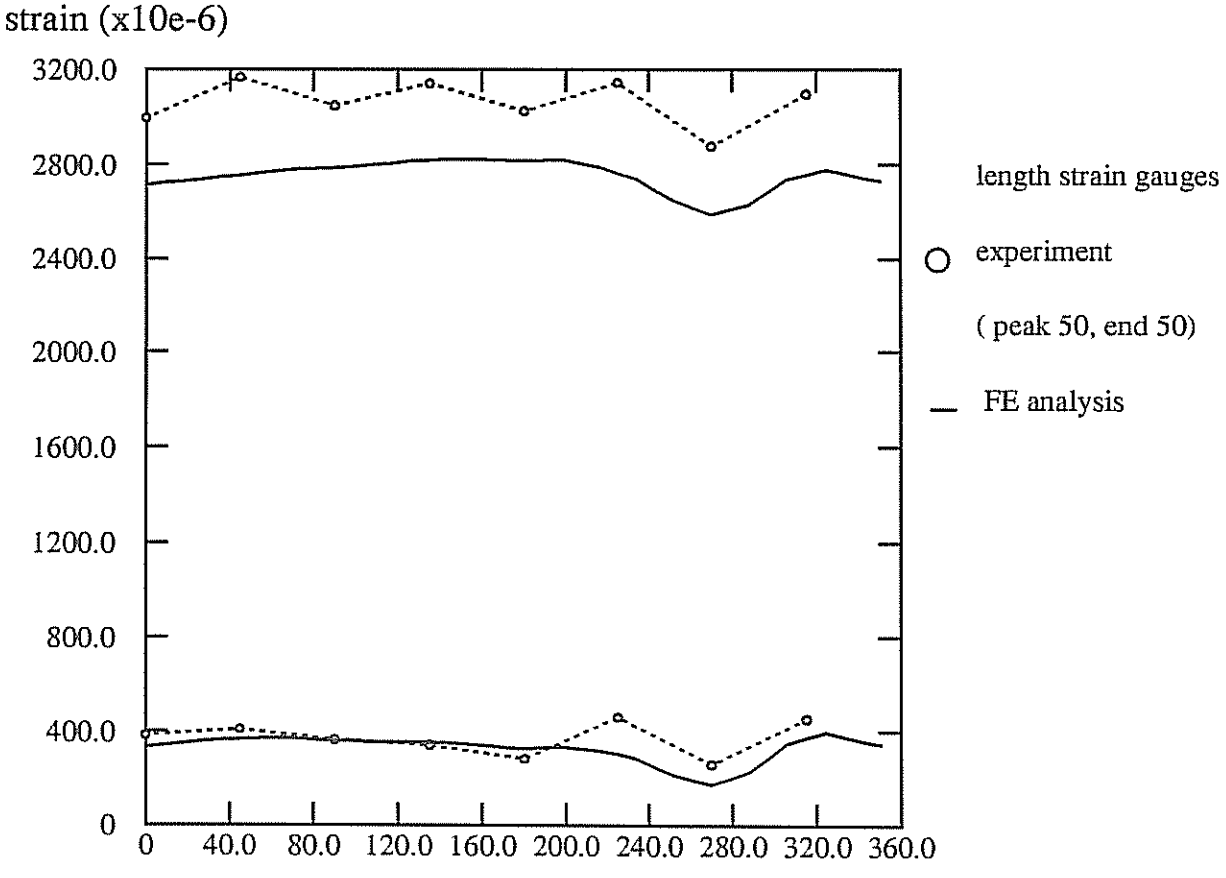
strain (x10e-6)
3200.0
2800.0
2400.0
2000.0
1600.0
1200.0
800.0
400.0
0
0
40.0
80.0
120.0
160.0
200.0
240.0
280.0
320.0
360.0
angle
length strain gauges
experiment
(peak 50, end 50)
FE analysis

Figure D.36.

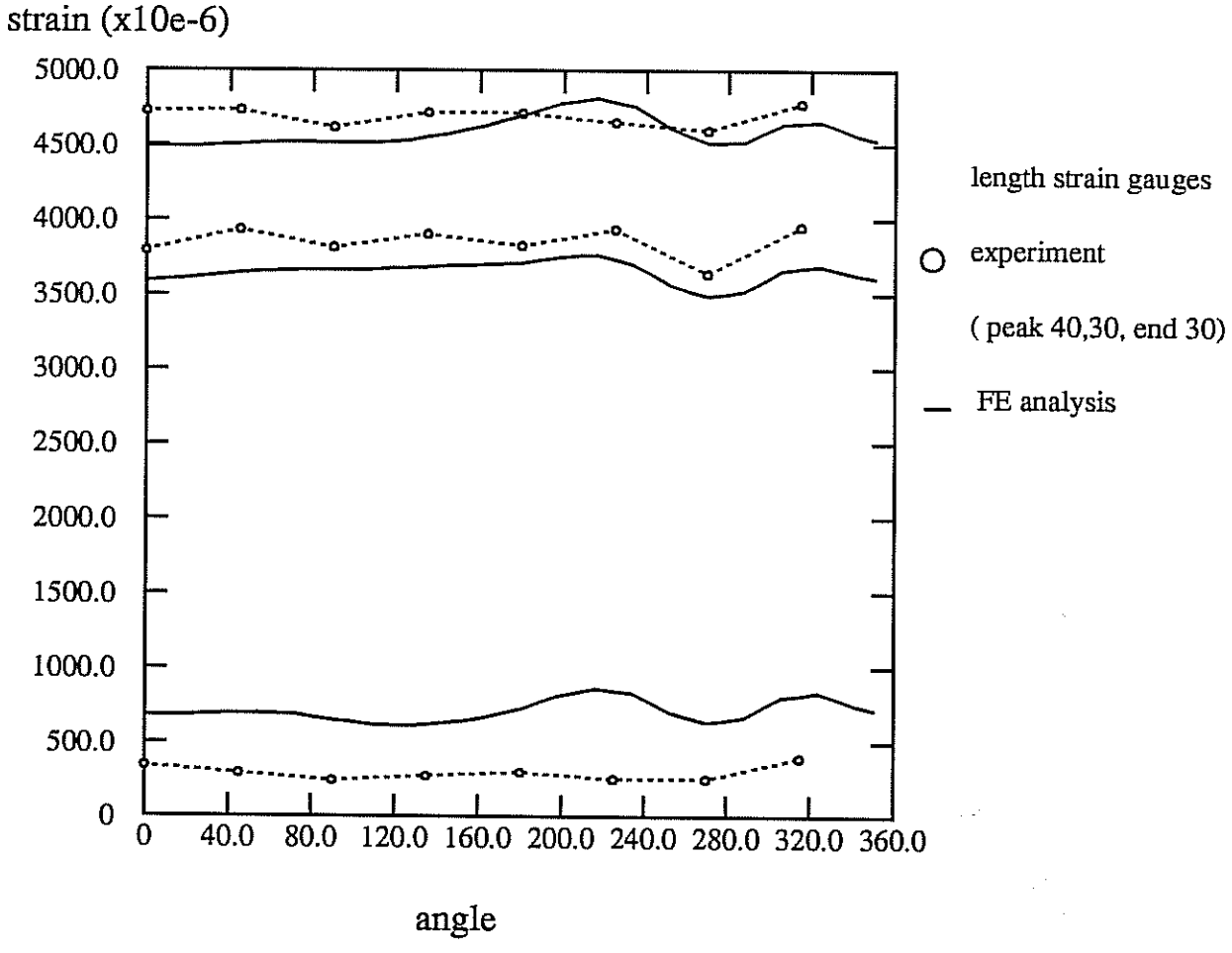
strain (x10e-6)
5000.0
4500.0
4000.0
3500.0
3000.0
2500.0
2000.0
1500.0
1000.0
500.0
0
0
40.0
80.0
120.0
160.0
200.0
240.0
280.0
320.0
360.0
angle
length strain gauges
experiment
(peak 40,30, end 30)
FE analysis

Figure D.37.

Figure D.38:
Tension-torsion test on a misoriented SC16 specimen.

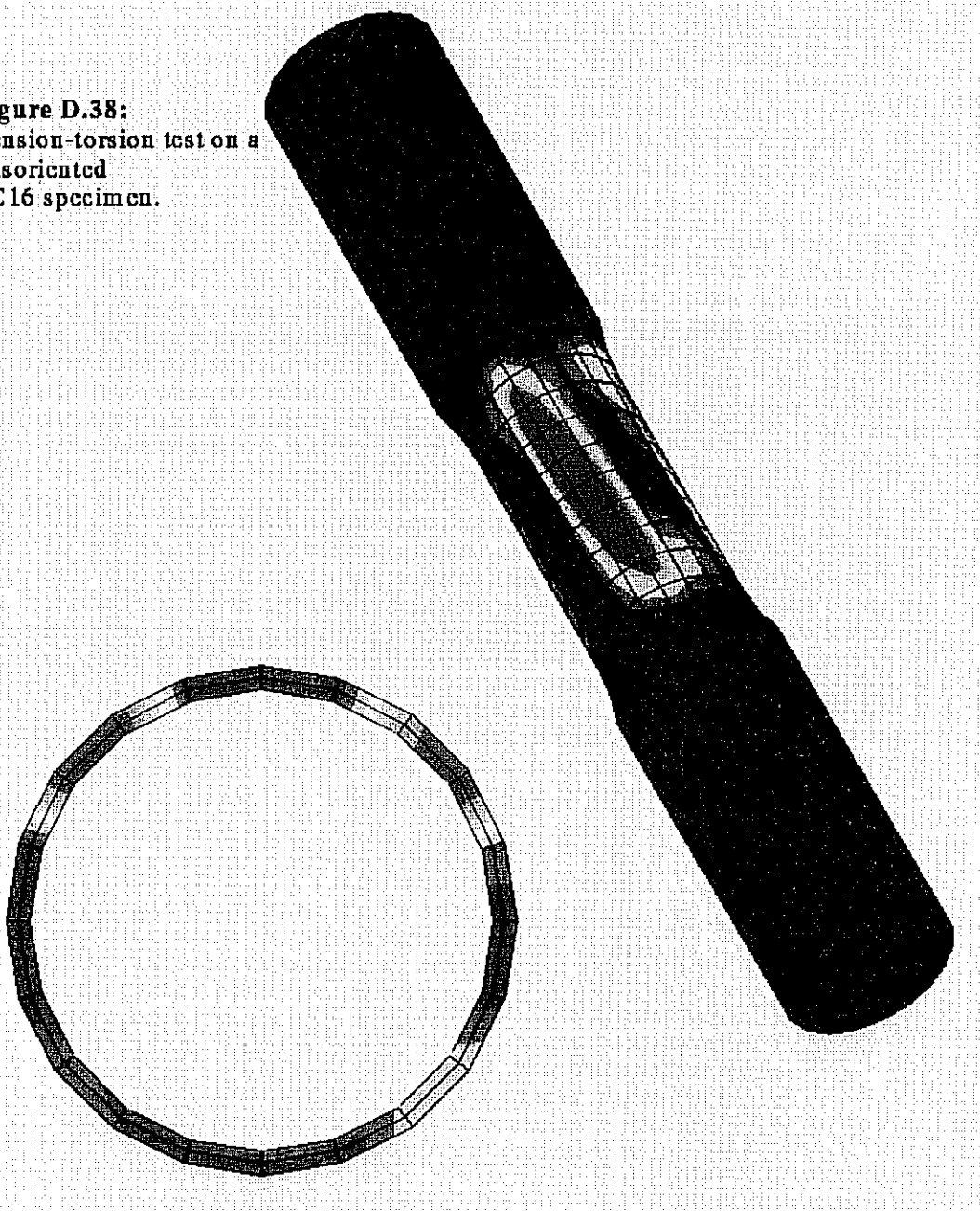

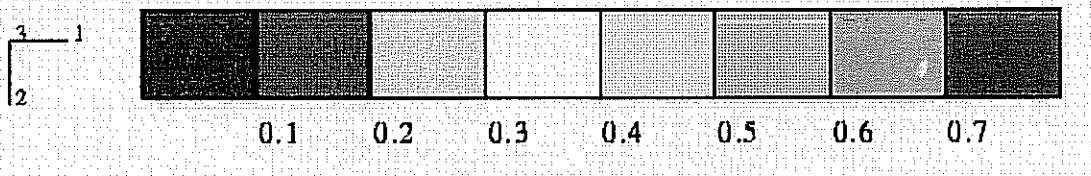

equivalent viscoplatic strain (%)

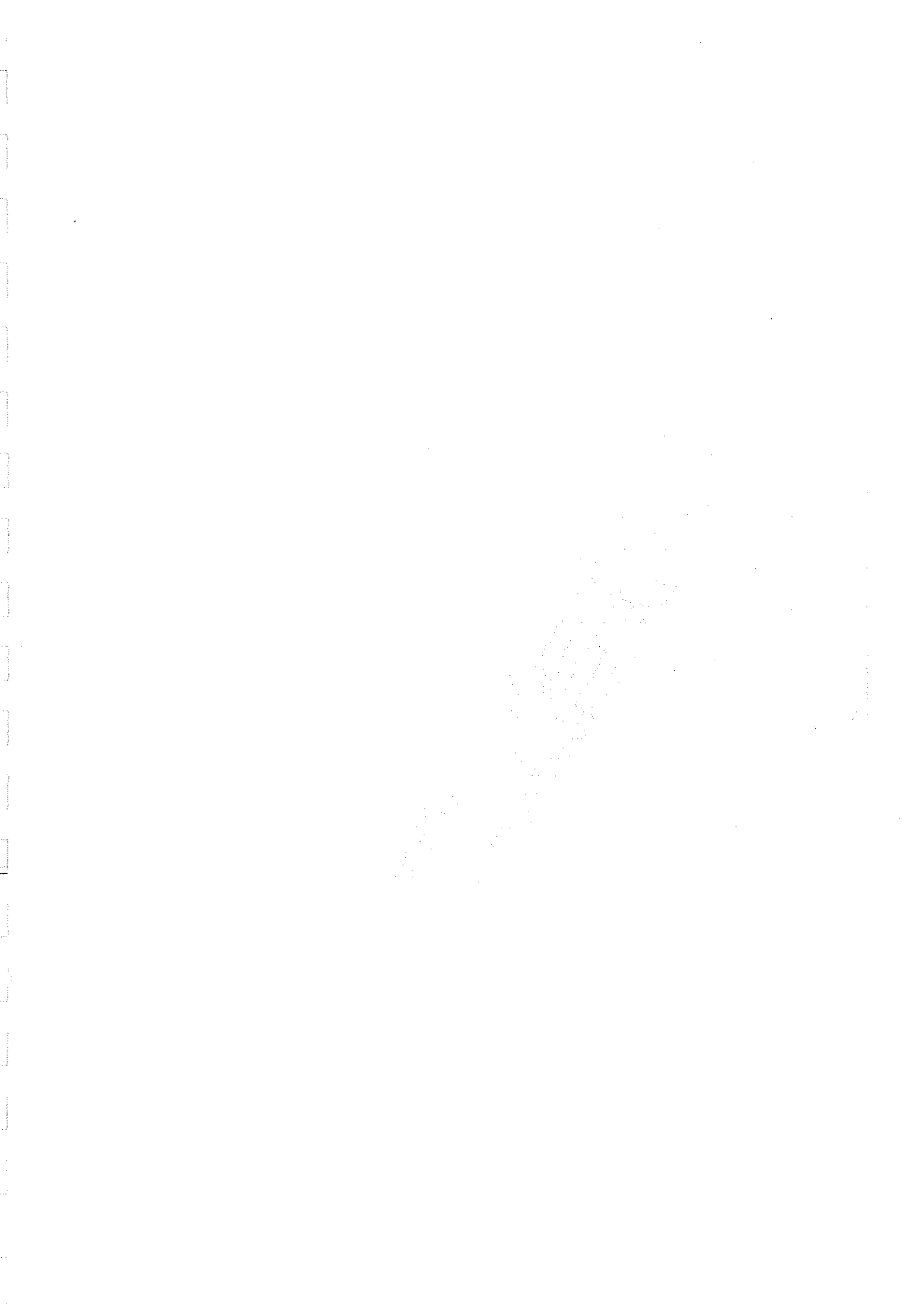

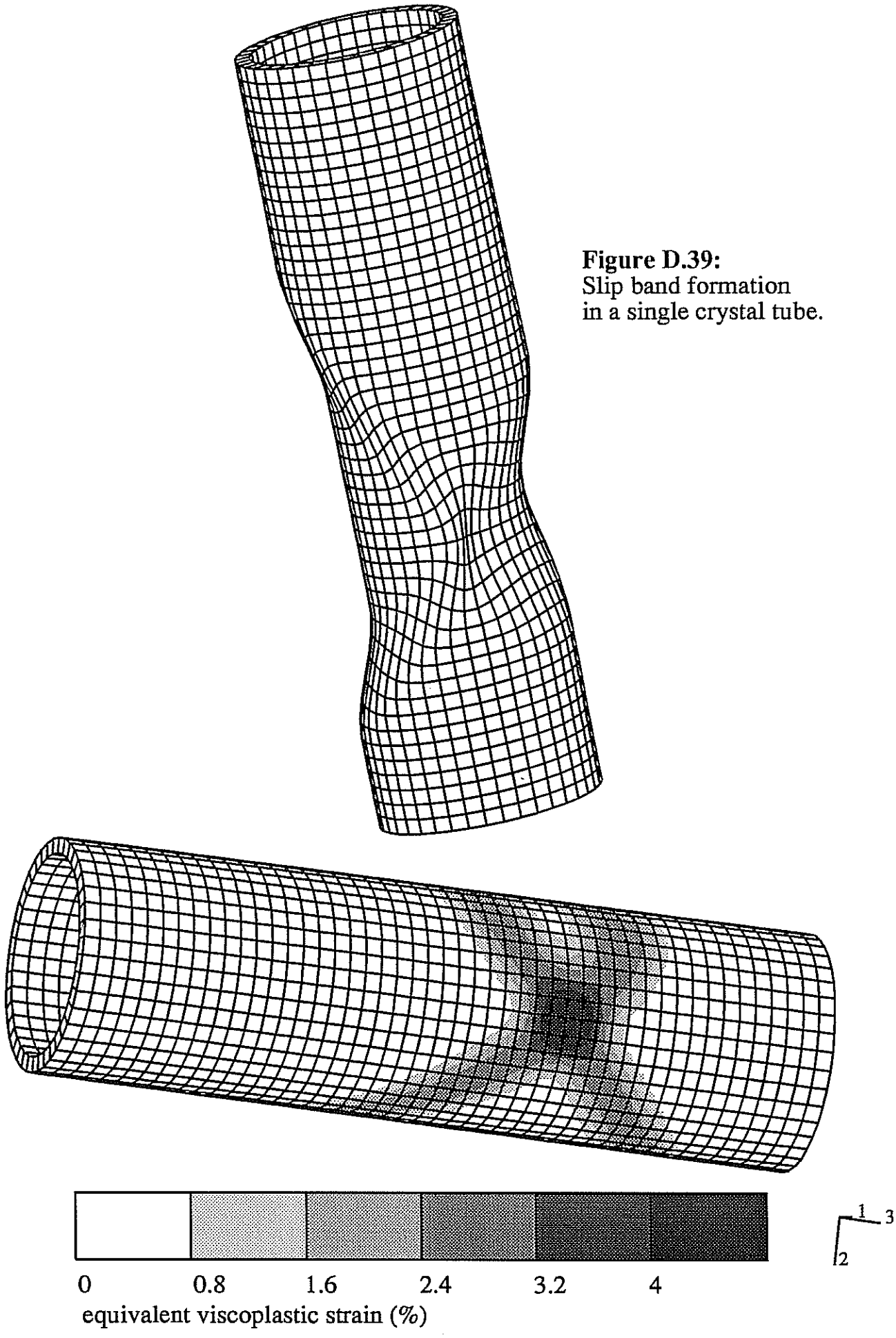

Figure D.39:
Slip band formation
in a single crystal tube.

Figure D.40: Developed surface of the single crystal tube (above), traces of the slip plane and of the kink plane (below).

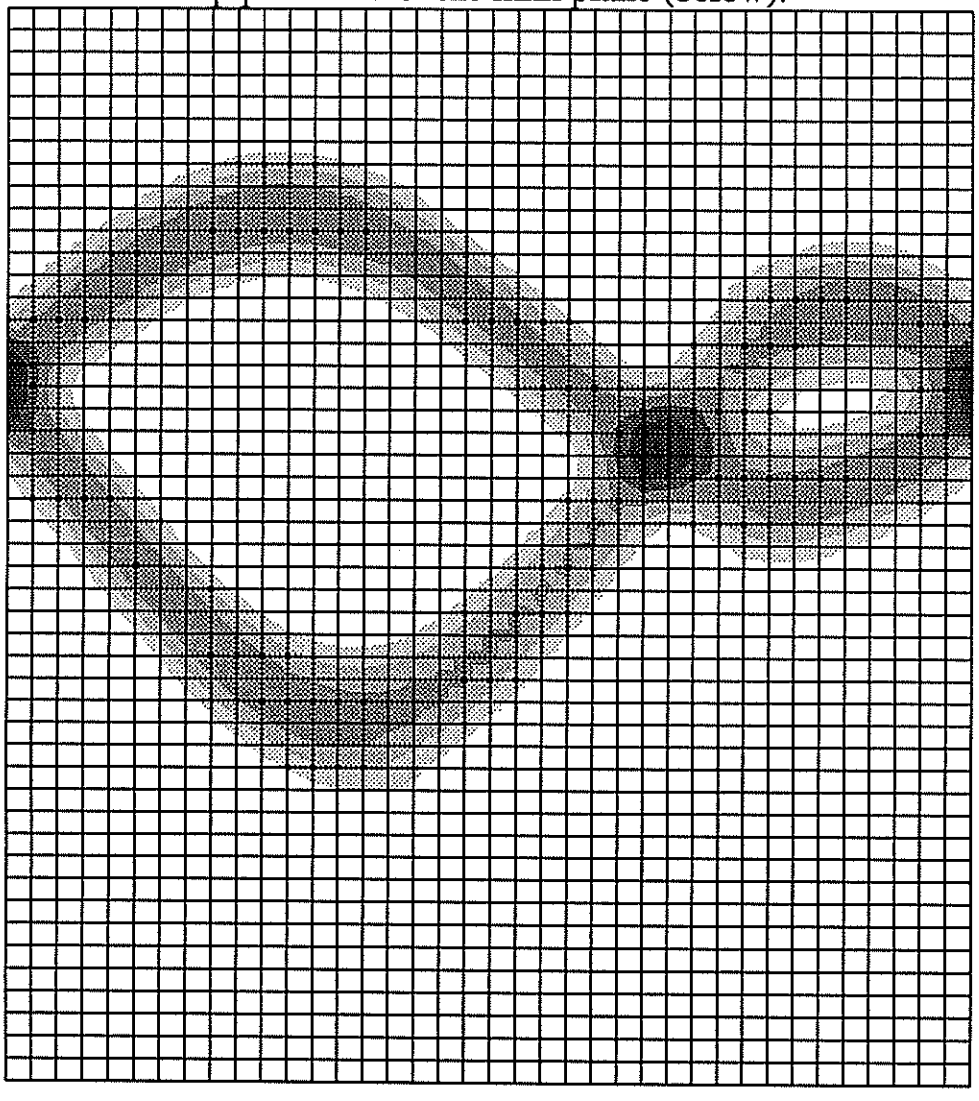

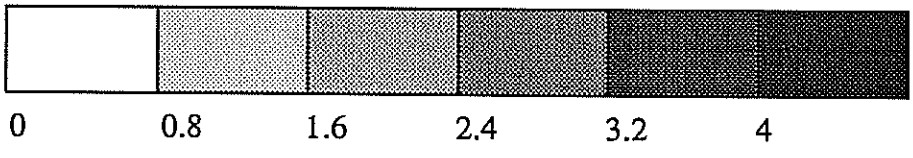

evequ (%)

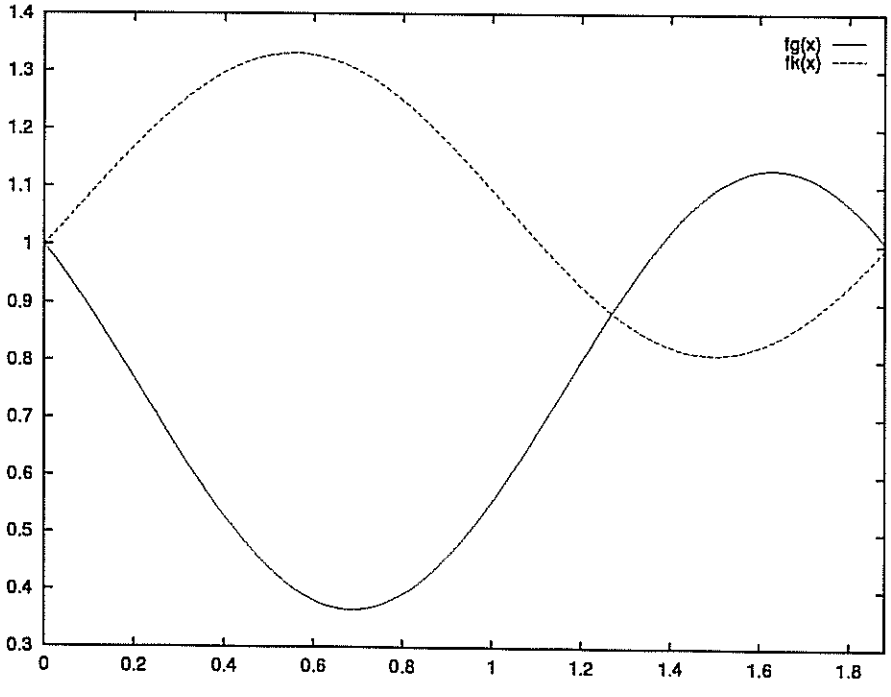

Figure D.41: Localization in a single crystal tube: large strain analysis, developed surface of the tube.

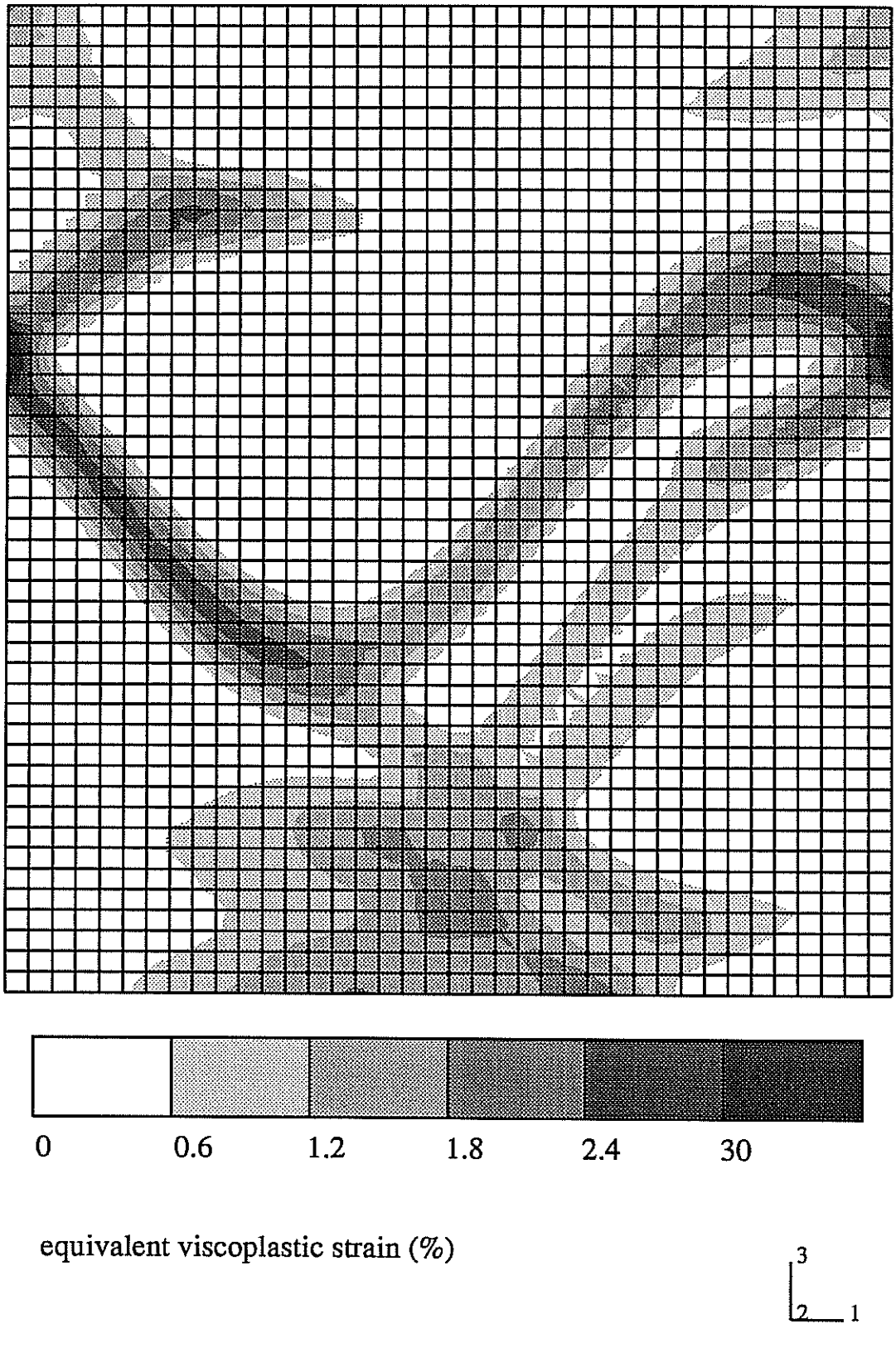

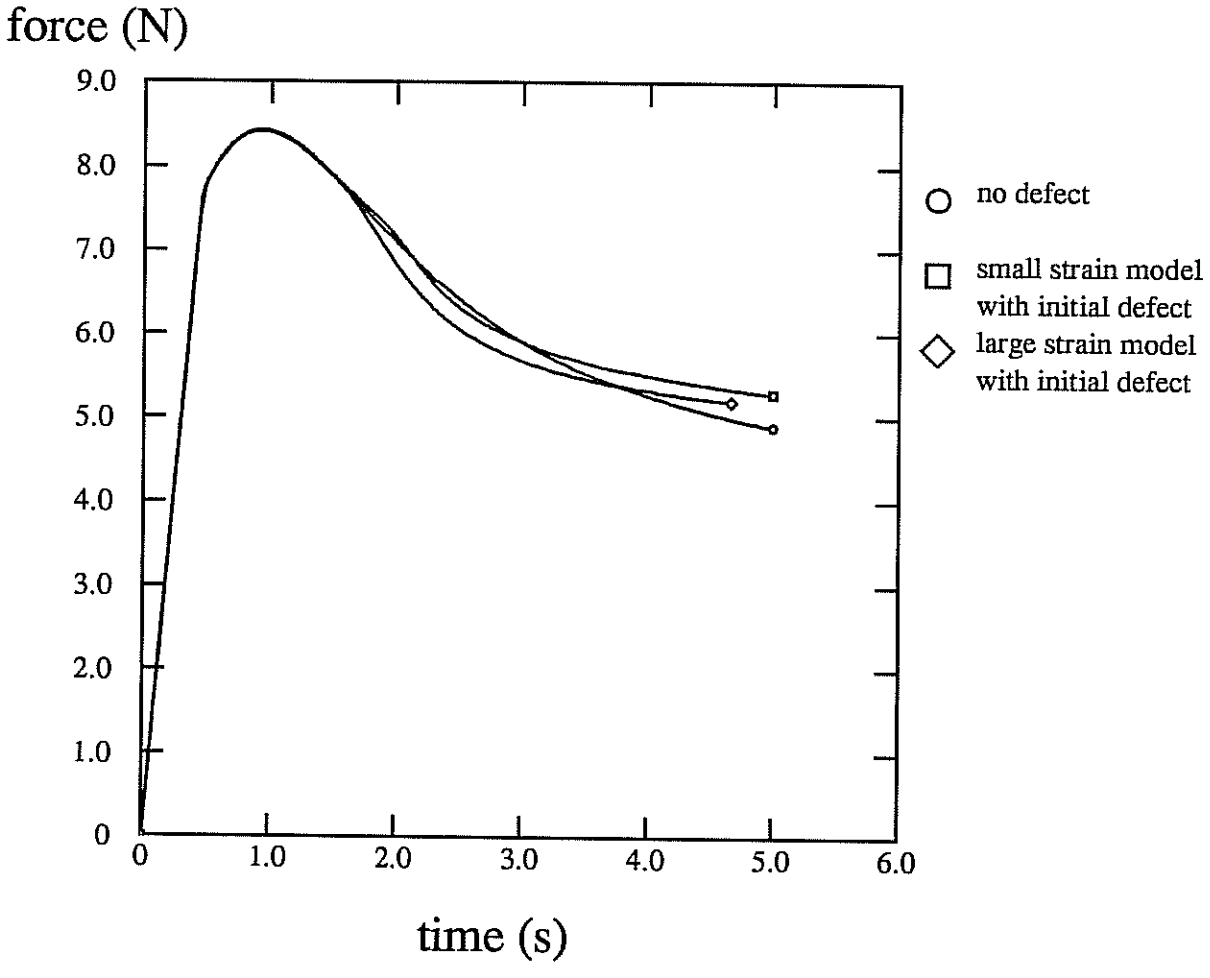

Figure D.42: Load displacement curve of the tension of a single crystal tube using the small and large strain version of the model.

3 Modelling the mechanical behaviour of SC16 at 950°C

3.1 Identification of the parameters of the two-phase model

We want to determine the parameters of the model presented in section C.4.3 to describe the behaviour of SC16 at 950°C under tension, low cycle fatigue and creep.

3.1.1 Simplified optimization scheme

It can not be expected that the material parameters describing the non-linear behaviour of phases γ and γ' in the two-phase alloy are identical to those accounting for bulk γ and bulk γ' alloys respectively ([Müller, Glatzel, Feller-Kniepmeier 1993] and [Feller-Kniepmeier, Glatzel, Link, Scheumann-Frerker 1990]). Similar conclusions have been drawn by Benyucef [1994] who has compared the behaviour of single crystal γ alone with the two-phase single crystal superalloy MC2. That is why they will be simultaneously identified looking at tension and low cycle fatigue tests.

The whole identification process has been described in section C.4.4 and also in [Forest, Pilvin 1995]. The optimization requires, on the one hand, FE calculations for the determination of the "geometric" parameters and, on the other hand, the simulation of the mechanical tests to be compared with experimental data.

However the entire optimization process is too time-consuming for the used workstations. That is why we have preferred a simplified version of the optimization process which has been described in section C.3.6. The identification of the "geometric" parameters (here we have used D only) is done independently of the identification of the material parameters, once reasonable values of the material parameters have been found. Then the value of D is fixed and better material parameters can be identified. At the end the FE calculations are performed again to check that the validity of the concentration rule is still ensured. If not, D must be identified again.

3.1.2 Identification

The experimental data retained for the identification contain 5 tension tests with prescribed strain rates ranging from 10^{-6} to 10^{-2} s^{-1}, 5 cyclic tests with various prescribed strain rates and amplitudes, and 3 creep tests for crystal orientation [001]. Recovery terms have been introduced in equations C.138 and also C.140, to describe the creep behaviour which is of the utmost importance for industrial purposes:

$$\dot{\alpha}_i^s = \dot{\gamma}_i^s - d_i \dot{v}_i^s \, \alpha_i^s - \left(\frac{| \alpha_i^s |}{M_i} \right)^{m_i} \operatorname{sign}(\alpha_i^s) \tag{3}$$

$$\dot{\underset{\sim}{\beta}}_i = \dot{\underset{\sim}{\xi}}_i - D \, \frac{2}{3} J_2(\dot{\underset{\sim}{\xi}}_i) \, \underset{\sim}{\beta}_i - \left(\frac{2 J_2(\underset{\sim}{\beta}_i)}{3L} \right)^{l} \frac{3 \underset{\sim}{\beta}_i}{2 J_2(\underset{\sim}{\beta}_i)} \tag{4}$$

Furthermore the FE computation of a tension test in direction [001] with the configuration of figure 43 is introduced in the optimization procedure.

The value of D obtained in section C.3.5.2 for the general self-consistent scheme is used as a starting value for the identification of the two-phase single crystal model. The final value

$$D = 110$$

ensures that the self-consistency condition is fulfilled up to 2%. A set of parameters can then be found, that satisfactorily describe the macroscopic experimental response and ensure the validity of the concentration rule (table 2 and figures 44 to 50). The elastic constants used for the simulation are

$$C_{11} = 254150 \text{ MPa}$$

$$C_{12} = 189000 \text{ MPa}$$

$$C_{44} = 95000 \text{ MPa}$$

These are only estimations since only few tests in other directions than $< 001 >$ were available and no torsion test has been performed at this temperature.

coefficient	γ	γ'
k ($MPa^{1/n}$)	560	545
n	3.24	4.76
r_0 (MPa)	36	90
q^1 (MPa)	33	11
q^2 (MPa)	-68	-83
b^1	420	280
b^2	575	83
c (MPa)	59224	637022
d	535	2877
M	0.11	2.9
m	2.7	2.7

Table 2: Material parameters of the two-phase model for SC16 at 950°C (octahedral slip).

The parameters intervening in the concentration rule are D, $L = 6.95$ and $l = 2.7$.

Only little is known about the elastoviscoplastic behaviour of each phase within the aggregate. At high temperatures deformation takes place essentially in matrix γ whereas γ' precipitates are only occasionaly sheared for slow strain rates. That is why some constraints have been imposed on the material parameters during the identificaton process

$$r_0^{\gamma'} = 2.5\ r_0^{\gamma}$$

$$c^{\gamma'}/d^{\gamma'} = 2\ c^{\gamma}/d^{\gamma}$$

3.2 Influence of the γ' morphology

The representative morphological pattern chosen for the previous identification is shown on figure 43. To spare computer time we have used spheres for the γ' precipitates. The behaviour of the inclusion and the shell are that of single crystals with the parameters used in the local constitutive equation of the proposed model. The whole two-phase model is implemented in the infinite matrix to model the homogeneous equivalent medium. This corresponds to the extension of the generalized self-consistent scheme to the anisotropic case and accounts for the inclusion-matrix morphology.

With the same set of parameters the influence of the real morphology on the previous results has been investigated. FE computations have been performed for spherical precipitates as seen previously but also for cubes and cuboides although with the same set of parameters as for spheres. For cuboides for instance the self-consistency condition is then fulfilled only up to 10% for the same tension test as previously. Some deviation from the prediction of the explicit concentration rule can be seen on figure 51. It means that the entire optimization process should be performed with the real morphology, which is much more computer-time consuming. The local strain heterogeneities within each phase can also be investigated, even though the proposed homogenized constitutive equations only give mean values. This can be done using the obtained FE computations (figure 53), because the proposed optimization procedure provides a reliable estimation of the homogeneous equivalent medium.

3.3 Predictions of the model

After identification the predictive capabilities of the model must be demonstrated.

3.3.1 Predictions at the macroscopic level

We consider firstly a cyclic test with the prescribed strain rate $10^{-3}s^{-1}$ and an amplitude $\pm 0.5\%$ that has not been used for the identification. Figure 54 shows the comparison simulation-experiment for the first and stabilized cycles. In figure 55 the simulation of a tensile test at $10^{-3}s^{-1}$ for a specimen with 5° deviation from $< 001 >$ is compared with experiment.

Only a few tests are available for the tensile and cyclic behaviour of SC16 at 950°C in other crystallographic directions than $< 001 >$. A tensile test at $10^{-3}s^{-1}$ on a near-$< 111 >$ specimen ($\theta = 35.8°$ and $\rho = 44°$) has been used to determine some material parameters associated with cubic slip. Since no cyclic test was available, it was not possible to distinguish correctly isotropic from kinematic hardening. Since tests with other strain rates are not available, the viscosity parameters are only trial values. The parameters given in table 3 are proposed for cubic slip.

coefficient	γ	γ'
k ($MPa^{1/n}$)	300	300
n	3	3
r_0 (MPa)	43	175
q (MPa)	0	0
c (MPa)	9258	172096
d	104	7984

Table 3: Material parameters of the two-phase model for SC16 at 950°C (cubic slip).

The comparison simulation/experiment after identification is given in figure 56. According to the simulation, one cubic slip system is predominantly activated.

Figure 57 shows then the predicted tensile behaviour for a specimen having a near-$< 011 >$ orientation ($\theta = 35°, \rho = 12.4°$) and the corresponding experiment. For this orientation both octahedral and cubic slip systems are significantly activated.

3.3.2 Predictions at the microscopic level

Figure 52 shows the strain heterogeneity in the alloy for a tension test simulated with the final set of parameters. For the same test we have compared in figure 51 the stresses in each phase given by direct application of the concentration rule with the averaged stresses in the inclusion and the shell according to the FE computation. It proves that for this test the self-consistency condition holds with good accuracy.

The anisotropic predictive capability of the model must now be checked at the scale of the representative volume element. In the identification process the fulfillment of the self-consistency condition has been ensured only for a tension test in direction $< 001 >$.

That is why a tension test on the aggregate presented in figure 43 has been considered for which the tensile direction coincides with a $< 011 >$ crystal direction. A strain of 3% has been prescribed at infinity at a strain rate of $10^{-3}s^{-1}$. At the end of the test, the mean strain in the shell-inclusion assembly was 2.99%, which means that the self-consistency condition holds also for this test. As a result, the mean stresses and viscoplastic strains in the shell and inclusion are correctly predicted by the explicit model (figures 58 and 59). For this simulation only octahedral slip systems have been taken into account as in the identification process.

In contrast the model provides only a poor prediction of the mean stresses in each phase for a tensile test in direction $< 111 >$ (figures 60 and 61). This is mainly due to the fact that for this orientation very high stresses must be reached in each phase to activate octahedral slip systems. In the FE calculation the complex multiaxial stresses in the shell lead to a premature activation of slip processes and strong strain localization in the shell. The inclusion undergoes only very small deformation. However the result must be interpreted with much caution, since we are working with a very coarse mesh. A finer mesh would make the computation untractable. But this could also indicate that the proposed concentration rule is too crude in the case of the three-phase model. In any case the predicted behaviour of the material is unrealistic when only octahedral slip systems are considered (compare figures 51 and 56).

As a conclusion, modifications of the identification procedure could give a better predictive character of the model. First of all, both octahedral and cubic slip systems must be taken into account for the identification of "geometric" and material parameters. This can only be done when enough experimental data are available for the direction $< 111 >$. Furthermore, since we are here interested in an approximation of the generalized self-consistent scheme, two parameters D_γ and $D_{\gamma'}$ instead of one single D should be introduced. This would break the symmetry of evolution rule C.141 that is inconsistent with the non-symmetric role played by each phase (inclusion-matrix). This identification process requires at least two FE calculations at each step (tension in $< 001 >$ and $< 111 >$ directions) and the whole procedure will be much more computer-time consuming. This is all the more true that a finer mesh should be used.

3.4 Simulation of torsion tests at 950°C

The experimental and numerical analysis of torsion tests on SC16 single crystals presented in section 2.2 has shown that plastic deformation is strongly non-homogeneous at room temperature. The question arises whether the result pertains at high temperature. That is why torsion tests at high temperatures must be performed. The main difficulty is that only scarce experimental techniques exist for local strain measurements at temperatures like 950°C and they are still in development.

However the simulation of the test can be performed since the material parameters of the two-phase model are now available for the temperature 950°C. Figure 62a shows the overall viscoplastic deformation in a section of the tube after torsion. Deformation is not homogeneous along the circumference of the tube and "soft" zones appear that coincide with $< 011 >$ directions. However the strain gradients are much smaller than at room temperature (compare figure 62a with figure 26).

Furthermore deformation contours can also be drawn for each phase. We can represent the mean deformation in each phase at a given Gauss point of the structure and build isovalues. Figure 62b (left) shows that deformation takes place mainly in the matrix γ and that the mean deformation of phase γ is almost homogeneous along the circumference of the tube. The analysis proves that all cubic slip systems are activated, some more than others. In spite of the very high critical shear stress, cubic slip systems are also activated in the phase γ' but the deformation in γ' is more heterogeneous than in γ (see figure 62c, right). Contrary to torsion at room temperature some octahedral slip systems are locally activated in the matrix γ.

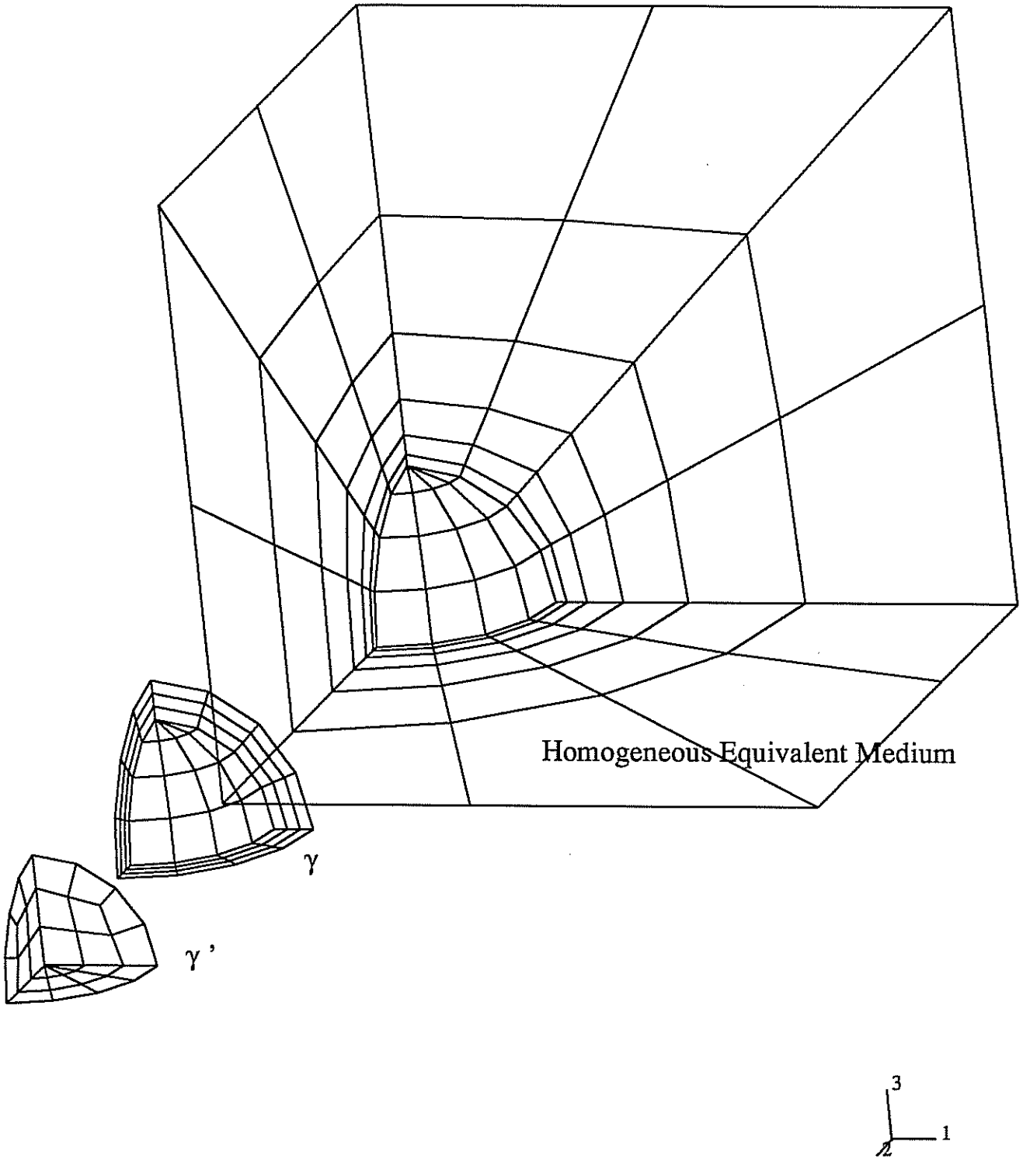

Figure D.43: Representative morphological pattern used in the modelling of two-phase single crystal superalloys.

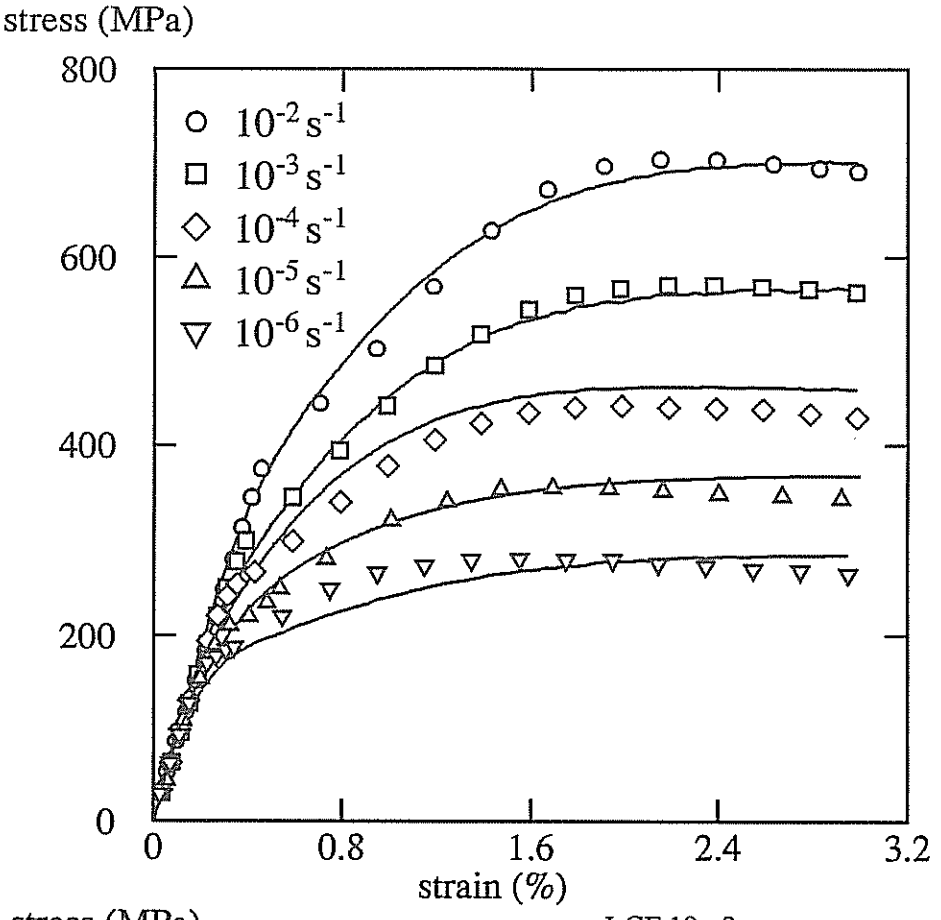

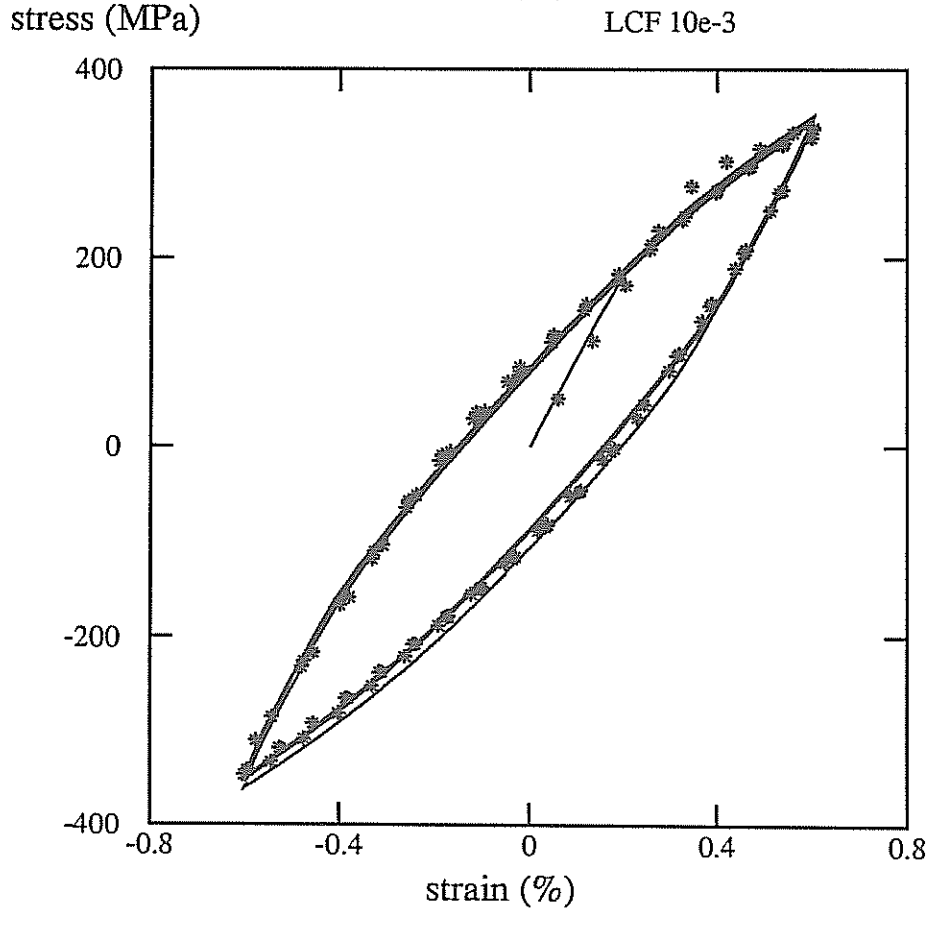

Figures D.44 and D.45: Tensile tests (above) and a LCF test (below, at 10e-3s-1) on SC16 near-<001> specimens: comparison simulation-experiment after identification. For the cyclic test, we give the first and the stabilized cycle.

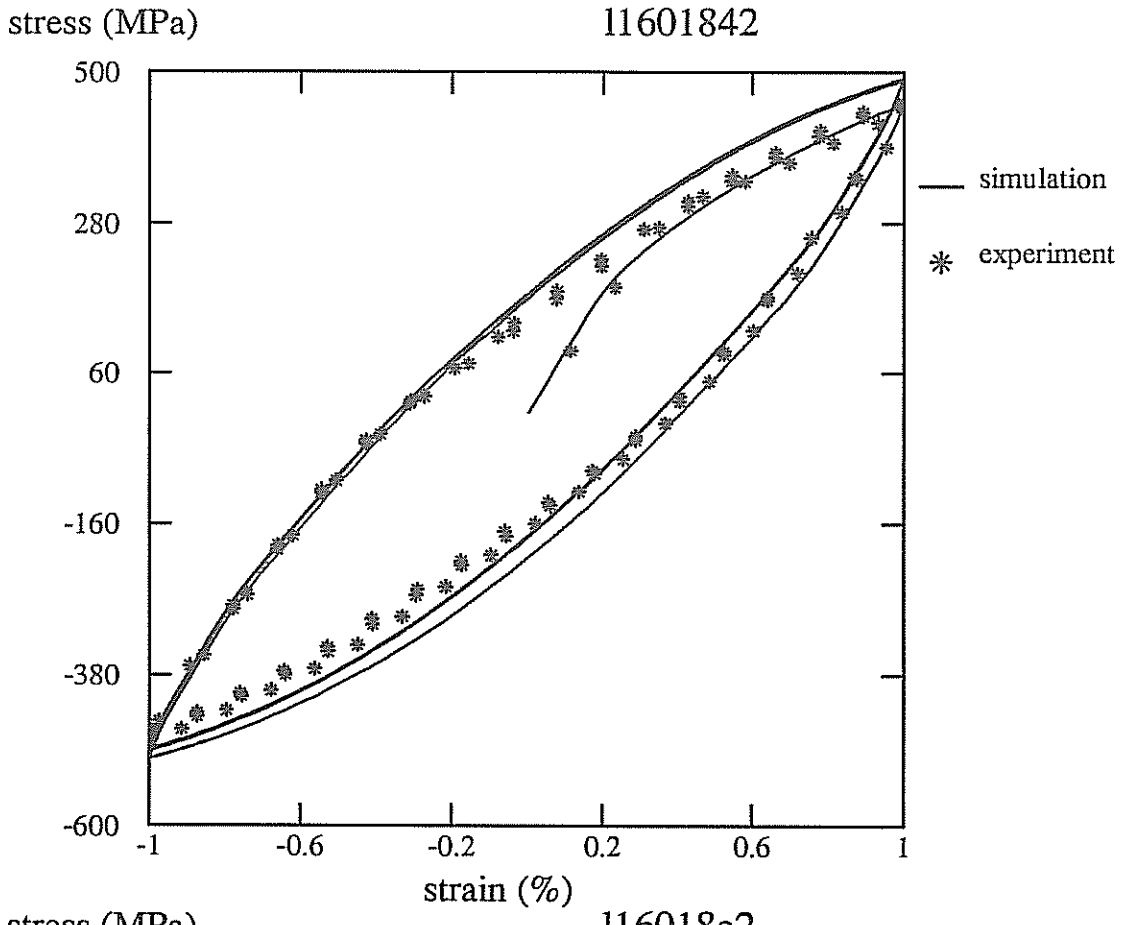

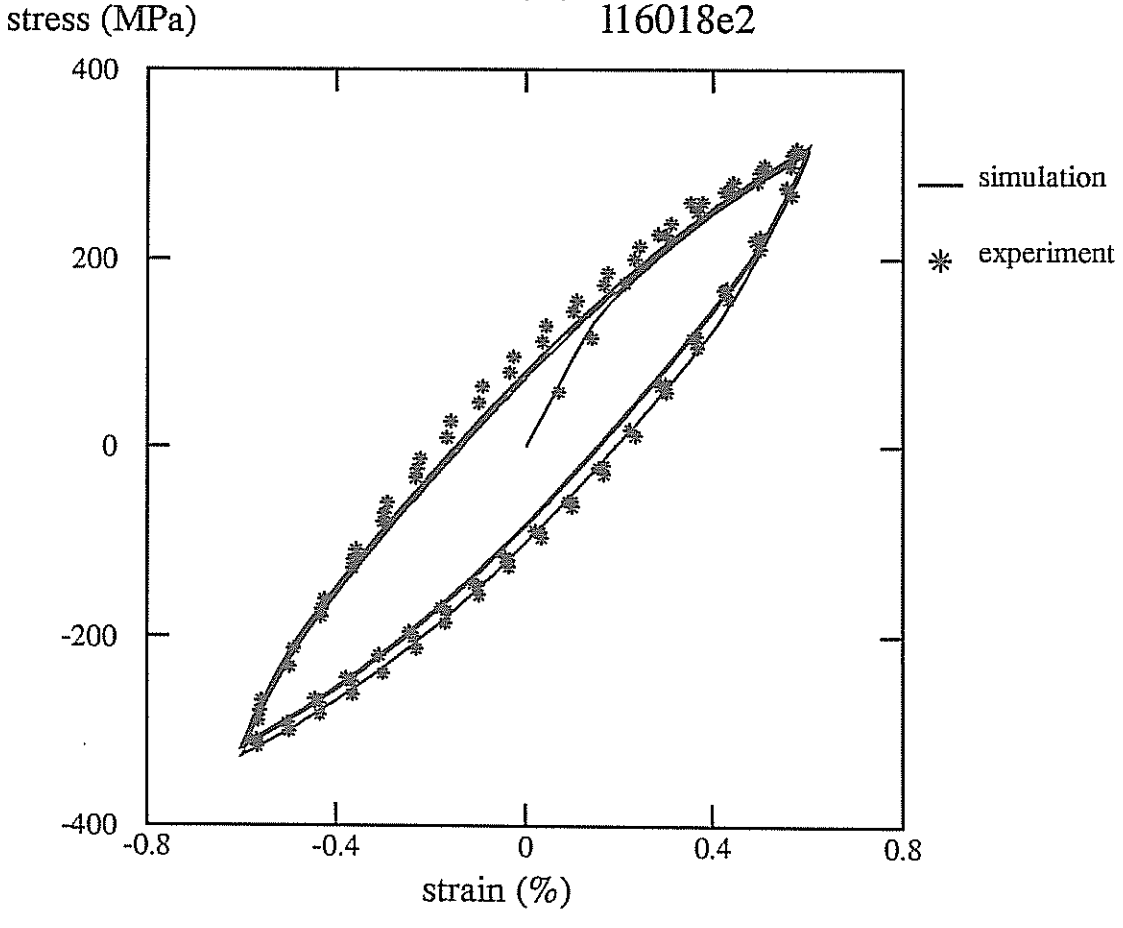

Figures D.46 and D.47: LCF test (at 10e-3s-1, above, and 10e-4s-1, below) on SC16 near-<001> specimens: comparison simulation-experiment after identification.

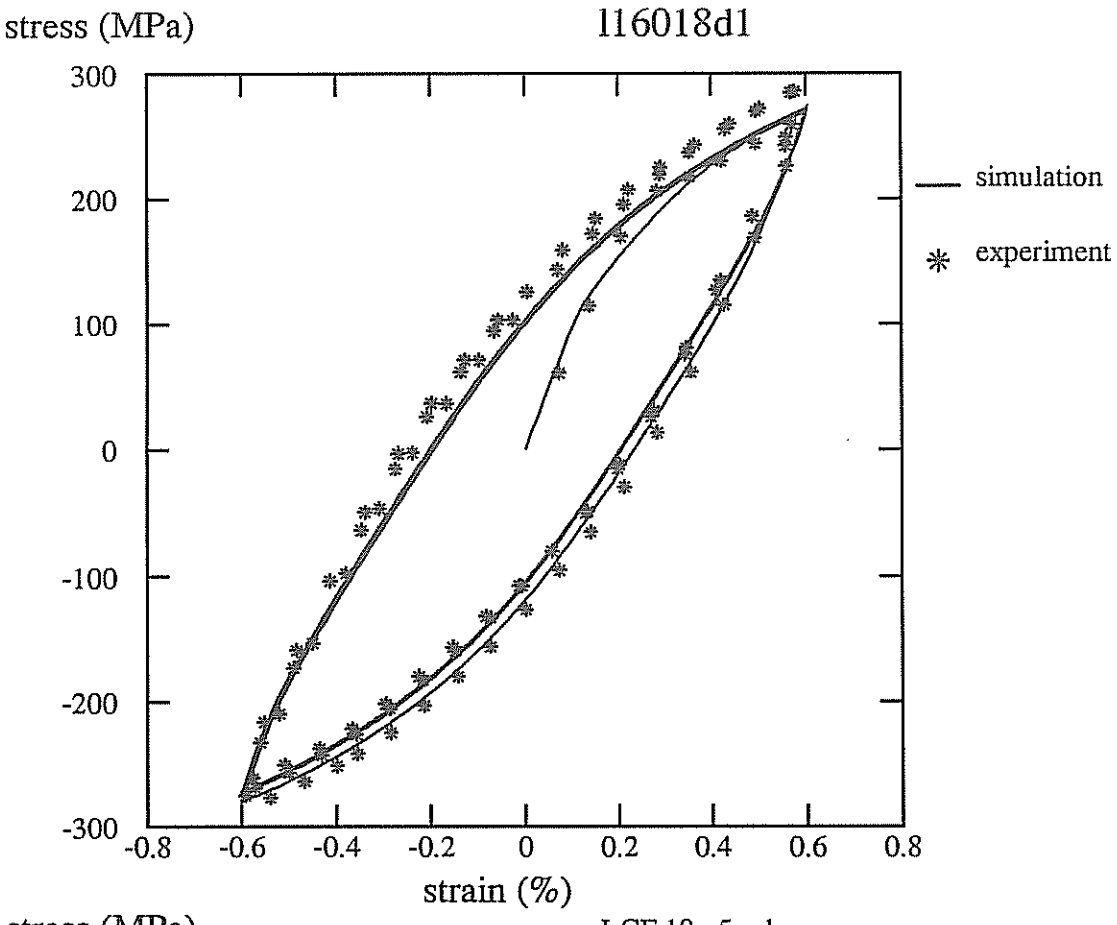

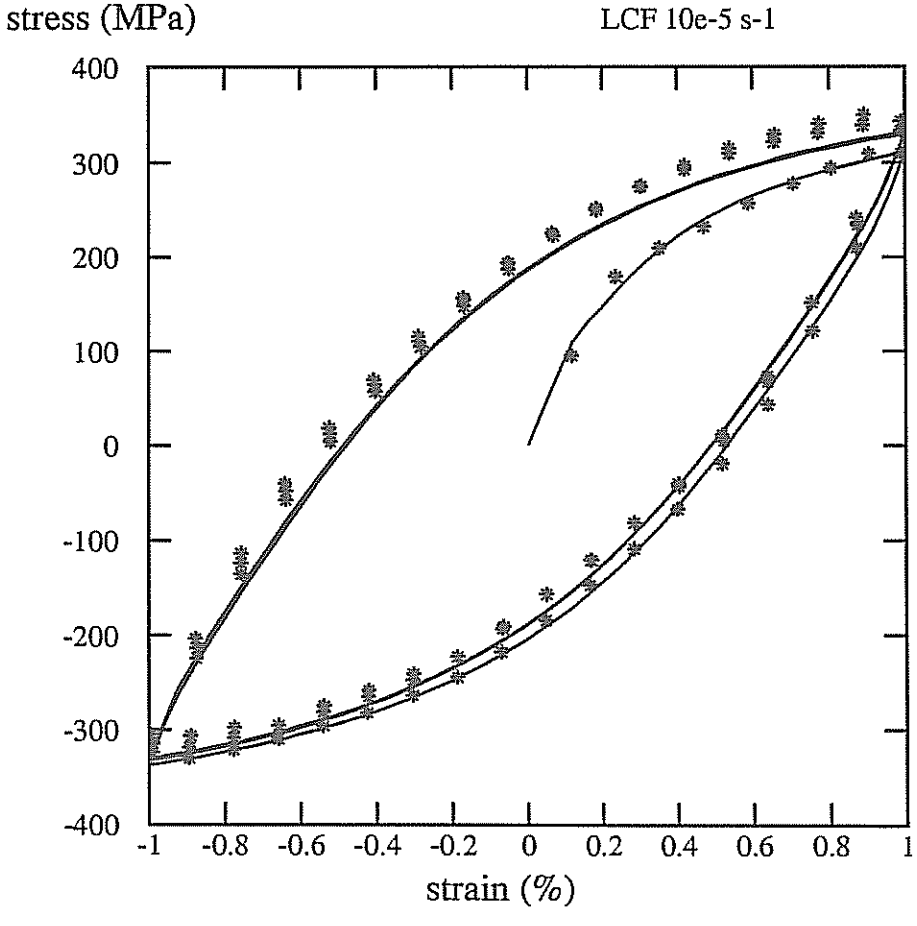

Figures D.48 and D.49: LCF test (at 10e-5s-1 for two amplitudes) on SC16 near-<001> specimens: comparison simulation-experiment after identification.

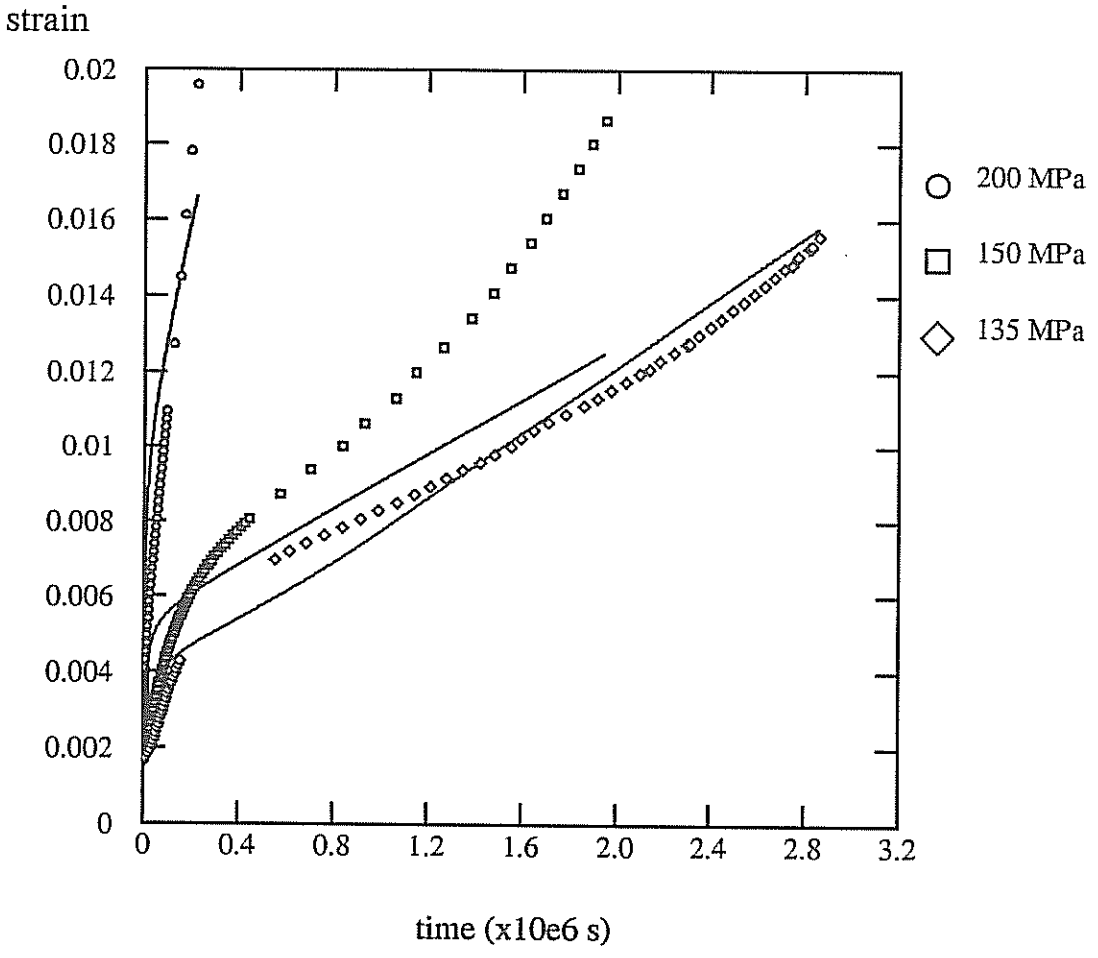

Figure D.50: creep tests at several loads on SC16 near-<001> specimens: comparison simulation-experiment after identification.

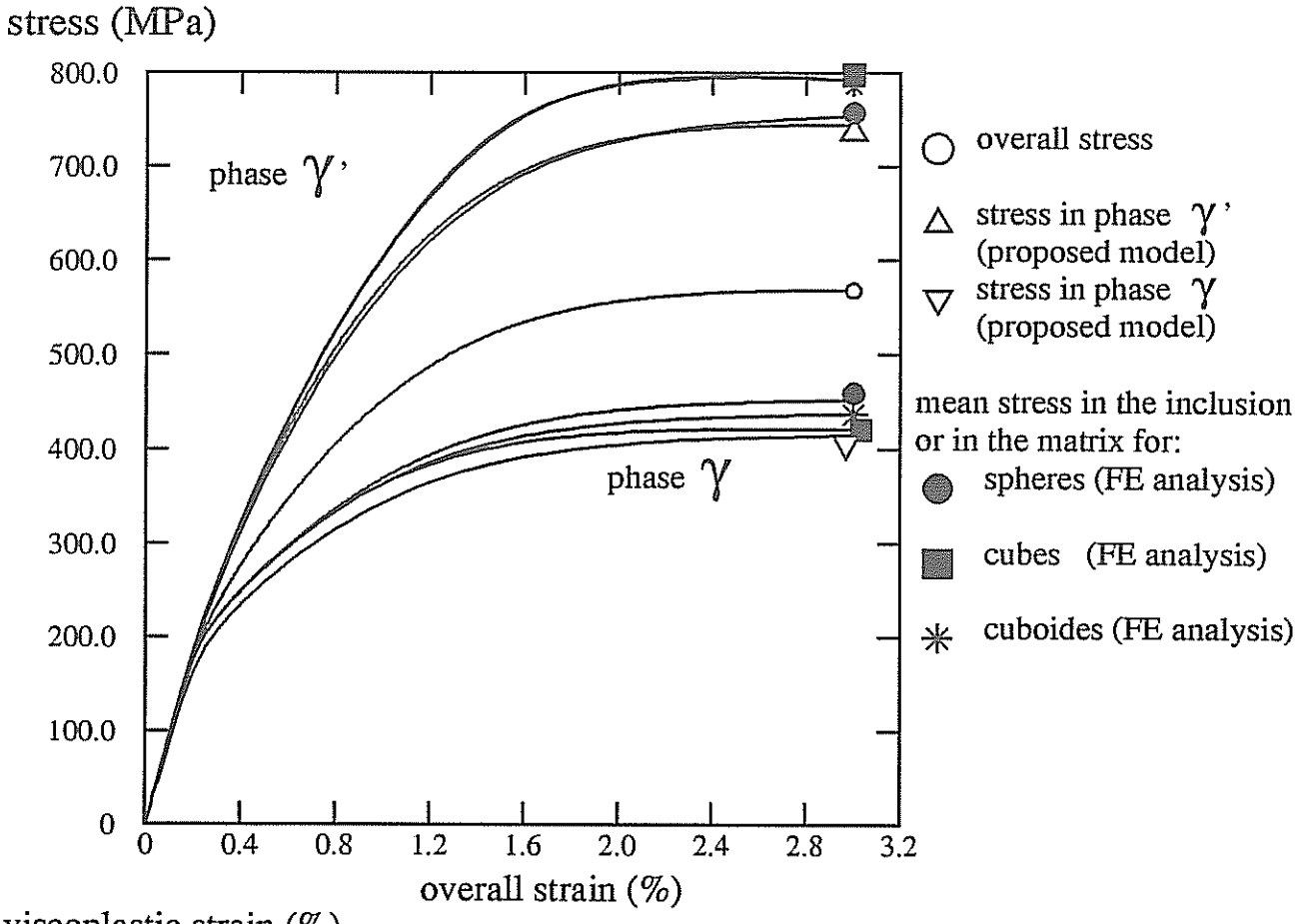

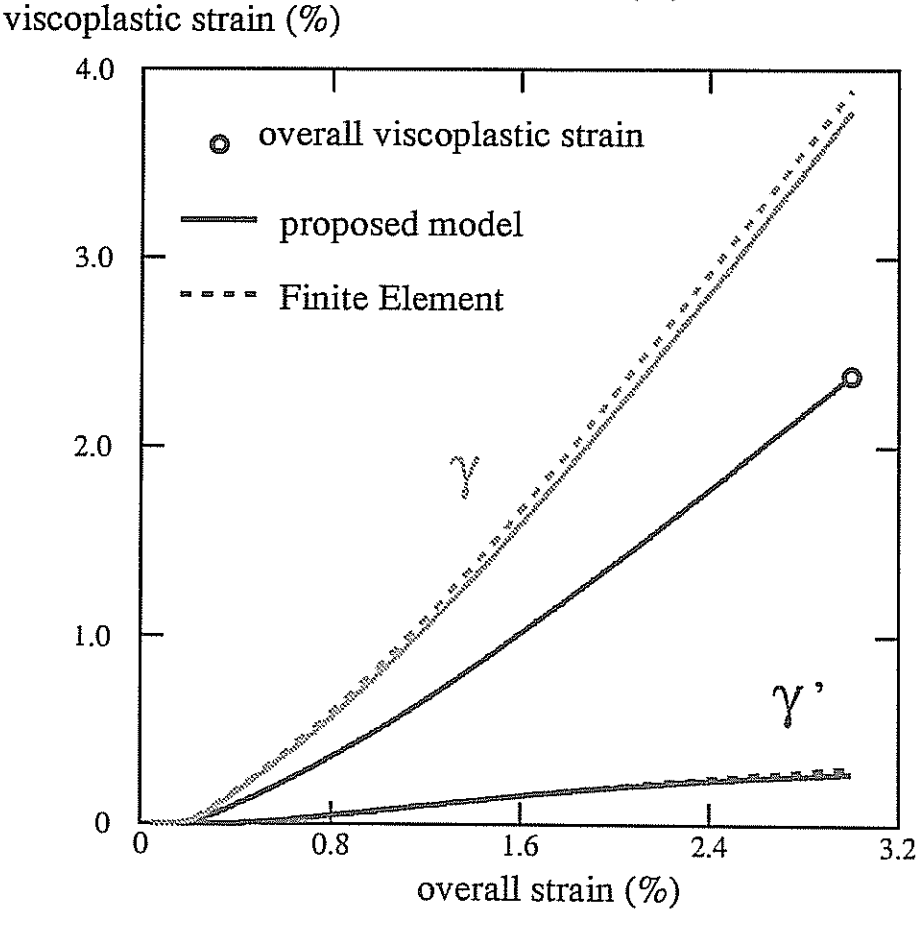

Figures D.51 and D.52: Influence on the precipitate morphology on the mean stresses in the inclusion and shell (above); mean viscoplastic strains in each phase (tension test at 10e-3s-1).

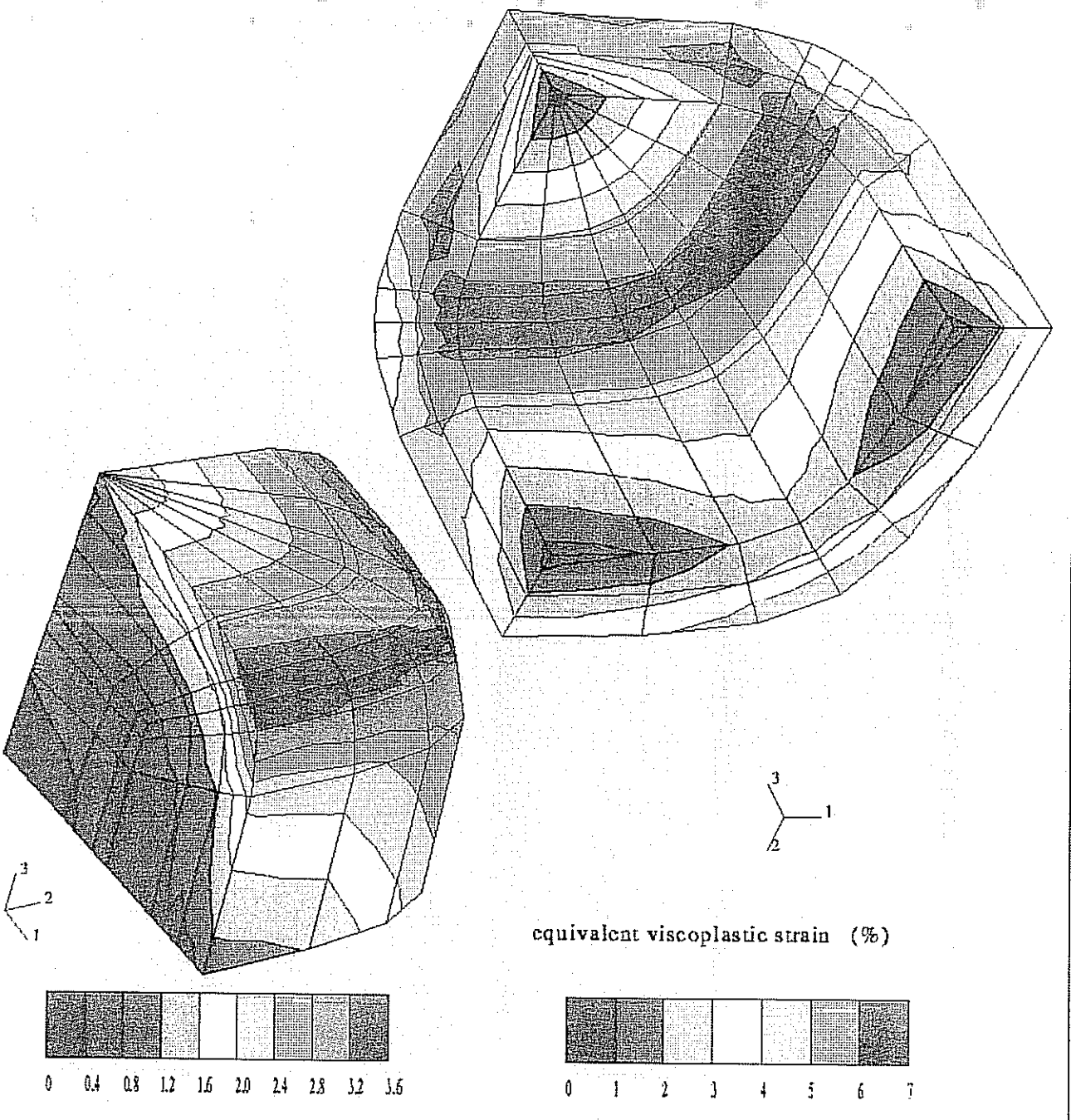

Figure D.53: Viscoplastic strain field in the cuboidal inclusion and in the shell; the surrounding homogeneous equivalent medium is not represented.

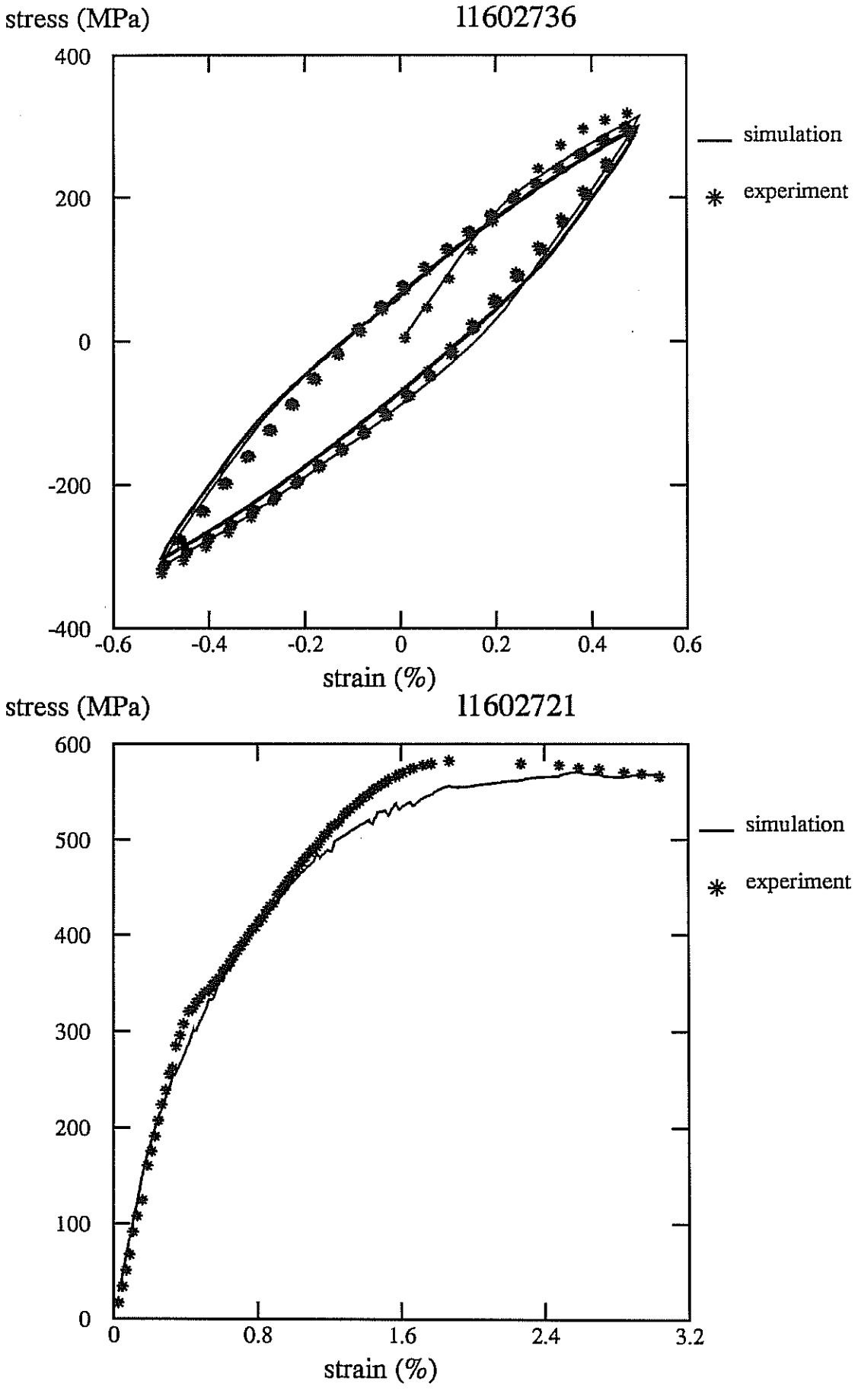

Figures D.54 and D.55: Model predictions: cyclic test at 10e-3s-1 (above), tensile test for a misoriented specimen (5 degree deviation from [001]).

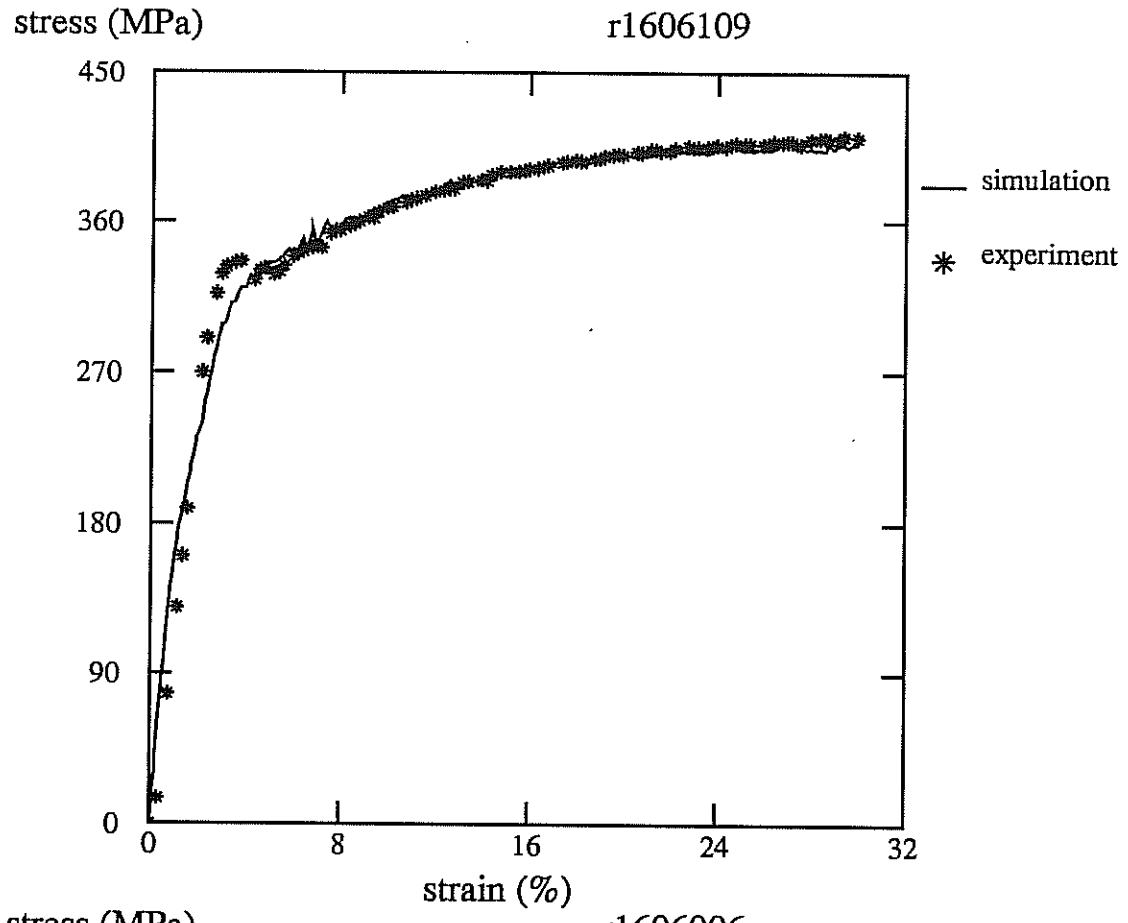

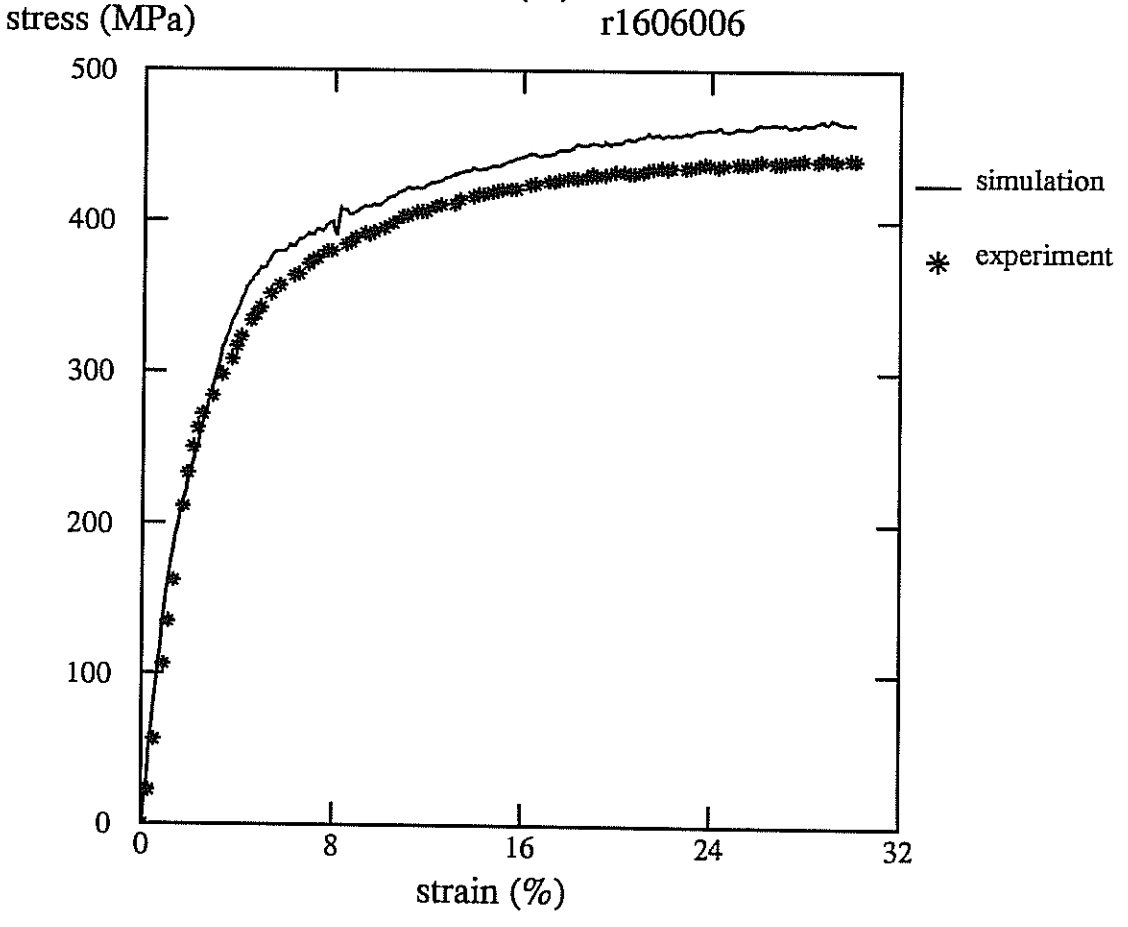

Figures D.56 and D.57: Model identification for a tensile test in a near-<111> direction (above) and model prediction for a near-<011> specimen (below).

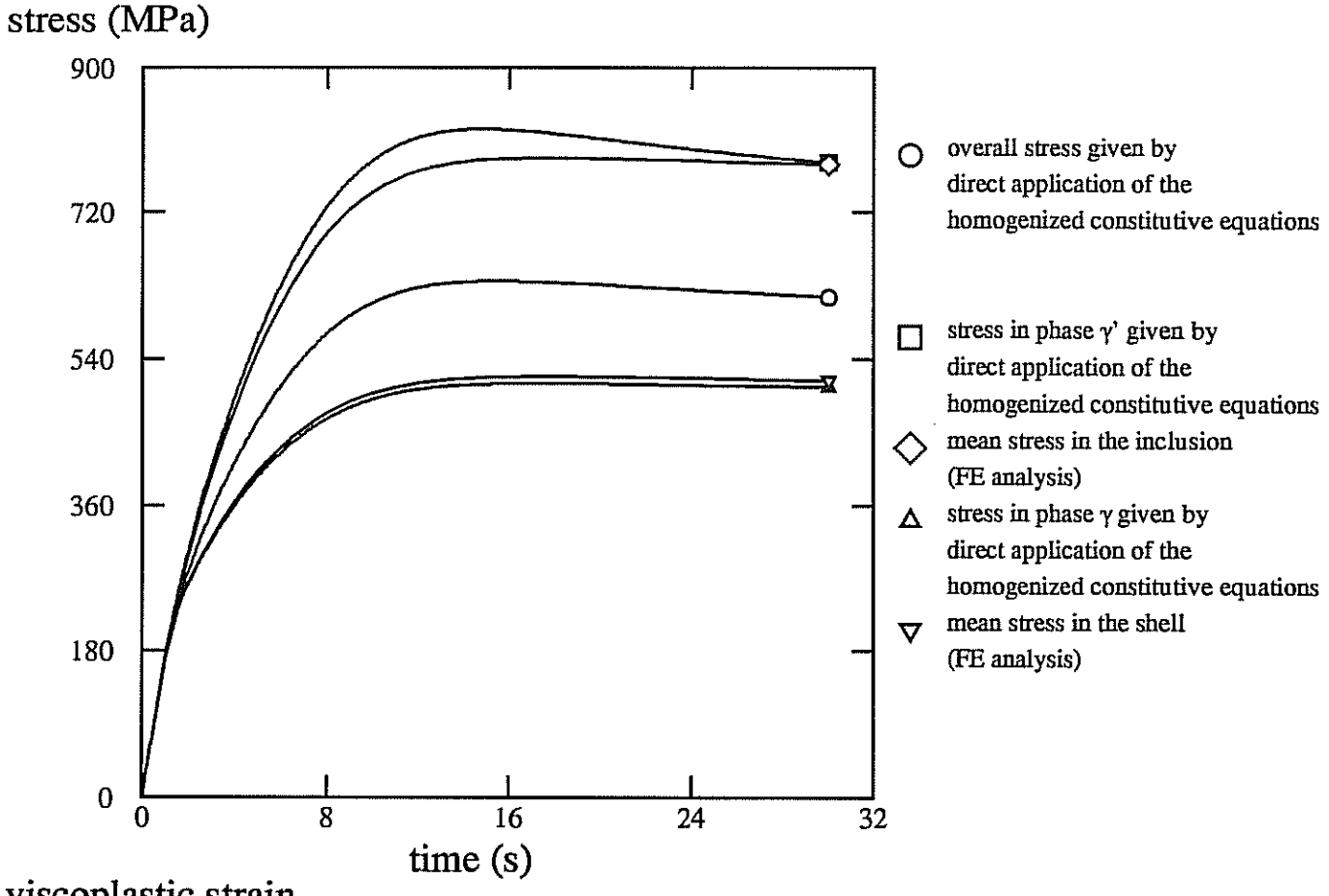

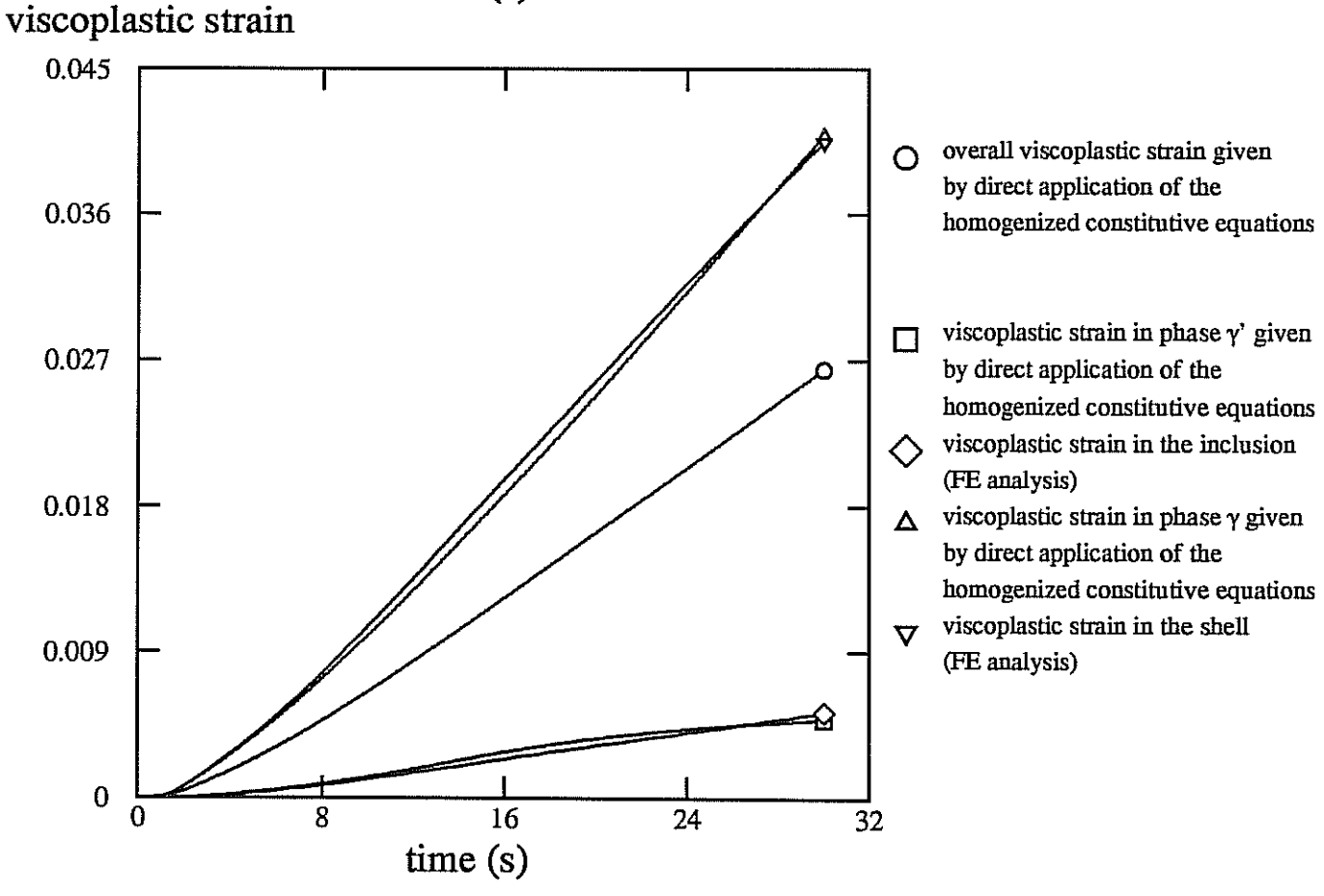

Figures D.58 and D.59: Mean stresses (above) and mean viscoplastic strains (below) given by the FE analysis and the direct application of the proposed model.
(tension test at 10e-3s-1, in crystal direction <011>).

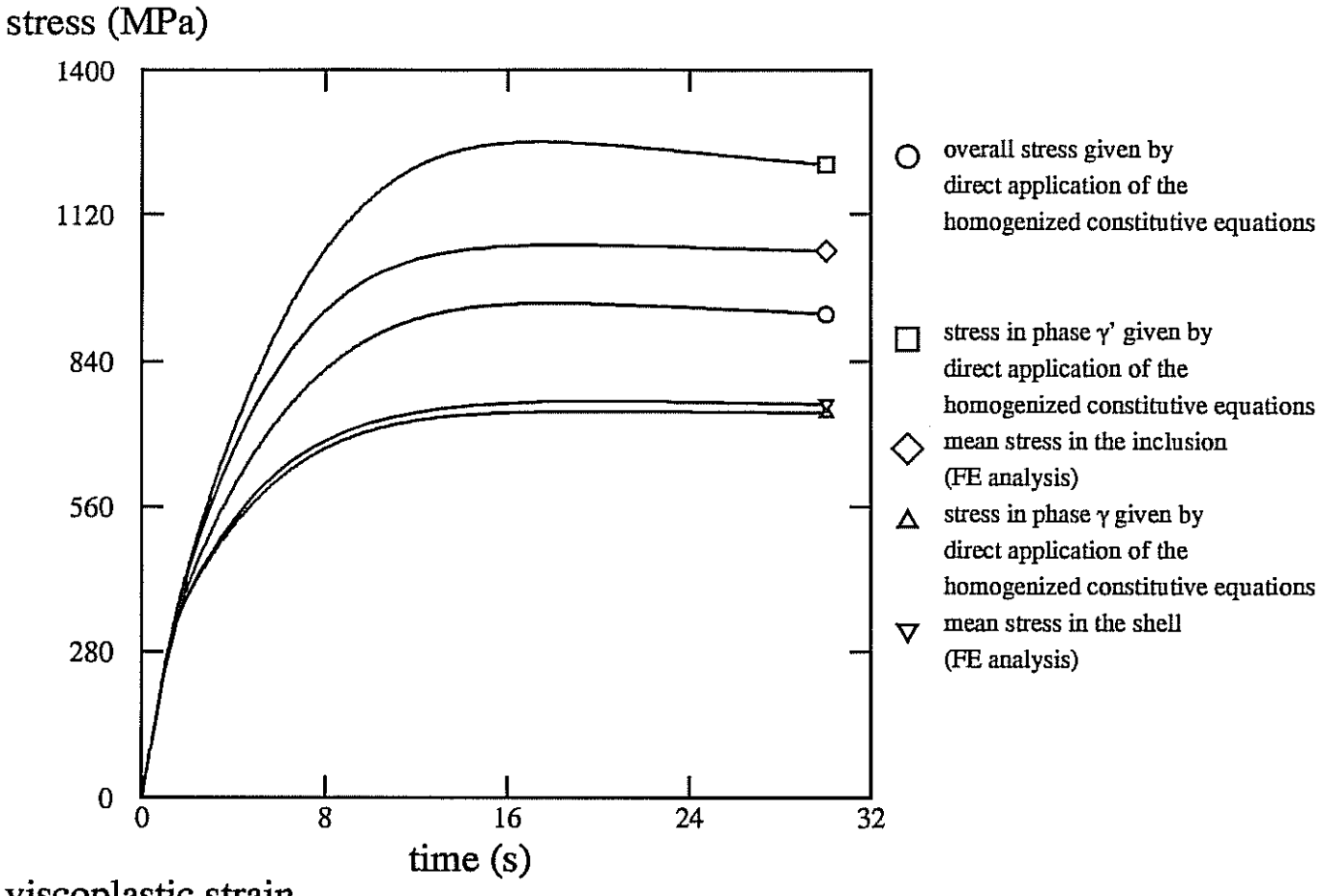

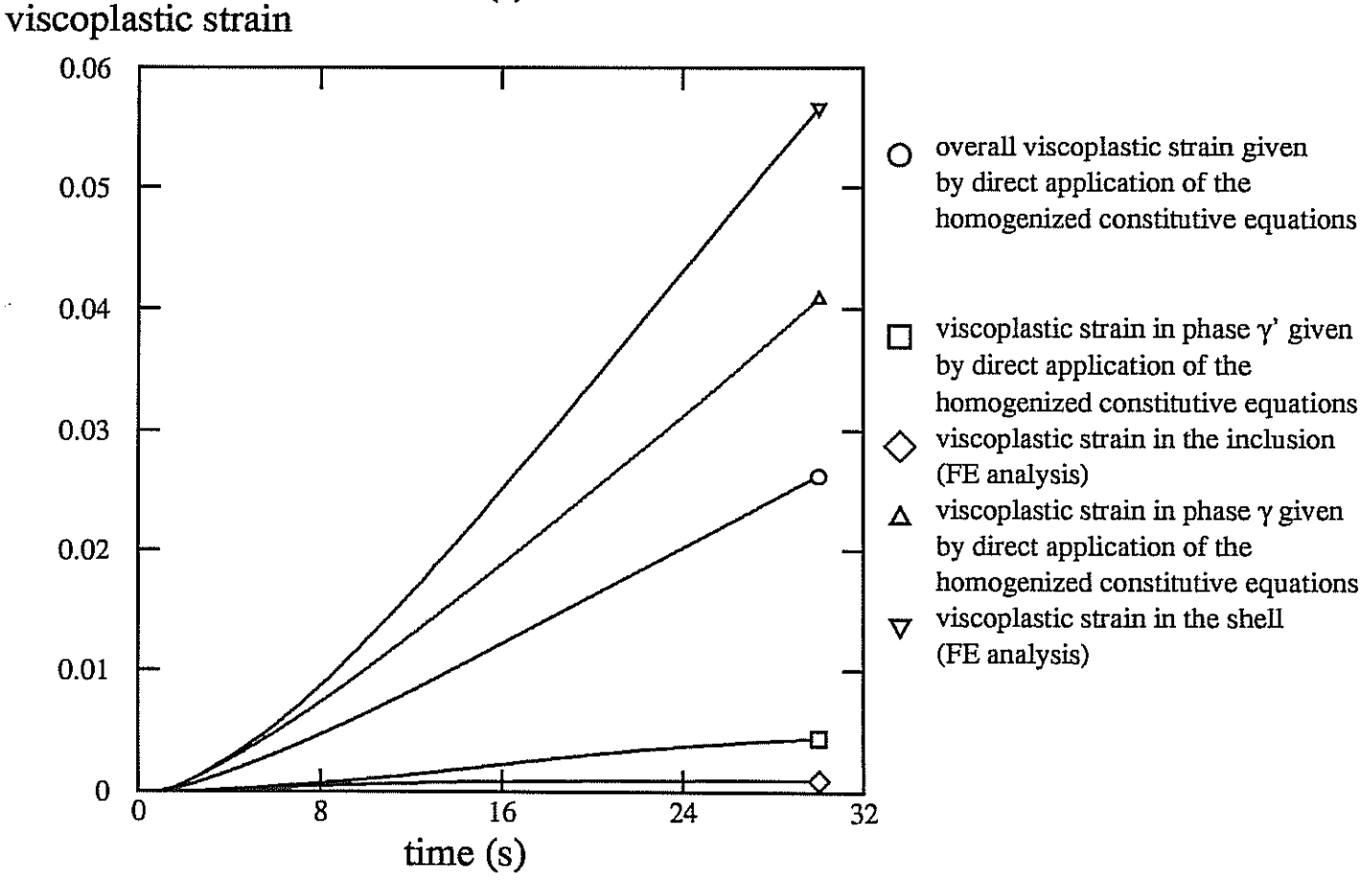

Figures D.60 and D.61: Mean stresses (above) and mean viscoplastic strains (below) given by the FE analysis and the direct application of the proposed model. (tension test at 10e-3s-1, in crystal direction <111>).

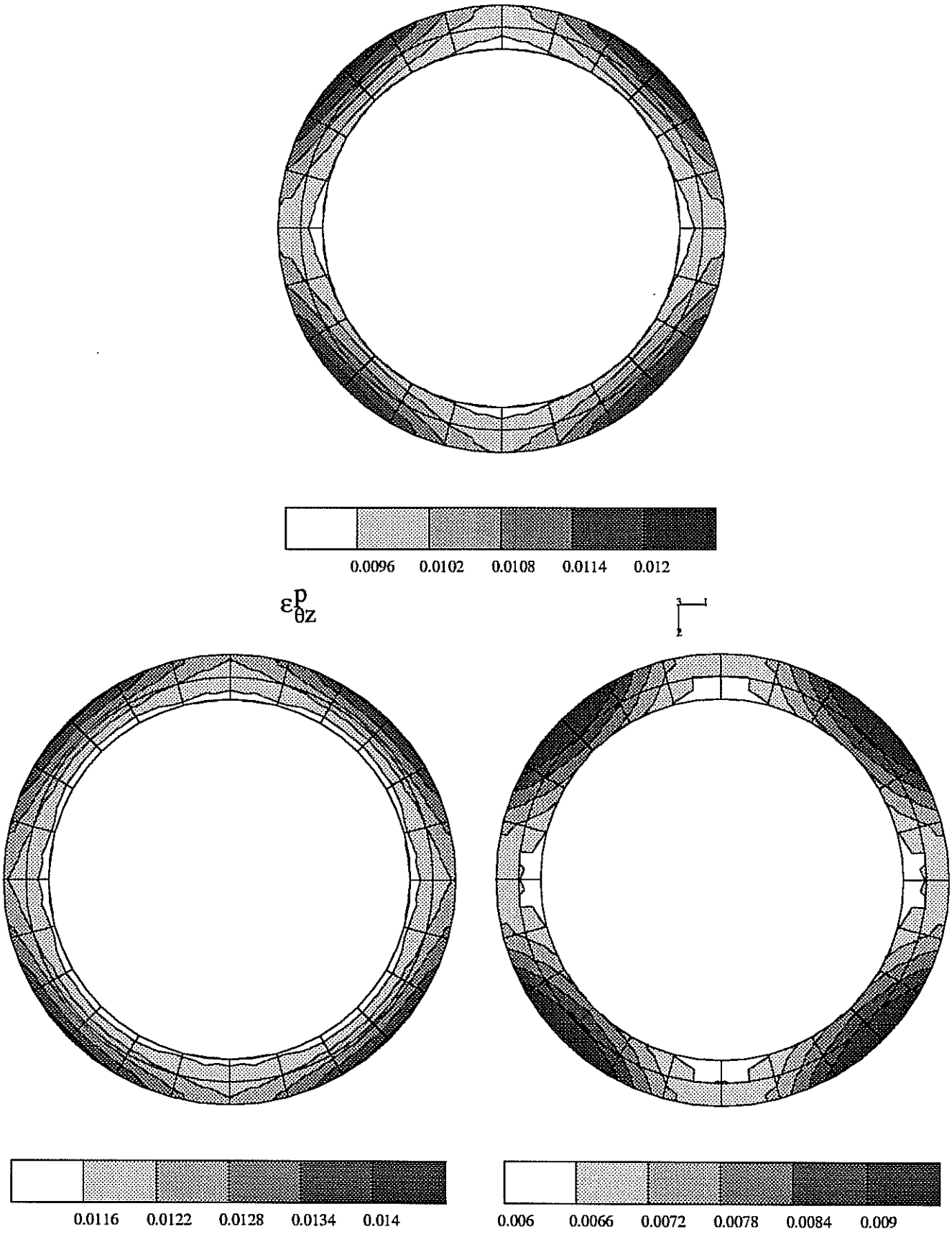

Figure D.62: Torsion test on SC16 at high temperature: overall viscoplastic deformation (above), deformation map in phase γ (left) and γ' (right) in a section of the tube.

Final discussion

1 Slip bands, kink bands, shear bands in f.c.c. single crystals

These localized deformation modes in single crystals have been interpreted as bifurcation modes for the non-linear boundary value problem, as done since [Hill, Hutchinson 1975]. A bifurcation analysis has been performed for single crystals undergoing symmetric multiple slip at small strain. The small strain framework allows us to consider situations for which 4, 6 or 8 slip systems are simultaneously activated. In contrast, Peirce [1983] studied double slip configurations at finite strain. For single slip the slip band and the kink band are equivalent bifurcation modes. Non crystallographic shear band orientations have been found for all other cases. For one and four slip systems, bifurcation may occur as soon as the hardening modulus vanishes. In all other cases the theoretical critical hardening modulus is strongly negative so that symmetry-breaking bifurcation modes may develop earlier. The predicted bifurcation modes have been simulated using the FE method. In each case the actual 3D geometry of f.c.c. single crystals has been considered. In contrast, most simulations of shear banding in literature make use of Asaro's planar model with 2 or more fictitious slip systems.

Local strain softening. Asaro and Rice [1977] have proved that bifurcation can occur in single crystals for single slip at finite strain with positive values of the hardening modulus. This is due to local geometrical softening and also non-Schmid effects. However this becomes possible only after significant straining and coarse slip bands are observed experimentally much earlier. Intense slip bands can appear at incipient plasticity and play a significant role in fatigue. This explains why strain softening must be introduced to trigger localization phenomena at the beginning of plastic flow. This choice is motivated by a stability analysis of evolution equation for dislocation populations from literature, which predicts two domains with negative hardening modulus, one at incipient plasticity, the other after large straining. The finite element simulations have then proved that a slip band can nucleate in a zone of local softening and cross surrounding hardening zones or subgrain boundaries and eventually the entire cross-section of the specimen. This is accompanied by a serration on the load-displacement curve. The introduction of subsequent hardening after the softening period into the constitutive behaviour leads to the formation of a slip band and the propagation of the localized deformation zone over the entire gauge length of the specimen in a way similar to Piobert-Lüders bands. A naïve view of these softening-hardening periods in single crystal behaviour could be the following: once some obstacles for dislocation motion have been freed on some slip planes, deformation localizes in them (softening period); afterwards, dislocations are more and more trapped on these planes and this leads to subsequent local hardening. Deformation will then take place in other virgin zones of the specimen. Nevertheless these effects have been introduced in a purely phenomenological manner. The adopted constitutive differential equations have a local character but describe non-local effects at the microscopic level where the evolution equations for dislocation populations are partial differential equations. In other words, microscopic bifurcation phenomena are replaced by deterministic softening-hardening rules at the volume element level. This underlines

the difficulty of the description of scale transitions, and extensions of the present work are necessary.

Effect of latent hardening. Dislocation interactions are represented in a phenomenological way by the interaction matrix h_{ij}. Strong effects of latent hardening on localization for symmetric double slip have been shown numerically. They can all be explained by the relation A.234. In particular, the usual case for aluminium and copper crystals for instance, that is $h_{11} < h_{12}$ (latent hardening strictly speaking), leads to stable symmetric double slip configurations in the softening regime. In the formed shear bands both slip systems are simultaneously activated, but their orientation is non crystallographic, which has not been observed experimentally. However Franciosi and Zaoui [1982] indicate that the interaction matrix is not fixed once and for all but that it strongly depends on the applied stress state. They have observed strong differences in the hardening behaviour at the beginning of plastic flow and at larger strains.

Effect of lattice rotation. The analysis with a formulation of the model at finite strain shows that, even though bifurcation occurs after only small straining, the final simulated bifurcation modes are different whether lattice rotation is taken into account or not. The macroscopic load-displacement curves are very similar for the two cases but, in the case of single slip, the final band can be a slip band or a kink band depending on the location of the defect and on the small or large strain framework. Large amounts of lattice rotation have been detected in the kink bands.

2 Description of lattice curvature and torsion within the framework of the mechanics of generalized continua

The gist of the continuum modelling of solids with microstructure consists in the choice of an Ersatz-continuum to represent the resulting properties of a heterogeneous microstructure in a continuum manner. The grade or order of this continuum depends on the refinement in the description of the microstructure. In particular the continuum is not bound to be a classical one (that is a first-gradient theory with only one symmetric stress tensor). Mandel [1971, 1973] has laid the basis for a classical treatment of finite deformations of single crystals. Some results of part A have led us to think that the classical framework is too restrictive to deal with non-homogeneous deformation of single crystals when strong lattice rotation gradients are present. The fact for instance that the slip band and kink band are equivalent bifurcation modes for single crystals undergoing single slip according to the analysis at small strains as well as the analysis at finite strains by Asaro and Rice [1977], should be regarded as a deficiency of the classical model of crystal plasticity. In fact, slip bands and kink bands are very different physical phenomena observed under different conditions. Slip bands are observed more frequently and earlier than kink bands in f.c.c. single crystals.

Contrary to slip bands, kink bands induce strong lattice rotation gradients. The associated strong lattice curvature is accommodated by geometrically necessary dislocations. A more precise description of dislocation populations within the representative volume element should distinguish geometrically necessary dislocations from statistically stored dislocations. The classical hardening variables are related only

to scalar dislocation densities measuring the total length of dislocations in the volume element. As for it the continuum theory of dislocations, since Nye [1953], considers only the dislocation density tensor which measures the resulting Burgers vector over a volume element.

In the present work, we have proposed to incorporate both aspects into the continuum modelling of single crystals. An even more refined description of dislocation distribution should include mobile and trapped dislocations or the density of dislocation loops. The main feature of the theory is that the description of lattice curvature associated with a non-vanishing dislocation density tensor and of the accompanying couple stresses requires the extension of the continuum to a Cosserat continuum (at least).

Finite elastoviscoplasticity of Cosserat crystals. Recent advances in the mechanics of generalized continua have been used to develop a Cosserat theory for single crystals at finite deformation and curvature. The decomposition of the deformation gradients into elastic and plastic parts is multiplicative as usual, whereas the wryness tensor admits the quasi-additive decomposition B.62. We have assumed that the plastic lattice curvature and torsion are accommodated respectively by edge and screw dislocations belonging to octahedral slip systems in f.c.c. single crystals. The curvature and torsion angles over a characteristic length due to each type of dislocation are internal variables in addition to the amounts of slip for each slip system. Ashby [1971] argues that the density of geometrically necessary dislocations can be directly calculated knowing the plastic strain heterogeneity, whereas the density of statistically stored dislocations can only be measured. The reason is that he works under the assumption of perfect plasticity for the curvature. In that case the plastic wryness tensor can be derived from the plastic deformation field. As soon as lattice elastic curvature is considered, constitutive equations are needed for the plastic curvature evolution rate. This allows a feedback of the curvature on the equilibrium through the effect of couple-stresses. Explicit constitutive equations have been proposed in the case of elastoviscoplasticity. An important consequence of the theory is that lattice rotation gradients are associated with dissipation. The production of geometrically necessary dislocations is clearly a dissipative process.

Renewal of the continuum theory of dislocations. The continuum theory of dislocations has been revisited. A great hope in the sixties was that it could bridge the gap between dislocation theory and plasticity theory. We have shown that the failure is due to its closure problem: it does not provide any constitutive equations and does not predict dislocation motion. The second reason is that the theory deals only with the dislocation density tensor which is not the relevant variable to describe the hardening of crystals. The links between the continously dislocated crystal and the Cosserat continuum has been seen since [Günther 1958] but most authors have worked with an inadequate constrained Cosserat continuum for which the directors are not lattice vectors but material vectors. As a result, the proposed Cosserat theory can be regarded, on the one hand, as the classical crystal plasticity theory complemented by the lacking lattice curvature and torsion variables and, on the other hand, as the continuum theory of dislocations closed by the missing hardening variables and constitutive equations within the appropriate Cosserat framework.

Hardening due to lattice curvature and torsion. A coupling between plastic curvature and plastic deformation has been introduced at the level of the hardening rule to represent the influence of slip plane curvature on further dislocation motion. Experimental evidence of such hardening effects have been provided in the fifties. Gilman [1955] investigated the bending of hexagonal single crystals and showed that the excess of dislocation of one sign leads after annealing to polygonization. As for him Jaoul [1956] and Jaoul, Bricot, Lacombe [1957] performed tensile tests on aluminium single crystals, annealed them and performed again the tensile tests. Due to annealing, statistically stored dislocations annihilate significantly, and the geometrically necessary dislocations generated by lattice rotation heterogeneities remain. When slip was rather homogeneous during the first test, no difference was noticed during the second test after recovery. In contrast for samples in which polygonized zones appeared, the yield stress was up to 75% bigger and the hardening behaviour was very different. The presence of locally curved slip planes led to the disparition of the easy glide part of the tensile curve. Similarly Paxton and Cottrell [1954] examined the effects of plastic twisting on the tensile deformation of aluminium crystals. They noticed an increased yield limit and work hardening. An interesting experiment would be to anneal the specimen after twisting and then perform a tensile test again in order to separate the hardening effect of local non-homogeneous lattice torsion from the interaction with stored dislocations belonging to the newly activated slip systems. An interesting aspect also is the hardening effect of geometrically necessary dislocations in the neighbourhood of a second phase as investigated by Ashby [1971]. Thermodynamical restrictions may exist to the hardening couplings effects so that an analysis similar to that of section A.3.2 must be performed. Some restrictions on the moduli H, H', and H_c, if uniqueness is to be ensured, can be worked out using the results of section B.4.2.

It is clear that the difference between the classical theory and the Cosserat theory can appear only if deformation and more precisely lattice rotation is not homogeneous. It means that the model must be implemented in a FE code to perform structural calculations. Contrary to the case of non-local or higher-grade theories, the implementation of a Cosserat model does not require fundamentally new developments. The nodes have twice as much degrees of freedom and the variational formulation must be complemented by the terms with couple-stresses. The torsion test will be an interesting first application of the theory. Much effort must now be concentrated, on the one hand, on the implementation of the model and, on the other hand, on the determination of estimates for parameters like H', H_c (equations B.197 and B.198). This will require additional experimental investigations like simple bending tests followed by tension and torsion-tension tests on single crystals (SC16 for instance) with annealing at larger strains.

3 Mesh dependence; physically motivated regularization methods

Results of calculations performed in a domain in which the uniqueness of the boundary value problem is not ensured must be interpreted with much caution. The predicted post-bifurcation behaviour in such cases is totally mesh-dependent. In particular, in our computations (part A and some sections of part D), the load drop (apparition and amplitude) and the post-bifurcation part of the load-displacement curves depend on the type and size of the elements, on the integration and resolution algorithms and precision.

The width of shear bands is also mesh-dependent. In contrast, the orientations of the obtained shear band turn out to be mesh-independent. In particular the localization bands do not coincide with the diagonal of square elements, as claimed sometimes in literature, provided quadratic elements are used. We could reproduce the whole variety of sometimes very peculiar predicted orientations. The main attention has been focused on the occurence or not of bifurcation modes and their orientation and not on the mesh-dependent post-bifurcation behaviour. In the case of slip band propagation (section D.2.1.2) the material displays strain hardening after a short softening period so that uniqueness is again ensured. Only the moment of apparition and amount of the load drop in this test remains questionable.

Role of viscoplasticity. A complete set of uniqueness and well-posedness theorems and localization criteria, as established in elastoplasticity, is still lacking in the case of viscoplasticity. Some regularization effects of viscoplasticity have been shown in literature. Loss of hyperbolicity is prevented by viscoplasticity in the dynamic case. In the static case the uniqueness of the solution has been proved in some one-dimensional cases. Our numerical investigations show the pseudo-regularization role played by viscoplasticity. Mesh-dependence turns out to decrease dramatically with increasing viscosity but the associated localization modes become more and more diffuse.

Regularization effects within the Cosserat framework. Many regularizing methods have been proposed in literature in the last ten years. The use of a Cosserat continuum is one of them. However they are often used in an *ad hoc* manner without a strong physical background. In contrast, we have developed our Cosserat theory in order to enrich the description of dislocation distribution at the continuum level and then inspected the possible regularizing capabilities of the model. The bifurcation analysis of section B.4.3 proves that the slip band and the kink band are two very different modes in the Cosserat framework. Regularization can be expected only if a strong coupling exists between lattice curvature and deformation. This is the case for kink bands but not for slip bands. It seems clear that more straightforward regularizing effects can be gained if non-locality or higher order gradients are introduced in the model. But we do not think at this moment that constitutive or kinematic restrictions can be derived from microstructural features as readily as for a Cosserat continuum. We think that the mechanics of generalized continua (including non-local, higher order, higher grade continua...) cannot be used as a regularization method for localization phenomena without strong physical motivations any longer. This is undoubtedly a new very attractive research field in micro-macro-mechanics of materials.

4 Between phenomenology and micromechanics...

Throughout this work we have tried to combine the efficiency of phenomenology with the sound basis of micro-mechanics and physics. The description of the kinematics of single crystals in both classical and Cosserat cases has its roots in crystallography and dislocation theory, whereas the hardening rules at the slip system level have a phenomenological character. Similarly, in the modelling of two-phase materials, we have adopted the phenomenologically motivated concentration law proposed by Pilvin

[1990] in order to overcome the tremendous difficulties of self-consistent modelling in elastoviscoplasticity under complex loading paths. Identification methods performed at the macroscopic level and at a more microscopic level, have been presented. They require heavy computations but, once the parameters have been determined, they provide explicit constitutive equations that can be used for structural calculations for industrial purposes.

Effective behaviour of multiphase materials. The method is based on the choice of one or more representative morphological patterns representing to some extent and in a statistical manner the microstructure of the material. According to the self-consistent scheme, this representative cell is embedded in the infinite unknown homogeneous equivalent medium. Homogeneous or mixed boundary conditions are prescribed at infinity. The corresponding calculations are performed using the FE method. Trial values of parameters characterizing the homogeneous equivalent medium must be chosen and can be some bounds in the elastic case. An optimization process runs then until the mean value of strain over the whole representative cell equals the macroscopic strain prescribed at infinity, up to a certain tolerance. This is the so-called "self-consistency condition", which has been derived by Hervé and Zaoui [1990] for the three-phase model. The method provides exact self-consistent estimates in the elastic case. The limitations of the method are the number of phases or representative cells and the refinement of the morphology description. It depends on the available ressources in computers.

The measurement of residual stresses or of stresses during testing by means of X-ray diffraction seems to be the suitable method to test the local predictions of the model for each phase. Although the misfit between the phases γ and γ' is very small, the two phases can be distinguished using this method [Zhou 1994]. The main advantage of the technique is that it does not give very local elastic strains in each precipitate or matrix channel, but mean values over a volume having the same size as our volume element. These are exactly the variables given by the homogenized constitutive equations. Such residual stresses measurements are now under process at the BAM-Berlin, as a result of this work.

Quasi-self-consistent modelling in the non-linear case. In the non-linear case we have assumed that the form of the constitutive equations for the homogeneous equivalent medium is known, which is of course an important restriction. Some parameters intervening in them are then determined using the same optimization procedure as previously, to best fulfill the self-consistency condition along some loading paths. If the proposed form of the homogenized constitutive equations is pertinent, this condition will then hold approximately also for other loading paths. This must of course be checked. We have shown for instance that the explicit concentration rule C.113 predicts with enough accuracy the mean stress state in each inclusion of phase i in the cyclic and non-proportional cases, even for elastoviscoplasticity. It must be noted that for the identification procedure we have considered a tension test only.

Extension to the anisotropic case: behaviour of SC16 at 950°C. Micromechanical modelling of single crystal nickel-base superalloy is usually based on an assumption of periodicity. The authors consider 2D or 3D cells containing one eightth of a cube or cuboidal γ' precipitate ([Müller, Glatzel, Feller-Kniepmeier 1993], [Benyucef 1994],

[Nouailhas, Cailletaud 1994]). In contrast, we have adopted the self-consistent approach which is appropriate mainly for totally disordered phase or pattern distributions. One of the reasons is that the phase distribution is quasi-periodic at the scale of some precipitates (some microns), but no space correlation subsists at the scale of 100 or more precipitates, which corresponds to the characteristic size retained for the volume element. The inclusion-matrix morphology has been taken into account via the generalized self-consistent scheme. The extension C.116 of concentration rule C.113 to the anisotropic case and constitutive equations for the two coherent single crystal phases have been proposed. In part C, the behaviour of each independent phase was assumed to be known and we wanted to model the effective behaviour. But in many situations the behaviour of one independent phase is different from the behaviour of the same phase within the aggregate. This holds for small grains in polycrystals and for the phases γ and γ' in single crystal nickel-base superalloys. This is due to hardening effects associated with the presence of interfaces and long-range internal stresses (due to dislocation pile-ups for instance). It means that the material parameters describing each phase must also be determined. For that purpose experimental data concerning, on the one hand, the macroscopic response of the material under tension and cyclic loading and, on the other hand, as much microscopic information as possible (local strains, activated slip systems...) must be introduced into the identification procedure. We have distinguished "geometrical" parameters from materials parameters: both sets of parameters must be identified simultaneously. The determination of the "geometrical" parameters requires large-scale FE computations over the representative cell embedded in the infinite homogeneous equivalent medium, whereas homogeneous mechanical tests are simulated and compared with experimental results for the identification of the material parameters. A simultaneous identification procedure is necessary because the "geometrical" parameters involved in the concentration rule depend also on the behaviour of each phase.

Only scarce information on the stress-strain state of each phase during straining was available. The only clear microstructural information is that at high temperature and for low strain rates deformation takes place mainly in the matrix channels. During the identification procedure, constraints have been imposed on the relative critical shear stresses and hardening moduli of the two-phases. A satisfying description of tension and cyclic tests in direction [001] has been obtained. In this work, creep has been modelled in a tentative manner and, in particular, no attention has been paid to the fulfillment or not of the "self-consistency" condition during the simulation of a creep test. This is an incentive for future work in the field: "quasi-self-consistent modelling" of creep. The tensile behaviour in directions [111] and [011] is also correctly accounted for, but additional experiments are needed. With the proposed parameters, the model fulfills the "self-consistency" condition for tension tests in directions [001](identification), [011](prediction) but not so well for [111](prediction). The discrepancy in the last case may indicate that the explicit concentration rule, well-suited for the purely self-consistent scheme, remains too crude to be used in the configuration of the three-phase model. However, we are using a very coarse mesh and it is surely not fine enough for the three-phase model. A finer mesh leads to too large computing time, unless parallel computers are used. The next step will be to perform again the whole identification procedure with, this time, two tension tests ([001] and [111] directions) on the representative cell in its infinite medium. Some modifications of the concentration rule have been proposed in section D.3.3.2. Lastly this identification process must also include the cubic slip systems,

as soon as enough experimental data are available.

5 Quantitative analysis of localized deformation

Sophisticated mechanical models accounting for non-homogeneous deformation of materials cannot develop without parallel advances in experimental techniques of local strain measurements. The use of microgrids has proved successfull to study the formation of shear bands ([Yang 1990], [Allais, Bornert, Bretheau, Caldemaison 1994]). The measurement of local relative lattice rotations with the EBSP method is also a very helpful tool. We have shown that strain gauges can be used if the location of strain heterogeneities are *a priori* known.

Local strain measurements in non-uniform fields. The analysis of tension-torsion tests on SC16 single crystals at room temperature presented in section D.2.2 proves that very complex strain distributions can be detected using a sufficient number of strain gauges. This requires constant exchanges between FE simulation, specimen preparation and final testing. Preliminary calculations are needed to choose carefully the number and location of the strain gauges. The feedback to the model has shown good prediction capabilities of the classical crystal plasticity framework. Tests on [011] and [111] specimens are planned and the comparison of local measurements with the FE analysis will be performed. Nevertheless, the use of strain gauges is not well-suited for torsion at larger strains. Furthermore experimental techniques are still lacking to investigate the strain field during torsion at high temperature and thus check the conjectures formulated in section D.3.4.

Interpretation of tensile curves for single crystals at low temperature. Some common features can be noticed between tensile curves of single crystal nickel-base superalloys at room temperature (see figures D.1, D.11 and D.12). The yield point is followed by a small load drop, a plateau and subsequent hardening. We would like to emphasize the fact that such load-displacement curves may well be systematically associated with non-homogeneous deformation of the specimen during testing. Experimental evidence of intense slip band propagation has been shown in some cases. A tentative modelling of this phenomenon has been proposed. It is likely that the actual hardening properties of the material can be read on the load-displacement curve only once slip bands have invaded the entire specimen gauge, which corresponds to the subsequent hardening period. A quantitative modelling of slip band propagation could integrate these hardening properties as the intrinsic hardening behaviour of the single crystal, after a short imperceptible local softening transition to trigger localization. However any quantitative analysis of post-bifurcation computations requires the use of a regularizing method as explained in section 3 of this discussion.

From localization to fracture. Void nucleation and growth within shear bands or necking zones lead to the final failure of ductile crystals. Under cyclic loading conditions, extrusion/intrusion mechanisms within intense slip bands lead to crack intitiation and final propagation. In the two cases, developments are needed to model the transition from the localized deformation modes presented in this work to final rupture. Similarly, strain

heterogeneities in two-phase single crystals play a significant role in damage mechanisms. The proposed model provides a large number of local variables (average viscoplastic strain in each phase, amount of slip for each slip system in each phase...) that may be the critical variables for the developments of damage models. An attempt in that direction is proposed in [Legait 1994]. But it is important to determine the relevant length scale for damage and fracture. For nickel-base superalloys, porosities play a significant role and are much bigger that the precipitates.

It is likely that all ressources of crystal plasticity, finite deformation theory, mechanics of generalized continua and homogenization techniques, together with a sound knowledge of physical mechanisms, will be required to better the description of material behaviour until final rupture. The breathtaking potentials of parallel computing now make possible the achievement of this ultimate goal.

Appendix 1

NOTATIONS

"The picturial approach motivates the mathematics;
the abstract approach makes the picturial ideas precise;
but to actually do complex calculations, we need components."

Misner, Thorne, Wheeler, Gravitation.

1 Tensor algebra

In the following, $\underline{\mathbf{a}}$ denotes a vector of the Euclidean space $\mathbf{E}$, $\underset{\sim}{\mathbf{A}}$ a second-rank Euclidean tensor, and $\underline{\underset{\sim}{\mathbf{A}}}$ (resp. $\underline{\underline{\mathbf{A}}}$) a third-rank tensor when operating on a vector (resp. a second-rank tensor). The same third-rank tensor is denoted $\underline{\underline{\underline{\mathbf{A}}}}$ when regarded as a 3-linear form. The tensor product of two vectors $\underline{\mathbf{a}}, \underline{\mathbf{b}}$ is such that, for all $\underline{\mathbf{x}} \in \mathbf{E}$,

$$\begin{aligned} \underline{\mathbf{x}}\,(\underline{\mathbf{a}} \otimes \underline{\mathbf{b}}) &= \underline{\mathbf{x}}.\underline{\mathbf{a}}\;\underline{\mathbf{b}} \\ (\underline{\mathbf{a}} \otimes \underline{\mathbf{b}})\,\underline{\mathbf{x}} &= \underline{\mathbf{b}}.\underline{\mathbf{x}}\;\underline{\mathbf{a}} \end{aligned} \tag{1}$$

where the dot denotes the inner product on $\mathbf{E}$.

Let $(\underline{\mathbf{e}}_1, \underline{\mathbf{e}}_2, \underline{\mathbf{e}}_3)$ be a direct orthonormal basis of oriented $\mathbf{E}$ with dimension 3. When written in components, the double contraction of second-rank tensors reads

$$\underset{\sim}{\mathbf{A}} : \underset{\sim}{\mathbf{B}} = A_{ij}B_{ij} \tag{2}$$

We note $\underline{\underline{\epsilon}}$ the Levi-Civita tensor

$$\underline{\underline{\underline{\epsilon}}} = \mathrm{Det}(\underline{\mathbf{e}}_j, \underline{\mathbf{e}}_k, \underline{\mathbf{e}}_l)\; \underline{\mathbf{e}}_j \otimes \underline{\mathbf{e}}_k \otimes \underline{\mathbf{e}}_l \tag{3}$$

Notice the useful identity

$$\epsilon_{ijk}\,\epsilon_{ilm} = \delta_{jl}\,\delta_{km} - \delta_{jm}\,\delta_{kl} \tag{4}$$

The following result concerning third-rank tensors will be used,

$$\begin{aligned} \text{If} \quad & \underset{\sim}{\mathbf{B}} = \tfrac{1}{2}\,\underline{\underline{\epsilon}} : \underline{\underline{\mathbf{A}}} = \tfrac{1}{2}\,\epsilon_{ikl}\,A_{klj}\;\underline{\mathbf{e}}_i \otimes \underline{\mathbf{e}}_j \\ \text{and} \quad & A_{ijk} = -A_{jik} \\ \text{then} \quad & \underline{\underline{\mathbf{A}}} = \underline{\underline{\epsilon}} \cdot \underset{\sim}{\mathbf{B}} = \epsilon_{ijm}\,B_{mk}\;\underline{\mathbf{e}}_i \otimes \underline{\mathbf{e}}_j \otimes \underline{\mathbf{e}}_k \end{aligned} \tag{5}$$

The cross product is defined by

$$\underline{\mathbf{a}} \times \underline{\mathbf{b}} = \underline{\underline{\epsilon}}\,(\underline{\mathbf{a}} \otimes \underline{\mathbf{b}}) = \epsilon_{ijk}\,a_j b_k\;\underline{\mathbf{e}}_i \tag{6}$$

The two following results are used in section B.1.2 and are derived in [Trostel 1993]. Let $\underset{\sim}{\mathbf{Q}}$ be an orthogonal tensor. Then

$$(\underset{\sim}{\mathbf{Q}}\,\underline{\mathbf{a}}) \times (\underset{\sim}{\mathbf{Q}}\,\underline{\mathbf{b}}) = \underset{\sim}{\mathbf{Q}}\,(\underline{\mathbf{a}} \otimes \underline{\mathbf{b}})\;\mathrm{Det}\underset{\sim}{\mathbf{Q}} \tag{7}$$

and

$$\begin{aligned} \underset{\sim}{\epsilon}\,(\underset{\sim}{Q}\,(\underline{a}\otimes\underline{b})\underset{\sim}{Q}^T) &= \epsilon_{ijk}\,Q_{jm}\,a_m\,b_n\,Q^T_{nk}\,\underline{e}_i \\ &= (\underset{\sim}{Q}\,\underline{a})\,\times\,(\underset{\sim}{Q}\,\underline{b}) \\ &= \underset{\sim}{Q}\,(\underline{a}\times\underline{b})\,\mathrm{Det}\underset{\sim}{Q} \\ &= \underset{\sim}{Q}\,\underset{\sim}{\epsilon}(\underline{a}\otimes\underline{b})\,\mathrm{Det}\underset{\sim}{Q} \end{aligned} \tag{8}$$

The symmetric and antisymmetric parts of tensor $\underset{\sim}{A}$ are respectively denoted $\{\underset{\sim}{A}\}$ and $\}\underset{\sim}{A}\{$. There is then one and only one vector $\overset{\times}{\underline{A}}$ such that, for all $\underline{x}$,

$$\}\underset{\sim}{A}\{\,\underline{x} = \overset{\times}{\underline{A}}\times\underline{x} \tag{9}$$

and

$$\overset{\times}{\underline{A}} = -\frac{1}{2}\,\underset{\sim}{\epsilon}\,\underset{\sim}{A} = -\frac{1}{2}\,\epsilon_{klm}\,A_{lm}\,\underline{e}_k \tag{10}$$

In matrix form,

$$\left[\,\}\underset{\sim}{A}\{\,\right] = \begin{bmatrix} 0 & -\overset{\times}{A}_3 & \overset{\times}{A}_2 \\ \overset{\times}{A}_3 & 0 & -\overset{\times}{A}_1 \\ -\overset{\times}{A}_2 & \overset{\times}{A}_1 & 0 \end{bmatrix} \tag{11}$$

Following Trostel [1993], we define a cross product between a second-rank tensor and a vector

$$\begin{aligned} (\underline{a}\otimes\underline{b})\times\underline{c} &= \underline{a}\otimes(\underline{b}\times\underline{c}) \\ \underline{a}\times(\underline{b}\otimes\underline{c}) &= (\underline{a}\times\underline{b})\otimes\underline{c} \end{aligned} \tag{12}$$

so that

$$\underset{\sim}{A}\times\underline{c} = -(\underline{c}\times\underset{\sim}{A}^T)^T \tag{13}$$

As a result

$$\}\underset{\sim}{A}\{ = \underset{\sim}{1}\times\overset{\times}{\underline{A}} = -\underset{\sim}{\epsilon}\,\overset{\times}{\underline{A}} \tag{14}$$

Rotations

Any element $\underset{\sim}{R}$ of the orthogonal group can be represented by the element $\underline{\Phi}$ of the associated Lie group such that

$$\underset{\sim}{R} = \exp(\underset{\sim}{1}\times\underline{\Phi}) = \exp(-\underset{\sim}{\epsilon}\,\underline{\Phi}) \tag{15}$$

and

$$\underline{\Phi} = \theta\,\underline{n} \tag{16}$$

where θ is the rotation angle with respect to rotation axis $\underline{n}$. Accordingly

$$\underset{\sim}{R} = \cos\theta\underset{\sim}{1} + \frac{1-\cos\theta}{\theta^2}\,\underline{\Phi}\otimes\underline{\Phi} + \frac{\sin\theta}{\theta}\,\underset{\sim}{1}\times\underline{\Phi} \tag{17}$$

Defining $\underset{\sim}{\Omega} = \dot{\underset{\sim}{R}}\underset{\sim}{R}^T$, a relation

$$\dot{\underline{\Phi}} = \underset{\sim}{T}^{-1}\,\overset{\times}{\underline{\Omega}} \tag{18}$$

can be derived, the matrix form of $\underset{\sim}{\mathbf{T}}$ being

$$\begin{bmatrix} \frac{\sin\theta}{\theta} + \frac{1-\frac{\sin\theta}{\theta}}{\theta^2}\Phi_1^2 & \frac{1-\frac{\sin\theta}{\theta}}{\theta^2}\Phi_1\Phi_2 - \frac{1-\cos\theta}{\theta^2}\Phi_3 & \frac{1-\frac{\sin\theta}{\theta}}{\theta^2}\Phi_1\Phi_3 + \frac{1-\cos\theta}{\theta^2}\Phi_2 \\ \frac{1-\frac{\sin\theta}{\theta}}{\theta^2}\Phi_1\Phi_2 + \frac{1-\cos\theta}{\theta^2}\Phi_3 & \frac{\sin\theta}{\theta} + \frac{1-\frac{\sin\theta}{\theta}}{\theta^2}\Phi_2^2 & \frac{1-\frac{\sin\theta}{\theta}}{\theta^2}\Phi_2\Phi_3 - \frac{1-\cos\theta}{\theta^2}\Phi_1 \\ \frac{1-\frac{\sin\theta}{\theta}}{\theta^2}\Phi_1\Phi_3 - \frac{1-\cos\theta}{\theta^2}\Phi_2 & \frac{1-\frac{\sin\theta}{\theta}}{\theta^2}\Phi_2\Phi_3 + \frac{1-\cos\theta}{\theta^2}\Phi_1 & \frac{\sin\theta}{\theta} + \frac{1-\frac{\sin\theta}{\theta}}{\theta^2}\Phi_3^2 \end{bmatrix}$$

The associated intrinsic formulation of which is

$$\underset{\sim}{\mathbf{T}} = \frac{\sin\theta}{\theta}\,\underset{\sim}{\mathbf{1}} + \frac{1-\frac{\sin\theta}{\theta}}{\theta^2}\,\underline{\mathbf{\Phi}}\otimes\underline{\mathbf{\Phi}} + \frac{1}{2}\left(\frac{\sin\theta/2}{\theta/2}\right)^2\underset{\sim}{\mathbf{1}}\times\underline{\mathbf{\Phi}} \tag{19}$$

This treatment of rotations is recommended in [Géradin 1992].

2 Tensor analysis

nabla operator

$$\underline{\nabla} = {}_{,i}\,\underline{\mathbf{e}}_i \tag{20}$$

gradient operator

$$\underline{\text{grad}}\, f = f\,\underline{\nabla} = f_{,i}\,\underline{\mathbf{e}}_i \tag{21}$$

$$\underset{\sim}{\text{grad}}\,\underline{\mathbf{u}} = \underline{\mathbf{u}}\otimes\underline{\nabla} = u_{i,j}\,\underline{\mathbf{e}}_i\otimes\underline{\mathbf{e}}_j \tag{22}$$

curl operator

$$\underline{\text{curl}}\,\underline{\mathbf{u}} = \underline{\mathbf{u}}\times\underline{\nabla} = \epsilon_{ijk}\,u_{j,k}\,\underline{\mathbf{e}}_i \tag{23}$$

$$\underset{\sim}{\text{curl}}\,\underset{\sim}{\mathbf{A}} = \underset{\sim}{\mathbf{A}}\times\underline{\nabla} = \epsilon_{hjk}\,A_{ij,k}\,\underline{\mathbf{e}}_i\otimes\underline{\mathbf{e}}_h \tag{24}$$

Note that

$$\}\underline{\mathbf{u}}\otimes\underline{\nabla}\{ = \frac{1}{2}\,\underset{\sim}{\epsilon}(\underline{\text{curl}}\,\underline{\mathbf{u}}) \tag{25}$$

The definition of the curl operator of a second-rank tensor is the same as in [Teodosiu 1982] but Kröner [1958] uses

$$\underset{\sim}{\text{curl}}\,\underset{\sim}{\mathbf{A}} = \underline{\nabla}\times\underset{\sim}{\mathbf{A}} = \epsilon_{ijk}\,A_{kh,j}\,\underline{\mathbf{e}}_i\otimes\underline{\mathbf{e}}_h \tag{26}$$

divergence operator

$$\text{div}\,\underline{\mathbf{u}} = \underline{\mathbf{u}}.\underline{\nabla} = u_{i,i} \tag{27}$$

$$\underline{\text{div}}\,\underset{\sim}{\mathbf{A}} = \underset{\sim}{\mathbf{A}}\,\underline{\nabla} = A_{ij,j}\,\underline{\mathbf{e}}_i \tag{28}$$

We now write the general version of Stokes' theorem as given in [Schouten 1954](index form)

$$\int_{\tau_{q+1}} \partial_{\}\mu} V_{\lambda_1\ldots\lambda_q\{}\, df^{\mu\lambda_1\ldots\lambda_q} = \int_{\tau_q} V_{\lambda_1\ldots\lambda_q}\, df^{\mu\lambda_1\ldots\lambda_q} \tag{29}$$

Direct applications are

$$\int_S \underline{\mathbf{u}}.\underline{\mathbf{n}}\; dS = \int_V \text{div}\,\underline{\mathbf{u}}\; dV \tag{30}$$

where the domain V is bounded by S.

$$\int_S \underset{\sim}{\mathbf{A}}\ \underline{\mathbf{n}}\ dS \ = \ \int_V \underline{\mathrm{div}}\ \underset{\sim}{\mathbf{A}}\ dV \tag{31}$$

and

$$\oint_L \underline{\mathbf{u}}.\underline{\mathbf{l}}\ dl \ = \ -\int_S (\underline{\mathrm{curl}}\ \underline{\mathbf{u}}).\underline{\mathbf{n}}\ dS \tag{32}$$

where the open surface S is bounded by the contour L.

$$\oint_L \underset{\sim}{\mathbf{A}}\ \underline{\mathbf{l}}\ dl \ = \ -\int_S (\underset{\sim}{\mathrm{curl}}\ \underset{\sim}{\mathbf{A}})\ \underline{\mathbf{n}}\ dS \tag{33}$$

For instance the last equation can be derived from 29 as follows

$$\begin{aligned}
\oint_L A_{ik}\ dl_k \ &= \ \int_S \partial_{\}\mu} A_{ik\{}\ dS^{\mu k} \\
&= \ \frac{1}{2}\int_S \epsilon_{\mu kl}\ (A_{ik,\mu} \ - \ A_{i\mu,k})\ dS^l \\
&= \ \int_S \epsilon_{\mu kl}\ A_{ik\mu}\ dS^l \\
&= \ -\int_S \epsilon_{lk\mu}\ A_{ik\mu}\ dS^l
\end{aligned} \tag{34}$$

where $d\underset{\sim}{\mathbf{S}} \ = \ \underset{\approx}{\epsilon}\ \underline{dS} \ = \ \epsilon_{\mu kl}\ dS^l\ \underline{\mathbf{e}}_\mu \otimes \underline{\mathbf{e}}_k$.

Appendix 2

DESCRIPTION OF FINITE INELASTIC DEFORMATIONS OF POLYCRYSTALS

1 Setting of the problem

The purpose of this section is to show that the quasi-systematic method to develop constitutive models at large strains for solids with microstructure, that we have proposed in section A.7, can be applied to even more complicated microstructures than that of single crystals. We now apply it to the extension at large strains of the model for polycrystalline aggregates presented in [Cailletaud 1992] and [Pilvin 1994].

In order to be still more precise and reliable, the material description must take the inner structure of the materials into account. Such microstructure-based models replace the ever increasing number of parameters in the usual phenomenological approach by a large number of internal variables that sometimes challenges computation capabilities. However the development of computers is now such that FE calculations using polycrystalline models are possible and will be of the utmost importance ([Legait 1994]). A compromise nevertheless must be found between the precision of the modelling and efficiency. That is why we give up building a mesh for each grain of the microstructure up to a certain grain size with respect to the size of the component to be computed. Instead we resort to homogenization techniques ([Hill 1965]). The classical volume element of continuum mechanics is now a representative volume element, representative of the microstructure.

From the microstructure of polycrystalline aggregates we retain only a certain number of crystal orientations called phases and we neglect other geometrical parameters like grain size or shape. Each phase represents the entire group of grains having the same orientation within a certain tolerance. Only average stresses and strains will be considered in each phase. Transition relations between local and overall levels are needed. The simplest transition rules are that of Sachs model for which local and overal stresses are equal, and that of Taylor model for which local and overall velocity gradients are equal. Taylor model has proved to be a crude but efficient approximation for qualitative texture evolution prediction and is used for instance in [Besdo, Müller 1992]. The self-consistent approximation turns out to be a more reliable and more ambitious attempt for modelling polycrystals behaviour. It is well adapted for the description of highly disordered microstructures (no spatial correlation between the orientations of individual grains). The method consists in solving for each phase the problem of a single crystal inclusion in a homogeneous matrix, the behaviour of which being that of the wanted homogeneous equivalent medium. This generally results in a complex implicit integral differential equation. However Berveiller and Zaoui [1979] could work out an explicit concentration rule in the case of isotropic elastoplasticity, radial monotonous loading and spherical grains (at small strains):

$$\underset{\sim}{\sigma}^g = \underset{\sim}{\Sigma} + 2\alpha\mu(1-\beta)(\underset{\sim}{\mathbf{E}}^p - \underset{\sim}{\varepsilon}^{pg}) \tag{1}$$

where $\underset{\sim}{\sigma}^g$ denotes the average stress in phase g, $\underset{\sim}{\Sigma}$ the overall stress, α the secant (or tangent) elastoplastic modulus, and $\beta \approx \frac{1}{2}$. Elasticity is assumed homogeneous so that

$$\underset{\sim}{\mathbf{E}}^p = < \underset{\sim}{\varepsilon}^{pg} > \tag{2}$$

Cailletaud [1987] and Pilvin [1990] adopt relation 1 for its simplicity and use a similar concentration rule within the framework of elastoviscoplasticity to simulate complex multiaxial cyclic loadings:

$$\underset{\sim}{\sigma}^g = \underset{\sim}{\Sigma} + \mu(\underset{\sim}{\mathbf{B}} - \underset{\sim}{\beta}^g) \tag{3}$$

with

$$\underset{\sim}{\mathbf{B}} = \sum_g f^g \, \underset{\sim}{\beta}^g \tag{4}$$

and

$$\dot{\underset{\sim}{\beta}}^g = \dot{\underset{\sim}{\varepsilon}}^{vg} - \frac{2}{3} D J_2(\dot{\underset{\sim}{\varepsilon}}^{vg}) \, \underset{\sim}{\beta}^g \tag{5}$$

f^g being the volume fraction of phase g. D is a geometrical parameter that must be determined to best fulfill the self-consistency condition. The main advantage of the model is that it is simple enough to allow calculations under complex cyclic loading paths and even FE calculations. However no textural development is predicted.

The formulation of the self-consistent scheme for polycrystals at large strains has been settled in [Lipinski, Berveiller 1989] and [Lipinski, Krier, Berveiller 1990] using Green's techniques. The behaviour of each grain is described by Mandel's model. An integral equation linking the local and overall velocity gradients is worked out but no explicit simple localization rule can be derived. Clearly the numerical methods required for solving the integral equation hamper an implementation in a FE code.

In contrast we propose here a model for polycrystals that transposes the simple concentration rule 3 into the framework of finite deformation and thus makes the problem numerically tractable, even for finite element calculations.

2 Local placement of the microstructure

In the case of polycrystals we see once more some privileged observers that could help simplifying the writing of constitutive equations. Using the corotational frame we get rid of local rotations that do not intervene in the material behaviour and we can follow the deformation of material fibers. This gives furthermore a priviledged point of view from which we can follow the evolution of the microstructure, namely the rotations of grains with respect to this frame. That is why we consider for each $X \in \mathcal{B}$ the corotational local placement K_c and a collection of local placements $K_\sharp^g$ in $E^{\sharp g}$, associated with the undistorted lattice of all grains having a common orientation.

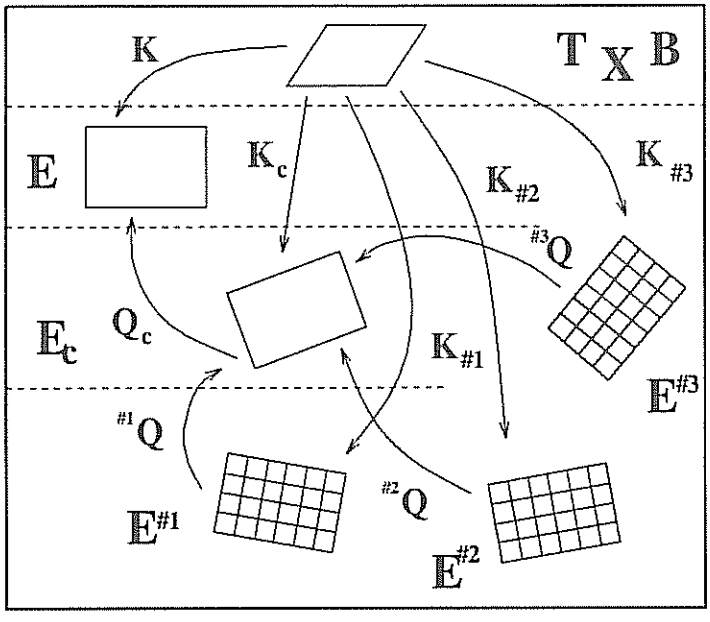

A finite number of orientations are taken into account, resulting from the discretization of the orientation distribution function that is given by pole figures. The discretization proceeds as follows: the standard triangle of the inverse pole figure is divided into several boxes and the retained orientation is that of the center of each box. The volume fraction f^g is attributed to each orientation after integration of the intensity function in the box it belongs to. Applying all the symmetries compatible with the crystallographic structure on the sample yields a discretized texture G: 4, 10 or 28 boxes give 40, 240 and 2016 orientations respectively for f.c.c. crystals (figure 33 for instance). The texture is isotropic when $f^g = \mathrm{C}^{\mathrm{st}}\ \forall g \in G$.

The different steps of the modelling are the following:

transport rules in the corotational frame

$$ {}^{c}\underset{\sim}{\mathrm{D}} = {}^{c}\underset{\sim}{\mathrm{Q}}^{T}\ {}^{c}\underset{\sim}{\mathrm{D}}\ {}^{c}\underset{\sim}{\mathrm{Q}} \tag{6} $$

$$ \underset{\sim}{\mathrm{S}} = {}^{c}\underset{\sim}{\mathrm{Q}}^{T}\ \underset{\sim}{\mathrm{T}}\ {}^{c}\underset{\sim}{\mathrm{Q}}\ \mathrm{Det}\ \underset{\sim}{\mathrm{F}} \tag{7} $$

strain rate additive decomposition

$$ {}^{c}\underset{\sim}{\mathrm{D}} = \dot{\underset{\sim}{\mathrm{e}}}^{e} + \dot{\underset{\sim}{\mathrm{e}}}^{p} \tag{8} $$

elastic law

$$ \underset{\sim}{\mathrm{S}} = \underset{\sim\sim}{\mathrm{C}} : \underset{\sim}{\mathrm{e}}^{e} \tag{9} $$

localization rules

$$ \underset{\sim}{\mathrm{S}}^{g} = \underset{\sim}{\mathrm{S}} + C(\underset{\sim}{\mathrm{B}} - \underset{\sim}{\beta}^{g}) \tag{10} $$

$$ \tau^{sg} = \underset{\sim}{\mathrm{S}}^{g} : ({}^{c}\underline{\mathrm{m}}^{sg} \otimes {}^{c}\underline{\mathrm{n}}^{sg}) \tag{11} $$

homogenization rules

$$\underset{\sim}{\mathbf{B}} = \sum_g f^g \, \underset{\sim}{\beta}^g \tag{12}$$

$$\underset{\sim}{\dot{\mathbf{e}}}^p = \sum_g f^g \, \underset{\sim}{\dot{\mathbf{e}}}^{pg} \tag{13}$$

intergranular kinematical hardening evolution rule

$$\underset{\sim}{\dot{\beta}}^g = \underset{\sim}{\dot{\mathbf{e}}}^{pg} - D\frac{2}{3}J_2(\underset{\sim}{\dot{\mathbf{e}}}^{pg}) \, \underset{\sim}{\beta}^g \tag{14}$$

intracrystalline behaviour

$$\underset{\sim}{\dot{\mathbf{e}}}^{pg} = \sum_s \dot{\gamma}^{sg} \, \{ {}^c\underline{\mathbf{m}}^{sg} \otimes {}^c\underline{\mathbf{n}}^{sg} \} \tag{15}$$

$$\dot{\gamma}^{sg} = < \frac{\mid \tau^{sg} - x^{sg} \mid - r^{sg}}{k} >^n \ \text{sign} \ (\tau^{sg} - x^{sg}) \tag{16}$$

$$r^{sg} = r_0 + q \sum_{r=1}^{N} h^{sr}(1 - \exp(-bv^{sg})) \tag{17}$$

$$\dot{v}^{sg} = \mid \dot{\gamma}^{sg} \mid . \tag{18}$$

$$x^{sg} = c \, \alpha^{sg} \tag{19}$$

$$\dot{\alpha}^{sg} = \dot{\gamma}^{sg} - d\dot{v}^{sg}\alpha^{sg} \tag{20}$$

rotation evolution equations

$${}^c\dot{\underset{\sim}{\mathbf{Q}}} \, {}^c\underset{\sim}{\mathbf{Q}}^T = \underset{\sim}{\mathbf{W}} \tag{21}$$

$${}^{\natural}\dot{\underset{\sim}{\mathbf{Q}}}^g \, {}^{\natural}\underset{\sim}{\mathbf{Q}}^{gT} = - \sum_s \dot{\gamma}^{sg} \, \} \, {}^c\underline{\mathbf{m}}^{sg} \otimes {}^c\underline{\mathbf{n}}^{sg} \, \{ \tag{22}$$

$${}^c\underline{\mathbf{m}}^{sg} = {}^{\natural}\underset{\sim}{\mathbf{Q}}^g \, {}^{\natural}\underline{\mathbf{m}}^{sg} \qquad {}^c\underline{\mathbf{n}}^{sg} = {}^{\natural}\underset{\sim}{\mathbf{Q}}^g \, {}^{\natural}\underline{\mathbf{n}}^{sg} \tag{23}$$

In the calculations that follow the initial texture is given by the Euler angles of all grains and their volume fraction. Contrary to most studies that deal with texture evolution ([Gilormini, Tòth, Jonas 1990], [Lipinski, Krier, Berveiller 1990]...), we do not write evolution equations for these Euler angles because of definition and uniqueness problems. Instead we still use the intrinsic representation of rotations (see Appendix 1). A vector ${}^{\natural}\underline{\Psi}^g$ tells at each instant the position of each grain with respect to E^c. Numerically equations 21 and 22 are replaced by

$${}^{\natural}\dot{\underline{\Psi}}^g = {}^{\natural}\underset{\sim}{\mathbf{T}}^{g-1} \, \overset{\times}{\underline{\mathbf{W}}}^{eg} \qquad \dot{\underline{\Psi}}_c = {}^c\underset{\sim}{\mathbf{T}}^{-1}\overset{\times}{\underline{\mathbf{W}}} \tag{24}$$

(operator $\underset{\sim}{\mathbf{T}}$ is given in Appendix 1).

When dealing with polycrystals, several coordinate systems can be used: one related to the frame of the laboratory E, another defined by the anisotropic axes of the material (think of rolling and transverse directions) and the lattice in each grain gives a new coordinate system. Loading conditions are usually given in the first one, the Euler angles defining the initial texture are given with respect to the second one, and the simplest

expression of the elastic moduli are obtained in the last ones! To avoid any confusion, we have chosen one single coordinate system, namely that of the laboratory frame, in which all components used in the program are expressed. The modelling requires indeed several changes of observers but not necessarily of coordinate systems!

The material parameters that we have used for the simulations correspond approximately to the behaviour of aluminium or copper and describe correctly the tensile curve given in figure 3 of [Lipinski, Krier, Berveiller 1990]:

$$E = 80000 \text{ MPa}$$

$$\nu = 0.33$$

$$k = 20 \text{ MPa s}^{1/n}$$

$$n = 5$$

$$r_0 = 140 \text{ MPa}$$

$$q = 120 \text{ MPa}$$

$$D = 50$$

$$h^{ii} = 1 \ \forall i \in \{1, ..., 12\}$$

$$h^{ij} = 3 \ \forall i \neq j.$$

3 Texture evolution

Some tests are now analysed and the pole figures obtained numerically for f.c.c. crystals are compared with experimental results or responses of other models. Situations are considered for which deformation gradient $\underset{\sim}{\mathbf{F}}$ is homogeneous. Some components are imposed, the other ones being found semi-analytically, so that no FE simulation is necessary.

3.1 Tension-compression

During tension or compression of an initially isotropic polycrystal along direction 3, the velocity gradient has the form:

$$\underset{\sim}{\mathbf{L}} = \frac{\dot{F}_{11}}{F_{11}}(\underline{\mathbf{e}}_1 \otimes \underline{\mathbf{e}}_1 + \underline{\mathbf{e}}_2 \otimes \underline{\mathbf{e}}_2) + \frac{\dot{F}_{33}}{F_{33}}\underline{\mathbf{e}}_3 \otimes \underline{\mathbf{e}}_3 \ = \ D \ = \underset{\sim}{\dot{\mathbf{e}}}^e + \underset{\sim}{\dot{\mathbf{e}}}^p \tag{25}$$

with $\operatorname{Tr} \underset{\sim}{\dot{\mathbf{e}}}^v = 0$ and $T = T_{33}\, \underline{\mathbf{e}}_3 \otimes \underline{\mathbf{e}}_3$. If $\dfrac{\dot{F}_{33}}{F_{33}}$ is imposed, equation

$$\frac{\dot{F}_{11}}{F_{11}} \ = \ \dot{e}^p_{11} - \nu(\frac{\dot{F}_{33}}{F_{33}} - \dot{e}^p_{33}) \tag{26}$$

can be included in the total set of differential equations to be integrated.

A random distribution of crystal orientations induces a quasi-isotropic behaviour as soon as it contains at least about 100 orientations. The first calculations are performed for 100 random grains. The direct and inverse pole figures corresponding to the initial

distribution are given in figure 1. After a tension test, figures 2 and 3 show that most $< 111 >$ and $< 001 >$ directions move towards the tensile direction. In contrast compression results in the alignment of $< 011 >$ directions along the tensile axis (figures 4 and 5). These results are compatible with those obtained in [Lipinski, Krier, Berveiller 1990] with a self-consistent scheme.

3.2 Rolling

The prediction of rolling textures is one of the main objectives of polycrystal modelling at large strains. Rolling is a complex process and to simplify we take the loading condition of a channel die test:

$$F = \underline{e}_1 \otimes \underline{e}_1 + F_{22}\underline{e}_2 \otimes \underline{e}_2 + F_{33}\underline{e}_3 \otimes \underline{e}_3 \tag{27}$$

If F_{33} is imposed, equation

$$\frac{\dot{F}_{22}}{F_{22}} = \dot{e}^p_{22} - \frac{\nu}{1-\nu}\left(\frac{\dot{F}_{33}}{F_{33}} - \dot{e}^p_{33} - \dot{e}^p_{11}\right) \tag{28}$$

must be added to the set of constitutive equations for the numerical integration.

The polycrystal represented by 1000 random orientations is now subjected to rolling in direction 2 ($F_{33} < 0$, $F_{22} > 0$). The $< 111 >$ and $< 200 >$ pole figures of figures 6 to 9 show that an anisotropic texture develops. They are also compared with experimental data (figure 10). The calculations have been carried out for an even larger set of 2016 grains obtained after a regular arrangement in the standard triangle (figures 11 and 12). Figures 13 to 15 show the formation of a similar anisotropic texture.

3.3 Simple shear of an initially textured polycrystalline sheet

The previous tests do not induce any global rotation so that the role played by the corotational frame could not be seen. In contrast the simple shear test involves both material and lattice rotations. In this section we consider the aluminium alloy studied in [Achon 1994] which has an initial anisotropic texture given in figures 16 and 17. When simple shear occurs in the plane 1-2 and direction 1, figures 18, 19, 20 and 21 show that the texture is not significantly altered but undergoes almost a global rotation around axis 3.

The experimental evidence of this phenomenon is provided in [Bacroix, Genevois and Teodosiu 1992] for a steel sheet (b.c.c. crystallographic structure, figure 22). Contrary to the case of rolling or tension-compression, the crystallographic structure does not play a major role at least for moderate straining, since simple shear involves more global material rotations than relative lattice rotations. Bacroix, Genevoix and Teodosiu notice also that a significant part of the initial texture pertains even after a large amount of shear. They are also interested in finding a priviledged frame where to write hardening rules for instance: it is surely not far from the frame with respect to which the loss of orthotropy seems to be minimized. In our modelling this is close to the corotational frame. Mandel [1982] proposed that the suitable frame for the study of inelastic deformation of polycrystals should have a spin equal to the average of the spins of individual grains. That is why Bacroix, Genevois and Teodosiu [1992] have determined experimentally the rotation rate of the quasi-orthotropy axes and compared it to that of the corotational

and that of Mandel's frame. The latter has been computed using a viscoplastic Taylor model. It seems that Mandel's frame displays a slight advantage. It would be interesting to perform the calculations with our model for the same material and compare the results with available experimental data.

Figures 23 to 27 show the result of a simple shear test in plane 1-3 and direction 1.

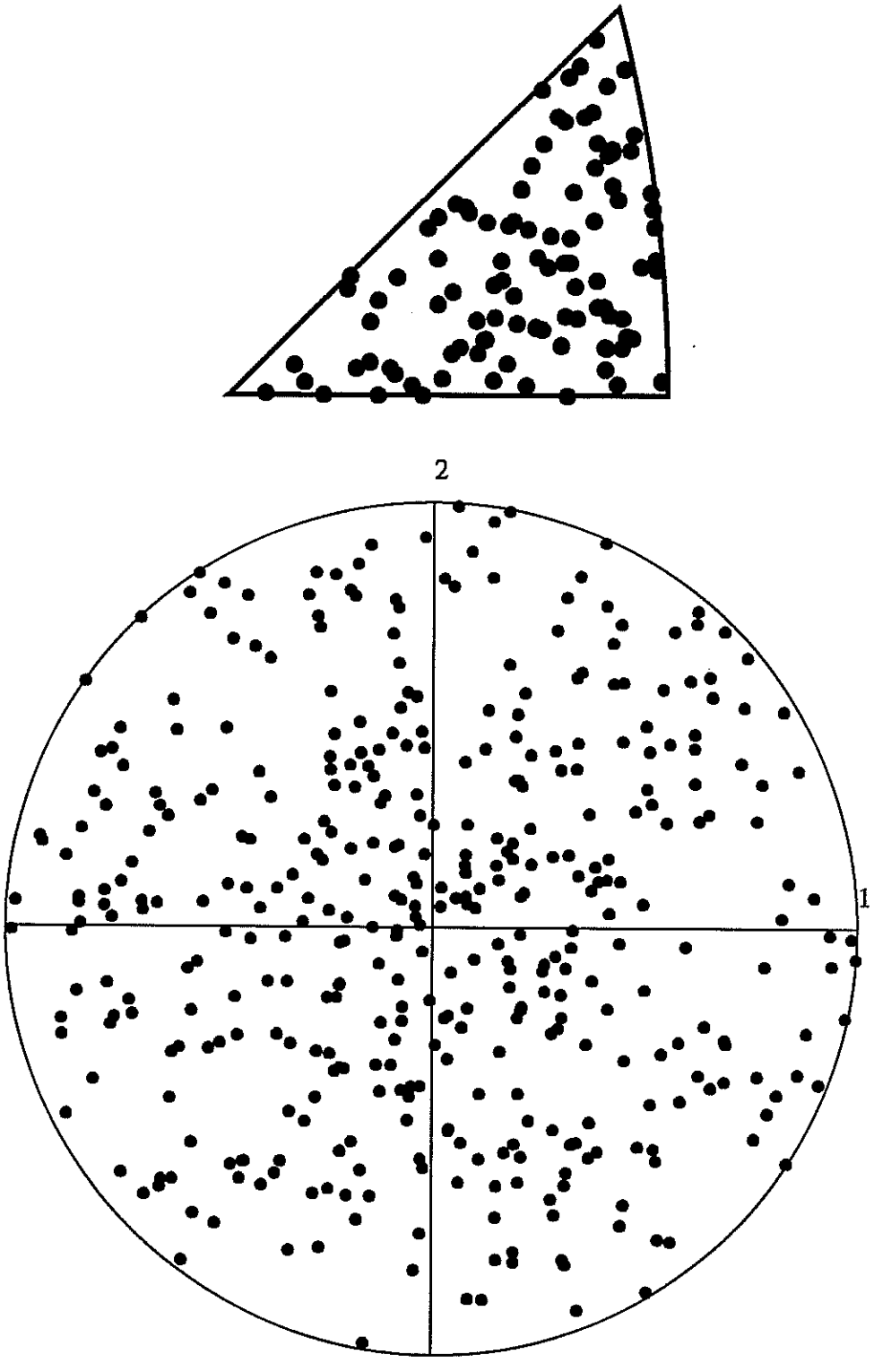

Figure A2.1: Random distribution of 100 grains; the inverse pole figure (above) gives the orientations of loading axis 3 with respect to all grains.

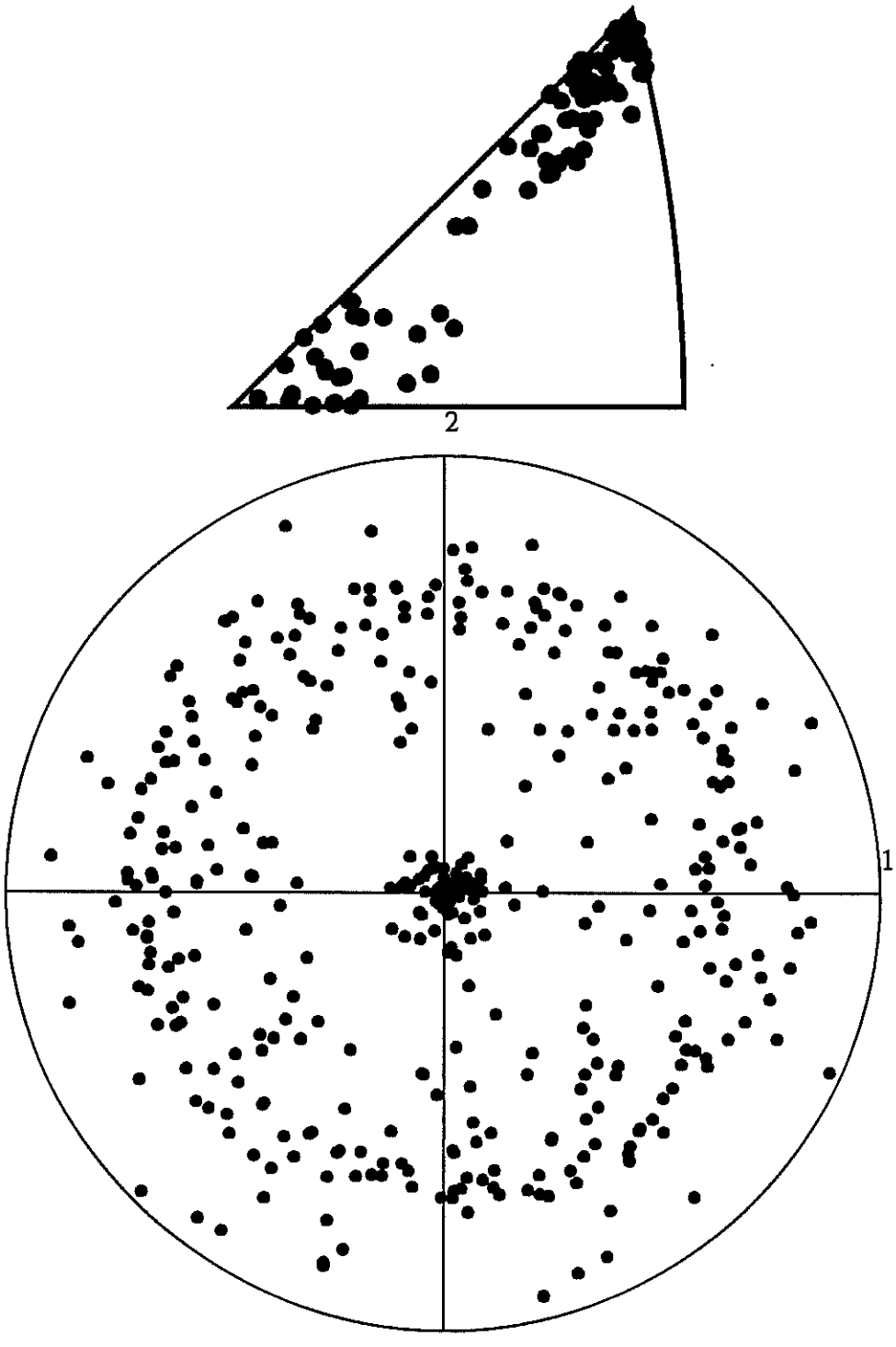

planes : 111

Figure A2.2: Direct and inverse pole figures {111} after a tension test (F33=1.7)

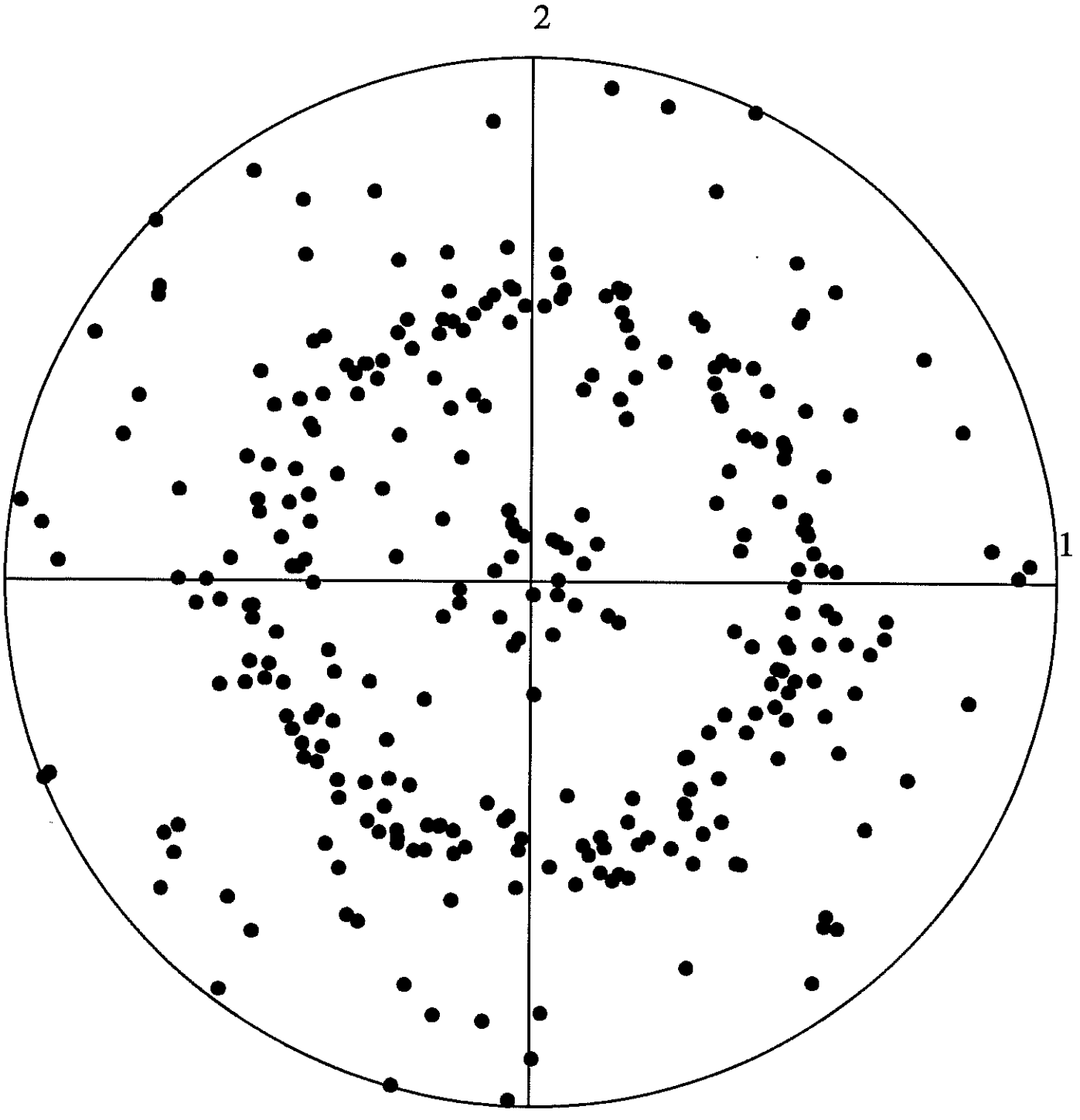

planes : 200

Figure A2.3: {200} pole figure after tension (F33=1.7).

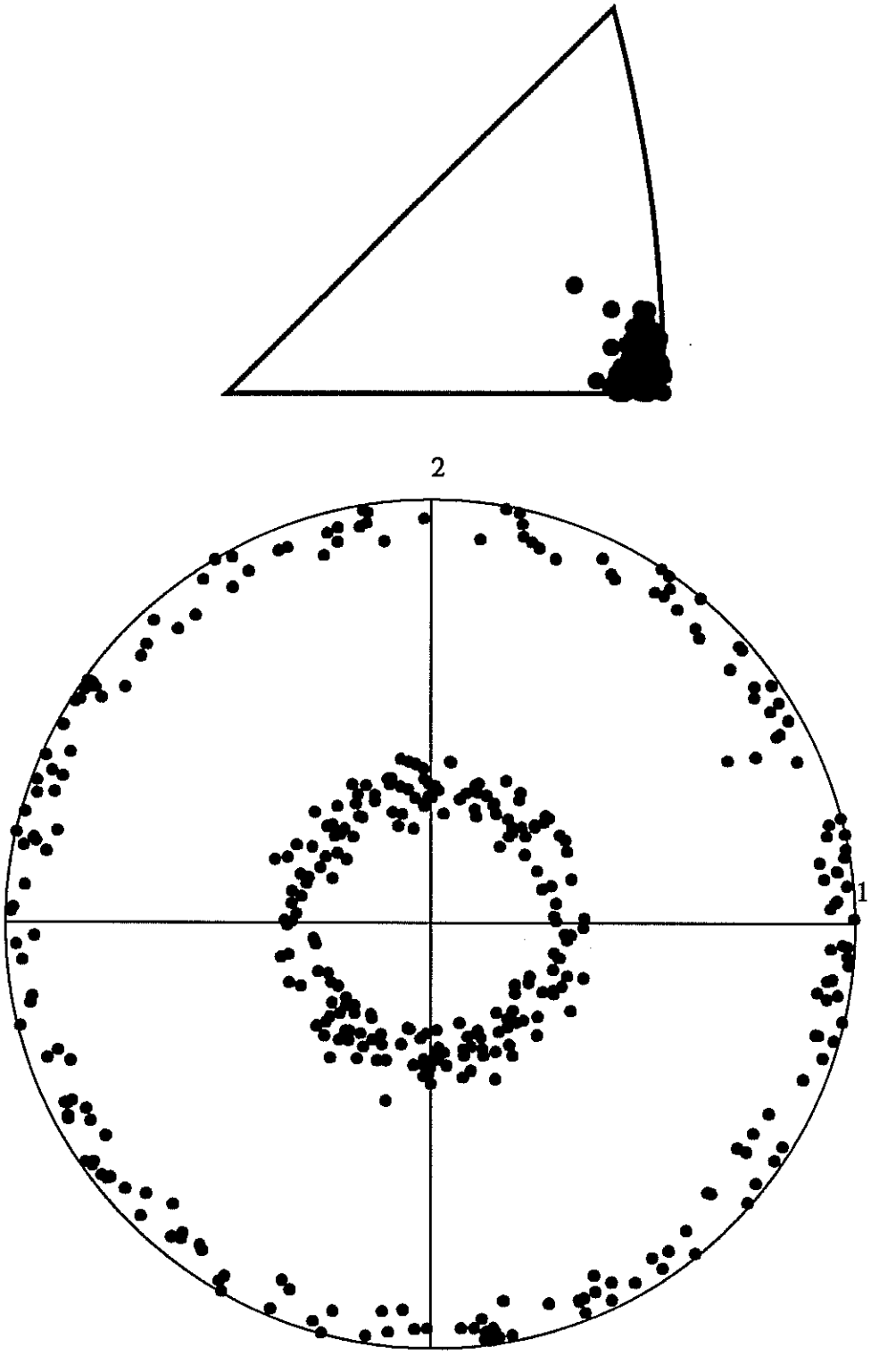

Figure A2.4: Direct and inverse pole figures {111} after a compression test (F33=0.3).

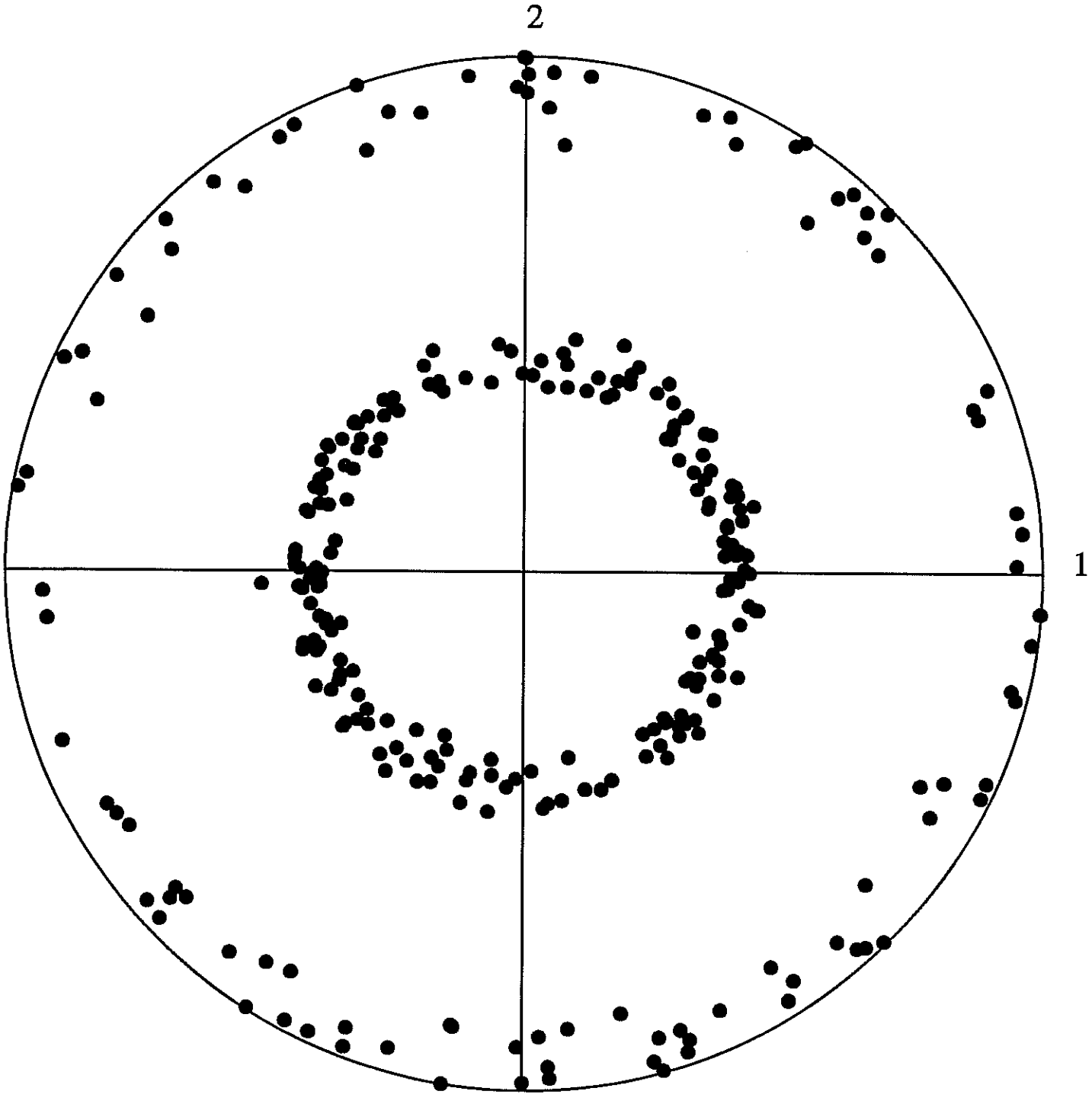

Figure A2.5: {200} pole figure after compression (F33=0.3).

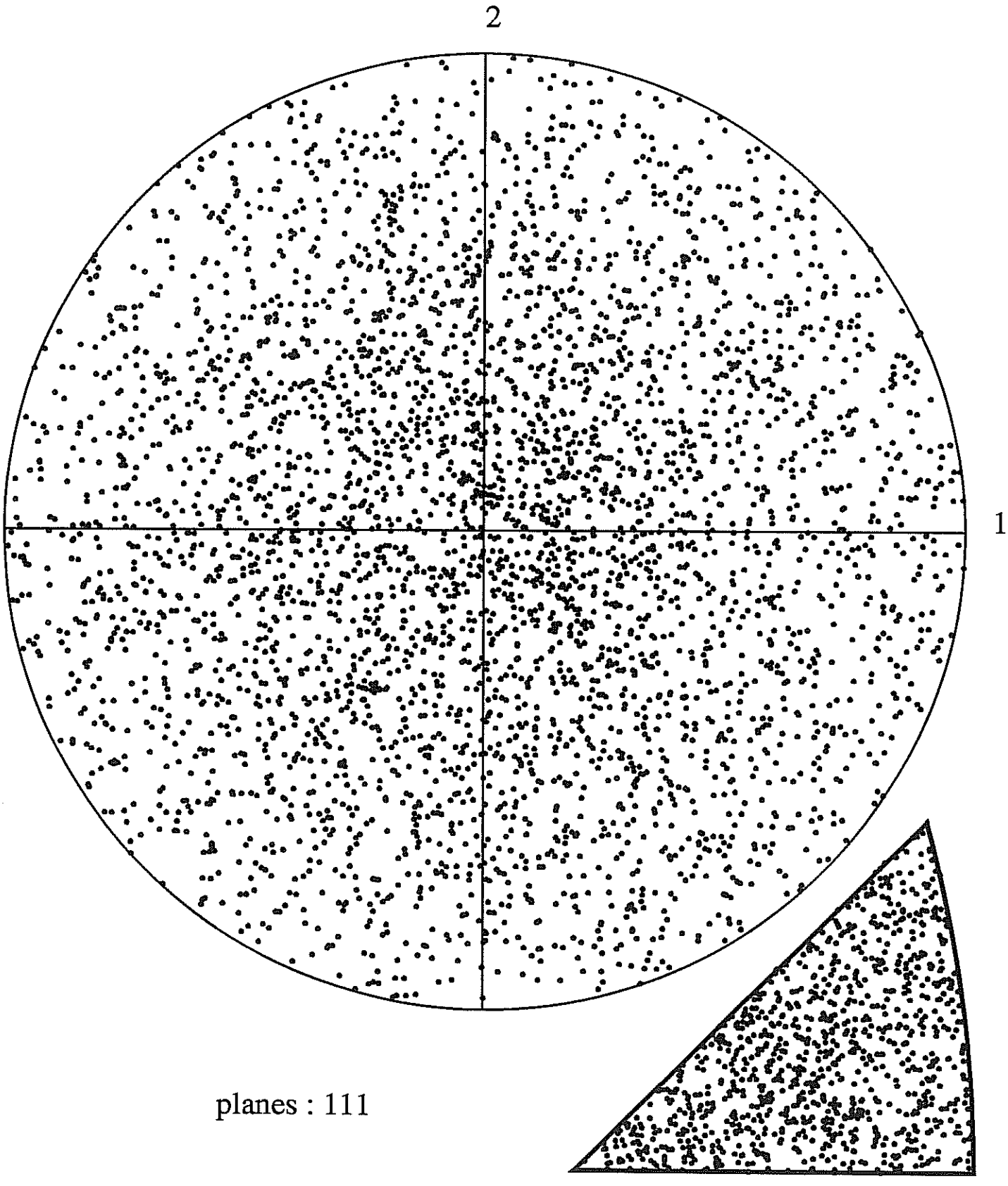

Figure A2.6: Random distribution of 1000 grains; the inverse pole figure (above) gives the orientations of loading axis 3 with respect to all grains.

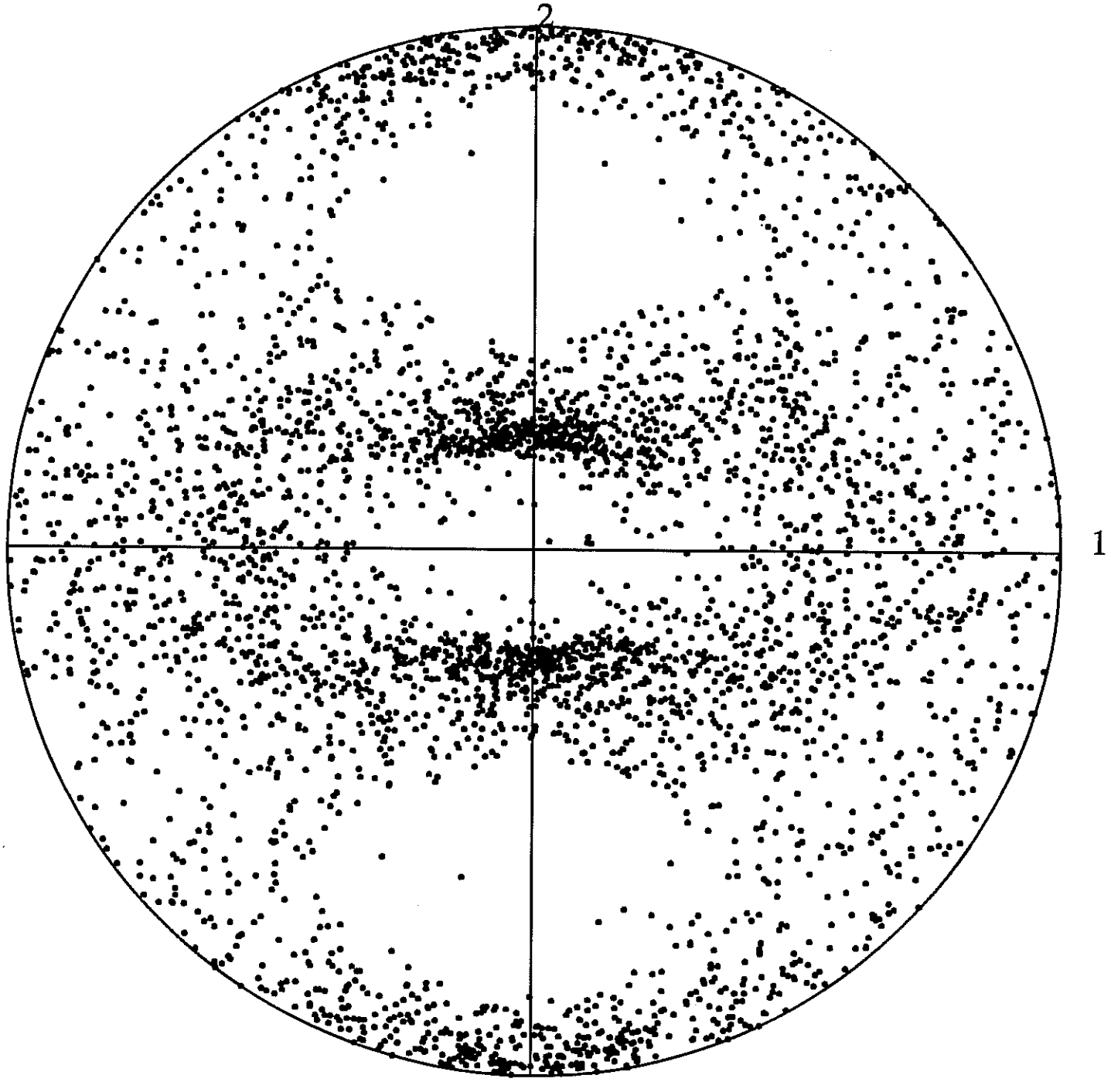

Figure A2.7: {111} pole figure after rolling (F33=0.66).

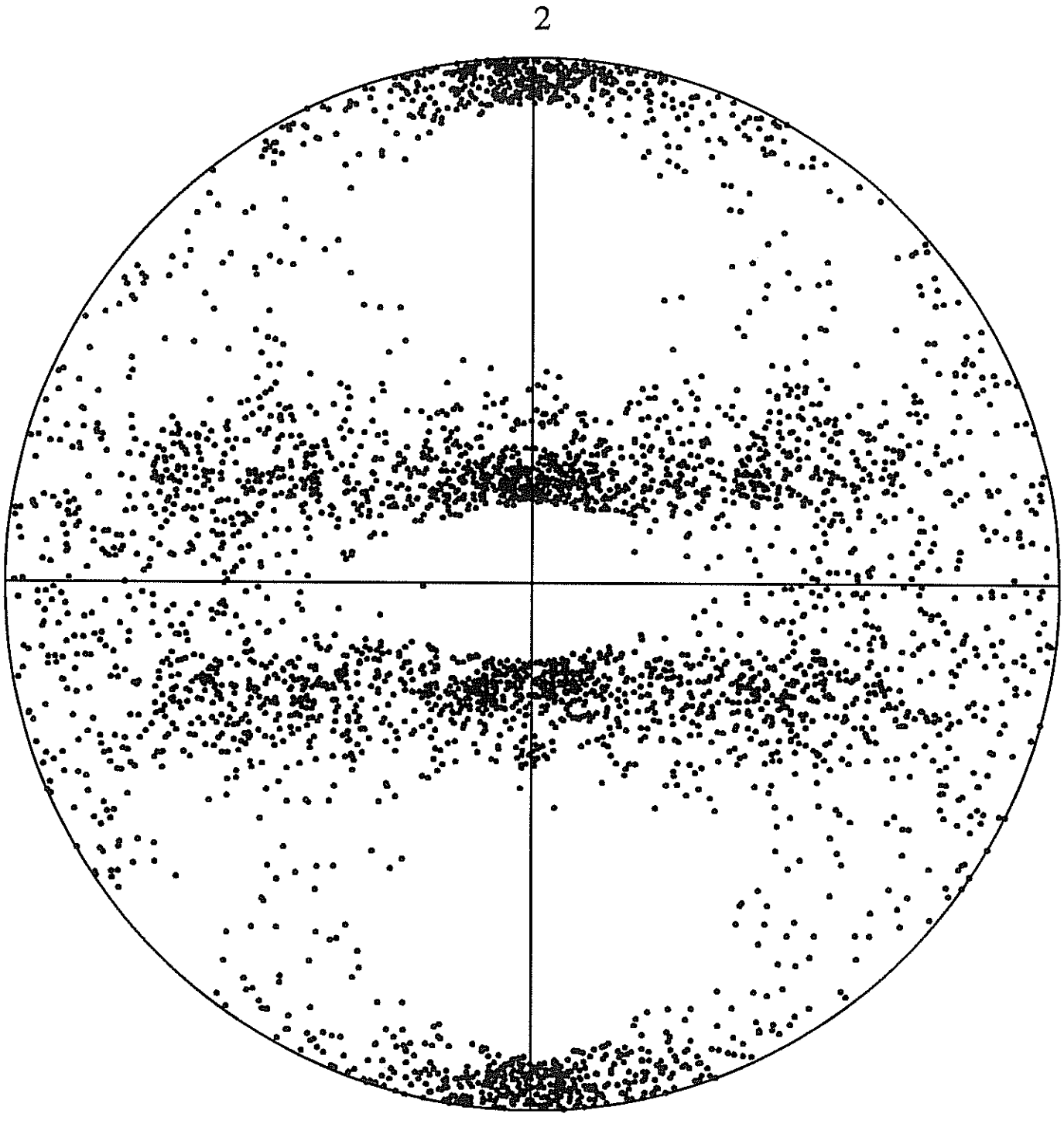

Figure A2.8: {111} pole figure after rolling (F33=0.43).

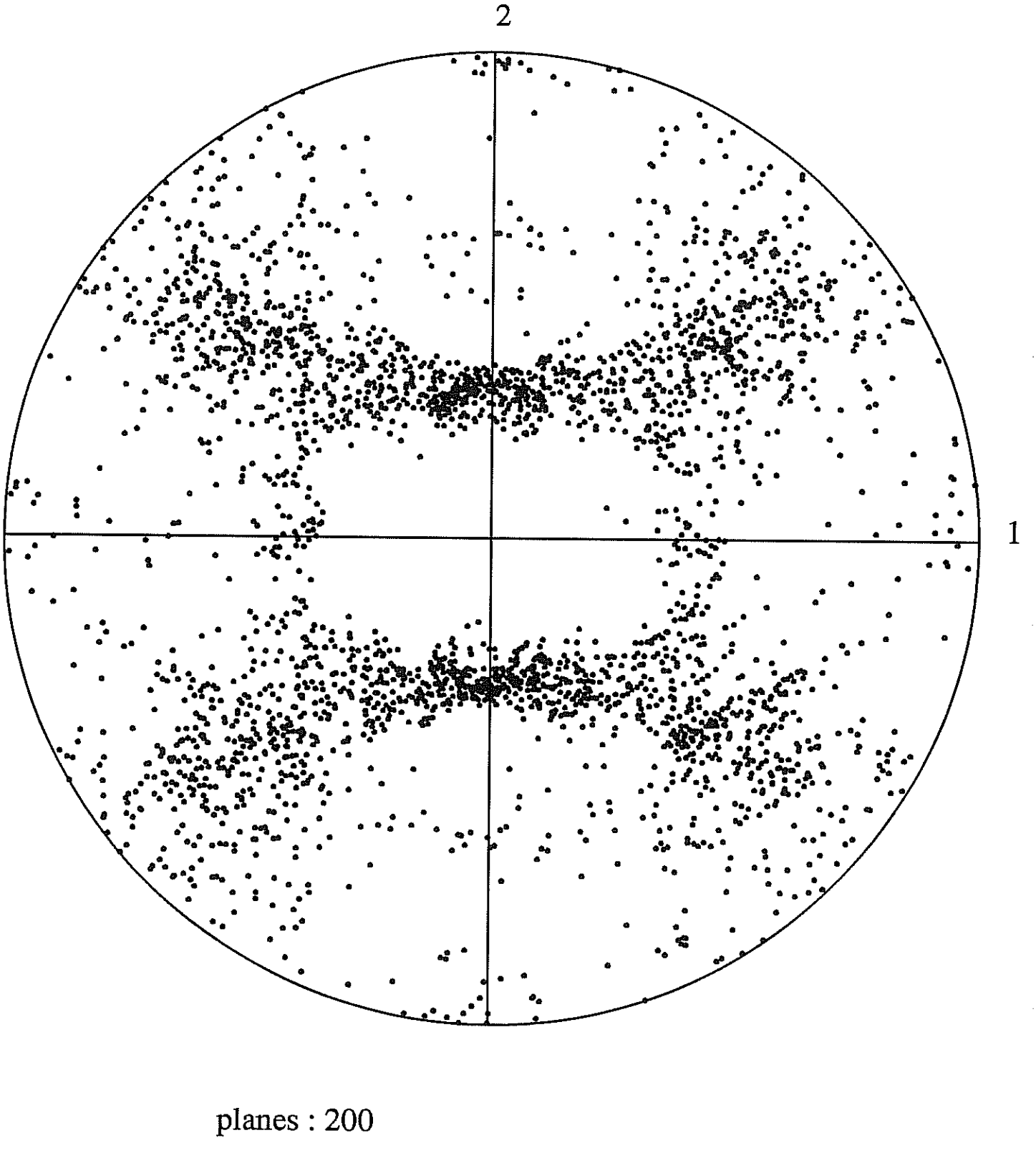

Figure A2.9: {111} pole figure after rolling (F33=0.43).

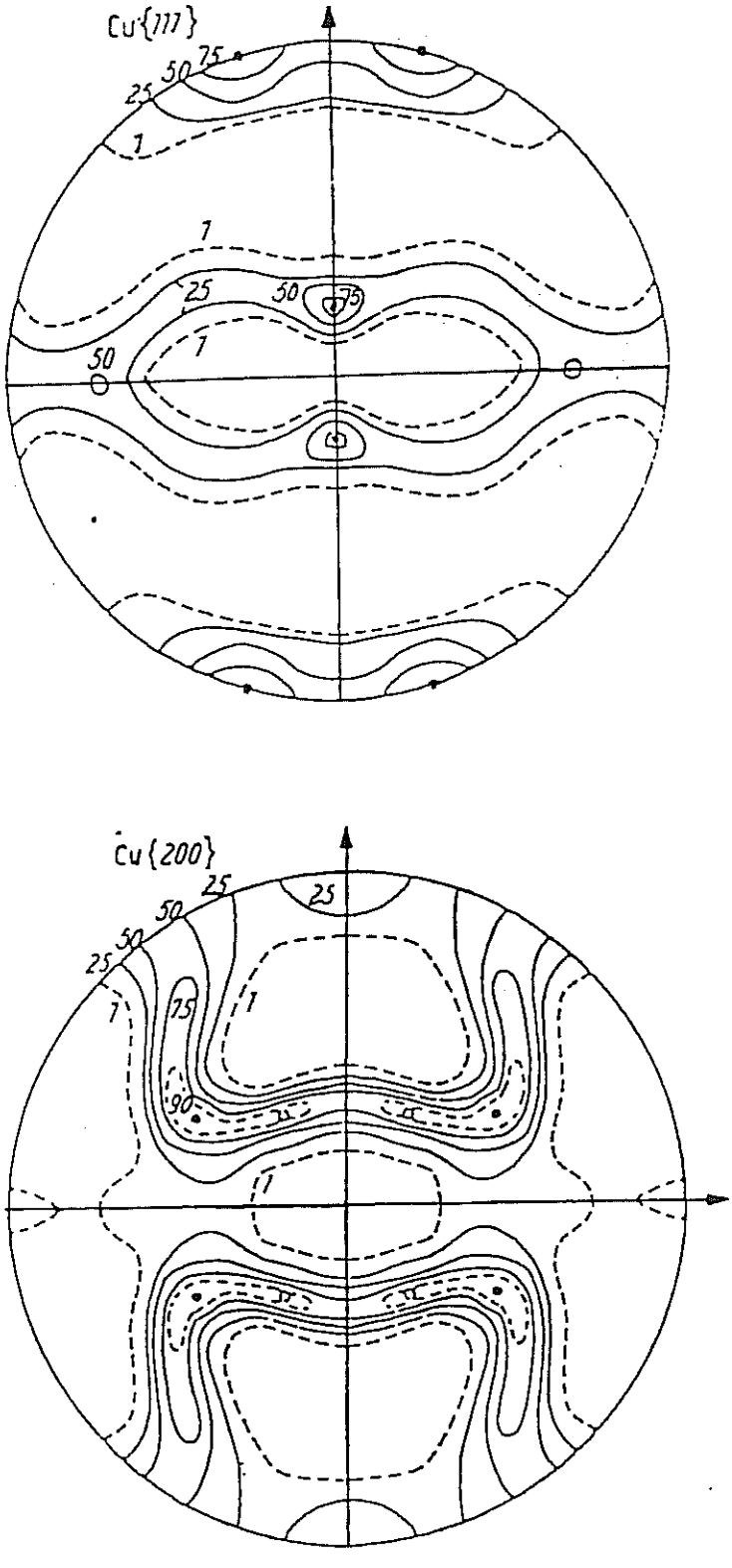

Figure A2.10: Experimental textures after rolling from [Bunge 1969].

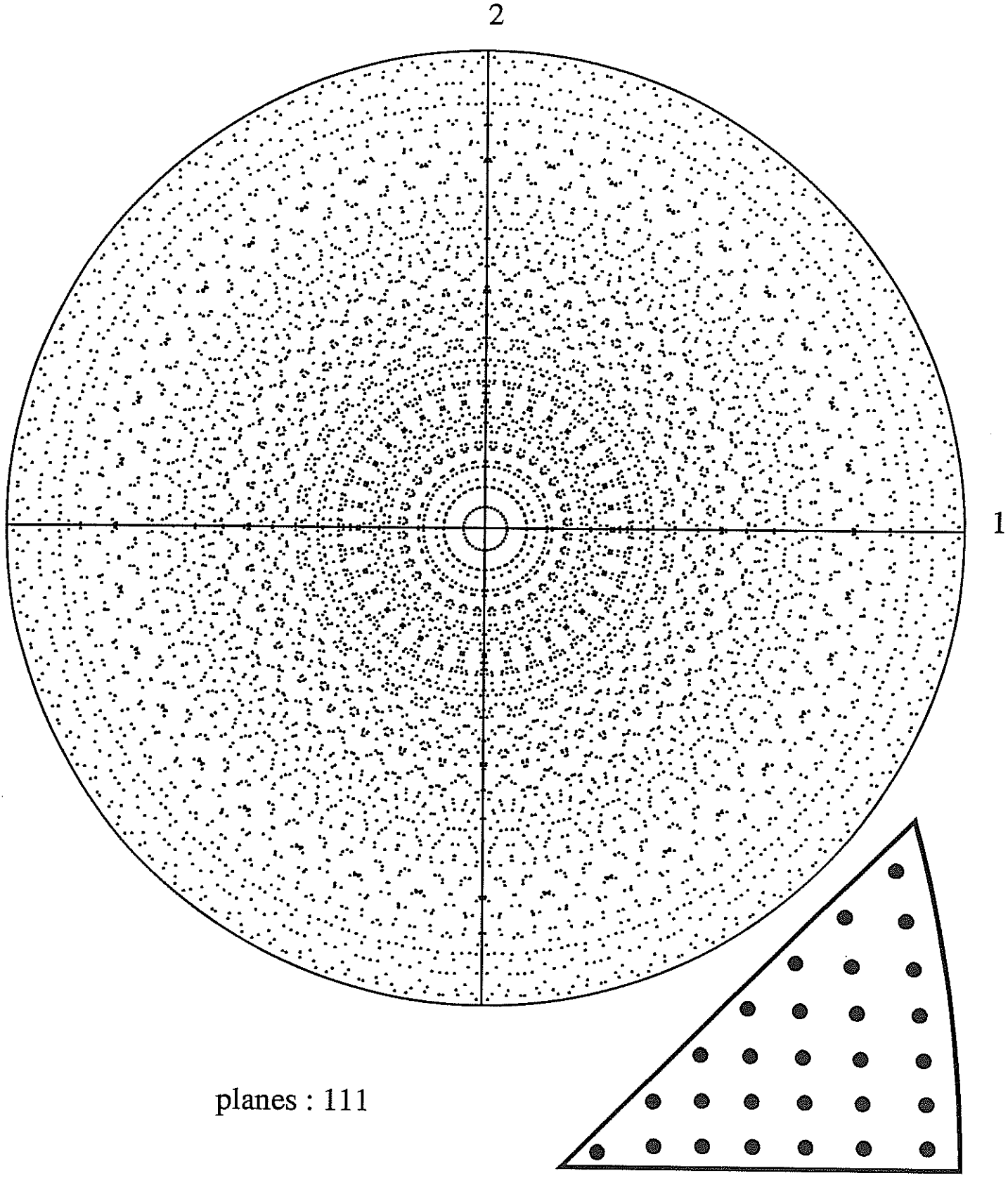

Figure A2.11: Isotropic distribution of 2016 grains.

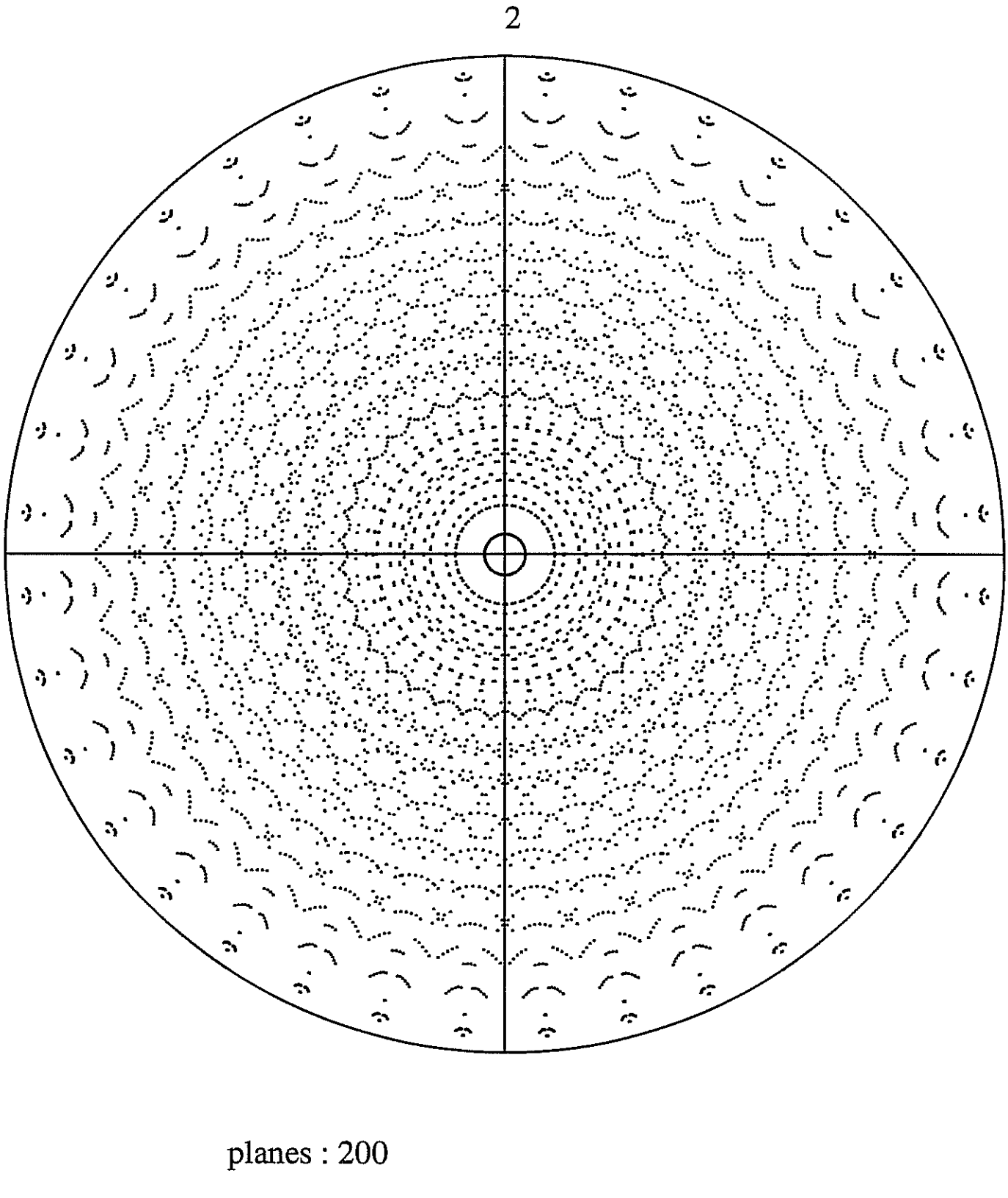

Figure A2.12: Isotropic distribution of 2016 grains.

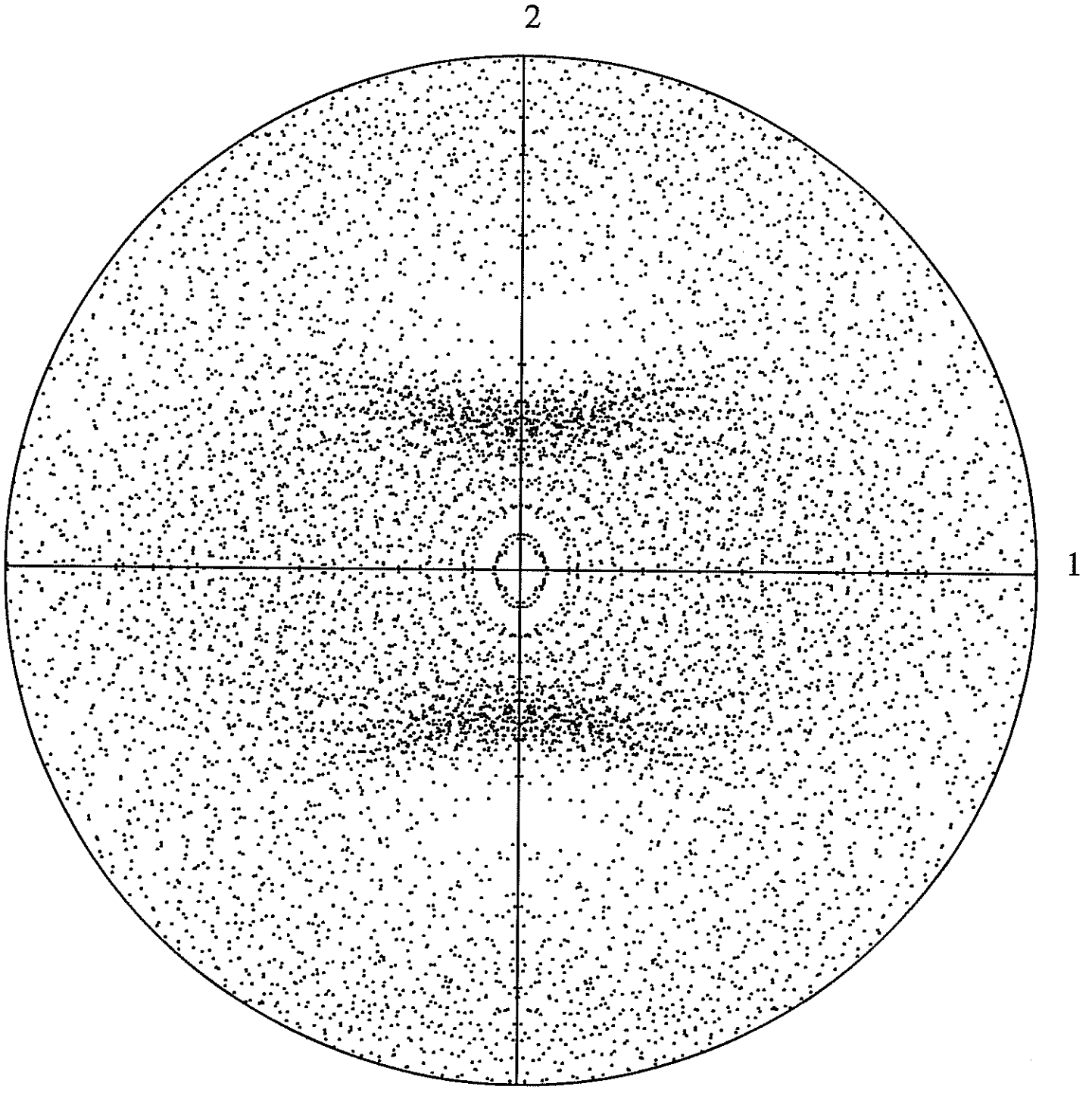

Figure A2.13: Texture formation during rolling (F33=0.88).

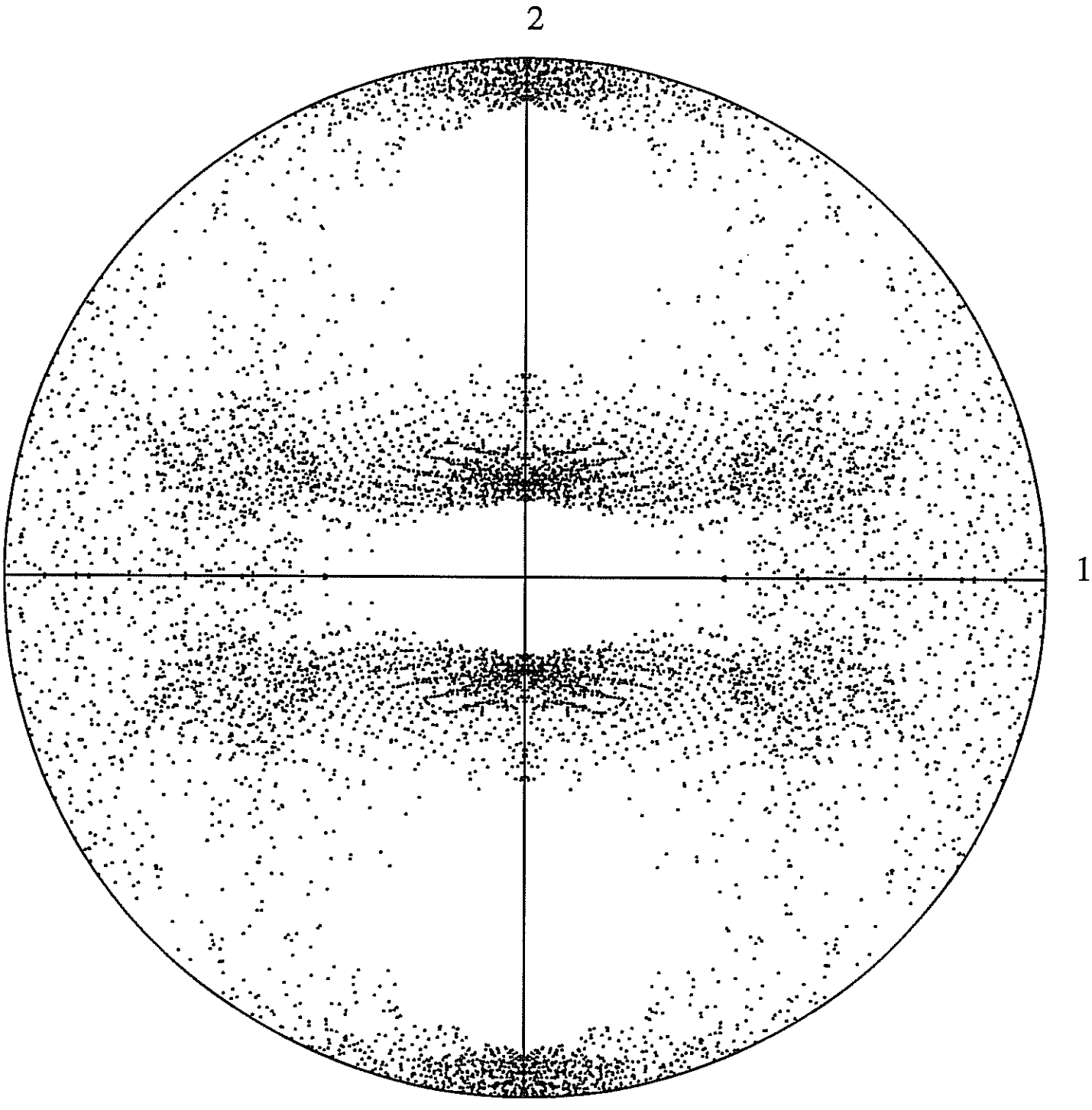

Figure A2.14: Texture formation during rolling (F33=0.43).

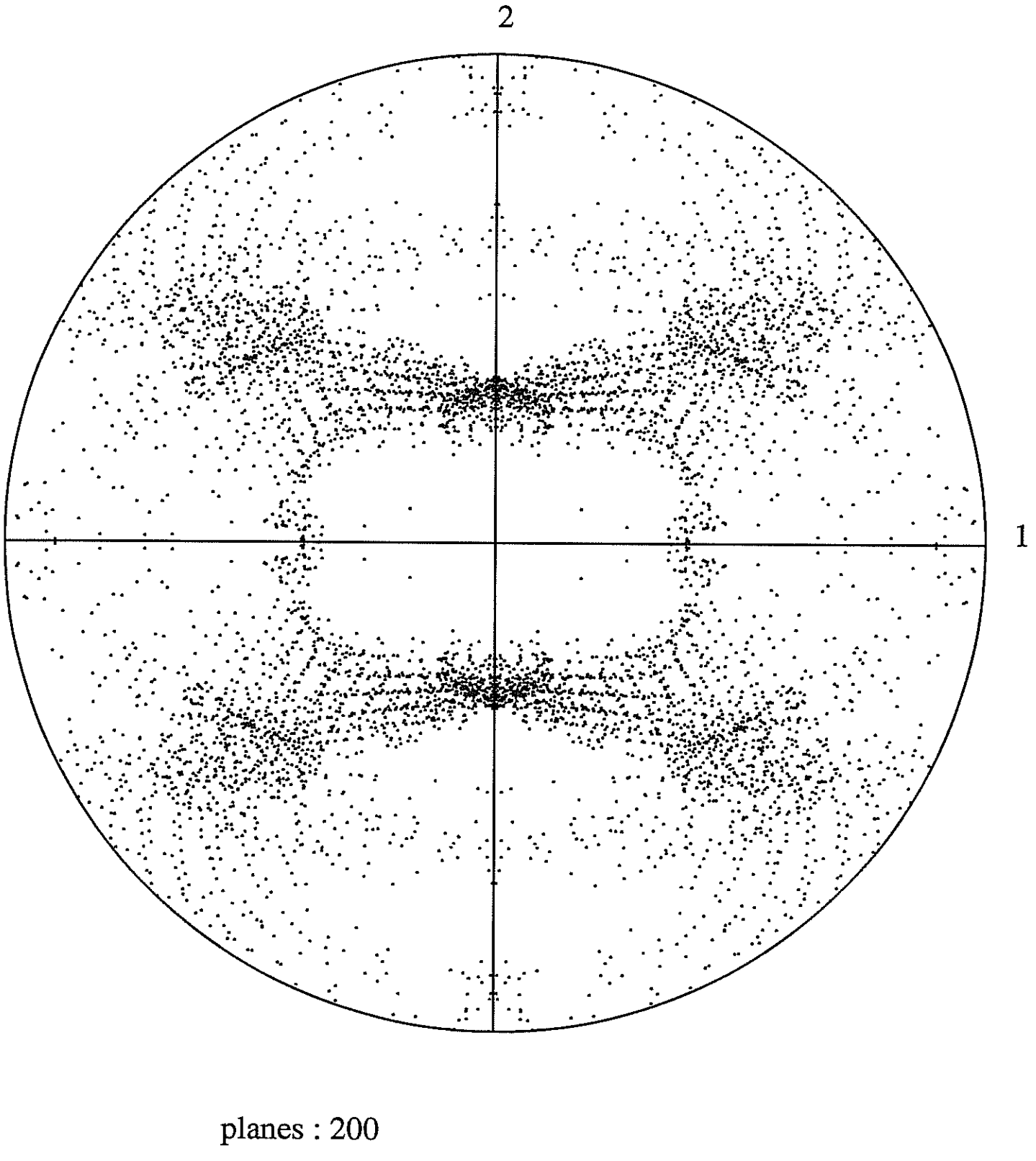

Figure A2.15: Texture formation by rolling.

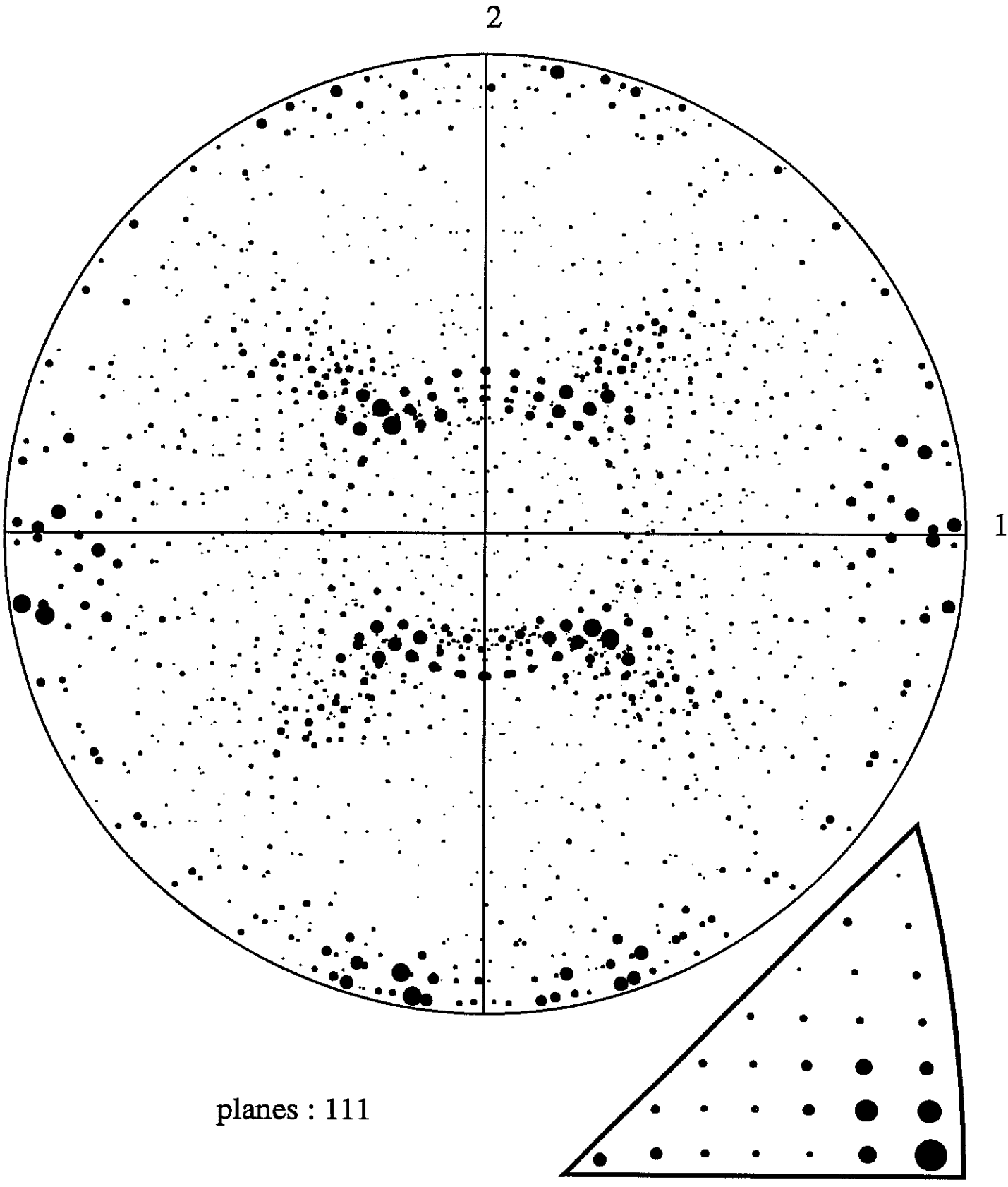

Figure A2.16: Direct and inverse pole figures of a textured Aluminium sheet.

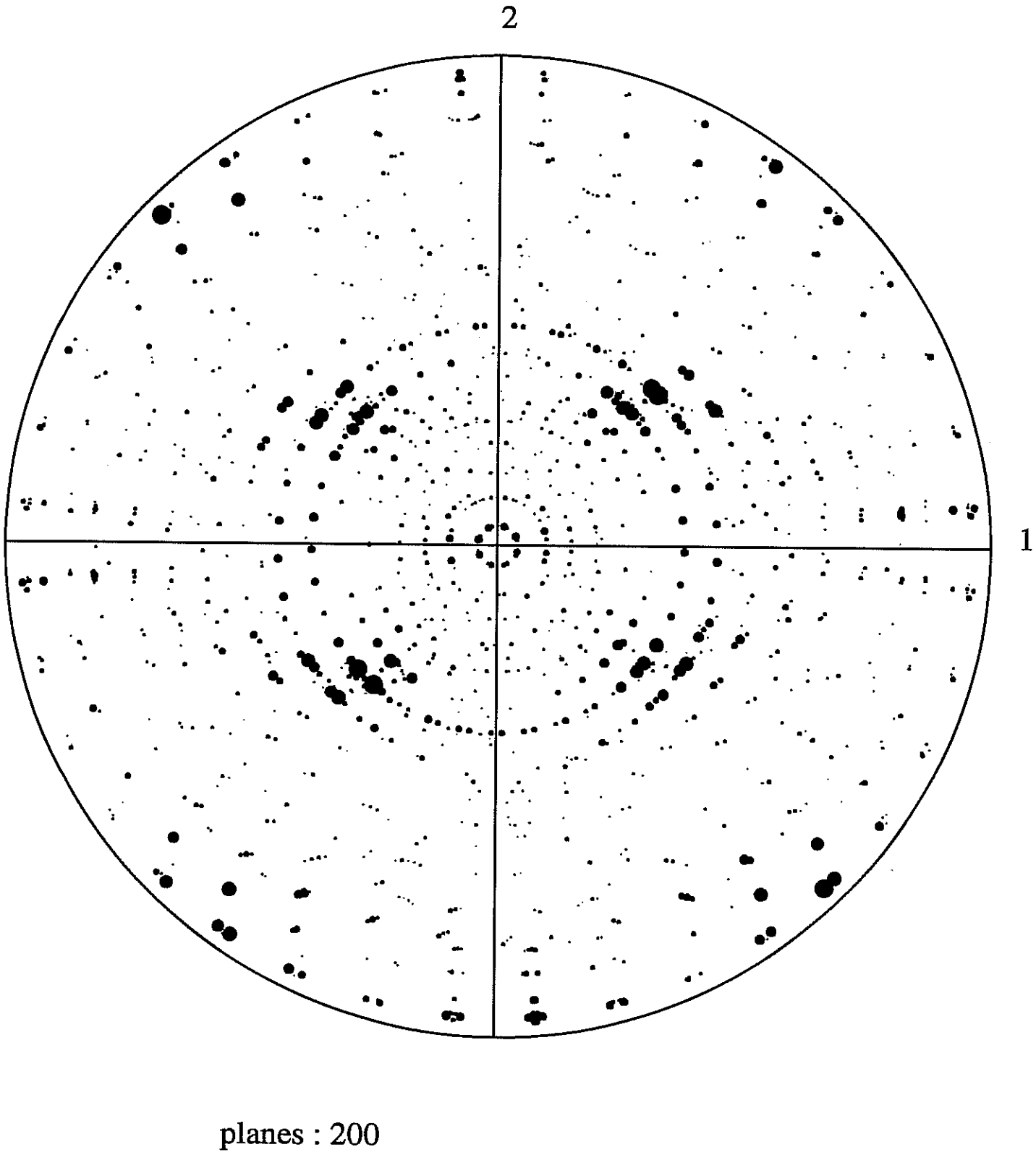

Figure A2.17: Direct pole figure {200} of a textured Aluminium sheet.

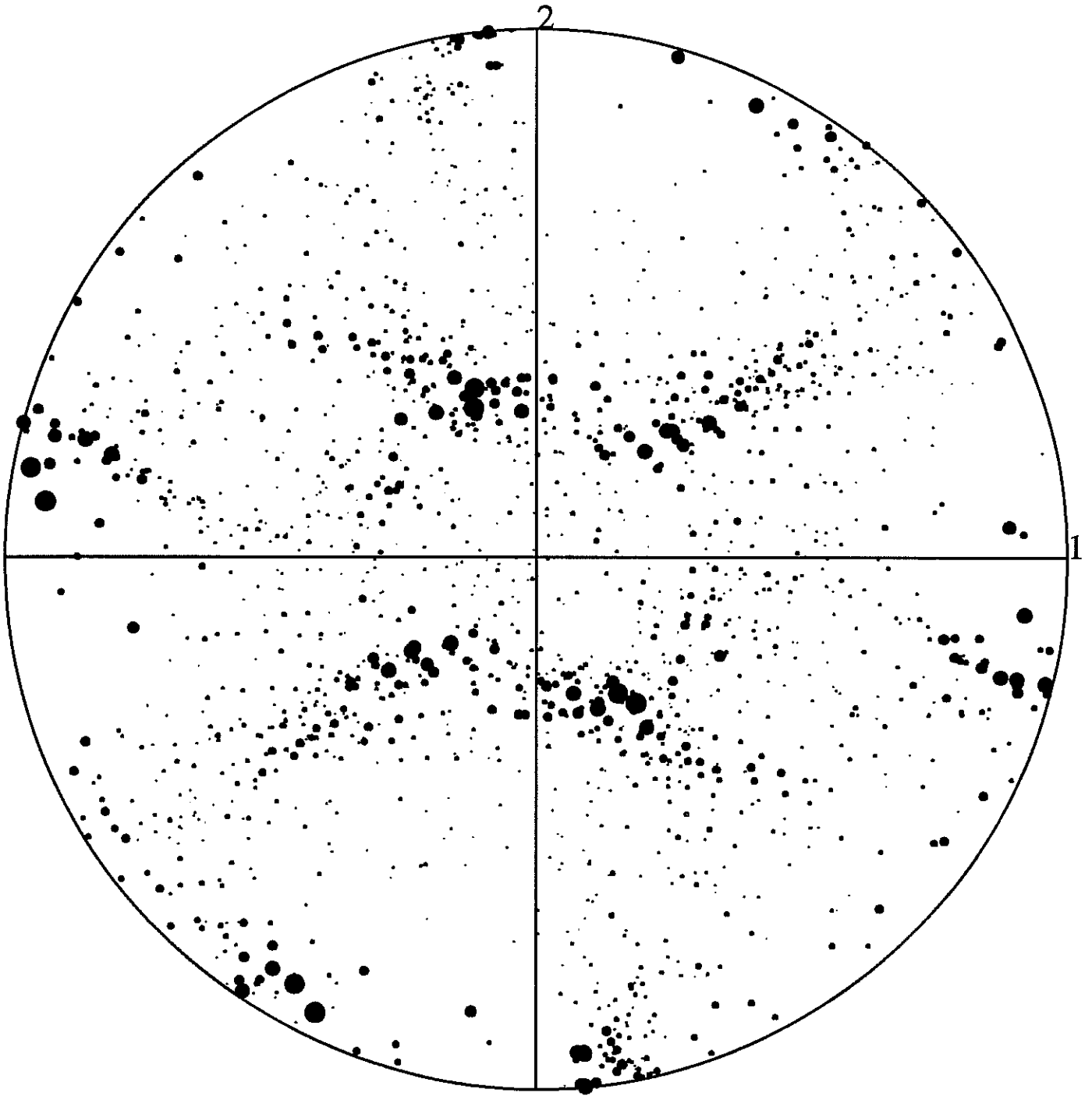

Figure A2.18: Texture evolution during simple shear (F12 = 0.33).

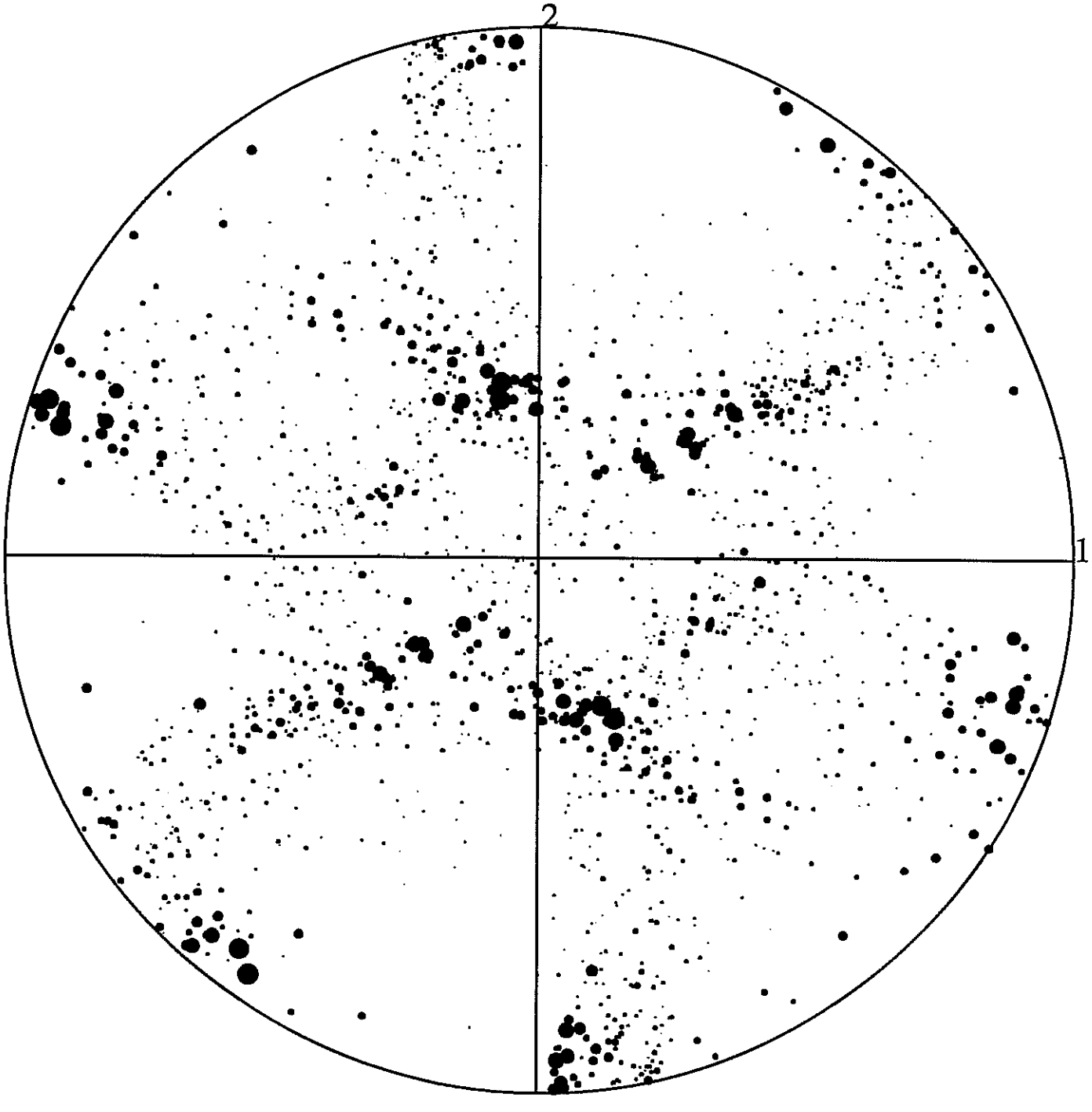

Figure A2.19: Texture evolution during simple shear (F12 = 0.55).

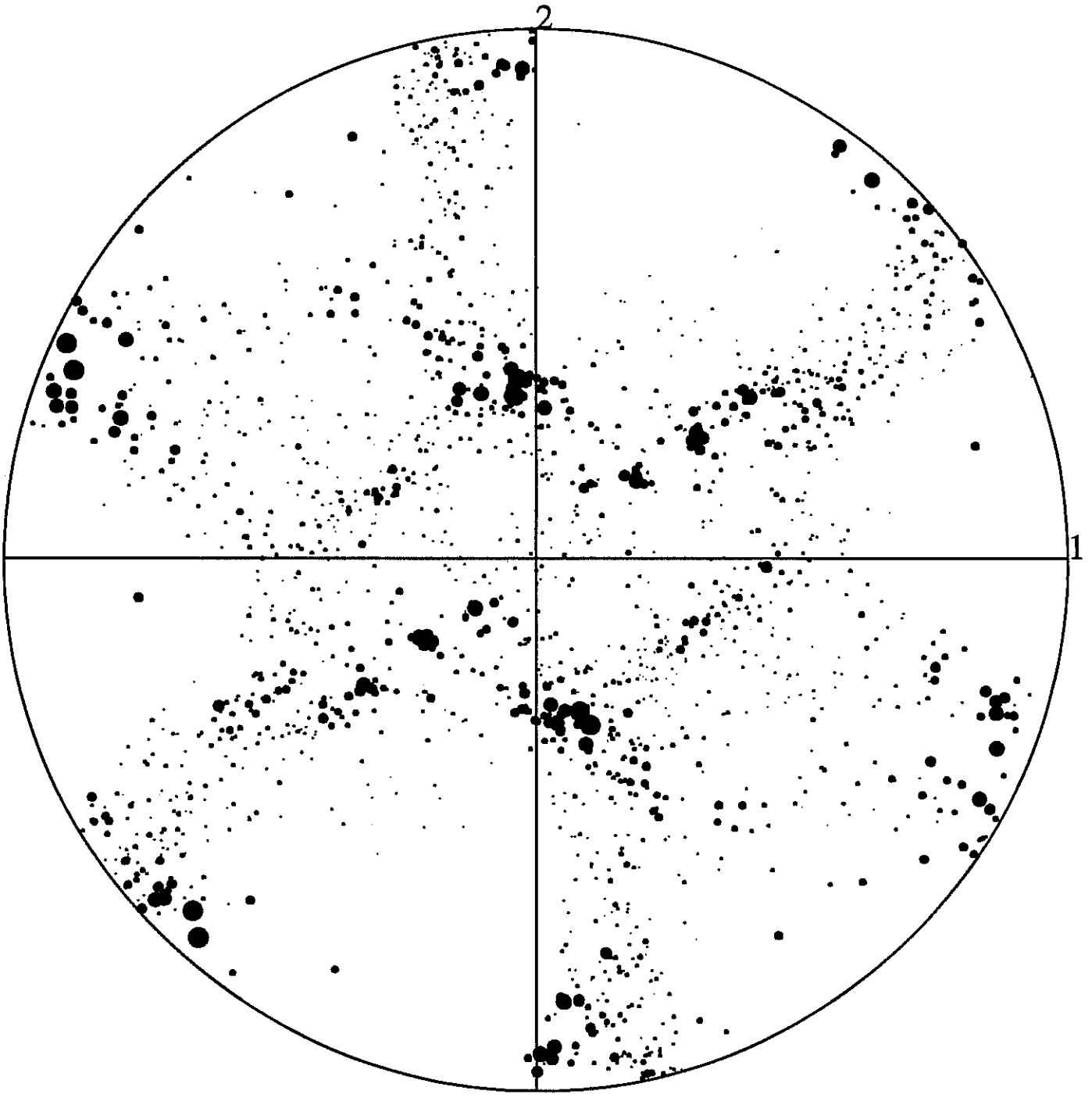

Figure A2.20: Texture evolution during simple shear (F12 = 0.77).

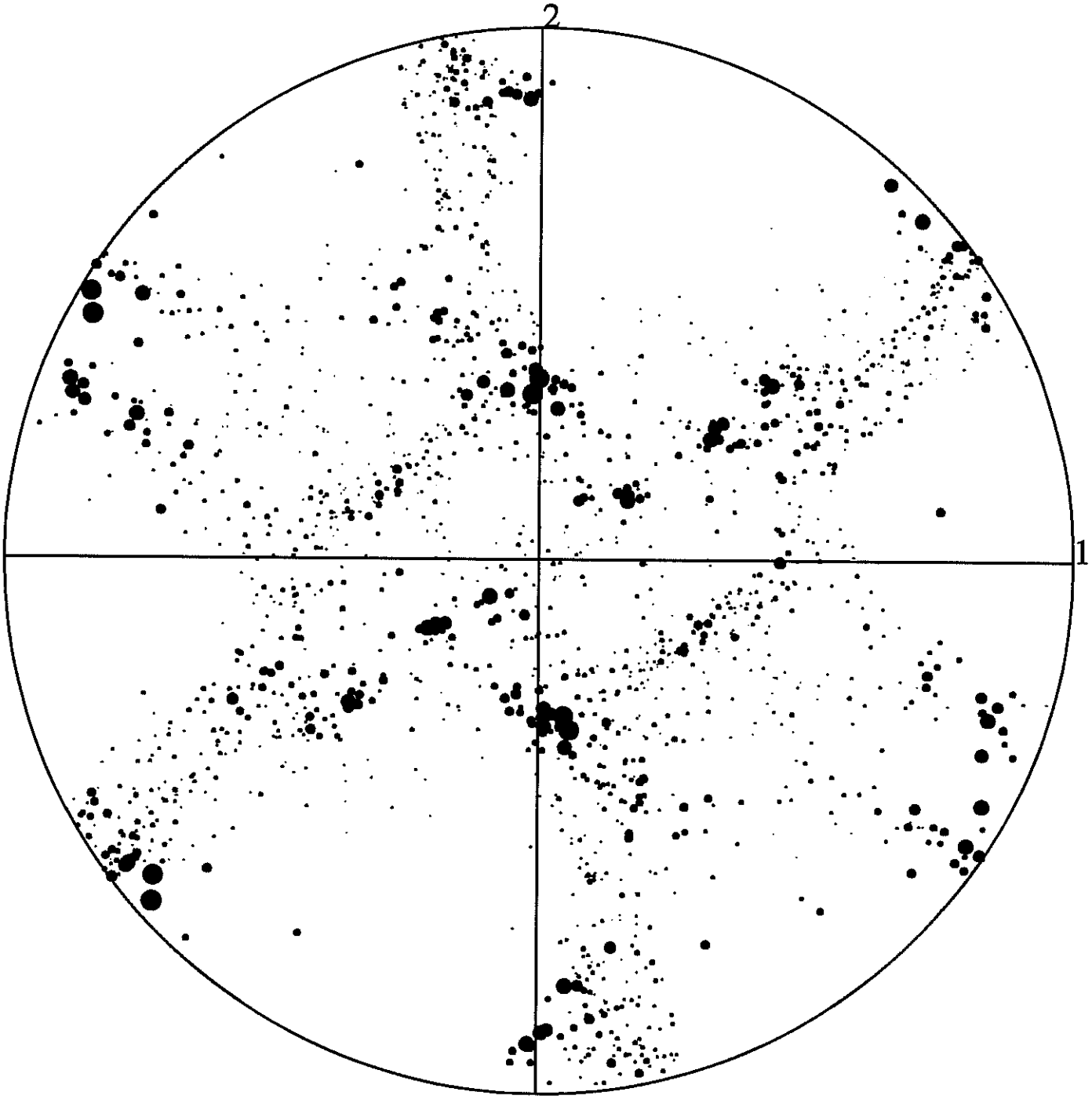

planes : 111

Figure A2.21: Texture evolution during simple shear (F12 = 1).

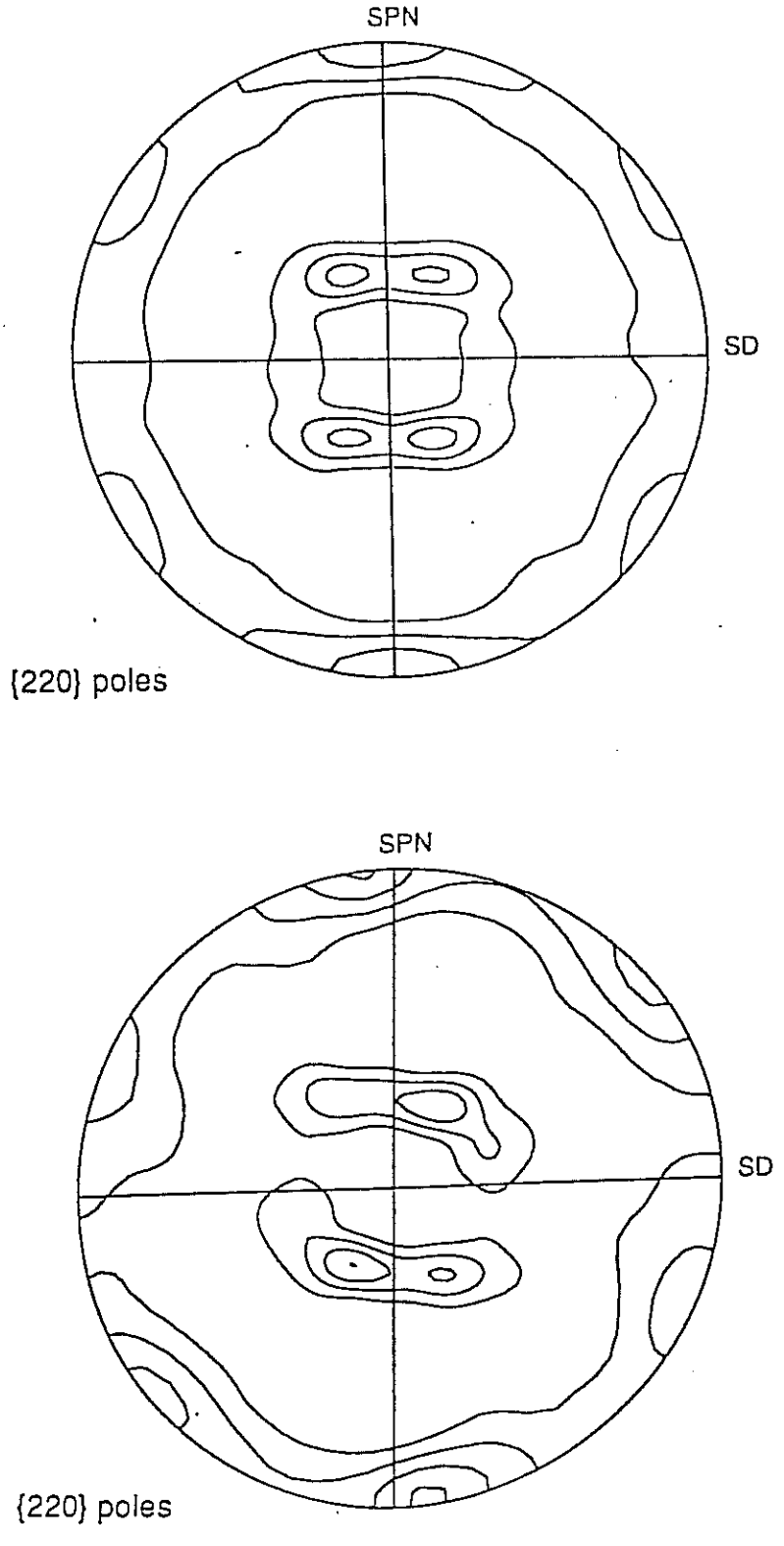

Figure A2.22: Experimental texture after a simple shear test on a steel sheet from [Bacroix *et al.* 1992]; initial texture (above), final texture (below).

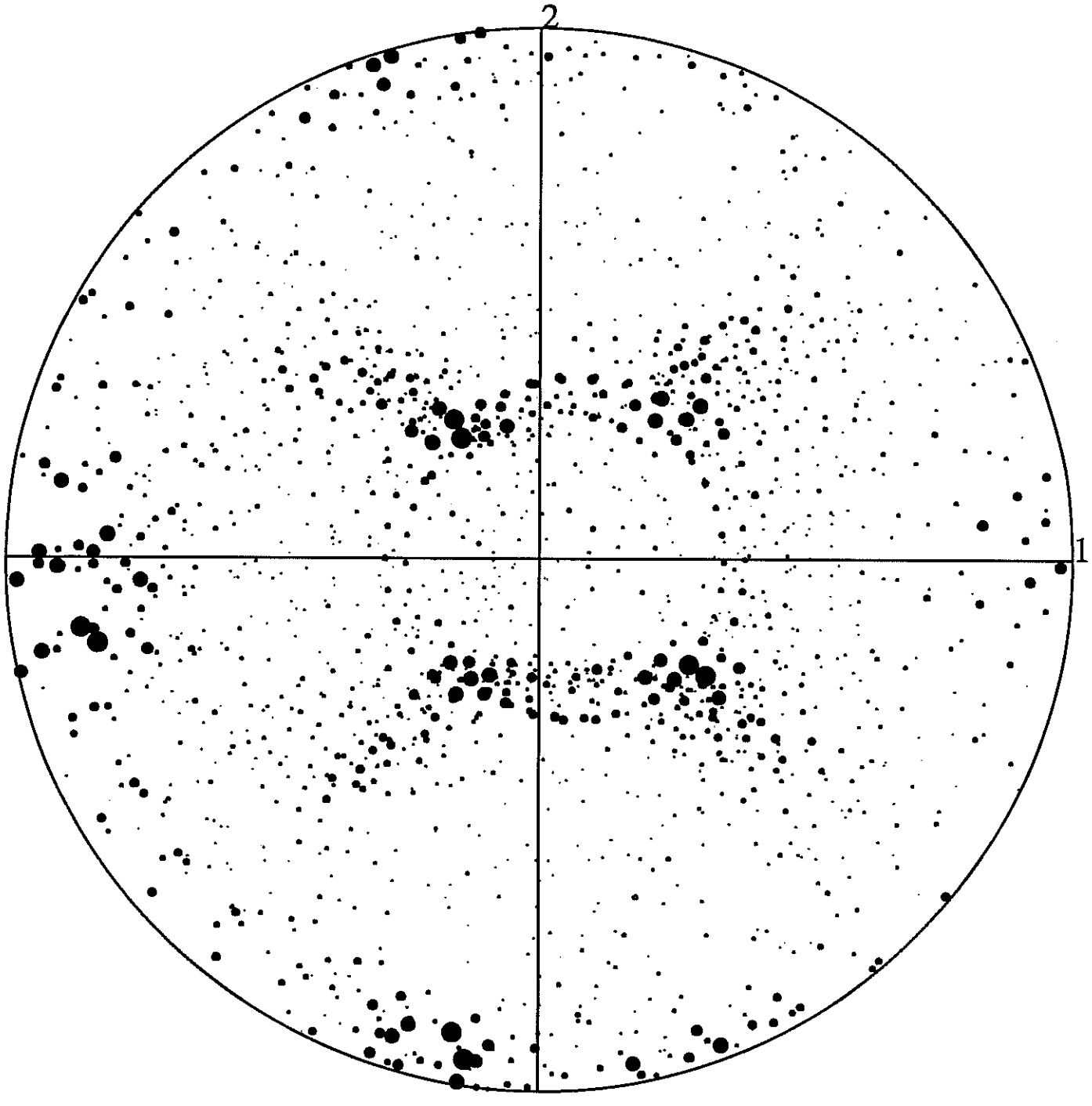

planes : 111

Figure A2.23: Texture evolution during simple shear (F13 = 0.11).

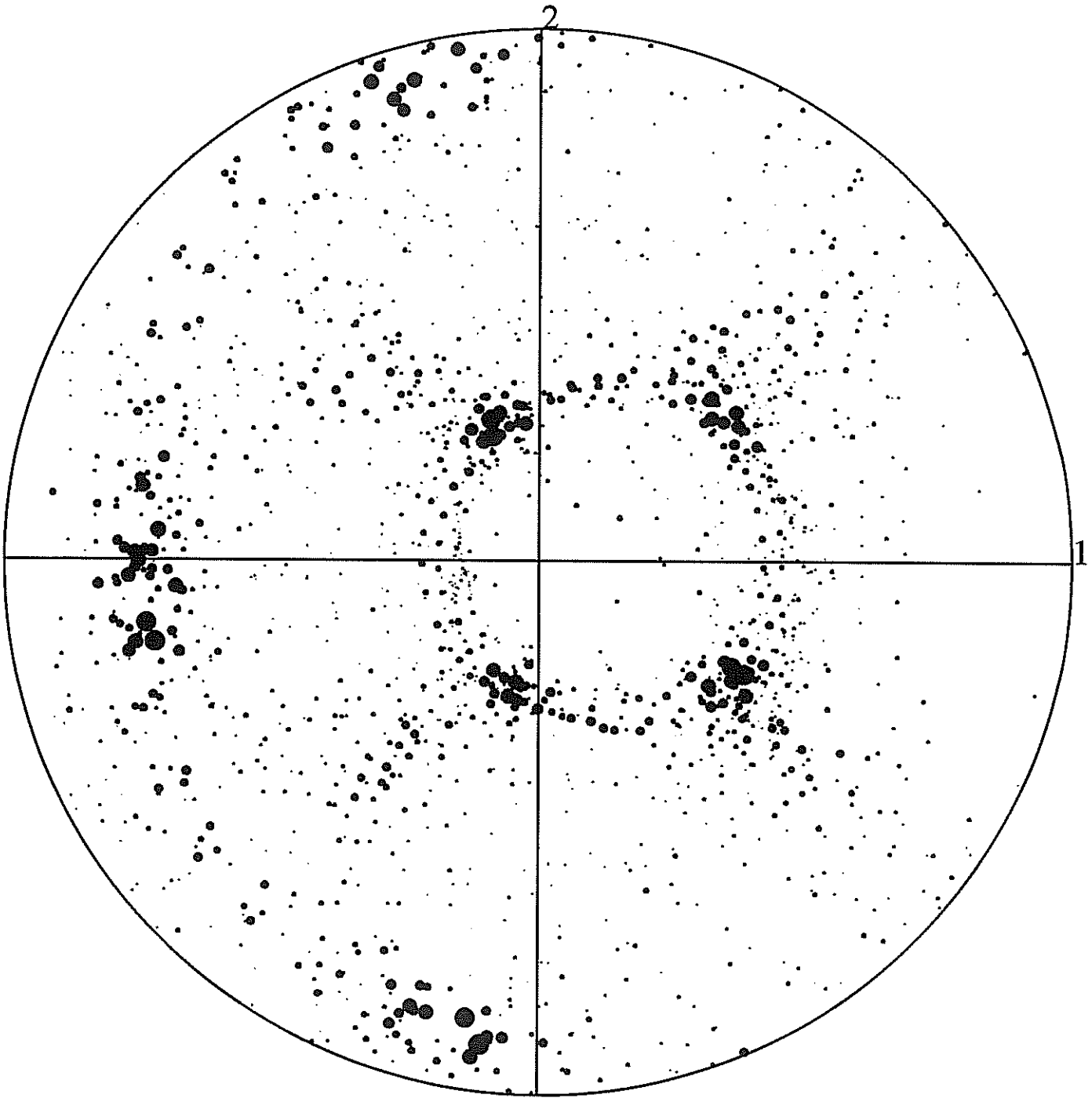

planes : 111

Figure A2.24: Texture evolution during simple shear (F13 = 0.33).

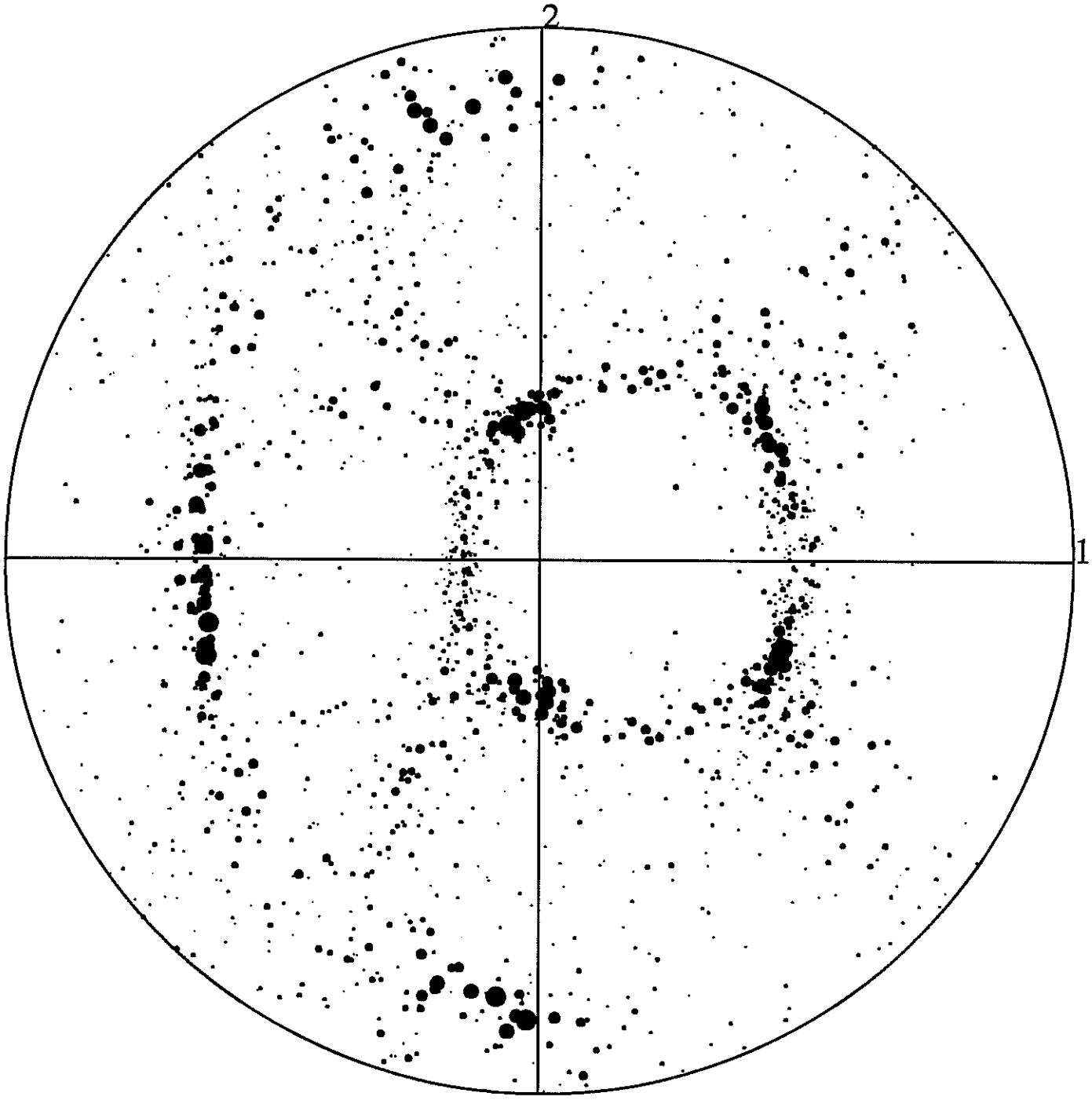

planes : 111

Figure A2.25: Texture evolution during simple shear (F13 = 0.66).

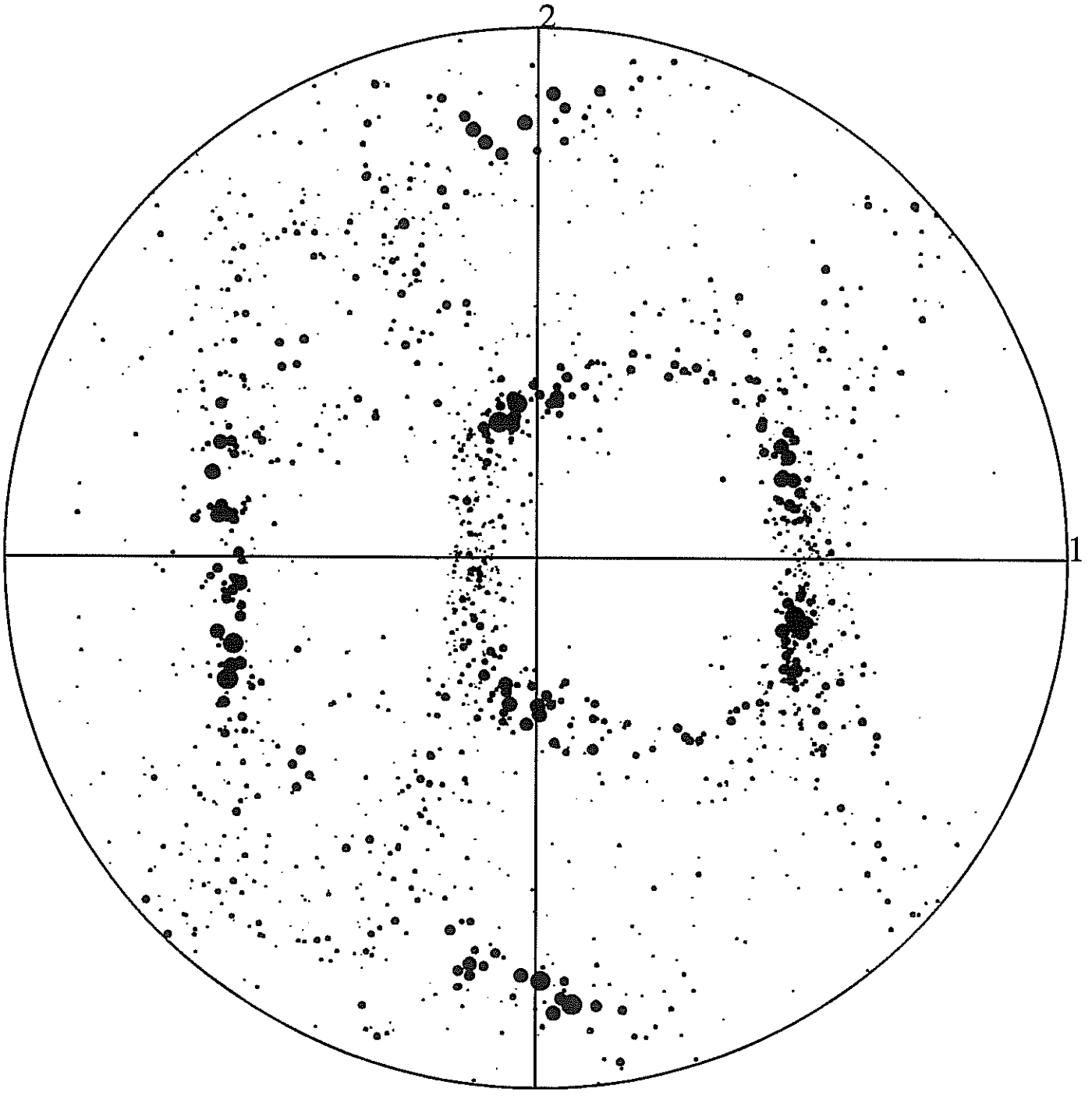

Figure A2.26: Texture evolution during simple shear (F13 = 1).

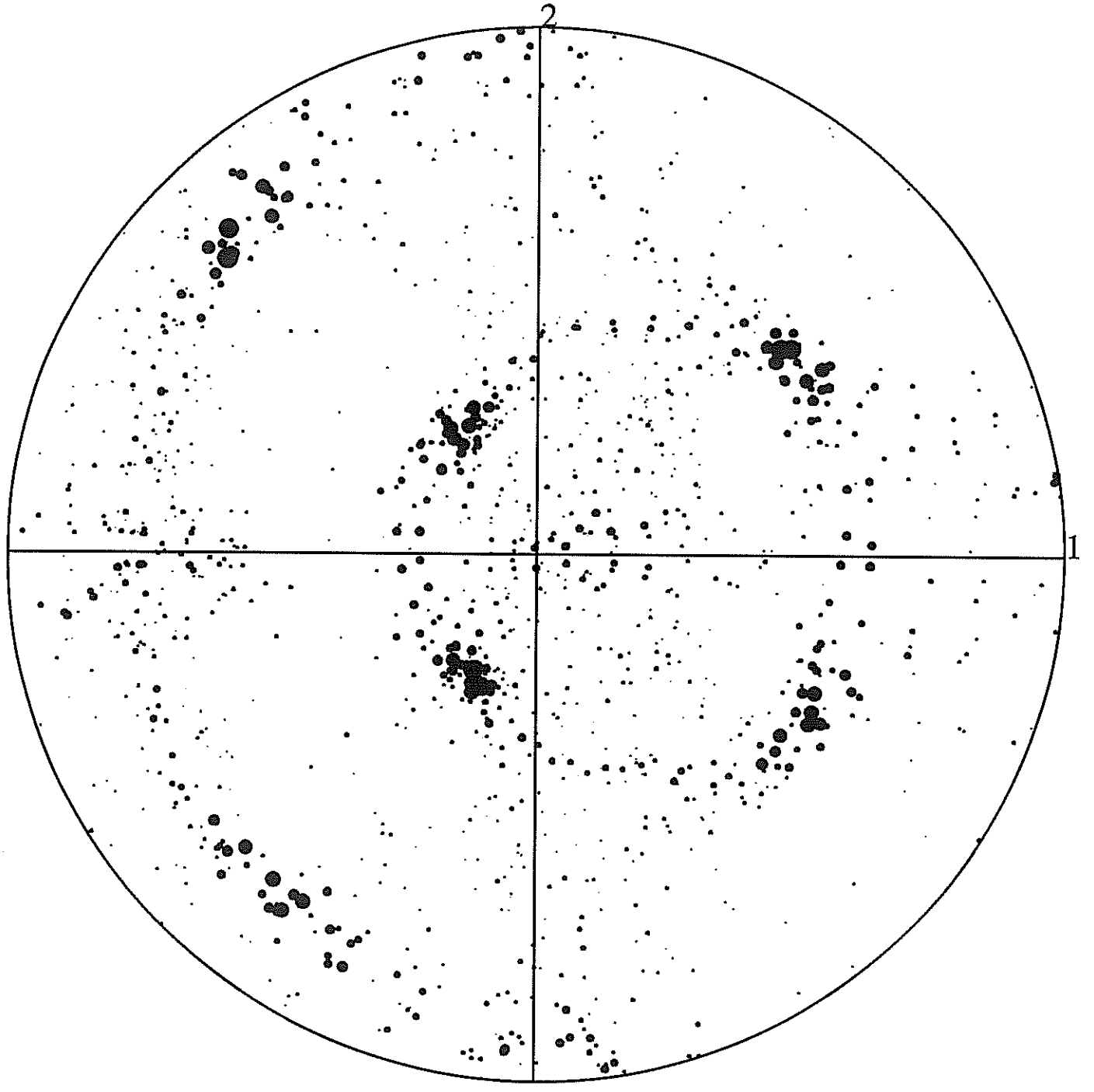

Figure A2.27: Texture evolution during simple shear (F13 = 0.44).

LEÇONS

SUR LA

PROPAGATION DES ONDES

ET LES

ÉQUATIONS DE L'HYDRODYNAMIQUE

PAR

JACQUES HADAMARD

ERGEBNISSE DER ANGEWANDTEN MATHEMATIK

UNTER MITWIRKUNG DER SCHRIFTLEITUNG DES „ZENTRALBLATT FÜR MATHEMATIK"

HERAUSGEGEBEN VON L. COLLATZ UND F. LOSCH

5

KONTINUUMSTHEORIE DER VERSETZUNGEN UND EIGENSPANNUNGEN

VON

DR. EKKEHART KRÖNER

MIT 39 ABBILDUNGEN

MECHANICS OF GENERALIZED CONTINUA

In Memoriam
of the three great French scientists
EUGÈNE and FRANÇOIS COSSERAT
who in 1909 developed the mechanical theory
of a continuum of oriented particles,
now known as the Cosserat continuum, and
ÉLIE CARTAN
who in 1922 introduced the notion of the torsion
of a space, a notion which 30 years later was
recognized to be isomorphic to the notion
of the crystal dislocation.

THÉORIE

DES

CORPS DÉFORMABLES

par MM. E. et F. COSSERAT

I. — CONSIDÉRATIONS GÉNÉRALES

1. Développement de l'idée de milieu continu. — La notion de corps déformable a joué, au siècle dernier, un rôle important dans le développement de la Physique théorique, et FRESNEL (1) doit être regardé, à l'égal de NAVIER, de Poisson et de CAUCHY (2), comme l'un des précurseurs de la théorie actuelle de l'élasticité. Sous l'influence des idées newtoniennes, on ne considérait encore au temps de ces savants que des systèmes discrets de points.

References

Aazizou K., *"Calcul par éléments finis en plasticité et viscoplasticité"*, Thèse ENSMP, Paris, 1990.

Achon P.,*"Comportement et tenacité d'alliages d'Aluminium"*, Thèse ENSMP, Paris, 1994.

Aifantis E.C.,*"The physics of plastic deformation"*, Int. J. of plasticity, Vol. 3, pp. 211-247, 1987.

Allais L., **Bornert** M., **Bretheau** T., **Caldemaison** D., *"Experimental characterization of the local strain field in a heterogeneous elastoplastic material"*, Acta Metall. Mater., Vol. 42, No. 11, pp. 3865-3880, 1994.

Anthony K., **Essmann** U., **Seeger** A., **Träuble** H., *"Disclinations and the Cosserat-continuum with incompatible rotations"*, in Mechanics of Generalized Continua, Proc. of the IUTAM-Symposium on the generalized Cosserat continuum and the continuum theory of dislocations with applications, Freudenstadt, Stuttgart, Springer-Verlag, 1967.

Argyris J., *"An excursion into large rotations"*, Comp. Meth. in Appl. Mech. and Eng., 32, pp. 85-155, 1982.

Asaro R.J., **Rice** J.R., *"Strain localization in ductile single crystals"*, J. Mech. Phys. Solids, Vol. 25, pp. 309-338, 1977.

Asaro R.J., *"Geometrical effect in the inhomogeneous deformation of ductile single crystals"*, Acta Metall., Vol. 27, pp. 445-453, 1979.

Asaro R.J., *"Crystal plasticity"*, J. of Appl. Mechanics, Vol. 50, pp. 921-934, 1983.

Ashby M.F.,*"The deformation of plastically non-homogeneous alloys"*, in Strengthening Methods in Crystals, edited by Kelly A. and Nicholson R.B., Applied Science Publishers, London, pp. 137-192, 1971.

Ayrault D., *"Fluage à haute température de superalliages base Ni monocristallins"*, Thèse ENSMP, Paris, 1989.

Bacroix B., **Genevoix** P., **Teodosiu** C., *"Plastic anisotropy induced by large strains"*, Mécamat 92, Multiaxial Plasticity, edited by Benallal A., Billardon R., Marquis D., ENS Cachan, pp. 774-803, 1992.

Balke H., **Estrin** Y., *"Micromechanical modelling of shear banding in single crystals"*, Int. J. Plasticity, Vol. 10, No. 2, pp. 133-147, 1994.

Batra R.C., *"The initiation and growth of and the interaction among adiabatic shear bands, in single and dipolar materials"*, Int. J. Plasticity, Vol. 3, pp. 75-89, 1987.

Beaude N., *"Etude théorique et expérimentale du comportement élastoplastique et de la localisation de la déformation dans les monocristaux"*, thèse Paris XIII, 1988.

Benallal A., **Billardon** R., **Geymonat** G., *"Conditions de bifurcation à l'intérieur et aux frontières pour une classe de matériaux non-standards"*, C. R. Acad. Sci. Paris, t. 308 série II, pp. 893-898, 1989.

Benallal A., **Billardon** R., **Geymonat** G.,*"Phénomènes de localisation à la frontière d'un solide"*, C.R. Acad. Sci. Paris, t. 310, Série II, pp. 679-684, 1990.

Benallal A., **Billardon** R., **Geymonat** G.,*"Localization at the boundaries and interfaces of solids"*, Proc. 3rd Int. Conf. on Constitutive Laws for Engineering Materials, University of Arizona, Tucson, 1991.

Benallal A., *"Quelques remarques sur le rôle du couplage thermomécanique dans les phénomènes de localisation"*, C.R. Acad. Sci. Paris, t. 312, Série II, pp. 117-122, 1991.

Benyoucef M., *"Etude par microscopie in situ des mécanismes de déformation du supéralliage MC2"*, Thèse CEMES, Toulouse, 1994.

Berger M., **Gostiaux** B., *"Géométrie différentielle: variétés, courbes et surfaces"*, PUF, Paris, 1987.

Bertram A., *"Axiomatische Einführung in die Kontinuumsmechanik"*, BI-Wissenschaftsverlag, 1989.

Bertram A.,*"Description of finite inelastic deformations"*, Mécamat 92, Multiaxial Plasticity, edited by Benallal A., Billardon R., Marquis D., ENS Cachan, pp. 821-835, 1992.

Bertram A., *"Description of finite inelastic deformations within crystal plasticity"*, Proceedings of 1. Asia-Oceania International Symposium on Plasticity, Beijing, pp. 105-110, 1993.

Bertram A., *"Elastizität großer Verformungen"*, BAM, Berlin, 1994a.

Bertram A., private communication, 1994b.

Bertram A., **Kraska** M., *"Beschreibung finiter plastischer Deformationen von Einkristallen mittels materieller Isomorphismen"*, to appear in ZAMM, 1995.

Berveiller M., **Zaoui** A., *"An extension of the self-consistent scheme to plastically-flowing polycrystals"*, J. Mech. Phys. Solids, Vol. 26, pp. 325-344, 1979.

Berveiller M., **Zaoui** A., *"Modeling of the plastic behavior of inhomogeneous media"*, J. of Engng Materials and Technology, Vol. 106, pp. 295-298, 1984.

Besdo D.,*"Ein Beitrag zur nichtlinearen Theorie des Cosserat-Kontinuums"*, Acta Mechanica, Vol. 20, pp. 105-131, 1974.

Besdo D., **Müller** M., *"The influence of texture development on the plastic behaviour of polycrystals"*, Finite Inelastic Deformations - Theory and Applications, edited by Besdo B. and Stein E., IUTAM Symposium, Hannover/Germany 1991, Springer Verlag, Berlin, Heidelberg, pp. 135-144, 1992.

Bigoni D., **Hueckel** T., *"Uniqueness and localization: I Associative and nonassociative elastoplasticity"*, Int. J. Solids Structures, Vol. 28, No. 2, pp. 197-213, 1991.

Bilby B.A., **Bullough** R., **Smith** E., *"Continuous distributions of dislocations : a new application of the methods of non-Riemannian geometry"*, Proc. Roy. Soc., A 231, pp. 263-273, 1955.

Bilby B.A., **Smith** E., *"Continuous distributions of dislocations III"*, Proc. Roy. Soc., A 236, pp. 481-525, 1956.

Bilby B.A., **Smith** E., *"The shapes of glide planes in bent zinc crystals"*, Acta Metall., Vol. 4, pp. 379-381, 1956.

Bilby B.A., **Bullough** R., **Gardner**, L.R.T., **Smith** E., *"Continuous distributions of dislocations IV: Single glide and plane strain"*, Proc. Roy. Soc., A 236, pp. 538-557, 1957.

Bilby B.A., **Lardner** L.R.T., **Smith** E., *"The relation between dislocation density and stress"*, Acta Metall., Vol. 6, pp. 29-33, 1958.

Bois F., *"Etude de superalliages base Nickel de structure monocristalline: solidification et fatigue à haute température"*, Thèse ENSMP, Paris, 1985.

Bornert M., **Hervé** E., **Stolz** C., **Zaoui** A.,*"Modelling the strain heterogeneities in a two-phase elastoplastic material"*, Mécamat 93, Int. Seminar on Micromechanics of Materials,

éditions Eyrolles, Paris, pp. 26-37, 1993.

Borré G., **Maier** G., *"On linear versus nonlinear flow rules in strain localization analysis"*, Meccanica Vol. 24, pp. 36-41, 1989.

Borst R. de, *"Simulation of strain localization: a reappraisal of the Cosserat continuum"*, Engineering Computations, Vol. 8, pp. 317-332, 1991.

Borst R. de, **Mühlhaus** H.B., *"Computational strategies for gradient continuum models with a view to localization of deformation"*, in Non Linear Engineering Computations, edited by Bićanić N., Owen D.R.J., Marović P., Jović V., Mihanović A., Pineridge Press, Swansea, 1991.

Borst R. de, **Sluys** L.J., *"Localization in a Cosserat continuum under static and dynamic loading conditions"*, Computer Methods in Applied Mechanics and Engineering, Vol. 90, pp. 805-827, 1991.

Borst R. de, **Mühlhaus** H.B., *"Finite deformation analysis of inelastic materials with microstructure"*, Finite Inelastic Deformations - Theory and Applications, edited by Besdo D. and Stein E., IUTAM Symposium, Hannover/Germany 1991, Springer-Verlag, pp. 313-322, 1992.

Borst R. de, *"A generalization of J_2-flow theory for polar continua"*, Computer Methods in Applied Mechanics and Engineering, Vol. 103, pp. 347-362, 1993.

Borst R. de, **Sluys** L.J., **Mühlhaus** H.B., **Pamin** J., *"Fundamental issues in finite element analyses of localization of deformation"*, Engineering Computations, Vol. 10, pp. 99-121, 1993.

Boukadia J., **Sidoroff** F., *"Simple shear and torsion of a perfectly plastic single crystal in finite transformations"*, Arch. Mech., Vol. 40, No. 5-6, pp. 497-513, 1988.

Boukadia J., **Chenaoui** A., **Sidoroff** F., *"Simple shear in FCC single crystals at large Deformations*, Large Plastic Deformations, edited by Raphanel J. L., Teodosiu C., Sidoroff F., Mécamat 91, pp. 109-116, 1993.

Cailletaud G., *"Une approche micromécanique phénoménologique du comportement inélastique des métaux*, Thèse d'Etat, Paris VI, 1987.

Cailletaud G., *"A Micromechanical approach to inelastic behavior"*, International Journal of Plasticity, Vol.8, pp. 55-73, 1992.

Cailletaud G., **Pilvin** P., *"Identification and inverse Problems: a modular approach"*, Material Parameter Estimation for Modern Constitutive Equations, edited by Bertram L.A., Brown S.B., Freed A.D., New Orleans, USA, 1993.

Canova G.R., **Molinari** A., **Fressengeas** C., *"Approach to the texture hardening of metals at high strain rates"*, edited by C. Huet, D. Bourgoin, S. Richemond, Rhéologie des matériaux anisotropes, CR 19e col. GFR Paris, Nov. 1984, éditions Cepadues, pp. 69-78, Toulouse, 1986.

Canova G., **Kubin** L.P., **Brechet** Y., *"Glide softening in alloys: a simulation"*, Large Plastic Deformations, edited by Raphanel J. L., Teodosiu C., Sidoroff F., Mécamat 91, pp. 27-38, 1993.

Cartan H., *"Calcul différentiel"*, Hermann, Paris, 1977.

Chambon R., *"Bifurcation par localisation en bande de cisaillement, une approche avec des lois incrémentales non linéaires"*, J. de Méc. Théo. Appl., Vol. 5, No. 2, pp. 277-298, 1986.

Chang Y.W., **Asaro** R.J., *"An experimental study of shear localization in Al-Cu single crystals"*, Acta Metall., Vol. 29, pp. 241-257, 1981.

Chieragatti R., *"Influence de l'orientation cristallographique sur le comportement en fatigue oligocyclique du MarM 200 monocristallin"*, Tthèse ENSMP, 1987.

Chrysochoos C.,*"Dissipation et blocage d'énergie lors d'un écrouissage en traction simple"*, thèse Université de Montpellier, 1987.

Cosserat E., **Cosserat** F., *"Sur la théorie de l'élasticité"*, Annales de la Faculté des Sciences de Toulouse, Tome X, 1896.

Cosserat E., **Cosserat** F., *"Théorie des corps déformables"*, Hermann, Paris, 1909.

Culioli J.C., *Introduction à l'optimisation*, Ellipses, 1994.

Dafalias Y.F., *"Corotational rates for kinematic hardening at large plastic deformations"*, J. of Appl. Mech., Vol. 50, pp. 561-565, 1983.

Dao M.,**Asaro** R.J.,*"Coarse slip bands and the transition to macroscopic shear Bands"*, Scripta Metall. et Mater., Vol. 30, pp. 791-796, 1994.

Dederichs P.H., **Zeller** R., *"Variational treatment of the elastic constants of disordered materials"*, Z. Physik, Vol. 259, pp. 103-116, 1973.

Demazure M., *Catastrophes et bifurcations*, Ellipses, Paris, 1989.

Dève H.E., **Asaro** R.J., *"The development of plastic failure modes in crystalline materials: shear bands in FCC polycrystals"*, Metallurgical Transactions, Vol. 20A, pp. 579-593, 1989.

Dreyer W., **Olschewski** J., *"Order-disorder transitions under load in single crystal superalloys"*, Mécamat 94, Solid-solid phase transformations of materials, 1994.

Dietsche A., **Steinmann** P., **Willam** K., *"Micropolar elastoplasticity and its role in localization analysis"*, Anisotropy and Localization of Plastic Deformation, Plasticity 91, edited by Boehler J.P., Khan A.S., Elsevier Applied Science, 1991.

Dietsche A., *"Lokale Effekte in linear-elastischen und elasto-plastischen Cosserat-Kontinua"*, Dissertation, Universität Karlsruhe, 1993.

Dietsche A., **Steinmann** P., **Willam** K., *"Micropolar elastoplasticity and its role in localization"*, Int. J. Plasticity, Vol. 9, pp. 1969-1994, 1993.

Dluzewski P.H., *"Finite deformations of polar media in angular coordinates"*, Arch. Mech., Vol. 43, No. 6, pp. 783-793, 1991.

Dluzewski P.H., *"Finite elastic-plastic deformations of oriented media"*, MECAMAT'92, Int. Seminar on Multiaxial Plasticity, Cachan, pp. 668-688, 1992.

Dogui A., **Sidoroff** F., *"Rhéologie anisotrope en grandes déformations"*, C. Huet, D. Bourgoin, S. Richemond, Rhéologie des matériaux anisotropes, CR 19e col. GFR Paris, Nov.1984, éditions Cepadues, pp. 69-78, Toulouse, 1986.

Dogui A., *"Plasticité anisotrope en grandes déformations"*, thèse d'Etat Lyon I, 1989.

Dubois P., *"Etude cristallographique de l'initiation et de la propagation des bandes de cisaillement dans les métaux purs"*, Thèse Université Paris Nord, 1988.

Duszek-Perzyna M.K., **Perzyna** P., *"Analysis of the influence of non-Schmid and thermal effects on adiabatic shear band localization in elastic-plastic single crystals"*, Finite Inelastic Deformations - Theory and Applications, edited by Besdo B. and Stein E., IUTAM Symposium, Hannover/Germany 1991, Springer Verlag, Berlin, Heidelberg, pp. 155-165, 1992.

Duszek-Perzyna M.K., **Perzyna** P., *"Adiabatic shear band localization in elastic-plastic single crystals"*, Int. J. Solids Structures, Vol. 30, No.1, pp. 61-89, 1993.

Duszek-Perzyna M.K., **Perzyna** P., *"A note on adiabatic shear band localization in elastic-plastic single crystals"*, Large Plastic Deformations, edited by Raphanel J. L., Teodosiu C., Sidoroff F., Mécamat 91, pp. 205-211, 1993.

Eisenberg M., *"On the relation between continuum plasticity and dislocation theories"*, Int. J. Engng. Sci., Vol. 8, pp. 261-271, 1970.

Eringen A.C., *"Polar and non local field theories"*, in Continuum Physics, edited by Eringen A.C., Volume IV, Academic Press, 1976.

Estrin Y., **Kubin** L.P., *"Local strain hardening and nonuniformity of plastic deformation"*, Acta Metall., Vol. 34, No. 12, pp. 2455-2464, 1986.

Estrin Y., **Kubin** L.P., *"Plastic instabilities: classification and physical mechanisms"*, Res Mechanica Vol. 23, pp. 197-221, 1988.

Feller-Kniepmeier M., **Glatzel** U., **Link** T., **Scheumann-Frerker** G., *"Entwicklung von Gefüge und Versetzungsstrukturen in der einkristallinen Nickelbasis-Legierung SRR99 während Wärmebehandlung und Hochtemperaturkriechen"*, 2. Werkstoffkolloquium des Sfb 339, VDI Verlag, Vol. 5, No. 203, 1990.

Fleck N.A., **Müller** G.M, **Ashby** M.F., **Hutchinson** J.W., *"Strain gradient plasticity: theory and experiment"*, Acta Metall. Mater., Vol. 42, No. 2, pp. 475-487, 1994.

Fleury E., *Endommagement du superalliage monocristallin AM1 en fatigue isotherme et anisotherme*, Thèse ENSMP, Paris, 1991.

Forest S., **Cailletaud** G., *"Modelling non homogeneous deformation of nickel based single crystal superalloys"*, mid-term progress report, Brite-Euram project BRE2-CT92-0176, Brussels, 1994.

Forest S., **Cailletaud** G., *"Strain localization in single crystals: effect of boundaries and interfaces"*, Eur. J. Mech., A/Solids, Vol. 14, No. 5, pp. 747-771, 1995.

Forest S., **Pilvin** P., *"Modelling the cyclic behaviour of two-phase single crystal nickel-base superalloys"*, to appear in the Proceedings of the IUTAM Symposium on Micromechanics of Plasticity and Damage of Multiphase Materials, Sèvres, France, 1995.

Fortunier R., *"Contribution à l'étude de la déformation plastique des cristaux et des polycristaux"*, thesis, Ecole des Mines de Saint-Etienne, 1987.

Franciosi P., **Berveiller** M., **Zaoui** A., *"Latent hardening in copper and aluminium single crystals"*, Acta Metall., Vol. 28, pp. 273-283, 1980.

Franciosi P., **Zaoui** A.,*"Multislip in FCC crystals: a theoretical approach compared with experimental data"*, Acta Metall., Vol. 30, pp. 1627-1637, 1982.

Franciosi P., **Zaoui** A.,*"Multislip tests on copper crystals: a junction hardening effect"*, Acta Metall.,Vol. 30,pp. 2141-2151, 1982.

François D., **Pineau** A., **Zaoui** A., *Comportement mécanique des matériaux*, tome 1, Hermès, Paris, 1991.

Fredholm A., *"Monocristaux d'alliages base nickel relation entre composition, microstructure et comportement en fluage à haute température"*, Thèse ENSMP, Paris, 1987.

Friedel J., *Dislocations*, Pergamon, 1964.

Gambin B., **Kröner** E., *"Convergence problems in the theory of random elastic media"*, Int. J. Engng Sci., Vol. 19, pp. 313-318, 1981.

Garstone J., **Honeycombe** R.W.K., **Greetham** G., *Easy glide of cubic metal crystals"*, Acta Metall., Vol. 4, pp. 485-494, 1956.

Gaspérini M., **Rey** C., *"Effect of initial orientation and of predeformation on shear banding in copper single crystals submitted to tensile tests"*, Large Plastic Deformations, edited by Raphanel J. L., Teodosiu C., Sidoroff F., Mécamat 91, pp. 229-237, 1993.

Géradin M., *"Aspects numériques et logiciels de l'approche éléments finis à l'analyse des systèmes articulés flexibles"*, Colloque national en calcul des structures, Giens, Hermès,

1992.

Germain P., *"The method of virtual power in continuum mechanics, Part 2: Microstructure"*, SIAM, J. Appl. Math., Vol. 25, No. 3, 1973.

Germain P., **Nguyen** Q.S., **Suquet** P., *"Continuum thermodynamics"*, J. of Applied Mechanics, Vol. 50, pp. 1010-1020, 1983.

Gilman J.J., *"Structure and polygonization of bent zinc monocrystals"*, Acta Metall., Vol. 3, pp. 277-288, 1955.

Gilormini P., **Tóth** L.S., **Jonas** J.J., *"An analytic method for the prediction of ODFs with application to the shear of polycrystals"*, Proc. R. Soc. Lond. A, Vol. 430, pp. 489-507, 1990.

Gouyet J.F., *"Physique et structures fractales"*, Masson, 1992. .

Günther W., *"Zur Statik und Kinematik des Cosseratschen Kontinuums"*, Abhandlungen der Braunschweig. Wiss. Ges., Vol. 10, pp. 195-213, 1958.

Günther H., *"Zur nichtlinearen Kontinuumstheorie bewegter Versetzungen"*, Schriftenreihe der Institute für Mathematik bei der deutschen Akademie der Wissenschaften zu Berlin, Akademie Verlag, Berlin, 1967.

Hadamard J., *"Leçons sur la propagation des ondes et les équations de l'hydrodynamique"*, Hermann, Paris, 1903.

Hahn H.T., **Jaunzemis** W., *"A dislocation theory of plasticity"*, Int. J. Engng. Sci., Vol. 11, pp. 1065-1078, 1973.

Halphen B., **Nguyen** Q.S., *"Sur les matériaux standards généralisés"*, Journal de Mécanique, Vol. 14, No. 1, pp. 39-63, 1975.

Hanriot F., *Etude du comportement du superalliage monocristallin AM1 sous sollicitations cycliques*, Thèse ENSMP, Paris, 1992.

Harirêche O., **Loret** B., *"3D dynamic strain-localization: shear band pattern transition in solids"*, Eur. J. Mech. A/Solids, Vol. 11, No. 6, pp. 733-751, 1992.

Hehl F., **Kröner** E., *"Zum Materialgesetz eines elastischen Mediums mit Momentenspannungen"*, Z. Naturforschg., Vol. 20a, pp. 336-350, 1965.

Hervé E., **Zaoui** A.,*"Modelling the effective behaviour of non-linear matrix-inclusion composites"*, Eur. J. Mech. A/Solids, Vol. 9, No. 6, pp. 505-515, 1990.

Hervé E., **Stolz** C., **Zaoui** A., *"A propos de l'assemblage des sphères composites de Hashin"*, C.R. Acad. Sci. Paris, t. 313, Série II, pp. 857-862, 1991.

Hervé E., **Stolz** C., **Zaoui** A., *"Morphological representative pattern-based micromechanical modelling"*, Mécamat 93, Int. Seminar on Micromechanics of Materials, éditions Eyrolles, Paris, pp. 3-13, 1993.

Hibbard W.R., **Dunn** C. G., *"A study of* $< 112 >$ *edge dislocations in bent silicon-iron single crystals"*, Acta Metall., Vol. 4, pp. 306-315, 1956.

Hihi A., **Berveiller** M., **Zaoui** A., *"Une nouvelle formulation de la modélisation autocohérente de la plasticité des polycristaux métalliques"*, J. de mécanique théorique et appliquée, Vol. 4, No. 2, pp. 201-221, 1985.

Hill R. *"A general theory of uniqueness and stability in elastic plastic solids"*, J. Mech. Phys. Sol., Vol. 6, pp. 236-249, 1958.

Hill R., *"Continuum micro-mechanics of elastoplastic polycrystals*, J. Mech. Phys. Solids, Vol. 13, pp. 89-101, 1965.

Hill R., **Hutchinson** J.W., *"Bifurcation phenomena in the plane tension test"*, J. Mech. Phys. Solids, Vol. 23, pp. 239-264, 1975.

Hirth J.P., **Lothe** J., *Theory of dislocations*, Wiley-Interscience, 1982.

Hu Z., **Teodosiu** C., *"Formation and evaluation of dislocation structures in f.c.c. single crystals"*, Large Plastic Deformations, edited by Raphanel J. L., Teodosiu C., Sidoroff F., Mécamat 91, pp. 239-245, 1993.

Ilcewicz L.B., **Narasimhan** M.N.L, **Wilson** J.B., *"Micro and macro material symmetries in generalized continua"*, Int. J. Engng. Sci., Vol. 24., No. 1, pp. 97-109, 1986.

Jaoul B., *"Influence de la sous-structure de monocristaux d'aluminium sur la forme des courbes de déformation plastique"*, C.R. Acad. Sci. Paris, t. 242, pp. 2372-2374, 1956.

Jaoul B., **Bricot** I., **Lacombe** P., *"Relation entre la géométrie de la déformation de monocristaux d'aluminium et leur structure après traitement thermique"*, Rev. de Métallurgie, Vol. 54, N0. 2, pp. 81-92, 1957.

Jaoul B., *"Etude de la plasticité et application aux métaux"*, Dunod, Paris, 1965.

Kafadar C.B., **Eringen** A.C., *"Micropolar media: I the classical theory"*, Int. J. Engng Sci., Vol. 9, pp. 271-305, 1971.

Kessel S., *"Lineare Elastizitätstheorie des anisotropen Cosserat-Kontinuums"*, Abhandlungen der Braunschweig. Wiss. Ges., Vol. 16, 1964.

Kessel S., *"Spannungsfelder einer Schraubenversetzung und einer Stufenversetzung im Cosseratschen Kontinuum"*, ZAMM, Vol. 50, No. 9, pp. 547-553, 1970.

Kluge G., *"Zur Dynamik der allgemeinen Versetzungstheorie bei Berücksichtigung von Momentenspannungen"*, Int. J. Engng. Sci., Vol. 7, pp. 169-182, 1969.

Kocks U.F., *"Polyslip in single crystals"*, Acta Metall., Vol. 8, pp. 345-352, 1960.

Kondo K., *"On the analytical and physical foundations of the theory of dislocations and yielding by the differential geometry of continua"*, Int. J. Engng. Sci., Vol. 2, pp. 219-251, 1964.

Kossecka E., **Wit** R. de, *"Disclination kinematics"*, Arch. of Mech., Vol. 29, No. 5, pp. 633-651, 1977.

Korbel A., *"The real nature of shear bands: plastons?"*, Plastic Instabilities, Considère Memorial, Presses de l'Ecole Nationale des Ponts et Chaussées, pp. 325-335, 1985.

Kraska M., *"Modellierung und Berechnung finiter inelastischer Verformungen von Einkristallen"*, Diplom-Arbeit, TU-Berlin, 1993.

Krawietz A., *"Materialtheorie"*, Springer Verlag, 1986.

Kröner E., *"Die Versetzung als elementare Eigenspannungsquelle"*, Z. Naturforschg., Vol. 11a, pp. 969-985, 1956.

Kröner E., **Rieder** G., *"Die Kontinuumstheorie der Versetzungen"*, Z. für Physik, Vol. 145, pp. 424-429, 1956.

Kröner E., *"Kontinuumstheorie der Versetzungen und Eigenspannungen"*, Ergebnisse der angewanten Mathematik, Vol. 5, Springer-Verlag, 1958.

Kröner E., *"Berechnung der elastischen Konstanten des Vielkristalls aus den Konstanten des Einkristalls"*, Z. Physik, Vol. 151, pp. 504-518, 1958.

Kröner E., **Seeger** A., *"Nicht-lineare Elastizitätstheorie der Versetzungen und Eigenspannungen"*, Arch. Rat. Mech. Anal., Vol. 3, pp. 97-119, 1959.

Kröner E., *"Allgemeine Kontinuumstheorie der Versetzungen und Eigenspannungen"*, Arch. Rat. Mech. Anal., Vol. 4, No.1, pp. 273-334, 1960.

Kröner E., *"Zur plastischen Verformung des Vielkristalls"*, Acta Metall., Vol. 9, pp. 155-161, 1961.

Kröner E., *"On the physical reality of torque stresses in continuum mechanics"*, Int. J. Engng. Sci., Vol. 1, pp. 261-278, 1963.

Kröner E., *"Das physikalische Problem der antimetrischen Spannungen und der sogenannten Momentenspannungen"*, Proc. of the 11th Int. Congress of Applied Mechanics, edited by Görtler H., Münich 1964, Springer-Verlag, 1966.

Kröner E., *"Mechanics of generalized continua"*, Proc. of the IUTAM-Symposium on the generalized Cosserat continuum and the continuum theory of dislocations with applications, Freudenstadt, Stuttgart, Springer-Verlag, 1967.

Kröner E., **Koch** H., *"Effective properties of disordered materials"*, SM Archives, Vol. 1, No. 2/3, pp. 183-238, 1976.

Kröner E., *"Bounds for effective moduli of disordered materials"*, J. Mech. Phys. Solids, Vol. 25, pp. 137-155, 1977.

Kröner E., *"Linear properties of random media- the systematic theory"*, Comportements rhéologiques et structure des matériaux, CR 15e Coll. GFR, Paris, pp. 15-40, 1980.

Kröner E., *"The internal mechanical state of solids with defects"*, Int. J. Solids Structures, Vol. 29, No 14/15, pp. 1849-1857, 1992.

Kröner E., *"A variational principle in non linear dislocation theory"*, Proc. of the second international conference of non linear mechanics, Beijing, pp. 59-64, 1993.

Ladevèze P., *"Sur la théorie de la plasticité en grandes déformations"*, rapport interne LMT No.9, 1980.

Lardner R.W., *"Dislocation dynamics and the theory of the plasticity of single crystals"*, ZAMP, Vol. 20, pp. 514-529, 1969.

Le K. C., **Stumpf** H., *"Finite elastoplasticity with microstructure"*, Mitteilung aus dem Institut für Mechanik der Ruhr-Universität Bochum, No. 92, 1994.

Leblond J.B., **Perrin** G., **Devaux** J., *"Bifurcation effects in ductile metals with non-local plasticity"*, J. of Appl. Mechanics, Vol. 61, pp. 236-242, 1994.

Legait J., *"Une approche micromécanique de l'endommagement des matériaux polycristallins"*, Thèse ENSMP, Paris, 1994.

Lehman D., **Sacré** C., *"Géométrie et topologie des surfaces"*, PUF, Paris, 1982.

Lemaitre J., **Chaboche** J.L., *"Mécanique des matériaux solides"*, Dunod, Paris, 1985.

Liebfried G., **Haasen** P., *"Zum Mechanismus der plastischen Verformung"*, Z. für Physik, Vol. 137, pp. 67-88, 1954.

Lipinski P., **Berveiller** M.,*"Elastoplasticity of micro-inhomogeneous metals at Large strains"*, Int. J. of Plasticity, Vol. 5, pp. 149-172, 1989.

Lipinski P., **Krier** J., **Berveiller** M., *"Elasto-plasticité des métaux en grandes déformations: comportement global et évolution de la structure interne"*, Revue physique appliquée Vol. 25, pp. 361-388, 1990.

Lippmann H., *"Eine Cosserat-Theorie des plastischen Fließens"*, Acta Mechanica, Vol. 8, pp. 255-284, 1969.

McClintock F.A., **André** P.A., **Schwerdt** K.R., **Stoeckly** R.E., *"Interface couples in crystals"*, Nature, No. 4636, pp. 652-653, 1958.

McClintock F.A., *"Contribution of interface couples to the energy of a dislocation"*, Acta Metall., Vol. 8, p. 127, 1960.

Mader S., *"Elektronenmikroskopische Untersuchung der Gleitlinienbildung auf Kupfereinkristallen"*, Z. für Physik, Vol. 149, pp. 73-102, 1957.

Mader S., **Seeger** A., *"Untersuchung des Gleitlinienbildes kubischflächenzentrierter Einkristalle"*, Acta Metall., Vol. 8, pp. 513-522, 1960.

Mandel J.,*"Ondes plastiques dans un milieu indéfini à trois dimensions"*, J. de Mécanique, Vol. 1, pp. 3-30, 1962.

Mandel J.,*"Généralisation de la théorie de la plasticité de W.T. Koiter"* Int. J. Solids Structures, Vol. 1, pp. 273-295, 1965.

Mandel J., *"Conditions de stabilité et postulat de Drucker"*, Rhéologie et mécanique des sols, edited by J. Kravtchenko et P.M. Sirieys, Springer Berlin, 1966.

Mandel J., *Plasticité classique et viscoplasticité*, CISM, Udine, Springer Verlag, 1971.

Mandel J., *"Equations constitutives et directeurs dans les milieux plastiques et viscoplastiques"*, Int. J. Solids Structures, Vol. 9, pp. 725-740, 1973.

Mandel J., *"Sur la définition de la vitesse de déformation élastique et sa relation avec la vitesse de contrainte"*, Int. J. Sol. Struct., Vol. 17, pp. 873-878, 1981.

Mandel J., *"Définition d'un repère privilégié pour l'étude des transformations anélastiques du polycristal"*, J. de Mécanique théorique et appliquée, Vol. 1, No.1; pp. 7-23, 1982.

Mandel J., *"Sur la vitesse de déformation élastique en grande déformation élastoplastique"*, Int. J. Solids Structures, Vol. 19, No. 7, pp. 573-578, 1983.

Martin A., *"Détermination des sysèmes des glissement actifs lors d'essais de traction sur des monocristaux SC16"*, training period at BAM-Berlin, 1995.

Méric L., *"Une modélisation mécanique du comportement des monocristaux"*, Thèse ENSMP, Paris, 1991.

Méric L., **Poubanne** E., **Cailletaud** G., *"Single crystal modeling for structural calculations: Part 1: Model presentation"*, Journal of Engineering Materials and Technology, Vol. 113, pp. 162-170, 1991.

Méric L., **Cailletaud** G., *"Single crystal modeling for structural calculations: Part 2: Finite Element implementation"*, Journal of Engineering Materials and Technology, Vol. 113, pp. 171-182, 1991.

Méric L., **Cailletaud** G., **Gaspérini** M.,*"F.E. calculations of copper bicrystal specimens submitted to tension-compression tests"*, Acta Metall. Mater., Vol. 42, No. 3, pp. 921-935, 1994.

Mescheryakov Y.I., **Prockuratova** E.I., *"Kinetic theory of continuously distributed dislocations"*, Int. J. Solids structures, Vol. 32, No. 12, pp. 1711-1726, 1995.

Morii K., **Mecking** H., **Nakayama** Y., *"Development of shear bands in FCC single crystals"*, Acta metall., Vol. 33, No.3, pp. 379-386, 1985.

Mühlhaus H.B., **Vardoulakis** I., *"The thickness of shear bands in granular materials"*, Géotechnique, Vol. 37, No. 3, pp. 271-283, 1987.

Mühlhaus H.B., *"Application of Cosserat theory in numerical solutions of limit load problems"*, Ingenieur-Archiv, Vol. 59, pp.124-137, 1989.

Müller L., **Glatzel** U., **Feller-Kniepmeier** M., *"Calculations of the internal stresses and strains in the microstructure of a single crystal nickel-base superalloy during creep"*, Acta Metal. Mater., Vol. 41, No. 12, pp. 3401-3411, 1993.

Mughrabi H., *"Cyclic plasticity of matrix and persistent slip bands in metals"*, Continuum models for discrete systems 4, edited by Brulin O. and Hsieh R.K.T., North-Holland, Amsterdam, pp. 241-245, 1981.

Mura T., *"On dynamic problems of continuous distribution of dislocations"*, Int. J. Engng. Sci., Vol. 1, pp. 371-381, 1963a.

Mura T., *"Continuous distribution of moving dislocations"*, Philosophical Magazine, Vol. 8, No. 89, pp. 843-857, 1963b.

Mura T., *"Continuous distribution of dislocations and the mathematical theory of plasticity"*, Phys. stat. sol., Vol. 10, pp. 447-453, 1965a.

Mura T., *"Continuous distribution of dislocations and the mathematical theory of plasticity II"*, Phys. stat. sol., Vol. 11, pp. 683-688, 1965b.

Mura T., *"Continuum theory of plasticity and dislocations"*, Int. J. Engng. Sci., Vol. 5, pp. 341-351, 1967.

Mura T., *"Micromechanics of defects in solids"*, Martinus Nijhoff, The Hague, 1987.

Needleman A., *"Material rate-dependence and mesh-sensitivity in localization problems"*, Comp. Meth. in Appl. Mech. and Eng., Vol. 67, pp. 805-827, 1988.

Needleman A., **Asaro** R.J., **Lemonds** J., **Peirce** D., *"Finite element analysis of crystalline solids"*, Comp. Meth. in Appl. Mech. and Eng., Vol. 52, pp. 689-708, 1985.

Needleman A., **Ortiz** M., *"Effects of boundaries and interfaces on shear-band localization"*, Int. J. Solids Structures, Vol. 28, No. 7, pp. 859-877, 1991.

Neilsen M.K., **Schreyer** H.L., *"Bifurcations in elastic-plastic materials"*, Int. J. Solids Structures, Vol. 30, No. 4, pp. 521-544, 1993.

Neuhäuser H., *"Slip-line formation and collective dislocation motion"*, Dislocation in Solids, Vol.6, Applications and Recent Advances, edited by Nabarro F.R.N., Holland Publishing Company, pp. 319-440, 1983.

Neuhäuser H., *"The dynamics of slip band formation in single crystals"*, Res Mechanica Vol. 23, pp. 113-135, 1988.

Noll W., *"A new mathematical theory of simple materials"*, Arch. Rat. Mech. Anal., Vol. 48, pp. 1-50, 1972.

Nouailhas D.,**Culié** J.P., **Méric** L., **Cailletaud** G., *"Finite element analysis of the stress-strain behaviour of single crystal tubes"*, Multiaxial Plasticity, Proc. Mécamat 92, Cachan, 1992.

Nouailhas D., **Cailletaud** G.,*"Multiaxial behaviour of Ni-base single crystals"*, Fourth International Conference on Biaxial/Multiaxial Fatigue, Paris, 1994.

Nouailhas D., **Cailletaud** G.,*"Microscopic and macroscopic behaviour of two-phase single crystal superalloys"*, Proc. of Plasticity'95, 1995.

Nouailhas D., **Cailletaud** G.,*Tension-torsion of single crystal superalloys: experiment and finite element analysis"*, Int. J. Plasticity, Vol. 11, No. 4, pp. 451-470, 1995.

Nye J.F., *"Some geometrical relations in dislocated crystals"*, Acta Metall., Vol. 1, pp. 153-162, 1953.

Ottosen N.S., **Runesson** K., *"Properties of discontinuous bifurcation solutions in elasto-plasticity"*, Int. J. Solids Structures, Vol. 27, No.4, pp. 401-421, 1991a.

Ottosen N.S., **Runesson** K., *"Acceleration waves in elastoplasticity"*, Int. J. Solids Structures, Vol. 28, No. 2, pp. 135-159, 1991b.

Paxton H.W., **Cottrell** A.H., *"Work-hardening in stretched and twisted aluminium crystals"*, Acta Metall., Vol. 2, pp. 3-8, 1954.

Peirce D. **Asaro** R.J., **Needleman** A., *"An analysis of non-uniform and localized deformation in ductile single crystals"*, Acta Metall., Vol. 30, pp. 1087-1119, 1982.

Peirce D. **Asaro** R.J., **Needleman** A., *"Material rate dependence and localized deformation in crystalline solids"*, Acta Metall., Vol. 31, No. 2, pp. 133-153, 1983.

Peirce D., *"Shear band bifurcation in ductile single crystals"*, J. Mech. Phys. Solids, Vol. 31, No.2, pp. 133-153, 1983.

Perić D., **Owen** D.R.J., *"Computational strategies for strain localization problems"*, Computational Methods in Applied Sciences, edited by Hirsch Ch., Elsevier, 1992.

Pilvin P., *"Identification des paramètres de lois de comportement"*, Proc. MECAMAT, Besançon, pp. 155-164, 1988.

Pilvin P., *"Approches multiéchelles pour la prévision du comportement anélastique des métaux"*, thèse Paris VI, 1990.

Pilvin P., *"The contribution of micromechanical approaches to the modelling of inelastic behaviour of polycrystals"*, Fourth International Conference on Biaxial/Multiaxial Fatigue, May 31-June 3, Paris, 1994.

Pilvin P., *"Contribution de la simulation numérique au développement des relations de comportement en mécanique des matériaux"*, mémoire d'habilitation, Université Pierre et Marie Curie, 1995.

Pineau A., *"Influence of uniaxial stress on the morphology of coherent precipitates during coarsening - Elastic energy considerations"*, Acta Metall., Vol. 24, pp. 559-564, 1976.

Pope D.P.,**Ezz** S.S.,*"Mechanical properties of* Ni_3Al *and nickel-base alloys with high volume fraction of* γ'*"*, Int. Metal Review. Vol. 29, No.3, 1984.

Potier-Ferry M., *"Towards a catastrophe theory for the mechanics of plasticity and fracture"*, Int. J. Solids Structures, Vol. 23, No. 8, pp. 821-837, 1985.

Poubanne P., *Etude et modélisation du comportement mécanique d'un superalliage monocristallin pour aube de turbine*, thèse Ecole Centrale de Paris, 1989.

Prigogine I., **Stengers** I., *"Order out of chaos"*, Bantam Books,1994.

Raniecki B., **Bruhns** O.T., *"Bounds to bifurcation stresses in solids with non-associated plastic flow law at finite strain"*, J. Mech. Phys. Solids, Vol. 29, No. 2, pp. 153-172, 1981.

Read W.T., *"Dislocation theory of plastic bending"*, Acta Metall., Vol. 5, pp. 83-88, 1957.

Rice J.R., *"The localization of deformation"*, Theoretical and Applied Mechanics, edited by W.T. Koiter, pp. 207-220, North Publishing Company, 1976.

Rice J.R., **Rudnicki** J.W., *"A note on some features of the theory of localization of deformation"*, Int. J. Solids Structures, Vol. 16, pp. 597-605, 1980.

Rougée P., *"Formulation lagrangienne intrinsèque en mécanique des milieux continus"*, Journal de Mécanique, Vol. 19, No.1, 1980.

Rougée P., *"A new Lagrangian intrinsic approach to large deformations in contiuous media"*, Eur. J. Mech., A/Solids, pp. 15-39, 1991.

Rougée P., *"The intrinsic lagrangian metric and stress variables"*, Finite Inelastic Deformations - Theory and Applications, edited by Besdo B. and Stein E., IUTAM Symposium, Hannover/Germany 1991, Springer Verlag, Berlin, Heidelberg, pp. 217-226, 1992a.

Rougée P., *"Kinematics of finite deformations"*, Arch. Mech., Vol. 44, No. 1, pp. 117-132, 1992b.

Rougée P., *"Material derivatives in large deformation theory"*, submitted to publication, 1994.

Rougier Y., **Stolz** C., **Zaoui** A.,*"Self-consistent modelling of elastic-viscoplastic polycrystals"*, C.R. Acad. Sci. Paris, t. 318, Série II, pp. 145-151, 1994.

Runesson K. **Mroz** Z., *"A Note on non-associated flow rules"*, Int. J. Plasticity, Vol. 5, pp. 639-658, 1989.

Runesson K., **Ottosen** N.S., **Peri/'c** D., *"Discontinuous bifurcations of elastic-plastic solutions at plane stress and plane strain"*, Int. J. Plasticity, Vol. 7, pp. 99-121, 1991.

Sansour C., **Keck** J., *"Zum elasto-viskoplastischen Cosserat Kontinuum"*, Große plastische Formänderungen, edited by O.T. Bruhns, Mitteilungen aus dem Institut für Mechanik,

No. 93, Ruhr-Universität Bochum, pp. 38-41, 1994.

Sawczuk A., *"On yielding of Cosserat continua"*, Arch. Mech. Stoso.,Vol. 3, No. 19, pp. 471-480, 1967.

Schäfer H., *"Das Cosserat-Kontinuum"*, ZAMM, Vol. 47, No. 8, pp. 485-498, 1967.

Schäfer H., *"Eine Feldtheorie der Versetzungen in Cosserat-Kontinuum"*, ZAMP, Vol. 20, pp. 891-899, 1969.

Schouten J.A., *"Ricci-calculus"*, Springer-Verlag, 1954.

Schwink Ch.,*"Über den Begriff 'aktives Gleitvolumen' und dessen Bedeutung"*,Phys. stat. sol., Vol. 18, pp. 557-567, 1966.

Seeger A., *"Theorie der Gitterfehler"*, in Handbuch der Physik, edited by S. Flügge, Band VII, Part 1, pp. 383-666, 1955.

Sievert R., *"Eine Systematik für elastisch-plastische Stoffgleichungen"*, Dissertation, Schriftenreihe Phys. Ing.-Wiss. No. 23, TU Berlin, 1992.

Sievert R., *"Zur Zerlegung der Verformungsmaße des Cosserat-Kontinuums bei großen inelastischen Deformationen"*, ZAMM, Vol. 75, pp. 205-206, 1995.

Sommerfeld A., *"Mechanik der deformierbaren Medien"*, Vorlesungen über Theoretiche Physik, Vol. 2, Verlag Harri Deutsch, 1978.

Steinmann P., **Willam** K., *"Localization within the framework of micropolar elastoplasticity"*, Advances in Continuum Mechanics, edited by Brüller O., Mannl V., Najar J., Springer-Verlag, 1991.

Steinmann P., *"A micropolar theory of finite deformation and finite rotation multiplicative elastoplasticity"*, Int. J. Solids Structures, Vol. 31, No. 8, pp. 1063-1084, 1994.

Steinmann P., **Miehe** C., **Stein** E., *"On the localization analysis of orthotropic Hill type elastoplastic solids"*, J. Mech. Phys. Sol., Vol. 42. No. 2, pp. 1969-1994, 1994.

Su X.M., **Lu** W.D., *"On the strain Localizations of Ductile Single Crystals Undergoing Single Slip"*, Int. J. Solids Structures, Vol. 27, No. 1, pp.49-58, 1991.

Suo Z., **Ortiz** M.,**Needleman** A.,*"Stability of solids with interfaces"*, J. Mech. Phys. Solids, Vol. 40, No.3, pp. 613-640, 1992.

Szczerba M., **Korbel** A.,*"Strain softening and instability of plastic flow in Cu-Al single crystals"*, Acta Metall., Vol. 35,No. 5,pp. 1129- 1135, 1987.

Teodosiu C., **Sidoroff** F., *"A theory of finite elastoviscoplasticity of single crystals"*, Int. J. Engng. Sci., Vol. 14, pp. 713-723, 1976.

Teodosiu C., *"Elastic models of crystal defects"*, Springer-Verlag, 1982.

Teodosiu C., **Raphanel** J.L., **Tabourot**, *"Finite element simulation of the large elastoplastic deformation of multi-crystals"*, Large Plastic Deformations, edited by Raphanel J. L., Teodosiu C., Sidoroff F., Mécamat 91, pp. 153-168, 1993.

Thom R., *Stabilité structurale et morphogénèse*, InterEditions, Paris, 1977.

Thomas T.Y., *"Plastic flow and fracture in solids"*, Academic Press, 1961.

Thompson J.M.T., **Stewart** H.B., *Non-linear dynamics and chaos*, Wiley, 1986.

Trostel R., *"Vektor- und Tensor- Algebra"*, Mathematische Grundlagen der technischen Mechanik I, Beiträge zur theoretische Mechanik, Vieweg 1993.

Truesdells C., *"Polar and oriented media"*, in Six Lectures on Natural Philosophy, Springer-Verlag, 1966.

Truesdells C., **Toupin** R. *"The classical field theories"*, in Handbuch der Physik, edited by S. Flügge, Vol. 3.1, Springer-Verlag, 1960.

Truesdells C., **Noll** W., *"The non-linear field theories of mechanics"*, in Handbuch der Physik, edited by S. Flügge, Vol. 3.3, Springer-Verlag, 1994.

Vardoulakis I., *"Potentials and limitations of softening models in geomechanics (the role of second order work)"*, Eur. J. Mech. A/Solids, Vol. 13, No. 4-suppl., pp. 195-226, 1994.

Wack B., **Tourabi** A., *Cyclic simple shear of metallic sheets: application to Aluminium-Lithium alloys*, J. Mat. Sci., Vol. 28B, pp. 4735-4 743, 1994.

Walgraef D., **Aifantis** E.C., *"Plastic instabilities, dislocation patterns and nonequilibrium phenomena"*, Res Mechanica Vol. 23, pp. 161-195, 1988.

Walpole L.J., *"Evaluation of the elastic moduli of a transversely isotropic aggregate of cubic crystals"*, J. Mech. Phys. Solids, Vol. 33, No. 6, pp. 623-636, 1985.

Weng G.J., **Phillips** A., *"On the kinematics of continuous distribution of dislocations in plasticity"*, Int. J. Engng. Sci., Vol. 14, pp. 65-73, 1976.

Wit R. de, *"A view of the relation between the continuum theory of lattice defects and non-Euclidean geometry in the linear approximation"*, Int. J. Engng. Sci., Vol. 19, No. 12, pp. 1475-1506, 1981.

Yang S.,*"Etude expérimentale et théorique de l'instabilité de déformation plastique en bande de cisaillement dans les matériaux métalliques"*, Thèse Université Paris Nord, 1990.

Yang S., **Rey** C., *"Analysis of deformation by shear Banding: a two-dimensional post-bifurcation model"*, Large Plastic Deformations, edited by Raphanel J. L., Teodosiu C., Sidoroff F., Mécamat 91, pp. 271-277, 1993.

Yu J., **Perić** D., **Owen** D.R.J., *"An assessment of the Cosserat continuum through the FE simulation of a strain localization problem"*, Finite Elements in the 90's, edited by Oñate E., Periaux J., Samuelsson A., Springer-Verlag/CIMNE, Barcelona, 1991.

Zaoui A., **Korbel** A., **Dubois** P., **Rey** C., *"Bifurcation analysis of shear banding in metals"*, Solid State Phenomena, Vol. 3&4, pp. 433-446, 1988.

Zaoui A., *"Approximate statistical modelling and applications"*, Homogenization techniques for composite media, edited by E. Sanchez-Palencia and A. Zaoui, Lecture notes in physics, No. 272, Springer-Verlag, 1985.

Zaoui A., **Raphanel** J.L., *"On the nature of the intergranular accommodation in the modelling of elastoviscoplastic behaviour of polycrystalline aggregates"*, Large plastic deformations, edited by Raphanel J. L., Teodosiu C., Sidoroff F., Mécamat 91, pp. 27-38, 1993.

Zaoui A., *"Matériaux hétérogènes"*, Cours de l'Ecole Polytechnique, 1993.

Zarka J, *"Généralisation de la théorie du potentiel plastique multiple en viscoplasticité"*, J. Mech. Phys. Solids, Vol. 20, No. 3, pp. 179-195, 1972.

Zbib H.M., **Aifantis** E.C., *"On the localization and postlocalization behaviour of plastic deformation: I, On the initiation of shear bands, II, On the evolution and thickness of shear bands, III, On the structure and velocity of the Portevin-Le Chatelier bands"*, Res Mechanicca, Vol. 23, pp. 261-305, 1988.

Zbib H.M., **Jubran** J.S., *"Dynamic shear banding: a 3D analysis"*, Int. J. Plasticity, Vol. 8, pp. 619-641, 1992.

Zhou Z., *"Détermination des déformations et des contraintes dans les matériaux polycristallins"*, Thèse ENSAM, Paris, 1994.

Zorski H, *"Statistical theory of dislocations"*, Int. J. Solids Structures, Vol. 4, pp. 959-974, 1968.